

PHYSICS  
OF FAST  
AND  
INTERMEDIATE  
REACTORS

II

Proceedings of a Seminar, Vienna, 3-11 August 1961



INTERNATIONAL ATOMIC ENERGY AGENCY - VIENNA 1962



PHYSICS OF FAST AND INTERMEDIATE REACTORS

VOL. II

The following States are Members of the International Atomic Energy Agency:

AFGHANISTAN	ISRAEL
ALBANIA	ITALY
ARGENTINA	JAPAN
AUSTRALIA	REPUBLIC OF KOREA
AUSTRIA	LEBANON
BELGIUM	LUXEMBOURG
BRAZIL	MALI
BULGARIA	MEXICO
BURMA	MONACO
BYELORUSSIAN SOVIET SOCIALIST REPUBLIC	MOROCCO
CAMBODIA	NETHERLANDS
CANADA	NEW ZEALAND
CEYLON	NICARAGUA
CHILE	NORWAY
CHINA	PAKISTAN
COLOMBIA	PARAGUAY
CONGO (LÉOPOLDVILLE)	PERU
CUBA	PHILIPPINES
CZECHOSLOVAK SOCIALIST REPUBLIC	POLAND
DENMARK	PORTUGAL
DOMINICAN REPUBLIC	ROMANIA
ECUADOR	SENEGAL
EL SALVADOR	SOUTH AFRICA
ETHIOPIA	SPAIN
FINLAND	SUDAN
FRANCE	SWEDEN
FEDERAL REPUBLIC OF GERMANY	SWITZERLAND
GHANA	THAILAND
GREECE	TUNISIA
GUATEMALA	TURKEY
HAITI	UKRAINIAN SOVIET SOCIALIST REPUBLIC
HOLY SEE	UNION OF SOVIET SOCIALIST REPUBLICS
HONDURAS	UNITED ARAB REPUBLIC
HUNGARY	UNITED KINGDOM OF GREAT BRITAIN AND NORTHERN IRELAND
ICELAND	UNITED STATES OF AMERICA
INDIA	VENEZUELA
INDONESIA	VIET-NAM
IRAN	YUGOSLAVIA
IRAQ	

The Agency's Statute was approved on 26 October 1956 at an international conference held at United Nations headquarters, New York, and the Agency came into being when the Statute entered into force on 29 July 1957. The first session of the General Conference was held in Vienna, Austria, the permanent seat of the Agency, in October, 1957.

The main objective of the Agency is "to accelerate and enlarge the contribution of atomic energy to peace, health and prosperity throughout the world".

PROCEEDINGS SERIES

PHYSICS OF FAST  
AND INTERMEDIATE  
REACTORS  
II

PROCEEDINGS OF THE SEMINAR  
ON THE PHYSICS OF FAST AND INTERMEDIATE REACTORS  
SPONSORED BY  
THE INTERNATIONAL ATOMIC ENERGY AGENCY  
AND HELD IN VIENNA, 3 — 11 AUGUST 1961

INTERNATIONAL ATOMIC ENERGY AGENCY  
VIENNA 1962

PHYSICS OF FAST AND INTERMEDIATE REACTORS, IAEA, VIENNA, 1962  
STI/PUB/49

## FOREWORD

It is generally agreed that the ultimate economic advantage of power produced by nuclear fission over that produced by conventional sources depends on the ability of a certain type of reactor to breed precious nuclear fuel out of the plentiful but not readily fissionable isotope of uranium. This fact is mainly responsible for the importance attached to the development of fast power reactors, but many other interesting properties of unmoderated or weakly moderated reactor systems have also been brought to light by reactor physicists.

In August 1961 the Agency organized in Vienna a Seminar on the Physics of Fast and Intermediate Reactors, at which all the topics relating to this important branch of reactor science were discussed. The main feature of this meeting was extensive discussion of the 66 written contributions, which set the stage for a wide exchange of experience and ideas throughout 13 half-day sessions. The Seminar was attended by 132 scientists from 22 Member States and two international organizations.

It is hoped that these Proceedings of the Seminar, which include both the papers presented and a record of the discussions, will be useful as a reference work both to research workers in the field and to newcomers to it for many years to come. The Agency's thanks are due to all the participating scientists for their written or oral contributions and especially to those among them who, as session chairmen, led the discussions and contributed greatly to the success of the meeting.



March 1962

Scientific Secretary  
Seminar on the Physics of Fast  
and Intermediate Reactors

## *EDITORIAL NOTE*

*The papers and discussions incorporated in proceedings published by the International Atomic Energy Agency are checked for scientific accuracy by the Agency's experts in the subjects concerned and edited by the Agency's editorial staff to the extent considered necessary for the reader's assistance. The views expressed and the general style adopted remain, however, the responsibility of the named authors or participants.*

*The units and symbols employed are to the fullest practicable extent those standardized or recommended by the competent international scientific bodies.*

*The affiliations of authors are those given at the time of nomination.*

*The use in these Proceedings of particular designations of countries or territories does not imply any judgement by the Agency as to the legal status of such countries or territories, of their authorities and institutions or of the delimitation of their boundaries.*

## CONTENTS OF VOLUME II

### III. REACTOR THEORY

#### III.1. CALCULATION METHODS

Методы расчета ядерных реакторов на промежуточных и быстрых нейтронах . . . . .	3
Г. И. Марчук	
Calculs multigroupes des piles rapides . . . . .	27
<i>P. Moinereau et M. Solanes</i>	
Multi-group neutron transport theory . . . . .	55
<i>R. Zelazny and A. Kuszell</i>	
The validity of the transport approximation in critical-size and reactivity calculations . . . . .	73
<i>E. D. Pendlebury and L. H. Underhill</i>	
The reactivity of a central air gap in a bare reactor . . . . .	85
<i>H. Häggblom</i>	

#### III.2. EFFECTS OF CROSS-SECTION ERRORS

The sensitivity of calculated critical masses of small fast systems to changes in the U <sup>235</sup> and U <sup>237</sup> neutron-scattering data . . . . .	97
<i>E. D. Pendlebury</i>	
The effects of errors in cross-section data on calculations for a large dilute fast reactor . . . . .	111
<i>T. P. Moorhead</i>	

#### III.3. REACTIVITY EFFECTS

Reactivity coefficients by perturbation theory . . . . .	149
<i>J. W. Webster</i>	
The reactivity effect of hydrogen addition in fast reactors . . . . .	165
<i>H. Soodak</i>	
Reactivity coefficients of sodium in some large fast reactors . . . . .	177
<i>M. G. Bhide and H. H. Hummel</i>	
Методы расчета выгорания поглотителей в реакторах на промежуточных нейтронах . . . . .	187
Г. И. Тошинский и А. Г. Калашников	

#### III.4. LONG-TERM EFFECTS

Long-time behaviour of fast breeders . . . . .	213
<i>K. Ott and A. Jansen</i>	
Fission gas pressure build-up and fast-breeder economy . . . . .	228
<i>P. Engelmann</i>	
Fission-product burn-up in fast reactors . . . . .	247
<i>M. M. Levine</i>	
Effect of the plutonium isotopic composition on the performance of fast reactors . . . . .	257
<i>S. Yiftah</i>	
Performance of large fast power reactors including effects of higher isotopes, recycling and fission products . . . . .	271
<i>D. Okrent</i>	

#### III.5. REACTOR CONCEPT STUDIES

Quelques études de piles rapides de puissance . . . . .	301
<i>A. Kania, P. Moinereau, G. Vendryès et C. P. Zaleski</i>	
Some physics aspects of cermet and ceramic fast systems . . . . .	357
<i>J. Codd, M. F. James and J. E. Mann</i>	
The physics aspects of a coupled fast-thermal steam superheating reactor . . . . .	373
<i>B. J. Toppel and R. Avery</i>	



### **III. REACTOR THEORY**

#### **1. CALCULATION METHODS**



# МЕТОДЫ РАСЧЕТА ЯДЕРНЫХ РЕАКТОРОВ НА ПРОМЕЖУТОЧНЫХ И БЫСТРЫХ НЕЙТРОНАХ

Г. И. МАРЧУК  
АКАДЕМИЯ НАУК СССР, МОСКВА,  
СССР

**Abstract — Résumé — Аннотация — Resumen**

**A review of calculation methods for fast and intermediate reactors.** This paper discusses the development of methods for calculating intermediate and fast reactors. It deals with various approaches to the problems of physical calculation. The calculation of resonance effects is discussed. Consideration is given to multi-group systems of fundamental and conjugate equations, various applications of perturbation theory to the problems of physical reactor calculation, and numerical methods of solving fundamental and conjugate reactor equations, which approximate the method of spherical harmonics.

The paper describes an application of the response method to the solution of critical-mass problems, and methods of calculating reactors with homogeneous moderators. The fundamental features of an effective one-group reactor model are described.

**Exposé des méthodes pour le calcul de réacteurs à neutrons rapides et intermédiaires.** L'auteur examine la mise au point de méthodes pour le calcul de réacteurs à neutrons rapides et intermédiaires. Il décrit diverses manières d'aborder les problèmes des calculs sur la physique des réacteurs, notamment le calcul des effets de résonance. Il s'attache particulièrement aux points suivants: systèmes d'équations fondamentales et conjuguées à plusieurs groupes; diverses applications de la théorie des perturbations aux problèmes de calculs sur la physique des réacteurs; méthodes numériques pour résoudre les équations fondamentales et conjuguées, voisines de la méthode des harmoniques sphériques.

L'auteur décrit ensuite une manière d'appliquer la méthode de la réponse aux problèmes de la masse critique ainsi que des méthodes pour le calcul de réacteurs ralentis à l'hydrogène. Il décrit les caractéristiques fondamentales d'un modèle de réacteur à un groupe effectif.

**Обзор методов расчета реакторов на промежуточных и быстрых нейтронах.** Обсуждается развитие методов расчета ядерных реакторов на промежуточных и быстрых нейтронах. Рассматриваются различные постановки задач физического расчета. Обсуждается учет резонансных эффектов. Вводятся в рассмотрение многогрупповые системы основных и сопряженных уравнений. Даётся различное применение теории возмущений к задачам физического расчета реактора. Рассматриваются численные методы решения основных и сопряженных уравнений реактора в приближении метода сферических гармоник.

Дается применение метода характеристик к решению задач на критическую массу реактора. Излагаются методы расчета реакторов с водородсодержащими замедлителями. Излагаются основы эффективной одногрупповой модели реактора.

**Estudio panorámico de los métodos de cálculo de los reactores rápidos e intermedios.** El autor analiza el desarrollo de los métodos de cálculo de los reactores nucleares que trabajan con neutrones rápidos y con neutrones intermedios. Examina diversos planteos de los problemas del cálculo físico. Indica la forma de tomar en cuenta los efectos de resonancia y menciona los sistemas de ecuaciones fundamentales y

conjugadas de la teoría de los multigrupos. Expone luego diversas aplicaciones de la teoría de la perturbación a los problemas del cálculo físico del reactor. Examina los métodos numéricos de resolución de las ecuaciones fundamentales y conjugadas que expresan el funcionamiento del reactor sobre la base del método de los armónicos esféricos.

Explica asimismo cómo se utiliza el método de las características en la solución de problemas relativos a la masa crítica del reactor. Describe los métodos de cálculo de los reactores con moderadores que contienen hidrógeno y, por fin, expone las bases de un modelo efectivo fundado en la teoría de un solo grupo, aplicable al reactor.

## **Введение**

Широкое применение в расчетах быстродействующей вычислительной техники создало благоприятные условия для развития многих областей науки и техники. Новейшие достижения вычислительной математики позволили пересмотреть алгоритмы решения многих задач математической физики и разработать новые алгоритмы, основанные на использовании численных методов, поддающихся эффективной реализации на вычислительных машинах.

Таким образом, аналитические методы решения задач, во многих случаях уступили место более эффективным численным методам.

Использование в расчетах быстродействующей вычислительной техники позволило поставить и решать новые задачи науки и техники, решение которых, вследствие большого объема вычислительных работ, казалось ранее практически неосуществимым.

В результате создались такие условия, при которых оказалось возможным решать сложнейшие математические и логические задачи. В связи с этим основное внимание приобрели вопросы, связанные с математической постановкой задач и разработкой эффективных вычислительных алгоритмов:

Успехи в области вычислительной математики оказали большое влияние на развитие теории и методов расчета ядерных реакторов. После книги С. Глесстона и М. Эдлунда [1], в которой были изложены элементарные основы теории реакторов на тепловых нейтронах, появилась монография А. Д. Галанина [2], посвященная вопросам теории реакторов на тепловых нейтронах. Теоретические основы атомной энергетики в дальнейшем были изложены в книгах А. Вейнберга и Е. Вигнера [3], а также Б. Дэвисона [4]. В монографиях Г. И. Марчука [5], [6] рассмотрены методы расчета ядерных реакторов. В последнее время вышла книга Р. Мегреблиана и Д. Холмса [7], которая также посвящена вопросам теории и методам расчета ядерных реакторов.

К настоящему времени не утратили своего теоретического значения работы раннего периода развития атомной энергетики. Это работы Е. Вигнера [3], Е. Пайерлса [8], Р. Маршака [9], [10], Н. Н. Боголюбова [11], И. И. Гуревича, И. Я. Померанчука [12], Г. Гурвича [13], [14], А. Вейнберга [3], [15] и др.

Дальнейшее развитие теории ядерных реакторов и методы расчета получили в докладах на первой и второй Женевской конференциях по мирному использованию атомной энергии.

Большое развитие теория и методы расчета ядерных реакторов получили в Советском Союзе.

Существенный прогресс имел место в теории и методах расчета тепловых реакторов в работах И. В. Курчатова [16], А. П. Александрова [17], А. И. Алиханова [18], Д. И. Блохинцева [19], [20], В. С. Фурсова [21], И. И. Гуревича и И. Я. Померанчука [12], С. М. Фейнберга [22], [23], [24], А. Д. Галанина [2], [25], В. В. Орлова [26], [27] и др. На основе этих работ научно обоснованы проекты ядерных реакторов для большого числа энергетических установок, таких как первая атомная электростанция Советского Союза, Воронежская, Белоярская атомные электростанции, ледокол „Ленин“ и др., а также большого числа экспериментальных реакторов с различными замедлителями и теплоносителями.

Теория и методы расчета реакторов на промежуточных нейтронах получили развитие в работах А. И. Лейпунского, А. С. Романовича, Л. Н. Усачева [28], В. Я. Пупко [29], [30], В. А. Кузнецова, Б. Ф. Громова, Г. И. Топшинского, В. В. Чекунова, В. В. Орлова [26]—[31] и др.

В 1949 году А. И. Лейпунский указал на возможность использования реактора на быстрых нейтронах с целью получения энергии при одновременном значительном воспроизведстве атомного горючего. В дальнейшем теория и методы расчета реакторов на быстрых нейтронах совершенствовались и развивались в работах А. И. Лейпунского [32], [33], [34], Д. И. Блохинцева [20], [34], Л. Н. Усачева [28], [35], О. Д. Казачковского [36], И. И. Бондаренко [37], [38], С. Б. Шихова [39], [40], Ю. А. Стависского [32], [33], а также В. С. Владимира [41], [42], Ю. А. Романова [43] и др.

Указанные работы позволили научно обосновать проекты атомных энергетических установок БР-1 и БР-2, построенных и пущенных в эксплуатацию соответственно в 1957 и 1959 гг.

Обзор работ иностранных ученых по теории и методам расчета реакторов дан в докладах на первой и второй Женевских конференциях.

Существенное развитие за последние годы получила также и вычислительная математика, основные результаты которой были получены коллективом Математического Института им. В. А. Стеклова АН СССР под научным руководством академика М. В. Келдыша. Наиболее существенные результаты этих работ относятся к решению конечно-разностных уравнений эллиптического типа, а также к построению конечно-разностных уравнений, аппроксимирующих дифференциальные уравнения с разрывными коэффициентами.

Для решения трехточечных конечно-разностных уравнений эллиптического типа И. М. Гельфандом и О. В. Локуциевским (см. [5]) и, независимо, А. С. Кронродом (см. [2]), а также Штарком [44], [45] был сформулирован метод линейной факторизации, который позволил краевую задачу свести к последовательному решению трех конечно-разностных уравнений первого порядка. В дальнейшем М. В. Келдыш, И. М. Гельфанд и О. В. Локуциевский вместе с К. И. Бабенко и Н. Н. Ченцовым существенно развили методы решения конечно-разностных уравнений, разработав аппарат матричной факторизации применительно к системам разностных уравнений. В частности, это позволило сформулировать новый метод решения многомерных дифференциальных уравнений эллиптического типа. Метод матричной факторизации оказал решающее влияние на развитие численных методов решения уравнений метода сферических гармоник применительно к задачам атомной энергетики.

Изучению конечно-разностных уравнений, аппроксимирующих дифференциальные уравнения эллиптического типа, посвящены работы А. Н. Тихонова и А. А. Самарского [46], [47]. В работах А. Н. Тихонова и А. А. Самарского весьма полно исследованы вопросы построения трехточечных конечно-разностных схем, даны практические алгоритмы наиболее рациональной аппроксимации дифференциальных уравнений конечно-разностными, а также устанавливаются общие свойства решений разностных уравнений. Ими вводится в рассмотрение понятие интегральной точности решения конечно-разностного уравнения по отношению к решению дифференциального уравнения и доказаны теоремы о сходимости решений конечно-разностного уравнения. В частности доказано, что построенные разностные уравнения в классе разрывных коэффициентов обладают вторым интегральным порядком точности.

Достижения вычислительной математики широко обсуждены в научной литературе, а также на конференциях и съездах.

В настоящем обзоре мы остановимся на рассмотрении некоторых принципиальных вопросов теории и методов расчета реакторов, получивших широкое распространение в практической деятельности научных коллективов Советского Союза.

## 1. Основные и сопряженные уравнения

Наиболее общая математическая формулировка задачи на расчет критического режима работы реактора дается с помощью интегро-дифференциального уравнения Больцмана при соответствующем граничном условии на внешней поверхности реактора  $S$ :

$$\Omega \nabla \varphi + \Sigma \varphi - \int dv' \int d\Omega' \varphi(r, \Omega', v') W(\mu_0, v' \rightarrow v) = 0 \quad (1)$$

$$\varphi(r, \Omega, v) = 0 \text{ на } S, \quad \Omega n < 0 \quad (2)$$

где  $\varphi = nv$  — поток нейтронов в точке с радиусом-вектором  $r$ , имеющих скорость  $v = v\Omega$ ,  $\Omega$  — единичный вектор направления полета нейтрона,  $\Sigma$  — полное макроскопическое сечение взаимодействия нейтрона с веществом,  $\mu_0 = \Omega \cdot \Omega$ . Штрихами отмечены величины  $v'$ ,  $\Omega'$ , характеризующие скорость нейтрона до столкновения с ядром. Функция  $W(\mu_0, v' \rightarrow v)$  является дифференциальным сечением ядерного процесса взаимодействия нейронов с веществом.

Граничное условие (2) выражает тот факт, что вылетевшие из реактора нейтроны, единичные векторы скоростей которых связаны с внешней нормалью  $n$  к поверхности соотношением  $\Omega \cdot n < 0$ , не возвращаются снова в реактор. Условие (2) равносильно предположению, что реактор граничит с вакуумом или с абсолютно черным телом.

Таким образом, пространственно-энергетическое и угловое распределение нейронов в критическом реакторе описывается однородной задачей (1), (2). Известно, что неотрицательное решение задачи (1), (2) возможно при вполне определенных размерах реактора, которые называются критическими размерами. В большинстве случаев решение задачи (1), (2) состоит в отыскании критического размера реактора. Однако, возможны различные видоизменения задачи на расчет критического реактора. Так, например, при фиксиро-

ванных размерах реактора можно изменять концентрацию ядер делящегося изотопа или замедлителя так, чтобы обеспечить существование неотрицательного решения задачи (1), (2). Возможны также и другие способы осуществления критического режима работы реактора.

Дальнейшее рассмотрение сводится к различным упрощениям в постановке и решении задачи (1), (2) применительно к тем или иным конкретным условиям физического расчета реактора.

Однако, прежде чем сформулировать приближенные методы решения уравнений реактора, мы остановимся на одном фундаментальном вопросе теории ядерных реакторов, а именно, на применении сопряженных уравнений в физическом расчете реакторов.

Для получения сопряженного уравнения по отношению к основному уравнению реактора (1) вводится в рассмотрение понятие скалярного произведения. Рассмотрим две функции  $f(\mathbf{r}, \Omega, v)$  и  $f^*(\mathbf{r}, \Omega, v)$ . Тогда скалярное произведение этих функций определим следующим образом:

$$(f, f^*) = \int d\mathbf{r} \int d\Omega \int dv f f^*, \quad (3)$$

где интегрирование производится по всей области изменения переменных ( $\mathbf{r}, \Omega, v$ ).

Уравнение (1) запишем формально в виде

$$L\varphi = 0 \quad (4)$$

где  $L$  — оператор, определенный формулой

$$L = \Omega \nabla + \Sigma - \int dv' \int d\Omega' W(\mu_0, v' \rightarrow v) \quad (5)$$

Предположим, что функция  $f(\mathbf{r}, \Omega, v)$  удовлетворяет граничному условию (2), а также что оператор  $L$  конечен. Тогда можно составить следующий функционал:

$$I = (f^*, Lf) \quad (6)$$

Если функционал (6) с помощью различных преобразований приведем к виду

$$(f^*, Lf) = (f, L^* f^*) \quad (7)$$

то оператор  $L^*$  называется сопряженным оператором по отношению к  $L$ . Непосредственной проверкой можно убедиться, что сопряженный оператор  $L^*$  имеет вид

$$L^* = -\Omega \nabla + \Sigma - \int dv' \int d\Omega' W(\mu_0, v \rightarrow v') \quad (8)$$

при этом требуется, чтобы функция  $f^*(\mathbf{r}, \Omega, v)$  удовлетворяла следующему условию на внешней поверхности реактора  $S$ :

$$f^*(\mathbf{r}, \Omega, v) = 0 \text{ на } S, \Omega n > 0 \quad (9)$$

Если в качестве функции  $f(\mathbf{r}, \Omega, v)$  в соотношении (6) выбрать решение уравнения (5), т.е. положить

$$f = \varphi(\mathbf{r}, \Omega, v)$$

а соответствующую этому случаю функцию  $f^*(\mathbf{r}, \Omega, v)$  обозначить через

$\varphi^*(\mathbf{r}, \Omega, v)$ , то равенство (8) приводит к сопряженному уравнению реактора

$$L^* \varphi^* = 0 \quad (10)$$

В результате мы приходим к следующей сопряженной задаче, по отношению к задаче (1), (2):

$$-\Omega \nabla \varphi^* + \Sigma \varphi^* - \int dv' \int d\Omega' \varphi^*(\mathbf{r}, \Omega', v') W(\mu_0, v \rightarrow v') = 0 \quad (11)$$

$$\varphi^*(\mathbf{r}, \Omega, v) = 0 \text{ на } S, \Omega n > 0 \quad (12)$$

Впервые простейшие сопряженные уравнения реактора в задачах на критический размер были введены в рассмотрение Е. Вигнером [3]. Для односкоростной задачи сопряженное уравнение в весьма общей постановке было сформулировано К. Фуксом [48] и Н. А. Дмитриевым (см. [28]). Наиболее полная запись сопряженного уравнения реактора с учетом замедления дана Л. Н. Усачевым [28]; им также дана физически наглядная интерпретация сопряженной функции, как ценности нейтронов. В дальнейшем теория сопряженных уравнений была обобщена Б. Б. Кадомцевым [49] на случай неоднородных уравнений переноса частиц. В работе Г. И. Марчука и В. В. Орлова [27] разработан метод получения сопряженных уравнений для широкого класса неоднородных линейных задач, а также в общем виде сформулирована теория возмущений для различных линейных функционалов.

При расчете критической массы и пространственно-энергетического распределения потока и ценности нейтронов в реакторе точное решение кинетического уравнения (1) при граничном условии (2) представляет задачу весьма сложную. Поэтому в большинстве случаев ограничиваются отысканием приближенных решений. Среди используемых для этой цели приближенных методов особое место занимает диффузационное приближение. Сущность метода состоит в том, что решение задачи (1), (2) ищется в виде ряда по сферическим функциям, ограничиваясь в разложении двумя первыми членами [10].

Итак, пусть

$$\varphi(\mathbf{r}, \Omega, v) = \frac{1}{4\pi} [\varphi_0(\mathbf{r}, v) + 3\Omega \varphi_1(\mathbf{r}, v)], \quad (13)$$

где функция  $\varphi_0$  является полным потоком нейтронов через единичную сферу с центром в точке  $\mathbf{r}$ , а  $\varphi_1$  — векторным током нейтронов в точке  $\mathbf{r}$ .

Функцию  $W(\mu_0, v' \rightarrow v)$  разложим в ряд по полиномам Лежандра и ограничимся двумя первыми членами. Тогда будем иметь

$$W(\mu_0, v' \rightarrow v) = \frac{1}{2} [W_0(v' \rightarrow v) + 3\mu_0 W_1(v' \rightarrow v)] \quad (14)$$

Подставляя выражения (13) и (14) в уравнение (1), приходим к системе интегро-дифференциальных уравнений

$$\left. \begin{aligned} \nabla \varphi_1 + \Sigma \varphi_0 - \int dv' W_0(v' \rightarrow v) \varphi_0(\mathbf{r}, v') &= 0, \\ \frac{1}{3} \nabla \varphi_0 + \Sigma \varphi_1 - \int dv' W_1(v' \rightarrow v) \varphi_1(\mathbf{r}, v') &= 0. \end{aligned} \right\} \quad (15)$$

Границное условие для системы уравнений (15) найдем следуя Р. Маршаку [10]:

$$2\varphi_1 n - \varphi_0 = 0 \text{ на } S \quad (16)$$

Система уравнений (15) вместе с граничным условием (16) образует замкнутую систему основных уравнений реактора в диффузионном приближении.

Аналогично, система сопряженных уравнений реактора в диффузионном приближении может быть получена в виде

$$\left. \begin{aligned} & -\nabla\varphi_1^* + \Sigma\varphi_0^* - \int dv' W_0(v \rightarrow v') \varphi_0^*(r, v') = 0 \\ & -\frac{1}{3}\nabla\varphi_0^* + \Sigma\varphi_1^* - \int dv' W_1(v \rightarrow v') \varphi_1^*(r, v') = 0 \end{aligned} \right\} \quad (17)$$

Границное условие для системы уравнений (17) имеет вид

$$2\varphi_1^* n + \varphi_0^* = 0 \text{ на } S \quad (18)$$

Система уравнений (17) вместе с граничным условием (18) образуют замкнутую систему сопряженных уравнений реактора в диффузионном приближении.

Аналогичные уравнения и граничные условия могут быть получены в различных более точных, чем  $P_1$ —приближениях метода сферических гармоник.

В связи с тем, что решение основных и сопряженных уравнений реактора в наименее общей постановке представляет собой задачу очень сложную, поддающуюся эффективному решению только в крайне редких случаях, появляется необходимость в разработке различных приближенных методов. Одним из наименее распространенных приближенных методов решения основных и сопряженных уравнений реактора является многогрупповой метод. Сущность метода состоит в том, что весь интервал скоростей нейтрона в реакторе разбивается на частичные интервалы, в пределах каждого из которых предполагается, что физические константы не изменяются.

Тогда на каждом интервале, где физические параметры задачи считаются постоянными, можно проинтегрировать уравнение (1) в пределах данной энергетической группы и в качестве неизвестных выбрать интегральные потоки нейтронов по группам.

В результате формально мы приходим к многогрупповым системам уравнений реактора. Так, многогрупповая система основных уравнений принимает вид [5], [6]

$$\Omega\nabla\varphi^j + \Sigma^j\varphi^j - \sum_l \int d\Omega' \Sigma^{l \rightarrow j}(\mu_0) \varphi^l(r, \Omega') = 0 \quad (19)$$

$$\varphi^j(r, \Omega) = 0 \text{ на } S, \Omega \cdot n < 0, \quad (20)$$

где

$$\varphi^j(r, \Omega) = \int_{v_{j-1}}^{v_j} dv \varphi(r, \Omega, v), \quad (21)$$

а  $\Sigma^j$  и  $\Sigma^{l \rightarrow j}(\mu_0)$  — групповые константы, которые будут определены в дальнейшем.

Сопряженная задача по отношению к многогрупповой задаче (20) может быть сформулирована с помощью изложенного выше метода с той только разницей, что для функций дискретного аргумента скалярное произведение следует определить формулой

$$(f, f^*) = \sum_j \int d\mathbf{r} \int d\Omega f^j f^{*j}, \quad (22)$$

где суммирование производится по всем группам, а интегрирование — по всей области изменения переменных  $\mathbf{r}$  и  $\Omega$ . В результате приходим к следующей сопряженной задаче:

$$-\Omega \nabla \varphi^{*j} + \Sigma^j \varphi^{*j} - \sum_l \int d\Omega' \Sigma^{j \rightarrow l}(\mu_0) \varphi^{*l}(\mathbf{r}, \Omega') \quad (23)$$

$$\varphi^{*j}(\mathbf{r}, \Omega) = 0 \text{ на } S, \Omega n > 0 \quad (24)$$

Для получения системы многогрупповых констант  $\Sigma^j$  и функций  $\Sigma^{l \rightarrow j}(\mu_0)$  необходимо воспользоваться теорией возмущений. С этой целью потребуем, чтобы при переходе от задачи (1), (2), которую будем называть невозмущенной, к многогрупповой возмущенной задаче (20), (21), критический размер реактора или любой другой характеристический параметр задачи не изменился. В результате нетрудно прийти к формулам усреднения констант [5], [6].

Если предположить, что решения основных и сопряженных уравнений не зависят от азимута, то приходим к следующим формулам для групповых констант:

$$\sum^j = \frac{\int_{G_n}^{\nu_j} d\mathbf{r} \int d\Omega \varphi^{*j} \int dv \Sigma \varphi}{\int_{G_n}^{\nu_{j-1}} d\mathbf{r} \int d\Omega \varphi^{*j} \int dv \varphi}, \quad (25)$$

$$\sum^{l \rightarrow j}(\mu_0) = \Delta v_j \cdot \sum_{m=0}^{\infty} \frac{2m+1}{2} W_m^{l \rightarrow j} \cdot P_m(\mu_0),$$

где

$$W_m^{l \rightarrow j} = \frac{\int_{G_n}^{\nu_l} d\mathbf{r} \varphi_m^{*j} \int_{\nu_{l-1}}^{\nu_l} dv \varphi_m \int_{\nu_{j-1}}^{\nu_j} dv' W_m(v \rightarrow v')}{\int_{G_n}^{\nu_{l-1}} d\mathbf{r} \varphi_m^{*j} \int_{\nu_{l-1}}^{\nu_l} dv \varphi_m} \quad (26)$$

Здесь  $\Delta v_j = v_j - v_{j-1}$ ,  $G_n$  — зона реактора, в которой ищутся групповые константы,  $\varphi_m^{*j}$  и  $\varphi_m(\mathbf{r}, v)$  — коэффициенты Фурье в разложении функции  $\varphi^{*j}(\mathbf{r}, \mu)$  и  $\varphi(\mathbf{r}, \mu, v)$  — в ряды по полиномам Лежандра.

Анализ формул (25), (26) показывает, что они представляют собой дробные функционалы со статистическими весами, в качестве которых выступают решения многогрупповых систем основных и сопряженных уравнений

реактора. Если в формулах (25), (26) принять  $\varphi_m^* = 1$  и  $\varphi_m = 1$ , то приходим к простейшему алгоритму усреднения групповых констант. Указанный простейший способ усреднения групповых констант широко используется в расчетах [5], [6], [39].

Аналогичным образом могут быть получены системы основных и сопряженных уравнений реактора в  $P_1$ -приближении. Так многогрупповая система основных уравнений реактора принимает вид

$$\left. \begin{aligned} \nabla \Phi_1^j + \Sigma_0^j \varphi_0^j - \sum_l \sum_{l \rightarrow j} \varphi_0^l &= 0 \\ \frac{1}{3} \nabla \varphi_0^j + \Sigma_1^j \Phi_1^j - \sum_l \sum_{l \rightarrow j} \Phi_1^l &= 0 \end{aligned} \right\} \quad (27)$$

при условии, что

$$2 \Phi_1^j n - \varphi_0^j = 0 \text{ на } S. \quad (28)$$

Многогрупповая система сопряженных уравнений представляется в виде

$$\left. \begin{aligned} -\nabla \Phi_1^{*j} + \Sigma_0^{*j} \varphi_0^{*j} - \sum_l \sum_{j \rightarrow l} \varphi_0^{*l} &= 0 \\ -\frac{1}{3} \nabla \varphi_0^{*j} + \Sigma_1^{*j} \Phi_1^{*j} - \sum_l \sum_{j \rightarrow l} \Phi_1^{*l} &= 0 \end{aligned} \right\} \quad (29)$$

причем, граничным условием на внешней поверхности будет следующее:

$$2 \Phi_1^{*j} n + \varphi_0^{*j} = 0 \text{ на } S. \quad (30)$$

Групповые константы в системе основных и сопряженных уравнений находятся с помощью следующих формул усреднения:

$$\begin{aligned} \Sigma_0^j &= \frac{\int_{G_n}^{v_j} dr \varphi_0^{*j} \int_{v_{j-1}}^{v_j} dv \Sigma \varphi_0}{\int_{G_n}^{v_j} dr \varphi_0^{*j} \int_{v_{j-1}}^{v_j} dv \varphi_0}, \\ \Sigma_1^j &= \frac{\int_{G_n}^{v_j} dr \varphi_1^{*j} \int dr \Sigma \varphi_1}{\int_{G_n}^{v_j} dr \varphi_1^{*j} \int dr \varphi_1}, \\ \Sigma_0^{l \rightarrow j} &= \Delta v_j \frac{\int_{G_n}^{v_l} dr \varphi_0^{*j} \int_{v_{l-1}}^{v_l} dv \varphi_0 \int_{v_{j-1}}^{v_j} dv' W_0(v \rightarrow v')}{\int_{G_n}^{v_l} dr \varphi_0^{*j} \int_{v_{l-1}}^{v_l} dv \varphi_0}, \end{aligned} \quad (31)$$

$$\Sigma_1^{l \rightarrow j} = \Delta v_j \frac{\int d\mathbf{r} \varphi_1 *^j \int dv \varphi_1 \int dv' W_1(v \rightarrow v')}{\int d\mathbf{r} \varphi_1 *^j \int dv \varphi_1} . \quad (31)$$

Формулы (31) предполагают, что спектр потока нейтронов в каждой точке реактора известен и известна многогрупповая ценность нейтронов. Стого говоря, ни потока нейтронов ни многогрупповой ценности мы заранее не знаем, так что точное значение групповых констант, определяемых формулами (31), нам неизвестно.

Тем не менее указанные формулы с успехом могут быть использованы для приближенного получения групповых констант. Так, например, в активной зоне реактора усреднение констант можно производить с учетом спектра эквивалентного реактора без отражателя, а в отражателе усреднение констант производить по интегральному потоку нейтронов, предварительно найденному из соотношения баланса нейтронов. Такие приближенные методы разработаны С. Б. Шиховым [40].

Возможны и другие методы усреднения, более точно учитывающие конкретные особенности реактора. Мы остановимся здесь на одном эффективном методе, сущность которого состоит в следующем.

Рассмотрим основные уравнения реактора. В диффузионно-возрастном приближении эта система представится в следующем виде

$$\frac{\partial q}{\partial u} + \frac{\Sigma_c}{\xi \Sigma_s} q = \nabla D \nabla \varphi_0 + \chi(u) Q(\mathbf{r}), \quad (32)$$

где

$$Q(\mathbf{r}) = \int_{-\infty}^{\infty} du v_f \Sigma_f \varphi_0, \quad q = \xi \Sigma_s \varphi_0 \quad (33)$$

а  $u$  — летаргия, связанная с переменной  $v$  соотношением  $u = 2 \ln(v_0/v)$ ,  $v_0$  — некоторая фиксированная скорость. Предполагая правую часть уравнения (33) известной, решим его в пределах группы  $(v_{j-1}, v_j)$  как линейное неоднородное дифференциальное уравнение первого порядка. В результате нетрудно прийти к решению [5], [6] уравнения (32).

$$\varphi_0(\mathbf{r}, u) = \frac{1}{\xi \Sigma_s} \left\{ \left[ P^j(u) - P^j \frac{A^j(u)}{A^j} \right] \xi \Sigma_s(u_{j-1}) \varphi_0(\mathbf{r}, u_{j-1}) + \right. \\ \left. + \Sigma^j A^j(u) \varphi_0(\mathbf{r}, u_j) + \frac{A^j(u)}{A^j} \chi^j Q(\mathbf{r}) \right\} \quad (34)$$

где

$$P^j(u) = e^{- \int_{u_{j-1}}^{u_j} \frac{\Sigma_c}{\xi \Sigma_s} du}, \quad A^j(u) = \int_{u_{j-1}}^{u_j} \eta \frac{\xi \Sigma_s(u)}{\xi \Sigma_s(u')} \frac{P^j(u)}{P^j(u')} du', \quad (35)$$

$$P^j = P^j(u_j), \quad A^j = A^j(u_j), \quad \eta = \int_{-\infty}^u \chi(u) du$$

Значения других физических констант общезвестны.

Таким образом, спектр нейтронов в пределах групп будет известен, если известны значения потока нейтронов на границах групповых интервалов. Как показано в работах [5], [6] значения потока нейтронов на границах интервалов определяются задачей:

$$\nabla D^j \nabla \varphi_0(\mathbf{r}, u_i) - \Sigma^j \varphi_0(\mathbf{r}, u_j) = -f^j, \quad (36)$$

где

$$\left. \begin{aligned} D^j &= \frac{\int_{u_{j-1}}^{u_j} \frac{D\eta}{\xi \Sigma_s} \frac{P^j}{P^j(u)} du}{\int_{u_{j-1}}^{u_j} \frac{\eta}{\xi \Sigma_s} \frac{P^j}{P^j(u)} du}, \\ \Sigma^j &= \xi \Sigma_s(u_j)/A^j, \\ f^j &= \frac{1}{A^j} \left[ P^j \xi \Sigma_s(u_{j-1}) \varphi_0(\mathbf{r}, u_{j-1}) + \chi^j Q(\mathbf{r}) \right] \end{aligned} \right\} \quad (37)$$

В результате решения уравнений (36) получаем потоки нейтронов при летаргиях  $u_i$ , соответствующих скоростям нейтронов  $v_i$ . Далее, с помощью интерполяционной формулы (34) находим спектр нейтронов в любой точке реактора. После того, как спектр нейтронов найден, алгоритм усреднения физических констант для реактора одномерной геометрии будет следующий.

Полагая в формулах (32)  $\varphi_0^* = 1$ ,  $\varphi_1^* = k$ , где  $k$ , совпадающий по направлению с нормалью к координатной поверхности, приходим к простейшей системе групповых констант, которые используются для решения сопряженной многогрупповой задачи (30), (31). После этого снова рассчитываются групповые константы и так далее. Этот процесс сходится очень быстро, так что уже после 2-х–3-х итераций групповые константы более не уточняются. Далее, с полученной системой групповых констант производится решение многогрупповой системы основных уравнений реактора (28), (29).

Если ширина групп так мала, что в пределах каждой из групп поток нейтронов изменяется слабо, то способ усреднения физических констант оказывается несущественным и в этом случае можно определить универсальную систему групповых констант, не зависящую от спектра нейтронов в реакторе. Однако, если интервалы групп велики, то для промежуточных и быстрых реакторов необходимо воспользоваться методом усреднения, изложенным выше.

В заключение необходимо сказать, что в более высоких приближениях метода сферических гармоник, чем  $P_1$ —приближение можно получить формулы группового усреднения аналогичные формулам (32). Для получения усредненных констант по этим формулам необходимо знание спектра нейтронов в каждой точке реактора, который находится с помощью различных приближенных методов, в том числе и в  $P_1$ —приближении.

## 2. Численные методы решения уравнений сферических гармоник

Среди приближенных методов решения кинетических уравнений видное место занимает метод сферических гармоник, разработанный Виком и развитый далее в работах Р. Маршака [10], Л. Н. Усачева [35], Б. Дэвисона [4], Г. Марка [40], В. С. Владимира [41], [42] и др. Сущность метода состоит в том, что решение кинетического уравнения ищется в виде ряда Фурье по сферическим функциям. В результате для получения неизвестных коэффициентов Фурье находится бесконечная система дифференциальных уравнений от геометрической координаты.

Рассмотрим для простоты односкоростное кинетическое уравнение, которое является элементом группового расчета. Если предположить, что рассеяние нейтронов в лабораторной системе координат определяется функцией  $g(\mu_0)$  задача плоско-параллельна, то уравнение переноса нейтронов будет иметь вид

$$\mu \frac{\partial \varphi}{\partial z} + \Sigma \varphi = \frac{\Sigma_s}{2} \int_{-1}^{+1} d\mu' g(\mu_0) \varphi'(z, \mu) + f(z, \mu), \quad (38)$$

где  $\mu_0 = \mu \mu' + \sqrt{1 - \mu^2} \sqrt{1 - \mu'^2} \cos \alpha$ ,  $\alpha$  — азимут.

Решение уравнения (38) будем искать в виде

$$\varphi(z, \mu) = \frac{1}{2} \sum_{l=0}^{\infty} (2l+1) \varphi_l(z) P_l(\mu), \quad (39)$$

где  $P_l(\mu)$  — полиномы Лежандра. Тогда приходим к системе обыкновенных дифференциальных уравнений

$$m \frac{d\varphi_{m-1}}{dz} + (m+1) \frac{d\varphi_{m+1}}{dz} + (2m+1) \Sigma_m \varphi_m = (2m+1) f_m, \quad (40)$$

где

$$\Sigma_m = \Sigma - g_m \Sigma_s,$$

а  $g_m$  и  $f_m$  — коэффициенты Фурье функции  $g(\mu)$  и  $f(z, \mu)$  в ряды по полиномам Лежандра.

На внешней границе области поставим условия Маршака

$$\int_{-1}^0 d\mu \cdot \mu^{2i+1} \varphi = 0 \text{ на } S \quad (i = 0, 1, 2, \dots) \quad (41)$$

Подставляя в условия (41) решение (39), приходим к граничным условиям коэффициентов Фурье

$$\sum_{m=0}^{\infty} a_{im} \varphi_m = 0 \quad (42)$$

где  $a_{im}$  — заданные числа.

Для решения системы обыкновенных дифференциальных уравнений (40) при условии (42) воспользуемся аппаратом матричного исчисления. С этой целью введем в рассмотрение векторы

$$\boldsymbol{\varphi} = \begin{vmatrix} \varphi_0 \\ \varphi_2 \\ \cdot \\ \cdot \\ \cdot \end{vmatrix}, \quad \mathbf{J} = \begin{vmatrix} \varphi_1 \\ \varphi_3 \\ \cdot \\ \cdot \\ \cdot \end{vmatrix}, \quad \mathbf{f} = \begin{vmatrix} f_2 \\ f_0 \\ \cdot \\ \cdot \\ \cdot \end{vmatrix}, \quad \mathbf{F} = \begin{vmatrix} f_1 \\ f_3 \\ \cdot \\ \cdot \\ \cdot \end{vmatrix}$$

и рассмотрим отдельно уравнения (40) для четных индексов  $m=0, 2, 4$  и нечетных  $m=1, 3, 5, \dots$

Тогда можно прийти к следующим матричным уравнениям

$$\begin{aligned} \alpha \frac{d\mathbf{J}}{dz} + a\boldsymbol{\varphi} &= \mathbf{f}, \\ \beta \frac{d\varphi}{dz} + b\mathbf{J} &= \mathbf{F}, \end{aligned} \quad (43)$$

где  $\alpha, \beta, a$  и  $b$  — известные матрицы, определяемые коэффициентами системы уравнений (40).

Одновременно, граничное условие может быть записано в виде

$$A\boldsymbol{\varphi} + B\mathbf{J} = 0 \text{ на } S. \quad (44)$$

Дальнейшая задача состоит в решении системы уравнений (43) при граничных условиях (44).

Методами хорошо разработанными в исчислении конечных разностей система уравнений (43) может быть представлена в случае кусочно-непрерывных коэффициентов в виде единой трехточечной матричной конечно-разностной системы уравнений.

$$\varphi_{k+1} - B_k \varphi_k + C_k \varphi_{k-1} = -g_k \quad (45)$$

где  $k$  — номер узловой точки по оси  $z$ ,  $B_k$  и  $C_k$  — матрицы, а  $g_k$  — вектор.

Решение уравнения (45)дается методом матричной факторизации в виде трех разностных уравнений первого порядка

$$\left. \begin{aligned} \beta_{k+1} &= C_{k+1} (B_k - \beta_k)^{-1} \\ Z_{k+1} &= \beta_{k+1} (Z_k + g_k) \\ \varphi_k &= C_{k+1}^{-1} (\beta_{k+1} \varphi_{k+1} + Z_{k+1}) \end{aligned} \right\} \quad (46)$$

Система уравнений (46) дополняется заданием „начальных“ условий, исходя из вида граничных условий [5], [6].

Метод матричной факторизации в применении к решению уравнений сферических гармоник оказался наиболее эффективным численным методом решения, позволяющим решать любые задачи в одномерных геометриях, как плоской, цилиндрической так и сферической. В качестве иллюстрации можно отметить, что решение кинетического уравнения для бесконечного цилиндра в  $P_3$ —приближении для пяти зон 60 узловых точек производится за 7 секунд. Решение многогрупповой задачи на критический размер сферического реактора в  $P_3$ —приближении на вычислительной машине производится за время, лишь в четыре раза превышающее время решения соответствующей задачи в  $P_1$ —приближении.

Повидимому, можно утверждать, что по крайней мере для одномерных задач решение кинетических уравнений с помощью метода сферических

гармоник в комбинации с численным методом матричной факторизации является наиболее эффективным по сравнению с другими численными методами.

Этот процесс сходится очень быстро, так что уже после 1—2-х итераций групповые константы более не уточняются. Далее, с полученной системой групповых констант производится решение многогрупповой системы основных уравнений реактора [28], [29].

Если ширина групп мала так, что в пределах каждой из групп поток нейтронов изменяется слабо, то способ усреднения физических констант оказывается несущественным и в этом случае можно определить универсальную систему групповых констант, не зависящую от спектра нейтронов в реакторе. Однако, если интервалы групп велики, то для промежуточных и быстрых реакторов необходимо воспользоваться методом усреднения, изложенным выше.

В заключение необходимо отметить, что в более высоких приближениях метода сферических гармоник, чем  $P_1$ —приближение можно получить формулы группового усреднения, аналогичные формулам (32). Для получения усредненных констант по этим формулам необходимо знание спектра нейтронов в каждой точке реактора, который находится с помощью различных приближенных методов, в том числе и в  $P_1$ —приближении.

### 3. Задачи физического расчета реакторов

Применение в математических расчетах быстродействующей вычислительной техники создало необходимые предпосылки для всестороннего физического расчета ядерных реакторов всевозможных спектров, различных композиций делящихся элементов и замедлителей. Для проведения указанных выше расчетов необходимо воспользоваться такими методами, которые позволили бы с единой точки зрения рассмотреть гомогенные реакторы всевозможных спектров от быстрых до тепловых. Естественно, что такой подход возможен только в том случае, когда разрабатываемый метод учитывает все основные особенности механизма замедления нейтронов различных энергий, а также структуру сечений ядерных процессов. Для указанных целей необходимо сформулировать в известном смысле универсальный метод расчета.

В большинстве случаев расчет критической массы и спектра нейтронов возможен в рамках  $P_1$  — приближения. Исключением являются реакторы, средняя длина свободных пробегов которых одного порядка с характерными размерами реактора, расчет которых в  $P_1$  — приближении может привести к существенным ошибкам как в критической массе, так и в спектре нейтронов. В этом случае для расчетов необходимо воспользоваться более высоким приближением, чем  $P_1$ . Таким приближением можно взять, например,  $P_3$ —приближение.

Проведение серийных многогрупповых расчетов реакторов в  $P_3$ —приближении связано с более или менее существенной затратой времени на вычислительных машинах. Поэтому для целей расчета критических масс можно воспользоваться эффективной одногрупповой теорией, сформулированной для расчетов в  $P_1$ —приближении.

Весьма существенное значение в расчетах имеет учет резонансной структуры сечений, а также термализации нейтронов.

Все указанные выше особенности должны быть учтены при построении математического алгоритма решения задачи на критический размер реактора.

В дальнейшем будет сформулированы некоторые алгоритмы решения основных задач физического расчета ядерных реакторов различных спектров, на основе которых составлены программы на вычислительные машины.

В США основные программы многогруппового расчета основаны на алгоритмах, разработанных Г. Гурвитцем и Р. Эрлихом [44], [45].

### ЗАДАЧА НА КРИТИЧЕСКИЙ РАЗМЕР РЕАКТОРА В $P_1$ -ПРИБЛИЖЕНИИ

Нейтроны всевозможных энергий разбиваются на группы, при этом нейтроны энергии ниже  $v_{ep}$  объединяются в одну группу, которой приписываются эффективные константы. В процессе рассеяния нейтронов учитываются как упругие, так и неупругие эффекты. При замедлении нейтронов принимаются во внимание резонансный характер сечений захвата и рассеяния. Рожденные в процессе деления ядер нейтроны распределяются по группам в соответствии со спектром деления. В функции рассеяния нейтронов учитываются нулевой и первый моменты.

Решение систем основных и сопряженных уравнений реактора находится с помощью метода последовательных приближений [5].

Решение уравнений реактора в одномерном и двумерном случаях для каждой группы производится с помощью метода конечных разностей. Для расчета удобно использовать простейшие разностные схемы, когда разрывы коэффициентов уравнений совпадают с расчетными узлами [5], [6], [46], [47]. Решение полученных конечно-разностных уравнений в случае одномерных областей производится с помощью метода факторизации, а в случае двумерных областей с помощью релаксационного метода Н. И. Булеева [50].

### ЗАДАЧА НА КРИТИЧЕСКИЙ РАЗМЕР РЕАКТОРА В $P_3$ – ПРИБЛИЖЕНИИ

В тех случаях, когда расчет критической массы одномерного реактора в  $P_1$  – приближении недостаточен, можно воспользоваться расчетом в  $P_3$  – приближении. Для этого формулируются многогрупповые системы основных и сопряженных уравнений для данной одномерной геометрии.

В большинстве случаев критическая масса удовлетворительно описывается при учете двух первых моментов в функции рассеяния. Следует, однако, отметить, что расчет спектра нейтронов на больших расстояниях от активной зоны предпочтительно осуществлять при учете четырех моментов в функции рассеяния, т.к. в этом случае более точно учитывается анизотропия нейтронного потока.

### РАСЧЕТ КРИТИЧЕСКОЙ МАССЫ И СПЕКТРА НЕЙТРОНОВ ДВУМЕРНЫХ ЦИЛИНДРИЧЕСКИХ РЕАКТОРОВ

Рассмотрим решение многогрупповой системы основных и сопряженных уравнений реактора методом характеристик Владимирова и  $S_n$  – методом Карлсона.

Рассматривается многогрупповая система кинетических уравнений реактора в транспортном приближении, где  $\Sigma^j_s$  заменено на  $\Sigma^j_s(1 - \mu_0)$  и рассеяние считается изотропным в лабораторной системе координат. Реактор по высоте разбивается на слои толщиной  $\Delta z$ . В пределах каждого слоя предполагается, что физические константы и решение задачи, усредненные

по данному слою, не зависят от координаты  $Z$ . В результате для каждой группы мы приходим к системе односкоростных кинетических уравнений, связанных друг с другом. Каждое такое уравнение зависит от координат  $r$ ,  $\psi$  и  $v$ , где  $r$  — расстояние от оси симметрии,  $\psi$  — высотный и  $v$  — азимутальный углы. Введем в рассмотрение гауссовой точки  $\psi_1$  на интервале  $[0, 2\pi]$  и систему уравнений для данной группы запишем применительно к гауссовым точкам. В результате приходим к системе односкоростных кинетических уравнений, каждое из которых по форме совпадает с кинетическим уравнением для сферической системы. В левой части каждого из полученных уравнений сохраним члены, относящиеся к данному слою  $\Delta Z$  и данной точке Гаусса, а все остальные члены отнесем к правой части уравнений, считая их заданными для каждой итерации. Полученные уравнения для каждого слоя, начиная с первого, примыкающего к торцу, решаются последовательно для всех точек Гаусса. Решение соответствующих уравнений может быть произведено либо методом характеристик Владимирова [42], либо  $S_n$  — методом Карлсона [51] с применением метода улучшения сходимости итерационного процесса, сформулированного В. Н. Морозовым [52]. Сущность метода Морозова состоит в следующем.

Ради простоты рассмотрим односкоростное кинетическое уравнение Больцмана в случае изотопного рассеяния

$$\Omega \nabla \varphi + \Sigma \varphi = \frac{\Sigma_s}{4\pi} \int d\Omega \varphi(r, \Omega) + \frac{1}{4\pi} S(r), \quad (47)$$

при условии, что

$$\varphi(r, \Omega) = 0 \text{ на } S, \quad \Omega n < 0 \quad (48)$$

Итерационный процесс определим обычным способом

$$\left. \begin{aligned} \Omega \nabla \varphi^{(n)} + \Sigma \varphi^{(n)} &= \frac{\Sigma_s}{4\pi} \int d\Omega \varphi^{(n-1)}(r, \Omega) + \frac{1}{4\pi} S(r) \\ \varphi^{(n)}(r, \Omega) &= 0 \text{ на } S \text{ при } \Omega n < 0 \end{aligned} \right\} \quad (49)$$

Решение задачи (47), (48) представим в виде

$$\varphi(r, \Omega) = \varphi^{(n)}(r, \Omega) + \varepsilon^{(n)}(r, \Omega), \quad (50)$$

где  $\varepsilon^{(n)}$  поправочный член в  $n$ -ой итерации.

Для приближенного нахождения поправки  $\varepsilon^{(n)}$  В. Н. Морозов предлагает следующий метод.

Соотношение (50) подставим в уравнение (47) и граничные условия (48). Тогда с учетом (49) получим

$$\left. \begin{aligned} \Omega \nabla \varepsilon^{(n)} + \Sigma \varepsilon^{(n)} - \frac{\Sigma_s}{4\pi} \varepsilon_0^{(n)} &= \frac{\Sigma_s}{4\pi} [\varphi_0^{(n)} - \varphi_0^{(n-1)}] \\ \varepsilon^{(n)}(r, \Omega) &= 0 \text{ на } S, \quad \Omega n < 0 \end{aligned} \right\} \quad (51)$$

где  $\varphi_0^{(n)}(r)$  и  $\varepsilon_0^{(n)}(r)$  — глобальные потоки.

Уравнение (42) будем называть уравнением итерационных процессов [52].

Однако, решение задачи (51) еще не упрощается по сравнению с решением задачи (47, 48), так как в левой части кинетического уравнения для  $\varepsilon^{(n)}$  стоит величина  $\varepsilon_0^{(n)}$ , получаемая интегрированием решения  $\varepsilon^{(n)}(r, \Omega)$  по всем углам.

Рассмотрим далее величину

$$\frac{1}{4\pi} \varepsilon_0^{(n)}(\mathbf{r}) = \frac{1}{4\pi} \int d\Omega \varepsilon^{(n)}(\mathbf{r}, \Omega) \quad (52)$$

Если решение задачи (51) представить в виде ряда по сферическим функциям

$$\varepsilon^{(n)}(\mathbf{r}, \Omega) = \frac{1}{4\pi} [\varepsilon_0^{(n)}(\mathbf{r}) + 3\Omega \varepsilon_1^{(n)}(\mathbf{r}) + \dots] \quad (53)$$

то в качестве первого приближения можно принять

$$\frac{1}{4\pi} \varepsilon_0^{(n)}(\mathbf{r}) = \varepsilon^{(n)}(\mathbf{r}, \Omega) \quad (54)$$

Если решение задачи изотропно, то последнее соотношение является точным.

Используя теперь приближенное равенство (54), задачу (51) перепишем в следующем виде

$$\left. \begin{aligned} \Omega \nabla \tilde{\varepsilon}^{(n)} + \Sigma_c \tilde{\varepsilon}^{(n)} &= \frac{\Sigma_s}{4\pi} [\varphi_0^{(n)} - \varphi_0^{(n-1)}], \\ \tilde{\varepsilon}^{(n)}(\mathbf{r}, \Omega) &= 0 \text{ на } S, \Omega n < 0 \end{aligned} \right\} \quad (55)$$

Очевидно, функция  $\varepsilon^{(n)}(\mathbf{r}, \Omega)$  будет приближенным решением задачи (51).

Таким образом, численный алгоритм решения задачи (47), (48) формулируется следующим образом.

Выбирается функция  $\varphi_0^{(n-1)}(\mathbf{r})$  и решается задача (49). В результате решения находим функцию  $\varphi_0^{(n)}(\mathbf{r})$ . Далее составляется выражение

$$Q(\mathbf{r}) = \frac{\Sigma_s}{4\pi} [\varphi_0^{(n)} - \varphi_0^{(n-1)}]$$

и производится решение задачи (55). В результате приходим к величине  $\tilde{\varepsilon}^{(n)}$ . Тогда приближенное решение задачи (47), (48) найдется в виде

$$\tilde{\varphi}(\mathbf{r}, \Omega) = \varphi^{(n)}(\mathbf{r}, \Omega) + \tilde{\varepsilon}^{(n)}(\mathbf{r}, \Omega) \quad (56)$$

Принимая, далее, полученное приближенное решение задачи (47), (48) за  $\varphi^{(n-1)}$  в (49), и подсчитывая  $\varphi_0^{(n-1)}(\mathbf{r})$ , мы можем весь цикл вычислений повторить и т.д.

Обратим внимание на следующее важное обстоятельство. А именно, метод улучшения сходимости, предложенный В. Н. Морозовым, не нарушает баланса нейтронов в реакторе, т.е. является балансным при каждой итерации и в этом случае выгодно отличается от метода итерации источников по столкновениям, который на каждом шаге итерационного процесса не является балансным.

#### 4. Малогрупповые приближения

При расчетах ядерных реакторов на вычислительных машинах зачастую создаются известные трудности, связанные с ограниченными возможностями машин. Прежде всего это относится к памяти машин и их быстродействию. Эти два наиболее существенных фактора необходимо принимать во внимание при формулировании математических задач, связанных с расчетом реакторов. В связи с этим возникает вопрос о наиболее рациональной в данных условиях математической постановке задач, обеспечивающей макси-

мальную информацию в решении. Заметим, что информация должна быть не только полной, но и достоверной.

При физическом расчете реактора желателен многогрупповой расчет двух- или трехмерного цилиндрического реактора, выполненный с возможно малым шагом с учетом резонансных эффектов, термализации и т.д., в рамках  $P_1$ —приближений. Однако, ясно, что современные вычислительные машины не могут оперативно осуществить решение поставленной задачи, даже при наличии соответствующей программы расчета.

Решение упомянутой задачи потребует столь больших затрат машинного времени, что указанный расчет в результате окажется экономически невыгодным и неоправданным.

Вместе с тем, рассматриваемая задача может быть расчленена на ряд простейших задач, решение которых не представляет труда. Набор решений соответствующих одномерных задач в комплексе с теорией возмущений позволяет получить весьма полную информацию, необходимую для проектирования реактора.

Таким образом, сложная задача может быть заменена набором более или менее простых задач, поддающихся оперативному решению на вычислительных машинах.

Это значит, что в каждом конкретном случае необходимо определять такой набор простейших задач, который доставлял бы необходимую информацию для целей проектирования.

В связи с соображениями, изложенными выше, оказывается весьма актуальным вопрос о малогрупповой системе уравнений реактора. В дальнейшем мы остановимся на рассмотрении одногруппового и трехгруппового методов.

Критическая масса реактора может быть найдена с помощью эффективной одногрупповой теории, которая может быть получена с помощью формул (19–31) в предположении, что все нейтроны объединены в одну группу. Для этой цели было предложено находить систему эффективных одногрупповых констант с использованием решения многогрупповой задачи в  $P_1$ —приближении. Полученное таким образом одногрупповое кинетическое уравнение в дальнейшем используется для уточнения расчетов критических параметров реактора в  $P_3$ —приближении. Таким образом, простейший метод учета кинетических эффектов состоит в следующем. Решается многогрупповая система уравнений реактора в  $P_1$ —приближении, затем производится усреднение констант для одногрупповой теории и, наконец, решается одногрупповая задача в  $P_3$ —приближении. Сопоставление расчетов критических масс в  $P_3$ —приближении в рамках многогруппового метода с соответствующим расчетом одногрупповой теории указывает на весьма высокую точность одногрупповых расчетов, вполне достаточную для практических целей (см. рис. 1, 2).

Если одногрупповая теория позволяет уточнить только критическую массу реактора, то трехгрупповой метод позволяет существенно уточнить поле энерговыделения в активной зоне реактора. В рассматриваемом методе быстрые нейтроны объединяются в одну группу, нейтроны промежуточных энергий — в другую и нейтроны тепловых энергий — в третью. В результате решение задачи снова начинается с решения одномерных многогрупповых уравнений реактора в  $P_1$ —приближении. Полученные потоки нейтронов используются далее для получения эффективных констант

трехгруппового метода. Полученная система уравнений используется как для уточненных расчетов критических масс и энерговыделений в  $P_8$ —приближении, так и для решения уравнений реактора в двумерной или трехмерной геометриях.

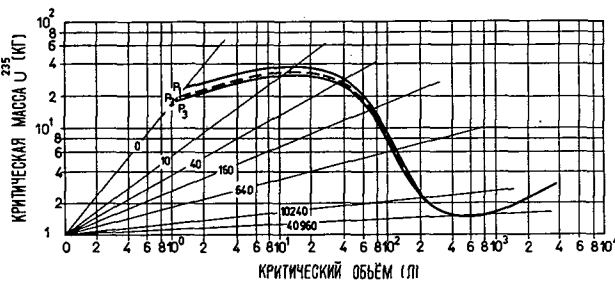


Рис. 1

Критические массы растворов  $\text{UO}_2\text{F}_2 \div \text{H}_2\text{O}$  с бесконечным водяным отражателем (25 групп).

— многогрупповой расчет в  $P_1$ -приближении.  
— многогрупповой расчет в  $P_3$ -приближении.  
— одногрупповой расчет в  $P_3$ -приближении.

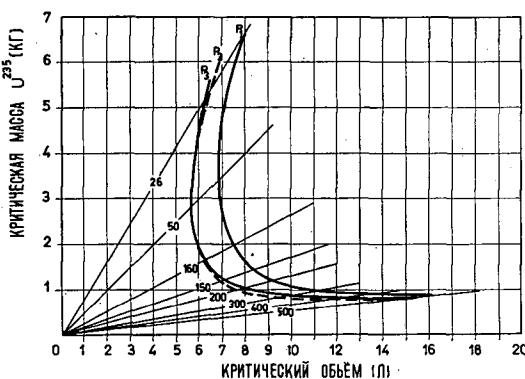


Рис. 2

Критические массы сферических уран-графитовых реакторов с бесконечным графитовым отражателем (25 групп).

— многогрупповой расчет в  $P_1$ -приближении.  
— многогрупповой расчет в  $P_3$ -приближении.  
— одногрупповой расчет в  $P_3$ -приближении.

## 5. Расчет гетерогенных реакторов

Теория расчета гетерогенных реакторов на тепловых нейтронах создана С. М. Файнбергом [22], А. Д. Галаниным [25], [54], Г. А. Бать [53] и др. Эта теория позволяет производить прямой расчет критических параметров гетерогенного реактора и спектра нейронов. В основу теории положены следующие предположения [22].

Поле тепловых нейронов в окрестности блока с делящимся изотопом осесимметрично так, что источники нейронов и их стоки можно рассматривать как нитевидные. Для описания диффузии тепловых нейронов между

блоками можно применять элементарное уравнение диффузии. Наконец, поглощающие способности урановых блоков характеризуются логарифмической производной потока нейтронов на поверхности блока. В этих предположениях задача на критическую массу гетерогенного реактора с помощью функций влияния сводится к системе однородных линейных алгебраических уравнений.

При расчетах критических масс реакторов можно также воспользоваться эффективными методами гомогенизации. Методы гомогенизации включают в себя расчет эффективных констант для быстрых, промежуточных и тепловых нейтронов.

Рассмотрим сначала расчет эффективных констант при энергиях спектра деления. В этом случае особое значение имеет расчет эффективного захвата с делением на уране-238, так как соответствующее сечение позволяет вычислить коэффициент размножения реактора на быстрых нейтронах. Расчет эффективных сечений захвата нейтронов с делением производится с учетом взаимной экранировки урановых блоков методом последовательных столкновений [1]. Расчет других констант производится с помощью формального метода гомогенизации [55].

Резонансные эффекты в области промежуточных энергий учитываются с помощью эффективных резонансных интегралов, а сечения плавно-изменяющиеся с энергией подвергаются процессу формальной гомогенизации. Если блок-эффект существенен, т.е. если поток нейтронов существенно изменяется по ячейке реактора, то необходимо воспользоваться эффективными методами гомогенизации, рассмотренными в главе 26 [6].

При расчете одногрупповых констант для тепловой группы нейтронов сначала рассматривается задача о нахождении пространственно-энергетического распределения нейтронов в ячейке реактора с учетом термализации. Расчет производится в  $P_1$ —приближении. Затем осуществляется одногрупповое усреднение констант. Полученные константы используются для одногруппового расчета интегрального спектра медленных нейтронов в  $P_1$  и  $P_3$ —приближениях по объему ячейки. В заключение производится усреднение сечений по ячейке с целью получения эффективных констант для эквивалентного гомогенизированного реактора. Если расчет в  $P_1$  и  $P_3$ —приближениях в рамках одногрупповой модели приводит к существенной разнице в результатах расчета гомогенизованных констант, то необходимо воспользоваться расчетом пространственно-энергетического распределения нейтронов в ячейке непосредственно  $P_3$ —приближения с учетом термализации.

После того как эффективные гомогенизованные константы получены, расчет гетерогенного реактора ничем не отличается от расчета реактора гомогенного и производится с помощью программы расчета гомогенного реактора.

## 6. Расчет компенсирующей способности регулирующих стержней

Расчет системы компенсации реактора относится к наиболее сложным вопросам физического расчета. Более или менее просто этот вопрос решается только в случае, когда компенсирующий стержень полностью введен в реактор без торцевых отражателей (которые могут быть заменены введением эффективных добавок по высоте) и совпадает с осью реактора. В этом

случае мы приходим к одномерному реактору. Задача решается в много-групповом приближении с использованием эффективного граничного условия на поверхности компенсирующего стержня. Пусть введение стержня привело к изменению характеристического числа задачи  $\lambda = 1/K_{\text{эфф}}$  на величину  $\delta\lambda$ . В диффузационном приближении для цилиндрического блока эта формула была получена Л. Н. Усачевым

$$\delta\lambda_0 = \frac{2\pi r_0}{\int dr Q^* Q} \sum_j \frac{D^j}{\gamma^j} \varphi_0^{*j} \varphi_0^j,$$

где  $\gamma_j$  — логарифмическая производная на интервале группы  $(v_{j-1}, v_j)$ ,  $r_0$  — радиус блока,  $G$  — объем реактора,  $Q(r)$  — полное число вторичных нейтронов, а  $Q^*(r)$  — ценность нейтронов деления.

Оценка величины  $\delta\lambda$  для стержня, помещенного на расстоянии  $r_j$  от центра найдется с помощью формулы теории возмущений, полученной Л. Н. Усачевым [35]

$$\delta\lambda_j = \delta\lambda_0 \frac{Q^*(r_j) Q(r_j)}{Q^*(0) Q(0)}$$

где  $Q^*(r)$  и  $Q(r)$  — невозмущенные функции, найденные в отсутствие стержней. Заметим кстати, что теория возмущений дает оценку только величины  $\delta\lambda_j$ , но она не позволяет вычислить потоки нейтронов или функцию  $Q(r)$  при наличии стержней. Для нахождения потока нейтронов даже в таком простейшем случае, когда стерженьмещен на расстоянии  $r_j$  от центра цилиндра связан с решением двумерной задачи в плоскости  $(r, z)$ .

Аналогичным образом, мы приходим к необходимости решения двумерных задач, когда стержень, помещенный в „точку“  $r=0$ , частично выведен из реакторов. Аналогичный случай имеет место при рассмотрении компенсирующего цилиндра или системы компенсирующих цилиндров, расположенных симметрично относительно начала координат.

Расчет еще более усложняется в том случае, когда рассматривается система компенсирующих стержней в реакторе при различных способах выведения стержней из реактора по мере выгорания делящегося изотопа. В этом случае необходим расчет серии трехмерных реакторов, с различным положением стержней в реакторе.

Указанные выше двумерные и трехмерные задачи можно решать в рамках эффективного трехгруппового метода в  $P_1$ -приближении при использовании эффективных граничных условий на поверхности компенсирующих стержней или цилиндров.

## 7. Основные программы физического расчета реактора

Разработанные алгоритмы решения задач физического расчета были положены в основу программ на вычислительные машины „БЭСМ-2“, „СТРЕЛА“, „УРАЛ“ и др. Ввиду того, что невозможно охватить всего комплекса разнообразных программ, составленных для целей физического расчета, остановимся на наиболее характерных программах расчета критических масс реакторов, получивших широкое распространение в научных учреждениях Советского Союза.

1. Программа 25-группового расчета реакторов в любой одномерной геометрии в  $P_1$ -приближении. Учитываются эффекты упругого и неупругого рассеяния нейтронов, резонансные эффекты на делящихся протонах и конструкционных элементах, термализация нейтронов учитывается в рамках газовой модели. В функции рассеяния учитываются два первых момента. Число зон до 9. Число точек по пространству до 200. Расчет по программе начинается с решения задачи на критический размер эквивалентного реактора без отражателя. После нахождения критического размера реактора с отражателем производится усреднение физических констант для одногрупповой модели. Далее производится уточненный расчет критического размера реактора в  $P_3$ -приближении. Полный расчет реактора на критический размер производится за 15 минут.

2. Программа решения 25-групповой системы сопряженных уравнений в  $P_1$ -приближении для одномерных реакторов плоской, цилиндрической и сферической геометрии. Учитываются те же эффекты, что и в программе для основных уравнений. Программа требует затраты времени на один вариант 15 минут.

3. Программа расчета критического размера реактора и потока нейтронов в  $P_2$ -приближении. Число групп до 25. Число зон и точек соответствует программам расчета реакторов в  $P_1$ -приближении. Программа используется для целей расчета защиты. Расчет одного варианта задачи на  $K_{\text{эфф}}$  производится за 5 минут.

4. Программа расчета реактора одномерной геометрии в  $P_3$ -приближении. Число групп до 25. Число зон до 6. Число точек по пространству до 100. Расчет одного варианта  $K_{\text{эфф}}$  производится за 10 минут.

5. Программа расчета компенсирующей способности регулирующих стержней в центре цилиндрической активной зоны. Расчет производится в многогрупповом приближении. Число групп до 25. Число зон реактора до 9. Расчет одного варианта  $K_{\text{эфф}}$  производится за 5 минут.

6. Программа расчета гетерогенного реактора. Число групп до 25. Решение производится методом эффективной гомогенизации. Для усреднения констант используется метод Вигнера-Зейца в  $P_3$ -приближении. Расчет критического размера реактора производится за 20 минут.

7. Программа расчета эффективного резонансного интеграла с учетом теплового движения ядер. Число резонансных уровней — произвольно. Расчет одного варианта смеси U-238 с замедлителем для 1 температуры производится за 20 минут.

8. Программа расчета промежуточных реакторов с учетом сильного поглощения замедляющихся нейтронов. Рассчитана на 18 групп и 3 зоны, 50 точек. Составлена на машину „УРАЛ-1“.

Указанные выше программы составлены Г. И. Марчуком вместе с коллективом сотрудников: В. П. Кочергиным, Е. И. Погудалиной, Л. И. Кузнецовой, Т. И. Журавлевой, В. В. Смеловым, Г. А. Илясовой, Ф. Ф. Михайлусом и др.

9. Программа расчета критической массы быстрого реактора с помощью  $S_4$  метода Карлсона. Число зон до 5, число точек до 60. Число групп до 9. Расчет одного значения  $K_{\text{эфф}}$  производится за 3 часа на машине „СТРЕЛА“.

Программа составлена В. П. Кочергиным, Е. И. Журавлевой и Анти-моник.

10. Программа расчета двумерного цилиндрического реактора в  $P_1$ —приближении. Число зон до 100, число точек до 900. Число групп 9. Расчет одного варианта  $K_{\text{эфф}}$  производится за 6—8 часов.

Программа составлена под руководством Е. С. Кузнецова, Т. А. Гермогеновой и В. Т. Торобцевой.

11. Программа расчета двумерного цилиндрического реактора в диффузионном двухгрупповом приближении. Составлена В. К. Саульевым. Расчет одного варианта  $K_{\text{эфф}}$  производится за 30 минут.

12. Программа расчета одномерного реактора в  $P_1$ —приближении, приспособленная для расчета критической массы и спектра нейтронов в промежуточном реакторе при сильном поглощении замедляющихся нейтронов с учетом водородсодержащихся компонентов. Число зон до 5, число точек до 100. Расчет одного варианта на критический размер осуществляется за 30 минут. Программа составлена Н. Я. Лищенко.

В настоящем обзоре нет возможности остановиться на всех программах физического расчета реактора. Число таких программ очень велико. Однако, в той или иной мере они используют в качестве составных элементов основные узлы рассмотренных выше программ. Это программы на расчет кинетики реактора, длительности кампаний, компенсацию реактивности в процессе кампаний, программы расчета динамических процессов в реакторах, программы теплофизического расчета, расчета защиты от излучения и многие другие.

## ЛИТЕРАТУРА

- [1] ГЛЕССТОН, С., ЭДЛУНД, М., „Основы теории ядерных реакторов“. ИЛ, 1954 г.
- [2] ГАЛАНИН, А. Д., „Теория ядерных реакторов на тепловых нейтронах“. Атомиздат, 1957 г.
- [3] WEINBERG, A., WIGNER, E., *The Physical Theory of Neutron Chain Reactors*, Chicago, 1958.
- [4] ДЭВИСОН, Б., Теория переноса нейтронов. Атомиздат, 1960 г.
- [5] МАРЧУК, Г. И., Численные методы расчета ядерных реакторов. Атомиздат, 1958 г.
- [6] МАРЧУК, Г. И., Методы расчета ядерных реакторов. Атомиздат, 1962 г.
- [7] MEGHREBLIAN, R. and HOLMES, D., *Reactor Analysis*, 1960.
- [8] PEIERLS, R., *Proc. Cambridge Phil. Soc.* 35 (1939) 610.
- [9] MARSHAK, R. E., BROOKS, H. and HURWITZ, H., *Nucleonics*, 4, No. 5, 6; 5, No. 1, 2 (1949).
- [10] MARSHAK, R. E., *Phys. Rev.* 71 (1947) 443.
- [11] БОГОЛЮБОВ, Н. Н., Проблемы динамической теории в статистической физике. Гостехиздат, 1946 г.
- [12] ГУРЕВИЧ, И. И., ПОМЕРАНЧУК, И. Я., Сб. Реакторостроение и теория реакторов, стр. 220, 1955 г.
- [13] HURWITZ, H., NELKIN, M. and HABATTER, G., *J. Nucl. Sci. Engng.* 1 (1956) 280.
- [14] HURWITZ, H. and ZWEIFEL, P., *J. appl. Phys.* 26 (1955) 923.
- [15] WEINBERG, A., *Amer. J. Phys.* 20 (1952) 401.
- [16] КУРЧАТОВ, И. В., *Атомная энергия* 3 (1956) 5.
- [17] АЛЕКСАНДРОВ, А. П. и др. Сб. Ядерные реакторы и ядерная энергетика. Атомиздат, стр. 60, 1959.
- [18] АЛИХАНОВ, А. И. и др., Сб. Реакторостроение и теория реакторов, стр. 105, 1955.
- [19] БЛОХИНЦЕВ, Д. И., НИКОЛАЕВ, Н. А., Сб. Реакторостроение и теория реакторов. стр. 3, 1955.
- [20] БЛОХИНЦЕВ, Д. И., МИНАШИН, М. Е., СЕРГЕЕВ, Ю. А. Атомная энергия, стр. 24, 1956.
- [21] ФУРСОВ, В. С. Сессия АН СССР по мирному использованию атомной энергии, 1—5 июля 1955, Пленарное заседание. Издат. АН СССР.
- [22] ФЕЙНБЕРГ, С. М., Сб. Реакторостроение и теория реакторов, стр. 152, 1955.
- [23] ФЕЙНБЕРГ, С. М. Доклад на сессии АН СССР, 1956.

- [24] ФЕЙНБЕРГ, С. М. и др., *Журн. Атомная энергия* 8 (1960) 493.
- [25] ГАЛАНИН, А. Д., *Журн. Атомная энергия* 9 (1960) 89.
- [26] ОРЛОВ, В. В., Сб. Нейтронная физика. Атомиздат (в печати), 1960.
- [27] МАРЧУК, Г. И., ОРЛОВ, В. В., Сб. Нейтронная физика. Атомиздат (в печати), 1961.
- [28] УСАЧЕВ, Л. Н., Сб. Реакторостроение и теория реакторов., стр. 251, 1955.
- [29] ПУПКО, В. Я., Приложение № 1 к *Журн. Атомная энергия*, 1958.
- [30] ПУПКО, В. Я., ЕРМАКОВА, Л. И., *Ж. Атомная энергия* 7 (1959) 560.
- [31] ОРЛОВ, В. В., ГОЛАШВИЛИ, Т. В., ВАСКИН, А. И., Сб. Нейтронная физика. Атомиздат (в печати), 1961.
- [32] ЛЕЙПУНСКИЙ, А. И. и др., Сб. Ядерные реакторы и ядерная энергетика. Атомиздат, стр. 377, 1959.
- [33] ЛЕЙПУНСКИЙ, А. И. и др., Сб. Ядерные реакторы и ядерная энергетика. Атомиздат, стр. 215, 1959.
- [34] БЛОХИН, Г. Е. и др., *Журн. Атомная энергия* 10 (1961) 437.
- [35] УСАЧЕВ, Л. Н., Методы расчета реакторов на быстрых нейтронах. Диссертация, 1954.
- [36] КАЗАЧКОВСКИЙ, О. Д., Сб. Ядерные реакторы и ядерная энергетика. Атомиздат, стр. 188, 1959.
- [37] БОНДАРЕНКО, И. И. и др., Доклад на II Международной конференции. Женева, 1958.
- [38] КУЗЬМИНОВ, Б. Д., КУЦАЕВА, Л. С., БОНДАРЕНКО, И. И., *Атомная энергия* 4 (1958) 187.
- [39] НОВОЖИЛОВ, А. И., ШИХОВ, С. Б., *Ж. Атомная энергия* 8 (1960) 209.
- [40] ШИХОВ, С. Б., *Ж. Атомная энергия* 6 (1959) 162.
- [41] ВЛАДИМИРОВ, В. С., Диссертация. Математический институт им. В. А. Стеклова, АН СССР, 1959.
- [42] ВЛАДИМИРОВ, В. С., Тр. Математического института им. В. А. Стеклова, АН СССР, 1961.
- [43] РОМАНОВ, Ю. А., Сб. Исследование критических параметров реакторных систем. Атомиздат, стр. 3, 1960.
- [44] EHRLICH, R. and HURWITZ, H., *Nucleonics* 12, N 2, 23 (1954).
- [45] HURWITZ, H. and EHRLICH, R., *J. Reactor Sci. Techn.*
- [46] ТИХОНОВ, А. Н., САМАРСКИЙ, А. А., ДАН СССР, т. 108, Вып. 3, 1956.
- [47] ТИХОНОВ, А. Н., САМАРСКИЙ, А. А., ДАН СССР, 124, № 4, 779, 1959.
- [48] FUCHS, K., *Proc. phys. Soc.* 62 (1949) 791.
- [49] КАДОМЦЕВ, Б. Б., ДАН, т. 113, № 3, 1957.
- [50] БУЛЕЕВ, Н. И., Математический сборник, т. 51, № 2, стр. 227, 1960.
- [51] КАРЛСОН, Б., БЕЛЛ ДЖ., Сб. Физика ядерных реакторов, стр. 408, Атомиздат, 1959.
- [52] МОРОЗОВ, В. Н., *Ж. Атомная энергия* (в печати), 1961.
- [53] БАТЬ, Г. А., Сб. Реакторостроение и теория реакторов, стр. 199, 1955.
- [54] ГАЛАНИН, А. Д., Сб. Нейтронная физика, Атомиздат (в печати), 1961.
- [55] СМЕЛОВ, В. В., *Ж. Атомная энергия* 6 (1959) 546.
- [56] ШЕВЕЛЕВ, Я. В., *Ж. Атомная энергия* 2 (1957) 224.
- [57] ЛАЛЕТИН, Н. И., Сб. Ядерные реакторы и ядерная энергетика. Атомиздат, стр. 634, 1959.
- [58] БАТЬ, Г. А., ЗАРЕЦКИЙ, Д. Ф., *Ж. Атомная энергия*, 4, (1958) 510.
- [59] МАРЧУК, Г. И. и др.. Сб. Исследование критических параметров реакторных систем. Атомиздат, 1960.
- [60] МАРЧУК, Г. И. и др., Сб. Исследование критических параметров реакторных систем, 1960.
- [61] МАРЧУК, Г. И. и др., Сб. Исследование критических параметров реакторных систем, 1960.

# CALCULS MULTIGROUPES DES PILES RAPIDES

P. MOINEREAU ET M. SOLANES  
CENTRE D'ÉTUDES NUCLÉAIRES DE SACLAY,  
FRANCE

**Abstract — Résumé — Аннотация — Resumen**

**Multi-group calculations for fast reactors.** The paper deals with various causes of error in calculations.

The first part sets out the mathematical approximations (diffusion approximation,  $S_n$  method, etc.), the numerical resolution methods (effect of integration step), the models used, and the implications of these various factors in the determination of the principal characteristics of a fast neutron reactor.

The second part studies the effect on reactivity of variations of element cross-sections, using various fuels, in a reactor of rather hard spectrum.

**Calculs multigroupes des piles rapides.** Les auteurs traitent des différentes causes d'erreur dans les calculs de piles rapides.

Dans la première partie sont exposées les approximations mathématiques (approximation de la diffusion, méthode  $S_n$ , etc.), les méthodes de résolution numérique (influence du pas d'intégration), les modèles utilisés, et l'incidence de ces différents facteurs sur la détermination des principales caractéristiques d'un réacteur à neutrons rapides.

La deuxième partie consiste en l'étude de l'effet sur la réactivité des variations des sections efficaces des éléments, dans le cas d'un réacteur à spectre assez dur, avec divers combustibles.

**Многогрупповой расчет реакторов на быстрых нейтронах.** В настоящем докладе разбираются различные причины, вызывающие погрешности в расчете реакторов на быстрых нейтронах.

В первой части даются математические приближения (диффузионное приближение, метод  $S_n$ , . . .), методы числового решения (влияние числа групп), использовавшиеся модели и влияние этих различных факторов на определение главных характеристик реактора на быстрых нейтронах.

Во второй части изучается влияние на реактивность колебания эффективного сечения элементов с различным топливом в случае реактора с довольно жестким спектром.

**Cálculos de grupos múltiples relativos a los reactores rápidos.** Los autores estudian las diferentes causas de error en el cálculo de los reactores rápidos.

En la primera parte de la memoria, exponen las aproximaciones matemáticas (aproximación de la difusión, método  $S_n$ , etc.), los procedimientos de resolución numérica (influencia de la etapa de integración), los modelos utilizados y el efecto de estos factores en la determinación de las principales características de un reactor de neutrones rápidos.

En la segunda parte de la memoria, examinan el efecto de las variaciones en las secciones eficaces de los elementos sobre la reactividad, en el caso de un reactor de espectro bastante duro, alimentado con diferentes combustibles.

## Introduction

Dans ce rapport, nous présenterons d'abord les méthodes de calcul que nous utilisons à la Section d'études de piles rapides de Saclay, en nous limitant aux calculs de criticalité (taille critique ou  $k_{\text{eff}}$ ). Ces méthodes étant bien connues, nous

ne ferons que les citer rapidement, le but essentiel de notre étude étant de rechercher et d'essayer de chiffrer les incertitudes de ces calculs. Nous pensons qu'il y a deux causes d'erreurs principales: d'une part la méthode de calcul, et d'autre part les constantes physiques, c'est-à-dire les sections efficaces.

En ce qui concerne la méthode de calcul, l'erreur peut provenir soit de la théorie physique choisie pour exprimer la conservation des neutrons (différence entre méthode  $S_n$  et diffusion), soit du procédé de résolution numérique (traitement des équations aux différences, influence du pas d'intégration, etc.), et plus sûrement d'ailleurs des deux à la fois. Nous montrerons, en nous appuyant sur quelques exemples, les incertitudes qui peuvent en découler.

Nous nous attacherons plus spécialement à l'influence des variations des sections efficaces sur la réactivité calculée, et nous présenterons une étude à peu près systématique faite sur le réacteur rapide RAPSODIE avec trois types de combustibles différents.

Il convient de signaler que:

1. Notre étude se limite à l'aspect criticalité, une étude sur les erreurs possibles dans le calcul des flux à longue distance faisant l'objet d'une autre communication [1]. L'influence des sections efficaces sur le taux de régénération n'a pas encore été étudiée.

2. Les exemples donnés se rapportant à peu près tous à un type de réacteur donné (RAPSODIE) ou à un lot de sections efficaces également donné, il faut se garder de généralisations trop hâtives des conclusions auxquelles nous aboutirons.

## 1. Méthodes de calcul

Les méthodes de calcul sont basées, soit sur l'approximation de la diffusion, soit sur l'approximation  $S_n$ , qui, on le sait, est plus proche de la théorie rigoureuse du transport.

### CODES UTILISANT L'APPROXIMATION DE LA DIFFUSION

Nous distinguerons entre codes à une et codes à deux dimensions, tous ayant pour objet le calcul de la réactivité ( $k_{\text{eff}}$ ).

#### *Codes à une dimension*

Le plus ancien et le plus utilisé pour les calculs de RAPSODIE a été PROD-II, programmé par HURWITZ et WALBRAN [2, 3, 4] pour l'ordinateur IBM-650. Ce code permet de traiter le ralentissement par l'hydrogène et la diffusion inélastique avec cependant une petite réserve: pas de diffusion inélastique au-delà du huitième groupe. Les inconvénients majeurs (limitation à 50 points et temps de calculs très longs) sont évidemment liés à la faible capacité de l'IBM-650.

A PROD-II ont été adjoints à Saclay divers petits programmes, sur IBM-650 également:

- a) Un programme de calcul des flux adjoints à 8 groupes;
  - b) Un programme d'itérations sur les termes de ralentissement élastique ( $f_i$ )
- $$\Sigma_{\text{er}i} = \frac{(\xi \Sigma_S)_i}{f_i \Delta u_i};$$
- c) Des programmes de calcul des intégrales de flux et de puissances, de calculs des constantes telles qu'elles doivent être présentées pour PROD-II, et de pondération des sections efficaces sur un spectre donné.

Nous avons programmé également, mais sur ordinateur Ferranti Mercury, deux codes (autocodes) de calculs des perturbations locales et intégrées dont nous dirons quelques mots dans la suite de l'exposé.

PROD-II est maintenant remplacé par un code aux possibilités supérieures et plus rapides sur ordinateur Ferranti et dû à LINDE [5]. Malheureusement, ce code ne comporte pas d'annexes, si ce n'est un calcul « adjoint », et ceci diminue un peu son intérêt. D'autre part, l'ordinateur Ferranti étant de capacité assez limitée, les possibilités de ce code sont parfois insuffisantes.

Un code multigroupe à une dimension est programmé à Saclay sur IBM-7090. Il permettra 50 groupes, 2 à 300 points et diffusion inélastique sans restriction.

Divers sous-programmes annexes sont prévus qui permettront notamment:

- a) Le calcul automatique des constantes;
- b) Des itérations sur les termes de ralentissement élastique;
- c) Le calcul de l'évolution du réacteur dans le temps (compositions et réactivité) avec étude possible des chaînes du thorium, de  $^{235}\text{U}$ , de  $^{238}\text{U}$  et des produits de fission;
- d) Le calcul des flux adjoints et son application au calcul du temps de vie des neutrons, du  $\beta_{\text{eff}}$  et des perturbations de réactivité.
- e) Le calcul de la propagation des flux à longue distance traité comme un problème inhomogène (flux donnés en un point);
- f) La pondération des sections efficaces sur le spectre déterminé par le programme principal.

La mise en service définitive du code est prévue pour la fin de l'année; d'ores et déjà les premiers essais ont donné des résultats satisfaisants.

### *Codes à deux dimensions*

Nous avons utilisé au début le code programmé sur Mercury par HASSITT [6]. Ce code est très limité (2 groupes pratiquement), et nous ne l'utilisons à peu près plus.

Le code que nous utilisons le plus, actuellement, est PDQ [7] sur IBM-704 ou 7090. Il présente les avantages d'être d'un emploi très facile et d'être très sûr; par contre, il est limité à 4 groupes, et le fait qu'il exige un spectre de fission nul dans le dernier groupe et ne permet pas de diffusion inélastique le limite pratiquement à 2 ou 3 groupes.

Citons pour mémoire CURE, sans diffusion inélastique également et moins pratique que PDQ, et CUREM, que nous utilisons depuis peu.

Un code à deux dimensions est actuellement programmé à Saclay et doit être en service bientôt. Ses caractéristiques seront les suivantes: 10 groupes ou plus, diffusion inélastique sans restrictions, et 9 à 10 000 points de maillage. Des sous-programmes annexes sont également prévus tels que: calcul des flux adjoints et leurs applications et étude de l'évolution du réacteur dans le temps.

### **CODES BASÉS SUR LA MÉTHODE $S_n$**

#### *Code $S_n$ pour Mercury*

Ce code a été programmé à Saclay pour l'ordinateur Mercury [8]. Il est composé, en fait, de trois programmes distincts: «  $\nu$  critique », qui calcule l'inverse du  $k_{\text{eff}}$ , «  $R$  critique », qui calcule une dimension critique, et «  $S_n$  complet », qui permet les calculs de perturbations de réactivité.

Les possibilités limites de ces programmes indiquées ci-dessous sont différentes selon qu'il s'agit des deux premiers ou du troisième:

	<i>v critique et R critique</i>	<i>S<sub>n</sub> complet</i>
<i>n</i> de la méthode	8	4
Nombre de milieux	8	4
Nombre de points	64	32
Nombre de groupes d'énergie	20	10
Géométries permises	Sphérique cylindrique	Sphérique

Signalons une particularité intéressante de ce code: il ne calcule pas  $\Phi_i(r_k, \mu_l)$  mais une valeur approchée de

$$\Phi_i\left(\frac{r_k + r_{k+1}}{2}, \frac{\mu_l + \mu_{l+1}}{2}\right)$$

qui est:

$$\frac{\Phi_i(r_k, \mu_l) + \Phi_i(r_{k+1}, \mu_l) + \Phi_i(r_k, \mu_{l+1}) + \Phi_i(r_{k+1}, \mu_{l+1})}{4}.$$

Ceci permet de diminuer l'erreur par rapport à la solution analytique  $\Phi_i(r, \mu)$ .

#### DSN et TDC

Ces deux codes [9] utilisent une approche différente de la méthode  $S_n$  appelée par Carlson « méthode  $S_n$  discrète ».

Ils ont été programmés initialement pour l'ordinateur IBM-704, mais des versions légèrement modifiées sont disponibles sur IBM-7090 au CEA.

Ils permettent de résoudre plusieurs types de problèmes (calcul du  $k_{eff}$ , d'une dimension critique, d'une concentration critique, calcul avec source, etc.), avec des approximations pouvant aller jusqu'à  $n=16$  avec DSN et  $n=6$  avec TDC. Toutefois, la présentation des données est assez complexe et en rend parfois l'emploi malaisé.

De plus, on se heurte aux difficultés devenues classiques de ces codes: convergence assez lente dans le cas de neutrons lents ou de piles de grandes dimensions avec des milieux juxtaposés très différents.

#### QUELQUES COMPARAISONS DES MÉTHODES DE CALCUL

Une méthode de calcul n'est vraiment cohérente que si les résultats auxquels elle conduit dépendent peu du découpage géométrique et de la division angulaire (dans le cas de la méthode  $S_n$ ). Nous mettrons à part la question du découpage en groupes d'énergie, obligatoirement liée à celle des sections efficaces, question que nous aborderons dans la deuxième partie de ce rapport. Nous ferons quelques comparaisons entre les résultats donnés par les différents codes dont nous venons de parler.

Il est évident que notre but n'est pas de faire une comparaison détaillée et complète de ces codes. Une telle étude, au surplus, ne présenterait qu'un intérêt assez académique, puisque seul compte en définitive l'accord ou le désaccord entre le résultat du calcul et l'expérience.

Les quelques comparaisons que l'on trouvera ci-après sont d'ailleurs limitées au seul problème de la criticalité: valeurs de rayons critiques ou de  $k_{eff}$ .

*Influence du pas d'intégration et du nombre d'intervalles angulaires ( $S_n$ )*

Le tableau I montre quelques exemples d'influence du pas d'intégration avec le code diffusion de Linde (géométrie sphérique). Le modèle de réacteur calculé comprend trois régions: cœur, couverture fertile et réflecteur acier. Les deux dernières régions ont la composition exacte des couverture radiale et réflecteur acier de RAPSODIE 59-1. Le cœur a une composition voisine du cœur de RAPSODIE 59-1 [10]. Les pas d'intégration ont été modifiés dans chaque région.

TABLEAU I

**INFLUENCE DU PAS D'INTÉGRATION GÉOMÉTRIQUE SUR LE COEFFICIENT DE MULTIPLICATION EFFECTIF (CODE LINDE)**

Nombre de pas			$k_{\text{eff}}$
Cœur (19,7 cm)	Couverture (44 cm)	Réflecteur acier (44 cm)	
30	30	30	1,000 34
30	18	30	1,001 70
24	24	30	1,000 45
20	11	11	1,004 56
15	15	15	1,001 80
15	13	15	1,001 97
5	15	15	0,983 67

On constate que le résultat est très sensible non seulement au pas d'intégration dans le cœur mais aussi au pas dans la couverture, et qu'il est inutile de choisir un pas très serré dans le cœur si celui qui a été choisi dans le second milieu est trop grand. D'une façon générale, il semble que les résultats fournis par le code de Linde dépendent beaucoup du découpage géométrique.

Un calcul de rayon critique du cœur, avec trois régions ayant la composition du cœur, de la couverture radiale et de l'écran acier de RAPSODIE 60-2 effectué avec le code  $S_n$  sur Mercury a conduit aux résultats suivants (approximation  $S_4$ ):

- avec 10 pas par région: 18,72 cm,
- avec 15 pas par région: 18,69 cm.

On peut en conclure que, du point de vue criticalité, il n'est pas indispensable de choisir un nombre de pas très élevé par région avec ce code.

L'influence du nombre d'intervalles angulaires et du découpage géométrique en calcul  $S_n$  a été également étudiée avec DSN pour le même problème que ci-dessus.

	Nombre de pas par milieu		
	10	20	30
$S_4$	18,731 cm	18,820 cm	18,830 cm
$S_8$	18,849 cm	—	18,934 cm
$S_{16}$	18,886 cm	—	18,950 cm

Quelques constatations s'imposent:

- Dans les mêmes conditions, la méthode  $S_n$  «classique» et la méthode «discrete» conduisent sensiblement au même résultat (18,72 cm contre 18,73 cm).
- Le rayon critique calculé augmente avec le nombre de pas, contrairement à ce qui se passe avec le code  $S_n$  pour Mercury.

c) Le rayon critique calculé augmente également avec l'ordre de l'approximation  $S_n$  (nombre d'intervalles angulaires), donc se rapproche du rayon critique fourni par l'approximation de la diffusion (19,6 cm dans ce cas).

d) Pour un calcul de rayon critique, l'approximation  $S_4$  est suffisante.

#### *Rayons critiques comparés en théorie $S_4$ et en théorie de la diffusion*

Le tableau II rassemble quelques exemples de rayons critiques calculés avec la méthode  $S_4$  et avec la théorie de la diffusion. Les calculs ont été faits dans des conditions aussi voisines que possible, en particulier avec les mêmes sections efficaces.

TABLEAU II  
RAYONS CRITIQUES COMPARÉS  $S_4$  — DIFFUSION

$S_4$ (cm)	Diffusion (cm)	Rayon diffusion Rayon $S_4$
18,72	19,6	1,047
18,87	19,7	1,044
19,75	20,5	1,038

Les valeurs indiquées dans ce tableau concordent avec les résultats donnés par OKRENT et AVERY [11]. Le rapport des rayons critiques obtenus en théorie de la diffusion et en théorie  $S_4$  augmente lorsque le rayon critique diminue. Pour des systèmes rapides de la taille de RAPSODIE, la théorie de la diffusion conduit à un rayon critique supérieur de 4 à 5% au rayon critique fourni par la méthode  $S_4$ .

#### *Rayons critiques en théorie de la diffusion*

Nous avons fait quelques comparaisons entre les deux programmes à une dimension que nous utilisons, PROD-II et LINDE. Les résultats obtenus sont d'autant plus voisins que le pas d'intégration géométrique est plus serré avec LINDE. Ainsi, un calcul de criticalité qui conduit à  $k_{\text{eff}} = 0,9997$  avec PROD-II conduit avec LINDE à 1,0020 ou 1,0010 suivant que le pas d'intégration choisi est le même qu'avec PROD-II ou trois fois plus faible.

D'une façon générale, le code de LINDE est plus sensible que PROD-II au pas d'intégration. Cela provient sans doute de la façon dont sont traitées numériquement les équations aux différences.

Nous avons comparé également les codes à deux dimensions, PDQ et HASSITT, et PROD-II utilisé en géométrie cylindrique, les fuites axiales y étant représentées par des termes d'absorption fictive (voir tableau III).

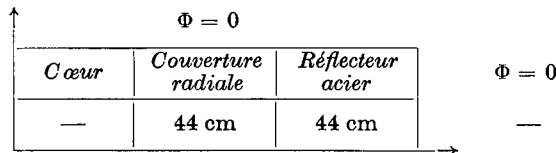
TABLEAU III  
COMPARAISON PDQ—HASSITT—PROD-II

Code	Rayon critique (cm)	
	Exemple 1	Exemple 2
PDQ	16,82	16,44
HASSITT	17,17	16,97
PROD-II	16,95	16,85

## Spectre de jeu à 8 groupes

$i$	1	2	3	4	5	6	7	8
$\Delta u_i$	2	0,5	0,5	0,5	0,5	1	2	—
$x_i$	0,575	0,178	0,116	0,064	0,034	0,025	0,0075	0,0005
$E_{min}$ (MeV)	1,35	0,825	0,5	0,3	0,18	0,0674	0,0091	0

Le modèle calculé dans l'exemple 1 est schématisé ci-dessous, les régions ayant la composition de RAPSODIE 59-1 :



Avec PROD-II, l'absorption fictive était dans chaque groupe  $\text{Di}B^2$  avec  $B^2 = [\pi/(2 \times 30)]^2 = 0,000\,274 \text{ cm}^2$ , ce qui suppose une distribution axiale des flux en cosinus indépendante de l'énergie des neutrons et de la position radiale.

Les calculs ont été faits à deux groupes avec les trois codes.

Dans l'exemple 2, le modèle calculé est RAPSODIE 59-1, supposé symétrique par rapport au plan médian du cœur et limité radialement à l'écran acier, axialement à la zone de transition supérieure. Les calculs ont été faits à 2 groupes avec PDQ et HASSITT, à 8 groupes avec PROD-II, les sections efficaces à 2 groupes ayant été obtenues par pondération du jeu à 8 groupes. Dans cet exemple, les fuites axiales sont représentées dans PROD-II par  $\text{Di}B^2(i, k)$ , où les  $B^2(i, k)$  dépendants dans une certaine mesure de l'énergie et des régions ont été calculés de la façon suivante : on a préalablement déterminé la forme des courbes de flux à 2 groupes avec PDQ, flux pris suivant des parallèles à Oz aux points moyens des régions radiales, puis on a calé des arches de cosinus sur ces courbes, alors  $B^2(i, k) = (\pi/H_{i, k})^2$ ,  $H_{i, k}$  étant la longueur de l'arche de cosinus pour le groupe  $i$  dans la région  $k$ .

Les exemples 1 et 2 montrent que PDQ conduit à un rayon critique plus petit que HASSITT. Nous avons d'ailleurs vérifié systématiquement ce résultat ; la différence est le plus souvent de 0,3 à 0,4 cm pour des systèmes de la taille de RAPSODIE. Nous pouvons aussi constater qu'un code à une dimension utilisé en géométrie cylindrique, avec des termes d'absorption fictive judicieux, peut conduire à de bons résultats pour le calcul du rayon critique.

En ce qui concerne la comparaison des résultats de PDQ et CURE, citons un exemple : le calcul de RAPSODIE 60-2 [10] avec un rayon du cœur fixé à 18,2 cm conduit à  $k_{eff} = 1,016\,70$  avec PDQ et à  $k_{eff} = 1,012\,65$  avec CURE, ce qui correspond à une différence de 0,15 cm environ sur le rayon critique.

Comparaisons des spectres calculés en méthode de la diffusion et en méthode  $S_n$ 

Nous avons calculé le modèle RAPSODIE 60-2 en géométrie sphérique radiale pour la méthode  $S_4$  avec trois milieux : cœur, couverture radiale et réflecteur acier. Le rayon critique trouvé est de 4,4% plus faible qu'en théorie de la diffusion.

Les courbes des figures 1 et 2 représentent les flux à 8 groupes obtenus avec les deux méthodes de calcul ; l'accord est excellent dans le cœur, mais devient de plus en plus mauvais lorsqu'on s'en éloigne.

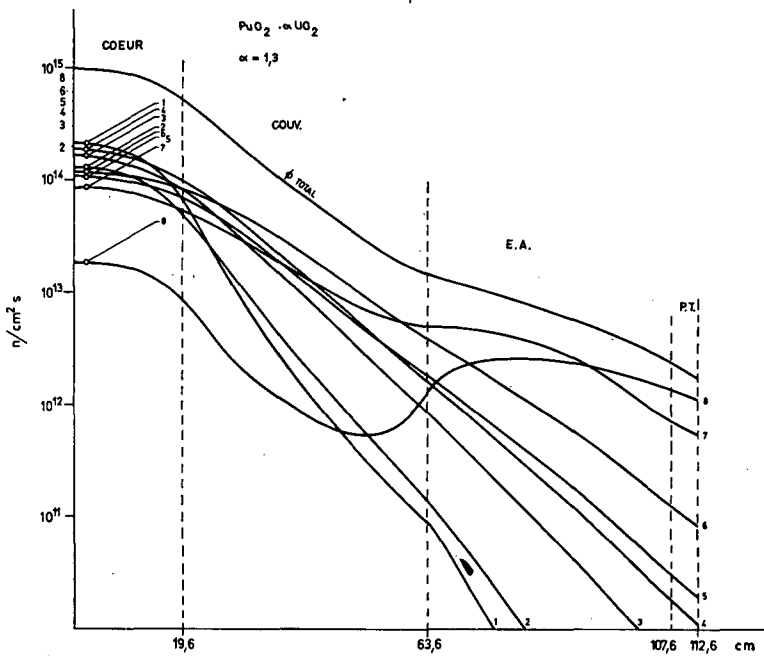


Figure 1  
RAPSODIE 60-2. Flux en GSR. Diffusion.

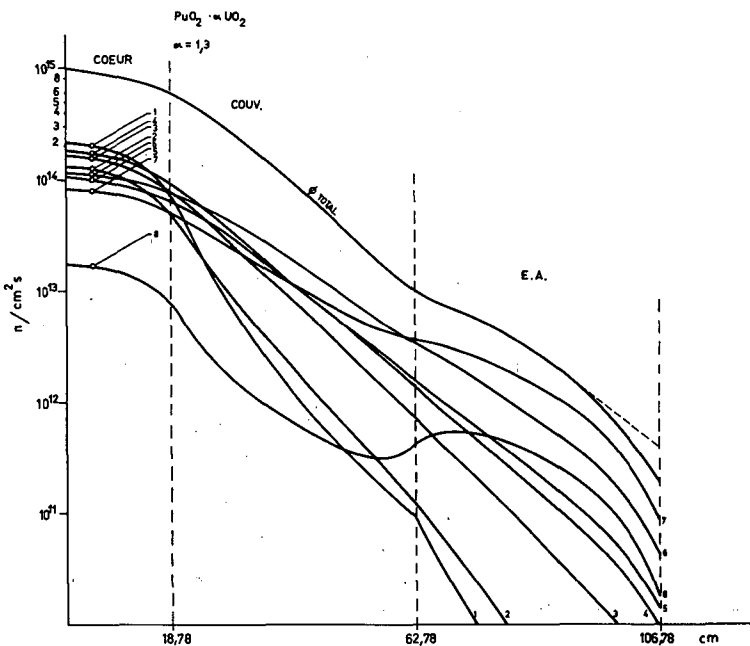


Figure 2  
RAPSODIE 60-2. Flux en GSR.  $S_4$ .

La décroissance du flux est plus rapide en méthode  $S_4$ ; il y a un facteur 1,5 pour le flux total à l'interface couverture-réflecteur acier, 2,5 au milieu du réflecteur acier, 13 à la limite externe de ce dernier milieu.

Ce phénomène est exagéré par la différence de conditions aux limites utilisées dans les deux méthodes. Le milieu qui succède au réflecteur acier est supposé avoir la composition infinie dans le cas d'un calcul en théorie de la diffusion; il est supposé un milieu vide donc sans aucun pouvoir de réflexion dans le cas du calcul  $S_4$ . Néanmoins, ceci ne suffit pas à expliquer la différence, et on peut estimer

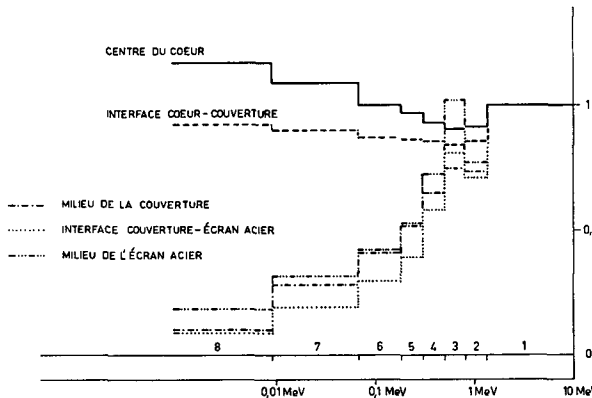


Figure 3  
RAPSODIE 59-1. Importance des neutrons.

qu'à la limite du réflecteur acier, le flux total calculé par la méthode  $S_4$  (en pointillés figure 3) est environ cinq fois plus faible que le flux calculé en théorie de la diffusion.

Les spectres moyens calculés (tableau IV) sont un peu plus durs en méthode  $S_4$ , mais cependant très voisins de ceux obtenus en théorie de la diffusion dans le cœur et la couverture; cet accord cesse d'exister dans le réflecteur acier surtout pour le groupe 8.

TABLEAU IV

**RAPSODIE 60-2 — SPECTRES CALCULÉS EN THÉORIE DE LA DIFFUSION ET EN THÉORIE  $S_4$**

Groupe	Cœur		Couverture radiale		Réflecteur acier	
	Diffusion	$S_4$	Diffusion	$S_4$	Diffusion	$S_4$
1	177	189	43	42	1,2	2
2	114	117	47	47	2,4	4
3	159	159	131	133	19,4	34
4	184	181	181	184	43	77
5	117	114	162	166	57	100
6	136	131	250	251	152	264
7	95	92	171	165	384	432
8	18	17	15	12	341	87

TABLEAU V  
BILAN DE NEUTRONS EN GÉOMÉTRIE SPHÉRIQUE

<b>[CŒUR]</b> $\ln.n.$		<b>FISSIONS</b> { $\begin{array}{l} \text{Pu} \\ \text{U}^{235} \\ \text{U}^{238} \end{array}$ } $\times \bar{\nu}$ ( $= 2,8019$ ) $\rightarrow \ln.n.$ $0,2076$ $0,1190$ $0,0303$ $\underline{\underline{\text{Total des fissions}}}$ $0,3569$
		<b>CAP-TURES</b> { $\begin{array}{l} \text{Pu} \\ \text{U}^{235} \\ \text{U}^{238} \end{array}$ } $0,0324$ $0,0178$ $0,0521$ <b>Matériaux de structure</b> $0,0097$ $\underline{\underline{\text{Total des captures}}}$ $0,1120$ $\underline{\underline{\text{Neutrons absorbés}}}$ $0,4689$
		<b>FUITES dans la couverture</b> $0,5311$
<b>[COUVERTURE RADIALE]</b> $0,2230 \text{ n.n.}$ $\rightarrow [0,7541] \rightarrow$		<b>FISSIONS</b> { $\begin{array}{l} \text{U}^{235} \\ \text{U}^{238} \end{array}$ } $\times \bar{\nu}$ ( $= 2,5721$ ) $\rightarrow 0,2230 \text{ n.n.}$ $0,0298$ $0,0569$ $\underline{\underline{\text{Total des fissions}}}$ $0,0867$
		<b>CAP-TURES</b> { $\begin{array}{l} \text{U}^{235} \\ \text{U}^{238} \end{array}$ } $0,0060$ $0,5544$ <b>Structures</b> $0,0531$ $\underline{\underline{\text{Total des captures}}}$ $0,6135$ $\underline{\underline{\text{Neutrons absorbés}}}$ $0,7002$
		<b>FUITES hors couverture</b> $0,0539$

TABLEAU VI  
BILAN DES NEUTRONS EN GÉOMÉTRIE ( $r, z$ )

<b>[CŒUR]</b> $\ln.n. \rightarrow$		<b>FISSIONS</b> { $\begin{array}{l} \text{Pu} \\ \text{U}^{235} \\ \text{U}^{238} \end{array}$ } $\times \bar{\nu}$ ( $= 2,7731$ ) $\rightarrow \ln.n.$ $0,2091$ $0,1218$ $0,0297$ $\underline{\underline{\text{Total des fissions}}}$ $0,3606$
		<b>CAP-TURES</b> { $\begin{array}{l} \text{Pu} \\ \text{U}^{235} \\ \text{U}^{238} \end{array}$ } $0,0341$ $0,0191$ $0,0545$ <b>Structures</b> $0,0046$ $\underline{\underline{\text{Total des captures}}}$ $0,1123$ $\underline{\underline{\text{Neutrons absorbés}}}$ $0,4729$
		<b>FUITES hors du cœur</b> $0,5271$
<b>[COUVERTURES RADIALE ET AXIALE]</b> $0,2017 \longrightarrow$		<b>FISSIONS</b> { $\begin{array}{l} \text{U}^{235} \\ \text{U}^{238} \end{array}$ } $\times \bar{\nu}$ ( $= 2,5925$ ) $\rightarrow 0,2017 \text{ n.n.}$ $0,0261$ $0,0517$ $\underline{\underline{\text{Total des fissions}}}$ $0,0778$
		<b>CAP-TURES</b> { $\begin{array}{l} \text{U}^{235} \\ \text{U}^{238} \end{array}$ } $0,0052$ $0,4872$ <b>Structures</b> $0,0555$ $\underline{\underline{\text{Total des captures}}}$ $0,5479$ $\underline{\underline{\text{Neutrons absorbés}}}$ $0,6257$
		<b>FUITES hors du cœur</b> $0,5271$

TABLEAU VII

**BILAN DE NEUTRONS EN GÉOMÉTRIE (r, z) DANS LES COUVERTURES  
(pour ln.n. dans le cœur)**

<b>COUVERTURE RADIALE</b>	FISSIIONS	$\left\{ \begin{array}{l} {}^{235}\text{U} \\ {}^{238}\text{U} \end{array} \right. \begin{array}{l} 0,0248 \\ 0,0494 \end{array} \right\} \times \bar{\nu} (= 2,5943) \rightarrow 0,1925\text{n.n.}$
	CAPTURES	$\begin{array}{l} \text{Total des fissions } 0,0742 \\ \\ \left\{ \begin{array}{l} {}^{235}\text{U} \\ {}^{238}\text{U} \\ \text{Structures} \end{array} \right. \begin{array}{l} 0,0049 \\ 0,4616 \\ 0,0521 \end{array} \right\} \\ \text{Total des captures } 0,5186 \\ \text{Neutrons absorbés } 0,5928 \end{array}$
<b>COUVERTURE AXIALE</b>	FISSIIONS	$\left\{ \begin{array}{l} {}^{235}\text{U} \\ {}^{238}\text{U} \end{array} \right. \begin{array}{l} 0,0013 \\ 0,0023 \end{array} \right\} \times \bar{\nu} (= 2,5556) \rightarrow 0,0092\text{n.n.}$
	CAPTURES	$\begin{array}{l} \text{Total des fissions } 0,0036 \\ \\ \left\{ \begin{array}{l} {}^{235}\text{U} \\ {}^{238}\text{U} \\ \text{Structures} \end{array} \right. \begin{array}{l} 0,0003 \\ 0,0256 \\ 0,034 \end{array} \right\} \\ \text{Total des captures } 0,0293 \\ \text{Neutrons absorbés } 0,0329 \end{array}$

*Bilan des neutrons — Comparaison une dimension, deux dimensions*

Nous avons calculé le nombre d'événements (captures, fissions, fuites) qui se produisent dans les régions actives de la pile pour un neutron naissant dans le cœur :

a) A une dimension, en géométrie sphérique, avec un cœur de 19,7 cm et une couverture de 44 cm d'épaisseur ayant la composition de la couverture radiale de RAPSODIE 59-1 (tableau V).

b) A deux dimensions (r, z) avec la configuration géométrique exacte de RAPSODIE 59-1 (tableaux VI et VII).

Les valeurs trouvées sont très comparables pour le cœur. Par contre, en géométrie sphérique, pour la couverture elles sont supérieures de 10 à 15% à celles fournies par le calcul à deux dimensions.

Ce résultat était prévisible pour plusieurs raisons :

1° Le rapport volume-couverture/volume-cœur est plus grand en géométrie sphérique qu'il ne l'est dans la réalité (32,8 contre 30,4).

2° Il n'est pas tenu compte des zones de transition en géométrie sphérique.

3° La géométrie sphérique ne tient pas compte de l'atténuation du flux lorsqu'on s'éloigne du plan médian dans la couverture radiale, à distance constante de l'axe.

4° Il y a également un effet dû aux sections efficaces (pondération à 2 ou 8 groupes) mais on ne peut prévoir dans quel sens il joue.

**TAUX DE RÉGÉNÉRATION**

Le taux de régénération est défini comme étant le rapport du nombre d'atomes de  ${}^{239}\text{Pu}$  formés, au nombre d'atomes précieux détruits :

$$R = \frac{\text{atomes Pu formés}}{p (\text{atomes Pu détruits}) + q (\text{atomes } {}^{235}\text{U cœur détruits}) + r (\text{atomes } {}^{238}\text{U couverture détruits})}$$

où

$p$ =prix d'un atome de plutonium,

$q$ =prix d'un atome de  $^{235}\text{U}$  du cœur,

$r$ =prix d'un atome de  $^{235}\text{U}$  de la couverture radiale.

Les résultats obtenus à une et deux dimensions sont les suivants:

	Cœur	Couverture	Total
Une dimension ( $p = q = 1$ $r = 0$ )	0,1378	1,4668	1,6046
Deux dimensions ( $p = q = 1$ $r = 0$ )	0,1419	1,2684	1,4103

Ils montrent que la part due au cœur dans le taux de régénération est environ le dixième de celle due aux couvertures et que le calcul à une dimension conduit à des valeurs trop optimistes.

#### CONCLUSION PRÉLIMINAIRE

Au vu de ces quelques résultats, et dans le cas d'une pile de la taille de RAPSODIE, il semble que les rayons critiques calculés en géométrie ( $r, z$ ) par la méthode de la diffusion puissent différer au maximum entre eux de 0,5 cm selon le code choisi et les pas d'intégration géométrique, soit une incertitude de 6 à 7 % environ sur la masse critique. Mais il y a d'autres causes d'incertitude: d'une part l'erreur apportée par la méthode de la diffusion elle-même (si l'on tient pour acquis que la méthode  $S_n$  conduit à des rayons critiques plus faibles et plus en accord avec l'expérience, on peut penser que les masses critiques calculées en approximation de la diffusion sont probablement surévaluées), et d'autre part l'erreur due aux sections efficaces. C'est à celle-ci que nous allons consacrer la deuxième partie de cet exposé.

#### 2. Sections efficaces

L'objet de la présente étude est d'essayer de déterminer quelles sont les constantes les plus influentes dans le calcul d'un réacteur rapide et la précision avec laquelle il serait souhaitable de les connaître.

Nous espérons ainsi pouvoir suggérer des mesures plus précises pour les constantes les plus sensibles; il serait alors possible d'ajuster les autres constantes de façon à obtenir un jeu de sections efficaces mieux adaptées au calcul d'un réacteur rapide dont le combustible serait semblable à celui de RAPSODIE. En effet, une des principales difficultés du calcul d'un tel réacteur est l'impossibilité de chiffrer l'erreur due aux sections efficaces.

Il est bien connu que les mesures de sections efficaces pour les neutrons rapides sont particulièrement délicates et difficiles:

1. Les interactions des neutrons rapides avec la matière sont en général très faibles.

2. Les sections efficaces sont relativement faibles et les libres parcours moyens associés grands.

3. Les effets dus aux résonances et aux neutrons thermiques sont souvent cent à mille fois plus grands que les effets dus aux neutrons rapides.

4. Certains domaines d'énergie sont très difficiles à explorer et on a dû faire appel à des théories approchées, à des formules empiriques.

5. On a construit de nombreux jeux de sections efficaces microscopiques, la plupart sont un mélange de résultats de mesures microscopiques directes et d'ajustements empiriques, ces ajustements étant réalisés de manière à trouver un accord raisonnable avec un groupe d'expériences critiques.

Pour nos calculs neutroniques, nous avons principalement fait appel à deux jeux de constantes: les constantes à 10 groupes d'Argonne [12], et les constantes à 10 groupes de Los Alamos [13]. Les premières semblent mieux adaptées à un calcul de criticalité, les secondes, dont le découpage en énergie est plus serré vers les basses énergies, conviennent mieux pour des calculs de flux à grande distance.

Dans l'étude qui suit, nous avons utilisé un jeu à 8 groupes d'énergie dérivé du jeu à 10 groupes d'Argonne.

Les études envisagées portent sur l'influence d'une variation d'une section efficace sur: a) la criticalité, b) le taux de régénération, c) la propagation des flux à grande distance. Ces trois études demandent la mise en œuvre de méthodes très différentes. Dans le présent mémoire, nous ne traiterons que la partie a), la partie b) restant à étudier et la partie c) faisant l'objet d'un autre mémoire [1].

## INFLUENCE D'UNE VARIATION D'UNE SECTION EFFICACE SUR LA CRITICALITÉ

### *Modèles utilisés*

Nous avons pris comme modèle de base un réacteur sphérique avec deux régions: cœur et couverture radiale.

Nous avons envisagé trois types de combustible:

$$\begin{array}{ll} \text{U—Pu—Mo} & \text{RAPSODIE 59-1} \\ \text{PuO}_2\text{—UO}_2 & \text{RAPSODIE 60-2} \\ \text{PuC—UC} & \text{RAPSODIE 60-3} \end{array}$$

Les dimensions adoptées sont:

$$\begin{array}{ll} \text{Rayon du cœur} & \left\{ \begin{array}{ll} \text{U—Pu—Mo} & R = 19,7 \text{ cm} \\ \text{PuC—UC} & \\ \text{PuO}_2\text{—UO}_2 & R = 19,6 \text{ cm} \end{array} \right. \\ \text{Epaisseur de la couverture radiale: } e & = 44 \text{ cm} \end{array}$$

La densité adoptée pour les oxydes et les carbures est 90% de la densité théorique.

Composition volumétrique:

Cœur	Combustible:	42,2%
	Structures:	18,58%
	Réfrigérant:	39,22%
Couverture radiale	Fertile:	56,05%
	Structures:	15,55%
	Réfrigérant:	28,40%

### *Méthodes de calcul*

Les calculs préliminaires ont été effectués sur IBM-650 à l'aide du programme PROD-II et du programme annexe de calcul des flux adjoints, ce qui explique notre choix de 8 groupes d'énergie, ce programme n'admettant pas de transfert au-delà du groupe 8.

On a également effectué certains calculs sur Mercury Ferranti à l'aide du programme à une dimension de Linde.

Les calculs de taille critique, flux, flux adjoints, fonction importance, ayant ainsi été effectués en théorie de la diffusion utilisant 8 groupes d'énergie, la méthode de calcul de perturbations au premier ordre était celle qui nous convenait le mieux. Cette méthode permet d'atteindre la variation de réactivité lorsqu'on connaît la variation des paramètres de la pile [14].

A partir des fonctions importance et des flux de neutrons pour une configuration sphérique, le programme autocode Mercury-116/34, perturbations intégrées, permet de calculer les expressions suivantes en fonction du rayon:

$$U = \sum_i \frac{\partial \Phi_i^*}{\partial r} \delta D_i \frac{\partial \Phi_i}{\partial r} \quad (\text{effet sur la réactivité du coefficient de la diffusion } D_i)$$

$$V = \sum_i \Phi_i^* \delta \Sigma_{ai} \Phi_i \quad (\text{effet sur la réactivité des sections efficaces d'absorption})$$

où:

$$\Sigma_{ai} = \Sigma_{ci} + \Sigma_{ti} + \Sigma_{ini} + \Sigma_{eri}$$

avec:

$$\sum_{ini} = \sum_{j>i} \Sigma_{ini \rightarrow j}$$

$$W = \sum_i \Phi_i^* \sum_{j < i} \delta B_{j \rightarrow i} \Phi_j \quad (\text{effet sur la réactivité de la variation des sections efficaces de diffusion inélastique et de passage élastique d'un groupe dans le suivant})$$

où:

$$B_{j \rightarrow i} = \Sigma_{inj \rightarrow i} + \Sigma_{erj} \delta_j^{i-1}$$

$$\delta_j^{i-1} = 0 \text{ pour } j \neq i-1$$

$$\delta_j^{i-1} = 1 \text{ pour } j = i-1$$

$$X = \sum_i \Phi_i^* \chi_i \sum_j \delta(\nu \Sigma_f)_j \Phi_j \quad (\text{effet sur la réactivité de la variation du produit } \nu \Sigma_f, \text{ c'est-à-dire ou } \Sigma_f \text{ ou } \nu \text{ si l'autre est constant})$$

$$\frac{\delta k}{k} = \frac{1}{F} (-U - V + W + X) \quad (\text{variation totale de réactivité due aux différentes perturbations})$$

$$F = \int \sum_i \Phi_i^* \chi_i \sum_j (\nu \Sigma_f)_j \Phi_j \quad (\text{importance des neutrons de fission})$$

tout le volume

Nous pouvons donc introduire des variations des sections macroscopiques dans chacun des 8 groupes d'énergie considérés.

Dans chaque calcul nous ferons varier les sections efficaces d'un seul groupe d'énergie. Le programme imprime  $\delta D_i$  et les intégrales:

$$\frac{1}{F} \int_U \text{d}V' \frac{1}{F} \int_V \text{d}V' \frac{1}{F} \int_W \text{d}V' \frac{1}{F} \int_X \text{d}V'$$

qui représentent la variation  $\delta k/k$  due à chaque variation. Le programme imprime également la variation globale:

$$\frac{\delta k}{k} = \frac{1}{F} \int_{\text{région}} (-U - V + W + X) \text{d}V'.$$

Dans notre calcul, nous avons introduit des variations macroscopiques  $\delta \Sigma = 8\% \Sigma$ . Nous avons introduit  $\delta D_i$  sous la forme:

$$\delta D_i = -\frac{\delta \Sigma_{tr}}{3 \Sigma_{tr}^2} \text{ calculé pour } \delta \Sigma_{tr} = 8\% \Sigma_{tr}.$$

Il nous a suffi ensuite, considérant une variation de  $\Sigma$  donnée à laquelle correspond une certaine valeur de  $\delta k/k$ , de supposer que la variation  $\delta \Sigma$  était due à la variation de la section efficace d'un seul des éléments. Un calcul très élémentaire permet ensuite de déterminer les valeurs  $\delta k/k$  correspondant à une variation de 10% d'une section efficace d'un élément.

Les valeurs ainsi trouvées sont consignées dans les tableaux IX et suivants.

*Remarque 1.* Le programme autocode Mercury-116/34 suppose la variation de réactivité linéaire en fonction du  $\delta \Sigma$ . Un calcul à l'aide du programme PROD-II sur IBM-650 nous a permis de vérifier cette linéarité dans la marge de variation que nous avons choisie:

a) Un premier calcul, avec les constantes à 8 groupes d'après ANL, appliqué à RAPSODIE 59-1, à deux régions, cœur, couverture radiale, en géométrie sphérique, sens radial, conduit à:

$$k_{\text{eff}} = 0,999841.$$

b) Un deuxième calcul, dans lequel les sections de fission sont diminuées de 4% dans le cœur, donne:

$$k'_{\text{eff}} = 0,991012.$$

c) Dans un troisième calcul, on a diminué les sections de fission de 8% dans le cœur:

$$k''_{\text{eff}} = 0,982191.$$

D'où:

$$\delta \Sigma_f = 4\% \Sigma_f \quad \delta k = 0,008829$$

$$\delta \Sigma_f = 8\% \Sigma_f \quad \delta k = 0,017650$$

La variation  $\delta k$  est pratiquement linéaire compte tenu de l'imprécision des dernières décimales.

*Remarque 2.* Le calcul de perturbations au premier ordre suppose que la forme du spectre change peu. Nous avons également vérifié à l'aide du programme PROD-II que le spectre n'était pas affecté par une variation de 8% d'une section macroscopique.

#### DISCUSSION DES RÉSULTATS OBTENUS

Nous avons appliqué l'accroissement de 10% aux constantes microscopiques des principaux éléments constituant les régions actives du réacteur, à savoir:  $^{239}\text{Pu}$ ,  $^{235}\text{U}$ ,  $^{238}\text{U}$ , Na, Fe, Mo, Cr, Ni, C, O.

Du point de vue criticalité, les éléments les plus influents sont les corps fissiles ou fertiles.

On remarquera, en particulier, l'importance du premier groupe de  $^{239}\text{Pu}$  et  $^{238}\text{U}$ .

Le terme prépondérant est le nombre moyen de neutrons émis par fission, puis viennent, dans l'ordre, la section efficace de fission, la section efficace de transport, les sections de diffusion inélastique de  $^{238}\text{U}$ .

*Premier cas: RAPSODIE 59-1, U-Pu-Mo*

L'influence sur la réactivité des sections efficaces de capture radiative est faible, celle des sections de passage par diffusion élastique est quasi nulle.

Il paraît donc inutile de chercher à évaluer avec plus de précision les  $\sigma_{er}$  lors de la recherche de la taille critique; bien entendu, cette conclusion serait erronée s'il y avait au voisinage du cœur des matériaux légers en quantité notable.

D'une façon générale, l'influence des sections efficaces décroît assez lentement avec le niveau d'énergie; pour  $\sigma_e$ , au contraire, le groupe le plus influent est le sixième.

*Matrices inélastiques.* Les matrices inélastiques ont été étudiées séparément avec PROD-II. On a multiplié successivement par 2 les sections inélastiques totales des principaux groupes diffusants (1.2.3) sans modifier le spectre de diffusion (tableau VIII).

TABLEAU VIII

**EFFET SUR LA RÉACTIVITÉ D'UNE VARIATION DE 100 % DE LA SECTION EFFICACE DE DIFFUSION INÉLASTIQUE D'UN MATÉRIAUX\***  
( $\delta k$  en pcm)

Elément	$i = 1$	$i = 2$	$i = 3$
$^{239}\text{Pu}$	—131	14,3	37,7
$^{235}\text{U}$	—163,1	16,3	46,0
$^{238}\text{U}$	—837,1	59,6	27,3
Mo	—180,2	10,0	—
Na	—136,9	12,0	25,9
Fe	—322,9	29,8	—
K	— 3,6	0,4	0,7
Cr	— 87,1	8,0	—
Ni	— 42,7	3,9	—

\* Région: cœur. Combustible: U, Pu, Mo.

Cet accroissement conduit à un effet négatif sur la réactivité pour le premier groupe, positif pour les suivants, dans le cœur. La diffusion inélastique dans

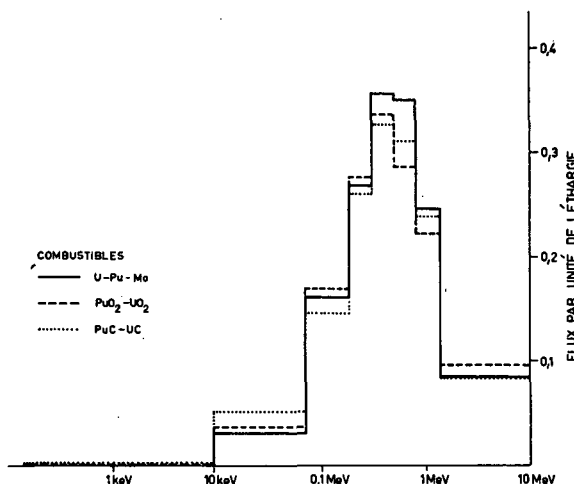


Figure 4  
RAPSODIE. Spectre moyen des neutrons dans le cœur.

le groupe 1 a en effet pour résultat d'envoyer les neutrons dans les groupes 2 et 3, pour lesquels l'importance des neutrons est minimale dans le cœur (fig. 4). Au contraire, l'importance croissant avec la léthargie au-dessous de 600 keV, la diffusion dans les groupes 2 et 3 amène les neutrons à des énergies où l'importance est plus grande.

Dans la couverture, l'importance décroît de façon régulière avec l'énergie; le ralentissement y a un effet toujours négatif sur la réactivité.

#### *Deuxième cas: RAPSODIE 60-1, RAPSODIE 60-3*

Ayant vérifié la linéarité de la variation de réactivité en fonction de la variation de section efficace introduite, on a fait uniquement des calculs en théorie des perturbations au premier ordre.

Les variations étudiées sont dans ce cas également de 10%. Nous nous bornerons à signaler les principaux points sur lesquels les résultats diffèrent de ceux de l'étude précédente.

a) L'influence de  $\sigma_{er}$  est globalement négligeable; toutefois, les  $\sigma_{er}$  de l'oxygène et du carbone sont assez importants, notamment pour le sixième groupe.

b) La présence d'oxygène dans le cœur conduit à un spectre moins dur et, pour le  $\sigma_c$ , le groupe le plus influent est le septième dans le cas de RAPSODIE 60-2; la dégradation du spectre est moins sensible dans le cas des carbures (fig. 4).

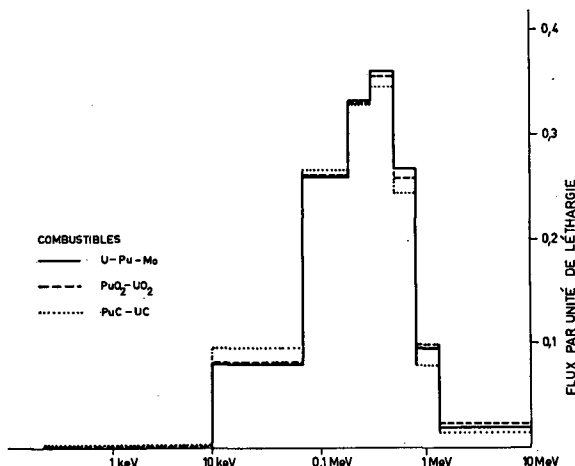


Figure 5  
RAPSODIE. Spectre moyen des neutrons dans la couverture radiale.

*Remarque.* Les résultats que nous présentons dans les tableaux IX et suivants sont spécifiques du réacteur choisi et ne pourraient être extrapolés à un réacteur de puissance de grand volume ( $> 1000$  l), pour lequel le spectre est beaucoup moins dur.

On peut seulement signaler que l'influence des groupes de basse énergie serait accrue; c'est ce que l'on note déjà lorsque l'on passe d'un combustible métallique à une céramique.

## Conclusion

Une étude telle que celle-ci ne peut apporter de renseignements utiles que si l'on connaît les marges d'incertitude sur chaque section efficace, ceci afin de prévoir les erreurs des calculs de neutronique et de suggérer d'éventuelles mesures aux expérimentateurs.

### *Précision des mesures fondamentales*

- $\nu(E)$  Ce terme est celui qu'il importe le plus de connaître avec précision. Si l'on se réfère aux travaux récents d'Argonne (ANL-5800), il apparaît que les valeurs de  $\nu(E)$  sont connues à  $\pm 4\%$  près, dans toute l'échelle des énergies.
  - $\sigma_f$  On dispose actuellement de beaucoup de renseignements quant à la variation des sections efficaces de fission avec l'énergie, sauf pour le plutonium-239 entre 9 keV et 30 keV (7e groupe) [15]. On peut donc penser que les erreurs dues aux  $\sigma_f$  sont faibles; il convient pourtant de remarquer que le plutonium n'a pas été utilisé dans les assemblages de ZPR-III sur lesquels les constantes ont été testées.
  - $\sigma_{tr}$  C'est la différence de deux termes:  $\sigma_{tot}$  et  $\mu\sigma_s$ . Les sections efficaces totales sont assez bien connues [16], sauf pour l'uranium-238, pour des énergies supérieures à 1 keV. L'imprécision est en général de  $\pm 1\%$ , elle peut atteindre au maximum  $\pm 5\%$ . L'erreur sur  $\sigma_{tr}$  vient surtout du terme  $\mu\sigma_s$ , dont l'évaluation est difficile; elle est d'autant plus faible que le rapport  $\mu\sigma_s/\sigma_{tot}$  est lui-même plus faible.
  - $\sigma_c$  Les mesures portent sur le rapport  $\alpha = \sigma_c/\sigma_f$ , et on ne peut guère espérer une précision supérieure à 25%. Les sections de capture doivent donc être considérées comme incertaines, mais nous avons vu que leur influence sur la réactivité est faible. Dans le cadre d'une étude du taux de régénération ou des sources de chaleur dans des régions éloignées du cœur, il y aurait lieu de suggérer des mesures plus précises de  $\sigma_c$ , surtout pour les noyaux fissiles ou fertiles et quelques noyaux de structure.
  - $\sigma_{er}$  L'influence du ralentissement élastique sur la réactivité est négligeable. Il n'y a pas lieu de ce point de vue, de rechercher plus de précision.
  - $\sigma_{in}$  Les éléments des matrices inélastiques sont calculés par référence aux modèles du noyau, les données expérimentales sont rares. Il est difficile d'évaluer les incertitudes sur les sections inélastiques totales  $\sigma_{in}$ ; et sur les spectres des neutrons diffusés après chocs inélastiques  $\sigma_{in:i \rightarrow j}$ . Les travaux de CRANBERG (Los Alamos) [17] laissent à penser que l'incertitude sur  $\sigma_{in}$  peut atteindre 100%.
- Des erreurs importantes pourraient résulter de telles incertitudes concernant l'uranium-238; il nous faut à ce sujet rappeler que la matrice inélastique de cet élément telle que nous l'avons adoptée n'est pas en accord avec les expériences les plus récentes.

### *Pondération des sections efficaces*

Nous ne nous sommes occupés jusqu'ici que de la précision que l'on peut attendre des mesures neutroniques fondamentales. Or les sections efficaces microscopiques obtenues à partir de ces mesures ne peuvent être utilisées telles quelles dans les calculs de piles: il est nécessaire de diviser l'énergie en intervalles plus ou moins nombreux et de moyenner les sections efficaces à l'intérieur de chacun de ces intervalles.

La pondération et, parfois, l'ajustement empirique des constantes à l'intérieur d'un groupe d'énergie peuvent constituer une source d'erreurs appréciable.

La méthode la plus généralement employée consiste à effectuer une pondération par le flux neutronique, de la forme :

$$\sigma_i = \frac{\int_{E_i}^{E_{i+1}} \sigma(E) \varphi(E) dE}{\int_{E_i}^{E_{i+1}} \varphi(E) dE}$$

avec une exception pour  $\sigma_{tri}$ :

$$\sigma_{tri} = \frac{\int_{E_i}^{E_{i+1}} \varphi(E) dE}{\int_{E_i}^{E_{i+1}} \frac{\varphi(E) dE}{\sigma_{tr}(E)}}$$

Ceci suppose que l'on a au départ une idée du spectre pour un réacteur donné.

Pour que les constantes d'un même jeu soient autant que possible indépendantes du spectre à l'intérieur d'un groupe, il faut que la résolution en énergie soit fine, et ceci est l'argument essentiel en faveur d'une théorie multigroupe lorsque le spectre de la pile que l'on veut étudier n'est pas connu.

Une autre méthode, employée par HANSEN et ROACH [18] et qui semble avoir donné des résultats satisfaisants, consiste à pondérer par  $dE/\sigma_{tot}E$ , où  $\sigma_{tot}$  est la section efficace totale d'un matériau.

Dans ce cas également, on pondère, non  $\sigma_{tr}$ , mais son inverse:

$$\frac{1}{\sigma_{tri}} = \frac{\int_{E_i}^{E_{i+1}} \frac{dE}{\sigma_{tr} \sigma_{tot} E}}{\int_{E_i}^{E_{i+1}} \frac{dE}{\sigma_{tot} E}}$$

Nous pensons que cette méthode peut donner de bons résultats, surtout lorsque l'on a affaire à des milieux où un matériau est nettement prépondérant, et nous avons l'intention de l'appliquer au calcul des sections efficaces de certains matériaux pour lesquels il nous sera possible de contrôler les résultats par l'expérience.

Les résultats consignés dans les tableaux IX et suivants nous permettent de dresser une première liste des mesures qui nous paraissent les plus importantes avec la précision souhaitée (tableau XIII), nos prétentions étant justifiées dans le cadre d'un réacteur du type RAPSODIE. Nous avons aussi porté sur cette liste certaines mesures de sections d'activation particulièrement précieuses pour des études de dégagement de chaleur dans les protections ou des détections de neutrons rapides.

Il est également nécessaire de faire un effort particulier dans la mesure des résonances pour les matériaux fissiles et fertiles; ce problème n'a pas été abordé ici, car nous avons étudié un réacteur de faible taille, mais il prend de l'importance dans le cas d'un réacteur plus dilué, de volume plus grand, pour lequel le coefficient Doppler doit être pris en compte.

Nous n'avons traité dans ce mémoire que l'aspect criticalité; ce n'est pas le seul, et notre étude devrait être complétée avant que l'on puisse en tirer des conclusions définitives.

Des calculs sont actuellement en cours pour déterminer l'influence des variations de sections efficaces sur les flux calculés loin des régions actives: les premiers résultats sont donnés dans un autre mémoire [1].

TABLEAU IX  
RÉSULTATS, RAPSODIE 59-1, U—Pu—Mo  
 $\delta k/k$  exprimé en pcm ( $10^{-5}$ ) pour une augmentation de 10 % des constantes considérées

Elé- ment	Groupe	Cœur						Couverture radiale					
		$\nu$	$\sigma_f$	$\sigma_c$	$\sigma_{in}$	$\sigma_{er}$	$\sigma_{tr}$	$\nu$	$\sigma_f$	$\sigma_c$	$\sigma_{in}$	$\sigma_{er}$	$\sigma_{tr}$
$^{239}\text{Pu}$	1	1058,39	701,21	—7,14	—18,36	—0,25	77,25	—	—	—	—	—	—
	2	766,25	532,92	—11,67	3,39	—0,05	39,9	—	—	—	—	—	—
	3	983,21	681,32	—24,15	3,25	0,17	32,14	—	—	—	—	—	—
	4	948,32	647,30	—36,12	2,13	0,4	28,4	—	—	—	—	—	—
	5	718,65	484,21	—46,89	0,49	0,22	17,62	—	—	—	—	—	—
	6	893,23	597,45	—102,53	—	0,54	15,24	—	—	—	—	—	—
	7	378,07	243,98	—57,31	—	0,08	2,15	—	—	—	—	—	—
	8	24,78	15,61	—4,58	—	—	0,087	—	—	—	—	—	—
$^{235}\text{U}$	1	441,48	265,03	—10,57	—23,96	—0,18	56,56	8,96	5,19	—0,23	—1,04	—0,003	2,61
	2	299,56	190,34	—8,7	0,88	—0,03	25,8	8,86	5,79	—0,24	—0,17	—0,004	1,48
	3	407,71	258,82	—16,38	3,11	0,09	19,7	19,08	12,50	—0,72	—0,28	—0,013	1,76
	4	438,89	274,47	—23,07	2,52	0,24	17,9	24,73	16,52	—1,15	—0,66	—0,035	1,8
	5	366,64	225,56	—22,6	0,69	0,15	11,6	23,43	16,37	—1,13	—0,18	—0,040	1,21
	6	508,27	306,54	—38,12	—	0,40	10,98	38,36	27,90	—1,98	—	—0,052	1,26
	7	284,18	165,25	—35,88	—	0,03	1,43	29,8	23,24	—1,97	—	—0,013	0,316
	8	25,62	14,44	—4,71	—	—	0,053	3,74	3,29	—0,191	—	—	0,0042
$^{238}\text{U}$	1	711,76	427,19	—19,01	—120,29	—1,79	223,6	501,5	288,1	—14,26	—180,01	—1,07	362,04
	2	39,44	25,4	—43,87	5,63	—0,18	106,3	41	17,12	—43,37	—21,79	—0,32	214,9
	3	—	—	—66,22	2,30	0,77	84,3	—	—	—102,69	—6,93	—2,51	263,9
	4	—	—	—65,51	3,92	1,49	75,45	—	—	—114,90	—18,96	—7,89	266,5
	5	—	—	—68,27	1,72	0,8	48,1	—	—	—119,91	—15,70	—8,26	175,4
	6	—	—	—118,61	2,15	1,82	43,4	—	—	—215,99	—	—9,06	175,5
	7	—	—	—74,67	—	0,22	5,74	—	—	—144,07	—	—3,47	43,92
	8	—	—	—8,85	—	—	0,209	—	—	—12,66	—	—	0,589
Mo	1	—	—	—2,82	25,88	—0,52	55,15	—	—	—1,33	—24,96	—0,50	55,97
	2	—	—	—3,73	1,07	—0,18	37,64	—	—	—2,31	—2,49	—0,21	47,70
	3	—	—	—7,38	—	0,97	35,95	—	—	—7,17	—	—1,81	70,58
	4	—	—	—8,92	—	1,70	29,14	—	—	—9,81	—	—5,50	70,63
	5	—	—	—7,94	—	0,80	18,57	—	—	—8,74	—	—5,22	42,47
	6	—	—	—12,75	—	1,49	14,84	—	—	—14,56	—	—4,80	37,61
	7	—	—	—7,85	—	0,12	1,42	—	—	—9,5	—	—1,30	7,12
	8	—	—	—6,652	—	—	0,046	—	—	—0,585	—	—	0,082

## CALCULS MULTIGROUPE

Na	1	—	—	—	-0,14	-19,63	-5,18	79,5	—	—	-0,03	-19,81	-2,25	42,75
	2	—	—	—	-0,15	1,10	-1,04	50,43	—	—	-0,05	-1,45	-0,59	33,87
	3	—	—	—	-0,25	2,12	4,79	54,11	—	—	-0,13	-2,17	-5,46	56,32
	4	—	—	—	-0,34	—	6,48	30,74	—	—	-0,20	—	-11,50	36,07
	5	—	—	—	-0,33	—	3,43	19,1	—	—	-0,19	—	-11,51	23,14
	6	—	—	—	-0,40	—	5,11	12,12	—	—	-0,24	—	-8,09	16,27
	7	—	—	—	-0,39	—	0,66	1,75	—	—	-0,25	—	-3,46	4,45
	8	—	—	—	-0,31	—	—	0,124	—	—	0,015	—	—	0,117
Fe	1	—	—	—	-1,88	-46,26	-2,65	114,4	—	—	-0,53	-25,9	-1,28	69,01
	2	—	—	—	-1,21	2,64	-0,45	57,6	—	—	-0,45	-4,26	-0,28	43,4
	3	—	—	—	-1,98	—	1,95	48,57	—	—	-1,14	—	-2,41	56,71
	4	—	—	—	-2,32	—	3,32	37,64	—	—	-1,52	—	-6,51	49,56
	5	—	—	—	-2,70	—	1,60	21,5	—	—	-1,77	—	-6,08	29,22
	6	—	—	—	-4,58	—	3,54	18,54	—	—	-3,10	—	-6,27	27,93
	7	—	—	—	-2,43	—	0,24	2,8	—	—	-1,74	—	-1,436	7,93
	8	—	—	—	-0,119	—	—	0,126	—	—	-0,063	—	—	0,13
K	1	—	—	—	-0,024	-0,529	-0,072	2,728	—	—	-0,004	-0,173	-0,028	0,96
	2	—	—	—	-0,059	0,038	-0,005	1,44	—	—	-0,013	-0,019	-0,012	0,63
	3	—	—	—	-0,083	0,05	0,076	1,04	—	—	-0,028	-0,060	-0,049	0,71
	4	—	—	—	-0,178	—	0,088	0,774	—	—	-0,07	—	-0,10	0,59
	5	—	—	—	-0,229	—	0,034	0,401	—	—	-0,088	—	-0,087	0,32
	6	—	—	—	-7,279	—	0,052	0,294	—	—	-2,88	—	-0,08	0,26
	7	—	—	—	-0,453	—	0,006	0,0378	—	—	-0,190	—	-0,017	0,063
	8	—	—	—	-0,0301	—	—	0,0013	—	—	-0,0094	—	—	0,0008
Cr	1	—	—	—	-0,67	-12,69	-0,64	47,78	—	—	-0,19	-7,05	-0,35	28,81
	2	—	—	—	-0,44	+0,63	-0,11	21,8	—	—	-0,16	-1,17	-0,070	16,42
	3	—	—	—	-0,69	—	0,61	15,71	—	—	-0,40	—	-0,70	18,33
	4	—	—	—	-0,78	—	0,90	11,55	—	—	-0,51	—	-1,77	15,2
	5	—	—	—	-0,85	—	0,42	5,98	—	—	-0,56	—	-1,65	8,12
	6	—	—	—	-1,53	—	0,92	4,38	—	—	-1,04	—	-1,66	6,6
	7	—	—	—	-0,78	—	0,05	0,47	—	—	-0,56	—	-0,39	1,34
	8	—	—	—	-0,039	—	—	0,027	—	—	-0,0207	—	—	0,028
Ni	1	—	—	—	-0,25	-6,81	-0,34	14,9	—	—	-0,07	-3,47	-0,18	8,99
	2	—	—	—	-0,16	0,27	-0,05	10,7	—	—	-0,06	-0,53	-0,03	8,06
	3	—	—	—	-0,26	—	1,61	8,18	—	—	-0,15	—	-0,46	9,54
	4	—	—	—	-0,31	—	0,43	6,1	—	—	-0,20	—	-0,82	8,02
	5	—	—	—	-0,36	—	0,21	4,1	—	—	-0,23	—	-0,79	5,58
	6	—	—	—	-0,61	—	0,46	6,8	—	—	-0,41	—	-0,80	10,26
	7	—	—	—	-0,321	—	0,03	1,18	—	—	-0,227	—	-0,183	3,38
	8	—	—	—	-0,016	—	—	0,036	—	—	-0,008	—	—	0,037

TABLEAU X  
RÉSULTATS, RAPSODIE 60-2,  $\text{PuO}_2$ — $\text{UO}_2$

Elément	Groupe	Cœur						Couverture radiale					
		$\nu$	$\sigma_f$	$\sigma_c$	$\sigma_{in}$	$\sigma_{er}$	$\sigma_{tr}$	$\nu$	$\sigma_f$	$\sigma_c$	$\sigma_{in}$	$\sigma_{er}$	$\sigma_{tr}$
$^{239}\text{Pu}$	1	1416	915,4	-9,3	-18,3	-0,2	109,8	—	—	—	—	—	—
	2	899,3	614	-14,3	3,7	0	38,6	—	—	—	—	—	—
	3	1130,4	769,1	-28,9	6	+0,3	35,1	—	—	—	—	—	—
	4	1244	829,2	-49,8	3,9	0,1	32,1	—	—	—	—	—	—
	5	791,5	526,6	-53	1,2	0,4	17,9	—	—	—	—	—	—
	6	952	625,7	-113,1	0	0,6	14,8	—	—	—	—	—	—
	7	775,1	490	-122	0	0,3	17	—	—	—	—	—	—
	8	248,5	148,5	-50	0	0	6,7	—	—	—	—	—	—
$\text{O}_2$	1	0	0	0	0	-11,6	129	—	—	—	—	—	—
	2	0	0	0	0	-4,7	121,4	—	—	—	—	—	—
	3	0	0	0	0	+18,4	82,1	—	—	—	—	—	—
	4	0	0	0	0	+2,5	118,5	—	—	—	—	—	—
	5	0	0	0	0	14,5	32,4	—	—	—	—	—	—
	6	0	0	0	0	35,7	22,1	—	—	—	—	—	—
	7	0	0	0	0	20,2	19,2	—	—	—	—	—	—
	8	0	0	0	0	0	5,9	—	—	—	—	—	—
$^{235}\text{U}$	1	215,8	132	-5	-9,2	0	29,4	10,3	6	0,2	-0,7	0	2,9
	2	128,5	79,7	-3,9	1,5	0	9,1	9	5,9	0,2	-0,1	0	1,4
	3	171,3	106,1	-7,2	2,8	0,1	7,9	19,1	12,4	0,7	-0,3	0	1,7
	4	210,4	127,7	-11,6	2,1	0,1	7,4	26,2	17,5	1,2	-0,3	0,1	1,9
	5	147,5	89,2	-9,3	0,5	0,1	4,3	23,5	16,2	1,2	-0,2	0,1	1,2
	6	197,9	116,6	-15,4	0	0,2	3,9	36,6	26,1	2	0	0,1	1,2
	7	212,8	120,5	-27,8	0	0,1	4,2	36,1	27,6	2,6	0	0,05	0,6
	8	93,9	49,3	-18,7	0	0	1,5	7,4	6,1	0,6	0	0	0,1
$^{238}\text{U}$	1	352	215,2	9,1	-46	-0,1	117,7	548,8	339,9	16,4	-196,5	-1,2	405
	2	17,1	10,8	19,8	5,7	0	38,1	41,4	27,4	43,8	-23,4	-0,1	204,7
	3	0	0	29,3	1,5	+0,5	34,1	0	0	105,1	-7,6	-3,3	261,8
	4	0	0	33,4	3	0,2	31,5	0	0	121,5	-18,7	-5,7	280,3
	5	0	0	28,5	1,6	0,5	18	0	0	124	-15,2	-7,8	170,8
	6	0	0	48,4	0,6	0,7	15,6	0	0	216,1	-10,7	-9,2	170,2
	7	0	0	58,7	0	0,3	16,7	0	0	186,3	0	-4,1	89,6
	8	0	0	35,7	0	0	5,9	0	0	36,7	0	0	13
Mo	1	—	—	—	—	—	—	—	—	1,5	-129,6	-0,6	62,6
	2	—	—	—	—	—	—	—	—	2,3	-41,3	-0,1	45,4
	3	—	—	—	—	—	—	—	—	7,3	0	-2,3	70
	4	—	—	—	—	—	—	—	—	10,4	0	-4	74,3
	5	—	—	—	—	—	—	—	—	9	0	-4,9	41,3

## CALCULS MULTIGROUPE

49

	6 7 8	—	—	—	—	—	—	—	—	—	14,6 12,6 1,7	0 0 0	—4,8 —1,6 0	36,5 14,5 1,8
K	1	—	—	—	—	—	—	—	—	—	0	—0,2	0	1,1
	2	—	—	—	—	—	—	—	—	—	0,01	—0,1	0	0,6
	3	—	—	—	—	—	—	—	—	—	0,02	—0,07	0	0,7
	4	—	—	—	—	—	—	—	—	—	0,06	0	0	0,6
	5	—	—	—	—	—	—	—	—	—	0,09	0	—0,1	0,3
	6	—	—	—	—	—	—	—	—	—	0,3	0	—0,1	0,2
	7	—	—	—	—	—	—	—	—	—	0,2	0	—0,1	0,1
	8	—	—	—	—	—	—	—	—	—	0,03	0	0	0,01
Na	1	—	—	0,1	—16	—2,1	88,5	—	—	—	0,03	—10,8	—2,5	47,8
	2	—	—	0,1	2,8	—0,9	38,2	—	—	—	0,04	—1,5	—0,1	32,2
	3	—	—	0,2	3,4	+6,9	46,2	—	—	—	0,1	—2,5	—7,2	55,9
	4	—	—	0,4	0	1,5	27,1	—	—	—	0,2	0	—8,3	37,9
	5	—	—	0,3	0	4,7	15,2	—	—	—	0,2	0	—11,1	22,5
	6	—	—	0,3	0	4,1	9,2	—	—	—	0,2	0	—8,4	15,8
	7	—	—	0,6	0	1,9	10,8	—	—	—	0,3	0	—4,2	9,1
	8	—	—	0,3	0	0	7,4	—	—	—	0,04	0	0	2,6
Fe	1	—	—	2,7	—22,6	—1,6	182,9	—	—	—	0,6	—29,6	—1,4	77,2
	2	—	—	1,7	4,6	—0,6	62,7	—	—	—	0,4	—4,7	—0,1	41,3
	3	—	—	2,7	0	+3,9	59,6	—	—	—	1,2	0	—3,2	56,2
	4	—	—	3,6	0	1,1	47,7	—	—	—	1,6	0	—4,8	52,1
	5	—	—	3,4	0	3,1	24,5	—	—	—	1,8	0	—5,8	28,5
	6	—	—	5,7	0	4	20,2	—	—	—	3,1	0	—6,5	27,1
	7	—	—	5,8	0	1	24,7	—	—	—	2,3	0	—1,7	16,3
	8	—	—	1,5	0	0	10,8	—	—	—	0,2	0	0	2,9
Cr	1	—	—	1,0	—13	—0,4	76,1	—	—	—	0,2	—7,6	—0,4	32,2
	2	—	—	0,6	2,6	—0,1	23,7	—	—	—	0,2	—1,1	0	15,6
	3	—	—	0,9	0	+1	19,2	—	—	—	0,4	0	—0,9	18,2
	4	—	—	1,2	0	+0,3	14,6	—	—	—	0,5	0	—1,2	16
	5	—	—	1,1	0	0,9	6,8	—	—	—	0,6	0	—1,5	7,9
	6	—	—	1,9	0	1,1	4,8	—	—	—	1	0	—1,8	6,4
	7	—	—	1,8	0	0,3	4,1	—	—	—	0,7	0	—0,6	2,7
	8	—	—	0,5	0	0	2,3	—	—	—	0,6	0	0	0,6
Ni	1	—	—	0,4	—6,5	—0,2	23,8	—	—	—	0,07	—3,8	—0,2	10,1
	2	—	—	0,2	1	0	11,6	—	—	—	0,05	—0,5	0	7,7
	3	—	—	0,4	0	+0,6	10	—	—	—	0,1	0	0,3	9,5
	4	—	—	0,5	0	0,2	7,7	—	—	—	0,2	0	0,5	8,4
	5	—	—	0,5	0	0,5	4,7	—	—	—	0,2	0	0,5	5,4
	6	—	—	0,7	0	0,6	7,4	—	—	—	0,4	0	0,7	9,9
	7	—	—	0,8	0	0,1	10,5	—	—	—	0,3	0	0,2	6,9
	8	*	—	0,2	0	0	3	—	—	—	0,2	0	0	0,8

TABLEAU XI  
RÉSULTATS, RAPSODIE 60-3, PuC—UC

Elément	Groupe	Cœur						Couverture radiale					
		$\nu$	$\sigma_f$	$\sigma_c$	$\sigma_{in}$	$\sigma_{er}$	$\sigma_{tr}$	$\nu$	$\sigma_f$	$\sigma_c$	$\sigma_{in}$	$\sigma_{er}$	$\sigma_{tr}$
$^{239}\text{Pu}$	1	1257	838	-8,4	-16,6	-0,2	93	—	—	—	—	—	—
	2	858	594	-13,2	3,3	0,1	46	—	—	—	—	—	—
	3	969	665	-24,3	5,4	0,2	30,2	—	—	—	—	—	—
	4	947	640	-37	3,3	0,5	28	—	—	—	—	—	—
	5	747	497	-50 <sup>b</sup>	1,1	0,4	19	—	—	—	—	—	—
	6	951	559	-101,4	0	0,6	13	—	—	—	—	—	—
	7	667	420	-105,5	0	0,2	13,5	—	—	—	—	—	—
	8	210	127	-41,6	0	0	5,1	—	—	—	—	—	—
C	1	0	0	0	0	-24,5	98,2	—	—	—	—	—	—
	2	0	0	0	0	0,6	62	—	—	—	—	—	—
	3	0	0	0	0	10	50	—	—	—	—	—	—
	4	0	0	0	0	20,7	42	—	—	—	—	—	—
	5	0	0	0	0	16,2	27,7	—	—	—	—	—	—
	6	0	0	0	0	39,5	17,3	—	—	—	—	—	—
	7	0	0	0	0	16,3	14,4	—	—	—	—	—	—
	8	0	0	0	0	—	4,3	—	—	—	—	—	—
$^{235}\text{U}$	1	336	203,3	-7,9	-13,3	-0,1	43,7	10,5	6,2	-0,3	-1	0	3
	2	215	135,7	-6,3	2,6	0	19,1	9,8	6,4	-0,3	-0,2	0	1,6
	3	257,5	161,5	-10,6	4,2	+0,1	12	19,5	12,8	-0,7	-0,3	0	1,7
	4	281	173,6	-15,1	2,6	+0,2	11,3	25,2	16,8	-1,2	-0,3	0	1,7
	5	244,2	147,7	-15,4	0,9	0,2	8	24	16,6	-1,2	-0,2	-0,1	1,2
	6	310,5	182,6	-24,2	0	0,3	6	38	27,3	-2	0	-0,1	1,2
	7	321,3	181,2	-42,3	0	0,1	5,8	35,7	27,5	-2,4	0	0	0,6
	8	139,2	74,2	-27,3	0	0	2	12	10,4	-0,6	0	0	0,1
$^{238}\text{U}$	1	254,2	331,8	-14,4	-69	-0,4	175	592,6	344,8	-16,5	-196,6	-1,2	411,6
	2	28,7	12,4	-32,2	10,7	0,1	79,4	45,3	29,9	-48,2	-23,8	-0,3	233,2
	3	0	0	-43,2	2,6	0,5	51,4	0	0	-105	-7,6	-2,2	253
	4	0	0	-43,3	3,7	1,2	48,2	0	0	-117,7	-18,3	-7,6	258,2
	5	0	0	-47,2	2,3	1	33,5	0	0	-125	-15,3	-7,8	176,2
	6	0	0	-76	1,1	1,2	24	0	0	-219	-10,8	-9,4	162,2
	7	0	0	-88,9	0	0,4	23,3	0	0	-182,4	0	-4,1	85,1
	8	0	0	-52	0	0	8	0	0	-41	0	0	12,8
Mo	1	—	—	—	—	—	—	—	—	1,5	-130,7	-0,5	63,6
	2	—	—	—	—	—	—	—	—	2,6	-42,9	-0,3	51,5
	3	—	—	—	—	—	—	—	—	7,3	0	-1,6	67,6
	4	—	—	—	—	—	—	—	—	10	0	-5,2	68,4
	5	—	—	—	—	—	—	—	—	9,1	0	-5	42,7

Na	6	7	8																	
	1	2	3	4	5	6	7	8												
Re	6	7	8	1	2	3	4	5	6	7	8									
K	1	2	3	4	5	6	7	8												
Cr	1	2	3	4	5	6	7	8												
Ni	1	2	3	4	5	6	7	8												

CALCULUS MULTIGROUPES

TABLEAU XII

Elément	Quantité à mesurer	Domaine d'énergie (MeV)	Précision souhaitée (%)
O	$\sigma_{n,n}(E, \theta)$	1—10	10
Na	$\sigma_{tot}$ $\sigma_{n,\gamma}$	0—0,1 0—0,1	10 5
P	$\sigma_{n,p}$	seuil —10	5
S	$\sigma_{n,p}$	seuil —10	2
Mn	$\sigma_{n,\gamma}$	0—10	5
Fe	$\sigma_{tot}$ $\sigma_{n,\gamma}$ $\sigma_{n,\gamma}$ $\sigma_{n,n'}(E, E')$	0—0,1 0—0,1 0,1—10 seuil —10	5 5 15 15
<sup>8</sup> C	$\sigma_{n,\gamma}$	0—10	5
Cu	$\sigma_{n,\gamma}$	0—10	5
Mo	$\sigma_{n,\gamma}$ $\sigma_{n,n'}(E, E')$	0—10 seuil —10	5 15
In	$\sigma_{n,\gamma}$	0—10	5
Au	$\sigma_{n,\gamma}$	0—10	5
<sup>232</sup> Th	$\nu$ $\sigma_f$	seuil —10 seuil —10	2 3
<sup>233</sup> U	$\nu$ $\sigma_f$	0—10 0—10	1 2
<sup>235</sup> U	$\nu$ $\sigma_f$ $\sigma_{n,n'}(E, E')$ $\sigma_{n,\gamma}$	0—10 0—10 seuil —10 0—10	1 2 10 5
<sup>238</sup> U	$\nu$ $\sigma_f$ $\sigma_{n,n'}(E, E')$ $\sigma_{n,\gamma}$	seuil —10 seuil —10 seuil —10 0—10	2 3 10 5
<sup>239</sup> Pu	$\nu$ $\sigma_f$ $\sigma_{n,n'}(E, E')$ $\sigma_{n,\gamma}$	0—10 0—10 seuil —10 0—10	0,5 1 10 5
<sup>240</sup> Pu	$\sigma_f$ $\sigma_{n,\gamma}$	seuil —10 0—10	2 5
<sup>241</sup> Pu	$\sigma_f$ $\sigma_{n,\gamma}$	0—10 0—10	2 5

## RÉFÉRENCES

- [1] KANIA, A. *et alii*, Vol. 1 des présents Comptes rendus, p. 387.
- [2] EHRLICH, R. et HURWITZ, H., Jr., *Nucleonics* 12, 2 (1954) 23.
- [3] HABETLER, G. J., KAPL-1415 (1955).
- [4] WALBRAN, W. A., KAPL-1531 (1956).
- [5] LINDE, S., The multigroup neutron-diffusion equation. One space dimension.
- [6] HASSITT, A., AERE T/R. 2487.
- [7] BILODEAU, G. G. *et alii*, WAPD-TM-70.
- [8] LAGO, B., Communication privée.
- [9] CARLSON, B., LEE, C. et WORLTON, J., LAMS-2346.
- [10] CAMPAN, J. L. *et alii*, Vol. III des présents Comptes rendus, p. 355.
- [11] OKRENT, D. *et alii*, Actes 1<sup>re</sup> Conf. Genève 5 (1956) 385.
- [12] ARGONNE NATIONAL LABORATORY, ANL-5800, p. 417.
- [13] KIEHN, R. M., NSE-4 (1958) 166—179.
- [14] CHAUMONT, J. M., MOINEREAU, P. et JAFFRES, J., Note interne CEA.
- [15] YIFTAH, S., OKRENT, D. et MOLDAUER, P. A., Fast reactor cross-sections. A study leading to a 16-group set. Pergamon Press, Oxford (1960).
- [16] HOWERTON, R. J., Tabulated neutron cross-sections, UCRL. (1958).
- [17] CRANBERG, L. et LEVIN, J. S., LA-2177.
- [18] ROACH, W. H., NSE-8 (1960) 621—651.



# MULTI-GROUP NEUTRON TRANSPORT THEORY

R. ZELAZNY AND A. KUSZELL

INSTITUTE OF NUCLEAR RESEARCH,  
POLISH ACADEMY OF SCIENCES, WARSAW,  
POLAND

Abstract — Résumé — Аннотация — Resumen

**Multi-group neutron transport theory.** In the paper the general theory of the application of the K. M. Case method to  $N$ -group neutron transport theory in plane geometry is given. The eigenfunctions (distributions) for the system of Boltzmann equations have been derived and the completeness theorem has been proved. By means of general solution two examples important for reactor and shielding calculations are given: the solution of a critical and albedo problem for a slab. In both cases the system of singular integral equations for expansion coefficients into a full set of eigenfunction distributions has been reduced to the system of Fredholm-type integral equations. Some results can be applied also to some spherical problems.

**Théorie du transport des neutrons en calculs multigroupes.** Les auteurs exposent la théorie générale de l'application de la méthode de K. M. Case à la théorie du transport des neutrons en calculs à  $N$  groupes, en géométrie plane. Ils ont obtenu les fonctions propres (distributions) relatives au système d'équation de Boltzmann et ont pu démontrer le théorème de fermeture. Ils montrent comment la solution générale peut être appliquée à deux calculs importants de réacteurs et de protection: un problème critique et un problème d'albédo pour les systèmes à géométrie plane. Dans l'un et l'autre cas, le système d'équations intégrales singulières correspondant aux coefficients de développement en ensembles complets de fonctions propres (distributions) a été ramené au système d'équations intégrales du type de Fredholm. Certains résultats peuvent s'appliquer également à des problèmes relatifs aux configurations sphériques.

**Теория многогруппового переноса нейтронов.** В докладе изложена общая теория применения метода К. М. Кейса к  $N$ -групповой теории переноса нейтронов геометрии плоскости. Выведены собственные функции (обобщенные) для системы уравнений Больцмана и доказана теорема о полноте (completeness theorem). Посредством общего решения даются два примера, которые имеют значение для реактора и для расчетов защиты: решение в плоской геометрии проблемы критичности и отражательной способности. В обоих случаях система однозначных интегральных уравнений для расширения коэффициентов до максимальных собственных функций распределения сведена к системе интегральных уравнений Фредхольма. Некоторые результаты могут быть также применены к некоторым сферическим проблемам.

**Teoría de varios grupos para el transporte neutrónico.** La memoria expone una teoría general de la aplicación del método de K. M. Case a la teoría de transporte de  $N$  grupos en geometría plana. Los autores han derivado las funciones propias (distribuciones) para el sistema de ecuaciones de Boltzmann y demuestran un teorema relativo al carácter completo del conjunto. Dan dos ejemplos importantes para el cálculo de reactores y de blindajes que han resuelto empleando una solución general: un problema de criticidad y un problema de albedo en una placa. En ambos casos, desarrollan el sistema de ecuaciones integrales singulares en conjuntos completos de funciones propias (distribuciones) cuyos coeficientes de expansión satisfacen el sistema anterior, y reducen estos conjuntos a un sistema de ecuaciones integrales de Fredholm. Algunos de los resultados son también aplicables a problemas de geometría esférica.

## Introduction

In the paper a general solution of the Boltzmann equation in the  $N$ -group approximation [1] in plane geometry for the case of isotropic scattering of neutrons is given. The concept of the solution is based upon the expansion of the solution into eigenfunctions of the system of multi-group Boltzmann equations, according to the ideas of Case [2] for the one-velocity Boltzmann equation, and according to the two-group generalization of these ideas given by the authors in [3].

The general solution has an explicit form of a sum consisting of an asymptotic (diffusion) part, which is constructed of the discrete eigenfunctions of the Boltzmann equations, and of a transport part constructed of the continuous eigenfunctions. The coefficients of the expansion into these continuous eigenfunctions satisfy the system of singular integral equations. On the basis of the theory of a system of singular integral equations, the consistency of the multi-group transport theory of neutrons has been proved.

The general solution enables us to solve the critical problems of a slab and multi-slab systems (according to [4,5]), as well as the problems of albedo-type (according to [6]) occurring in reactor and shielding calculations. In all these problems the systems of singular integral equations can be reduced to the system of one-dimensional integral equations of the Fredholm-type, which can be treated by simple, classical numerical methods.

By means of a special theorem on the equivalents of the slab and spherical systems some of these results can be applied to some problems concerning spherical reactors.

The method given in this paper can be extended without any essential difficulty to anisotropic scattering of arbitrary order [7, 8].

This work is in preparation. The method described here will be very useful in photon transport theory and in shielding calculations.

### 1. Eigenfunctions (distributions) of the system of Boltzmann equations

The system of Boltzmann equations for the  $N$ -group approach in neutron transport theory in plane geometry and in the case of isotropic scattering of neutrons has the form:

$$\mu \frac{\partial \psi_i(x, \mu)}{\partial x} + \sigma_i \psi_i(x, \mu) = \sum_{j=1}^N c_{ij} \int_{-1}^1 \psi_j(x, \mu') d\mu' \quad (1)$$

where index  $i$  denotes the  $i$ th group of neutrons,  $\sigma_i$  denotes the total cross-section for the  $i$ th group and  $c_{ij}$  describes the transfer of neutrons from the  $j$ th group to the  $i$ th one. The groups are labelled in such a way that  $\sigma_1 > \sigma_2 > \dots > \sigma_k > \sigma_{k+1} > \dots > \sigma_N = 1$  (with a proper choice of units for  $x$ ).

According to Case's ideas [2], used already in the two-group approach [3], let us seek the solution of system (1) among functions of the form:

$$\psi_i(x, \mu) = e^{-\frac{x}{\nu}} \Phi_i(\mu, \nu). \quad (2)$$

Functions  $\Phi_i(\mu, \nu)$  should satisfy the following equations:

$$\left( \sigma_i - \frac{\mu}{\nu} \right) \Phi_i(\mu, \nu) = \sum_{j=1}^N c_{ij} \int_{-1}^1 \Phi_j(\mu', \nu) d\mu'. \quad (3)$$

The right side of Eq. (3) forms a set of functions of  $\nu$ , hence

$$\left( \sigma_i - \frac{\mu}{\nu} \right) \Phi_i(\mu, \nu) = b_i(\nu) \quad (4)$$

where:

$$b_i(\nu) = \sum_{j=1}^N c_{ij} \int_{-1}^1 \Phi_j(\mu', \nu) d\mu' \quad (5)$$

Eq. (4) can be easily solved:

$$\Phi_i(\mu, \nu) = \frac{\nu b_i(\nu)}{\sigma_i \nu - \mu} + \lambda_i(\nu) \delta(\sigma_i \nu - \mu). \quad (6)$$

The conditions (5) give the following equations for the unknown functions  $b_i(\nu)$  and  $\lambda_i(\nu)$ :

$$\sum_{j=1}^N c_{ij} \int_{-1}^1 \frac{\nu b_j(\nu)}{\sigma_j \nu - \mu} d\mu + \sum_{j=1}^N c_{ij} \lambda_j(\nu) \int_{-1}^1 \delta(\sigma_j \nu - \mu) d\mu = b_i(\nu). \quad (7)$$

Let us assume that  $c = \det c_{ij} \neq 0$ . This assumption enables us to use a matrix  $c_{ij}^{-1}$  which is an inverse matrix to a matrix  $c_{kl}$ , i.e.  $\sum_{j=1}^N c_{ij} c_{jk}^{-1} = \sum_{j=1}^N c_{ij}^{-1} c_{jk} = \delta_{ik}$ .

Multiplying Eq. (7) by  $c_{ki}^{-1}$  and summing over index  $i$  we obtain:

$$\nu f_k(\nu) b_k(\nu) + \lambda_k(\nu) \chi_k(\nu) = \sum_{i=1}^N c_{ki}^{-1} b_i(\nu) \quad (8)$$

where we have introduced the following notation:

$$f_k(\nu) = \int_{-1}^1 \frac{d\mu}{\sigma_k \nu - \mu} \quad (9)$$

$$\chi_k(\nu) = \int_{-1}^1 \delta(\sigma_k \nu - \mu) d\mu. \quad (10)$$

Defining a new matrix:

$$\omega_{ki}(\nu) = c_{ki}^{-1} - \delta_{ki} \nu f_k(\nu) \quad (11)$$

we can rewrite Eq. (8):

$$\lambda_k(\nu) \chi_k(\nu) = \sum_{i=1}^N \omega_{ki}(\nu) b_i(\nu). \quad (12)$$

Now two cases should be considered.

CASE A

Let us take into consideration the region consisting of two intervals:

$$\frac{1}{\sigma_{n-1}} < \nu < \frac{1}{\sigma_n} \quad \text{and} \quad -\frac{1}{\sigma_n} < \nu < -\frac{1}{\sigma_{n-1}}$$

which will be denoted below as region (n). Let us observe that for  $\nu \in (n)$ :

$$\chi_k(\nu) = \begin{cases} 0 & k < n \\ 1 & k \geq n \end{cases}$$

Thus the system of Eq. (12) has for  $\nu \epsilon(n)$  the following form:

$$\sum_{l=1}^N \omega_{kl}(\nu) b_l^{(n)}(\nu) = 0 \quad k < n \quad (13)$$

$$\lambda_k^{(n)} = \sum_{l=1}^N \omega_{kl}(\nu) b_l^{(n)}(\nu) \quad k \geq n. \quad (14)$$

In the system of Eqs. (13) and (14) there are  $N + N - n + 1 = 2N - n + 1$  unknown functions. Thus it is evident that  $N - n + 1$  functions must remain unknown. The choice of functions is quite arbitrary. Let them be the functions  $b_s(\nu)$  for  $s \geq n$ . Then Eqs. (13) and (14) may be rewritten in the form:

$$\sum_{\varrho=1}^{n-1} \omega_{\eta\varrho} b_{\varrho}^{(n)}(\nu) = - \sum_{s=n}^N \omega_{\eta s} b_s^{(n)}(\nu) \quad \eta < n \quad (15)$$

$$\lambda_k^{(n)}(\nu) = \sum_{l=n}^N \omega_{kl} b_l^{(n)}(\nu) + \sum_{\varrho=1}^n \omega_{k\varrho} b_{\varrho}^{(n)}(\nu) \quad k \geq n. \quad (16)$$

From Eq. (15) we obtain:

$$b_{\eta}^{(n)}(\nu) = -[\Omega^{(n)}]^{-1} \sum_{\varrho=1}^{n-1} \sum_{s=n}^N \Delta_{\eta\varrho}^{(n)} \omega_{\varrho s} b_s^{(n)}(\nu) = - \sum_{\varrho=1}^{n-1} \sum_{s=n}^N \Delta_{\eta\varrho}^{(n)} \omega_{\varrho s} h_s^{(n)}(\nu) \quad (17)$$

where  $\Delta_{\eta\varrho}^{(n)}$  is an algebraic complement of the element  $\omega_{\eta\varrho}$  of the matrix  $\omega_{\sigma\tau}$  ( $\sigma, \tau = 1, 2, \dots, n-1$ ). According to the notation used in Appendix B it can be written in the form:

$$\Delta_{\eta\varrho}^{(n)}(\nu) = (-1)^{\eta+\varrho} \left\{ \omega_{\sigma\tau}; \frac{1}{1}, \dots, \frac{\eta-1}{\varrho-1}, \frac{\eta+1}{\varrho+1}, \dots, \frac{n-1}{n-1} \right\}$$

and

$$\Omega^{(n)}(\nu) = \det \omega_{\sigma\tau}(\nu) (\sigma, \tau = 1, 2, \dots, n-1) = \left\{ \omega_{\sigma\tau}; \frac{1}{1}, \frac{2}{2}, \dots, \frac{n-1}{n-1} \right\}$$

$$\Omega^{(1)}(\nu) \equiv 1$$

is a determinant of this same matrix and  $h_s^{(n)}(\nu) = [\Omega^{(n)}]^{-1} b_s^{(n)}(\nu)$ . From Eqs. (16) and (17) we obtain:

$$\begin{aligned} \lambda_k^{(n)}(\nu) &= \sum_{l=n}^N \omega_{kl} \Omega^{(n)}(\nu) h_l^{(n)}(\nu) - \sum_{\varrho=1}^{n-1} \omega_{k\varrho} \sum_{\eta=1}^{n-1} \sum_{l=n}^N \Delta_{\eta\varrho}^{(n)} \omega_{\eta l} h_l^{(n)}(\nu) = \\ &= \sum_{l=n}^N h_l^{(n)}(\nu) \left[ \Omega^{(n)}(\nu) \omega_{kl} - \sum_{\varrho=1}^{n-1} \sum_{\eta=1}^{n-1} \omega_{k\varrho} \Delta_{\eta\varrho}^{(n)} \omega_{\eta l} \right] = \\ &= \sum_{l=n}^N h_l^{(n)}(\nu) P \left\{ \omega_{\sigma\tau}; \frac{1}{1}, \frac{2}{2}, \dots, \frac{n-1}{n-1}, \frac{k}{l} \right\}^{(n)} \end{aligned} \quad (18)$$

In this way the functions  $\Phi_k^{(n)}(\mu, \nu)$  ( $k \geq n$ ) for fixed but arbitrary  $n$  can be written:

$$\begin{aligned}\Phi_k^{(n)}(\mu, \nu) = & \left[ \frac{\nu \Omega^{(n)}(\nu)}{\sigma_k \nu - \mu} + A_{kk}^{(n)}(\nu) \delta(\sigma_k \nu - \mu) \right] h_k^{(n)}(\nu) + \\ & + \sum_{s=n}^N A_{ks}^{(n)}(\nu) \delta(\sigma_k \nu - \mu) h_s^{(n)}(\nu)\end{aligned}\quad (19)$$

where to shorten the formula the following notation has been used

$$A_{ks}^{(n)}(\nu) = P \left\{ \omega_{\sigma\tau} ; \begin{array}{l} 1, 2, \dots, n-1, k \\ 1, 2, \dots, n-1, s \end{array} \right\}^{(n)} \quad (20)$$

and  $(k)$  by the summation sign denotes that the term  $A_{kk}^{(n)}$  should be omitted. The same functions for the group index smaller than  $n$  (in this case we use Greek letters for this index) will be:

$$\Phi_\varrho^{(n)}(\mu, \nu) = -\nu \sum_{\eta=1}^{n-1} \sum_{s=n}^N \frac{A_{\eta\varrho}^{(n)} \omega_{\eta s}(\nu) h_s^{(n)}(\nu)}{\sigma_\varrho \nu - \mu} \quad \varrho < n. \quad (21)$$

#### CASE B

Finally let us calculate functions  $\Phi_k(\mu, \nu)$  for  $\nu$  belonging to the cut plane with a cut along the interval  $(-1, 1)$ . In this case the system of Eq. (12) is reduced to:

$$\sum_{i=1}^N \omega_{ki} b_i(\nu) = 0. \quad (22)$$

The solutions of this system of homogeneous equations are non-trivial only when:

$$\Omega(\nu) = \Omega^{(N+1)}(\nu) = 0. \quad (23)$$

Since the function  $\Omega(\nu)$  is an even function of the variable  $\nu$ , Eq. (23) has an even number of roots, say  $2M$ . The system of Eq. (22) can be written in the form:

$$\sum_{l=1}^{N-1} \omega_{kl}(\nu_s) b_l(\pm \nu_s) = -\omega_{kN}(\nu_s) b_N(\pm \nu_s) \quad (24)$$

where it has been assumed that  $A_{NN}^{(N+1)}(\nu_s) = \Omega^N(\nu_s) \neq 0$  (in the opposite case the functions  $b_l(\pm \nu_s)$  should be expressed by another  $b_k(\pm \nu_s)$  for which  $A_{kk}^{(N+1)}(\nu_s) \neq 0$ ) and the  $N$ th equation has been omitted from system (22). System (24) has the following solutions:

$$b_l(\pm \nu_s) = [\Omega^{(N)}(\nu_s)]^{-1} \sum_{r=1}^{N-1} A_{rl}^{(N)}(\nu_s) \omega_{rN}(\nu_s) b_N(\pm \nu_s) = g_l(\nu_s) h(\pm \nu_s) \quad (25)$$

where

$$h(\pm \nu_s) = [\Omega^{(N)}(\nu_s)]^{-1} b_N(\pm \nu_s) \quad (26)$$

$$g_l(\nu_s) = \sum_{r=1}^{N-1} A_{rl}^{(N)}(\nu_s) \omega_{rN}(\nu_s) \quad (27)$$

(The evenness of functions  $A_{i,l}^{(N)}(\nu)$  and  $\omega_{r,N}(\nu)$  has been made use of.) Hence the discrete eigenfunctions have the following form:

$$\Phi_k(\mu, \pm \nu_s) = \frac{\nu_s g_k(\nu_s) h(\pm \nu_s)}{\sigma_k \nu_s \pm \mu}. \quad (28)$$

In this way we have derived the full set of continuous and discrete eigenfunctions (distributions) for the system of multi-group Boltzmann equations.

## 2. Completeness theorem

Now let us formulate the theorem which will be the basis of our further considerations: the completeness theorem.

Every system of  $N$  functions  $\psi_i(\mu)$  satisfying the Hölder conditions can be expanded into a full set of continuous and discrete eigenfunctions (distributions) derived in the preceding section. In other words the following system of singular integral equations has unique solutions:

$$\psi_k(\mu) = \sum_{s=1}^M \{\Phi_k(\mu, +\nu_s) + \Phi_k(\mu, -\nu_s)\} + \sum_{n=1}^N \int \Phi_k^{(n)}(\mu, \nu) d\nu; \mu \in \sum_{n=1}^N (n') \quad (29)$$

where  $(n')$  has the following meanings:

- (1)  $(n') = (n)$  (see preceding section, case A);
- (2)  $(n') = \left(\frac{1}{\sigma_{n-1}}, \frac{1}{\sigma_n}\right).$

It is worth noting that on the basis of Eqs. (19) and (20) the functions  $\Phi_\varrho^{(n)}(\mu, \nu)$  for  $\varrho < n$  have no singularities and do not contain terms with the  $\delta$ -function; therefore the integration operation over the interval  $(n')$  leads to Fredholm-type integrals. This observation enables us to write system (29) in the following form:

$$\psi'_k(\mu) = \sum_{n=1}^k \int \Phi_k^{(n)}(\mu, \nu) d\nu \quad (30)$$

where

$$\psi'_k(\mu) = \psi_k(\mu) - \sum_{n=k+1}^N \int_{(n')} \Phi_k^{(n)}(\mu, \nu) d\nu - \sum_{l=1}^M \{\Phi_k(\mu, \nu_l) + \Phi_k(\mu, -\nu_l)\} \quad (31)$$

In system (30) the following change of the independent variable may be performed:  $\mu = \sigma_k \mu'$ . Then  $\mu' \in \sum_{n=1}^k (n')$  and system (30) can be written in the form:

$$\sum_{n=1}^k \int_{(n')} \sigma_k \Phi_k^{(n)}(\sigma_k \mu, \nu) d\nu = \sigma_k \psi'_k(\sigma_k \mu) \quad (32)$$

where

$$\begin{aligned} \sigma_k \Phi_k^{(n)}(\sigma_k \mu, \nu) = & \left[ \frac{\nu \Omega^{(n)}(\nu)}{\nu - \mu} + A_{kk}^{(n)}(\nu) \delta(\nu - \mu) \right] h_k^{(n)}(\nu) + \\ & + \sum_{s=n}^N \int_{(k)} A_{ks}^{(n)} \delta(\nu - \mu) h_s^{(n)}(\nu). \end{aligned} \quad (33)$$

It is convenient to rewrite the system of singular integral equations (32) in the form:

$$\sum_{n=1}^k \sum_{l=n}^N K_{kl}^{(n)} h_l^{(n)}(\mu) = \sigma_k \psi'_k(\sigma_k \mu), \quad (k = 1, \dots, N), \quad (34)$$

where

$$K_{kl}^{(n')} h_l^{(n)}(\mu) = A_{kl}^{(n)}(\mu) H^{(n')}(\mu) h_l^{(n)}(\mu) - \frac{1}{\pi i} \int_{(n')} \frac{\delta_{kl}(-i\pi\nu) \Omega^{(n)}(\nu) h_l^{(n)}(\nu)}{\nu - \mu} d\nu \quad (35)$$

$$H^{(n')}(\mu) = \int_{(n')} \delta(\nu - \mu) d\nu. \quad (36)$$

Let us write the first equation from system (34):

$$\sum_{l=1}^N K_{1l}^{(1')} h_l^{(1)}(\mu) = \sigma_1 \psi'_1(\sigma_1 \mu) \quad (37)$$

or in the form:

$$K_{11}^{(1')} h_1^{(1)}(\mu) = \sigma_1 \psi'_1(\sigma_1 \mu) - \sum_{l=2}^N K_{1l}^{(1')} h_l^{(1)}(\mu). \quad (38)$$

The solution of this integral equation may be written in the form (see formula (A8) in Appendix A):

$$h_1^{(1)}(\mu) = [K_{11}^{(1')}]^{-1} [\sigma_1 \psi'_1(\sigma_1 \mu) - \sum_{l=2}^N K_{1l}^{(1')} h_l^{(1)}(\mu)] \quad (39)$$

and can be inserted into the remaining  $N-1$  Eq. (34):

$$\begin{aligned} & \sum_{l=2}^N \left\{ K_{kl}^{(1')} - K_{kl}^{(1')} \left[ K_{11}^{(1')} \right]^{-1} K_{1l}^{(1')} \right\} h_l^{(1)}(\mu) + \sum_{n=2}^k \sum_{l=n}^N K_{kl}^{(n')} h_l^{(n)}(\mu) + \\ & + \sigma_1 K_{k1}^{(1')} \left[ K_{11}^{(1')} \right]^{-1} \psi_1'(\sigma_1 \mu) = \left[ K_{11}^{(1')} \right]^{-1} \sum_{l=2}^N \left[ K_{11}^{(1')} \oplus K_{kl}^{(1')} - K_{k1}^{(1')} \oplus K_{ll}^{(1')} \right] \\ & h_l^{(1)}(\mu) + \left[ K_{11}^{(1')} \right]^{-1} \sum_{l=2}^N \left[ K_{11}^{(1')} \wedge K_{kl}^{(1')} - K_{k1}^{(1')} \wedge K_{1l}^{(1')} \right] h_l^{(1)}(\mu) + - \sum_{l=2}^N \left[ K_{k1}^{(1')}, K_{11}^{(1')} \right]^{-1} \\ & K_{11}^{(1')} h_l^{(1)}(\mu) + \sum_{n=2}^k \sum_{l=n}^N K_{kl}^{(n')} h_l^{(n)}(\mu) + \sigma_1 K_{k1}^{(1')} \left[ K_{11}^{(1')} \right]^{-1} \psi_1'(\sigma_1 \mu) = \sigma_k \psi'_k(\sigma_k \mu) \\ & \text{for } k \geq 2. \end{aligned} \quad (40)$$

Eqs. (40) can be rewritten in a more compact way by introducing the definition of operatorial determinants in  $\oplus$ -algebra (see Appendices A and B):

$$\left( K_{\varrho\delta}^{(m+1)} ; m+1, \dots, m+p, k \right) \underset{\text{def}}{=} \begin{vmatrix} K_{m+1, m+1}^{(m+1)} & \cdots & K_{m+1, m+p}^{(m+1)} & K_{m+1, l}^{(m+1)} \\ \vdots & & \vdots & \vdots \\ K_{m+p, m+1}^{(m+1)} & & K_{m+p, m+p}^{(m+1)} & \\ & & & \vdots \\ K_{k, m+1}^{(m+1)} & & & K_{kl}^{(m+1)} \end{vmatrix} \quad (41)$$

in the form:

$$\left[ K_{11}^{(1')} \right]^{-1\oplus} \sum_{l=2}^N (K_{\varrho\delta}^{(1')}; {}_{1l}^{1k}) h_l^{(1)}(\mu) = \Psi_k(\mu) - \sum_{n=2}^k \sum_{l=n}^N K_{kl}^{(n')} h_l^{(n')}(\mu), \quad (42)$$

where

$$\begin{aligned} \Psi_k(\mu) &= \sigma_k \psi_k'(\sigma_k \mu) - \sigma_1 K_{k1}^{(1')} \left[ K_{11}^{(1')} \right]^{-1} \psi_1'(\sigma, \mu) - \left[ K_{11}^{(1')} \right]^{-1} \sum_{l=2}^N \left[ K_{11}^{(1')} \wedge K_{kl}^{(1')} \right. \\ &\quad \left. - K_{k1}^{(1')} \wedge K_{1l}^{(1')} \right] h_l^{(1)}(\mu) - \sum_{l=2}^N \left[ K_{k1}^{(1')}, \left[ K_{11}^{(1')} \right]^{-1} \right] K_{1l}^{(1')} h_l^{(1)}(\mu) - \\ &\quad - \left[ K_{11}^{(1')} \right]^{-1} \wedge \sum_{l=2}^N K_{\varrho\delta}^{(2')}; {}_{1l}^{1k}) h_l^{(1)}(\mu) \end{aligned} \quad (43)$$

and contains Fredholm-type integrals only with respect to  $h_l^{(1)}(\mu)$ .

Let us consider now Eq. (42) for  $k=2$  and for  $\mu \in (1')$ :

$$\begin{aligned} \left[ K_{11}^{(1')} \right]^{-1\oplus} (K_{\varrho\delta}^{(1')}; {}_{1,2}^{1,2}) h_2^{(1)}(\mu) &= \Psi_2(\mu) - \left[ K_{11}^{(1')} \right]^{-1\oplus} \sum_{l=3}^N (K_{\varrho\delta}^{(1')}; {}_{1,2}^{1,2}) h_l^{(1)}(\mu) - \\ &\quad - \sum_{l=2}^N K_{kl}^{(2')} h_l^{(2)}(\mu). \end{aligned} \quad (44)$$

Solving Eq. (44) we find:

$$\begin{aligned} (K_{\varrho\delta}^{(1')}; {}_{1,2}^{1,2}) h_2^{(1)}(\mu) &= \left( \left[ K_{11}^{(1')} \right]^{-1\oplus} \right)^{-1} \left\{ \Psi_2(\mu) - \left[ K_{11}^{(1')} \right]^{-1\oplus} \sum_{l=3}^N (K_{\varrho\delta}^{(1')}; {}_{1,2}^{1,2}) h_l^{(1)}(\mu) - \right. \\ &\quad \left. - \sum_{l=2}^N K_{kl}^{(2')} h_l^{(2)}(\mu) \right\} \equiv \xi_2^{(1)}(\mu). \end{aligned} \quad (45)$$

It should be emphasized that since  $x(K) = -x(K^{-1})$  in both operations (39) and (45), additional conditions equal in number to arbitrary constants in the polynomial  $P_{x-1}$  had to be introduced. It is easily seen from Appendix B that:

$$(K_{\varrho\delta}^{(1')}; {}_{1,2}^{1,2}) = (\omega_{\varrho\delta}; {}_{1,2}^{1,2})^{(1')}. \quad (46)$$

Now let us consider Eq. (42) for  $k=2$  but for  $\mu \in (2')$ . It can be written in the form:

$$\begin{aligned} K_{22}^{(2')} h_2^{(2)}(\mu) &= \Psi_2(\mu) - \left[ K_{11}^{(1')} \right]^{-1\oplus} (K_{\varrho\delta}^{(1')}; {}_{1,2}^{1,2}) h_2^{(1)}(\mu) - \\ &\quad - \left[ K_{11}^{(1')} \right]^{-1\oplus} \sum_{l=3}^N (K_{\varrho\delta}^{(1')}; {}_{1,2}^{1,2}) h_l^{(1)}(\mu) - \sum_{l=3}^N K_{2l}^{(2')} h_l^{(2)}(\mu) \equiv \xi_2^{(2)}(\mu) \end{aligned} \quad (47)$$

where  $\xi_2^{(2)}(\mu)$  contains, at most, Fredholm-type integrals only with respect to  $h_2^{(2)}(\mu)$  and  $h_2^{(1)}(\mu)$ .

Using the definition of  $K_{22}^{(2')}$  one can write Eqs. (45) and (46) in the form:

$$\begin{aligned} (\omega_{\varrho\delta}; {}_{1,2}^{1,2})^{(1')} h_2^{(1)}(\mu) &= \xi_2^{(1)}(\mu) \\ (\omega_{\varrho\delta}; {}_{1,2}^{1,2})^{(2')} h_2^{(2)}(\mu) &= \xi_2^{(2)}(\mu). \end{aligned} \quad (48)$$

Such a system of two singular integral equations was discussed already in [3] by the authors. The total index of the systems is given by values of

$$\frac{1}{\pi} \arg \left\{ \omega_{\theta\delta} ; \begin{smallmatrix} 1, 2 \\ 1, 2 \end{smallmatrix} \right\}^{(l')} - \quad (49)$$

at the ends of the interval  $(1') + (2')$ . The points of junction between the intervals  $(1')$  and  $(2')$  give no contributions. It is worth while to observe that the ends of the interval  $(1') + (2')$  are special ends from the point of view of the general theory of singular integral equations.

Having determined the functions  $h_2^{(1)}(\mu)$  and  $h_2^{(2)}(\mu)$ , we can insert them into Eq. (42) for  $k=3$  and obtain the set of equations for  $h_3^{(1)}(\mu)$ ,  $h_3^{(2)}(\mu)$ ,  $h_3^{(3)}(\mu)$ . Reducing necessary operations to those in the sense of  $\oplus$ -algebra, we get a system of singular integral equations with operators:

$$(\omega_{\theta\delta} ; \begin{smallmatrix} 1, 2, 3 \\ 1, 2, 3 \end{smallmatrix})^{(n')} \quad \text{where } n' = 1', 2', 3'. \quad (49)$$

To obtain this result the reciprocal operators have been used in such a way that the arbitrary constants entering explicit forms of functions  $h_2^{(1)}(\mu)$  and  $h_2^{(2)}(\mu)$  have been determined. The procedure of elimination described above is completely analogous to the Gauss algorithm well known in the theory of linear algebraic equations.

The ultimate result of this procedure is

$$(\omega_{\theta\delta} ; \begin{smallmatrix} 1, 2, \dots, N \\ 1, 2, \dots, N \end{smallmatrix})^{(l)} h_N^{(l)}(\mu) = \xi_N^{(l)}(\mu), \quad (l = 1, 2, \dots, N) \quad (50)$$

where functions  $\xi_N^{(l)}(\mu)$  contain only the Fredholm-type integrals. It must be emphasized that all arbitrary constants and additional conditions introduced during the elimination cancel each other. Let us consider now two cases:

$$(1) \quad (l') = - \left( \frac{1}{\sigma_l}, \frac{1}{\sigma_{l-1}} \right) + \left( \frac{1}{\sigma_{l-1}}, \frac{1}{\sigma_l} \right)$$

$$(2) \quad (l') = \left( \frac{1}{\sigma_{l-1}}, \frac{1}{\sigma_l} \right).$$

In the first case the total index of the system (50) is equal to

$$x = \frac{1}{\pi} \arg \left\{ \omega_{\theta\delta} ; \begin{smallmatrix} 1, 2, \dots, N \\ 1, 2, \dots, N \end{smallmatrix} \right\}^{(N)} - \int_{\mu=1}^{\infty} - - - - - \quad (51)$$

$$- \frac{1}{\pi} \arg \left\{ \omega_{\theta\delta} ; \begin{smallmatrix} 1, 2, \dots, N \\ 1, 2, \dots, N \end{smallmatrix} \right\}^{(N)} - \int_{\mu=-1}^{-\infty} - - - - -$$

which, according to the argument principle [3, 7], is equal to the number of roots of the function  $\left\{ \omega_{\theta\delta} ; \begin{smallmatrix} 1, 2, \dots, N \\ 1, 2, \dots, N \end{smallmatrix} \right\} \equiv \Omega(v)$  in the cut plane with the opposite sign.

In this way all the arbitrary constants entering the discrete solutions can be uniquely determined. Going backwards with our elimination procedure we can obtain the Fredholm-type equations for coefficients  $h_k^{(l)}(\mu)$  ( $l=1, \dots, k$ ;  $k=1, \dots, N$ ). In the second case one can make use of the well-known fact that the function  $\Omega(v)$  is an even function of  $v$  and thus prove that  $x' = \frac{1}{2}x$ . Hence only half of a full set of the expansion coefficients with respect to the discrete set of eigen-

functions can be determined. The remaining expansion coefficients with respect to the discrete eigenfunctions must be determined in another way.

On the basis of this theorem the general solution of the system of Boltzmann equations (1) can be written in the form:

$$\psi_k(x, \mu) = \sum_{l=1}^M \left\{ \Phi_k(\mu, \nu_l) e^{-\frac{x}{\nu_l}} + \Phi_k(\mu, -\nu_l) e^{\frac{x}{\nu_l}} \right\} + \sum_{l=1}^N \int \Phi_k^{(l)}(\mu, \nu) e^{-\frac{x}{\nu}} d\nu. \quad (52)$$

The expansion coefficients enter the functions  $\Phi_k$ ,  $\Phi_k^{(l)}$  according to the results given in section 1.

### 3. Examples of application

In this section the method of applying the expansion into eigenfunctions (distributions) will be outlined. Let us consider, for example, two important problems: the critical problem and the albedo problem for a slab.

#### THE CRITICAL PROBLEM FOR A SLAB

The general solution of the form (52) should satisfy the following boundary conditions:

$$\begin{aligned} \psi_k(d, \mu) &= 0 & \text{for } \mu < 0 \\ \psi_k(-d, \mu) &= 0 & \text{for } \mu > 0 \end{aligned} \quad (53)$$

To avoid the necessity of solving  $2N$  singular integral equations derived from conditions (53) let us use the following property of the functions  $\psi_k^s(x, \mu)$  (being the solutions of the critical problem for a slab)

$$\psi_k^s(x, \mu) = \psi_k^s(-x, -\mu). \quad (54)$$

Such functions must be sought in the symmetric part of the general solution (53). It can be written in the form:

$$\begin{aligned} \psi_k^s(x, \mu) &= \sum_{l=1}^M \left\{ [\Phi_k(\mu, \nu_l) + \Phi_k(-\mu, -\nu_l)] e^{-\frac{x}{\nu_l}} + [\Phi_k(\mu, -\nu_l) + \right. \\ &\quad \left. + \Phi_k(-\mu, \nu_l)] e^{\frac{x}{\nu_l}} \right\} + \sum_{l=1}^N \int \left\{ \Phi_k^{(l)}(\mu, \nu) + \Phi_k^{(l)}(-\mu, -\nu) \right\} e^{\frac{-x}{\nu}} d\nu. \end{aligned} \quad (55)$$

Now the symmetric parts of the functions  $\Phi_k(\mu, \nu_l)$  and  $\Phi_k^{(l)}(\mu, \nu)$  can be calculated:

$$\Phi_k(\mu, \nu_l) + \Phi_k(-\mu, -\nu_l) = [h(\nu_l) + h(-\nu_l)] \frac{\nu_l g_k(\nu_l)}{\sigma_k \nu_l - \mu} \equiv \Phi_k^s(\mu, \nu_l)$$

where the only change in the shape of  $\Phi_k^s(\mu, \nu_l)$  in comparison with  $\Phi_k(\mu, \nu_l)$  is that  $h(\nu_l) \rightarrow h^s(\nu_l) = h(+\nu_l) + h(-\nu_l)$ . A similar procedure should be applied also to the functions where the functions  $h_n^{(l)}(\nu)$  should be replaced by the functions  $h_n^{(l)s}(\nu) = h_n^{(l)}(\nu) + h_n^{(l)}(-\nu)$ . Further, the change of the integration variable can be performed which results in the following expression for  $\psi_k^s(x, \mu)$ :

$$\begin{aligned}\psi_k^s(x, \mu) = & \sum_{l=1}^M \left\{ \Phi_k^{(l)s}(\mu, v_l) e^{-\frac{x}{v_l}} + \Phi_k^{(l)s}(\mu, -v_l) e^{\frac{x}{v_l}} \right\} + \\ & + \sum_{l=1}^N \int \left\{ \Phi_k^{(l)s}(\mu, v) e^{-\frac{x}{v}} + \Phi_k^{(l)s}(\mu, -v) e^{\frac{x}{v}} \right\} dv.\end{aligned}\quad (56)$$

It can be easily verified that conditions (53 a, b) are equivalent to only one of them, for instance

$$\psi_k^s(d, -\mu) = 0 \quad \text{for } \mu > 0. \quad (57)$$

Inserting the expression (56) into the condition (57) we obtain

$$\begin{aligned}& \sum_{l=1}^N \int \left\{ \Phi_k^{(l)s}(-\mu, v) e^{-\frac{d}{v}} + \Phi_k^{(l)s}(-\mu, -v) e^{\frac{d}{v}} \right\} dv = \\ & = - \sum_{l=1}^M \left\{ \Phi_k^s(-\mu, v_l) e^{-\frac{d}{v_l}} + \Phi_k^s(-\mu, -v_l) e^{\frac{d}{v_l}} \right\} \equiv \Phi_k^d(\mu).\end{aligned}\quad (58)$$

Using the evident property of the functions

$$\Phi_k^{(l)s}(\mu, v) = \Phi_k^{(l)s}(-\mu, -v) \quad (59)$$

we can rewrite Eq. (58) in the following form

$$\sum_{l=1}^N \int \Phi_k^{(l)s}(\mu, v) e^{\frac{d}{v}} dv = \Phi_k^d(\mu) - \sum_{l=1}^M \int \Phi_k^{(l)s}(\mu, -v) e^{-\frac{d}{v}} dv. \quad (60)$$

In the system (60), the following change of unknown functions should be performed:

$$\tilde{h}_k^{(l)}(v) = h_k^{(l)s}(\nu) e^{\frac{d}{v}} \quad (61)$$

which results in the following system of singular integral equations

$$\sum_{l=1}^N \int \tilde{\Phi}_k^{(l)}(\mu, v) dv = \Phi_k^d(\mu) - \sum_{l=1}^N \int \tilde{\Phi}_k^{(l)}(\mu, -v) e^{-\frac{2d}{v}} dv \quad (62)$$

where the functions  $\Phi_k^{(l)s}$  with  $h_k^{(l)s}$  changed according to Eq. (61) are denoted by  $\tilde{\Phi}_k^{(l)}$ .

Transferring the Fredholm-type integrals from the left-hand side of Eq. (62) to the right-hand side and denoting the resulting right-hand side by  $\psi_k(\mu)$  a system of equations

$$\sum_{l=1}^k \int \tilde{\Phi}_k^{(l)}(\mu, v) dv = \psi_k(\mu) \quad (63)$$

can be obtained, which is identical in the form with a system (30), case (2), treated in Section 2.

After an elimination identical with the one described above, the system of Fredholm-type integral equations is obtained which should be treated by means of classical methods. Besides this,  $M$  additional conditions must be satisfied which, after substitution of the expansion coefficients calculated from the above-mentioned system of Fredholm-type integral equations, form a system of homogeneous, linear algebraic equations with respect to  $M$  unknown constants entering the functions  $\Phi_k^{(l)}(\mu)$ . The sufficient and necessary condition of existence of non-trivial solutions of this system of algebraic equations is that the characteristic determinant must vanish. This is a  $N$ -group exact critical condition determining the critical thickness  $d$  of a slab.

#### THE ALBEDO PROBLEM FOR A SLAB

The general solution of the form (52) should satisfy the following boundary conditions:

$$\begin{aligned}\psi_k(o, \mu) &= f_1(\mu) & \mu > 0 \\ \psi_k(d, \mu) &= f_2(\mu) & \mu < 0.\end{aligned}\quad (64)$$

It is convenient to present the general solution (52) in the following form

$$\begin{aligned}\psi_k(x, \mu) &= \sum_{l=1}^M \left\{ \Phi_k(\mu, \nu_l) e^{-\frac{x}{\nu_l}} + \Phi_k(\mu, \nu_l) e^{\frac{x}{\nu_l}} \right\} + \sum_{l=1}^N \int_{(l')} \Phi_k^{(l)}(\mu, \nu) e^{-\frac{x}{\nu}} d\nu = \\ &= \sum_{l=1}^M \left\{ \Phi_k(\mu, \nu_l) e^{-\frac{x}{\nu_l}} + \Phi_k(\mu, \nu_l) e^{\frac{x}{\nu_l}} \right\} + \sum_{l=1}^N \left\{ \int_{(l')} \Phi_k^{(l)}(\mu, \nu) e^{-\frac{x}{\nu}} d\nu + \right. \\ &\quad \left. + \int_{(l')} \tilde{\Phi}_k^{(l)}(-\mu, \nu) e^{\frac{x-d}{\nu}} d\nu \right\},\end{aligned}$$

where the following change of the expansion coefficient has been performed

$$\tilde{h}_n^{(l)}(\nu) = h_n^{(l)}(-\nu) e^{\frac{d}{\nu}} \quad (\text{for every } n) \quad (66)$$

and  $\tilde{\Phi}_k^{(l)}(-\mu, \nu)$  denotes the usual  $\Phi_k^{(l)}(-\mu, \nu)$  with  $\tilde{h}_k^{(l)}(\nu)$  instead of  $h_k^{(l)}(\nu)$ .

On inserting the expression (65) into (64 a, b) (with a change of sign in (64 b)), the following system of equations has been obtained

$$\begin{aligned}\sum_{l=1}^N \left\{ \int_{(l')} \Phi_k^{(l)}(\mu, \nu) d\nu + \int_{(l')} \tilde{\Phi}_k^{(l)}(-\mu, \nu) e^{-\frac{d}{\nu}} d\nu \right\} + \sum_{l=1}^M \left\{ \Phi_k(\mu, \nu_l) + \right. \\ \left. + \Phi_k(\mu, -\nu_l) \right\} &= \psi_k(o, \mu) = f_1(\mu) & \mu > 0 \\ \sum_{l=1}^N \left\{ \int_{(l')} e^{-\frac{d}{\nu}} \Phi_k^{(l)}(-\mu, \nu) d\nu + \int_{(l')} \tilde{\Phi}_k^{(l)}(\mu, \nu) d\nu \right\} + \sum_{l=1}^M \left\{ \Phi_k(-\mu, \nu_l) e^{-\frac{d}{\nu_l}} + \right. \\ \left. + \Phi_k(\mu, \nu_l) e^{\frac{d}{\nu_l}} \right\} &= \psi_k(d, -\mu) = f_2(-\mu), & \mu > 0.\end{aligned}\quad (67)$$

Transferring all Fredholm-type integrals and discrete parts of the expansion to the right-hand side, the system (67) can be rewritten in the form:

$$\begin{aligned}
 & \sum_{l=1}^k \int \Phi_k^{(l)}(\mu, \nu) d\nu = f_1(\mu) - \sum_{l=1}^M \{\Phi_k(\mu, \nu) + \Phi_k(\mu, -\nu_l)\} - \\
 & - \sum_{l=1}^N \int e^{-\frac{d}{\nu}} \tilde{\Phi}_k^{(l)}(-\mu, \nu) d\nu - \sum_{l=k+1}^N \int \Phi_k^{(l)}(\mu, \nu) d\nu \quad \mu > 0 \\
 & \sum_{l=1}^k \int \tilde{\Phi}_k^{(l)}(\mu, \nu) d\nu = f_2(-\mu) - \sum_{l=1}^M \{\Phi_k(-\mu, \nu_l) e^{-\frac{d}{\nu_l}} + \\
 & + \Phi_k(\mu, \nu_l) e^{\frac{d}{\nu_l}}\} - \sum_{l=1}^N \int e^{-\frac{d}{\nu}} \Phi_k^{(l)}(-\mu, \nu) d\nu - \sum_{l=k+1}^N \int \tilde{\Phi}_k^{(l)}(\mu, \nu) d\nu \\
 & \mu > 0. \tag{68}
 \end{aligned}$$

In this way we obtain two systems of singular integral equations discussed as (2) in Section 2. Each system of singular integral equations (68 a, b) can be reduced to a system of Fredholm-type integral equations with  $M$  additional conditions. Thus  $2M$  arbitrary constants occurring in the discrete part of the expansion can be uniquely determined.

#### 4. Conclusions

The method presented here allows us to formulate the general solution of the  $N$ -group Boltzmann equations in plane geometry. In every physical problem the boundary conditions give the system of singular integral equations for the expansion coefficients with respect to the full set of eigenfunctions. The method of reduction of this system of singular integral equations to the system of Fredholm-type integral equations has been given, but the general shape of these integral equations is not given explicitly. This difficulty can be easily avoided in each particular case using this approach. The above-mentioned system of Fredholm-type integral equations can be treated by means of classical numerical methods. It is worth while to mention that according to the theorem given in DAVISON's monograph [1], the spherical problems are equivalent (on the level of neutron flux and Peierls integral equation) to the appropriate slab problems. This fact implies a large extension of the possible applications of the presented theory. It should be emphasized that according to the discussed example of application this method can be used in the critical and shielding calculations of the reactors. For example, the critical dimensions of a bare sphere in the multi-group transport theory can be evaluated. This method can be easily extended to the case of anisotropic scattering of neutrons, according to the ideas given in [7, 8].

The transport calculations for photons would then also be based on a more realistic ground.

#### ACKNOWLEDGEMENT

The authors are very grateful to Miss K. Kowalska for valuable help during the preparation of the manuscript.

## APPENDIX A

## Algebra of the singular integral operators

Let us consider the singular operators of the form:

$$K\varphi(\mu) \underset{\text{def}}{=} A(\mu)\varphi(\mu) - \frac{1}{\pi i} \int_L^{} \frac{B(v)\varphi(v)}{v-\mu} dv \quad (\text{A1})$$

where  $A(\mu)$  and  $iB(\mu)$  are arbitrary real functions satisfying the Hölder conditions superposition of two such singular integral operators has the form:

$$\begin{aligned} K_1 K_2 f(\mu) &= [A_1(\mu)A_2(\mu) + B_1(\mu)B_2(\mu)]f(\mu) - \frac{1}{\pi i} \int \frac{A_1(v)B_2(v) + B_1(v)A_2(v)}{v-\mu} f(v) dv + \\ &\quad + \frac{1}{\pi i} \int \frac{F_1(v) - F_1(\mu)}{v-\mu} B_2(v)f(v) dv \end{aligned} \quad (\text{A2})$$

where

$$F_1(v) = A(v) - \frac{1}{\pi i} \int_L^{} \frac{B_1(\eta)d\eta}{\eta-v} \equiv K_1 I(v) \quad (\text{A3})$$

with  $I(v) \equiv 1$  for  $v \in L$

Let us introduce now the following operation of multiplication of singular integral operators:

$$K_1 \oplus K_2 \varphi(\mu) \underset{\text{def}}{=} [A_1(\mu)A_2(\mu) + B_1(\mu)B_2(\mu)]\varphi(\mu) - \frac{1}{\pi i} \int \frac{A_1(v)B_2(v) + B_1(v)A_2(v)}{v-\mu} \varphi(v) dv \quad (\text{A4})$$

which satisfies all axioms of a commutative multiplication. The formula (A2) can be rewritten in the form:

$$K_1 K_2 \varphi(\mu) = K_1 \oplus K_2 \varphi(\mu) + K_1 \wedge K_2 \varphi(\mu). \quad (\text{A5})$$

Let us observe that the integral expression

$$K_1 \wedge K_2 \varphi(\mu) = \frac{1}{\pi i} \int_L^{} \frac{F_1(v) - F_1(\mu)}{v-\mu} B_2(v)\varphi(v) dv \quad (\text{A6})$$

has no Cauchy singularity. Thus it is the Fredholm-type integral. It is worthwhile to calculate the commutator

$$\begin{aligned} [K_1, K_2] \varphi(\mu) &\underset{\text{def}}{=} (K_1 K_2 - K_2 K_1) \varphi(\mu) = (K_1 \wedge K_2 - K_2 \wedge K_1) \varphi(\mu) \\ &= \frac{1}{\pi i} \int_L^{} \frac{[F_1(v) - F_1(\mu)]B_2(v) - [F_2(v) - F_2(\mu)]B_1(v)}{v-\mu} \varphi(v) dv \end{aligned} \quad (\text{A7})$$

which, as is easily seen, is a Fredholm-type integral. The singular integral operators of type (A2) with multiplication of type  $\oplus$  and with the usual addition define the commutative algebra over the field of real numbers. This algebra is isomorphic with an algebra of the complex functions of the form  $A(\mu) + iB(\mu)$ , where  $A(\mu)$  and  $iB(\mu)$  are real functions, satisfying the Hölder conditions on  $L$ .

From the general theory of singular integral equations [9] it is well known that the reciprocal operator  $K^{-1}$  is given in the form:

$$K^{-1}g(\mu) = A^*(\mu)g(\mu) + \frac{1}{\pi i Z(\mu)} \int_L^{} \frac{B^*(v)Z(v)g(v)dv}{v-\mu} + \frac{P_{n-1}(\mu)}{Z(\mu)} \quad (\text{A8})$$

where

$$A^*(\mu) = \frac{A(\mu)}{A^2(\mu) - B^2(\mu)}; \quad B^*(\mu) = \frac{B(\mu)}{A^2(\mu) - B^2(\mu)}; \quad (\text{A9})$$

$$Z(\mu) = [A(\mu) - B(\mu)] X^-(\mu) = \sqrt{A^2(\mu) - B^2(\mu)} \prod_{k=1}^m (\mu - a_k)^{\left[ \frac{1}{2\pi i} \ln G(a_k) \right]} \cdot \\ \cdot \prod_{k=1}^m (\mu - b_k)^{-\left[ \frac{1}{2\pi i} \ln G(b_k) \right]} \exp \left\{ \frac{1}{2\pi i} \int_L \frac{\ln G(v)}{v - \mu} dv \right\} \quad (A10)$$

(Here  $a_k$  and  $b_k$  denote the starting and the end points of contours  $L_k$  which constitute the contour  $L$ :  $L = \sum_{k=1}^m L_k$ ).

$$G(\mu) = \frac{A - B}{A + B} \quad (A11)$$

$$\nu = \sum_{k=1}^m \left\{ \left[ \frac{1}{2\pi i} \ln G(b_k) \right] - \left[ \frac{1}{2\pi i} \ln G(a_k) \right] \right\}. \quad (A12)$$

This formula is valid only for  $\nu > 0$ . Then  $P_{\nu-1}$  is an arbitrary polynomial of the degree  $\nu-1$ . For  $\nu \leq 0$   $P_{\nu-1} = 0$  and the additional conditions of the following form should be used

$$\int_L \frac{\mu^r g(\mu)}{Z(\mu)} d\mu = 0 \quad r = 0, 1, \dots, -\nu - 1. \quad (A13)$$

The operator  $K^{-1}$  may be split into two parts: a dominant and a Fredholm-type part, according to the following formula:

$$K^{-1}g(\mu) = A^*(\mu)g(\mu) + \frac{1}{\pi i} \int_L \frac{B^*(v)g(v)dv}{v - \mu} + \\ + \frac{1}{\pi i Z(\mu)} \int_L \frac{B^*(v)[Z(v) - Z(\mu)]}{v - \mu} g(v)dv + \frac{P_{\nu-1}(\mu)}{Z(\mu)}. \quad (A14)$$

Now we can construct an operator  $K^{-1}\oplus$  defined as follows:

$$K^{-1}\oplus K = I$$

where  $I$  is an identical operator ( $A(\mu) = 1$ ,  $B(\mu) = 0$ ).

By means of simple algebraic calculations based on formula (A4) one can find that

$$K^{-1}\oplus g(\mu) = A^*(\mu)g(\mu) + \frac{1}{\pi i} \int_L \frac{B^*(v)g(v)dv}{v - \mu}. \quad (A15)$$

Hence formula (A14) can be written simply as

$$K^{-1}g(\mu) = K^{-1}\oplus g(\mu) + K^{-1}\wedge g(\mu),$$

where

$$K^{-1}\wedge g(\mu) = \frac{1}{\pi i Z(\mu)} \int_L \frac{B^*(v)[Z(v) - Z(\mu)]}{v - \mu} g(v)dv + \frac{P_{\nu-1}(\mu)}{Z(\mu)}. \quad (A16)$$

It can be easily proved that the following formula is valid

$$(K_1 \oplus K_2)^{-1}\oplus = K_1^{-1}\oplus \oplus K_2^{-1}\oplus \quad (A17)$$

and that the index  $\nu(K^{-1}\oplus) = \nu(K^{-1}) = -\nu(K)$ .

## APPENDIX B

## Operatorial determinants

Let us introduce the following notation:

$$\left\{ \gamma_{\varrho\delta} ; \frac{\alpha_1, \dots, \alpha_n}{\beta_1, \dots, \beta_n} \right\} \underset{\text{def}}{=} \begin{vmatrix} \gamma_{\alpha_1 \beta_1}, \dots, \gamma_{\alpha_n \beta_n} \\ \vdots \\ \gamma_{\alpha_n \beta_1}, \dots, \gamma_{\alpha_n \beta_n} \end{vmatrix} \quad (\text{B1})$$

where  $\gamma_{\varrho\delta}$  are arbitrary matrix elements of the  $N$ th rank. Using the determinant theorem [10] one can prove the following relation easily:

$$\begin{aligned} & \left\{ \gamma_{\varrho\delta} ; \frac{1, \dots, m, \sigma}{1, \dots, m, \tau} ; \frac{m+1, \dots, m+p, k}{m+1, \dots, m+p, l} \right\} \\ &= \left\{ \gamma_{\varrho\delta} ; \frac{1, \dots, m}{1, \dots, m} \right\}^r \left\{ \gamma_{\varrho\delta} ; \frac{1, \dots, m+p, k}{1, \dots, m+p, l} \right\} \end{aligned} \quad (\text{B2})$$

where  $0 \leq p \leq N-m$ .

Now let us construct a determinant of type (B1) from the elements  $\omega_{\varrho\delta}$  defined by Eq. (11):

$$\left\{ \omega_{\varrho\delta} ; \frac{\alpha_1, \dots, \alpha_n}{\beta_1, \dots, \beta_n} \right\} \quad (\text{B3})$$

This determinant is an analytic function in an appropriate cut plane of  $\nu$ , according to the analytic properties of the functions  $f_{\varrho}(\nu)$  entering into the definition of  $\omega_{\varrho\delta}$ . Since on the upper and lower sides of the cuts the functions  $f_{\varrho}(\nu)$  have the respective limits  $f_{\varrho}^{\pm}(\nu)$  we can define the following determinants

$$\left\{ \omega_{\varrho\delta} ; \frac{\alpha_1, \dots, \alpha_n}{\beta_1, \dots, \beta_n} \right\}^{(m)\pm} = \left\{ \omega_{\varrho\delta}^{(m)\pm} ; \frac{\alpha_1, \dots, \alpha_n}{\beta_1, \dots, \beta_n} \right\} \quad (\text{B4})$$

where the index  $(m)$  denotes that an appropriate limit of  $f_{\varrho}(\nu)$  is taken in the region  $(m)$ . In other words we must use the formula:

$$\omega_{\varrho\delta}^{(m)\pm} = P \omega_{\varrho\delta}^{(m)\pm} i \pi \mu \delta_{\varrho\delta} \gamma_{m\rho} \quad (\text{B5})$$

where  $P$  is a symbol of the principal value and

$$\gamma_{m\rho} = \begin{cases} 1 & \text{for } m \leq \rho \\ 0 & \text{for } m > \rho \end{cases}.$$

The determinant (B4) with a sign  $\pm$  can be evidently split into a real and imaginary part. On the basis of Appendix A it is isomorphic with a particular singular integral operator (on the ground of  $\oplus$ -algebra). This operator will be denoted as follows:

$$\left\langle \omega_{\varrho\delta} ; \frac{\alpha_1, \dots, \alpha_n}{\beta_1, \dots, \beta_n} \right\rangle^{(m)} \quad (\text{B6})$$

and the isomorphic relation should be written in the form:

$$\left\{ \omega_{\varrho\delta} ; \frac{\alpha_1, \dots, \alpha_n}{\beta_1, \dots, \beta_n} \right\}^{(m)\pm} \xleftrightarrow{\text{is}} \left\langle \omega_{\varrho\delta} ; \frac{\alpha_1, \dots, \alpha_n}{\beta_1, \dots, \beta_n} \right\rangle^{(m)}. \quad (\text{B7})$$

It can be easily seen that

$$\begin{aligned} \left\{ \omega_{\varrho\delta} ; \frac{1, \dots, n-1, k}{1, \dots, n-1, l} \right\}^{(n)\pm} &= P \left\{ \omega_{\varrho\delta} ; \frac{1, \dots, n-1, k}{1, \dots, n-1, l} \right\}^n \pm \pi i \mu \delta_{kl} \\ \left\{ \omega_{\varrho\delta} ; \frac{1, \dots, n-1}{1, \dots, n-1} \right\}^{(n)} &= P \left\{ \omega_{\varrho\delta} ; \frac{1, \dots, n-1, k}{1, \dots, n-1, l} \right\}^{(n)} \pm i \pi \mu \Omega^{(n)} \delta_{kl}, \end{aligned} \quad (\text{B8})$$

according to the definition of  $\Omega^{(n)}$  given in Eq. (17). This fact enables us to formulate the following theorem. The function

$$\left\{ \omega_{\theta\delta}; \begin{matrix} 1, \dots, n-1, k \\ 1, \dots, n-1, l \end{matrix} \right\}^{(n)} -$$

is isomorphic with the following singular integral operator of the form

$$P \left\{ \omega_{\theta\delta}; \begin{matrix} 1, 2, \dots, n-1, k \\ 1, 2, \dots, n-1, l \end{matrix} \right\}^{(n)} H^{(n)}(\mu) \varphi(\mu) + \delta_{kl} \int \frac{\nu \Omega^{(n)}(\nu) \varphi(\nu)}{\nu - \mu} d\nu \equiv K_{kl}^{(n)} \varphi(\mu). \quad (\text{B9})$$

It must be emphasized that this theorem is valid only for determinants of  $n$  rank and in  $(n)$  region.

Similarly the following theorem can be formulated without any difficulty on the basis of the isomorphic relation (B7):

$$\begin{aligned} & \left( \left\{ \omega_{\theta\delta}; \begin{matrix} 1, \dots, m, \sigma \\ 1, \dots, m, \tau \end{matrix} \right\}; \begin{matrix} m+1, \dots, m+p, k \\ m+1, \dots, m+p, l \end{matrix} \right)^{(n)} = \\ & = \left( \left\{ \omega_{\theta\delta}; \begin{matrix} 1, \dots, m, \sigma \\ 1, \dots, m, \tau \end{matrix} \right\}^{(n)}; \begin{matrix} m+1, \dots, m+p, k \\ m+1, \dots, m+p, l \end{matrix} \right) \end{aligned} \quad (\text{B10})$$

where the expression on the right-hand side denotes a determinant constructed of operators

$$\left( \omega_{\theta\delta}; \begin{matrix} 1, \dots, m, \sigma \\ 1, \dots, m, \tau \end{matrix} \right)^{(n)}$$

in the formalism of  $\oplus$ -algebra.

The particular case of formula (B10) is

$$\begin{aligned} & \left( \left\{ \omega_{\theta\delta}; \begin{matrix} 1, \dots, m, \sigma \\ 1, \dots, m, \tau \end{matrix} \right\}; \begin{matrix} m+1, \dots, m+p, k \\ m+1, \dots, m+p, l \end{matrix} \right)^{(m+1)} = \\ & = \left( K_{\theta\delta}^{(m+1)}; \begin{matrix} m+1, \dots, m+p, k \\ m+1, \dots, m+p, l \end{matrix} \right). \end{aligned} \quad (\text{B11})$$

On the other hand, on the basis of Eq. (B2) and the isomorphic relation (B7), the right-hand side of Eq. (B11) may be written also in the form:

$$\begin{aligned} & \left( K_{\theta\delta}^{(m+1)}; \begin{matrix} m+1, \dots, m+p, k \\ m+1, \dots, m+p, l \end{matrix} \right) = \\ & = \left[ \left( \omega_{\theta\delta}; \begin{matrix} 1, \dots, m \\ 1, \dots, m \end{matrix} \right)^{(m+1)} \right]^p \oplus \left( \omega_{\theta\delta}; \begin{matrix} 1, \dots, m+p, k \\ 1, \dots, m+p, l \end{matrix} \right)^{(m+1)} \end{aligned} \quad (\text{B12})$$

where it must be noted that according to the analytic properties of the functions  $\omega_{\theta\delta}$  in the region  $(m+1)$  the operator

$$\left( \omega_{\theta\delta}; \begin{matrix} 1, \dots, m \\ 1, \dots, m \end{matrix} \right)^{(m+1)}$$

is an operator of multiplication by function  $\left\{ \omega_{\theta\delta}; \begin{matrix} 1, \dots, m \\ 1, \dots, m \end{matrix} \right\}^{(m+1)}$ .

## REFERENCES

- [1] DAVISON, B., Neutron Transport Theory, Oxford University Press (1957).
- [2] CASE, K. M., *Ann. Phys.* 9 (1960).
- [3] ZELAZNY, R. and KUSZELL, A., *Ann. Phys.* 16 (1961) 81.
- [4] ZELAZNY, R., *J. Math. Phys.* 2 (1961) 538.
- [5] KUSZELL, A., *Acta phys. polon.* 20 (1961) 567.
- [6] ZELAZNY, R. and KUSZELL, A., *Physica* 27 (1961) 797.
- [7] ZELAZNY, R., KUSZELL, A. and MIKA, J., *Ann. Phys.* 16 (1961) 69.
- [8] MIKA, J., In preparation.
- [9] MUSKHELISHVILI, N. J., Singular Integral Equations, Nordhoff, Netherlands (1952).
- [10] GROSSMAN, D. P., *Progr. math. Sci. (Moscow)* 5 (1950) 87.



# THE VALIDITY OF THE TRANSPORT APPROXIMATION IN CRITICAL-SIZE AND REACTIVITY CALCULATIONS

E. D. PENDLEBURY AND L. H. UNDERHILL

ATOMIC WEAPONS RESEARCH ESTABLISHMENT, ALDERMASTON,  
UNITED KINGDOM

**Abstract — Résumé — Аннотация — Resumen**

**The validity of the transport approximation in critical-size and reactivity calculations.** Elastically scattered neutrons are, in general, not distributed isotropically in the laboratory system, and a convenient way of taking this into account in neutron-transport calculations is to use the transport approximation. In this, the elastic cross-section is replaced by an elastic transport cross-section with an isotropic angular distribution. This leads to a considerable simplification in the neutron-transport calculation.

In the present paper, the theoretical bases of the transport approximation in both one-group and many-group formalisms are given. The accuracy of the approximation is then studied in the multi-group case for a number of typical systems by means of the  $S_n$  method using the isotropic and anisotropic versions of the method, which exist as alternative options of the machine code SAINT written at Aldermaston for use on IBM-709/7090 machines. The dependence of the results of the anisotropic calculations on the number of moments used to represent the angular distributions is also examined. The results of the various calculations are discussed, and an indication is given of the types of system for which the transport approximation is adequate and of those for which it is inadequate.

**Validité de l'approximation de transport dans le calcul des dimensions critiques et de la réactivité.** La diffusion élastique des neutrons ne s'effectue pas, en général, d'une manière isotrope dans les dispositifs expérimentaux; un moyen pratique d'en tenir compte dans les calculs de transport des neutrons consiste à utiliser l'approximation de transport. Dans cette méthode, on remplace la section efficace de diffusion élastique par une section efficace de transport élastique à distribution angulaire isotrope, ce qui simplifie beaucoup les calculs de transport.

Les auteurs exposent les fondements théoriques de l'approximation de transport pour les formalismes à un groupe et à plusieurs groupes. Ils étudient ensuite la validité de l'approximation dans le cas des formalismes à plusieurs groupes, pour un certain nombre de modèles classiques, au moyen de la méthode  $S_n$ ; on utilise les deux variantes, isotrope et anisotrope, de la méthode, que l'on trouve dans le code SAINT, établi à Aldermaston pour être utilisé sur les calculatrices IBM 709 et 7090. Les auteurs examinent aussi dans quelle mesure les résultats des calculs par la méthode anisotrope sont fonction du nombre de moments utilisés pour représenter les distributions angulaires. Ils passent en revue les différents résultats des calculs et indiquent les modèles pour lesquels l'approximation de transport est valable et ceux pour lesquels elle ne l'est pas.

**Использование транспортного приближения в расчетах критических размеров и реактивности.** Как правило, упруго рассеиваемые нейтроны не распределяются изотропически в лабораторной системе, и использование транспортного приближения является подходящим способом учета этого при вычислениях переноса нейронов. В данном случае сечение упругого процесса заменяется сечением переноса упругого процесса с изотропным угловым распределением. Это значительно упрощает вычисления переноса нейронов.

В настоящем докладе даются теоретические основы транспортного приближения как в одногрупповых, так и в многогрупповых формализмах. Затем точность приближения изучается в многогрупповом случае для ряда типичных систем путем использования метода  $S_n$  с применением изотропного и анизотропного вариантов для этого метода, являющихся альтернативой машинного кода SAINT, записанного в Олдермastonе для использования на машинах IBM 709/7090. Изучается также зависимость результатов анизотропных вычислений от числа моментов, использовавшихся для воспроизведения углового распределения. Обсуждаются результаты различных вычислений и указываются типы системы, для которой транспортное приближение является адекватным, а также типы системы, для которой они не адекватны.

**Validez de la aproximación de transporte en los cálculos de dimensiones críticas y de reactividades.** Por regla general, la distribución de los neutrones dispersados elásticamente no es isotrópica en los dispositivos experimentales; un medio práctico para tener en cuenta ese factor en los cálculos de transportes neutrónicos consiste en utilizar la aproximación de transporte. Con arreglo a ésta, la sección eficaz de dispersión elástica es sustituida por una sección eficaz de transporte elástico con distribución angular isotrópica, con lo cual el cálculo se simplifica considerablemente.

La memoria expone los fundamentos teóricos de la aproximación de transporte para los formalismos de un grupo y de varios grupos. Seguidamente, estudia la validez de la aproximación alcanzada mediante este último formalismo para cierto número de sistemas típicos con ayuda del método  $S_n$ ; se emplean las variantes isotrópica y anisotrópica, que se encuentran en la clave SAINT establecida en Aldermaston para las calculadoras IBM 709/7090. También examina la relación que existe entre los resultados de los cálculos anisotrópicos y el número de momentos empleados para representar las distribuciones angulares. Por último, discute los resultados de los diversos cálculos e indica los sistemas a los cuales la aproximación de transporte es aplicable y a cuáles no lo es.

## Introduction

In neutron-transport calculations it is usually adequate to assume that the emergent neutrons from non-elastic processes, for example  $(n, n')$  and  $(n, f)$ , are distributed isotropically in the laboratory system, but it is nearly always essential to take into account the anisotropic distribution of neutrons emergent from elastic scatters — an anisotropy which is particularly pronounced for incident neutron energies greater than a few hundred keV. This can always be done accurately in principle by solving the transport equation incorporating the appropriate angular distributions but it is considerably simpler, and more usual, to take the anisotropy into account by means of the transport approximation. In this the elastic cross-section is replaced by the elastic transport cross-section in conjunction with which the scattering is assumed isotropic.

The theoretical basis of the transport approximation is discussed in section 1 below with particular reference to one-energy group and multi-group methods. The accuracy of the approximation is then studied in the multi-group case (cf. section 2) for a number of typical systems by means of the  $S_n$  method [1] using the isotropic and anisotropic versions of the method, which exist as alternative options of the machine code SAINT written at Aldermaston for use on IBM 709/7090 machines. The dependence of the results of the anisotropic calculations on the number of moments used to represent the angular distributions is also examined. The results of the calculations presented in section 2 are discussed in section 3 and an indication is given of the types of system for which the transport approximation is adequate and of those for which it is inadequate.

For completeness and to assist with the understanding of the results given in section 2, a brief account of the anisotropic version of the Carlson method and of the machine code SAINT is given in the Appendix.

### 1. The theoretical basis of the transport approximation

The theoretical basis of the transport approximation is most conveniently illustrated by expanding the neutron flux in the transport equation in terms of spherical harmonics of the angular variable. In the following paragraphs, spherical geometry is considered for simplicity but it must be emphasized that the transport approximation is quite general and applies to any geometry. In spherical geometry and with anisotropic scattering the steady-state Boltzmann transport equation can be written in the form:

$$\left\{ \mu \frac{\partial}{\partial r} + \frac{(1-\mu^2)}{r} \frac{\partial}{\partial \mu} + \varrho(r) \alpha_g \right\} \Phi_g(r, \mu) = \left. \begin{aligned} &= \frac{1}{2\pi} \int_{\eta=0}^{2\pi} \int_{\mu'=-1}^{+1} \sum_{g'} \varrho(r) \beta_{g'g}(\bar{\mu}) \Phi_{g'}(r, \mu') d\mu' d\eta + \text{Source Terms} \end{aligned} \right\} \quad (1)$$

where  $g (=1, 2, 3 \dots)$  refers to energy group, the groups being numbered in order of decreasing energy

$r$  is the radius

$\mu$  is the cosine of the angle between the radius vector and the direction of the neutron

$\bar{\mu}$  is the cosine of the angle between the incident ( $\mu'$ ) and emergent ( $\mu$ ) directions of a neutron

$\eta$  is the azimuth angle between the initial and scattered neutron directions. ( $\bar{\mu} = \mu\mu' - \sqrt{(1-\mu^2)(1-\mu'^2)} \cos \eta$ )

$\varrho(r)$  is the material density at  $r$

$\alpha_g$  is the inverse mean free path of neutrons in group  $g$  for material at unit density.

$\frac{1}{2\pi} \beta_{g'g}(\bar{\mu})$  is the probable number of neutrons created in group  $g$ , per unit solid angle about a direction  $\cos^{-1} \bar{\mu}$  with the direction of the neutron in group  $g'$ , per unit path of a neutron in group  $g'$  in material at unit density. It follows that

$$\sum_g \int \beta_{g'g}(\bar{\mu}) d\bar{\mu} / \alpha_g,$$

is the average number of neutrons produced at a collision of a neutron in group  $g'$ .  $\beta_{g'g}(\bar{\mu})$  contains contributions from all processes (elastic scatter, (n, n'), (n, f), etc.) except absorptions.

$\Phi_g(r, \mu)$  is the flux of group  $g$  neutrons per unit area at  $r$  normal to  $\mu$ , per unit solid angle about the direction  $\mu$ .

The "Source Terms" on the right-hand side of equation (1) can often be taken into account by application of suitable boundary conditions, but as their explicit consideration does not affect the approximation under consideration they are omitted from the equations below. First it is useful to develop equation (1) a little by expansion of the  $\beta_{g'g}(\bar{\mu})$  in terms of Legendre polynomials, as this step

is common to both the present illustration of the basis of the transport approximation and the anisotropic  $S_n$  method discussed in the Appendix.

Writing

$$\left. \begin{aligned} \beta_{g'g}(\bar{\mu}) &= \sum_{l=0}^{\infty} \frac{(2l+1)}{2} \beta_{g'g}^l P_l(\bar{\mu}) \\ \text{which implies } \beta_{g'g}^l &= \int_{-1}^{+1} \beta_{g'g}(\bar{\mu}) P_l(\bar{\mu}) d\bar{\mu} \end{aligned} \right\} \quad (2)$$

and using the relation

$$P_l(\bar{\mu}) = P_l(\mu) P_l(\mu') + 2 \sum_{m=1}^l \frac{(l-m)!}{(l+m)!} P_m(\mu) P_m(\mu') \cos(m\eta) \quad (3)$$

where  $P_l^m$  are the associated Legendre polynomials, one obtains from equation (1)

$$\begin{aligned} &\left\{ \mu \frac{\partial}{\partial r} + \frac{(1-\mu^2)}{r} \frac{\partial}{\partial \mu} + \varrho(r) \alpha_g \right\} \Phi_g(r, \mu) \\ &= \sum_{g'} \sum_l \frac{(2l+1)}{2} \beta_{g'g}^l P_l(\mu) \varrho(r) \int_{-1}^{+1} P_l(\mu') \Phi_{g'}(r, \mu') d\mu' \end{aligned} \quad (4)$$

If we proceed now with the Legendre polynomial expansion of  $\Phi_g(r, \mu)$ ,

$$\Phi_g(r, \mu) = \frac{1}{4\pi} \sum (2l+1) \psi_g^l(r) P_l(\mu). \quad (5)$$

Substitution of (5) in (4) gives, after some manipulation, an infinite set of differential difference equations for the  $\psi_g^l(r)$ :

$$\begin{aligned} &\frac{(l+1)}{(2l+1)} \left\{ \frac{d}{dr} + \frac{(l+2)}{r} \right\} \psi_g^{l+1}(r) + \frac{l}{(2l+1)} \left\{ \frac{d}{dr} - \frac{(l-1)}{r} \right\} \psi_g^{l-1}(r) + \varrho(r) \alpha_g \psi_g^l(r) \\ &= \varrho(r) \sum_{g'} \beta_{g'g}^l \psi_{g'}^l(r). \end{aligned} \quad (6)$$

The transport approximation is obtained by assuming that  $\psi_g^l(r)=0$  for  $l=2$  and neglecting the contribution from  $\psi_g^l(r)$  with  $l>2$ . This assumption leads to what is usually called diffusion theory, but in the terminology of the spherical harmonics method it is referred to as the  $P_1$  approximation [2]. First consider one-group theory; suffices  $g'$  and  $g$  can be omitted and in the  $P_1$ -approximation equations (6) reduce to

$$\left. \begin{aligned} &\left\{ \frac{d}{dr} + \frac{2}{r} \right\} \psi^1(r) + \varrho(r) \alpha \psi^0 = \varrho(r) \beta^0 \psi^0(r) \\ &\frac{1}{3} \frac{d\psi^0(r)}{dr} + \varrho(r) \alpha \psi^1(r) = \varrho(r) \beta^1 \psi^1(r) \end{aligned} \right\} \quad (7)$$

With

$$\left. \begin{aligned} \alpha^* &= \alpha - \beta^1 \\ \beta^* &= \beta - \beta^1 \end{aligned} \right\} \quad (8)$$

equations (7) become

$$\left. \begin{aligned} & \left\{ \frac{d}{dr} + \frac{2}{r} \right\} \psi^1(r) + \varrho(r) \alpha^* \psi^0(r) = \varrho(r) \beta^* \psi^0(r) \\ & \frac{1}{3} \frac{d\psi^0(r)}{dr} + \varrho(r) \alpha^* \psi^1(r) = 0 \end{aligned} \right\} \quad (9)$$

which are just the equations which obtain if, in the  $P_1$  approximation to the original transport equation,  $\alpha$  is replaced by  $\alpha^*$  and  $\beta$  by  $\beta^*$  and all scattering is assumed to be isotropic. The use of the modified cross-sections  $\alpha^*$  and  $\beta^*$  with isotropic scattering is known as the transport approximation. It is exact in the  $P_1$  or diffusion approximation but in practice it is found to work well in higher order approximations such as obtain in accurate numerical solutions of the transport equation. Physically it is equivalent to replacing an anisotropic distribution by an isotropic component plus a  $\delta$ -function forward-scattering component such that the mean value of the cosine of the scattering angle is the same as in the actual distribution; if the actual distribution is either isotropic ( $\beta^l \equiv 0$  for all  $l > 0$ ) or a  $\delta$ -function along its original direction ( $\beta^l \equiv \text{const.}$  for all  $l > 0$ ) then the transport approximation is exact, as is readily verified from equations (6).

Consider now the multi-group case. The transport approximation again follows from the  $P_1$  approximation in which equations (6) reduce to

$$\left. \begin{aligned} & \left\{ \frac{d}{dr} + \frac{2}{r} \right\} \psi_g^1(r) + \varrho(r) \alpha_g \psi_g^0(r) = \varrho(r) \sum_{g'} \beta_{g'g}^0 \psi_{g'}^0(r) \\ & \frac{1}{3} \frac{d}{dr} \psi_g^0(r) + \varrho(r) \alpha_g \psi_g^1(r) = \varrho(r) \sum_{g'} \beta_{g'g}^1 \psi_{g'}^1(r). \end{aligned} \right\} \quad (10)$$

From these equations it follows that the modifications given by (8) generalize to

$$\left. \begin{aligned} \alpha_{g'g}^* &= \alpha_g \delta_{g'g} - \beta_{g'g}^1 \\ \beta_{g'g}^* &= \beta_{g'g}^0 - \beta_{g'g}^1 \end{aligned} \right\} \quad (11)$$

where the  $\alpha_{g'g}^*$  operating on  $\Phi_{g'}$  involves a summation over  $g'$  to replace the term  $\alpha_g \Phi_g$  in the transport equation. As in the one-group case, the transport approximation is equivalent to representing the actual angular distribution by an isotropic component and a  $\delta$ -function forward-scattering component such that the mean cosine of the scattering angle is the same as in the actual distribution. In particular the term  $\alpha_{g'g}^*$  for  $g' \neq g$  represents a collision in which the neutron changes group without changing direction. The transport approximation is again exact in the diffusion approximation.

The modifications (11) are referred to as the *full transport correction* but methods of calculation and in particular, machine codes, which can only deal with isotropic scattering cannot immediately accommodate (11), and modification to the methods and to the machine codes may be necessary. In the case when only slowing-down collisions are anisotropic, as is nearly always true,  $\beta_{g'g}^1 = 0$  for  $g' > g$  and the handling of the full transport approximation, in the  $S_n$  method for instance, does not present any fundamental difficulty. If, however, the only contribution to anisotropy is elastic scattering from heavy nuclei, the effect of scattering to lower energy groups is negligible and the transport correction becomes

$$\left. \begin{aligned} \alpha_g^* &= \alpha_g - \beta_{gg}^1 \\ \beta_{g'g}^* &= \beta_{g'g}^0 - \beta_{g'g}^1 \delta_{g'g} \end{aligned} \right\}. \quad (12)$$

This particular form of the transport correction is known as the *diagonal transport correction*, and it will be noted that this can be used with any method or machine code which can only deal with isotropic scattering. While (12) is only strictly applicable to heavy nuclei, it can be expected to be fairly reliable as long as the major contribution to elastic scattering retains the neutrons in the same energy group.

In view of the great practical advantage of the diagonal transport correction over the full transport correction from the user point of view, only the diagonal transport correction is considered in the present paper.

At this point a few *a priori* comments about its expected accuracy can be made. The diagonal transport correction is not expected to work well where scattering by very light elements is concerned, in particular by hydrogen and deuterium, since most of the scattering is to lower energy groups. For heavy elements the transport approximation is exact in the diffusion approximation and hence can be expected to work well in problems where diffusion theory works well; this occurs when the dimensions of the system are large compared with the mean free path of the neutrons. For small systems whose dimensions are only about a neutron mean free path or so, it is not so obvious whether the transport correction will be a good approximation and at first sight might be considered bad. However, it must be remembered that it is accurate for  $\delta$ -function scattering along the original direction as well as isotropic scattering and, fortunately, many angular distributions approximate to one or the other of these extremes.

TABLE I

**A COMPARISON OF CRITICAL RADII CALCULATED WITH THE ANISOTROPIC CODE USING DIFFERENT NUMBERS OF MOMENTS  $\beta^l$**

System (composition by nuclei)	Group constants used	$S_n$ approxi- mation	Critical radii (cm)			
			Highest moment $\beta^l$ used in the calculation			
			$L = 1$	$L = 2$	$L = 3$	$L = 5$
Bare sphere 93.9% U <sup>235</sup> ) 6.1% U <sup>238</sup> ) at 18.75 g/cm <sup>3</sup>	4-group Set 5	S <sub>4</sub>	8.786	8.762	8.739	8.739
	4-group Set 5	S <sub>8</sub>	8.827	8.796	8.783	8.783
Sphere 93.9% U <sup>235</sup> ) 6.1% U <sup>238</sup> ) at 18.75 g/cm <sup>3</sup> with nat. U reflector at 19 g/cm <sup>3</sup> and 23 cm thick	4-group Set 5	S <sub>4</sub>	6.164	—	6.075	6.071
Sphere 93.9% U <sup>235</sup> ) 6.1% U <sup>238</sup> ) at 18.75 g/cm <sup>3</sup> with C reflector at 2.25 g/cm <sup>3</sup> and 23 cm thick	4-group Set 5	S <sub>4</sub>	5.800	—	5.754	5.754
Sphere with cavity of radius 1.05 cm 93.9% U <sup>235</sup> ) 6.1% U <sup>238</sup> ) at 18.75 g/cc in H <sub>2</sub> O reflector at 1.0 g/cm <sup>3</sup> and 10 cm thick	8-group Set 5	S <sub>4</sub>	7.169	—	6.996	6.995

## 2. Results of calculations

In the first instance, calculations have been carried out to examine the effect of using different numbers of moments  $\beta^l$  in the representation of  $\beta_{g'g}(\bar{\mu})$  (cf. equation (2) and equation (A3) of the Appendix). In Table I the critical radii of several systems are given for different values of  $L$ , the maximum value of  $l$  considered. In Table II a comparison is made between critical radii calculated by means of the isotropic code with the transport correction and corresponding radii obtained with the anisotropic code with  $L=1$  and  $L=5$ . In the last two columns of Table II the percentage errors in the critical radii calculated by means of the isotropic code with the transport correction, and with the anisotropic code and  $L=1$ , are given—assuming that the critical radii obtained with  $L=5$  to be exact. In some instances the calculated critical radii do not agree with experimental values because the basic data have not been adjusted to the extent necessary to give these agreements, but it does not affect the comparisons made in the present paper. The systems considered are those given in Table I together with a few others.

It should be appreciated that the accuracy obtained in a reactivity calculation on a near-critical system is proportional to the accuracy obtained in the corresponding critical-size calculation.

For completeness a brief description is now given of the group constants used in these calculations. The references to the group constants used are included in Tables I and II and are described in detail by PARKER [3]. The "set number" refers to the weighting spectrum used in their derivation. The group constants used are basically either a 13- or 8-group set covering the range from thermal to 11 MeV, and the energy boundaries are as follows:

13-group: 11.0 MeV, 2.4 MeV, 1.1 MeV, 0.55 MeV, 0.26 MeV, 0.13 MeV, 43 keV, 10 keV, 1.6 keV, 0.26 keV, 42 eV, 5.5 eV, 0.4 eV. The thermal (13th) group contains neutrons with energies below 0.4 eV.

8-group: 11.0 MeV, 1.6 MeV, 0.78 MeV, 0.18 MeV, 10 keV, 0.26 keV, 15 eV, 0.4 eV. The thermal (8th) group contains neutrons with energies below 0.4 eV.

The neutron-scattering data used in the calculation of these group constants are those given by BUCKINGHAM *et al.* [4], except for the carbon data which are those given by PARKER [5]. The weighting spectra used are either a fission or degraded-fission spectrum in the top energy groups with a weighting proportional to  $(E)^{-1}$  in the lower energy groups, except for the thermal group for which appropriate thermal group-constants are used.

The 7-group set 4 constants are the top seven groups of the 13-group set 5 modified such that all transfers from groups 7 and above to groups below 7 are replaced by transfers to group 7. In this way neutrons are not allowed to slow down below group 7. Similarly, the 4-group set 5 constants consist of the top four groups of the 8-group set 5 with corresponding modifications.

In the original data all non-elastic processes are assumed to be isotropic in the laboratory system—only elastic scatter leading to anisotropy. To give an idea of the degree of anisotropy in the elastic scattering from the various elements considered, the mean cosine of the scattering angle in the laboratory system are given in Table III at a few representative energies.

TABLE II

**A COMPARISON OF CRITICAL RADII CALCULATED USING THE TRANSPORT CORRECTION WITH THE CORRESPONDING VALUES OBTAINED USING THE ANISOTROPIC  $S_n$  CODE**

System (composition by nuclei)	Group constants used	$S_n$ approxi- mation	Critical radius (cm)			Error in $L = 1$ solution [(a) - (b)] (b)	Error in transport solution [(c) - (b)] (b)
			Anisotropic code		(c) Trans- port correc- tion		
			(a) $L = 1$	(b) $L = 5$			
Bare sphere 93.9% $U^{235}$ } at 18.75 6.1% $U^{238}$ } g/cm <sup>3</sup>	4-group Set 5	$S_4$	8.786	8.739	8.716	+0.54%	-0.26%
	4-group Set 5	$S_8$	8.827	8.783	8.760	+0.50%	-0.26%
Bare sphere 30% $U^{235}$ } at 18.75 70% $U^{238}$ } g/cm <sup>3</sup>	7-group Set 4	$S_4$	17.171	17.119	17.101	+0.30%	-0.11%
Sphere 93.9% $U^{235}$ } at 18.75 6.1% $U^{238}$ } g/cm <sup>3</sup> with nat. U reflector at 19 g/cm <sup>3</sup> and 23 cm thick	4-group Set 5	$S_4$	6.164	6.071	6.029	+1.5%	-0.69%
Sphere 93.9% $U^{235}$ } at 18.75 6.1% $U^{238}$ } g/cm <sup>3</sup> with C reflector at 2.25 g/cm <sup>3</sup> and 23 cm thick	4-group Set 5	$S_4$	5.800	5.754	5.807	+0.80%	+0.92%
	8-group Set 5	$S_4$	5.777	5.731	5.799	+0.80%	+1.2%
Sphere with cavity of radius 1.05 cm 93.9% $U^{235}$ } at 18.75 6.1% $U^{238}$ } g/cm <sup>3</sup> in $H_2O$ reflector at 1.0 g/cm <sup>3</sup> and 10 cm thick	8-group Set 5	$S_4$	7.169	6.995	6.284	+2.5%	-10.2%
ZPR III Assembly No 6F [7] (Spherical) Core: 15.3% $U^{235}$ , 17.3% $U^{238}$ , 43.2% Al, 17.8% Fe, 4.6% Cr, 1.8% Ni at 7.44 g/cm <sup>3</sup> Reflector: 83.9% $U^{238}$ , 2.9% Al, 9.7% Fe, 2.5% Cr, 1.0% Ni at 16.3 g/cm <sup>3</sup> ~30 cm thick	13-group Set 5	$S_4$	23.779	23.670	23.637	+0.46%	-0.14%

TABLE III

## MEAN COSINE OF THE ELASTIC SCATTERING ANGLE IN THE LABORATORY SYSTEM

Incident neutron energy (MeV)	Mean cosine							
	Element or isotope							
	$U^{235}$	C	H	O	Al	Fe	Cr	Ni
0.5	0.315	0.056	0.661	0.154	0.270	0.201	0.196	0.125
1.0	0.377	0.056	0.661	0.154	0.270	0.201	0.196	0.125
2.0	0.571	0.200	0.661	0.480	0.341	0.201	0.406	0.405
4.0	0.814	0.032	0.661	0.534	0.341	0.631	0.406	0.786

## 3. Discussion and conclusions

The results given in Table I for the bare sphere of  $\sim 94\%$   $U^{235}$  show much the same degree of convergence with increasing  $L$  in both the  $S_4$  and  $S_8$  approximations. This, together with the remaining results given in Table I, indicates that it is not necessary to take  $L > 5$  in calculations using the anisotropic code. An examination of the angular distributions and the evaluation of the  $\beta^l$  for  $L > 5$  clearly indicate that the truncation occurs because  $\psi^l \rightarrow 0$  for  $L > 5$ , not because  $\beta^l \rightarrow 0$  for  $L > 5$ . This is consistent with the fact that the spherical harmonics method in  $P_5$  approximation has been found to give quite accurate results.

It is seen from the last column in Table II that for all the systems considered, except the water-reflected one, the transport approximation gives results of adequate accuracy—the errors being less than the errors in experimental critical-size determinations. It is gratifying to note, in particular, that the transport correction gives an excellent result for the bare sphere of  $\sim 94\%$   $U^{235}$ . This is no doubt due to the fortunate coincidence that angular distributions are well represented by an isotropic component together with a  $\delta$ -function forward-scattering component, and under these circumstances the transport correction is exact (cf. section 1). It was noted in section 1 that the transport approximation is not expected to work well in cases where scattering by hydrogen is important and this is clearly indicated in the case of the water-reflected sphere, the error on critical mass in this case being  $\sim 30\%$ .

The DSN code written by CARLSON and co-workers [6] has an anisotropic option up to  $L = 1$  and it is interesting to note from the figures given in Table II that, in all the cases considered, the anisotropic code with  $L = 1$  gives results of acceptable accuracy. The transport correction gives results of similar accuracy for all but the water-reflected case and requires rather less computational effort than the anisotropic ( $L = 1$ ) calculation.

The results of the present calculations show that the transport approximation is in general better than the *a priori* predictions of section 1 would indicate and it is concluded that one can have a fairly high degree of confidence in its use for all systems except those in which moderation by hydrogen (or deuterium) is important. There is no reason to believe that the particular choice of group constants affects these conclusions in any way.

## ACKNOWLEDGEMENTS

We are indebted to the various past and present members of the Mathematical Physics Division at the Atomic Weapons Research Establishment, Aldermaston, whose work has made it possible for us to write this paper and in particular to Mr. J. H. Bird who has carried out the calculations reported in section 2.

## APPENDIX

The anisotropic  $S_n$  method and the machine code SAINT

The starting point of the anisotropic  $S_n$  method is equation (4) which is reproduced below;

$$\left\{ \mu \frac{\partial}{\partial r} + \frac{(1-\mu^2)}{r} \frac{\partial}{\partial \mu} + \varrho(r) \alpha_g \right\} \Phi_g(r, \mu) = \sum_{g'} \sum_l \frac{(2l+1)}{2} \beta_{g'g}^l P_l(\mu) \varrho(r) \int_{-1}^{+1} P_l(\mu') \Phi_{g'}(r, \mu') d\mu' \quad (\text{A1})$$

$$\text{where } \beta_{g'g}^l = \int_{-1}^{+1} \beta_{g'g}(\mu) P_l(\mu) d\mu. \quad (\text{A2})$$

In the  $S_n$  formulation, the anisotropic source term is required to be averaged over an angular interval  $(\mu_{j-1}, \mu_j)$ \* and integrated over a radial interval  $(r_i, r_{i+1})$ . Denoting this averaged source term by  $S_g(i, j)$  and using the basic assumption of the  $S_n$  method that  $\Phi(r, \mu)$  is a linear function of  $\mu$  in an angular interval,  $\mu_{j-1} < \mu < \mu_j$ , a set of scalar products for all "i" can be derived of the form

$$S_g(i, j) = \sum_{g'=1}^G \sum_{l=0}^L \sum_{j'=1}^J A_{jl} \beta_{g'g}^l B_{j'l} F_{g'}(i, j'). \quad (\text{A3})$$

$J$  and  $L$  are the total number of angles and Legendre moments respectively.  
 $A_{jl}$ ,  $B_{j'l}$  and  $F_{g'}(i, j')$  are defined as follows:

$$A_{jl} = \frac{1}{(\mu_j - \mu_{j-1})} \int_{\mu_{j-1}}^{\mu_j} P_l(\mu) d\mu \text{ for } j > 1$$

$$A_{1l} = P_l(-1).$$

$$B_{j'l} = \frac{(2l+1)}{2} \left\{ \int_{\mu_{j'-1}}^{\mu_{j'+1}} \left( \frac{\mu_{j'+1}-\mu}{\mu_{j'+1}-\mu_{j'}} \right) P_l(\mu) d\mu + \int_{\mu_{j'-1}}^{\mu_{j'}} \left( \frac{\mu-\mu_{j'-1}}{\mu_j-\mu_{j'-1}} \right) P_l(\mu) d\mu \right\} \text{ for } 1 < j' < J.$$

$$B_{1l} = \frac{(2l+1)}{2} \int_{\mu_1}^{\mu_2} \left( \frac{\mu_2-\mu}{\mu_2-\mu_1} \right) P_l(\mu) d\mu.$$

$$B_{jl} = \frac{(2l+1)}{2} \int_{\mu_{j-1}}^{\mu_j} \left( \frac{\mu-\mu_{j-1}}{\mu_j-\mu_{j-1}} \right) P_l(\mu) d\mu$$

$$F_{g'}(i, j') = \int_{r_i}^{r_{i+1}} \varrho(r) \Phi_{g'}(r, \mu_{j'}) dr.$$

\* For  $\mu_1 = -1$  the source term required is the value at  $\mu = -1$ .

Note:  $\varrho(r)$  is required to be constant between  $r_i$  and  $r_{i+1}$ . Hence

$$F_{g'}(i, j') = \frac{1}{2} \varrho_{i+\frac{1}{2}} [\Phi_{g'}(r_i, \mu_j') + \Phi_{g'}(r_{i+1}, \mu_j')].$$

The form of equation (A3) is the same as given by CARLSON in LA 1891 [1].

The machine code SAINT has been developed by one of us (L.H.U.) and his group at AWRE, Aldermaston, to deal with the anisotropic source term given by equation (A3) above. SAINT is a multipurpose one-dimensional  $S_n$  code, with options for isotropic- and anisotropic-scatter calculation; versions exist for use on 32K IBM 704, 709 and 7090 machines. An account is now given of the salient features of the anisotropic-scatter option.

In SAINT, the nuclear data is supplied in the form  $\beta_{g'g}^l$  up to any reasonable order of  $l$  on binary cards of a standard format. The summation over  $l$  in (A3) is carried out once and for all during the input stage of a calculation, so during the course of a calculation, the source term is evaluated by

$$S_g(i, j) = \sum_{g'} \sum_{j'} C(g, g', j, j') \Phi_{g'}(i, j'). \quad (A4)$$

This decreases the amount of computation needed at the expense of increasing the amount of storage required. In particular, calculation time is effectively independent of the number of moments used.

The procedure adopted during the solution is the "fission generation" iterative technique. Here the fission component of the scattering term is split off from the rest of the scattering terms and it is assumed that fission neutrons are emitted isotropically with an energy spectrum independent of material or incident neutron energy. The contribution by fission is thus handled by a "fission source term" which is recomputed from the neutron scalar fluxes at the end of each "outer iteration". Within each outer iteration, the fission source term is unchanging and the neutron scalar fluxes appropriate to the fission source term are calculated. Thus in equation (A4) only slowing-down neutron processes occur and so the  $g'$  summation is over the range  $g' = 1(1)g$ .

For the purposes of calculation within each outer iteration, the right-hand side of (A4) is split up into an off-diagonal and a diagonal component,

$$S_g(i, j) = \sum_{g'=1}^{g-1} \sum_{j'} C(g, g', j, j') \Phi_{g'}(i, j') + \sum_{j'} C(g, g, j, j') \Phi_g(i, j'), \quad (A5)$$

and each outer iteration starts with  $g = 1$ . In this case, the first term of the right-hand side of (A5) is zero and a one-group iterative process ("inner iteration") is used to calculate  $\Phi_1$  to the required degree of convergence. If one proceeds to  $g = 2$ , the first term on the right-hand side of (A5) is evaluated by means of the already calculated  $\Phi_1$ , followed by another set of one-group iterations until  $\Phi_2$  is calculated to the required degree of convergence.

This process is repeated, always evaluating the first term of the right-hand side of (A5) once for each  $g$  in terms of the already calculated  $\Phi$ 's until the scalar flux for the final group has been calculated. The outer iteration is then completed by the evaluation of a new fission source term.

The whole process is terminated when two successive fission source terms differ by less than some predetermined value.

This iterative scheme is particularly useful for problems where no fission processes are involved, for example, in the calculating of the transmission of neutrons through a shield. Here only one outer iteration is needed to complete the calculation, the inner iteration being taken to finality for each group in turn.

For problems involving a fission process, for example a critical-size calculation, the degree of convergence to which each inner iteration is carried is determined by the degree of convergence attained by the outer iteration. This works reasonably well but a completely satisfactory scheme has not yet been devised.

The code can be used for critical-size calculation (no imposed source present), or an imposed source can be specified either as an isotropic source distributed over desired energy groups and regions of the system, as a shell source from which neutrons

are emitted into specified groups with specified angular distributions or as the virtual source arising from first collisions. In calculations with imposed sources, vector flux analyses allow one to calculate any multiplication which may be required. In all cases, either plane or spherical (but not cylindrical) geometries can be specified.

In general, an anisotropic calculation takes about four times as long as a similar isotropic calculation. For calculations on systems without fissile material, anisotropic calculations are quite fast, a transmission problem involving eight neutron groups in  $S_4$  approximation with 50 radial points taking about ten minutes on the IBM-709.

The code uses five tapes, distributed for the IBM-709, 7090 machines over channels A, B and C.

#### REFERENCES

- [1] CARLSON, B. G., LA-1891 (1955).
- [2] DAVISON, B., *Transport Theory of Neutrons*, Oxford University Press, London (1956).
- [3] PARKER, K., AWRE Report 0—1/61 (1961).
- [4] BUCKINGHAM, B. R. S., PARKER, K. and PENDLEBURY, E. D., AWRE Report 0—28/60 (1960).
- [5] PARKER, K., AWRE Report 0—71/60 (1960).
- [6] CARLSON, B. G., LEE, C. and WORLTON, J., LAMS-2346 (1959).
- [7] KOCH, L. J. and PAXTON, H. C., *Annu. Rev. nucl. Sci.* 9 (1959) 437.

# THE REACTIVITY OF A CENTRAL AIR GAP IN A BARE REACTOR

H. HÄGGBLOM

AKTIEBOLAGET ATOMENERGI,  
SWEDEN

**Abstract — Résumé — Аннотация — Resumen**

**The reactivity of a central air gap in a bare reactor.** Two methods are presented for calculation of the reactivity equivalence of a central gap in a bare reactor with rectangular cross-section. The first is a perturbation theory and has been developed by Friedman in an unpublished paper. The second method is an application of variation calculus. In both cases the eigenvalue is solved for the transport equation in integral form. The principal difference between the two methods is in the assumption for the flux shape. In the perturbation theory, it is assumed that the flux is unperturbed and has the form  $A \cos \pi x/L$ . The reactivity as a function of the gap width is expressed in closed form in one and two energy groups, but the expression is valid only for reactivity changes less than about 8 %. The variation calculus is developed only for one energy group, but the accuracy is approximately independent of the gap width. This is obtained by varying the expression for the flux in order to optimize the functional integral.

The results are compared with those obtained by Chernick and Kaplan by diffusion theoretical methods.

**Incidence d'une fente centrale sur la réactivité dans un réacteur sans réflecteur.** L'auteur expose deux méthodes permettant de calculer l'incidence d'une fente centrale à section rectangulaire sur la réactivité dans un réacteur sans réflecteur. Il s'agit, dans le premier cas, d'une théorie de la perturbation du transport, formulée par Friedman dans une communication qui n'a pas été publiée et, dans le second cas, d'une application du calcul des variations. Dans les deux cas, la valeur propre relative à l'équation de transport est obtenue sous la forme d'une intégrale. La principale différence entre les deux méthodes réside dans l'hypothèse relative à la forme du flux. Dans la théorie de la perturbation, on suppose que le flux est non perturbé et qu'il a la forme  $A \cos \pi x/L$ . La réactivité en fonction de la largeur de la fente est exprimée sous forme fermée pour un et deux groupes d'énergie, mais cette expression n'est valable que pour les modifications de la réactivité inférieures à 8 % environ. La méthode du calcul des variations n'est appliquée que dans le cas d'un groupe d'énergie, mais la précision est pratiquement indépendante de la largeur de la fente. Dans cette dernière méthode, on fait varier l'expression du flux pour optimiser l'intégrale fonctionnelle.

L'auteur compare les résultats indiqués avec ceux qui ont été obtenus par Chernick et Kaplan au moyen de la théorie de la diffusion.

**Реактивность центрального воздушного зазора в реакторе без отражателя.** В докладе изложены два метода подсчета реактивной эквивалентности центрального зазора в реакторе без отражателя с прямоугольным сечением. Первый метод представляет собой теорию возмущений и разработан Фридманом в неопубликованном докладе. Второй метод является применением вариационного расчета. В обоих случаях найдено собственное значение уравнения переноса в интегральной форме. Основное различие между двумя методами состоит в предположении относительно формы потока. По теории возмущений мы предполагаем, что поток невозмущенный и имеет форму  $A \cos \pi x/L$ . Реактивность как функция ширины зазора имеет закрытую форму в одной из двух энергетических групп, но эта форма

годится только для изменений реактивности менее примерно восьми процентов. Вариационный расчет выведен только для одной энергетической группы, но приближенно точность независима от ширины зазора. Это получено путем изменения формы потока для выведения оптимального функционального интеграла. Данные результаты сравниваются с результатами, полученными Черником и Капланом с помощью теоретических методов диффузии.

**Reactividad de un espacio central lleno de aire en un reactor sin reflector.** La memoria presenta dos métodos para calcular la equivalencia en reactividad de una separación central en un reactor sin reflector, de sección rectangular. El primero se basa en una teoría de la perturbación que expone Friedman en un artículo todavía no publicado. El segundo método constituye una aplicación del cálculo de variaciones. En ambos casos se resuelve el valor propio para la ecuación integral de transporte. La diferencia principal entre ambos métodos estriba en las características que se asignen teóricamente al flujo. En la teoría de la perturbación, se supone que el flujo no es perturbado y tiene la forma  $A \cos \pi x/L$ . La reactividad en función del ancho de la separación se expresa en forma cerrada en uno y dos grupos de energía, pero la expresión es válida solamente para cambios de reactividad inferiores a 8 por ciento aproximadamente. El cálculo de variaciones sólo se ha desarrollado para un grupo de energía, pero su precisión es prácticamente independiente del ancho de la separación. Se obtiene variando la expresión correspondiente al flujo con el fin de encontrar valores óptimos para la integral funcional.

El autor compara esos resultados con los obtenidos por Chernick y Kaplan por métodos de la teoría de la difusión.

### The transport equation for a reactor with a central air gap

A transverse air gap in a bare reactor with rectangular cross-section has been treated previously by CHERNICK and KAPLAN [1], who refer to an unpublished work by Friedman. Friedman starts from the transport integral equation and transforms it so that the air-gap width,  $\delta$ , only enters into the integrand. He solves this equation by perturbation theory to obtain a value  $\Delta L_0$ , which is the required change in reactor length to maintain criticality. The calculations are performed in one-group formalism.

Because most of the mathematical part of the perturbation theory will be used later, we will first give a derivation of Friedman's formula. For completeness, we will also extend the perturbation theory to include two energy groups. In this section we will transform the integral equation to a form suitable for further treatment, either using perturbation theory or variational calculus.

First we consider the transport equation in one-group formalism, which can be written:

$$\psi(x, y, z) = \frac{c}{4\pi\lambda} \int \int \int \frac{e^{-\bar{\rho}/\lambda} \Psi(x', y', z') dx' dy' dz'}{\rho^2}. \quad (1)$$

Here  $\bar{\rho}$  is the "optical" distance between the points  $x, y, z$  and  $x', y', z'$ , and  $\rho$  is the corresponding geometrical distance;  $c$  is the multiplication constant for an infinite medium, and  $\lambda$  is the mean free path. We assume that the reactor consists of only one medium and that it has a square cross-section. Without an air gap the flux is separable and can be written:

$$\psi(x, y, z) = \Phi(z) \cos \alpha x \cos \beta y.$$

We assume that this expression holds approximately also in the presence of an

air gap.  $\Phi(z)$  can be most conveniently calculated by putting  $x=y=0$ . In spherical co-ordinates, we then get from Eq. (1):

$$\Phi(z) = \frac{c}{4\pi\lambda} \int_0^{2\pi} \int_0^\pi \sin\theta d\varphi \int_0^{R(\theta)} \frac{e^{-\eta/\lambda} \Phi(r', \varphi, \theta) e^{1/\eta} r' \sin\theta \cos\varphi r'^2 dr'}{\eta^2} \quad (2)$$

where  $\eta^2 = \alpha^2 + \beta^2$ .

Now we make the following transformation:

$$(r', \varphi, \theta) \rightarrow (z', \varphi, \mu)$$

with  $\mu = \cos(z, \rho)$ .

An air gap of width  $\delta$  is assumed to separate the two equal halves of the reactor, where total material length is  $L$ .

The Jacobian is then

$$\frac{\partial(r', \varphi, \cos\theta)}{\partial(z', \varphi, \mu)} = \frac{\eta^2}{\mu r'^2} \quad (3)$$

and the transformed form of the one-group transport equation is for  $z > 0$ :

$$\begin{aligned} \Phi(z) = & \frac{c}{2\lambda} \int_0^1 \int_0^{L/2} dz' \Phi(z') \left\{ e^{-\frac{|z-z'|}{\mu\lambda}} J_0 \left[ \frac{\eta|z-z'|\sqrt{1-\mu^2}}{\mu} \right] + \right. \\ & \left. + e^{-\frac{z+z'}{\mu\lambda}} J_0 \left[ \frac{\eta(z+z'+\delta)\sqrt{1-\mu^2}}{\mu} \right] \right\}. \end{aligned} \quad (4)$$

This expression was derived by Friedman. Above we assumed that  $z > 0$ . For  $z < 0$ , the absolute value of  $z$  must be inserted as a consequence of the reactor symmetry.

In multi-group theory we introduce the following symbols:

$l_i$  = mean free path in group  $i$

$\chi_i$  = fraction of fission neutrons born in group  $i$

$v_j$  = number of neutrons per fission caused by a neutron of group  $j$

$\Sigma_{tj}$  = macroscopic fission cross-section in group  $j$

$\Sigma_{s,j \rightarrow i}$  = macroscopic elastic and inelastic removal cross-section from group  $j$  into group  $i$ .

The eigenvalue of the transport equation and the criticality value of the reactor are then related through the equation:

$$\frac{c_{i,tj \rightarrow i}}{l_j} = \chi_i v_j \Sigma_{tj} + \Sigma_{s,j \rightarrow i}. \quad (5)$$

For kinetic studies, we are interested in the quantity  $\Delta \nu/\nu = \Delta v_j/v_j$  (independent of  $j$ ). This quantity is not proportional to the change of the  $e_j$ 's when the air gap changes. The integral equation for the flux is in analogy with Eq. (4):

$$\begin{aligned} \Phi_i(z) = & \frac{1}{2} \sum_j \frac{c_j f_{j \rightarrow i}}{l_j} \int_0^1 \int_0^{L/2} dz' \Phi_j(z') \left\{ e^{-\frac{|z-z'|}{\mu\lambda}} J_0 \left[ \frac{\eta|z-z'|\sqrt{1-\mu^2}}{\mu} \right] + \right. \\ & \left. + e^{-\frac{z+z'}{\mu\lambda}} J_0 \left[ \frac{\eta(z+z'+\delta)\sqrt{1-\mu^2}}{\mu} \right] \right\}. \end{aligned} \quad (6)$$

A corresponding equation holds for the adjoint flux  $\Phi_i^*(z)$ .

For solving Eqs. (4) and (6), it is convenient to expand the second Bessel function in the following way:

$$J_0[a(z+z'+\delta)] = J_0[a(z+z')] J_0(a\delta) + 2 \sum_{n=1}^{\infty} (-1)^n J_n[a(z+z')] J_n(a\delta) \quad (7)$$

where

$$a = \frac{\eta \sqrt{1-\mu^2}}{\mu}. \quad (8)$$

### Perturbation theory

First we treat the problem in one-group formalism. We put

$$\varphi(\delta, z, z', \mu) \equiv J_0[a(z+z'+\delta)] - J_0[a(z+z')] \quad (9)$$

where  $a(\mu)$  is defined in Eq. 8. For  $\eta\delta \ll 1$  we have

$$e^{-\frac{z+z'}{\mu\lambda}} \varphi(\delta, z, z', \mu) \ll 1.$$

We consider this function as a perturbation, whose effect on  $\Delta\nu/\nu$  will be calculated. Eq. (4) can then be written:

$$\begin{aligned} \Phi(z) = & \frac{c}{2\lambda} \int_0^1 \frac{d\mu}{\mu} \int_0^{L/2} dz' \Phi(z') \left\{ e^{-\frac{|z-z'|}{\mu\lambda}} J_0 \left[ \frac{\eta|z-z'|\sqrt{1-\mu^2}}{\mu} \right] + \right. \\ & \left. + e^{-\frac{z+z'}{\mu\lambda}} J_0 \left[ \frac{\eta z+z'\sqrt{1-\mu^2}}{\mu} \right] + e^{-\frac{z+z'}{\mu\lambda}} \varphi(\delta, z, z', \mu) \right\}. \end{aligned} \quad (10)$$

The first approximation to the flux when  $\delta=0$  is

$$\Phi(z) = \cos \frac{\pi z}{L}.$$

A straight-forward application of perturbation theory, together with Eq. (5), then gives:

$$\frac{\Delta\nu}{\nu} = \frac{(\Sigma_s + \nu\Sigma_f)^2}{\nu\Sigma_f} \left( \frac{2}{L} \right) \int_0^1 \frac{d\mu}{\mu} \int_0^{L/2} \cos \frac{\pi z}{L} dz \int_0^{L/2} \cos \frac{\pi z'}{L} e^{-\frac{z+z'}{\mu\lambda}} \varphi(\delta, z, z', \mu) dz'. \quad (11)$$

We will now derive the corresponding formula in two-group theory. Here the starting point is Eq. (6) with  $i$  and  $j=1, 2$ . We assume that the eigenvalues for  $\delta \neq 0$  are obtained by multiplying  $\nu_1$  and  $\nu_2$  by  $(\nu + \Delta\nu)/\nu$ , which is  $=1$  for  $\delta=0$ . Physically, this means that the "average effect" of the air gap is cancelled by a change in all  $\nu$ -values. The "average effect" can be assumed to be the power of the reactor. A temporary change in the energy spectrum of the flux cannot be avoided, and during this time the flux is time dependent. The constancy of the power, according to USSACHOFF and HENRY [2, 3] can be expressed by the equation:

$$\frac{\partial}{\partial t} \int_V \int_E \frac{\Phi_0^*(r, E) \Phi(r, E, t)}{v(E)} dE dV = 0. \quad (12)$$

Here,  $E$  is the energy,  $V$  the reactor volume,  $v$  the neutron velocity,  $\Phi$  the neutron flux and  $\Phi_0^*$  the stationary adjoint flux for the unperturbed reactor.  $\Phi$  is

the solution of the time-dependent integral equation, which can be written:

$$l(v) \frac{\partial}{\partial t} \left( \frac{\Phi}{v} \right) = -\Phi(r, v, t) + \\ + \frac{1}{4\pi} \int \int \int \frac{dV'}{|r - r'|^2} e^{-\frac{|r - r'|}{l(v)}} \int \frac{c(v') f(v \rightarrow v')}{l(v)} \Phi(r', v', t) dv'. \quad (13)$$

In the stationary case,  $\Phi(r, v_i)$  corresponds to  $\Phi_i(z)$  in Eq. (6). The condition expressed in Eq. (13) can then be fulfilled in the following way. The integral equation for  $\Phi_1(z)$  is multiplied by  $\Phi_1^*/l_1$ , the corresponding equation for  $\Phi_2(z)$  is multiplied by  $\Phi_2^*/l_2$ , and the expressions are added. The remaining procedure is straight forward if we accept the diffusion theory solutions as a first approximation to the fluxes.

We adopt the following notations:

$D_i$ =diffusion coefficient for group  $i$

$B^2$ =material buckling

$\Sigma_{a,i}$ =macroscopic absorption cross-section in group  $i$

$\Sigma_{11} = \Sigma_{a,i} - \chi_1 \nu_1 \Sigma_{f1}$

$\Sigma_{12} = \chi_1 \nu_2 \Sigma_{f2}$

$\Sigma_{21} = \chi_2 \nu_1 \Sigma_{f1} + \Sigma_{s,1 \rightarrow 2}$

$C = \frac{D_1 B^2 + \Sigma_{11}}{\Sigma_{12}}$

$C^* = \frac{D_1 B^2 + \Sigma_{11}}{\Sigma_{21}}$ .

$$S_i = -\frac{2}{l_i^2} \int_0^1 \frac{d\mu}{\mu} \int_0^{L/2} \cos \frac{\pi z}{L} dz \int \cos \frac{\pi z'}{L} e^{-\frac{z+z'}{\mu l_i}} \varphi(\delta, z, z', \mu) dz'. \quad (14)$$

The formula for the change in criticality is then:

$$\frac{\Delta \nu}{\nu} = \frac{\frac{1}{L} [S_1 (1 + l_1 D_1 B^2) + S_2 (1 + l_2 D_2 B^2) C C^*]}{\nu_1 \chi_1 \Sigma_{f1} + \Sigma_{11} + D_1 B^2 + \chi_2 (C^* \nu_1 \Sigma_{f1} + \nu_2 \Sigma_{f2})}. \quad (15)$$

As before,  $\varphi(\delta, z, z', \mu)$  is expressed by Eq. (9). For a practical application of Eq. (11) and (15), there remains to solve the integral in the identity (14). Setting  $z+z'=x$  and integrating over  $z'$ , we have:

$$S_i = -\frac{1}{l_i^2} \int_0^1 \frac{d\mu}{\mu} \int_0^L e^{-\frac{x}{\mu l_i}} \varphi(\delta, x, \mu) \left( \frac{L}{\pi} \sin \frac{\pi x}{L} + x \cos \frac{\pi x}{L} \right) dx. \quad (16)$$

Now we approximate the integral over  $x$  by changing the upper limit from  $L$  to  $\infty$ . Then, because of Eq. (7), we have only integrals over  $x$  of the following type:

$$\int_0^\infty e^{-b_1 x} J_n(b_2 x) dx.$$

The solution of this as well as of the remaining integrals in expression (16)

can be found e.g. in Ref. [4]. The integration over  $\mu$  is performed with the aid of the following transformation:

$$w = \frac{\sqrt{1-\mu^2}}{\mu}.$$

It is convenient to expand the integrand in a series in  $l_i/L$  and  $\eta L_i$ . Keeping terms up to third degree in these quantities, we then obtain:

$$S_i = C_0 + C_1 + C_2 \quad (17)$$

$$C_0 = [1 - \zeta K_1(\zeta)] (1 - \eta^2 l_i^2) + \frac{l_i^2}{2} \left( \frac{\eta^2}{2} - \frac{\pi^2}{L^2} \right) + \frac{l_i^2}{4} \left( \frac{\pi^2}{L^2} - \frac{\eta^2}{2} \right) \zeta^2 K_2(\zeta) \quad (18)$$

$$C_1 = \frac{4}{3} \eta l_i \left[ \zeta e^{-\zeta} \left( 1 - \frac{3}{4} \eta^2 l_i^2 \right) + l_i^2 \left( \frac{3\eta^2}{20} - \frac{4\pi^2}{5L^2} \right) \zeta (1 + \zeta) e^{-\zeta} \right] \quad (19)$$

$$C_2 = \frac{3}{8} (\eta l_i)^2 \zeta^2 K_0(\zeta) \quad (20)$$

$$\zeta = \eta \delta.$$

$C_0$  originates from the first term on the right side in Eq. (7),  $C_1$  from the next and so on.

The first approximation for  $S_i$  is:

$$S_i = \frac{4}{3} \eta l_i \zeta e^{-\zeta} + 1 - \zeta K_1(\zeta). \quad (21)$$

This formula, together with the definition in Eq. (14), can also be inserted in the one-group formula Eq. (11), if we put  $l_i = \lambda$ . The first approximation in one-group theory is then:

$$\frac{\Delta \nu}{\nu} = \frac{(\Sigma_{st} + \nu \Sigma_f)^2}{\nu \Sigma_f} \frac{\lambda^2}{L} \left[ \frac{4}{3} \eta \lambda \zeta e^{-\zeta} + 1 - \zeta K_1(\zeta) \right]. \quad (22)$$

Eq. (22) is identical with Friedman's formula if transformation is made from  $\Delta \nu$  to  $\Delta L$ . Higher approximations may be of value for small reactors.

CARLVIK [6] has made more extensive calculation of the contributions of the terms of higher order in  $\eta \lambda$  and  $\lambda/L$ . For a cylindrical reactor with  $\lambda = 3$  cm,  $L = 40$  cm and  $R = 20$  cm, he finds that the term linear in  $\delta$  is reduced by about 15%. The derivation above of Friedman's formula is partly due to him.

### The variational method

For the background of the method, see e.g. DAVISON [5]. We seek for the eigenvalue to the integral equation (4). As a trial function we use

$$\Phi(z) = \cos(kz - \varphi). \quad (23)$$

The quantities  $k$  and  $\varphi$  are parameters, which will maximize the following functional:

$$I(k, \varphi) = \frac{c}{2\lambda} \frac{\int_0^{L/2} \cos(kz - \varphi) dz \int_0^{L/2} \frac{d\mu}{\mu} \int_0^L K(z, z', \mu) \cos(kz' - \varphi) dz'}{\int_0^{L/2} \cos^2(kz - \varphi) dz} \quad (24)$$

where

$$K = e^{-\frac{|z-z'|}{\mu \lambda}} J_0 \left[ \frac{\eta |z-z'| \sqrt{1-\mu^2}}{\mu} \right] + e^{-\frac{z+z'}{\mu \lambda}} J_0 \frac{\eta (z+z'+\delta) \sqrt{1-\mu^2}}{\mu} = \\ = K_1(|z-z'|, \mu) + K_2(z+z', \delta, \mu). \quad (25)$$

First we consider:

$$\int_0^{L/2} K_1(|z-z'|, \mu) \cos(kz' - \varphi) dz' = \\ = \int_0^z K_1(x, \mu) \cos(kz - kx - \varphi) dx + \int_0^{L/2-z} K_1(x, \mu) \cos(kz + kx - \varphi) dx. \quad (26)$$

The following approximation is made:

$$K_1(x, \mu) = e^{-\frac{x}{\mu \lambda}} \left[ 1 - \left( \frac{\eta x \sqrt{1-\mu^2}}{2\mu} \right)^2 \right]. \quad (27)$$

This approximation is reasonable because of the rapidly decreasing exponential. All integrations in the first part of the functional  $I(k, \varphi)$  are then elementary, and we obtain:

$$\int_0^{L/2} \cos(kz - \varphi) dz \int_0^1 \frac{d\mu}{\mu} \int_0^{L/2} K_1(z, z', \mu) \cos(kz' - \varphi) dz' \approx \\ \approx \frac{\lambda L}{2} \left[ 1 - \frac{\lambda^2 (k^2 + \eta^2)}{3} \right] \left[ 1 + \frac{1}{kL} \sin 2\varphi + \frac{1}{kL} \sin(kL - 2\varphi) \right] - \\ - \frac{\lambda^2}{4} [2 + \cos 2\varphi + \cos(kL - 2\varphi)]. \quad (28)$$

The integrations in the second part of the functional  $I(k, \varphi)$  is performed in the same way as the integration of the expression (14). To condense the expressions, we define a quantity  $\varepsilon$  in the following way:

$$\varepsilon = 1 - \frac{I}{c} - \frac{\lambda^2 \eta^2}{3}.$$

The calculated first approximation to  $\varepsilon$  is then:

$$\varepsilon = \frac{\lambda^2 k^2}{3} + \frac{\lambda k}{2[kL + \sin 2\varphi + \sin(kL - 2\varphi)]} \left\{ 1 + \cos(kL - 2\varphi) + \right. \\ \left. + (1 + \cos 2\varphi) \left[ \frac{3}{2} \eta^2 \lambda^2 + \frac{4}{3} \eta \lambda \zeta e^{-\zeta} + 1 - \zeta K_1(\zeta) \right] \right. \\ \left. - \frac{2}{3} k \lambda \sin 2\varphi (1 + \zeta) e^{-\zeta} \right\}. \quad (29)$$

As before,  $\zeta = \eta \delta$ .

We have to maximize  $\varepsilon$  with respect to  $k$  and  $\varphi$ . This has been done numerically for a reactor with the following data:

Composition 20% U<sup>235</sup>, 80%U<sup>238</sup>

$$\begin{aligned}\lambda &= 2.98 \text{ cm} \\ \Sigma_s &= 0.3097 \text{ cm}^{-1} \\ \nu \Sigma_f &= 0.0446 \text{ cm}^{-1} \\ L &= 39.5 \text{ cm}\end{aligned}$$

If we further assume a cubic reactor,  $\eta = \frac{\pi\sqrt{2}}{L}$ .

The optimum values are called  $k_0$ ,  $\varphi_0$  and  $\varepsilon_0$ . For  $\delta=0$ ,  $k_0 L=0.85 \pi$ ,  $\varphi_0=0$  and  $\varepsilon_0=0.0279$ . When  $\delta$  increases,  $k_0$  and  $\varphi_0$  will first stay constant, probably dependent upon the approximations made in the calculations of  $\varepsilon$ . At  $\delta \approx 4$  cm,  $k_0 L$  and  $\varphi_0$  jump to  $1.35 \pi$  and  $\pi/4$ , respectively. This optimum point is then constant up to very large values of  $\delta$  ( $\delta \approx 20$  cm), whereafter it jumps to  $k_0 L=2 \pi$  and  $\varphi_0=\pi/2$ .  $\varepsilon_0$  varies continuously until  $k_0 L$  reaches the value  $2 \pi$ . From this point  $\varepsilon_0$  assumes the constant value

$$\lim_{\delta \rightarrow \infty} \varepsilon_0 = \frac{4\pi^2 \lambda^2}{3L^2}. \quad (30)$$

The reactivity as a function of  $\delta$  can be calculated if we substitute  $\gamma c$  for  $c$  in Eq. (24) and consider  $\gamma$  as the eigenvalue of the integral equation. Then the maximum value of  $I$  is equal to  $1/\gamma$ .

If  $\gamma=1$  for  $\delta=0$ , we obtain

$$c = \lambda (\nu \Sigma_f + \Sigma_s) = \frac{1}{1 - \frac{\eta^2 \lambda^2}{3} \varepsilon_0(0)}. \quad (31)$$

When  $\delta \neq 0$ , we have  $\varepsilon(\delta) = \varepsilon_0(0) + \Delta \varepsilon_0$  and  $\gamma = 1 + \Delta \gamma$ . Then

$$\frac{1}{1 + \Delta \gamma} = 1 - c \Delta \varepsilon_0 \quad (32)$$

and

$$\frac{\Delta \nu}{\nu} = c \left( \frac{\Sigma_s + \nu \Sigma_f}{\nu \Sigma_f} \right) \left( \frac{\Delta \varepsilon_0}{1 - c \Delta \varepsilon_0} \right). \quad (33)$$

TABLE I

**THE REACTIVITY EQUIVALENCE OF AN AIR GAP ACCORDING TO DIFFERENT THEORIES FOR A REACTOR WITH COMPOSITION GIVEN IN THE TEXT**

$\delta$ (cm)	$\left( \frac{\Delta \nu}{\nu} \right)_V$	$\left( \frac{\Delta \nu}{\nu} \right)_P$	$\left( \frac{\Delta \nu}{\nu} \right)_D$	$\left( \frac{\Delta \nu}{\nu} \right)_L$
2	0.078	0.078	0.047	0.047
4	0.127	0.160	0.087	0.078
5	0.143	0.199	0.104	0.090
10	0.214	0.355	0.160	0.135
12	0.236	0.399	0.175	0.147
15	0.262	0.453	0.190	0.161
20	0.288	0.508	0.205	0.180

Index  $V$  refers to variational calculus,  $P$  to perturbation theory,  $D$  to diffusion theory and  $L$  to direct leakage calculus.

For  $\delta=0$ , we get  $\varepsilon_0(0)=0.0279$ . Assuming  $\lambda=2.98$  cm and  $\Sigma_s=0.3097 \text{ cm}^{-1}$ , Eq. (31) gives for  $\Sigma_s + \nu\Sigma_f$  the value  $0.3591 \text{ cm}^{-1}$ . The difference between this value and the sum of  $\Sigma_s$  and  $\nu\Sigma_f$  earlier given depends upon the assumed value of  $L$ , which is calculated by diffusion theory. The values of  $\Delta\nu/\nu$  at different values of  $\delta$  is given in Table I. The actual value has the index  $V$ .

### Comparison with other theories

Chernick and Kaplan have solved the gap problem using diffusion theory and using what they call "direct leakage calculation". The result of both methods is given by the following formula:

$$\frac{L_0 + \Delta L_0}{L_0} = \frac{2}{\pi} \cot^{-1} \left[ -3 L_0 C_2 \left( C_1 + \frac{N \lambda \xi^2 e^{-\xi}}{3 \delta} \right) (2\pi\lambda)^{-1} \right]. \quad (34)$$

Here,

$L_0$ =the extrapolated length of a cubic reactor at criticality

$L$ =corresponding material length of a reactor with air gap, whereby the length has been changed in a direction perpendicular to the air gap

$\delta$ =length of the air gap

$\lambda$ =mean free path

$$\xi = \frac{\pi \delta \sqrt{2}}{L_0}$$

$N=2$  by diffusion theory and 3 by "direct leakage calculation"

$C_1$  and  $C_2$  are functions of  $\delta$  and are tabulated in Ref. [1].

$\Delta L_0/L_0$  can be transformed to  $\Delta\nu/\nu$  by the following formulae:

$$\frac{\Delta L_0}{L_0} = \left( \frac{x}{y} \right) \left( \frac{\Delta\nu}{2\nu} \right) \left[ 1 + \frac{1}{\gamma^2_0 L^2} (1 + L^2 B^2_t) \right] \quad (35)$$

$$\operatorname{tg} x = \frac{\pi + 2y}{\pi} \operatorname{tg} y \quad (36)$$

$$x = \frac{\pi}{2} \frac{\Delta L_0}{L_0}$$

$L^2$ =migration surface

$\gamma^2_0$ =buckling coefficient in the direction perpendicular to the air gap

$B^2_t$ =buckling coefficient in the direction parallel to the air gap.

The result using diffusion theory will be called  $(\Delta\nu/\nu)_D$ , and the result from "direct leakage calculation" will be called  $(\Delta\nu/\nu)_L$ . Further, the result from perturbation theory will be called  $(\Delta\nu/\nu)_P$ , and from variational calculus  $(\Delta\nu/\nu)_V$ . These quantities for different values of  $\delta$  are given in Table I and in Fig. 1.

The perturbation theory gives of course wrong values for large  $\delta$ . There are also errors in the result from the variational method because of the rather coarse approximations in performing the integrations and because of the "image pile" effect [1]. The "image pile" effect can be appreciated by comparing the values from diffusion theory with the values from "direct leakage calculation". In the latter method, this error does not exist, and the values differ from the diffusion theoretical values by about 15% at large  $\delta$ -values. This is about half of the difference between  $(\Delta\nu/\nu)_V$  and  $(\Delta\nu/\nu)_D$ . The rest of the difference can be assumed to depend upon other approximations in both methods.

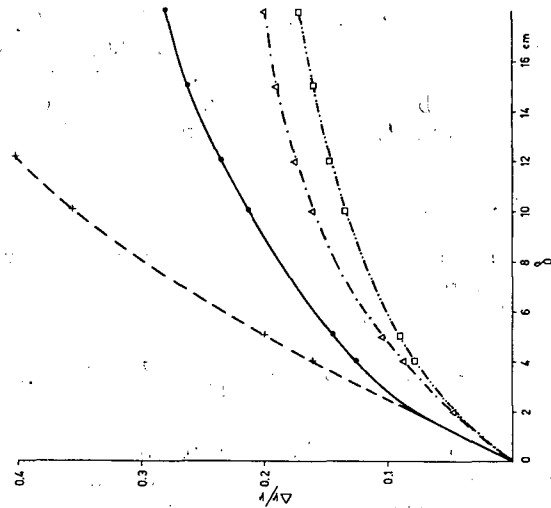


Fig. 1

The reactivity equivalence of an air gap for a reactor with composition given in the text.

- Variational method
- - - Perturbation theory
- · - Diffusion theory
- · - · Direct leakage calculation

## REFERENCES

- [1] CHERNICK, J. and KAPLAN, I., *J. nucl. Energy* **2** (1955) 41-51.
- [2] USSACHOFF, L. N., Proc. UN Int. Conf. PUAE **5** (1955) 503.
- [3] HENRY, A. F., *Nucl. Sci. and Engng* **3** (1958) 52-70.
- [4] WATSON, G. N., *A Treatise on the Theory of Bessel Functions*, Cambridge University Press (1952).
- [5] DAVISON, B., *Neutron Transport Theory*, Oxford (1958).
- [6] CARLVIK, I., Private communication.

### **III. 2. EFFECTS OF CROSS-SECTION ERRORS**



# THE SENSITIVITY OF CALCULATED CRITICAL MASSES OF SMALL FAST SYSTEMS TO CHANGES IN THE U<sup>235</sup> AND U<sup>238</sup> NEUTRON-SCATTERING DATA

E. D. PENDLEBURY

ATOMIC WEAPONS RESEARCH ESTABLISHMENT, ALDERMASTON,  
UNITED KINGDOM

**Abstract — Résumé — Аннотация — Resumen**

The sensitivity of calculated critical masses of small fast systems to changes in the U<sup>235</sup> and U<sup>238</sup> neutron-scattering data. The sensitivity of the calculated critical masses of a number of simple systems, to changes in the basic neutron scattering data, have been investigated. The systems considered are spheres of 29% U<sup>235</sup> and 93½% U<sup>235</sup>, both bare, and reflected by thick natural uranium. The calculations have been carried out using the Carlson  $S_n$  method with 4 energy groups, and the percentage changes in the calculated critical masses of the different systems, due to specified changes in the various aspects of the neutron scattering data, have been obtained. The results are presented and discussed with particular reference to the adjustment of the basic data to give good agreement with experimental critical sizes.

The basic data on which these calculations have been based are those given in AWRE Report 0—28/60.

Influence de la précision des données relatives à la diffusion des neutrons par <sup>235</sup>U et <sup>238</sup>U sur le calcul des masses critiques de petits modèles à neutrons rapides. L'auteur a étudié, pour plusieurs modèles simples, quelle était la sensibilité des masses critiques calculées aux modifications des données fondamentales relatives à la diffusion des neutrons. Les systèmes considérés sont deux sphères d'uranium enrichi à 30% et à 94%, respectivement, tantôt nues, tantôt entourées d'un réflecteur épais en uranium naturel. Pour faire les calculs, l'auteur a utilisé la méthode  $S_n$  de Carlson avec quatre groupes d'énergie; il a obtenu ainsi les variations en pourcentages des masses critiques calculées pour les différents modèles en fonction de modifications déterminées des différentes données relatives à la diffusion. L'auteur présente les résultats et les examine en insistant particulièrement sur le problème que pose l'ajustement des données de base nécessaire pour obtenir un bon accord entre les dimensions critiques calculées et celles qui sont déterminées par l'expérience.

Les données de base d'après lesquelles ces calculs ont été établis sont celles qui figurent dans le rapport 0—28/60 de l'Atomic Weapons Research Establishment.

Чувствительность вычисленных критических масс небольших систем на быстрых нейтронах к изменениям в данных рассеяния нейтронов урана-235 и урана-238. Изучалась чувствительность вычисленных критических масс ряда простых систем к изменениям в основных данных рассеяния нейтронов. Изучавшиеся системы представляют собой сферы урана-235 с 30% обогащением и урана-235 с 94% обогащением как без экранирования, так и с отражателем из тонкого слоя природного урана. При вычислениях применяется метод Карлсона  $S_n$  с 4 энергетическими группами и были получены процентные изменения в вычисленных критических массах различных систем, вызываемые заданными изменениями в некоторых данных рассеяния нейтронов. В докладе даются и обсуждаются результаты, причем особое внимание придается приведению основных данных в соответствие с экспериментально установленными критическими размерами.

Основные данные, на которых были основаны эти вычисления, взяты из доклада AWRE 0-28/60.

**Influencia de la precisión de los datos relativos a la dispersión de neutrones en el  $^{235}\text{U}$  y el  $^{238}\text{U}$  sobre la masa crítica calculada de sistemas rápidos de pequeñas dimensiones.** El autor ha estudiado la sensibilidad de las masas críticas, calculadas para varios sistemas sencillos, a los cambios de los datos básicos relativos a la dispersión neutrónica. Los sistemas estudiados consisten en esferas de uranio enriquecido al 29 por ciento y al 93,5 por ciento, respectivamente, en el isótopo 235, desnudas o provistas de un grueso reflector de uranio natural. Los cálculos se han realizado por el método  $S_n$  de Carlson, referido a cuatro grupos energéticos, obteniéndose así las variaciones porcentuales de las masas críticas en función de las modificaciones de los diversos datos relativos a la dispersión neutrónica. El autor presenta y examina los resultados, insistiendo particularmente en la adaptación de los datos básicos necesarios para lograr una concordancia satisfactoria con las dimensiones críticas calculadas y determinadas experimentalmente.

En los cálculos se emplearon los datos básicos que figuran en el informe 0—28/60 del Atomic Weapons Research Establishment.

## Introduction

In the present state of knowledge, it is most unlikely that a compilation of neutron cross-sections for fissile isotopes, based on the best available experimental data, with the gaps filled in accordance with the predictions of current nuclear theory, will lead to calculated critical sizes in agreement with the experimental values. It is then necessary to adjust the cross-sections, preferably within the stated experimental errors of the microscopic measurements, to give cross-sections (and corresponding group cross-sections) which reproduce critical sizes of a range of experimental systems appropriate to the (neutron) energy range and material of interest. Whilst these adjustments can be decided upon, in principle, by trial and error, it is preferable to make a systematic approach to the problem, and it is then necessary to know the sensitivity of the critical masses of various systems to changes in the cross-section data. In the present paper this sensitivity has been studied for some simple  $\text{U}^{235}/\text{U}^{238}$  systems.

The systems considered are:

- (a) Bare sphere of (94%  $\text{U}^{235} + 6\% \text{U}^{238}$ )\* at 18.75 g/cm<sup>3</sup>
- (b) Bare sphere of (29%  $\text{U}^{235} + 71\% \text{U}^{238}$ ) at 18.75 g/cm<sup>3</sup>
- (c) Sphere of (94%  $\text{U}^{235} + 6\% \text{U}^{238}$ ) reflected by 15 cm of natural uranium at 18.7 g/cm<sup>3</sup>
- (d) Sphere of (30%  $\text{U}^{235} + 70\% \text{U}^{238}$ ) reflected by 15 cm of natural uranium at 18.75 g/cm<sup>3</sup>

and the changes in the critical masses of these systems due to specified changes in the cross-section data have been calculated by the  $S_n$  method [1]. The results of the calculations are given in Section 1 and discussed in Section 2. The discussion in Section 2 is aimed at giving some qualitative understanding of the results, and in Section 3 they are then considered with particular reference to the problem of adjusting the data to give agreement between the calculated and experimental critical sizes.

---

\* Compositions refer to percentages by nuclei.

The results in Section 1 can also be interpreted as giving the accuracy to which it is necessary to measure the basic data in order that critical masses can be calculated to some specified accuracy.

### 1. Calculations and results

When a partial cross-section in a set of neutron-scattering data is altered, either one or more other partial cross-sections must also be changed in order to preserve the value of the total cross-section, or the total cross-section itself must be changed. The total cross-section for U<sup>235</sup> and U<sup>238</sup> is fairly well established (at least in the region above 1 keV), and it is usual to calculate the elastic cross-section as the difference between the total and non-elastic cross-sections. Hence, in the present paper, where a change in a non-elastic partial cross-section is considered, the elastic cross-section is changed to preserve the value of the total cross-section. It must be realized however that this leads to a change in the *total transport cross-section*. When the effect of a change in the elastic cross-section is considered, the total cross-section is then changed in order to maintain consistency between the partial and total cross-sections.

Each of the following changes in the data have been considered separately for U<sup>235</sup> and U<sup>238</sup>, except where the change is explicitly referred to one or other of these isotopes;

- 10% decrease in  $\sigma_{n\gamma}$  ( $\sigma_{el}$  increased to preserve the value of  $\sigma_{tot}$ )
- 10% increase in  $\sigma_{nn'}$  ( $\sigma_{el}$  decreased to preserve the value of  $\sigma_{tot}$ )
- 10% increase in  $\sigma_{nf}$  ( $\sigma_{el}$  decreased to preserve the value of  $\sigma_{tot}$ )
- 10% decrease in  $\sigma_{el}$  ( $\sigma_{tot}$  decreased to preserve consistency between the partial and total cross-sections)
- 10% increase in  $\bar{\mu}^*$
- 10% increase in  $\bar{\nu}$  for U<sup>238</sup>
- 7.5% increase in  $\bar{\nu}$  for U<sup>235</sup>.

The above changes have been made uniformly at all energies above 10 keV. In addition, the effects of using data including each of the following in turn have also been considered

- $\bar{\nu}(U^{235}) = 2.42$  (constant at all energies)
- Softer (n, n') spectra (see text below)
- Harder (n, n') spectra (see text below).

The percentage changes in the critical masses of the four systems listed in the Introduction have been calculated for the changes in the data given above. The calculations have been carried out using the  $S_n$  method [1] in the  $S_4$  approximation with four energy groups between 10 keV and 11 MeV. The original data on which these calculations have been based are those given by BUCKINGHAM *et al.* [2], and appropriate group cross-sections have been calculated from these [3], using an energy weighting given by a degraded fission spectrum. Anisotropic scattering is treated by the transport approximation [4], and changes in the anisotropy are thus taken into account by changes in  $\mu$ .

The results of the calculations are given in Tables I—IV in the form of the percentage change in critical mass due to the various changes in the U<sup>235</sup> and U<sup>238</sup> scattering data, each table corresponding to a different system.

At this point it is necessary to comment on the soft and hard spectra which have been used to obtain the results quoted in Tables I—IV.

---

\*  $\bar{\mu}$  = mean cosine of the scattering angle in the laboratory system.

The  $(n, n')$  spectra were altered in a way which was primarily of convenience in calculating the new group constants. The changes in spectra considered were quite large, and one should think about them carefully before drawing conclusions from the results as presented in Tables I—IV. To get an idea of just how much the spectra have been altered and to obtain a parameter which is a measure of the hardness or softness of any given spectrum, it is useful to compute the mean energy of the emergent neutrons following  $(n, n')$  reactions with fission-spectrum neutrons. The mean energy  $\langle E \rangle$  defined in this way is given in group constant notation [3] by

$$\langle E \rangle = \sum_{g'} \sum_g [f_{g'} \beta_{g'g} E_g] / \sum_{g'} \sum_g [f_{g'} \beta_{g'g}] . \quad (1)$$

TABLE I  
VARIATION OF THE CRITICAL MASS OF THE 94%  $U^{235}$  BARE SPHERE  
due to specified changes in the nuclear data

Change in data	Change in critical mass due to change in data for	
	$U^{235}$	$U^{238}$
10% decrease in $\sigma_{n\gamma}$	— 1.5 %	— 0.1 %
10% increase in $\sigma_{nn'}$	— 0.3 %	0.0 %
10% increase in $\sigma_{nf}$	— $18^{1/2}$ %	— 0.2 %
10% decrease in $\sigma_{el}$	+ 4.5 %	+ 0.36 %
10% increase in $\mu$	+ 3.0 %	+ 0.2 %
10% increase in $\bar{v}$	—	— 0.4 %
7.5% increase in $\bar{v}$ $\bar{v} (U^{235}) \equiv 2.42$ (constant at all energies)	— 23 % + 1.4 %	— —
Softer $(n, n')$ spectra (cf. Section 1)	— 16 %	— 1.7 %
Harder $(n, n')$ spectra (cf. Section 1)	+ 6.1 %	+ 0.2 %

TABLE II  
VARIATION OF THE CRITICAL MASS OF THE 29%  $U^{235}$  BARE SPHERE  
due to specified changes in the nuclear data

Change in data	Change in critical mass due to change in data for	
	$U^{235}$	$U^{238}$
10% decrease in $\sigma_{n\gamma}$	— 1.8 %	— 3.7 %
10% increase in $\sigma_{nn'}$	+ 0.34 %	+ 1.6 %
10% increase in $\sigma_{nf}$	— 18 %	— 4.1 %
10% decrease in $\sigma_{el}$	+ 1.8 %	+ 5.7 %
10% increase in $\mu$	+ 1.0 %	+ 2.7 %
10% increase in $\bar{v}$	—	— 6.8 %
7.5% increase in $\bar{v}$ $\bar{v} (U^{235}) \equiv 2.42$ (constant at all energies)	— 22 % — 2.0 %	— —
Softer $(n, n')$ spectra (cf. Section 1)	— 8.0 %	— 16 %
Harder $(n, n')$ spectra (cf. Section 1)	+ 1.0 %	— 5.2 %

TABLE III  
**VARIATION OF THE CRITICAL MASS OF THE 94% U<sup>235</sup> SPHERE WITH NATURAL URANIUM REFLECTOR**  
due to specified changes in the nuclear data

Change in data	Change in critical mass due to change in data for	
	U <sup>235</sup>	U <sup>238</sup>
10% decrease in $\sigma_{n\gamma}$	— 1.7 %	— 2.2 %
10% increase in $\sigma_{nn'}$	— 0.20 %	+ 0.75 %
10% increase in $\sigma_{nf}$	— 18 %	— 1.6 %
10% decrease in $\sigma_{el}$	—	—
10% increase in $\bar{\nu}$	+ 1.3 %	+ 3.1 %
10% increase in $\bar{\nu}$	—	— 2.8 %
7.5% increase in $\bar{\nu}$ $\bar{\nu}$ (U <sup>235</sup> ) ≡ 2.42 constant at all energies)	— 23 % — 1.9 %	— —
Softer (n, n') spectra (cf. Section 1)	— 15 %	— 2.7 %
Harder (n, n') spectra (cf. Section 1)	+ 5.5 %	— 5.7 %

TABLE IV  
**VARIATION OF THE CRITICAL MASS OF THE 30% U<sup>235</sup> SPHERE WITH NATURAL URANIUM REFLECTOR**  
due to specified changes in the nuclear data

Change in data	Change in critical mass due to change in data for	
	U <sup>235</sup>	U <sup>238</sup>
10% decrease in $\sigma_{n\gamma}$	— 2.0 %	— 6.3 %
10% increase in $\sigma_{nn'}$	— 0.47 %	+ 2.8 %
10% increase in $\sigma_{nf}$	— 20 %	— 5.1 %
10% decrease in $\sigma_{el}$	—	—
10% increase in $\bar{\mu}$	+ 0.56 %	+ 3.9 %
10% increase in $\bar{\nu}$	—	— 8.4 %
7.5% increase in $\bar{\nu}$ $\bar{\nu}$ (U <sup>235</sup> ) ≡ 2.42 (constant at all energies)	— 24 % — 9.3 %	— —
Softer (n, n') spectra (cf. Section 1)	— 7.4 %	— 8.3 %
Harder (n, n') spectra (cf. Section 1)	+ 0.26 %	— 18 %

TABLE V  
**MEAN ENERGIES OF (nn') SCATTERED NEUTRONS GIVEN BY Eq. (1)**  
(in MeV)

Element	Unadjusted data	Softened spectrum (cf. Section 1)	Hardened spectrum (cf. Section 1)
U <sup>235</sup>	0.93	0.31	1.81
U <sup>238</sup>	1.05	0.36	1.78

Here  $\beta_{g'g}$  is the transfer matrix for neutrons transferred from group  $g'$  to  $g$  for the  $(n, n')$  reaction,  $E_g$  is the mean energy of neutrons in group  $g$ ,  $f_{g'}$  is the fraction of fission neutrons produced in group  $g'$ . This mean energy is thus a measure of the hardness or softness of the spectrum, and when considered relative to the unaltered value gives an indication of the amount by which the spectrum has been altered. If the mean energy is changed by a factor  $p$  say, this means that the same result could have been achieved by assuming that the nuclear temperature in the basic data were changed by the same factor  $p$ .

The mean energies as defined above for the spectral variations considered are given in Table V, together with the values which obtain for the unadjusted data. It will be seen that the altered spectra correspond to quite large changes—by a factor of  $\sim 2-3$  in the nuclear temperature. (The nuclear temperature used in the basic data has a value of 0.25 MeV for incident neutrons of 1 MeV energy.)

## 2. Discussion of the results in Tables I—IV

### *Change in $\sigma_{n\gamma}$*

When  $\sigma_{n\gamma}$  is decreased and  $\sigma_{el}$  correspondingly increased (as in these calculations), this means that some neutrons which would otherwise have been captured are scattered instead. The consequence of this must therefore be a decrease in the critical mass, which is in accord with the results in the first row of Tables I—IV. The percentage decrease in critical mass is not large, because the average value of  $\sigma_{n\gamma}$  over the spectra of the systems is not large. The effect would of course be greater in systems further diluted, with, say, graphite.

Since the  $U^{235}$  ( $n, \gamma$ ) cross-section is roughly the same as the  $U^{238}$  ( $n, \gamma$ ) cross-section, one would expect the percentage change in the critical mass of the bare systems, corresponding to the 10% change in  $\sigma_{n\gamma}$  for either isotope, to be approximately proportional to the percentage of that isotope present in the system. Thus in Table II for example

$$\frac{\% \text{ change in crit. mass due to } 10\% \text{ change in } U^{235} \sigma_{n\gamma}}{\% \text{ change in crit. mass due to } 10\% \text{ change in } U^{238} \sigma_{n\gamma}} = \frac{1.8}{3.7} = 0.49 \simeq \frac{29}{71} = 0.41,$$

As would be expected, the effect of the change in  $U^{238}$  ( $n, \gamma$ ) is greater in the reflected systems.

### *Change in $\sigma_{nn'}$*

The direct consequence of an increase in  $\sigma_{nn'}$  is an increase in moderation, whilst the indirect consequence is an increase in the transport cross-section, since the increase in  $\sigma_{nn'}$  is taken up by an equivalent decrease in  $\sigma_{el}$ . If  $\Delta\sigma$  represents the increase in  $\sigma_{nn'}$ , the change in the *transport cross-section* is given by

$$\Delta\sigma - \Delta\sigma(1-\bar{\mu}) = \bar{\mu}\Delta\sigma$$

where  $\bar{\mu}$  is the mean cosine of the scattering angle (in the laboratory system) in an elastic collision. For  $U^{235}$  and  $U^{238}$ ,  $\bar{\mu} \geq 0$  at all energies, and hence the total transport cross-section is increased by the amount  $\bar{\mu}\Delta\sigma$ . The effect of the increased transport cross-section is a tendency to decrease the critical mass, but the effect of the increased moderation depends on the  $U^{235}$  enrichment in the system. This arises because of the threshold in the  $U^{238}$  fission cross-section. In Fig. 1, the

fission cross-sections for  $[0.94 \text{ U}^{235} + 0.06 \text{ U}^{238}]$  and for  $[0.29 \text{ U}^{235} + 0.71 \text{ U}^{238}]$  are plotted as a function of energy. The cross-section corresponding to the low enrichment of  $\text{U}^{235}$  shows a very marked increase due to the onset of the  $\text{U}^{238}$

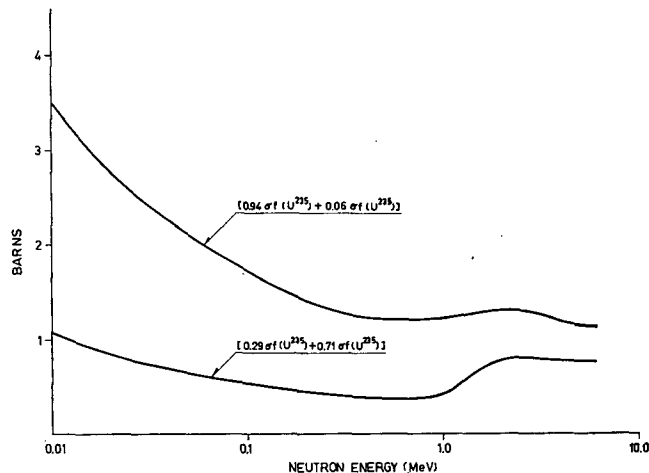


Fig. 1  
Fission cross-sections.

fission. In this case, the increased moderation of the neutrons due to the increased  $(n, n')$  cross-section leads to a lower effective fission cross-section, with the consequent tendency towards a greater critical mass. It is seen from Table II that, for the bare 29%  $\text{U}^{235}$  sphere, this more than compensates the tendency towards a smaller critical mass due to the increased transport cross-section. In the case of the high-enriched bare sphere, the effect due to the onset of the  $\text{U}^{238}$  fission is less marked, and any tendency towards a greater critical mass—if there is any tendency at all—due to the increased moderation clearly does not cancel the tendency towards a smaller critical mass due to the increased transport cross-section (see Table I).

In the reflected systems, the increased  $(n, n')$  cross-section leads to a reasonable increase in the critical mass, indicating that the reduced fission in  $\text{U}^{238}$  in these cases has a significantly greater effect than the increased transport cross-section.

#### *Change in $\sigma_{nf}$*

An increase in the fission cross-section produces an increase in the total transport cross-section for the same reason as an increase in  $\sigma_{nn'}$  leads to an increase in the total transport cross-section (see paragraph above). Both the direct and indirect consequences of the increased fission cross-section are therefore decreases in the critical mass. As might be expected, the critical mass is fairly sensitive to changes in  $\sigma_f$ —though not quite as sensitive as to changes in  $\bar{\nu}$ .

If one assumes that the  $\text{U}^{238}$  in these systems contributes only a small fraction of the fissions, then from simple diffusion theory one would expect the critical mass (of all the systems considered) to be governed largely by  $[(\bar{\nu} - 1) \sigma_f]_{\text{U}^{235}}$ , whence

$$\frac{\Delta \bar{\nu}}{\bar{\nu} \left(1 - \frac{1}{\bar{\nu}}\right)} \Bigg|_{U^{235}} \simeq -\frac{\Delta \sigma_f}{\sigma_f} \Bigg|_{U^{235}}$$

for a fixed critical mass.

For  $\nu \sim 2\frac{1}{2}$  this becomes

$$\frac{5}{3} \frac{\Delta \nu}{\nu} \Bigg|_{U^{235}} \simeq -\frac{\Delta \sigma_f}{\sigma_f} \Bigg|_{U^{235}}.$$

This implies that the critical mass is approximately 5/3 times more sensitive to a given percentage change in  $\bar{\nu}$  ( $U^{235}$ ) than to the same percentage change in  $\sigma_f$  ( $U^{235}$ ). This simple relationship is in accord with the results given in Tables I—IV.

It is interesting to note from the results in Tables I—IV that the percentage change in the critical masses of all the systems due to the 10% change in  $\sigma_{nf}$  ( $U^{235}$ ) are approximately the same. In the case of the bare spheres, this similarity can easily be demonstrated on the basis of simple diffusion theory, assuming that the large majority of fission events take place in the  $U^{235}$ .

It will be noted that the decrease of the critical mass in the 30%  $U^{235}$  reflected sphere, due to the 10% increase in  $\sigma_{nf}$  for  $U^{238}$ , is three times the corresponding decrease in the case of the 94%  $U^{235}$  reflected sphere (cf. Tables III and IV). Since the thickness of the reflector is the same in both cases, this indicates that the variation of the critical mass is much more dependent on the  $U^{238}$  in the core—provided there is sufficient  $U^{238}$  in the core—than the  $U^{238}$  in the reflector.

#### *Change in $\sigma_{el}$*

When  $\sigma_{el}$  is decreased and  $\sigma_{tot}$  is correspondingly decreased by the same amount to preserve the balance between partial and total cross-sections, the net effect is to give neutrons a better chance to escape, and so the calculated critical mass is increased.

It is seen from Tables I and II that the critical masses of the bare systems are only moderately sensitive to changes in  $\sigma_{el}$ . Corresponding calculations have not been carried out on the reflected systems, but there is no reason to suppose that the sensitivity of the critical masses in these cases to changes in  $\sigma_{el}$  is much different than in the bare systems. This is supported by the results relating to the changes in  $\bar{\mu}$ .

#### *Change in $\bar{\mu}$*

An increase in  $\bar{\mu}$  decreases the elastic transport cross-section and hence the total transport cross-section, thus leading to an increase in the calculated critical mass. The critical masses are however not very sensitive to changes in  $\bar{\mu}$  (cf. Tables I — IV).

#### *Change in $\bar{\nu}$*

This is the parameter — for  $U^{235}$  — on which the critical mass is most sensitive. The percentage change in critical mass for a given percentage change in  $\bar{\nu}$  ( $U^{235}$ ) is roughly the same for all the four systems under consideration. This is consistent with the variation of critical mass due to changes in  $\sigma_{nf}$ , and also with the discussion in the paragraph above on the change in  $\sigma_{nf}$ .

The 7.5% increase in  $\bar{\nu}$  ( $U^{235}$ ) [cf. Tables I — IV] leads to:

$$\bar{\nu} (U^{235}) = 2.42 + 0.141 E$$

(previously,  $\bar{\nu} = 2.25 + 0.132 E$ ), where  $E$  is the incident neutron energy in mega-electron-volts. When the critical masses calculated with these values of  $\bar{\nu}$  are taken in conjunction with the values for  $\bar{\nu} (U^{235}) = 2.42$ , they represent the variation of critical mass as the slope of the  $\bar{\nu}$ -versus-energy curve is varied — assuming that the curve remains linear — keeping the thermal values fixed.

It is interesting to note the critical masses with  $\bar{\nu} (U^{235}) = 2.42$ , for all except the 30%  $U^{235}$  reflected sphere, are only slightly different from the values obtained with  $\bar{\nu} = 2.25 + 0.132 E$ . This indicates that the spectra in these systems are such that with  $\bar{\nu} = 2.25 + 0.132 E$  the effective average value of  $\bar{\nu}$  is  $\approx 2.42$ . In the 30%  $U^{235}$  reflected sphere, the spectrum must be significantly softer, leading to a smaller effective value of  $\bar{\nu}$  when  $\bar{\nu} = 2.25 + 0.132 E$  is used — thus the critical mass is decreased when  $\bar{\nu}$  is set equal to 2.42 at all energies.

The slight increase in the critical mass of the high-enriched bare sphere when  $\bar{\nu} = 2.42$  and the decrease in the critical mass of the other systems is consistent with the fact that the hardest spectrum is expected in the 94%  $U^{235}$  bare sphere.

#### Change in the $(n, n')$ spectra

In the case of the 94%  $U^{235}$  bare sphere, the softer spectra must lead to a more efficient exploitation of the  $U^{235}$  fission reaction whilst the harder spectra have the opposite effect and there is insufficient  $U^{238}$  present to offset the effect of this. In the case of the 29%  $U^{235}$  bare sphere the softer spectra again must lead to more efficient exploitation of the  $U^{235}$  fission reaction at the possible expense of some  $U^{238}$  fission, whilst the reduced  $U^{235}$  fission due to a harder spectrum may be more than compensated for by the increased fission in  $U^{238}$ . This is best illustrated by considering the  $U^{235}$  and  $U^{238}$  results together. The  $U^{238} \sigma_{nn'}$  is about

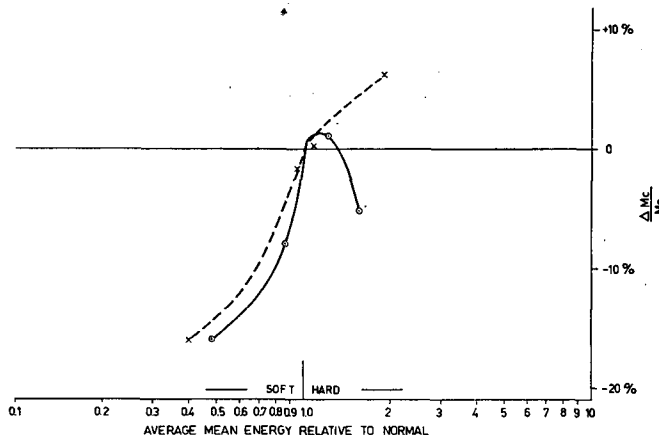


Fig. 2  
Variation of critical mass with  $(n, n')$  spectrum.

○ 25%  $U^{235}$  bare sphere  
× 94%  $U^{235}$  bare sphere

$\frac{1}{3}$  times the  $U^{235} \sigma_{nn'}$ , and so for a bare system with say  $x\%$   $U^{235}$ ,  $(100-x)\%$   $U^{238}$  an average mean energy denoted by  $\langle E \rangle_{AV}$  can be defined as

$$\langle E \rangle_{AV} = [3x \langle E \rangle_5 + 4(100-x) \langle E \rangle_8] / 700$$

where  $\langle E \rangle_5$  and  $\langle E \rangle_8$  are the mean energies for  $U^{235}$  and  $U^{238}$  respectively as defined by equation (1). In Fig. 2 the percentage change in critical mass for the two bare systems considered is represented as a function of  $\langle E \rangle_{AV}$  expressed relative to its unadjusted value. For the 29%- $U^{235}$  sphere it is seen that as the hardness of spectrum increases the critical mass increases to a maximum, and as the  $U^{238}$  fission is exploited by further hardening it begins to fall again. Over the range considered and because of the low amount of  $U^{238}$  the critical mass of the 94%- $U^{235}$  sphere does not show this same variation.

It is interesting to note that the changes in the critical mass of the reflected systems due to the changes in spectra from the  $U^{235}(n, n')$  reaction are approximately the same as in the corresponding bare system. The variation of the critical mass of the reflected 30%- $U^{235}$  sphere due to the spectral changes in  $U^{238}$  are much greater than the corresponding variations in the critical mass of the 94%- $U^{235}$  sphere (cf. Tables III and IV), and since the thickness of the reflector is the same in both cases, this indicates that the critical masses are more sensitive to changes of the  $U^{238}(n, n')$  spectrum in the core — provided there is a sufficient amount of  $U^{238}$  — than to changes in the  $U^{238}(n, n')$  spectrum in the reflector.

### 3. Application of the results of Section 1 to the adjustment of the basic data to give consistency with experimental critical sizes

In 1959, a set of neutron-scattering data for  $U^{235}$  and  $U^{238}$  for calculation purposes was compiled at AWRE, using the then currently available experimental data. *Simple* adjustments were included in these data, so that they gave the correct critical masses — to within  $\pm 3\%$  of the experimental values — for 94%- $U^{235}$  spheres, bare and reflected by up to 23 cm of natural uranium. The adjustments consisted only of a uniform reduction in the  $\bar{\nu}$  values for both  $U^{235}$  and  $U^{238}$ , and the values obtained (after adjustment) were;

$$U^{235}: \bar{\nu} = 2.25 + 0.132 E \text{ (before adjustment; } \bar{\nu} = 2.46 + 0.144 E)$$

$$U^{238}: \bar{\nu} = 2.32 + 0.129 E \text{ (before adjustment; } \bar{\nu} = 2.53 + 0.141 E).$$

(The reduction in the  $\bar{\nu}$  value for  $U^{235}$  alone was not sufficient to give agreement with the experimental values for the reflected systems.) These data for  $U^{235}$  and  $U^{238}$  are included in AWRE Report 0-28/60 [2].

The data described above lead to calculated critical sizes for low-enriched  $U^{235}$  systems which are significantly at variance with experimental values, and due to the growing interest in fast-reactor calculations this disagreement becomes a serious deficiency. This deficiency could obviously be remedied by a readjustment of the current data in a more elaborate way than hitherto, but in view of the time lapse since the previous compilation was made and the additional experimental data which is now available, it has been decided to do a full revision of the  $U^{235}$  and  $U^{238}$  neutron cross-sections in the region above 1 keV\*, and then to adjust these revised data so that they give the correct critical masses, to within say  $\pm 3\%$  of the experimental values, for a range of high- and low-enriched  $U^{235}/U^{238}$  systems. The results presented in this paper should be of

\* This work is now in progress.

assistance in deciding these adjustments, although a multi-group perturbation code\* for the IBM-7090 has now been written at AWRE which should further assist with this problem. It is however interesting and instructive at this stage to make a *preliminary* examination of the problem of adjusting the data, and to get some appreciation as to how far the results given in the present paper can be used in deciding these adjustments. For this purpose, it is convenient to begin with the current AWRE data and to examine how these might be adjusted in a fairly simple way to give better — though not necessarily adequate — agreement between the calculated and experimental critical sizes for the systems considered in the present paper.

The experimental values for the critical masses of the systems considered in the present paper are given in Table VI, along with the values calculated from

TABLE VI  
COMPARISON OF THE EXPERIMENTAL AND CALCULATED CRITICAL SIZES  
using the current AWRE data for  $U^{235}$  and  $U^{238}$

System	Experimental critical mass (kg)	Calculated critical mass (20 energy groups) (kg)	Error in calculated value
94%- $U^{235}$ bare sphere	51.9 [8]	51.9	0
29%- $U^{235}$ bare sphere	377 [9]	437	+16%
94%- $U^{235}$ reflected sphere	18.25* [8]	18.01	— 1.3%
30%- $U^{235}$ reflected sphere	130* [9]	165	+26%

\* These values are deduced by the author from experimental values for slightly different systems.

the current AWRE data using twenty energy groups between 1.6 keV and 11 MeV. A large number of groups were used to eliminate, as far as possible, errors due to the group approximation. The calculations were carried out by the  $S_n$  method in the  $S_8$  approximation [1], using the transport approximation [4]. It will be noted that the errors in the calculated values for the low-enriched systems are quite large.

In deciding the adjustments which must be made to the current AWRE data to give better agreement between the calculated and experimental critical sizes for the low- and high-enriched systems. (simultaneously) it is desirable to exploit some of the changes suggested by recent experimental evidence, but without going into much detail.

The current "world consistent" value of  $\bar{v}$  ( $U^{235}$ ) at thermal energies is  $2.43 \pm 0.02$  [5]; one finds that with  $\bar{v} = 2.43 + 0.143 E$  (this corresponds to in-

\* The code takes the output from  $S_n$  calculations as its input, and calculates various functions required in the application of perturbation theory. It is then a simple matter to calculate by perturbation theory the effect on critical mass or reactivity due to specified changes in the neutron-scattering data.

creasing the current AWRE values by 8%) the calculated critical masses of the high-enriched systems are gross underestimates, though the calculated critical masses of the low-enriched systems are greatly reduced in error. A slightly lower value of  $\bar{\nu}$  helps to reduce the *maximum* error which occurs. Alteration of the slope of the variation of  $\bar{\nu}$  with energy, assuming a linear variation and keeping the thermal value fixed, will itself not produce simultaneous agreement between the calculated and experimental critical sizes for the low- and high-enriched systems considered, but a slope of  $0.08 \text{ MeV}^{-1}$ , for instance, does help to reduce the maximum error which occurs. Once the range of errors has been brought within reasonable limits by adjustment of the  $\bar{\nu}(\text{U}^{235})$  value, it is not as difficult to reduce them to acceptable values by reasonable adjustments of other aspects of the data. From the above considerations, it is suggested that  $\bar{\nu}(\text{U}^{235}) = 2.42 + 0.08 E$  is a reasonable choice for the present investigation; in order to obtain the effect of this on the critical masses from the results given in Section 1, it is necessary to think of it arising as the result of two independent changes, first a  $7\frac{1}{2}\%$  increase in  $\bar{\nu}$  leading to  $\bar{\nu} = 2.42 + 0.142 E$ , and then a change of slope. The effect of the first change is obtained directly from Tables I — IV, and the effect of the second is obtained by interpolation between the entry just referred to (slope  $0.142 \text{ MeV}^{-1}$ ) and the entry corresponding to  $\bar{\nu} = 2.42$  (zero slope). The effects of taking  $\bar{\nu} = 2.42 + 0.08 E$  are summarized in Table VII.

From a recent survey of  $\bar{\nu}$  values for  $\text{U}^{238}$  by HANNA [6], there is an indication that  $\bar{\nu}(\text{U}^{238})$  in the AWRE data should be increased by 4%. There is also considerable uncertainty in the  $\text{U}^{238}(n, \gamma)$  cross-section, and evidence — mainly

TABLE VII  
THE EFFECT ON CRITICAL MASS OF MAKING PARTICULAR ADJUSTMENTS  
TO THE DATA\*

System	Change in calculated critical mass resulting from					(v) Net change in critical mass due to (i), (ii), (iii), (iv) and (vi) (%)	(vi) New estimate of calculated critical mass based on (v) (kg)	(vii) New calculated critical mass after making changes (i) — (iv) in data (see Section 4) (kg)	(viii) Error in new calculated critical mass (%) relative to experimental values (%)
	(i) $\bar{\nu}(\text{U}^{235}) = 2.42 + 0.08 E$ (%)	(ii) $\bar{\nu}(\text{U}^{235})$ increased by 4% (%)	(iii) $\sigma_{\gamma}(\text{U}^{238})$ decreased by 15% (%)	(iv) $\sigma_{\text{nif}}(\text{U}^{235})$ decreased by 5% (%)					
94% - $\text{U}^{235}$ bare sphere	-12.3	-0.2	-0.2	+9.3	-	3.4	50.1	50.0	-3.7
29% - $\text{U}^{235}$ bare sphere	-13.3	-2.7	-5.6	+9.0	-	12.6	382	378	+0.3
94% - $\text{U}^{235}$ reflected sphere	-13.8	-1.1	-3.3	+9.0	-	9.2	16.4	16.7	-8.5
30% - $\text{U}^{235}$ reflected sphere	-17.6	-3.4	-9.5	+9.0	-	21.5	130	134	+3.1

\* Cf. Section 3.

from integral measurements in reactor systems — suggests that the present curve should be reduced by 15%. The effect of this and of the increased  $\bar{\nu}$  ( $U^{238}$ ) are summarized in Table VII.

The combined effects of the above changes to  $\bar{\nu}$  ( $U^{235}$ ),  $\bar{\nu}$  ( $U^{238}$ ) and to the  $U^{238}$  ( $n, \gamma$ ) cross-section should lead to calculated critical masses which are too low (cf. Table VII). If, however,  $\sigma_f(U^{235})$  is uniformly reduced by 5% over the energy range of the present systems, that is, a few keV — 11 MeV, then the calculated critical masses of all except the 94%- $U^{235}$  reflected sphere should be within  $\pm 3\%$  of the experimental values. The 5% change in  $\sigma_f(U^{235})$  is within its experimental error over most of the relevant energy range [7]. The effect of the 5% reduction in  $\sigma_f(U^{235})$  on the systems considered is given in Table VII, together with the combined effects of all four adjustments considered. The expected values of the calculated critical masses on the basis of these adjustments are listed in the same Table. For comparison, the critical masses listed in the last but one column are obtained by direct calculation\*, after making the adjustments to  $\bar{\nu}$  ( $U^{238}$ ),  $\sigma_f(U^{238})$  and  $\sigma_{n\gamma}(U^{238})$  as described, but with  $\bar{\nu}$  ( $U^{235}$ ) given by:

$$\begin{aligned}\bar{\nu} &= 2.42 + 0.08 E & 0 < E < 6 \text{ MeV} \\ &= 1.1 + 0.3 E & 6 \text{ MeV} < E < 9 \text{ MeV} \\ &= 2.90 + 0.10 E & 9 \text{ MeV} < E\end{aligned}$$

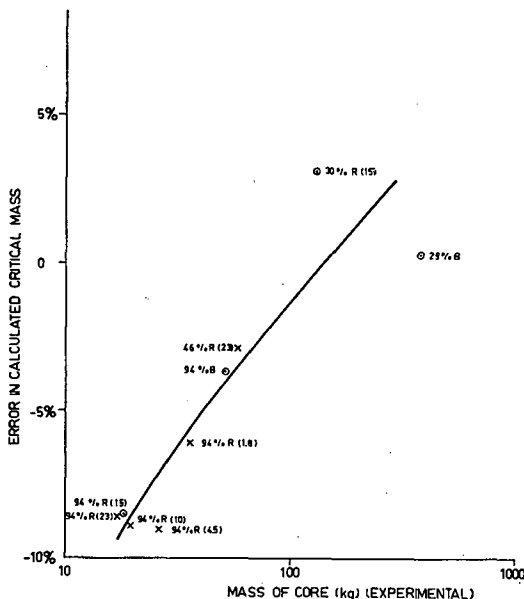


Fig. 3

Error in calculated critical mass (using adjusted data) as a function of core mass.

$x\% B = x\% U^{235}$  bare sphere  
 $x\% R(y) = x\% U^{235}$  sphere reflected by  $y$  cm of natural uranium  
 ○ Systems studied in present paper  
 × Other systems

\* Using eighteen energy groups between 10 keV and 11 MeV with the  $S_n$  method in  $S_8$  approximation.

in order to be consistent with experimental values at 14 MeV. This further modification to  $\bar{\nu}$  ( $U^{235}$ ) should not have much effect on the calculated critical masses, since only a small fraction of neutrons have energies greater than 6 MeV.

The agreement between the masses in columns (vi) and (vii) in Table VII clearly demonstrates the satisfactory use of the results in Tables I-IV in predicting the effect on critical mass of changes in the basic data. A comparison of the critical masses obtained by direct calculation using the adjusted data, with the experimental values (cf. last column of Table VII), indicates that it should be possible to obtain simultaneous agreement between calculated and experimental critical sizes by making reasonable adjustments to the basic data. The adjusted data which lead to the results in Table VII are not sufficiently accurate for general use in computations involving low- and high-enriched systems, as is shown by the  $-8\frac{1}{2}\%$  discrepancy which still exists in the case of the 94-%  $U^{235}$  reflected sphere. The inadequacy of the data is more clearly demonstrated by Fig. 3, in which the error on the critical masses — calculated using this adjusted data — of a wide range of high- and low-enriched systems (including those already studied) are plotted as a function of core mass. If the cross-section data were absolutely correct, then the points in Fig. 3 should be more or less randomly distributed about the line corresponding to zero error; instead, they appear to be random about a curve. This emphasizes the need to consider a large number of experimental systems, covering as wide a range as possible when making data adjustments; for instance, in the present case, if only the systems (a) and (b), or (a), (b) and (d) had been considered, one might have been led to conclude from the results in Table VII that the adjusted data were sufficiently accurate for general use.

#### ACKNOWLEDGEMENTS

Thanks are due to Dr. K. Parker of the Mathematical Physics Division, AWRE, for helpful comments during the preparation of the manuscript, and to Mr. J. H. Bird for organizing the calculations reported in Section 1.

#### REFERENCES

- [1] CARLSON, B. G., Solution of the transport equation by  $S_n$  approximations, LA-1891 (1955).
- [2] BUCKINGHAM, B. R. S., PARKER, K. and PENDLEBURY, E. D., Neutron cross-sections of selected elements and isotopes for use in neutronics calculations in the range 0.025 eV—15 MeV, AWRE Report 0-28/60 (1960).
- [3] PARKER, K., Machine production of group cross-sections for use in Carlson  $S_n$  and other multi-group neutronics calculations on high speed computers, AWRE Report 0-1/61 (1961).
- [4] PENDLEBURY, E. D. and UNDERHILL, L. H., *These proceedings*, vol. I, p. 73.
- [5] HUGHES, D. J., MAGURNO, B. A. and BRUSSEL, M. K., Neutron cross-sections, BNL-325, 2nd ed., Suppl. I (1960.)
- [6] HANNA, G. C., A survey of published values of  $\bar{\nu}$  in the fast fission of  $U^{238}$ , CPR-936 (1960).
- [7] HOWERTON, R. J., Tabulated neutron cross-sections, Part 1, Vol. 3, UCRL-5226 (Revised) (1959).
- [8] HANSEN, G. E., PAXTON, H. C., and WOOD, D. P., Critical masses of orraloy in thin reflectors, LA-2203 (1958).
- [9] PAXTON, H. C., Critical masses of fissionable metals as basic nuclear safety data, LA-1958 (1957).

# THE EFFECTS OF ERRORS IN CROSS-SECTION DATA ON CALCULATIONS FOR A LARGE DILUTE FAST REACTOR

T. P. MOORHEAD

ATOMIC ENERGY ESTABLISHMENT, WINFRITH,  
UNITED KINGDOM

**Abstract — Résumé — Аннотация — Resumen**

**The effect of errors in cross-section data on calculations for a large dilute fast reactor.** The neutron physics of a large power fast reactor with a 1500 l core containing about 1000 kg of plutonium have been calculated using five-group diffusion theory. The effect on the critical size and breeding ratio of varying each cross-section in turn has been determined. The most important use of the results is to indicate the accuracy required for the cross-section data used in this type of calculation, but they can also be used to estimate the effect on the reactor of small changes in core composition or neutron spectrum.

**Effet des erreurs sur les sections efficaces dans les calculs d'un grand réacteur à neutrons rapides.** L'auteur calcule dans une théorie de diffusion à cinq groupes la physique neutronique d'un grand réacteur de puissance à neutrons rapides dont le cœur de 1500 l contient environ 1000 kg de plutonium. Il fait varier successivement chaque section efficace, et détermine l'effet sur les dimensions critiques et le taux de surgénération. L'intérêt primordial des résultats est d'indiquer la précision requise pour les valeurs des sections efficaces dans ce genre de calcul, mais ils peuvent également servir à évaluer les effets sur le réacteur de faibles modifications dans la composition du cœur ou dans le spectre neutronique.

**Влияние ошибок в данных о поперечном сечении на расчеты для большого быстрого реактора на разбавленном топливе.** Физический расчет большого энергетического реактора на быстрых нейтронах с активной зоной реактора 1.500 литров, содержащего около 1.000 кг плутония, осуществляется путем использования 5-групповой теории диффузии. Влияние на критические размеры и коэффициент воспроизведения определяется в свою очередь колебанием каждого поперечного сечения. Наиболее важное использование результатов состоит в том, чтобы указать на точность, требуемую для данных поперечного сечения, используемых в этом типе расчета, но они могут быть также использованы, чтобы оценить влияние на реактор небольших изменений в строении активной зоны реактора или нейтронного спектра.

**Influencia de errores en los datos de secciones eficaces sobre los cálculos de un reactor rápido diluido de grandes dimensiones.** Con ayuda de una teoría de difusión de cinco grupos, el autor ha efectuado una serie de cálculos de física neutrónica relativos a un reactor de potencia rápida de grandes dimensiones cuyo cuerpo, de 1500 l, contiene unos 1000 kg de plutonio. Determinó la influencia ejercida sobre la masa crítica y la razón de reproducción al modificar sucesivamente cada una de las secciones eficaces. Estos resultados permiten ante todo evaluar la exactitud que han de presentar los datos sobre secciones eficaces que se utilicen en cálculos de este tipo, pero también sirven para calcular los efectos que ejercen sobre el reactor ligeras modificaciones de la composición del cuerpo o del espectro neutrónico.

## Introduction

Nuclear cross-sections for fast-neutron reactions suitable for use in multi-energy-group calculations are difficult to determine with accuracy. Further, no fully detailed assessment of the degree of accuracy desirable for studies of future large dilute systems has yet been made.

An attempt is made in this report to correlate the effects of many individual cross-section variations on calculations for a typical large fast power reactor. The reactivity and breeding ratios of the system were the properties chosen for study, but these may be related to other properties such as critical mass and power distribution by means of the various data recorded. The results provide a guide to the accuracy needed in cross-section measurements, and also make possible some estimate of the degree of error likely in calculations based on the cross-sections. In later parts of the work various other useful inferences are drawn, and consideration is given to reactors of differing composition.

Computer methods employing five-group diffusion theory applied to true cylindrical geometry were used. Sufficient data and details of the methods are included to enable calculations to be repeated, if desired.

## 1. Methods

1.1. The methods used are based on the use of the HASSITT programme [1], for the Mercury computer. The following reasons guided this choice:

(a) It enables consideration of a short cylindrical core, which may be desirable in future highly-rated fast reactors.

(b) It uses as input macroscopic cross-sections, upon which our correlation method is based.

(c) There are no restrictions on the number of inelastic transfer cross-sections, except by flexible storage limits.

(d) A complete mechanized system has been developed [2, 4, 5] in connection with the Hassitt programme, to obtain the required input parameters quickly, and to obtain flux integrals, breeding ratios, neutron balance, etc., simply, in any number of groups.

The use of five energy groups was a reasonable compromise between what was desirable and what was practical in terms of effort and machine time. The results can be referred back to the original multi-group cross-sections.

The method of use of the Hassitt programme is described in Ref. [2]. The restrictions mentioned in that memorandum have since been eased by larger storage capacity on Mercury.

1.2. The basic cross-sections used were the ANL 11-group set, [3], and the 5-group constants required were produced by the usual flux-weighting process, which is described in Section 3.

1.3. The Hassitt programme uses as input total macroscopic cross-sections for the composite material. Having established a critical basic case, these macroscopic cross-sections were varied one at a time, and the change in reactivity obtained. If  ${}^M\Sigma$  is any type macroscopic cross-section for the isotope  $M$ , and  $T\Sigma$  is the corresponding total cross-section for the core or blanket material,

$$T\Sigma = \sum_M ({}^M\Sigma) = \sum_M ({}^M A \cdot {}^M \sigma)$$

where  $\sum_M$  indicates summation over the isotopes  $M$ ,  ${}^M A$  is the number of atoms per cubic centimetre and  ${}^M \sigma$  the microscopic cross-section of each isotope  $M$  in the composition.

Hence if  $T\Sigma$  is changed by  $P\%$ , this is equivalent to a change of  $P \times {}^T \Sigma / {}^M \Sigma \%$  in any individual  ${}^M \Sigma$ , and to a similar change in  ${}^M \sigma$  (or  ${}^M A$ ). Thus changes can be correlated for each isotope  $M$ . This is the basis of the methods used, but complications arise in allowing for effects from both core and blanket, and in dealing with transport and fission cross-sections. Further details are given in Section 6. Blanket effects obviously could not be neglected because breeding ratios were to be considered.

1.4. The Hassitt 'NU' tape facility was used in most of the many cases considered, substantially reducing computer time in iteration. A complete flux print was obtained from each case, for subsequent integration, and production of breeding ratios, etc. The method of correlating the breeding-ratio changes is dealt with in Section 10.

## 2. Reactor model

2.1. The system studied has a cylindrical core with height equal to radius, and a heat rating of 1000 MW, using the carbides of plutonium and uranium as fuel, with iron structure, sodium coolant and metallic-uranium blankets. Details are set out in Table I. The size of the core was decided by the coolant conditions, assuming a temperature rise of 200°C in each core channel, and limiting the maximum coolant speed at the core centre to about 10 m/s. Criticality was then achieved by varying the fuel enrichment.

Two points should be noted about the figures in Table I:

TABLE I  
FIXED PARAMETERS OF MODEL STUDIED

Core diameter (cm)		156.2
Core height (cm)		78.1
Core volume (l)		~1,500
Axial and radial blankets, thickness (cm)		45
Composition (volume per cent)		
Core	{ Fuel Fe Na	45% 20% 35%
Blankets	{ Natural uranium metal Fe Na	60% 20% 20%
Fuel		PuC and UC
using irradiated Pu	{ Pu <sup>239</sup> Pu <sup>240</sup>	80% 20%
and natural U, allowing 0.7% U <sup>235</sup> .		
Theoretical density of PuC and UC (mol./cm <sup>3</sup> )		0.0328 × 10 <sup>24</sup>
Assumed density of PuC and UC, 80% of theoretical (mol./cm <sup>3</sup> )		0.02624 × 10 <sup>24</sup>

(a) In practice, the axial blankets could hardly have less sodium fraction than the core, assuming axial coolant flow (for this study, however, two different blanket compositions would have been an unnecessary complication).

(b) Carbide density fractions better than 80% may be possible.

These are considered in Section 16.5 and Section 14.3 respectively.

### 3. Cross-section data

3.1. The basic cross-section data used was that given by LOEWENSTEIN and OKRENT [3], who use eleven groups with energy ranges well suited to fast-reactor work. To reduce the number of groups to five, an approximate 11-group spectrum is necessary for a similar composition. In this case, a spectrum was available for a similar composition, though with a smaller and less dilute core, considered in Ref. [3], model 7, Table XII. The integrated spectra given there for core and blanket were used to produce the 5-group constants used for this study. Effects of the spectrum assumption made are considered in Section 16 (8 and 9).

3.2. The relation between the 5-group system used and the 11-group system is shown in Table II, together with the integrated spectra normalized to total 1 in core and blanket.

3.3. The flux-weighting processes used to produce 5-group constants from 11-group are defined in Ref. [4]. Based on the spectra of Table II, the sets of 5-group cross-sections produced for core and blanket are given in Table III. It will be seen that for five groups the effect of the different averaging spectra

TABLE II  
5-GROUP AND 11-GROUP SYSTEMS AND MULTI-GROUP SPECTRA

5-group system	11-group system				
	Group No.	Lower energy boundary (MeV)	Lethargy interval	Normalized integrated spectra for averaging	
5-group system				Core	Blanket
1	1	2.25	—	0.046	0.012
	2	1.35	0.5	0.056	0.018
2	3	0.825	0.5	0.076	0.038
	4	0.5	0.5	0.114	0.107
	5	0.3	0.5	0.129	0.146
3	6	0.18	0.5	0.115	0.141
	7	0.11	0.5	0.104	0.128
	8	0.067	0.5	0.092	0.124
4	9	0.025	1.0	0.119	0.159
	10	0.0091	1.0	0.075	0.080
5	11	0	—	0.074	0.046

for core and blanket is fairly small, but whether it may or may not be neglected is considered in Section 16 (8 and 9).

The group-transfer cross-sections quoted are the total of inelastic and elastic transfer where appropriate, but the contribution of elastic transfer is also shown separately.

3.4. A difficulty must be noted regarding the transport cross-sections. Evidence both from transport theory [6] and from comparative calculation indicates that, instead of "averaging"  $\sigma_{tr}$  or  $T\Sigma_{tr}$  over the energy range, the average of transport mean free paths ( $1/T\Sigma_{tr}$ ) should be taken, equivalent to averaging the diffusion coefficient  $D$ . This latter process was used in this study. However, those processes, which depend on summing the averaged cross-sections, are complicated by the averaging of the reciprocals, and it is easily shown that in general the correct average value of  $D$  for a mixture of isotopes cannot be obtained from values of the microscopic cross-sections of the individual isotopes, averaged either directly or by reciprocals.

In Table III, the transport cross-sections quoted are the reciprocals of the averaged mean free paths for each isotope separately. If these are used with the appropriate atomic densities (Table V) to produce the total macroscopic transport cross-sections, it will be found that these do not agree exactly with  $\Sigma_{tr}$  and  $D$  as given in Table IV. However, with five groups the discrepancies are generally insignificant. The effect would become important where large cross-section variations are hidden within a broad group, say for 1-, 2-, or 3-group calculations.

The correct method is to start all calculations from the basic set of multi-group data being used, to find the  $D$ -values, and to average these; not to average the transport cross-sections of the separate isotopes. The averaging of  $D$  gives the best agreement between few-group and multi-group calculations; but it should be recalled that the usual definition of  $D$  is itself only an approximation.

#### 4. Basic case

4.1. The size and composition of the basic case was fixed as explained, excepting only the proportion of Pu to U in the fuel. This proportion was adjusted, keeping total fuel atoms constant, to bring the basic case very close to critical, as calculated by the Hassitt programme. The full flux output at all groups and mesh points was obtained and fed to programme 255 for production of flux integrals and form factors and subsequent calculation of breeding ratios and neutron balance.

4.2. The critical atomic composition is given in Table V. This composition applies to the basic case and throughout all the cases of cross-section changes recorded in Tables VII, VIII, etc. Critical mass, breeding ratios and other details are also given in Table V.

4.3. Table VI gives flux and flux-integral details, showing also for comparison the spectrum from Table II, which had been used in reducing the number of groups. The slightly softer spectrum of our basic case reflects the higher degree of dilution of the fuel; but the agreement between the assumed and calculated spectra is good enough to give confidence that the 5-group cross-sections obtained (Table III) are compatible with the spectrum of our basic case.

4.4. The necessary 5-group constants for data for the Hassitt programme were obtained from programme 228, with also sets of macroscopic cross-sections for the individual isotopes throughout core and blanket. The 5-group *total* macro-

TABLE III  
5-GROUP MICROSCOPIC CROSS-SECTIONS APPLYING TO BASIC CASE  
Cross-sections in barns

	Isotope	Group No. S	Group transfer cross-sections												Cross-sections for elastic transfer only	
			$\sigma_{tr}$		$\sigma_c$		$\sigma_f$		$\nu$ neutrons/fission		$\sigma_{R \leftarrow S}$					
			Core	Blanket	Core	Blanket	Core	Blanket	Core	Blanket	Core	Blanket	Core	Blanket	Core	Blanket
Pu <sup>239</sup>	1	4.60	—	—	0.061	—	1.97	—	3.13	—	0.814	—	0.126	—	0.0	—
	2	6.14	—	—	0.135	—	1.76	—	2.97	—	—	—	0.330	—	0.038	—
	3	9.42	—	—	0.392	—	1.73	—	2.92	—	—	—	—	—	0.061	—
	4	13.62	—	—	0.863	—	2.10	—	2.91	—	—	—	—	—	0.043	—
	5	16.80	—	—	2.100	—	3.50	—	2.91	—	—	—	—	—	—	0.043
Pu <sup>240</sup>	1	4.60	—	—	0.053	—	1.54	—	2.60	—	1.13	—	0.224	—	0.0	—
	2	6.16	—	—	0.195	—	0.644	—	2.47	—	—	—	0.271	—	0.0	—
	3	9.42	—	—	0.307	—	0.011	—	2.47	—	—	—	—	—	0.124	—
	4	13.62	—	—	0.816	—	0.0	—	—	—	—	—	—	—	0.0	—
	5	16.80	—	—	1.500	—	0.0	—	—	—	—	—	—	—	0.050	—
U <sup>235</sup>	1	4.50	4.50	0.100	0.100	1.29	1.29	2.70	2.70	1.45	1.47	0.215	0.220	0.0	0.0	0.0
	2	5.44	5.59	0.153	0.162	1.24	1.25	2.53	2.53	—	—	0.541	0.583	0.066	0.071	0.0018
	3	9.21	9.25	0.342	0.346	1.62	1.63	2.48	2.48	—	—	—	—	0.076	0.078	0.0018
	4	12.70	12.64	0.884	0.857	2.73	2.67	2.47	2.47	—	—	—	—	—	0.029	0.025
	5	14.30	14.30	2.520	2.520	6.00	6.00	2.47	2.47	—	—	—	—	—	—	0.029
U <sup>238</sup>	1	4.59	4.58	0.041	0.044	0.513	0.504	2.60	2.60	1.81	1.84	0.361	0.367	0.0	0.0	0.0
	2	5.78	5.96	0.135	0.135	0.0007	0.0004	2.48	2.49	—	—	0.310	0.330	0.0	0.0	0.0
	3	9.38	9.42	0.211	0.214	0.0	0.0	—	—	—	—	—	—	0.168	0.180	0.0
	4	12.70	12.64	0.481	0.470	0.0	0.0	—	—	—	—	—	—	—	0.054	0.049
	5	14.30	14.30	0.800	0.800	0.0	0.0	—	—	—	—	—	—	—	—	0.042

TABLE IV  
TOTAL MACROSCOPIC CROSS-SECTIONS APPLYING TO BASIC CASE  
Cross-sections in  $\text{cm}^{-1}$

Group Transfer Cross-Sections $\Sigma_R \leftarrow S$											
Group No.	S	Fission neutron distribution $\chi_r$	Diffusion coefficient $D$	$\Sigma_{tr}$	$\Sigma_c$	$\Sigma_f$	$\Sigma_a$	$\nu \Sigma_f$	R = 2		
									R = 2		
									3	4	5
									Elastic Total	Elastic Total	Elastic Total
									Elastic only	Total	Elastic only
Core	1	0.574	2.6732	0.1247	0.00060	0.00828	0.00888	0.02285	0.03726	0.00574	0.00563
	2	0.360	1.9831	0.09171	0.00171	0.00422	0.00422	0.00733	—	0.01331	0.00863
	3	0.058	1.3019	0.2560	0.00289	0.00230	0.00520	0.00667	—	—	0.00957
	4	0.008	0.9894	0.3389	0.00665	0.00284	0.00949	0.00817	—	—	0.00833
	5	0	0.7637	0.4364	0.01170	0.00484	0.01655	0.01390	—	—	0.00597
Blanket	1	0.574	1.8941	0.1760	0.00136	0.01468	0.01604	0.03814	0.06600	0.00221	0.01198
	2	0.360	1.4603	0.2233	0.00398	0.00424	0.00424	0.00666	—	0.01347	0.00454
	3	0.058	0.9306	0.3552	0.00631	0.00033	0.00634	0.00081	—	—	0.00736
	4	0.008	0.6863	0.4887	0.01398	0.00053	0.01452	0.00132	—	—	0.00435
	5	0	0.5637	0.5914	0.02364	0.00120	0.02484	0.00296	—	—	0.00284

TABLE V  
PHYSICAL DETAILS RELATING TO BASIC CASE

Critical composition, atoms $\times 10^{24}$ per cubic centimetre of core of blanket material			
<i>Isotope</i>	<i>Core</i>		<i>Blanket</i>
$Pu^{239}$	0.001260	Total	—
$Pu^{240}$	0.000315	fuel	—
$U^{235}$	0.000072	atoms	0.00020
$U^{238}$	0.010161	0.011808	0.02860
Fe	0.016940		0.01694
Na	0.007700		0.00440
C	0.011808		—

General details of system, initial clean conditions			
Hassitt "NU"			0.99970
$k_{eff}$ (See 7.2)			1.00030
Concentration of $Pu^{239}$ (gm/cm <sup>3</sup> of core)			0.4998
Concentration of irrad. Pu (gm/cm <sup>3</sup> of core)			0.6248
Atomic ratio, $U^{238}/Pu^{239}$ in core			8.064
Critical mass of $Pu^{239}$ (kg)			748
Mass of irradiated Pu (kg)			935
$k_\infty$ for core { centre spectrum			1.349
integrated spectrum			1.336
Median fission energy (MeV)			0.28
Ratio $Pu^{239}$ captures to fissions			0.248

Breeding ratios, thermally fissile atoms			
<i>Produced</i>	<i>Destroyed</i>	<i>Internal</i>	<i>Total</i>
$Pu^{239}$	$Pu^{239}$	0.872	1.681
$Pu^{239}, Pu^{241}$	$Pu^{239}$	0.916	1.725
$Pu^{239}, Pu^{241}$	$Pu^{239}, U^{235}$	0.866	1.556

Breeding ratios in parts of blankets, $Pu^{239}$ produced in blanket to $Pu^{239}$ destroyed in core			
Radial blanket			0.319
Axial blanket			0.423
Corner blanket			0.066
<i>Total blankets</i>			<u>0.808</u>

scopic cross-sections corresponding with the data of Table V are shown in Table IV. These are the actual constants to which all the cross-section changes of Table VII refer. The transport cross-sections quoted are those obtained by averaging  $D$ , as explained in Section 3.4.

- 4.5. The number and size of mesh spacings used in the Hassitt data, for the

TABLE VI  
FLUX DETAILS FOR BASIC CASE

Group $R$	Spectrum at core centre $\Phi_R$	Normalized flux integrals $\Phi_R$			
		Core		Blanket	
		Cylindrical basic case	Assumed spectrum from Table II	Cylindrical basic case	Assumed spectrum from Table II
1	0.094	0.088	0.102	0.034	0.030
2	0.325	0.322	0.319	0.299	0.291
3	0.322	0.328	0.312	0.397	0.394
4	0.193	0.198	0.194	0.230	0.239
5	0.065	0.064	0.074	0.041	0.046
Total flux integral ratios, Core					1.000
Radial blankets					0.128
Axial blankets					0.170
Corner blankets					0.026
<i>Total blankets</i>					0.324
Core flux, radial form factor					0.57
Core flux, overall form factor					0.46
Core flux, axial form factor					0.81
Aggregate flux integrals (n/cm s) producing 1.0000 fission/s in core and 0.0894 fission/s in blankets (from Table XIV)			<i>Core</i>	<i>Blanket</i>	
			315.8	102.2	
<i>For total heat output of 1000 MW</i>					
Core heat production (MW)					918
Blanket heat production (MW)					82
Average core flux (n/cm <sup>2</sup> )					$6.0 \times 10^{15}$
Max. flux at core centre (n/cm <sup>2</sup> )					$1.3 \times 10^{16}$

basic case and all cases of Table VII etc., were as follows:

Core: radial, 11 at 7.1 cm; axial, 8 at 4.88125 cm.

Blankets: radial, 5 at 9.0 cm; axial, 6 at 7.5 cm.

A fairly small number of points was taken to economize on computer time, but large changes of mesh at boundaries were avoided. The calculation assumes symmetry about the centre plane, so that the axial mesh refers to half the height.

A full neutron balance for the basic case is given in Tables XIV, XV (Section 15) and effects of finer mesh are recorded in Section 16.3.

## 5. Mass-reactivity correlations

5.1. Many of the results are given in terms of reactivity changes, but the following expressions, obtained from extra computer cases, correlate changes in  $k_{\text{eff}}$  with changes of critical mass  $C$  of  $\text{Pu}^{239}$ , for various ways of adjusting the mass.

5.2. Varying enrichment, keeping total fuel atoms constant (Table V):

TABLE VII  
CHANGES IN  $k_{\text{eff}}$  PRODUCED BY CHANGES IN TOTAL MACROSCOPIC CROSS-SECTIONS\*

Group	$D$	$k_{\text{eff}}$	$\Sigma_e$	$k_{\text{eff}}$	$\Sigma_f$	$k_{\text{eff}}$	$\nu$	$k_{\text{eff}}$	Group transfers $R \leftarrow S$	$\Sigma_{R \leftarrow S}$	$k_{\text{eff}}$
Core cross-section changes											
1	-9.09%	+0.002 60	-20%	+0.001 27	+~5%	+0.007 04	+5%	+0.011 03	2 $\leftarrow$ 1	-10%	+0.008 03
2	-9.09%	+0.004 82	-10%	+0.005 26	+~5%	+0.009 07	+5%	+0.012 80	3 $\leftarrow$ 1	-20%	+0.003 05
3	-9.09%	+0.002 84	-10%	+0.008 38	+~5%	+0.008 38	+5%	+0.011 57	3 $\leftarrow$ 2	-10%	+0.003 64
4	-9.09%	+0.001 30	-10%	+0.010 63	+~5+	+0.006 42	+5%	+0.008 64	4 $\leftarrow$ 2	-100%	+0.002 05
5	-9.09%	+0.000 45	-10%	+0.006 63	+~5%	+0.003 54	+5%	+0.004 86	4 $\leftarrow$ 3	-10%	+0.002 80
1			-10%	+0.000 63	+~5%	+0.006 28	+2½%	+0.005 45	5 $\leftarrow$ 4	+20%	+0.000 61
2	+9.09%	-0.004 50	+10%	-0.005 20	-	-	-	-	3 $\leftarrow$ 1	-10%	+0.001 53
									5 $\leftarrow$ 4	-10%	-0.000 35
									2 $\leftarrow$ 1	+10%	-0.007 08
Blanket cross-section changes											
1	-9.09%	+0.000 73	-20%	+0.000 11	+~5%	+0.000 43	+5%	+0.000 76	2 $\leftarrow$ 1	-10%	+0.000 80
2	-9.09%	+0.002 02	-10%	+0.000 92	+~20%	+0.000 20	+20%	+0.000 32	3 $\leftarrow$ 1	-20%	+0.000 36
3	-9.09%	+0.001 16	-10%	+0.001 35	+~20%	+0.000 38	+20%	+0.000 52	3 $\leftarrow$ 2	-10%	+0.000 75
4	-9.09%	+0.000 42	-10%	+0.001 25	+~20%	+0.000 40	+20%	+0.000 49	4 $\leftarrow$ 2	-100%	+0.000 21
5	-9.09%	+0.000 10	-10%	+0.000 40	+~20%	+0.000 18	+20%	+0.000 22	4 $\leftarrow$ 3	-10%	+0.000 51
1			-10%	+0.000 05	-	-	+10%	+0.001 54	5 $\leftarrow$ 4	+20%	-0.000 07
2	+9.09%	-0.001 91	-	-	-	-	-	-	3 $\leftarrow$ 1	-10%	+0.000 22
									5 $\leftarrow$ 4	-10%	+0.000 03
Core and blanket cross-section changes											
1	-9.09%	-	-	-	+~5%	+0.006 72	+5%	+0.011 79	2 $\leftarrow$ 1	-10%	+0.008 89
2	-9.09%	+0.006 72	-10%	+0.006 21	-	-	-	-	3 $\leftarrow$ 1	-20%	+0.003 61
									5 $\leftarrow$ 4	+20%	+0.000 55

\*  $k_{\text{eff}}$  for basic case 1.000 30.

$$\frac{dk}{k} = 0.54 \frac{dC}{C}. \quad (1)$$

Other relations of this type can be obtained from Table XIII.

5.3. Varying core radius only:

$$\frac{dk}{k} = 0.08 \frac{dC}{C} \quad (2)$$

5.4. Varying core height only:

$$\frac{dk}{k} = 0.18 \frac{dC}{C}. \quad (3)$$

5.5. Varying core size, keeping shape constant,  $H = 1/2D$ :

$$\frac{dk}{k} = 0.11 \frac{dC}{C}. \quad (4)$$

5.6. In obtaining these relations, height and/or radius were altered by 4% in (2), (3) and (4), and atoms of  $\text{Pu}^{239}$  by  $\sim 4\%$  in (1). Within these limits, the changes are linear within a few per cent. (4) may be used to show that changes like (2) and (3) are additive within  $\sim 3\%$ .

## 6. Calculation details

6.1. The intention of this study was not merely to record results of cross-section changes, but to correlate them in such a way that use can be made of them in estimating errors and effects of variations of the system. Essential requirements were: (a) that changes of cross-section should be approximately proportional to the changes produced in reactivity and breeding ratios, and (b) that the effects of several or many separate small changes should be approximately additive. The size of the changes made in the various cross-sections was chosen with these requirements in mind. Extra computer cases were run and cross-checks applied, to provide evidence on how far these requirements were upheld.

6.2. From the point of view of the multi-group diffusion equations, a change may be regarded as "small" if the proportional change in a given total macroscopic cross-section is small, and (a) and (b) of (6.1) should hold. Such a change may however be equivalent to much larger proportional changes in individual isotopic cross-sections (Section 1.3).

6.3. The ratios  ${}^T\Sigma/M\Sigma$  (Section 1.3) are not the same in the blanket as in the core; but an error, say in a capture cross-section of  $\text{U}^{238}$ , must be allowed for throughout the system. This raises a difficulty in correlation which was overcome by making changes separately in core and in blanket cross-sections. Results from these are useful in themselves (Table VII). The "proportional" and "additive" requirements of section 6.1 were then relied upon, with suitable checks, in allowing for both core and blanket effects when obtaining the results given in Table VIII.

6.4. From the "proportional" checks, it was found that  $k_{\text{eff}}$  was much more nearly proportional to  $D$  than to  ${}^T\Sigma_{\text{tr}}$ . It was, therefore, necessary to allow for this in the correlations, and in Table VII the changes shown of  $-9.09\%$  in  $D$  result from the original changes of  $+10\%$  in  ${}^T\Sigma_{\text{tr}}$ , while the changes of  $+0.09\%$

TABLE VIII  
PERCENTAGE CHANGES IN MICROSCOPIC CROSS-SECTIONS THROUGHOUT  
CORE AND BLANKET to produce 0.001 change in  $k_{\text{eff}}$

Isotope	Group	$\sigma_{\text{tr}}$ (%)	$\sigma_c$ (%)	$\sigma_f$ (%)	$\nu$ (%)	Group transfer $R \leftarrow S$	$\sigma_{R \leftarrow S}$ (%)
$\text{Pu}^{239}$	1	+ 75	— 120	+ 2.1	+ 1.3	2 $\leftarrow$ 1	— 48
	2	+ 41	— 19	+ 0.61	+ 0.44	3 $\leftarrow$ 1	— 230
	3	+ 69	— 7.0	+ 0.62	+ 0.45	3 $\leftarrow$ 2	— 87
	4	+ 140	— 5.7	+ 0.83	+ 0.66	4 $\leftarrow$ 2	— 390
	5	+ 420	— 6.7	+ 1.5	+ 1.1	4 $\leftarrow$ 3 5 $\leftarrow$ 4	— 430 + 3900
$\text{Pu}^{240}$	1	+ 300	— 560	+ 14	+ 8.2	2 $\leftarrow$ 1	— 140
	2	+ 160	— 52	+ 9	+ 5.7	3 $\leftarrow$ 1	— 530
	3	+ 280	— 34	+ 510	+ 320	3 $\leftarrow$ 2	— 410
	4	+ 550	— 24	—	—	4 $\leftarrow$ 2	—
	5	+ 1700	— 38	—	—	4 $\leftarrow$ 3 5 $\leftarrow$ 4	— 850 + 9800
$\text{U}^{238}$	1	+ 6.0	— 20	+ 1.2	+ 0.69	2 $\leftarrow$ 1	— 2.3
	2	+ 2.8	— 2.0	+ 220	+ 140	3 $\leftarrow$ 1	— 8.7
	3	+ 4.7	— 1.3	—	—	3 $\leftarrow$ 2	— 7.2
	4	+ 11	— 1.1	—	—	4 $\leftarrow$ 2	—
	5	+ 41	— 2.0	—	—	4 $\leftarrow$ 3 5 $\leftarrow$ 4	— 12 + 1000
$\text{U}^{235}$ (0.7% of nat. U)	1	+ 870	— 1200	+ 62	+ 37	2 $\leftarrow$ 1	— 420
	2	+ 430	— 240	+ 16	+ 10	3 $\leftarrow$ 1	— 1700
	3	+ 680	— 110	+ 12	+ 7.9	3 $\leftarrow$ 2	— 570
	4	+ 1600	— 85	+ 11	+ 8.4	4 $\leftarrow$ 2	— 2400
	5	+ 5800	— 91	+ 17	+ 12	4 $\leftarrow$ 3 5 $\leftarrow$ 4	— 2400 + 160 000
$\text{Fe}$	1	+ 11	— 110	—	—	2 $\leftarrow$ 1	— 4.3
	2	6.0	— 34	—	—	3 $\leftarrow$ 1	— 22
	3	9.0	— 25	—	—	3 $\leftarrow$ 2	— 13
	4	21	— 17	—	—	4 $\leftarrow$ 2	— 130
	5	56	— 71	—	—	4 $\leftarrow$ 3 5 $\leftarrow$ 4	— 15 + 270
$\text{Na}$	1	+ 23	— 4700	—	—	2 $\leftarrow$ 1	— 15
	2	+ 11	— 620	—	—	3 $\leftarrow$ 1	— 220
	3	+ 26	— 420	—	—	3 $\leftarrow$ 2	— 13
	4	+ 55	— 360	—	—	4 $\leftarrow$ 2	— 83
	5	+ 100	— 460	—	—	4 $\leftarrow$ 3 5 $\leftarrow$ 4	— 24 + 180
$\text{C}$	1	+ 23	—	—	—	2 $\leftarrow$ 1	— 15
	2	+ 9.5	—	—	—	3 $\leftarrow$ 1	—
	3	+ 17	—	—	—	3 $\leftarrow$ 2	— 7.4
	4	+ 46	—	—	—	4 $\leftarrow$ 2	—
	5	+ 170	—	—	—	4 $\leftarrow$ 3 5 $\leftarrow$ 4	— 7.5 + 62

Notes: 1. Refer to text under Sections 7, 8, 9.

2. A minus sign indicates that the change of cross-section and change of reactivity are opposite in sign.

were made for comparison. Further, the relation between individual isotopic transport cross-sections  ${}^M\Sigma_{tr}$  and the diffusion coefficient 'D' is less simple than that given in (1.3), bearing in mind also that average 'D' is taken (3.4). An approximate relation was obtained connecting  ${}^M\Sigma_{tr}$  and  $D$ , and this was used in arriving at the figures under  $\sigma_{tr}$  in Table VIII.

6.5. For other cross-sections, the proportional and additive requirements held usually within a few per cent of the small changes. "Additive" checks included superimposing core and blanket changes, combining several cross-section changes, and combining changes of different types of cross-section. In the transfer cross-section  $\Sigma_{2 \leftarrow 1}$ , which is large, changes of +10% and -10% were sufficient to show some departure from linearity (Table VII). A mean figure was taken in correlating for Table VIII.

A further difficulty arose in dealing with the fission cross-sections, for which the simple treatment of Section 1.3 could not be applied directly. This was because  $\Sigma_f$  is involved in  $\Sigma_a$  and also in  $\bar{\nu}\Sigma_f$ , where  $\nu$  also varies with the isotope considered. The "approximate" signs in Table VII are a consequence of this difficulty, as also are the two results given for group 1; the first was corrected to suit  $Pu^{239}$  fission cross-section, the second to suit  $U^{238}$ .

## 7. Reactivity correlations

7.1. Table VII shows the relation between the changes in total macroscopic cross-sections and the effective reproduction constant for the system,  $k_{eff}$ , as obtained from the Hassitt programme. The percentage changes applied to the cross-sections are shown, the cross-sections being those of the basic case, Table IV, and corresponding changes of  $k_{eff}$  are recorded, showing the differences from the basic case, 1.00030.

7.2. It will be remarked that these changes are recorded to five places of decimals. It was not expected that this order of accuracy would be possible, but during progress of the work considerable care was exercised regarding the convergence of the Hassitt 'NU' (output to six places) and the ability of the programme to produce consistent results.

The "proportional" and "additive" checks required by Section 6.1 give evidence of the excellent agreement obtained. See, for example, the results in Table VII for  $\nu$ , group 1, giving  $2\frac{1}{2}\%$  and 5% changes in the core, 5% and 10% changes in the blanket, and 5% changes in core and blanket together.

Hence, it is considered that the results shown, regarded as differentials, and with no changes in mesh, may be relied upon within 1% (or to 1 in the fifth decimal place if this is larger). It is not suggested, of course, that the absolute value of  $k_{eff}$  could be correct to five places; the truncation error alone is much larger than this, apart from the general approximations of diffusion theory.

The change of 0.00672 quoted for  ${}^T\Sigma_{f,1}$  change in core and blanket, is the result of combining blanket case (0.00043) with second group-1 core case (0.00628), showing good agreement.

7.3. Table VIII shows the relation between the various individual isotopic cross-sections, and  $k_{eff}$ , deduced as previously explained from Table VII. A small "standard" change of 0.001 in  $k_{eff}$  is taken throughout; the figure entered for a given cross-section shows the percentage change, or error, in that microscopic cross-section, necessary to produce this change of 0.001 in  $k_{eff}$ . Hence the relative importance of the various cross-sections is made evident; the smaller the percentage change, the more important the cross-section.

The figures for  $U^{235}$  are included for completeness. Since  $U^{235}$  is present only in small proportions, the changes in cross-sections necessary to produce 0.001 change in  $k_{\text{eff}}$  are large.

The microscopic cross-sections to which the percentage changes refer are those given in Table III.

## 8. Discussion

8.1. Table VII shows that  $k_{\text{eff}}$  is not very sensitive to some of the cross-section changes. However, the critical mass is a more sensitive parameter, and in Section 5 relations are given connecting  $k_{\text{eff}}$  and critical mass for various ways of adjusting the mass.

8.2. In Table VII,  $\nu$ , and then  $\Sigma_f$ , are, of course, the most sensitive parameters with  $\Sigma_c$  next. In observing the results, the relative fluxes in each group should be kept in mind (Table VI). This would explain, e.g., the  $\Sigma_{\text{tr}}$  results — if the flux in each group were equal, the importance of  $\Sigma_{\text{tr}}$  would drop off sharply from the highest-energy group to the lowest, as might be expected from considerations of leakage, with a “kink” at the last group, where the cross-sections increase sharply. In considering other cross-sections in this way, their relative sizes (Table IV), as well as the fluxes, must be allowed for.

8.3. The effect of the transfer cross-sections on  $k_{\text{eff}}$  is fairly small, except from group 1, where fast fission in  $U^{238}$  and inelastic transfer compete. The  $\Sigma_{R \leftarrow S}$  results show the general effect of spectrum changes — the less the transfer and the harder the spectrum, the higher the reactivity. This trend however is reversed in  $\Sigma_{5 \leftarrow 4}$ , though this cross-section has a very small effect indeed in this system. The reason for this can be seen from Section 18.4 and Table XV (Section 15.2).

The blanket changes are generally small but not negligible in relation to the core changes.

8.4. In considering the figures for changes in microscopic cross-sections given in Table VIII, the group fluxes, the relative size of the cross-sections (Table III) and the relative atomic abundance of the isotopes in our composition (Table V) must be kept in mind.

The most important transport cross-sections are those of  $U^{238}$ , followed by those of iron, then carbon and sodium.  $\sigma_{\text{tr}}$  for  $Pu^{239}$  has only a small effect. Naturally also, the fertile isotope  $U^{238}$  has the most important capture cross-sections, but it should be noted that capture in  $Pu^{239}$  is next in importance. Note also that capture in sodium affects reactivity hardly at all, but capture in iron cannot be neglected.

The effects of changes in  $\nu$  and  $\sigma_f$  are similar, the latter having less nett effect because it varies neutron absorption as well as production. The importance of  $\nu$  and  $\sigma_f$  for  $U^{238}$  in the top group is evident, the effects being nearly twice those for  $Pu^{239}$ ; the latter is of course most important in the other groups. The effects of  $Pu^{240}$  and of  $U^{235}$ , even in such small proportion, are not negligible.

8.5. In the transfer cross-sections, the importance of transfer out of group 1 to below the  $U^{238}$ -fission threshold is emphasized.  $\sigma_{2 \leftarrow 1}$  for  $U^{238}$  and iron is of comparable importance to the fission cross-sections. The peculiarity of transfers from group 4 to 5 has already been noted; these figures may be misleading (Section 18.4). In the other transfers, only the figures for  $U^{238}$  and carbon show much importance, with smaller effects from iron and sodium. Plutonium has little effect here.

The transfer cross-sections referred to include both elastic and inelastic effects, but these effects may be separated, if desired, with the aid of data given in Tables III (microscopic) and IV (macroscopic). For the heavy isotopes, transfers in the upper groups are mainly inelastic and have considerable effect on reactivity. Transfer in carbon is all elastic, while in iron and sodium elastic effects predominate, except from the important top group. The most important effects are: (a) inelastic transfers out of group 1, (b) elastic transfers from group 2 to 3 and group 3 to 4. Transfer from group 4 to 5 is almost all elastic, but is of small importance in this composition.

## 9. Cross-section inter-relations

9.1. Throughout this study, cross-sections have been treated as being independent of one another, i.e. the relation between transport cross-sections and capture, fission, and scattering cross-sections has been ignored. Sufficient details are given, however, to enable the effects of this inter-relation to be obtained, by superposition of two effects.

9.2. If a capture or fission cross-section is increased, the corresponding transport cross-section ought to be increased by the same small increment, leading to a small decrease in  $D$ . The effect on reactivity can be obtained from Tables VII and IV, and for all capture and fission cross-sections it is very small, the largest effect arising from a change in the core of  $\Sigma_f$  for group 1. The change of  $k_{eff}$  quoted is +0.00704, to which the transport effect would add +0.00009. In the case of variations in capture cross-sections, the small transport effects subtract from the figures quoted.

9.3. For transfer cross-sections, the transport effect is a significant proportion, order 10%, of the  $k_{eff}$  changes quoted in Table VII, but they tend to decrease the changes shown. For example, a  $k_{eff}$  change of +0.00803 is quoted for  $\Sigma_{2 \leftarrow 1}$ , for a decrease of 10% in the core cross-section, and the transport effect is found to be -0.00083 on  $k_{eff}$ . In the single case of  $\Sigma_{5 \leftarrow 4}$  (core), the two effects add, but both are very small. In the top group, transfer in the blankets +0.00080 is reduced by -0.00030 by the transport effect.

9.4. When a transport cross-section is changed, the increment may be ascribed to the elastic-scattering cross-section,  $\Sigma_s$ . The change in the elastic transfer out of the group (given by  $\xi \Sigma_s / U$ , where  $\xi$  is a mean lethargy increment for an elastic collision, and  $U$  the lethargy interval in the group) ought then to be allowed for. When this is done, the effects may be surprisingly large in the core, but again decrease the reactivity changes shown for  $D$ . The decreases can be 50% or even more, but will vary according to which isotope we consider to be in error — larger effects from carbon, smaller from heavy isotopes. In the blanket, these effects are less but in the same direction. Thus the net effect of  $\Sigma_{tr}$  changes is even less than is indicated by the tables.

9.5. Similar adjustments can be made to the figures in Table VIII, but it is simpler to think about them as they are given, relating to independent changes, and to remember that separate small effects may be superimposed. For the lighter isotopes, the sign of the changes may be reversed by this superposition.

9.6. One essential point arises from all of the foregoing: where significant effects arise from these inter-relations, the tabulated figures are on the "safe" side, i.e. they over-estimate the importance of the relevant cross-sections.

## 10. Method for correlating the breeding ratios

10.1. Throughout this report, unless otherwise explicitly stated, the breeding ratio is defined as the ratio of neutron capture in  $U^{238}$  to absorption in  $Pu^{239}$ , calculated for the initial clean conditions of the reactor. This very simple definition may be justified for a study of this type. In Table V, the effects are shown of considering the production of  $Pu^{241}$ , and also the destruction of  $U^{235}$ , and it will be seen that the loss of  $U^{235}$  out-weighs the gain in  $Pu^{241}$ .

In determining small changes, a problem arises in that any calculated breeding ratio is fictitious unless the system is critical. In changing the cross-sections, small changes of reactivity as well as breeding ratio are produced, and it would be incorrect to compare these breeding-ratio changes without allowing for the reactivity changes. If a system is super-critical, the excess neutrons could be absorbed in extra  $U^{238}$ ; or, if the system were sub-critical, it would be necessary to increase the fissile material present, or decrease the absorption. In each case there would be an apparent change in the breeding ratio.

It might be thought that this effect would be small, but in fact it was found that, for a given increment in reactivity, the increment in the internal breeding ratio was twice as great, and the increment in the total breeding ratio 3.5 times as great. These *apparent* changes in breeding ratio are of opposite sign to the changes of reactivity. These effects are, therefore, much too large to be neglected, and in many cases they were in fact the main factors operating in changing the breeding ratios, so it was necessary to devise a correlation method to compare the true breeding ratios in each case for a critical system.

10.2. A non-critical system may be adjusted in various ways to criticality. It is assumed here that the adjustment for errors in critical mass will be by adjusting the enrichment of the system, as in the Dounreay fast reactor, and the correlation is based on the following composite adjustment:

A macroscopic cross-section is adjusted as in Section 1.3, then the enrichment (the proportion of plutonium in the fuel) is varied to bring the system back to criticality, while the total number of fuel atoms is kept constant. The new breeding ratio for the critical system is calculated, and the changes for individual isotopes are then correlated by a method similar to that explained in Section 1.3.

Exceptional calculation accuracy was necessary to obtain the small differences of breeding ratio, and considerable care was exercised in the development and checking of the methods of calculation.

10.3. Another difference from the reactivity correlations should be noticed. If a macroscopic capture cross-section is changed, the change produced in the breeding ratio will depend on whether we ascribe this change of capture cross-section to  $U^{238}$ ,  $Pu^{239}$ , or to materials such as iron not considered in the fertile conversion. This additional complication should be borne in mind when studying the tables, and it applies also to the fission-cross-section changes.

## 11. Breeding ratio correlations

11.1. Changes in the breeding ratios produced by the composite adjustments detailed in Section 10.2 are set out in Table IX. The breeding ratio in the core (i.e. the internal breeding ratio) and the breeding ratio for core and blanket together (i.e. the total breeding ratio) are both tabulated. The numbers should be used with considerable care, since in a sense some of them are fictitious,

TABLE IX

## CHANGES IN BREEDING RATIOS PRODUCED BY MACROSCOPIC CROSS-SECTIONS CHANGES, ADJUSTED FOR CRITICALITY

Group	<i>D</i> (%)	Int. <i>BR</i>	Total <i>BR</i>	$\Sigma_c^*$ (%)	Int. <i>BR</i> *	Total <i>BR</i> *	$\Sigma_f^{**}$ (%)	Int. <i>BR</i> **	Total <i>BR</i> **	$\nu$ (%)	Int. <i>BR</i>	Total <i>BR</i>	Group transfers	$\Sigma_{R \leftarrow S}$ (%)	Int. <i>BR</i>	Total <i>BR</i>
Core changes																
1	-9.09	+0.005	-0.001	-20	+0.003	+0.005	+~ 5	+0.013	+0.020	+ 5	+0.022	+0.037	2 ← 1	- 10	+0.013	+0.028
2	-9.09	+0.011	+0.002	-10	+0.011	+0.017	+~ 5	+0.018	+0.031	+ 5	+0.026	+0.044	3 ← 1	- 20	+0.003	+0.012
3	-9.09	+0.006	-0.001	-10	+0.019	+0.028	+~ 5	+0.016	+0.026	+ 5	+0.027	+0.040	3 ← 2	- 10	-0.001	+0.013
4	-9.09	+0.003	<0.001	-10	+0.027	+0.036	+~ 5	+0.012	+0.022	+ 5	+0.017	+0.030	4 ← 2	- 100	-0.001	+0.007
5	-9.09	+0.001	<0.001	-10	+0.016	+0.020	+~ 5	+0.006	+0.012	+ 5	+0.010	+0.016	4 ← 3	- 10	-0.002	+0.008
1							+~ 5	+0.014	+0.023				5 ← 4	+ 20	-0.001	-0.005
Blanket changes																
1	-9.09	+0.001	+0.001	-20	<0.001	+0.001	+~ 5	+0.001	+0.005	+ 5	+0.005	+0.007	2 ← 1	- 10	+0.001	+0.007
2	-9.09	+0.004	+0.004	-10	+0.002	+0.012	+~ 20	<0.001	+0.003	+ 20	<0.001	+0.005	3 ← 1	- 20	<0.001	+0.002
3	-9.09	+0.003	+0.003	-10	+0.003	+0.027	+~ 20	+0.001	+0.004	+ 20	+0.001	+0.007	3 ← 2	- 10	+0.001	-0.001
4	-9.09	+0.001	<0.001	-10	+0.004	+0.035	+~ 20	+0.001	+0.004	+ 20	+0.001	ø 0.007	4 ← 2	- 100	<0.001	<0.001
5	-9.09	<0.001	-0.001	-10	+0.002	+0.011	+~ 20	<0.001	+0.022	+ 20	<0.001	+0.003	4 ← 3	- 10	+0.001	-0.001
1										+ 10	+0.003	+0.015	5 ← 4	+ 20	<0.001	-0.001
2	-9.09	-0.004	+0.005													
Core and blanket changes																
1										+ 5	+ 0.021	+ 0.040	2 ← 1	- 10	+ 0.013	+ 0.033
2	-9.09	+0.014	+0.003	-10	+0.013	+0.030										

\* Relevant to isotopes other than U<sup>238</sup> and Pu<sup>239</sup>.\*\* Relevant to isotopes other than Pu<sup>239</sup>.

Cont. following page

TABLE IX, cont.

**CHANGES IN BREEDING RATIO PRODUCED BY CHANGES IN CAPTURE AND FISSION MACROSCOPIC CROSS-SECTIONS when applied to  $U^{238}$  and  $Pu^{239}$**

Group	Applied to $U^{238}$ (Capture)						Applied to $Pu^{239}$ (Capture)			Applied to $Pu^{239}$ (Fission)		
	Core changes			Blanket changes			Core changes			Core changes		
	$\Sigma_c$ (%)	Int. $BR$	Total $BR$	$\Sigma_c$ (%)	Int. $BR$	Total $BR$	$\Sigma_c$ (%)	Int. $BR$	Total $BR$	$\Sigma_f$ (%)	Int. $BR$	Total $BR$
1	-20	-0.001	+0.001	-20	<0.001	<0.001	-20	+0.006	+0.011	+~5	+0.005	+0.005
2	-10	-0.008	-0.001	-10	+0.002	-0.001	-10	+0.027	+0.049	+~5	+0.007	+0.009
3	-10	-0.013	-0.003	-10	+0.003	-0.001	-10	+0.048	+0.084	+~5	+0.006	+0.006
4	-10	-0.018	-0.009	-10	+0.004	-0.001	-10	+0.070	+0.117	+~5	+0.004	+0.007
5	-10	-0.010	-0.007	-10	+0.002	<0.001	-10	+0.040	+0.065	+~5	+0.002	+0.004

Note: This table must be interpreted in conjunction with text, Sections 10, 11, 12. Reactivity adjustment is included as explained in Section 10.2.

being simply a step towards the correlation of each isotope. For example, in fact the capture cross-section of  $Pu^{239}$  could not alone cause a 10% error in the *macroscopic* capture cross-section. Smaller changes, however, would be in proportion within very close limits. The proportional and additive properties of the small changes were checked, as previously described in Section 6.1.

11.2. The changes are recorded to three places of decimals, and again, regarding these as differentials, it is believed that most of these figures are correct to this order of accuracy. The proportional and additive checks (Section 6.1) show less accuracy than those in the reactivity correlations.

11.3. Table X shows the relation between the various individual isotopic cross-sections and the total breeding ratio, deduced from the changes in Table IX, and tabulated in the manner described in Section 7.3. Table XI similarly correlates the individual cross-sections with the internal breeding ratio. The assumption of independent cross-sections (Section 9.1) also applies throughout the breeding-ratio studies.

## 12. Discussion

12.1. In critically observing the figures in the breeding-ratio tables, many underlying features must be kept in mind. Some of these points are mentioned in Section 8 (2 and 4). Other points complicating interpretation of these tables are the reactivity adjustment (Section 10, 1 and 2), the difference explained in section 10.3, the larger effect resulting in some cases from blanket changes, and the fact that even the internal breeding ratio is not independent of blanket changes, since the latter affect reactivity and core flux distributions. Thus the reasons underlying some apparent anomalies may be quite subtle.

12.2. Table IX will not be considered in detail, but a few points are briefly noted.

As might be foreseen from neutron-balance considerations,  $\nu$  is a very sensitive parameter. The fission-cross-section changes, if applied to  $U^{235}$ , are also sensitive, but if the changes are applied to  $Pu^{239}$  opposing effects come into operation, leading to reduced sensitivity of breeding ratio to  $Pu^{239}$  fission-cross-section. The changes for  $U^{235}$  are, however, "fictitious" in the sense used in Section 11.1.

TABLE X

**PERCENTAGE CHANGES IN MICROSCOPIC CROSS-SECTIONS THROUGHOUT  
CORE AND BLANKET to produce 0.001 change in total breeding ratio**

Isotope	Group	$\sigma_{tr}$ (%)	$\sigma_c$ (%)	$\sigma_f$ (%)	$\nu$ (%)	Group transfer $R \leftarrow S$	$\sigma_{R \leftarrow S}$ (%)
$Pu^{239}$	1	— 300	— 15	+ 3.0	+ 0.4	2 $\leftarrow$ 1	— 13
	2	+ 100	— 2.1	+ 0.6	+ 0.13	3 $\leftarrow$ 1	— 60
	3	— 300	— 0.7	+ 0.6	+ 0.13	3 $\leftarrow$ 2	— 25
	4	— 2 000	— 0.5	+ 0.8	+ 0.18	4 $\leftarrow$ 2	— 120
	5	— 900	— 0.7	+ 1.4	+ 0.35	4 $\leftarrow$ 3	— 160
$Pu^{240}$	1	— 1 300	— 150	+ 5	+ 2.5	2 $\leftarrow$ 1	— 40
	2	+ 400	— 15	+ 2.5	+ 1.6	3 $\leftarrow$ 1	— 140
	3	— 1 100	— 10	+ 140	+ 90	3 $\leftarrow$ 2	— 120
	4	— 7 000	— 7	—	—	4 $\leftarrow$ 2	—
	5	— 3 500	— 13	—	—	4 $\leftarrow$ 3	— 300
	5	— 4	—	—	—	5 $\leftarrow$ 4	— 1 600
$U^{238}$	1	+ 30	— 20	+ 0.3	+ 0.17	2 $\leftarrow$ 1	— 0.5
	2	+ 2.5	+ 6	+ 50	+ 30	3 $\leftarrow$ 1	— 2.0
	3	+ 5.0	+ 2.9	—	—	3 $\leftarrow$ 2	— 4.0
	4	+ 80	+ 1.3	—	—	4 $\leftarrow$ 2	—
	5	— 19	+ 2.0	—	—	4 $\leftarrow$ 3	— 13
	5	— 4	—	—	—	5 $\leftarrow$ 4	— 20
$U^{235}$ (0.7% of nat. U)	1	+ 4 000	— 300	+ 17	+ 9	2 $\leftarrow$ 1	— 90
	2	+ 400	— 40	+ 4	+ 2.0	3 $\leftarrow$ 1	— 500
	3	+ 800	— 18	+ 2.0	+ 1.4	3 $\leftarrow$ 2	— 300
	4	+ 11 000	— 10	+ 2.5	+ 1.5	4 $\leftarrow$ 2	— 1 500
	5	— 3 000	— 15	+ 3.5	+ 2.5	4 $\leftarrow$ 3	— 5 000
	5	— 4	—	—	—	5 $\leftarrow$ 4	— 10 000
Fe	1	— 300	— 28	—	—	2 $\leftarrow$ 1	— 1.1
	2	+ 8	— 7	—	—	3 $\leftarrow$ 1	— 6
	3	+ 30	— 5	—	—	3 $\leftarrow$ 2	— 5
	4	+ 300	— 4	—	—	4 $\leftarrow$ 2	— 40
	5	— 50	— 18	—	—	4 $\leftarrow$ 3	— 8
	5	— 4	—	—	—	5 $\leftarrow$ 4	— 20
Na	1	— 200	— 120	—	—	2 $\leftarrow$ 1	— 4
	2	+ 17	— 160	—	—	3 $\leftarrow$ 1	— 60
	3	+ 200	— 100	—	—	3 $\leftarrow$ 2	— 4
	4	+ 1 000	— 80	—	—	4 $\leftarrow$ 2	— 30
	5	— 100	— 100	—	—	4 $\leftarrow$ 3	— 10
	5	— 4	—	—	—	5 $\leftarrow$ 4	— 17
C	1	— 100	—	—	—	2 $\leftarrow$ 1	— 4
	2	+ 20	—	—	—	3 $\leftarrow$ 1	—
	3	— 70	—	—	—	3 $\leftarrow$ 2	— 2.0
	4	— 600	—	—	—	4 $\leftarrow$ 2	—
	5	— 400	—	—	—	4 $\leftarrow$ 3	— 2.5
	5	— 4	—	—	—	5 $\leftarrow$ 4	— 8

Notes: 1. See text under Sections 10, 11, 12. Reactivity adjustment is included, Section 10.2.

2. A minus sign indicates that the change of cross-section and change of breeding ratio are opposite in sign.

TABLE XI

**PERCENTAGE CHANGES IN MICROSCOPIC CROSS-SECTIONS THROUGHOUT  
CORE AND BLANKET to produce 0.001 change in internal breeding ratio**

Isotope	Group	$\sigma_{tr}$ (%)	$\sigma_c$ (%)	$\sigma_f$ (%)	$r$ (%)	Group transfers $R \leftarrow S$	$\sigma_{R \leftarrow S}$ (%)
$Pu^{239}$	1	+ 40	— 30	+ 2.8	+ 0.7	2 $\leftarrow$ 1	— 30
	2	+ 18	— 4	+ 0.8	+ 0.2	3 $\leftarrow$ 1	— 200
	3	+ 30	— 1.2	+ 0.9	+ 0.2	3 $\leftarrow$ 2	+ 600
	4	+ 60	— 0.9	+ 1.3	+ 0.3	4 $\leftarrow$ 2	+ 1 100
	5	+ 200	— 1.1	+ 2.5	+ 0.5	4 $\leftarrow$ 3	+ 700
$Pu^{240}$	1	+ 160	— 250	+ 8	+ 4	2 $\leftarrow$ 1	— 80
	2	+ 70	— 25	+ 4	+ 3.0	3 $\leftarrow$ 1	— 500
	3	+ 130	— 16	+ 200	+ 130	3 $\leftarrow$ 2	+ 3 000
	4	+ 200	— 9	—	—	4 $\leftarrow$ 2	—
	5	+ 700	— 15	—	—	4 $\leftarrow$ 3	+ 1 400
$U^{238}$	1	+ 3.0	+ 50	+ 0.6	+ 0.35	2 $\leftarrow$ 1	— 1.3
	2	+ 1.3	+ 2.5	+ 100	+ 70	3 $\leftarrow$ 1	— 8.0
	3	+ 2.0	+ 1.6	—	—	3 $\leftarrow$ 2	— 20
	4	+ 4.5	+ 1.0	—	—	4 $\leftarrow$ 2	—
	5	+ 20	+ 2.0	—	—	4 $\leftarrow$ 3	— 140
$U^{235}$ (0.7% of nat U)	1	+ 500	— 600	+ 30	+ 18	2 $\leftarrow$ 1	— 250
	2	+ 200	— 120	+ 8	+ 5	3 $\leftarrow$ 1	— 2 000
	3	+ 300	— 50	+ 6	+ 3.5	3 $\leftarrow$ 2	— 1 500
	4	+ 600	— 16	+ 8	+ 4	4 $\leftarrow$ 2	— 20 000
	5	+ 3000	— 30	+ 10	+ 6	4 $\leftarrow$ 3	— 30 000
$Fe$	1	+ 6	— 50	—	—	2 $\leftarrow$ 1	— 2.5
	2	+ 3.0	— 16	—	—	3 $\leftarrow$ 1	— 20
	3	+ 4	— 11	—	—	3 $\leftarrow$ 2	— 150
	4	+ 8	— 7	—	—	4 $\leftarrow$ 2	+ 600
	5	+ 25	— 30	—	—	4 $\leftarrow$ 3	+ 60
$Na$	1	+ 13	— 200	—	—	2 $\leftarrow$ 1	— 9
	2	+ 5	— 300	—	—	3 $\leftarrow$ 1	— 200
	3	+ 12	— 180	—	—	3 $\leftarrow$ 2	— 500
	4	+ 20	— 140	—	—	4 $\leftarrow$ 2	+ 400
	5	+ 50	— 180	—	—	4 $\leftarrow$ 3	+ 60
$C$	1	+ 12	—	—	—	2 $\leftarrow$ 1	— 9
	2	+ 4	—	—	—	3 $\leftarrow$ 1	—
	3	+ 8	—	—	—	3 $\leftarrow$ 2	+ 50
	4	+ 20	—	—	—	4 $\leftarrow$ 2	—
	5	+ 80	—	—	—	4 $\leftarrow$ 3	+ 12
						5 $\leftarrow$ 4	— 60

Notes: 1. See text under Sections 10, 11, 12. Reactivity adjustment is included, Section 10.2.

2. A minus sign indicates that the change of cross-section and change of breeding ratio are opposite in sign.

The capture cross-section changes show considerable differences according to whether the changes are applied to  $U^{238}$ ,  $Pu^{239}$ , or other isotopes in the composition. When capture in  $Pu^{239}$  is decreased, the breeding-ratio changes are proportionally much larger than changes due to a corresponding decrease in the absorption in non-fissile isotopes. On the other hand, a capture change in  $U^{238}$  has effects of the opposite sign, but proportionally very much smaller. Put another way, decreased capture in  $U^{238}$  lowers the breeding ratios, but, when the system is readjusted to critical as explained, there is an apparent increase in the breeding ratios, the two effects opposing and resulting in small net changes.

Changes in  $D$  or  $\Sigma_{tr}$  are in general not very sensitive, and similarly the transfer cross-sections are of low sensitivity, except as before the transfer from group 1 to lower groups. It is important to notice from these results that generally (where significant) hardening of the spectrum improves the breeding ratios, particularly the total breeding ratio, and *vice versa*.

12.3. Table X, correlating microscopic cross-sections and total breeding ratio, shows the great importance of the neutron production terms, even for  $U^{235}$  and  $Pu^{240}$ , which are present in the model in only small proportion. There is an appreciable contribution to the breeding ratio from the  $U^{235}$  in the natural uranium. Both  $\nu$  and  $\sigma_f$  need to be known to great accuracy for all groups for  $Pu^{239}$  and for the highest-energy group for  $U^{238}$ .

In capture cross-sections, it should be noticed that the capture in  $Pu^{239}$  is the most sensitive parameter, the capture in  $U^{238}$ , though sensitive, being less important because of the opposing effects previously mentioned. Capture in iron is also important.

Nearly all the transport cross-sections are quite unimportant, except only the  $U^{238}$  figures. The apparent anomaly here may be explained from the original calculations, and is largely due to the high proportion of  $U^{238}$  in the blanket. Group 2 shows some importance in the non-fissile isotopes.

In the transfer cross-sections, generally the importance increases with neutron energy. Great sensitivity is again shown for  $U^{238}$  and iron, top-group inelastic transfers, in spite of the small flux in this group. Elastic transfer in carbon is also of high importance.

12.4. Table XI, correlating microscopic cross-sections and internal breeding ratio, indicates effects generally similar to the effects on total breeding ratio. It indicates a lesser importance of the neutron production terms, and transfer terms, but increased importance of the transport cross-sections. The latter is fairly readily explained in that the leakage from core to blanket is an appreciable fraction of the neutrons present, while the leakage or escape from the blanket is an order of magnitude smaller. Hence an increase in leakage leads to a decrease in core breeding, but an increase in blanket breeding, so that the total breeding ratio changes little.

### 13. Combination of small errors

13.1. The "standard" change or increment of 0.001 taken for Tables VIII, X, and XI, is quite small, but there are many possible errors which could add together. The number of small errors possible is sufficient to justify statistical investigation.

It is not reasonable to assume that errors on *all* the cross-sections might add together. The total error could then approach 10% on  $k_{eff}$ , but the probability

against this occurring is of the order  $10^{30}$  or greater. A rough consideration showed that, if all the cross-sections were known within the degrees of accuracy given in Table VIII,  $k_{\text{eff}}$  might be calculated within 1% to 2%, with 90% confidence. This can be a 10% to 20% error on critical mass.

13.2. On the same rough basis, the accuracy required in the breeding-ratio tables is rather higher than necessary. For the total breeding ratio (Table X), the accuracy may be relaxed by a factor of three, with the expectation of calculating the total breeding ratio within about 0.05. The internal breeding ratio (Table XI) affects the calculation of reactivity changes with burn-up. Hence the accuracy required in this table should be relaxed by not more than a factor of 2, giving internal breeding ratio within about 0.03.

13.3. Thus, referring to the figures in the body of the tables, it is suggested that the figures in Table VIII indicate suitable orders of accuracy for cross-sections to be used in reactivity calculations for this system (accuracy to be better where possible); that the figures in Table X could be multiplied by 3, and those in Table XI multiplied by 2, for breeding-ratio calculations. With these adjustments, the cross-section accuracies required for reactivity calculations and for breeding-ratio calculations are of similar magnitude.

The foregoing remarks apply to systems very similar to our basic case. Extension to other systems will be considered later.

#### 14. Additional reactivity correlations

14.1. Extensions of the reactivity calculations, still applying to the basic reactor studied, are presented in Table XII. The body of the table presents the reactivity effect of altering a given cross-section parameter over the whole energy range by 1%, for each material listed. Thus the figures may be regarded as showing the sensitivity of  $k_{\text{eff}}$  to spectrum-averaged 1-group cross-sections, except for the figures applying to transfer cross-sections. The latter indicate the extent of spectrum effects on the reactivity, though this nett effect might be expected to be greater numerically if calculations were made in more than the five groups used. Effects are listed separately for core and blanket.

From this table, the most important cross-sections are very quickly picked out.  $\nu$  and  $\sigma_f$  for  $\text{Pu}^{239}$  have much the largest effect, followed by capture and then fission in  $\text{U}^{238}$ . The importance of capture in  $\text{Pu}^{239}$  is again emphasized. In both transport and transfer cross-sections,  $\text{U}^{238}$  and iron show comparable effects, with smaller contributions from carbon and sodium.

It is important to notice that the spectrum effect in reactivity is negative, i.e. if the transfer cross-sections are increased — so degrading the spectrum — reactivity decreases. Hence carbon or other moderator is a liability, not an asset, in this type of system. The effect on the breeding ratios is also negative, as has been shown.

The remarks of Section 9 apply to this table also.

14.2. In the last column of Table XII, the effects of changes in all the types of cross-section have been combined for each material, giving the nett effect of changes in the atomic density of each of the materials present.

A figure for the sodium temperature coefficient (isothermal) results from the figures in this last column for sodium. The figure  $-0.011 (\times 10^{-3})$  is the result of combining  $+0.175$ ,  $-0.177$  and  $-0.0089$ , so that we cannot expect good accuracy, especially since these latter figures were the result of combining

TABLE XII  
CHANGES IN  $k_{\text{eff}}$

Material	Core or blanket	Changes in $k_{\text{eff}}$ produced by 1 % increase in given cross-sections, in all groups, in core or blanket ( $\times 10^{-3}$ )					Changes in $k_{\text{eff}}$ produced by 1 % increase in atoms/cm <sup>3</sup> in core or blanket ( $\times 10^{-3}$ )
		$\sigma_{\text{tr}}$	$\sigma_{\text{c}}$	$\sigma_{\text{f}}$	$\nu$	$\sigma_{R \leftarrow S}$	
Pu <sup>239</sup>	C	+0.062	-0.527	+5.57	+7.67	-0.041	+5.06
Pu <sup>240</sup>	C	+0.016	-0.118	+0.182	+0.299	-0.013	+0.067
Irrad. Pu	C	—	—	—	—	—	+5.13
U <sup>238</sup>	C	+0.480	-2.33	+0.750	+1.32	-0.605	-1.71
	B	+0.364	-0.384	+0.085	+0.150	-0.167	-0.102
U <sup>235</sup>	C	+0.0033	-0.032	+0.254	+0.374	-0.0042	+0.221
	B	+0.0025	-0.0047	+0.059	+0.080	-0.0014	+0.056
Nat. U	C	—	—	—	—	—	-1.48
	B	—	—	—	—	—	-0.047
Fe	C	+0.345	-0.142	—	—	-0.382	-0.179
	B	+0.093	-0.0088	—	—	-0.043	+0.042
Na	C	+0.175	-0.0089	—	—	-0.177	(-0.011)
	B	+0.027	-0.0003	—	—	-0.019	(+0.008)
C	C	+0.233	—	—	—	-0.321	-0.088

- Notes: 1. The figures in this table represent small changes from the basic case, and must be interpreted in conjunction with the atomic composition, Table V.  
 2. Figures for core and blanket changes may be added together.  
 3. Bracketed figures are less accurate.

the figures for the separate groups. An extra computer case was run allowing a 10% increase of sodium density in the core, giving a result equivalent to 0.004 ( $\times 10^{-3}$ ) in place of the 0.011 in the table, both figures being negative. This provides a good cross-check of the many steps in the calculation, and in general on the methods used.

The result is equivalent to a small positive temperature coefficient about  $+1.2 \times 10^{-7} \Delta k/\text{ }^{\circ}\text{C}$ . The effect of sodium in the blanket is slightly positive (i.e. its temperature coefficient in the blanket is negative), and in fact, in this system, the blanket effect slightly outweighed the very small core effect. When the sodium density was decreased by 10% over core and blanket, the reactivity change was -0.00004. This result was not proportional to the result of a case in which all sodium was lost from core and blanket, which produced a decrease in reactivity of -0.0014.

TABLE XIII: See following page

TABLE XIV  
NEUTRON BALANCE BY ISOTOPES FOR BASIC CASE  
normalized to one neutron produced in the core

	Core	Blanket
<b>Production reactions</b>		
Pu <sup>239</sup> neutron production	0.7978	—
Pu <sup>240</sup> neutron production	0.0303	—
U <sup>235</sup> neutron production	0.0391	0.0342
U <sup>238</sup> neutron production	0.1328	0.0452
<i>TOTAL</i>	<u>1.0000</u>	<u>0.0794</u>
<b>Absorption reactions</b>		
Pu <sup>239</sup> fission	0.2704	—
Pu <sup>239</sup> capture	0.0670	—
Pu <sup>240</sup> fission	0.0119	—
Pu <sup>240</sup> capture	0.0149	—
U <sup>235</sup> fission	0.0158	0.0138
U <sup>235</sup> capture	0.0037	0.0036
U <sup>238</sup> fission	0.0510	0.0174
U <sup>238</sup> capture	0.2942	0.2730
Fe capture	0.0177	0.0061
Na capture	0.0014	0.0002
C capture	0.0000	—
<i>Neutron surplus</i>	0.0003	—
Leakage from core to blanket	0.2516	—
Leakage from blanket to void	—	0.0168
<i>TOTALS</i>	<u>1.0000</u>	<u>0.331</u>
<i>Aggregate flux integrals (n/cm s), producing above reactions per second (see Table VI)</i>	110.2	35.7

It is interesting to note that the choice of reactor model gives by chance a core in which the sodium coefficient is almost zero. It may be expected, however, that if more groups were used the coefficient would be slightly more positive, and also the coefficient will be sensitive to errors in the cross-section data. The small magnitude of the blanket effect would not be greatly changed by different size or composition, and so it would usually be negligible in cases where the core coefficient is of a larger order. From Table VIII the contribution of each cross-section to the temperature coefficient may be seen, and the opposing spectrum and leakage effects studied. The capture effect is small.

14.3. A further step in the calculations provides the figures given in Table XIII, which allow estimates of the effects of composition changes. The table shows the reactivity worth of a distributed 1% by volume of the various materials, and allows various useful inferences to be drawn.

The value of the constant given in Section 5.2, connecting enrichment and reactivity variations, may be obtained from the figures in this table, and it was in fact found to agree to better than 1%. Though such close agreement may be partly fortuitous, it does provide an excellent cross-check on the accuracy and validity of the calculations made for this study, since the figures in Table XIII were produced *via* the many steps of our general correlations, while the figure in Section 5.2 was obtained directly from extra computer cases. Correlation

TABLE XIII  
REACTIVITY WORTH OF 1% BY VOLUME OF MATERIALS SHOWN  
evenly distributed throughout core or blanket, for small changes from basic case

Region	Material	Pu <sup>239</sup>	Pu <sup>240</sup>	Irrad. Pu	U <sup>238</sup>	U <sup>235</sup>	Nat. U	Fuel as table 5.21	Fe	Na	C (alone)
Core	Metal 80 % monocarbide as Table I	+0.193	+0.010	+0.156	-0.0081	(+0.147)	-0.0070	—	-0.00089	(-0.00003)	-0.00063
		+0.105	+0.0054	+0.085	-0.0046	(+0.080)	-0.0040	+0.0079	—	—	—
Blanket	Metal	—	—	—	-0.00017	(+0.013)	-0.00008	—	+0.00021	(+0.00004)	-0.00005

Notes: 1. Bracketed figures are less accurate.

2. Many useful inferences may be drawn from this table, and cross-checks are possible on the accuracy and validity of the calculations—see Section 15.3.

TABLE XV  
NEUTRON BALANCE BY ENERGY GROUPS FOR BASIC CASE normalized to one neutron produced in core

Group	Born into group	Leakage from core in group	Scattered into group	Scattered out of group	Captured in group	Causing fissions in group	Leaking to blanket from group	Leaking to void from group	Produced by group	Absorbed in group (capture+fission)	Absorption +leakage in group	Capture + leakage in group
Neutron fractions in core												
1	0.5740	—	0	0.4175	0.0058	0.0806	0.0700	—	0.2225	0.0864	0.1564	0.0758
2	0.3600	—	0.3627	0.4852	0.0606	0.0890	0.0879	—	0.2598	0.1496	0.2373	0.1483
3	0.0580	—	0.5265	0.3462	0.1045	0.0836	0.0500	—	0.2412	0.1881	0.2381	0.1545
4	0.0080	—	0.3596	0.1304	0.1452	0.0621	0.0300	—	0.1784	0.2073	0.2373	0.1752
5	0	—	0.1304	0	0.0826	0.0341	0.0137	—	0.0981	0.1167	0.1304	0.0963
Totals	1.0000	—	1.3792	1.3793	0.3987	0.3494	0.2516	—	1.0000	0.7481	0.9995	0.6501
Neutron fractions in blanket												
1	0.0455	0.0700	0.0	0.0935	0.0016	0.0176	—	0.0023	0.0458	0.0192	0.0215	0.0039
2	0.0286	0.0879	0.0792	0.1457	0.0424	0.0028	—	0.0046	0.0070	0.0452	0.0498	0.0470
3	0.0047	0.0500	0.1580	0.1129	0.0893	0.0047	—	0.0058	0.0115	0.0940	0.0998	0.0951
4	0.0007	0.0300	0.1148	0.0233	0.1148	0.0044	—	0.0030	0.0109	0.1192	0.1222	0.1178
5	0	0.0137	0.0233	0	0.0346	0.0017	—	0.0007	0.0043	0.0363	0.0370	0.0353
Totals	0.0795	0.2516	0.3753	0.3754	0.2827	0.0312	—	0.0164	0.0795	0.3139	0.3303	0.2991

for other ways of varying the enrichment may be obtained, for example, varying the Pu<sup>239</sup> content without keeping the total fuel atoms constant, or varying the Pu<sup>240</sup> content of the plutonium.

It is possible also to obtain from this table and Table 1 the effects of variation of the fuel-carbide density. An increase from 80% to 90% of theoretical density would increase reactivity by 4.4%. Pu<sup>239</sup> as a fuel is seen to be about 1.3 times as effective as U<sup>235</sup> (this equivalence must of course vary with the reactor spectrum). Pu<sup>240</sup> is shown to be about 5% as effective as a fuel as Pu<sup>239</sup>. Iron is shown to be a liability in the core, but an asset in the blanket, while U<sup>238</sup> is, for reactivity (i.e. disregarding its breeding effect), a liability both in core and blanket. Its negative effect is nine times as high as iron in the core. Thus iron considered solely as a neutron reflector should be better than uranium, an inference which is supported by other evidence. As previously noted, sodium has a very small net effect, and the moderating property of graphite is a liability in this system. Addition of carbon even in the blanket produced a small decrease in reactivity.

The effect of using depleted uranium instead of natural may be estimated from this table, and the adverse effect on breeding ratios, which is small but not negligible, may also be inferred from the breeding-ratio tables.

Composition changes based on Table XIII may not be extrapolated too far from our basic system, since the changes would no longer be proportional. The results may be expected to differ considerably in systems fuelled with U<sup>235</sup> instead of plutonium, and in much smaller systems, or those in which the fertile/fissile ratio is greatly different from that used here.

## 15. Neutron balance data

15.1. Much useful information on a reactor system can be obtained from tables showing the proportion of neutrons involved in the various reactions. Table XIV presents neutron production and absorption in each isotope in both core and blanket, with the leakage fractions, each figure showing the fraction of neutrons involved in that reaction relative to each neutron produced in the core.

The production terms show that 20% of all core neutrons are provided by U<sup>238</sup>, U<sup>235</sup> and Pu<sup>240</sup>, and further that an extra 8% of neutrons are produced in the natural uranium in the blanket.

The total of structural and coolant capture throughout core and blanket is only 2½%, this being less than half the capture in the fuel. From the absorption figures given, fission ratios, breeding ratios and effective  $\alpha$  and  $\eta$  for the fuel are all simply obtained.

Even in this large reactor, 25% of core neutrons leak to the blanket, and neutron escape from the blanket, though small at 1½%, would need to be further reduced by reflecting material (e.g. iron or sodium), in order to minimize shielding problems.

Also from figures in Tables XIV and VI, flux levels and blanket-heat production for any given power level may be obtained.

15.2. A different type of neutron balance is given in Table XV. The figures show the fraction of neutrons involved in different reactions in each energy group, and are normalized, as before, to one neutron produced in the core. In observing the figures, the proportions of flux in each group (Table VI) should be kept in mind.

The large effects of inelastic scattering are well shown in the large scattering fraction for the upper groups. Only 14% of the neutrons born into group 1 stay long enough in that group to produce a fission. In spite of this, 22% of all neutrons born are produced by this top group. Substantial variation with energy of leakage from each group is clearly shown, as may be expected. Neutron production and absorption can be compared in each group, and it will be seen that only the upper groups produce more neutrons than they absorb, even in the core. If the column headed "produced by group" is compared with the column "absorption plus leakage in group", it will be seen that the top group alone has a substantial surplus of neutrons produced over neutrons lost, groups 2 and 3 being nearly balanced, while in the last two groups more neutrons are lost than are produced. It is possible to gain considerable insight into the neutron processes occurring in the system from study of these tables.

## 16. Effects of other kinds of small changes

16.1. Results of various other types of small changes from our basic case are recorded below, and provide a useful guide to the magnitude of calculation errors, in comparison with the effects of cross-section errors. Changes in the size and enrichment of the core are discussed in Section 5, and changes in the sodium density in Section 14.2.

16.2. *Input data accuracy.* The macroscopic data in the input tape for the Hassitt programme were originally entered to five places of decimals, rounding the  $D$  values to three places. It was, however, found that roundings in the sixth place of decimals on some of the more sensitive cross-sections could produce small errors in the eigenvalue "Nu" in the fourth place of decimals. Roundings from six places to five in the basic case produced a difference in reactivity of 0.00013, with a corresponding small change in the breeding ratios. Though the error is small, it is an unnecessary error, and so it is recommended, particularly where small changes are looked for, that the cross-sections should be entered to six places of decimals, or say five significant figures. Such accuracy cannot, of course, be justified from the basic microscopic-cross-section data, but there is no need to introduce additional small errors within the calculations themselves by unnecessary roundings. The effect might be significant, for instance, in calculating the effects of loss of sodium, and particularly the effect of a small change in the sodium density.

16.3. *Mesh effects — Truncation error.* Fairly coarse mesh spacings were used generally in this study to economize on computer time, as recorded in Section 4.5. Another case was run with a larger number of mesh intervals, the data being in all other respects the same as our basic case. In this extra case the mesh spacings used were as follows:

Core: radial, 16 at 4.88 125 cm; axial, 11 at 3.55 cm

Blankets: radial, 9 at 5.0 cm; axial, 10 at 4.5 cm.

The result showed a reactivity increase of 0.0034, so that truncation error alone may be responsible for errors comparable to, or in many cases larger than, errors in single cross-sections. The apparent effect on the breeding ratios was a decrease of 0.008 on the total breeding ratio, with negligible change of the internal breeding ratio. If, however, the system is readjusted for criticality, the true effect on the breeding ratios is an increase of about 0.007 in the internal breeding ratio, and an increase of about 0.004 in the total breeding ratio.

Usually, the effect of using a finer mesh through the core region is to increase slightly the calculated reactivity.

**16.4. Blanket changes.** An attempt was made to find the sensitivity of this system to changes in the blanket thickness, by increasing separately the end blanket, and the radial blanket, from 45 to 54 cm thickness. The change was made simply by increasing the blanket mesh spacing, without increasing the number of points. In both cases the reactivity indicated was *less* by about 0.001. Two other cases were run in which the mesh spacing was not changed, but instead an extra point was added to increase the blanket thicknesses, this being equivalent to adding 9 cm to radial blanket, and 7.5 cm to the axial blanket. The results then obtained were, in the change of axial blanket a reactivity decrease of 0.0002, and in the radial blanket case a very small reactivity increase, 0.00001.

We must conclude from these results that the blanket mesh spacings used are too coarse for these small changes to be reliably calculated. These results are recorded to show the errors which may occur if the effect of mesh changes is not taken into consideration. The 45-cm blankets used are thick enough for variation in their thickness to have little effect on reactivity, but on the other hand the effect on leakage of fast flux may not be negligible (see Section 16.6).

**16.5. Different axial blanket.** In most real reactors, the axial blanket is likely to be different in composition from the radial blanket. The basic model (Section 1) was varied by putting in axial blankets containing 35% sodium, 20% iron, 45% uranium, i.e. these blankets having the same coolant-volume fraction as the core, while keeping the radial blanket and other details including the mesh the same as before.

The loss of reactivity in this case was 0.0023; the changes in breeding ratios were, apparently, nil in the internal breeding ratio and 0.029 less in the total breeding ratio, but when corrected to criticality these changes would be respectively -0.005 and -0.037. In this short core —  $H=1/2 D$  — changes in the axial blanket may have larger effects than changes in the radial blanket because of the higher fluxes in the axial blanket. Breeding in the axial blankets is greater than breeding in the whole of the radial and "corner" blankets (Table V).

**16.6. Non-zero boundary conditions.** Throughout this study, the condition of zero flux at the outer boundary of the blankets was imposed. This artificial condition slightly depresses the flux over the outer part of the system generally, but it does not impose zero leakage from the blanket, since, although the flux is zero, the flux gradient is not zero.

The Hassitt programme allows outer boundary conditions to satisfy for each group  $g$  the equation

$$Dg \frac{\partial \varphi_g}{\partial N} + \beta_g \cdot \varphi_g = 0$$

where  $N$  stands for  $R$  or  $Z$ . The  $\beta$  values for each group are to be supplied in the data. The results are not sensitive, however, to the values of  $\beta$ , and as no proper multi-group treatment of this parameter is available, it was set to 0.45 for each group (this figure comes from simple extrapolation length consideration, with a rough correction). With all other details again as the basic case, but with this new boundary condition, the reactivity showed a very small increase of 0.00002. The internal breeding ratio was unchanged beyond the fourth place of decimals, but, as might be expected, since the blanket flux is allowed to rise slightly, the total breeding ratio showed an increase of 0.008. The leakage from the blanket

was apparently decreased from 1.68% of core neutrons to 1.46%, but the former figure is in error due to the method of calculation and artificial zero boundary flux. The flux levels compared to the core centre were at the radial blanket edge 0.1% and at the axial blanket edge 0.3%, the figures being quoted for the centre lines. 0.1% corresponds to a flux of  $10^{13}$  n/cm<sup>2</sup> at 1000-MW output.

16.7. *More groups.* A case was run using nine groups in two-dimensional geometry, in which only groups 4 and 5, and 6 and 7, of the original 11-group set [3] were combined. The reactivity figure showed a decrease of 0.0017, and the integrated spectrum showed excellent agreement ( $\leq 1\%$ ). It should be emphasized that calculations in fewer groups can only be made to agree as well as this by carefully choosing the averaging spectrum and the groups to be combined.

16.8. *Effect of different averaging spectra.* A case was run in which the same averaging spectrum was used throughout the blanket as well as the core, which means that the same microscopic cross-sections were used throughout the system, instead of slightly different ones in core and blanket. The reactivity figure for this case was increased by 0.0003, the internal breeding ratio remained the same, and the total breeding ratio decreased by about 0.004.

In another case, different averaging spectra were used, from case 4 instead of case 7 of Table XII of Ref. [3], this case 4 being a less dilute oxide-fuelled core, though still using Pu<sup>239</sup> fuel. The effects of this case were a reactivity increase of 0.0023, changes in the breeding ratios (corrected) of -0.003 in the internal, and +0.004 in the total breeding ratio, with changes in the group-flux integrals of up to 5%.

Considering that these results refer to 5-group calculations, and that the averaging spectra were not greatly different, the reactivity change of 0.0023 is by no means insignificant, and is of similar order to the effects of our cross-section changes (Table VII). Calculations in only three groups or less would be much more sensitive to the effects of the averaging spectrum used. The apparent small effects of using the same averaging spectrum throughout blanket and core, as recorded above, should not lead to the assumption that this effect is negligible. If only reactivity is to be calculated, it may be good enough not to average differently for different regions. But the effect is, as explained below, to produce incorrect spectra, and therefore calculation of such parameters as detector ratios will be in error in the region considered.

16.9. *Postscript on calculation methods.* It may be shown from this study that analyses of the 1-group type may be easily be subject to errors equal to or greater than those expected from cross-section inaccuracies. In the so-called fundamental-mode type of calculation, a multi-group spectrum for the centre of a core is produced and used to obtain averaged 1-group cross-sections. This technique may be inadequate for these dilute cores in which the results are sensitive to the assumed spectrum, for this theory can calculate the spectrum only at the centre of a core, cannot produce a spectrum for absorbing regions, and assumes inaccurately that the spectrum remains constant over the whole core. When only reactivity is to be calculated, approximate methods may suffice. If, however, breeding or detector ratios, neutron balance, leakage, etc., are to be calculated, true multi-group methods become essential. Further, these multi-group methods must attempt to eliminate all unnecessary errors introduced within the calculation itself. It is pointless to try to investigate with a spherical-geometry programme a real reactor system which is cylindrical in shape and has different axial

and radial blankets, particularly if the height of the core is not equal to its radius. It is equally pointless to try to calculate the coolant temperature coefficient using a multi-group programme which does not allow a full transfer matrix.

The desirable calculation accuracy is approached by multi-group analysis with group lethargy intervals of about 0.5, in true two-dimensional geometry, with full transfer matrix. Where this ideal is not attainable, it is believed that the following procedure is an acceptable alternative.

Auxiliary data programmes must be available.

(a) Make a multi-group calculation of a spherical system, simulating the real system as nearly as possible, with correct composition. More than one case of this sort may be necessary (e.g. two different blankets).

(b) Take multi-group-flux integrals from the spherical cases, from the different regions, and using these reduce the number of groups by spectrum-weighting the cross-sections, as discussed, to a number acceptable for a two-dimensional programme. At least five groups are recommended, this still allowing a fair degree of spectrum variation. The groupings must be carefully chosen to reduce sensitivity to the averaging spectrum, e.g. the  $U^{238}$  fission threshold obviously should not occur in the middle of a group.

(c) Now perform a few-group calculation in geometry as true to life as possible, and with no transfer restrictions. By taking flux integrals from this, which are needed anyway for breeding ratios, etc., comparison may be made with the original multi-group spectra, which may be adjusted if desired, even using an iterative technique.

It is possible to choose the groupings (b) to reduce the importance of the averaging spectra, but it is easily shown that the transfer cross-sections must always be sensitive to this averaging process. The effect of incompatible averaging spectra will, therefore, be inaccurate transfer cross-sections, leading to incorrect spectra, and hence incorrect fission ratios, or other spectral indices, and poor estimation of temperature coefficients and blanket-heat distribution.

It is possible to formulate a cross-section set in only five or six groups, which would be adequate for calculation of all types of fast neutron systems. Twelve groups may be sufficient, but more may be needed where moderator is present.

The degree of error arising from use of diffusion theory instead of transport theory is adequately dealt with in other work [3], and will not be discussed here.

## 17. Application of the results of this study

17.1. This study has two basic aims: (a) to provide a sound basis for establishing the accuracy needed in cross-section measurements for fast reactor work, and (b) to enable an estimate to be made of the probable error in calculations based upon cross-section data of known accuracy.

(a) cannot be satisfied without considering various types of system beside the one chosen here.

(b) has been considered briefly in Section 13. In the system chosen, if it were possible at present to specify the limits of error on all the various cross-sections, then it would be possible from Table VIII to estimate the reactivity effect of each separate cross-section error. Then, by applying statistical methods to combine the many small errors, an estimate could be obtained of the total probable error on the reactivity of the complete system. Similar remarks apply to the breeding ratios.

In a system similar to that studied, an estimate could still be made by comparing the atomic densities and macroscopic cross-sections of the two systems, and making proportionate allowance for differences. For systems considerably different from the one studied, other factors need to be taken into account, and some consideration is given to these factors in the next section.

In general, when studying small changes or comparing differences in systems, it is best to compare reactivities rather than critical masses, because the latter can be adjusted in so many different ways to criticality.

## 18. Consideration of other systems

18.1. The principal factors which would affect the results of this study when different types of system are considered are listed below, roughly in order of importance:

- (a) The atomic proportion of the fissile isotope in the core;
- (b) The atomic proportions of the other isotopes;
- (c) The type of fissile material, i.e.  $\text{Pu}^{239}$ ,  $\text{U}^{235}$ , or  $\text{U}^{233}$ ;
- (d) Uranium or thorium fertile material;
- (e) The fertile/fissile atomic ratio;
- (f) The blanket configuration and composition;
- (g) The physical size of the core, or more strictly the fraction of neutron leakage therefrom.

The energy spectrum in the reactor is also of importance, but the spectrum is a dependent variable determined by the factors given above.

All the above features will not be considered in detail, but in the following paragraphs some suggestions are made to facilitate comparison of other systems.

18.2. The main effect of differing atomic proportions of materials is fairly obvious; for example, if a carbide cermet system has twice as much iron as the carbide system studied, then errors in the iron cross-section data will have roughly twice the effect shown in our Table VIII, etc. However, the sensitivity of  $\nu$  for the main fuel is likely to remain roughly constant for any type of system.

The effect of using different fuels is less obvious but of considerable importance, because of the substantial differences between the fission cross-sections and the  $\nu$  and  $\eta$  values for the main fissile isotopes. The largest differences will be in the transfer cross-sections, where even the sign of the changes may be reversed, e.g. in a  $\text{U}^{235}$ -fuelled system moderation may produce an increase in reactivity instead of the decrease which we have noted in this plutonium-fuelled system. The fertile/fissile ratio also affects this strongly.

18.3. A simple approximate means of making a general comparison is to formulate the macroscopic cross-sections for the reactor compositions, in the same form and number of groups as those given in Table IV, so that direct comparison can be made with the figures quoted there. In addition, the macroscopic cross-sections of each isotope separately may be formulated, these operations being very quick and simple if computer-data programmes are available. It is possible to estimate roughly the effect of each isotope from its individual macroscopic cross-section compared to the total or mixed macroscopic cross-section. The following considerations then apply, comparing the mixed macroscopic cross-sections for the new system with those quoted in Table IV, and estimating the effects of changes from Tables VII and IX.

The transport cross-sections and diffusion coefficients are unlikely to differ by large factors from those shown in Table IV, and, as their effects are generally small, they may be roughly estimated by remembering that larger transport cross-sections or smaller diffusion coefficients will mean lower leakage, and hence less importance of errors in the transport cross-sections, while in smaller cores with greater leakage the importance will be increased.

Changes expressed as percentages in  $\bar{v}$  and  $\Sigma_f$  and  $\Sigma_e$  are expected to produce reactivity changes similar to those in Table VII, varying only slowly with the size of core, but with "local" variations between groups because of different proportions of the cross-sections to one another, and different proportions of flux in the groups. Approximate allowance can be made for these by simple proportion.  $\Sigma_e$  should show less importance in a smaller, higher-leakage core.

18.4. There is much more difficulty in understanding the transfer cross-section effects, and here a method is suggested which is of fairly general use in understanding qualitatively what is happening in a given system. In Table IV it will be seen that the macroscopic absorption cross-sections and  $\bar{v}\Sigma_f$  — that is the macroscopic production terms — are placed side by side. Looking at the figures for the core, it will be seen that in group 1 the neutron production greatly outweighs the absorption (due to the effect of fast fission in U<sup>238</sup>). In groups 2 and 3, the production still outweighs absorption, though by a much smaller amount, but in group 4 the absorption is larger than the production, and similarly in group 5. This is not a complete picture, since leakage of the neutrons produced from the higher groups is larger. But while keeping this in mind and making some approximate allowance, it will be seen that only the upper groups are multiplying, while the lower ones are in fact absorbing to a small extent. This comparison of absorption and production in the different groups is a quick qualitative method of observing the variation of neutron importance with energy, though in this other factors are involved.

Observing the figures, we could predict the great importance previously noted of transfers from the top group to lower groups, and the fact that moderation in general has an adverse effect in this system. Also if we take the ratios of production to absorption in groups 4 and 5, making some slight allowance for different leakage which for this purpose slightly adds to absorption, we find that these ratios are very nearly the same in these two groups, and it matters little whether a neutron is in group 4 or 5. Therefore, the transfer cross-section from group 4 to group 5 is of very little importance in this system, as previously noted.

Hence it is suggested that if the ratio of production to absorption be taken in each group, the importance of a transfer cross-section or its effect on reactivity (as shown in Table VII) will mainly depend, first on the difference between these ratios for a given pair of groups; and, second on the magnitude of the transfer cross-section between these two groups. A correction is needed to allow for the differential effects of neutron leakage from the different energy groups, and an idea of the magnitude of this correction can be obtained from the table of neutron balance by groups (Table XV), by comparing the neutron fraction leaking from the core to the fraction absorbed in any particular group. See also the column headed "absorption plus leakage in group". The correction is substantial in the upper groups (see also Section 15.2).

18.5. The foregoing discussion is not intended either to be precise or exhaustive, and it may be inaccurate where resonances modify the spectrum effects. It is hoped, however, that it does offer a means whereby the cross-sections for a

different system may be compared with those quoted in the tables, and the correct sign and approximate order of magnitude determined for the reactivity changes expected from cross-section errors. The importance of a given isotopic cross-section may be established, once the importance of the total macroscopic cross-section has been roughly determined, by comparing the size of the individual macroscopic cross-section with the total macroscopic cross-section, as previously mentioned. It may be possible to make slight corrections for blanket effects, but these generally are not large, assuming an efficient blanket. The only substantial effect of different blankets is likely to be, of course, on the total breeding ratio. Little has been said in the foregoing about breeding-ratio changes, and though it may be possible to estimate these, in the majority of cases the importance of cross-sections with reference to the breeding ratios is similar to their importance with reference to reactivity effects.

### 19. Accuracy desirable in cross-section measurements

19.1. The results given in Tables VIII, X and XI have been considered in relation to other types of system, as discussed in the foregoing paragraphs. From this consideration, Table XVI has been drawn up. This table suggests orders of accuracy for cross-sections measurements which should be adequate for most types of fast-reactor systems, containing the isotopes shown in any likely proportions, with emphasis on the larger dilute power reactors. From this table, orders of accuracy for other isotopes, e.g. nickel or oxygen, may be reasonably estimated.

A few of the figures ask for exceptional accuracy, probably better than it is possible to obtain with present methods. It must be realized however that even if the orders of accuracy on this table were achieved, it would not guarantee that reactivity could be calculated to better than 1% and breeding ratios to 2% and 5%. Even if accuracy can be improved on those cross-sections where large limits are shown in the table, the importance of the neutron-production and absorption terms in the fertile and fissile isotopes is so high that a total error on reactivity of 1% may still arise only too easily. It is suggested, therefore, that these accuracies must be attained to make it possible to predict with confidence, by calculation alone, systems which are very different from any on which experimental data are available. It should be realized that in the system studied the volume fraction equivalent to the amount of  $\text{Pu}^{239}$  present is less than 3%; no fast-reactor system has yet been built or simulated approaching this order of fuel dilution. Further, experimental simulation of dilute-system spectra by adding moderator in more concentrated systems *cannot* reproduce certain important effects arising in a real dilute system.

19.2. The orders of accuracy quoted may be interpreted as applying to the range of energy defined by the group boundaries. Strictly, in this study they refer to the cross-section assigned to a group, i.e. the average cross-section within a group, listed in Table III. It is a fairly simple matter to refer back these limits to the original set of multi-group cross-sections, i.e. those of Ref. [3].

Some further work is required in considering whether the accuracies quoted would be adequate for other types of calculation, for example, for composition and reactivity changes in burn-up, for activation rates (for the latter, obviously, some of the capture cross-sections should be known to better accuracy), for perturbation- and reaction-rate calculations. In fast-thermal systems, better

TABLE XVI  
ACCURACY REQUIRED IN MEASUREMENTS OF CROSS-SECTIONS FOR FAST,  
REACTOR WORK DILUTE SYSTEMS

Isotope	Group S	$\sigma_{tr}$ (%)	$\sigma_c$ (%)	$\sigma_f$ (%)	$\nu$ (%)	Group transfers R $\leftarrow$ S	$\sigma_{inel}$ R $\leftarrow$ S (%)	$S + \sigma_{el}$ 1 $\leftarrow$ S (%)
$Pu^{239}$	1	10	20	2	1	2 $\leftarrow$ 1	10	100
	2	10	5	1	$1/2$	3 $\leftarrow$ 1	40	—
	3	10	2	1	$1/2$	3 $\leftarrow$ 2	20	50
	4	10	2	1	$1/2$	4 $\leftarrow$ 2	50	—
	5	20	2	2	1	4 $\leftarrow$ 3	100	50
$Pu^{240}$	1	20	20	8	5	2 $\leftarrow$ 1	30	100
	2	20	10	8	5	3 $\leftarrow$ 1	100	—
	3	20	10	100	100	3 $\leftarrow$ 2	50	100
	4	20	10	—	—	4 $\leftarrow$ 2	—	—
	5	40	10	—	—	4 $\leftarrow$ 3	100	100
$U^{238}$	1	5	20	1	1	2 $\leftarrow$ 1	2	20
	2	3	2	50	50	3 $\leftarrow$ 1	5	—
	3	5	1	—	—	3 $\leftarrow$ 2	5	20
	4	10	1	—	—	4 $\leftarrow$ 2	—	—
	5	20	2	—	—	4 $\leftarrow$ 3	10	10
$U^{235}$	1	10	10	3	1	2 $\leftarrow$ 1	7	100
	2	10	5	1	$1/2$	3 $\leftarrow$ 1	30	—
	3	10	2	1	$1/2$	3 $\leftarrow$ 2	10	50
	4	10	2	1	$1/2$	4 $\leftarrow$ 2	30	—
	5	20	2	1	1	4 $\leftarrow$ 3	50	50
Fe	1	5	30	—	—	2 $\leftarrow$ 1	2	10
	2	3	15	—	—	3 $\leftarrow$ 1	10	—
	3	5	10	—	—	3 $\leftarrow$ 2	10	5
	4	10	7	—	—	4 $\leftarrow$ 2	50	—
	5	20	20	—	—	4 $\leftarrow$ 3	—	8
Na	1	10	100	—	—	2 $\leftarrow$ 1	10	10
	2	5	100	—	—	3 $\leftarrow$ 1	50	—
	3	10	100	—	—	3 $\leftarrow$ 2	10	10
	4	10	100	—	—	4 $\leftarrow$ 2	40	—
	5	20	100	—	—	4 $\leftarrow$ 3	—	10
C	1	10	—	—	—	2 $\leftarrow$ 1	—	10
	2	5	—	—	—	3 $\leftarrow$ 1	—	—
	3	10	—	—	—	3 $\leftarrow$ 2	—	5
	4	10	—	—	—	4 $\leftarrow$ 2	—	—
	5	20	—	—	—	4 $\leftarrow$ 3	—	5
						5 $\leftarrow$ 4	—	10

5-group system	Energy boundaries (MeV)	Lethargy increment from 10 MeV
1	— $\infty$ —	2.0
2	— 1.35 —	1.5
3	— 0.30 —	1.5
4	— 0.067 —	2.0
5	— 0.0091 —	—
	— 0 —	—

accuracy and resolution may be required in the energy region covered by our group 5.

Evidence is accumulating that the fission-neutron energy distribution may vary for different isotopes, and with the energy of the neutron causing fission. The effects of this variation should also be studied, since the neutron-production terms have been shown to be of high importance.

### Conclusion

Table XVI presents the orders of accuracy needed in cross-section measurements to ensure that the reactivity of most types of fast-reactor system can be calculated within 1%, and breeding ratios within 2% to 5%. The accuracy required for other isotopes not listed may also be estimated.

A basis is provided for estimating the total probable error due to cross-section inaccuracies for a complete system, and much other useful data are provided on the system examined, and on the effects of other small changes in the calculations.

### ACKNOWLEDGEMENTS

The author is indebted to Dr. R. D. Smith, under whose direction this study was initiated; to Miss G. Holman and Miss L. V. Wragg, for their efficient and methodical computational work; to Dr. A. Hassitt, Mr. E. B. Fossey, and the computer operating staffs at Harwell and Winfrith; and, for some later assistance, to Mr. A. S. B. Belcher.

### REFERENCES

- [1] HASSITT, A., AERE T/R 2487 and T/R 2859.
- [2] MOORHEAD, T. P., AERE M/597.
- [3] LOEWENSTEIN, W. B. and OKRENT, D., Proc. 2nd UN Int. Conf. PUAE **12** (1958) 16.
- [4] MOORHEAD, T. P., AERE R/3055.
- [5] MOORHEAD, T. P., AERE M/576.
- [6] WEINBERG, A. M. and WIGNER, E. P., *The Physical Theory of Neutron Chain Reactors*, ch. 8 and 11, Chicago, The Chicago University Press (1958).



### III. 3. REACTIVITY EFFECTS



# REACTIVITY COEFFICIENTS BY PERTURBATION THEORY

J. W. WEBSTER  
INTERNATIONAL ATOMIC ENERGY AGENCY

## Abstract — Résumé — Аннотация — Resumen

**Reactivity coefficients by perturbation theory.** The development of the formulae of perturbation theory provides a good opportunity to use one of the principal devices of mathematical heuristics, i.e. proceeding by analogy from something that is simple to something that is more complicated.

This paper:

(a) Reviews the formulation of perturbation theory as a method of calculating reactivity coefficients; this consists mainly of developing the differential equation for the adjoint flux, as a continuous function of position and lethargy, by proceeding by analogy from the one-group differential equation for adjoint flux.

(b) Presents an application of the two-group form of perturbation theory to a boiling-mercury-cooled fast-breeder reactor (MCBR).

It is seen that the net Hg density coefficient of reactivity for the first-design-try for the MCBR is negative for some regions and positive for others. However, it is negative for regions of highest statistical weight and where the density change for a power change would be the greatest. The overall Hg density coefficient is thus negative, i.e. the void coefficient is positive—an unsafe condition.

It can be easily seen from the two-group formulation what design changes had to be made to obtain a design which would have a negative void coefficient. It developed in subsequent investigations that there were such design changes that could be made and a design of the MCBR with a negative void coefficient was eventually achieved.

**Calcul des coefficients de réactivité par la théorie des perturbations.** La mise au points des formules de la théorie des perturbations fournit une bonne occasion d'employer en mathématiques une des principales règles de la méthode heuristique, celle qui consiste à procéder par analogie du simple au complexe.

L'auteur du mémoire:

a) Expose une méthode permettant de calculer les coefficients de réactivité en utilisant les formules de la théorie des perturbations; en substance, cette méthode consiste à développer l'équation différentielle relative au flux adjoint en fonction continue de la position et de la léthargie, en procédant par analogie à partir de l'équation différentielle à un groupe relative au flux adjoint.

b) Montre comment appliquer la forme à deux groupes de la théorie des perturbations au cas d'un réacteur surgénérateur à neutrons rapides, refroidi au mercure.

Lors de l'essai préliminaire du réacteur, on a constaté que la variation de réactivité accompagnant une variation de densité du mercure est telle que le coefficient net de la réactivité est négatif pour certaines régions et positif pour d'autres. Il est négatif pour les régions de poids statistique le plus élevé et où une variation de puissance entraînerait le changement de densité le plus important. Le coefficient global de densité du mercure est donc négatif, et par conséquent le coefficient cavitaire est positif, ce qui est dangereux.

On peut facilement voir, en employant la forme à deux groupes, quelles modifications doivent être apportées aux plans du réacteur étudié pour obtenir un coefficient cavitaire négatif. Au cours de recherches ultérieures, il s'est révélé possible d'apporter certaines de ces modifications, et l'on est finalement parvenu à établir des plans tels que le coefficient cavitaire du réacteur soit négatif.

**Коэффициенты реактивности, определенные при помощи теории возмущений.** Развитие формулы теории возмущений дает хорошую возможность использовать один из главных методов математического исследования, т.е. произвести действие по аналогии от простого к более сложному.

В этом докладе:

*a)* Рассматривается формулировка теории возмущений в качестве метода расчета коэффициентов реактивности. Он состоит, главным образом, из развития дифференциального уравнения для сопряженного потока как постоянной функции положения и летаргии, выводимое по аналогии от одной группы дифференциального уравнения для сопряженного потока.

*b)* Даётся применение двухгрупповой формы теории возмущений для кипящего реактора-размножителя на быстрых нейтронах с ртутным теплоносителем (MCBR).

Видно, что коэффициент реактивности ртути низшей плотности в ходе первого испытания проекта MCBR является отрицательным для некоторых областей и положительным для других. Однако он является отрицательным для областей наивысшего статистического веса и там, где изменение плотности с изменением энергии оказывается наибольшим. Общий коэффициент плотности ртути является, таким образом, отрицательным, т.е. коэффициент порозности является положительным, что представляет собой опасное условие.

Можно легко видеть из двухгрупповой формы, какие изменения в проекте должны быть сделаны, чтобы получить проект с отрицательным коэффициентом порозности. Проект получил дальнейшее развитие в последующих исследованиях, в ходе которых определены осуществимые изменения для проекта, и проект MCBR с отрицательным коэффициентом порозности был, в конечном счете, достигнут.

**Determinación de coeficientes de reactividad con ayuda de la teoría de las perturbaciones.** Las fórmulas de la teoría de las perturbaciones pueden establecerse empleando uno de los procedimientos más importantes de la heurística matemática, que consiste en partir de una expresión sencilla para llegar por analogía a una expresión más compleja.

La presente memoria:

*(a)* Formula la teoría de las perturbaciones como método para calcular los coeficientes de reactividad. Consiste principalmente en desarrollar la ecuación diferencial del flujo adjunto como función continua de la posición y del letargo, procediendo por analogía a partir de la ecuación diferencial de un solo grupo para el flujo adjunto.

*(b)* Presenta una aplicación de la forma de dos grupos de la teoría de las perturbaciones a un reactor reproductor rápido, refrigerado por mercurio hirviente (MCBR).

Al calcular la reactividad, se comprueba que el coeficiente correspondiente a la densidad neta del mercurio en el primer proyecto del MCBR es negativo en algunas regiones, y positivo en otras. Es negativo en las regiones de peso estadístico máximo y en las que los cambios de densidad serían mayores al variar la potencia. Por lo tanto, el coeficiente global de densidad del mercurio es negativo, esto es, el coeficiente de vacíos es positivo, lo que constituye una condición que implica peligro.

En la formulación de dos grupos, se aprecia fácilmente qué modificaciones es preciso introducir en el diseño para que el coeficiente de cavidad sea negativo. Nuevas investigaciones demostraron que era posible introducir dichas modificaciones, lográndose establecer para el MCBR un diseño cuyo coeficiente de vacíos es negativo.

## Introduction

The development of the formulae of perturbation theory provides a good opportunity to use one of the principle devices of mathematical heuristic, i.e. proceeding by analogy from something that is simple to something that is more complicated. I would like to propose in this connection a definition of "analogy"

as being a similarity in the arrangement of the elements of two sets, where the word "set" has the broad meaning of modern mathematics of being a group of numbers or functions or ideas or almost anything.

We encounter this device of heuristic early in our technical schooling in all countries. Perhaps geometry provides some of the most beautiful examples. An example which comes to mind is the problem of proving that in a tetrahedron the lines which join a vertex to the mid-point of an opposite face all meet in a point. This is analogous to a simpler problem in that, in a triangle, the lines which join a vertex to the mid-point of the opposite side also meet in a point. When one sees how to prove the simpler problem in the plane he can by analogy see how to prove the more complicated problem in space.

In this paper I shall:

(a) Review the formulation of perturbation theory as a method of calculating reactivity coefficients. This consists mainly of a review of the development of the differential equation for the adjoint flux, as a continuous function of position and lethargy, starting with the one-group differential equation for adjoint flux. Once the forward flux and the adjoint flux, as a continuous function of position and lethargy, or any group approximation to them, are known, it is quite easy to write down formulae for the reactivity coefficients for various compositional perturbations. These formulae are not new and have been derived in various ways by various people in various countries.

(b) Present an application of the two-group form of perturbation theory to a boiling-Mercury-Cooled fast-Breeder Reactor (MCBR). The application was part of a kinetics evaluation of the MCBR performed by the Advanced Technology Laboratories (a division of American-Standard) for the United States Atomic Energy Commission.

The accurate computation of reactivity coefficients is of particular importance in the design of fast reactors because of the crucial aspects of kinetics and safety, or perhaps one should say, because of the exceptional opportunity for safety offered by fast reactors.

Perturbation theory provides a way of computing these coefficients when the compositional perturbation is spatially non-uniform, a task that is difficult with the straightforward use of the neutron-group solutions of the diffusion equation.

The differential equation for the flux,  $\varphi(\mathbf{r}, u)$ , in a critical reactor as a function of position,  $\mathbf{r}$ , and lethargy,  $u$ , is given by the familiar equations:

$$\begin{aligned} & -D(\mathbf{r}, u) \nabla^2 \varphi(\mathbf{r}, u) + \Sigma_a(\mathbf{r}, u) \varphi(\mathbf{r}, u) + \frac{\partial q(\mathbf{r}, u)}{\partial u} + \frac{\partial \eta(\mathbf{r}, u)}{\partial u} - \\ & - \int_0^u g(\mathbf{r}, u' \rightarrow u) \varphi(\mathbf{r}, u') du' - v_c \chi(u) \left[ \sum_{f_i} \varphi_i(\mathbf{r}) + \int_0^{u_f} \sum_i \varphi_i(\mathbf{r}, u) \varphi(\mathbf{r}, u) du \right] = 0 \\ & -D_t(\mathbf{r}) \nabla^2 \varphi_t(\mathbf{r}) + \Sigma_{a_t}(\mathbf{r}) \varphi_t(\mathbf{r}) - q_t(\mathbf{r}) - \eta_t(\mathbf{r}) = 0 \\ & q(\mathbf{r}, u) = \xi \sum_s (\mathbf{r}, u) \varphi(\mathbf{r}, u); \quad \frac{\partial \eta(\mathbf{r}, u)}{\partial u} = \Sigma_{s_H}(\mathbf{r}, u) \varphi(\mathbf{r}, u) - \eta(\mathbf{r}, u). \end{aligned} \quad (1)$$

This differential equation is solved by various codes for various machines in various countries.

In the present paper, a process of generalizing by analogy is used, going from one-group to  $N$ -group to continuous lethargy, to derive the equivalent differential

equation for the adjoint flux,  $\varphi^*(\mathbf{r}, u)$ , the lowest eigenfunction of the set  $\psi_m^*(\mathbf{r}, u)$  which is orthogonal to the set  $\psi_n(\mathbf{r}, u)$  of which  $\varphi(\mathbf{r}, u)$  is the lowest eigenfunction. This orthogonality is of the type

$$\int_V \frac{1}{v} \psi_m^*(\mathbf{r}, u) \psi_n(\mathbf{r}, u) d\mathbf{v} = \delta_{mn} \quad (2)$$

Once the  $\varphi(\mathbf{r}, u)$  and  $\varphi^*(\mathbf{r}, u)$  or any group-approximation to them, are known it is quite easy to write down formulae for the reactivity coefficients for various compositional perturbations.

### Adjoint flux

#### ONE-GROUP THEORY

The time-dependent equation is

$$D(\mathbf{r}) \nabla^2 \varphi(\mathbf{r}, t) + [k(\mathbf{r}) - 1] \Sigma_a(\mathbf{r}) \varphi(\mathbf{r}, t) = \frac{1}{v} \frac{\partial \varphi(\mathbf{r}, t)}{\partial t} \quad (3)$$

if delayed neutrons are ignored.

Any expression of the form  $\psi_n(\mathbf{r}) e^{\lambda_n t}$  is a solution of Eq. (3), because when this form is substituted and  $e^{\lambda_n t}$  is cancelled from both sides, the resulting equation, i.e.

$$D(\mathbf{r}) \nabla^2 \psi_n + [k(\mathbf{r}) - 1] \Sigma_a(\mathbf{r}) \psi_n(\mathbf{r}) = \frac{\lambda_n}{v} \psi_n(\mathbf{r}) \quad (4)$$

has a solution. For example, suppose we have a slab reactor with core and reflector. For any value of  $\lambda_n$  there exists a solution consisting of a cosine function in the core and a linear combination of hyperbolic functions in the reflector which would satisfy the conditions of zero slope at the centre of core and continuity of flux and current at the interface between core and reflector. For a certain set of numbers,  $\lambda_1, \lambda_2, \dots, \lambda_n$ , the corresponding solutions,  $\psi_1, \psi_2, \dots, \psi_n$ , vanish at the outer surface of the reflector. This set of  $\lambda_n$  is the set of eigenvalues; the set of  $\psi_n$  is the set of eigenfunctions.

The  $\psi_n$  form a self-orthogonal set over the volume of the reactor, with respect to  $1/v$ . This can be seen as follows. Consider two eigenfunctions,  $\psi_n(\mathbf{r})$  and  $\psi_m(\mathbf{r})$  of the set. The former obeys Eq. (4), the latter the following equation:

$$D(\mathbf{r}) \nabla^2 \psi_m + [k(\mathbf{r}) - 1] \Sigma_a(\mathbf{r}) \psi_m(\mathbf{r}) = \frac{\lambda_m}{v} \psi_m(\mathbf{r}). \quad (5)$$

Multiplying Eq. (4) by  $\psi_m$  and Eq. (5) by  $\psi_n$ , subtracting and integrating over the reactor volume, we obtain the result

$$\int D(\mathbf{r}) [\psi_n(\mathbf{r}) \nabla^2 \psi_n(\mathbf{r}) - \psi_m(\mathbf{r}) \nabla^2 \psi_m(\mathbf{r})] d\mathbf{v} = (\lambda_m - \lambda_n) \int \frac{1}{v} \psi_n(\mathbf{r}) \psi_m(\mathbf{r}) d\mathbf{v}. \quad (6)$$

The left-hand side is zero by Green's second theorem. Thus the right-hand side must be zero:

$$(\lambda_m - \lambda_n) \int \frac{1}{v} \psi_n(\mathbf{r}) \psi_m(\mathbf{r}) d\mathbf{v} = 0. \quad (7)$$

When  $n \neq m$ ,  $\lambda_m \neq \lambda_n$ , it follows that

$$\int \frac{1}{v} \psi_n(\mathbf{r}) \psi_m(\mathbf{r}) d\mathbf{v} = 0 \quad (8)$$

When  $n=m$ ,

$$\int \frac{1}{v} \psi_n^2(\mathbf{r}) dv \neq 0 \quad (9)$$

because the squared integrand cannot be negative anywhere and it is not zero everywhere.

Thus, in one-group theory, the desired set of functions,  $\psi_m^*$ , which is to be orthogonal to the set,  $\psi_n$ , is just the set,  $\psi_n$ , itself, because the set,  $\psi_n$ , is self-orthogonal. The lowest eigenfunction of the set,  $\psi_m^*$ , or  $\psi_1^*$  or  $\varphi^*$  is just  $\varphi$  ( $\equiv \psi_1$ ) itself. In other words the adjoint flux is the same as the flux in one-group theory.

## TWO-GROUP THEORY

The one-group treatment will now be generalized to two groups. The time-dependent equations are

$$D_1 \nabla^2 \varphi_1 - \Sigma_{a_1} \varphi_1 - \Sigma_{r_1} \varphi_1 + \chi_1 v_1 \Sigma_{f_1} \varphi_1 + \chi_1 v_2 \Sigma_{f_2} \varphi_2 = \frac{1}{v_1} \frac{\partial \varphi_1}{\partial t} \quad (10)$$

$$D_2 \nabla^2 \varphi_2 - \Sigma_{a_2} \varphi_2 + \Sigma_{r_1} \varphi_1 + \chi_2 v_1 \Sigma_{f_1} \varphi_1 + \chi_2 v_2 \Sigma_{f_2} \varphi_2 = \frac{1}{v_2} \frac{\partial \varphi_2}{\partial t}. \quad (11)$$

The  $\varphi_1(\mathbf{r}, t)$  and  $\varphi_2(\mathbf{r}, t)$  have solutions of the form

$$\varphi_1(\mathbf{r}, t) \sim \psi_{1m} e^{\lambda_m t}$$

$$\varphi_2(\mathbf{r}, t) \sim \psi_{2n} e^{\lambda_n t}$$

where  $\psi_{1m}/\psi_{2n}$  is the ratio of  $n$ th mode fluxes.

The  $\psi_{1m}$  and  $\psi_{2n}$  are the eigenfunctions of

$$D_1 \nabla^2 \psi_{1m} - \Sigma_{a_1} \psi_{1m} - \Sigma_{r_1} \psi_{1m} + \chi_1 v_1 \Sigma_{f_1} \psi_{1m} + \chi_1 v_2 \Sigma_{f_2} \psi_{2n} = \frac{\lambda_m}{v_1} \psi_{1m} \quad (12)$$

$$D_2 \nabla^2 \psi_{2n} - \Sigma_{a_2} \psi_{2n} + \Sigma_{r_1} \psi_{1m} + \chi_2 v_1 \Sigma_{f_1} \psi_{1m} + \chi_2 v_2 \Sigma_{f_2} \psi_{2n} = \frac{\lambda_m}{v_2} \psi_{2n} \quad (13)$$

Although analogy is the most important tool of discovery and understanding, it can often lead to a conjecture which is incorrect. Analogy, we agreed earlier, is a similarity in the arrangement of the elements of two sets. It is clear that there may be several arrangements of the elements of Set B which are similar to the arrangement of the elements of Set A.

At this point a strictly analogous procedure to the one-group leads one astray. The strictly analogous procedure would be to write the equations for  $\psi_{1m}$  and  $\psi_{2m}$ ; i.e.,

$$D_1 \nabla^2 \psi_{1m} - \Sigma_{a_1} \psi_{1m} - \Sigma_{r_1} \psi_{1m} + \chi_1 v_1 \Sigma_{f_1} \psi_{1m} + \chi_1 v_2 \Sigma_{f_2} \psi_{2m} = \frac{\lambda_m}{v_1} \psi_{1m} \quad (14)$$

$$D_2 \nabla^2 \psi_{2m} - \Sigma_{a_2} \psi_{2m} + \Sigma_{r_1} \psi_{1m} + \chi_2 v_1 \Sigma_{f_1} \psi_{1m} + \chi_2 v_2 \Sigma_{f_2} \psi_{2m} = \frac{\lambda_m}{v_2} \psi_{2m} \quad (15)$$

then multiply Eq. (12) by  $\psi_{1m}$ , Eq. (13) by  $\psi_{2m}$ , Eq. (14) by  $\psi_{1n}$  and Eq. (15) by  $\psi_{2n}$ ; subtract the last two from the sum of the first two; and then integrate over the reactor volume. The result is

$$\begin{aligned}
& \int D_1 (\psi_{1m} \nabla^2 \psi_{1n} - \psi_{1n} \nabla^2 \psi_{1m}) dv + \int D_2 (\psi_{2m} \nabla^2 \psi_{2n} - \psi_{2n} \nabla^2 \psi_{2m}) dv + \\
& + \int \chi_1 v_2 \Sigma_{f_2} (\psi_{2n} \psi_{1m} - \psi_{2m} \psi_{1n}) dv + \int (\Sigma_{r_1} + \chi_2 v_1 \Sigma_{f_1}) (\psi_{1n} \psi_{2m} - \psi_{1m} \psi_{2n}) dv = \\
& = (\lambda_n - \lambda_m) \left( \frac{\psi_{1n} \psi_{1m}}{v_1} + \frac{\psi_{2n} \psi_{2m}}{v_2} \right) dv. \tag{16}
\end{aligned}$$

The analogous thing to one group would be for the left-hand side to be zero and then the orthogonality would be expressed by the right-hand side being zero for  $n \neq m$ ; i.e.,

$$\int \left( \frac{\psi_{1n} \psi_{1m}}{v_1} + \frac{\psi_{2n} \psi_{2m}}{v_2} \right) dv \stackrel{?}{=} 0 \tag{17}$$

A close look at the left-hand side, however, shows that, although the first and second terms are zero by Green's theorem, the third and fourth terms are not zero. The orthogonality expressed by Eq. (17) does not therefore hold.

We have just seen that the set of functions  $(\psi_{1n}, \psi_{2m})$  is not self-orthogonal. The logical question to ask, then, is: "Is there some other set  $(\psi_{1n}^*, \psi_{2m}^*)$  which is orthogonal to the set  $(\psi_{1n}, \psi_{2m})$ ?" More particularly, "What changes could be made in Eqs. (14) and (15) which would lead to the third and fourth terms on the left-hand side of Eq. (16) being zero?" It can be seen that if the coefficient of  $\psi_{2m}$  in Eq. (14) and the coefficient of  $\psi_{1m}$  in Eq. (15) are interchanged, the desired result is accomplished; i.e., Eqs. (14) and (15) are replaced by

$$D_1 \nabla^2 \psi_{1m} - \Sigma_{a_1} \psi_{1m} - \Sigma_{r_1} \psi_{1n} + \chi_1 v_1 \Sigma_{f_1} \psi_{1m} + (\Sigma_{r_1} + \chi_2 v_1 \Sigma_{f_1}) \psi_{2m} = \frac{\lambda_m}{v_1} \psi_{1m} \tag{18}$$

$$D_2 \nabla^2 \psi_{2m} - \Sigma_{a_2} \psi_{2m} + \chi_2 v_2 \Sigma_{f_2} \psi_{2m} + \chi_1 v_2 \Sigma_{f_2} \psi_{1m} = \frac{\lambda_m}{v_2} \psi_{2m}. \tag{19}$$

An alternative way of expressing this is afforded by the concept of adjoint matrices. Let us write Eqs. (12) and (13) as

$$\begin{pmatrix} D_1 \nabla^2 - \Sigma_{a_1} - \Sigma_{r_1} + \chi_1 v_1 \Sigma_{f_1} - \frac{\lambda_n}{v_1} & \chi_1 v_2 \Sigma_{f_2} \\ \Sigma_{r_1} + \chi_2 v_1 \Sigma_{f_1} & D_2 \nabla^2 - \Sigma_{a_2} + \chi_2 v_2 \Sigma_{f_2} - \frac{\lambda_n}{v_2} \end{pmatrix} \begin{pmatrix} \psi_{1n} \\ \psi_{2n} \end{pmatrix} = \begin{pmatrix} 0 \\ 0 \end{pmatrix}. \tag{20}$$

Replacing the matrix on the left by its adjoint, we have

$$\begin{pmatrix} D_1 \nabla^2 - \Sigma_{a_1} - \Sigma_{r_1} + \chi_1 v_1 \Sigma_{f_1} - \frac{\lambda_n^*}{v_1} & \Sigma_{r_1} + \chi_2 v_1 \Sigma_{f_1} \\ \chi_1 v_2 \Sigma_{f_2} & D_2 \nabla^2 - \Sigma_{a_2} + \chi_2 v_2 \Sigma_{f_2} - \frac{\lambda_n^*}{v_2} \end{pmatrix} \begin{pmatrix} \psi_{1m}^* \\ \psi_{2m}^* \end{pmatrix} = \begin{pmatrix} 0 \\ 0 \end{pmatrix}. \tag{21}$$

It can be shown that the set,  $\lambda_m^*$ , is identical to the set,  $\lambda_n$ , so we drop\*.

The demonstration of orthogonality of the set  $(\psi_{1n}, \psi_{2m})$  with the set  $(\psi_{1m}^*, \psi_{2m}^*)$  is as follows:

$$\begin{aligned}
& D_1 \nabla^2 \psi_{1m} - \Sigma_{a_1} \psi_{1m}^* - \Sigma_{r_1} \psi_{1m}^* + \chi_1 v_1 \Sigma_{f_1} \psi_{1m}^* \\
& - \frac{\lambda_m}{v_1} \psi_{1m}^* + \Sigma_{r_1} \psi_{2m}^* + \chi_2 v_1 \Sigma_{f_1} \psi_{2m}^* = 0. \tag{21}
\end{aligned}$$

$$D_2 \nabla^2 \psi_{2m}^* - \Sigma_{a_2} \psi_{2m}^* + \chi_2 v_2 \Sigma_{f_2} \psi_{2m}^* - \frac{\lambda_m}{v_2} \psi_{2m}^* + \chi_1 v_2 \Sigma_{f_2} \psi_{1m}^* = 0.$$

Multiplying the first by  $\psi_{1n}$  and the second by  $\psi_{2n}$ , we have

$$\begin{aligned} D_1 \psi_{1n} \nabla^2 \psi_{1m}^* - \sum_{a_1} \psi_{1n} \psi_{1m}^* - \sum_{r_1} \psi_{1n} \psi_{1m}^* + \chi_1 v_1 \sum_{f_1} \psi_{1n} \psi_{1m}^* - \frac{\lambda_m}{v_1} \psi_{1n} \psi_{1m}^* \\ + \sum_{r_1} \psi_{1n} \psi_{2m}^* + \chi_2 v_1 \sum_{f_1} \psi_{1n} \psi_{2m}^* = 0. \end{aligned} \quad (22)$$

$$\begin{aligned} D_2 \psi_{2n} \nabla^2 \psi_{2m}^* - \sum_{a_2} \psi_{2n} \psi_{2m}^* + \chi_2 v_2 \sum_{f_2} \psi_{2n} \psi_{2m}^* \\ - \frac{\lambda_m}{v_2} \psi_{2n} \psi_{2m}^* + \chi_1 v_2 \sum_{f_2} \psi_{2n} \psi_{1m}^* = 0. \end{aligned}$$

Similarly, from Eq. (12) and (13), we have

$$\begin{aligned} D_1 \psi_{1m}^* \nabla^2 \psi_{1n} - \sum_{a_1} \psi_{1m}^* \psi_{1n} - \sum_{r_1} \psi_{1m}^* \psi_{1n} + \chi_1 v_1 \sum_{f_1} \psi_{1m}^* \psi_{1n} - \frac{\lambda_m}{v_1} \psi_{1m}^* \psi_{1n} \\ + \chi_1 v_2 \sum_{f_2} \psi_{1m}^* \psi_{2n} = 0. \end{aligned} \quad (23)$$

$$\begin{aligned} D_2 \psi_{2m}^* \nabla^2 \psi_{2n} - \sum_{a_2} \psi_{2m}^* \psi_{2n} + \chi_2 v_2 \sum_{f_2} \psi_{2m}^* \psi_{2n} - \frac{\lambda_n}{v_2} \psi_{2m}^* \psi_{2n} \\ + \sum_{r_1} \psi_{2m}^* \psi_{1n} + \chi_2 v_1 \sum_{f_1} \psi_{2m}^* \psi_{1n} = 0 \end{aligned}$$

Subtracting Eq. (23) from the sum of Eq. (22), it follows that

$$(\lambda_n - \lambda_m) \int \left( \frac{1}{v_1} \psi_{1n} \psi_{1m}^* + \frac{1}{v_2} \psi_{2n} \psi_{2m}^* \right) dv = 0. \quad (24)$$

If  $n \neq m$ ,  $\lambda_n \neq \lambda_m$ , and the orthogonality follows:

$$\int \left( \frac{1}{v_1} \psi_{1n} \psi_{1m}^* + \frac{1}{v_2} \psi_{2n} \psi_{2m}^* \right) dv = 0 \quad (25)$$

If  $n = m$ ,  $\lambda_n = \lambda_m$  and

$$\int \left( \frac{1}{v_1} \psi_{1n} \psi_{1n}^* + \frac{1}{v_2} \psi_{2n} \psi_{2n}^* \right) dv \neq 0. \quad (26)$$

The desired functions, the adjoint fluxes, are thus

$$\psi_{11}^* = \varphi_1^*$$

$$\psi_{21}^* = \varphi_2^*$$

#### *N*-GROUP THEORY

The *N*-group equations for the *n*th eigenfunction of the time-dependent flux are:

$$\begin{aligned} D_1 \nabla^2 \psi_{1n} - \sum_{a_1} \psi_{1n} - \sum_{r_1} \psi_{1n} + \chi_1 v_1 (\sum_{f_1} \psi_{1n} + \dots + \sum_{f_N} \psi_{Nn}) = \frac{\lambda_n}{v_1} \psi_{1n} \\ D_2 \nabla^2 \psi_{2n} - \sum_{a_2} \psi_{2n} - \sum_{r_2} \psi_{2n} + \sum_{r_1} \psi_{1n} + g_{1 \rightarrow 2} \psi_{1n} \\ + \chi_2 v_2 (\sum_{f_1} \psi_{1n} + \dots + \sum_{f_N} \psi_{Nn}) = \frac{\lambda_n}{v_2} \psi_{2n} \end{aligned} \quad (27)$$

$$\begin{aligned} D_N \nabla^2 \psi_{Nn} - \sum_{a_N} \psi_{Nn} + \sum_{r_{N-1}} \psi_{N-1,n} + g_{1 \rightarrow N} \psi_{1n} + \dots + g_{N-1 \rightarrow N} \psi_{N-1,n} \\ + \chi_N v_N (\sum_{f_1} \psi_{1n} + \dots + \sum_{f_N} \psi_{Nn}) = \frac{\lambda_n}{v_N} \psi_{Nn} \end{aligned}$$

where the notation is standard.

The *N*-group equations for the *n*th adjoint-flux eigenfunction can be established by analogy with the few-group development. The result is

$$\begin{aligned}
D_1 \nabla^2 \psi_{1m}^* - (\Sigma_{a_1} + \Sigma_{r_1}) \psi_{1m}^* + \Sigma_{r_1} \psi_{2m}^* + g_{1 \rightarrow 2} \psi_{2m}^* + g_{1 \rightarrow 3} \psi_{3m}^* + \cdots + g_{1 \rightarrow N} \psi_{Nm}^* \\
+ v_1 \Sigma_1 (\chi_1 \psi_{1m}^* + \cdots + \chi_N \psi_{Nm}^*) = \frac{\lambda_m}{v_1} \psi_{1m}^* \\
D_2 \nabla^2 \psi_{2m}^* - (\Sigma_{a_2} + \Sigma_{r_2}) \psi_{2m}^* + \Sigma_{r_2} \psi_{3m}^* + g_{2 \rightarrow 3} \psi_{3m}^* + \cdots + g_{2 \rightarrow N} \psi_{Nm}^* \\
+ v_2 \Sigma_{f_2} (\chi_1 \psi_{1m}^* + \cdots + \chi_N \psi_{Nm}^*) = \frac{\lambda_m}{v_2} \psi_{2m}^* \quad (28) \\
D_{N-1} \nabla^2 \psi_{N-1,m}^* - (\Sigma_{a_{N-1}} + \Sigma_{r_{N-1}}) \psi_{N-1,m}^* + \Sigma_{r_{N-1}} \psi_{Nm}^* + g_{N-1 \rightarrow N} \psi_{Nm}^* \\
+ v_{N-1} \Sigma_{f_{N-1}} (\chi_1 \psi_{1m}^* + \cdots + \chi_N \psi_{Nm}^*) = \frac{\lambda_m}{v_{N-1}} \psi_{N-1,m}^* \\
D_N \nabla^2 \psi_{Nm}^* - \Sigma_{a_N} \psi_{Nm}^* + v_N \Sigma_{f_N} (\chi_1 \psi_{1m}^* + \cdots + \chi_N \psi_{Nm}^*) = \frac{\lambda_m}{v_N} \psi_{Nm}^*
\end{aligned}$$

The desired functions, the adjoint fluxes, are then

$$\begin{aligned}
\varphi_1^* &= \psi_{11}^* \\
\varphi_2^* &= \psi_{21}^* \\
&\vdots \\
\varphi_N^* &= \psi_{N1}^*
\end{aligned}$$

#### CONTINUOUS LETHARGY THEORY

The differential equation for the  $n$ th eigenfunction for flux is

$$\begin{aligned}
D(\mathbf{r}, u) \nabla^2 \psi_n(\mathbf{r}, u) - \Sigma_a(\mathbf{r}, u) \psi_n(\mathbf{r}, u) - \frac{\partial q_n(\mathbf{r}, u)}{\partial u} - \frac{\partial \eta_n(\mathbf{r}, u)}{\partial u} \\
+ \int_0^u g(\mathbf{r}, u' \rightarrow u) \psi_n(\mathbf{r}, u') du' + v(u) \chi(u) \left[ \Sigma_{f_t} \psi_{n_t}(\mathbf{r}) + \int_0^{u_t} \Sigma_f(\mathbf{r}, u) \psi_n(\mathbf{r}, u) du \right] \\
= \frac{\lambda_n}{v} \psi_n(\mathbf{r}, u) \quad (29)
\end{aligned}$$

with the special case at thermal being

$$D_t(\mathbf{r}) \nabla^2 \psi_{n_t}(\mathbf{r}) - \Sigma_{a_t}(\mathbf{r}) \psi_{n_t}(\mathbf{r}) + q_{n_t}(\mathbf{r}) + \eta_{n_t}(\mathbf{r}) = \frac{\lambda_n}{v_t} \psi_{n_t}(\mathbf{r}) \quad (30)$$

where

$$q_n(\mathbf{r}, u) = \xi \Sigma_s(\mathbf{r}, u) \psi_n(\mathbf{r}, u) \quad (31)$$

and where

$$\frac{\partial \eta_n(\mathbf{r}, u)}{\partial u} = \Sigma_{s_H}(\mathbf{r}, u) \psi_n(\mathbf{r}, u) - \eta_n(\mathbf{r}, u) \quad (32)$$

When Eq. (25) is generalized, it is seen that we wish to find a set of functions,  $\psi_n^*(\mathbf{r}, u)$ , which have the following properties:

$$\begin{aligned}
\int_{\text{Reactor volume}} \left\{ \frac{1}{v_t} \psi_{n_t}(\mathbf{r}) \psi_{m_t}^*(\mathbf{r}) + \int_0^{u_t} \frac{1}{v(u)} \psi_n(\mathbf{r}, u) \psi_m^*(\mathbf{r}, u) du \right\} dv = 0 \quad (n \neq m) \\
\neq 0 \quad (n = m) \quad (33)
\end{aligned}$$

This could be written more compactly as

$$\begin{aligned}
\int_V \int_U \frac{1}{v} \psi_n(\mathbf{r}, u) \psi_m^*(\mathbf{r}, u) du dv = 0 \quad (n \neq m) \\
\neq 0 \quad (n = m) \quad (34)
\end{aligned}$$

When the differential equations for the eigenfunctions were in the group form, it was fairly easy to discover the corresponding differential equations for the importance functions, i.e., the adjoint system. To discover the differential equations for the importance function expressed in continuous lethargy,  $u$ , (i.e., the equations corresponding to Eqs. 29, 30, 31 and 32) is also not difficult but is more involved.

The most straightforward way is to pass by analogy from the  $N$ -group equations (Eq. 28) for the importance function to the desired continuous lethargy equation. Space does not permit presentation of the details, but the procedure is to express the  $N$ -group equations in terms of infinitesimals by analogy, and let  $N$  go to infinity, and pass to the limit. The final result is:

$$\begin{aligned} D(\mathbf{r}, u) \nabla^2 \psi_m^*(\mathbf{r}, u) - \Sigma_a(\mathbf{r}, u) \psi_m^*(\mathbf{r}, u) + \xi \Sigma_s(\mathbf{r}, u) \frac{\partial \psi_m^*(\mathbf{r}, u)}{\partial u} \\ = \psi_m^*(\mathbf{r}, u) \Sigma_{sH}(\mathbf{r}, u) + \frac{\Sigma_{sH}(\mathbf{r}, u)}{e^{-u}} \left\{ \psi_m^*(\mathbf{r}) e^{-u_t} + \int_0^{u_t} \psi_m^*(\mathbf{r}, u') e^{-u'} du' \right\} \\ + \left\{ g(\mathbf{r}, u \rightarrow \text{th}) \psi_m^*(\mathbf{r}) + \int_0^{u_t} g(\mathbf{r}, u \rightarrow u') \psi_m^*(\mathbf{r}, u') du' \right\} \\ + \nu(u) \Sigma_f(\mathbf{r}, u) \int_0^{u_t} \chi(u') \psi_m^*(\mathbf{r}, u') du' = \frac{\lambda_m}{v} \psi_m^*(\mathbf{r}, u) \end{aligned} \quad (35)$$

By observing the last equation of Eq. 28, one sees that the special case of the above equation at thermal is

$$D_t(\mathbf{r}) \nabla^2 \psi_{m_t}^*(\mathbf{r}) - \Sigma_{a_t}(\mathbf{r}) \psi_{m_t}^*(\mathbf{r}) + \nu_t \Sigma_{f_t}(\mathbf{r}) \int_0^{u_t} \chi(u') \psi_{m_t}^*(\mathbf{r}, u') du' = \frac{\lambda_m}{v} \psi_{m_t}^*(\mathbf{r}) \quad (36)$$

The desired function is, then,

$$\varphi^*(\mathbf{r}, u) = \psi_1^*(\mathbf{r}, u)$$

### Reactivity coefficients

From a study of Eq. 29 and 30, it will be seen that the various kinds of perturbation of constants that can be made are

$$\begin{aligned} D(\mathbf{r}, u) &\rightarrow D(\mathbf{r}, u) + \delta D(\mathbf{r}, u) \\ \Sigma_a(\mathbf{r}, u) &\rightarrow \Sigma_a(\mathbf{r}, u) + \delta \Sigma_a(\mathbf{r}, u) \\ \xi \Sigma_s(\mathbf{r}, u) &\rightarrow \xi \Sigma_s(\mathbf{r}, u) + \delta [\xi \Sigma_s(\mathbf{r}, u)] \\ \Sigma_{sH}(\mathbf{r}, u) &\rightarrow \Sigma_{sH}(\mathbf{r}, u) + \delta \Sigma_{sH}(\mathbf{r}, u) \\ g(\mathbf{r}, u' \rightarrow u) &\rightarrow g(\mathbf{r}, u' \rightarrow u) + \delta g(\mathbf{r}, u' \rightarrow u) \\ \Sigma_f(\mathbf{r}, u) &\rightarrow \Sigma_f(\mathbf{r}, u) + \delta \Sigma_f(\mathbf{r}, u) \\ \nu_c &\rightarrow \nu_c + \delta \nu_c \end{aligned}$$

where we shall define

$$\Sigma_f(\mathbf{r}, u) \equiv \frac{\nu(u)}{\nu_c} \Sigma_f(\mathbf{r}, u).$$

The last change is an artificial one which will be utilized in a later formula. For the moment we seek a formula for the stable period,  $\lambda_1$ , (assuming, as throughout this paper, there are no delayed neutrons). Substituting these changes of constants into Eqs. 29 and 30, letting  $n=1$ , multiplying through by  $\psi_m^*(\mathbf{r}, u)$ ; then letting  $m=1$  in Eqs. 35 and 36, multiplying through by  $\psi_n(\mathbf{r}, u)$ , subtracting these equations and integrating over lethargy and volume, the result is

$$\begin{aligned}
 & \int_V \int_U \psi_1^*(\mathbf{r}, u) \operatorname{div} \delta D(\mathbf{r}, u) \operatorname{grad} \psi_1(\mathbf{r}, u) du dv \\
 & \quad - \int_V \int_U \delta \Sigma_s(\mathbf{r}, u) \psi_1^*(\mathbf{r}, u) \psi_1(\mathbf{r}, u) du dv \\
 & - \int_V \int_0^{u_t} \psi_1^*(\mathbf{r}, u) \frac{\partial}{\partial u} [\delta \{\xi \Sigma_s(\mathbf{r}, u)\} \psi_1(\mathbf{r}, u)] du dv \\
 & \quad - \int_V \psi_{1t}^*(\mathbf{r}) \delta \{\xi \Sigma_s(\mathbf{r}, u_t)\} \psi_1(\mathbf{r}, u_t) dv \\
 & - \int_V \int_0^u \psi_1^*(\mathbf{r}, u) \varphi_1(\mathbf{r}, u) \delta \Sigma_{sH}(\mathbf{r}, u) du dv \\
 & \quad + \int_V \int_0^{u_t} \psi_1^*(\mathbf{r}, u) e^{-u} \int_0^u \frac{\psi_1(\mathbf{r}, u') \delta \Sigma_{sH}(\mathbf{r}, u')}{e^{-u'}} du' du dv \\
 & + \int_V \psi_{1t}^*(\mathbf{r}) e^{-u_t} \int_0^{u_t} \frac{\psi_1(\mathbf{r}, u') \delta \Sigma_{sH}(\mathbf{r}, u')}{e^{-u'}} du' dv \\
 & \quad + \int_V \int_0^{u_t} \psi_1^*(\mathbf{r}, u) \int_0^u \delta g(\mathbf{r}, u' \rightarrow u) \psi_1(\mathbf{r}, u') du' du dv \\
 & + \int_V \psi_{1t}^*(\mathbf{r}) \int_0^{u_t} \delta g(\mathbf{r}, u' \rightarrow \text{th}) \psi_1(\mathbf{r}, u') du' dv \\
 & \quad + \int_V \int_U \delta \nu_c \psi_1(\mathbf{r}, u) \chi(u) \int_U \Sigma_f(\mathbf{r}, u) \psi_1(\mathbf{r}, u') du' du dv \\
 & + \int_V \int_U \nu_c \psi_1^*(\mathbf{r}, u) \chi(u) \int_U \delta \Sigma_f(\mathbf{r}, u') \psi_1(\mathbf{r}, u') du' du dv \\
 & + \int_V \int_U \delta \nu_c \psi_1^*(\mathbf{r}, u) \chi(u) \int_U \delta \Sigma_f(\mathbf{r}, u') \psi_1(\mathbf{r}, u') du' du dv \\
 & = \lambda_1 \int_V \int_U \frac{1}{v} \psi_1^*(\mathbf{r}, u) \psi_1(\mathbf{r}, u) du dv \quad (37)
 \end{aligned}$$

Eq. 37 provides an expression for  $\lambda_1$ , after dividing through by the double integral on the left.

Eq. 37 also provides an expression for  $\delta \nu_c/\nu_c$ , which is by definition the reactivity effect. To obtain this,  $\lambda_1$  is set equal to zero, the last term on the left is neglected since it contains the product of two increments, and the quantity  $-\delta \nu_c/\nu_c$  is

solved for. (It is clear that  $\delta \nu_c$  is the artificial change in  $\nu_c$  which offsets the actual changes.)

The result is

$$\begin{aligned} \delta \varrho \equiv -\frac{\delta \nu_c}{\nu_c} = & \frac{1}{\int_V \int_U \varphi^*(\mathbf{r}, u) \chi(u) \int_U \nu_c \Sigma_f(\mathbf{r}, u') \varphi(\mathbf{r}, u') du' du dv} \\ & \cdot \left[ - \int_V \int_U \delta \Sigma_a(\mathbf{r}, u) \varphi^*(\mathbf{r}, u) du dv + \int_V \int_U \varphi^*(\mathbf{r}, u) \operatorname{div} \delta D(\mathbf{r}, u) \operatorname{grad} \varphi(\mathbf{r}, u) du dv \right. \\ & - \int_V \int_0^{u_t} \varphi^*(\mathbf{r}, u) \frac{\partial}{\partial u} [\delta \{ \xi \Sigma_s(\mathbf{r}, u) \} \varphi(\mathbf{r}, u)] du dv - \int_V \varphi_t^*(\mathbf{r}) \delta \{ \xi \Sigma_s(\mathbf{r}, u_t) \} \varphi(\mathbf{r}, u_t) dv \\ & - \int_V \int_0^{u_t} \varphi^*(\mathbf{r}, u) \varphi(\mathbf{r}, u) \delta \Sigma_{sH}(\mathbf{r}, u) du dv + \int_V \int_0^{u_t} \varphi^*(\mathbf{r}, u) e^{-u} \int_0^u \frac{\varphi(\mathbf{r}, u') \delta \Sigma_{sH}(\mathbf{r}, u')}{e^{-u'}} du' du dv \\ & \quad + \int_V \varphi_t^*(\mathbf{r}) e^{-u_t} \int_0^{u_t} \frac{\varphi(\mathbf{r}, u') \delta \Sigma_{sH}(\mathbf{r}, u')}{e^{-u'}} du' dv \\ & + \int_V \int_0^{u_t} \varphi^*(\mathbf{r}, u) \int_0^u \delta g(\mathbf{r}, u' \rightarrow u) \varphi(\mathbf{r}, u') du' du dv \\ & \quad + \int_V \varphi_t^*(\mathbf{r}) \int_0^{u_t} \delta g(\mathbf{r}, u' \rightarrow \text{th}) \varphi(\mathbf{r}, u') du' dv \\ & \left. + \int_V \int_U \nu_0 \varphi^*(\mathbf{r}, u) \chi(u) \int_U \delta \Sigma_f(\mathbf{r}, u') \varphi(\mathbf{r}, u') du' du dv \right]. \end{aligned}$$

### Physical interpretations

It was, I believe, originally pointed out by Professor Eugene Wigner that  $\varphi^*(\mathbf{r}, u)$  has the physical interpretation of a neutron-importance function in the sense that, if a neutron with velocity corresponding to lethargy  $u$  is inserted in a critical reactor at the point  $\mathbf{r}$ , the power level of the reactor will rise by some fractional increment which is proportional to  $\varphi^*(\mathbf{r}, u)$ .

Thus, each term of Eq. 38 is proportional to the eventual increase in total neutron population due to a change in neutron reaction rate for one second through some change in a macroscopic constant over some perturbed volume.

The first term has to do with the extra neutron absorption.

The second term has to do with the additional flow of neutrons from the region of  $\delta D$  and their deposition at the boundary of the region.

The third term has to do with the additional accrual of neutrons in each  $\Delta u$  where the accrual is due to the difference between the slowing-down density into  $\Delta u$  and the slowing-down density out of  $\Delta u$  caused by elastic scatterings other than hydrogen. The fourth term takes care of this for the thermal group.

The fifth term has to do with the additional neutrons being degraded out of each  $\Delta u$  due to hydrogen scatterings. The sixth term has to do with the additional

neutrons being degraded into each  $\Delta u$  due to hydrogen scatterings. The seventh term takes care of this for the thermal group.

The eighth term has to do with the additional neutrons being degraded into  $\Delta u$  due to inelastic scattering. The ninth term is this for the thermal group. (The additional neutrons leaving each  $\Delta u$  due to inelastic scattering is taken care of in the first term.)

The tenth term has to do with the additional neutrons created by fission.

### Application to the MCBR

The remainder of the paper will be devoted to the results of an application of perturbation theory to the boiling-Mercury-Cooled fast-Breeder Reactor (MCBR) [12], a design study performed by the Advanced Technology Laboratories.

The MCBR design is, briefly, a cylindrical core of rather conventional fuel elements surrounded by a top, bottom and radial breeding-blanket of depleted uranium; forced recirculation of the coolant is required to insure a constant mercury vapour quality in the core; the lower blanket and the lower part of the core contain single-phase mercury; the upper part of the core and the upper blanket contain two-phase mercury having an average density of about  $0.75 \text{ g/cm}^3$ ; the fuel enrichment in the core is about 26%; in the application treated here the fuel is metallic but in later studies oxide fuel was considered; the coolant volume-fraction in the core is 62%.

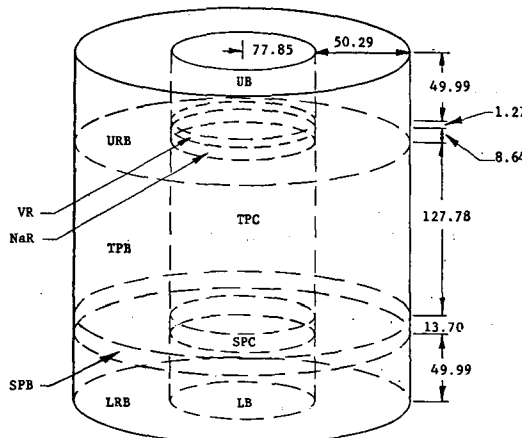


Fig. 1  
Regions of MCBR reference design core and blanket.

LB	Lower blanket
SPC	Single-phase portion of core
TPC	Two-phase portion of core
NaR	Region just above core where interior of fuel tubes is Na
VR	Region just above Region NaR where interior of fuel tubes is void
UB	Upper blanket
LRB	Portion of radial blanket that lies below level of core
SPB	Portion of radial blanket that lies at level of core and that has single-phase Hg
TPB	Portion of radial blanket that lies at level of core and that has two-phase Hg
URB	Portion of radial blanket that lies above level of core

Fig. 1 shows the idealized geometrical configuration of the reactor which was assumed for computational purposes.

When the two group specialization of perturbation theory is used, the reactivity change caused by a compositional perturbation in some arbitrary region of a reactor can be expressed as follows:

$$\delta \varrho = -\frac{\delta \nu}{\nu} = \frac{\alpha_1}{W} \delta \Sigma_{a_1} + \frac{\alpha_2}{W} \delta \Sigma_{a_2} + \frac{\beta}{W} \delta \Sigma_{r_1} + \frac{(\gamma_1 + \delta_1)}{W} \delta D_1 + \frac{(\gamma_2 + \delta_2)}{W} \delta D_2$$

where

$$-\frac{\delta \nu}{\nu} = \delta \varrho = \text{reactivity effect};$$

$\delta \Sigma_{a_1}$  = change in fast-group macroscopic-absorption cross-section in the region of perturbation;

$\delta \Sigma_{a_2}$  = change in slow-group macroscopic-absorption cross-section in the region of perturbation;

$\delta \Sigma_{r_1}$  = change in macroscopic-removal cross-section in the region of perturbation;

$\delta D_1$  = change in fast-group diffusion coefficient in the region of perturbation;

$\delta D_2$  = change in slow-group diffusion coefficient in the region of perturbation;

$\alpha_1, \alpha_2, \beta, \gamma_1, \delta_1, \delta_2, \gamma_2$  = quantities involving integrals over the perturbed region of products of flux and adjoint flux;

$W$  = a quantity involving integrals over the entire reactor of products of flux and adjoint flux.

The fast group is defined as those neutrons having energy above the threshold of the fission cross-section of  $U^{238}$ . Multi-group calculations were performed for each region of the reactor separately in order to determine good average values for the two-group constants.

Since the object of the computations reported here was to determine the effect of Hg on reactivity, the Hg cross-sections were of special importance. Before the computation for the reference design was started, letters were sent to everyone who could be expected to have made measurements, or might have knowledge of measurements, of Hg cross-sections in the high-energy range. Data on the capture cross-section proved to be especially scarce. The greatest amount of information in this regard was contained in a letter from Dr. R. D. Smith, of the UKAEA, Harwell [3].

Dr. Smith quoted the average capture cross-section of Hg in various fast-reactor spectra as 62 mb for the Russian reactor BR 1 with copper reflector and 117 mb with uranium reflector; 120 mb for Zephyr Core 1; 79 mb for Zeus Core 1.

Zeus Core 1 is a larger core with a more degraded spectrum than some of the others. The MCBR would probably correspond more to Zeus than to the smaller assemblies.

The distribution of the cross-section over the various groups was determined by using known data on neighbouring heavy isotopes as a guide. The magnitude was determined so that when the distribution was averaged over the spectrum for MCBR the average was close to that of Zeus (see Table I).

TABLE I  
CAPTURE CROSS-SECTION OF MERCURY ( $\sigma_c$ )\*

Group number	Energy limits (eV)		$\sigma_{cf}$ (mb)	Computed spectrum in core of MCBR $v_j \Delta u_j$
1	$2.25 \times 10^6$	—	13	5.68
2	$8.25 \times 10^5$	$2.25 \times 10^6$	21	17.14
3	$3 \times 10^5$	$8.25 \times 10^5$	62.5	39.46
4	$1.1 \times 10^5$	$3 \times 10^5$	120	26.30
5	$2.5 \times 10^4$	$1.1 \times 10^5$	153.5	13.36
6	$9.1 \times 10^3$	$2.5 \times 10^4$	220	0.86
7	0	$9.1 \times 10^3$	800	0.10

$$* \text{ Average cross-section: } \sigma_c = \frac{\sum_j \sigma_{cf} v_j \Delta u_j}{\sum_j v_j \Delta u_j} = 81 \text{ mb.}$$

The results for the reactivity change which would occur following an increase in Hg density by 1 g/cm<sup>3</sup> in the various regions of the MCBR (first-design) are presented in Table II.

TABLE II  
REACTIVITY CHANGE,  $-\delta\nu/\nu$  DUE TO INCREASE IN Hg DENSITY BY 1 g/cm<sup>3</sup>  
in various regions of MCBR reference design

Region*	$\delta\Sigma_{a_1}$ and $\delta\Sigma_{a_2}$ terms	$\delta\Sigma_{rl}$ term	$\delta D_1$ and $\delta D_2$ terms	Net $-\frac{\delta\nu}{\nu} = \delta\rho$
LB	-0.000 098	-0.000 013	+0.000 061	-0.000 050
SPC	-0.000 552	-0.000 083	+0.000 271	-0.000 36
TPC	-0.017 170	-0.004 182	+0.005 667	-0.016
NaR	-0.000 266	-0.000 034	+0.000 794	+0.000 49
VR	-0.000 032	-0.000 003	+0.000 380	+0.000 35
UB	-0.000 440	-0.000 054	+0.000 624	+0.000 13
LRB	-0.000 001	-0.000 000	NC**	NC
SPB	-0.000 003	-0.000 001	NC	NC
TPB	-0.000 271	-0.000 076	NC	NC
URB	-0.000 014	-0.000 001	NC	NC

\* For key to regions, see Fig. 1.

\*\* NC = not computed.

It may be seen that the net effect for this first design as shown in the column to the far right is negative for some regions and positive for others. However, it is negative for the regions of highest statistical weight and where the density change for a power change would be the greatest, i.e. the single-phase and two-phase regions of the core. It thus must be concluded that the overall coefficient is negative. This means, in other words, that the void coefficient is positive — an unsafe condition.

One important advantage of using a simple two-group model in preliminary computations of a design concept is that it is easy to use the method to decide what changes must be made in a design to correct some undesirable condition of the first try. Looking at Table II, one realizes that the terms concerning increased absorption (the first column of numbers) will always be negative; the term concerning increased slowing-down (the second column of numbers) can be either positive or negative depending on whether the fast neutrons or the slow neutrons are most important; and the terms concerning decreased leakage from important regions (the third column of numbers) will always be positive.

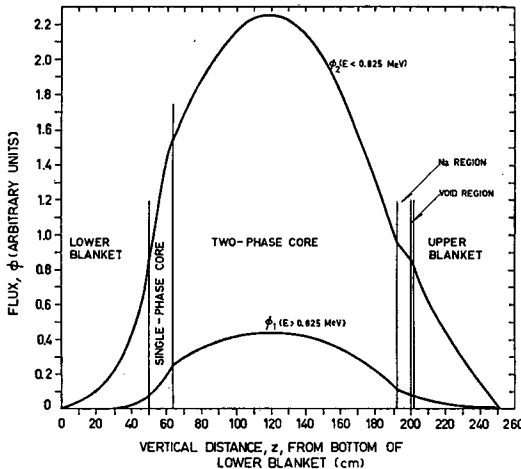


Fig. 2  
Vertical flux distribution!

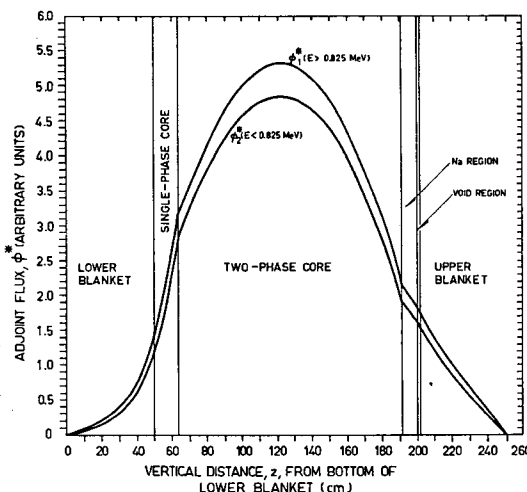


Fig. 3  
Vertical adjoint-flux distribution.

To make the density coefficient positive (void coefficient negative), design changes have to be made which make the numbers in the leakage column larger or which make the numbers in the slowing-down column more positive, i.e. which make the slow neutrons relatively more important compared to the fast neutrons.

It developed in the subsequent investigations that there were such design changes that could be made and a negative void-coefficient was eventually achieved.

Figs. 2 and 3 show the vertical flux distribution and the vertical adjoint-flux distribution that was obtained for the first design.

#### REFERENCES

- [1] ATL-A-102 (1959).
- [2] ATL-A-116 (1961).
- [3] SMITH, R. D., Personal communication (1959).

# THE REACTIVITY EFFECT OF HYDROGEN-ADDITION IN FAST REACTORS\*

H. SOODAK

UNITED NUCLEAR CORPORATION, WHITE PLAINS, N. Y.,  
UNITED STATES OF AMERICA

Abstract — Résumé — Аннотация — Resumen

**The reactivity effect of hydrogen-addition in fast reactors.** The addition of small amounts of hydrogen into a fast reactor results in two competing reactivity effects. On the one hand, there is a reactivity gain due mainly to the decreased leakage at lower energies; and on the other, there is a reactivity loss due to the decrease in  $k_{\infty}$  at the lower energies. In large reactors with high ratios of fertile to fissionable material, the leakage effect may be smaller than the  $k_{\infty}$  effect leading to a decrease in reactivity due to the addition of small amounts of hydrogen. In smaller reactors with lower ratios of fertile to fissionable material, the leakage effect is larger than the  $k_{\infty}$  effect, and the hydrogen coefficient is positive.

For larger amounts of hydrogen-addition, neutrons are thrown into the resolved resonance region where  $k_{\infty}$  increases because of the greater self-protection in fertile material than in fissionable material. As a result, the reactivity effect becomes more positive.

Illustrative results concerning these effects are presented along with some comments on the effect of the addition of large amounts of hydrogen (flooding).

**Incidence de l'introduction d'hydrogène sur la réactivité dans les réacteurs à neutrons rapides.** L'introduction d'une petite quantité d'hydrogène dans un réacteur à neutrons rapides a deux effets contraires sur la réactivité. Aux basses énergies, elle entraîne simultanément un accroissement de la réactivité par suite d'une réduction des fuites et une diminution de la réactivité due à une diminution de  $k_{\infty}$ . Dans les grands réacteurs, où les rapports matière fertile/produit fissile sont élevés, l'effet de fuite peut être inférieur à l'effet  $k_{\infty}$ , et l'introduction de petites quantités d'hydrogène entraîne une diminution de la réactivité. Dans les petits réacteurs, où les rapports matière fertile/produit fissile sont peu élevés, l'effet de fuite est supérieur à l'effet  $k_{\infty}$  et le coefficient d'hydrogène est positif.

Si l'hydrogène est introduit en plus grandes quantités, l'énergie des neutrons est déplacée dans le domaine où les résonances sont bien résolues et où  $k_{\infty}$  augmente du fait que l'autoprotection est plus grande dans la matière fertile que dans le produit fissile. De ce fait, l'effet de réactivité est plus positif.

L'auteur présente des exemples qui mettent ces effets en évidence et formule des observations sur l'effet de l'introduction de très grandes quantités d'hydrogène (engorgement).

**О реактивном эффекте водородной примеси в реакторах на быстрых нейтронах.** Добавление небольших количеств водорода в реактор на быстрых нейтронах имеет своим результатом два конкурирующих реактивных эффекта. С одной стороны, происходит накопление реактивности, вызываемое, главным образом, уменьшением утечки при более низких энергиях; с другой стороны, происходит потеря реактивности, вызываемая уменьшением величины  $k_{\infty}$  при более низких энергиях. В больших реакторах с большим отношением количества воспроизводящего материала к расщепляющемуся материалу эффект утечки может быть меньше, чем эффект  $k_{\infty}$ , что ведет к уменьшению в реактивности,

\* Based on work performed under United States Atomic Energy Commission Contract.

вызываемой добавлением небольших количеств водорода. В малых реакторах с низким отношением количества воспроизводящего материала к расщепляющемуся материалу эффект утечки является большим, чем эффект  $k_{\infty}$ , а коэффициент водорода — положительным.

При больших количествах водорода нейтроны выбрасываются в область разрешенного резонанса, где  $k_{\infty}$  увеличивается в связи с тем, что воспроизводящий материал обладает большей самозащитой, чем расщепляющийся материал. В результате этого эффект реактивности становится более положительным.

Представлены иллюстрирующие результаты, касающиеся этих эффектов, а также некоторые замечания о влиянии добавления больших количеств водорода (захлебывание).

**Efectos de la introducción de hidrógeno en los reactores rápidos sobre la reactividad.**  
 La introducción de pequeñas cantidades de hidrógeno en un reactor rápido da lugar a dos efectos de reactividad competitivos. Por una parte, la reactividad aumenta debido principalmente a la disminución del escape a bajas energías; por otra parte, se produce una pérdida de reactividad debido a que  $k_{\infty}$  decrece a energías bajas. En los reactores grandes, en los que la razón de material fértil a material fisiónable es elevada, el efecto de escape puede ser menos pronunciado que la disminución de reactividad debida a  $k_{\infty}$  al introducir en un reactor pequeñas cantidades de hidrógeno. En los reactores pequeños, cuya razón de material fértil a material fisiónable es más baja, el efecto de escape es mayor que el producido por  $k_{\infty}$ , y el coeficiente de hidrógeno es positivo.

Al añadir cantidades mayores de hidrógeno, se introducen neutrones en la región de resonancia resuelta, donde  $k_{\infty}$  aumenta porque la autoprotección es mayor en el material fértil que en el material fisiónable. Como consecuencia aumenta el valor absoluto de la reactividad, que es positiva.

La memoria presenta resultados que ilustran estos efectos y formula algunos comentarios sobre el efecto de la introducción de grandes cantidades de hidrógeno (inundación).

## Introduction

Apart from their intrinsic interest, the reactivity effects of hydrogen-addition are basic in the study of the dynamics and safety of steam-cooled fast reactors [1, 2] and also play a role in safety studies on other fast reactors [3]. Experimental results [4] exist on the effect of small amounts of hydrogen in the highly enriched Los Alamos fast assemblies.

Presented below are the results of preliminary calculations on the reactivity effects of various amounts of hydrogen added into uranium reactors with various amounts of enrichment. The results are quite sensitive to the cross-sections used, and especially so for energies at a few kV and lower where self-protection effects are important.

It is planned to continue the study of the self-protection effects, to extend the calculations to reactors fuelled with other combinations of fissionable and fertile materials, and to use other cross-section sets [5, 6, 7.] with finer group structures.

## Some general results

The major reactivity effects of small amounts of hydrogen-addition are caused by the softening of the spectrum. On the one hand, the leakage is decreased because of the generally higher cross-sections at the lower energies; and on the

other, the number of neutrons produced per neutron absorbed is decreased because of the reduced  $\nu$ -values and the increased ratios of capture-to-fission cross-sections. In short, the addition of small amounts of hydrogen causes a reactivity loss due to a decrease in  $k_\infty$  and a gain due to a decreased leakage. In the small reactors with low ratios of fertile-to-fissionable atoms, the leakage effect predominates and the hydrogen reactivity effect is positive. In the larger reactors with high ratios of fertile-to-fissionable atoms, the  $k_\infty$  effect may predominate and the hydrogen reactivity effect may be negative. The occurrence and location of the change-over from positive to negative effect is a sensitive function of the cross-sections used for energies in the neighbourhood of a kilovolt. In the present calculations, the change-over occurs at about eight U<sup>238</sup> atoms per U<sup>235</sup> atom.

The insertion of larger amounts of hydrogen throws neutrons down to the 100-V range where the greater self-protection in U<sup>238</sup> as compared with U<sup>235</sup> causes  $k_\infty$  to be larger than in the kV range. As a result, the hydrogen effect turns positive when more than a small amount is added. For still larger amounts, increasing numbers of neutrons are thrown into the thermal and epithermal energy range where  $k_\infty$  is even larger, and the hydrogen effect remains positive.

### The cases calculated

The reactors considered are bare uniform spheres containing only U<sup>235</sup>, U<sup>238</sup> and H. The atom ratio  $N^{28}/N^{25}$  of U<sup>238</sup> atoms to U<sup>235</sup> atoms varies from 0 to 13. The hydrogen content is measured by the parameter  $N^H/N^U$  which is the ratio of hydrogen atoms to total uranium atoms and varies from 0 to 7. Thus, equal values of  $N^H/N^U$  correspond to unequal values of the number of H atoms per U<sup>235</sup> atom.

The reactors are all sized to be critical with no hydrogen, and the  $k$ -values are then obtained for the reactors with hydrogen. Thus, the reactor radii are independent of  $N^H/N^U$  and depend only on  $N^{28}/N^{25}$  and on a uranium density parameter. The parameter chosen is the ratio of the density of U (U<sup>235</sup> plus U<sup>238</sup>) in the reactor to 18.6 g/cm<sup>3</sup> (U metal density),

$$\varrho = \frac{\text{density of U}}{18.6}.$$

The reactor radii are inversely proportional to  $\varrho$ .

Forty-nine cases were calculated, running through the values

$$N^H/N^U = 0, 0.1, 0.2, 0.5, 1.2, 3, 7$$

$$N^{28}/N^{25} = 0, 1, 2, 4, 7, 10, 13.$$

### The method of calculation

The multiplication constant  $k$  (criticality factor) is here defined as the number of fission neutrons starting the next generation due to one fission neutron born in this generation. It is given by

$$k = \sum k_{\alpha g} A_g \quad (1)$$

where  $A_g$  is the number of neutrons absorbed in group  $g$  due to one fission neutron

starting a cycle, and  $k_{\infty g}$  is the number of fission neutrons produced per neutron absorbed in group  $g$ . It may also be expressed as

$$k = \sum k_g (A_g + L_g) \quad (2)$$

where  $A_g + L_g$  is the sum of absorptions and leakage in group  $g$ , and  $k_g$  is the number of neutrons produced per neutron lost in group  $g$  due to either absorption or leakage.

The neutron cycle is followed in two stages using seven groups. In the high-energy stage consisting of the first four groups, neutrons are traced using the equations

$$\left( D_g B_g^2 + \mu_{a,g} + \sum_{j>g} \mu_{gj} \right) \varphi_g = f_g + \sum_{j<g} \mu_{js} \varphi_j \quad (3)$$

where  $\varphi$  is the group flux,  $f$  is the fraction of fission neutrons born into the group,  $D = \frac{1}{3}/\mu_{tr}$  is the diffusion coefficient,  $\mu_a$  is the absorption (fission plus capture) cross-section,  $\mu_{gj}$  is the transfer cross-section from group  $g$  to group  $j$ ,  $B_g^2$  is the buckling, and the group number increases with decreasing energy. The equations are solved successively for the  $\varphi_g$ , and the quantities  $A_g$  and  $L_g$  are evaluated from

$$A_g = \mu_{a,g} \varphi_g \quad L_g = D_g B_g^2 \varphi_g. \quad (4)$$

The quantities  $k_{\infty g}$  and  $k_g$  depend only on the cross-sections and the buckling, and are given by

$$k_{\infty g} = \left( \frac{\nu \mu_f}{\mu_a} \right)_g \quad (5)$$

$$k_g = \left( \frac{\nu \mu_f}{\mu_a + DB^2} \right)_g \quad (6)$$

where  $\mu_f$  and  $\nu$  are the fission cross-section and number of neutrons emitted per fission. The buckling is obtained from

$$B_g^2 = \frac{\pi^2}{(R + \lambda_g)^2} \quad (7)$$

where the extrapolation length  $\lambda_g$  is given by

$$\lambda_g = 2D_g. \quad (8)$$

In the low-energy region consisting of the last three groups, leakage is neglected and the absorptions are evaluated using resonance-escape formulae. Thus, the number of neutrons,  $q$ , slowing down to below group 4, is obtained from

$$q = 1 - \sum_{g<5} (A_g + L_g) \quad (9)$$

and the absorptions in the low-energy groups are evaluated from

$$A_5 = q(1 - p_5) \quad (10)$$

$$A_6 = qp_5(1 - p_6) \quad (11)$$

$$A_7 = qp_5 p_6 = q - A_5 - A_6 \quad (12)$$

where  $p_5$  and  $p_6$  are the resonance-escape probabilities in groups 5 and 6. They are calculated by use of

$$p_g = \exp \left( -\frac{N^{28}}{N^H} \frac{I^{28}}{\sigma^H} - \frac{N^{25}}{N^H} \frac{I^{25}}{\sigma^H} \right)_g \quad (13)$$

where  $I^{28}$  and  $I^{25}$  are the absorption-resonance integrals in the group in b per indicated atom, and  $\sigma^H$  is the hydrogen cross-section in b. The group  $k$  values are obtained from

$$k_{\infty g} = k_2 = \left( \frac{N^{25} I^{25}}{N^{25} I^{25} + N^{28} I^{28}} \eta \right)_g \quad (14)$$

where  $\eta = \nu/(1 + \alpha)$  and  $\alpha$  is the capture-to-fission ratio in  $U^{235}$ . In the last group, the present calculations simply use a constant value (2.05) for  $k_{\infty g} = k_g$ .

The high-energy-stage equations were solved on a Datatron-205 computer, and the low-energy group quantities were evaluated by hand computation.

### Perturbation

For very small amounts of H-addition, the  $k$  change may be evaluated by a perturbation method. Thus, neglecting the direct effect of hydrogen collisions in reducing leakage, or in other words, taking into account only the softening of the spectrum, the  $k$  change is

$$\delta k = \sum_g \sum_{j > g} \varphi_g \delta \mu_{gj} (m_j - m_g) \quad (15)$$

where  $\delta \mu_{gj}$  is the change due to hydrogen addition, and  $m_g$  is the "importance" of a neutron in the indicated group, here defined as the number of fission neutrons resulting from one neutron thrown into the group. Thus, for a group out of which there is no slowing-down,  $m_g = k_g$ . As a result, the reactivity change is given approximately by

$$\delta k \approx \sum_g \sum_{j > g} \varphi_g \delta \mu_{gj} (k_j - k_g) \quad (16)$$

when the major effects occur in the groups in which there is negligible slowing-down in the absence of hydrogen. The  $\varphi_g$  in the above formulae are the fluxes in the reactors without hydrogen.

### Group structure and cross-sections

The group structure and cross-sections used for the high-energy stage of the neutron cycle are those of the first four groups of a ten-group set of cross-sections recorded on a tape unit for use with the Datatron computer. The three low-energy groups are contracted from the lower six groups. The group structure used here is presented in Table I. The cross-sections for capture and fission, transport, and transfer in groups 1—4 are listed in Tables II, III, and IV. The values used for the quantities of interest in groups 5—7 are listed in Table V.

TABLE I  
GROUP STRUCTURE

Group No., $g$	Bottom energy	Lethargy width	Fission fraction, $f_g$
1	2.23 MeV	1.5	0.344
2	1.05 MeV	0.75	0.321
3	11.7 keV	4.5	0.333
4	555.4 eV	3.05	0.002
5	30.5 eV	2.9	—
6	5.04 eV	1.8	—
7	Thermal	—	—

TABLE II  
CAPTURE AND FISSION CROSS-SECTIONS IN GROUPS 1-4  
(barns per atom)

Group No.	$\sigma_f^{25}$	$\nu\sigma_f^{25}$	$\sigma_c^{25}$	$\sigma_f^{28}$	$\nu\sigma_f^{28}$	$\sigma_c^{28}$
1	1.29	3.76	0.0541	0.597	1.72	0.021
2	1.29	3.44	0.0886	0.258	0.694	0.0816
3	1.65	4.12	0.384	0.0009	0.0023	0.224
4	6.58	16.3	3.14	0	0	1.35

NOTES. 25 denotes  $U^{235}$ . 28 denotes  $U^{238}$ . Hydrogen absorption cross-sections are negligible.

Although self-protection effects occur in group 4, they are much smaller than in groups 5 and 6, and have not been taken into account in the present calculations. Although self-protection is appreciable in the epithermal part of group 7, its effect is unimportant in the present calculations because almost all neutrons in this group are absorbed in  $U^{235}$ . Thus,  $k_7$ , the only quantity for group 7 that is used in the calculations is always close to 2.05. The effect of self-protection in group 7 becomes important in the case that a resonance-absorber is incorporated into the reactor to eliminate the reactivity effects of flooding.

The resonance integrals used in groups 5 and 6 are only illustrative. They take no account of the effects of spatial self-protection or of the presence of atoms other than H and U. The resonance integrals used for  $U^{238}$  are based on calculations [8] performed in connection with uranium-lattice reactors by translating surface-to-mass ratio (or rod radius) to the equivalent amount of moderating diluent cross-section homogeneously mixed with the  $U^{238}$ , and are assumed proportional to the square root of the diluent cross-section per  $U^{238}$  atom. It is also assumed that the only moderating cross-section is that of hydrogen. The resonance integrals used for  $U^{235}$  are based on the  $U^{238}$  values used and on the ratios resulting from calculations [9] on a case with  $N^{28}/N^{25}$  equal to one, performed in connection with the Doppler coefficient in fast and slightly moderated fast reactors. Again, the resonance integral is assumed proportional to the square root of the hydrogen cross-section per atom of resonance-absorber. In this case, however, the square-

TABLE III  
TRANSPORT CROSS-SECTIONS IN GROUPS 1-4  
(barns per atom)

Group No.	$\sigma_{tr}^{25}$	$\sigma_{tr}^{28}$	$\sigma_{tr}^H$
1	4.41	4.25	0.57
2	4.59	4.94	1.18
3	9.40	8.80	3.43
4	24.2	17.4	6.57

TABLE IV  
TRANSFER CROSS-SECTIONS IN GROUPS 1-4  
(barns per atom)

$U^{235}$	$U^{238}$	$H$	
$\sigma_{12} = 0.50$	$\sigma_{12} = 0.42$	$\sigma_{12} = 0.892$	$\sum \sigma_{1j} = 0.0004$
$\sigma_{13} = 1.38$	$\sigma_{13} = 2.00$	$\sigma_{13} = 0.789$	$j > 4$
$\sigma_{23} = 1.08$	$\sigma_{23} = 1.47$	$\sigma_{14} = 0.0084$	$\sum \sigma_{2j} = 0.001$
All others are negligible	All others are negligible	$\sigma_{23} = 2.59$	$j > 4$
		$\sigma_{24} = 0.028$	$\sum \sigma_{3j} = 0.18$
		$\sigma_{34} = 3.63$	$j > 4$
			$\sum \sigma_{4j} = 6.24$
			$j > 4$

TABLE V  
RESONANCE INTEGRALS (capture + fission in barns per atom),  
 $\alpha$  VALUES, AND OTHER QUANTITIES FOR  
GROUPS 5-7

Group	Values of quantities
5	$I^{25} = \min \left[ 13 \left( \frac{N^H \sigma^H}{N^{25}} \right)^{1/2}, 110 \right] \quad \alpha^{25} = 0.5$ $I^{28} = 0.9 \left( \frac{N^H \sigma^H}{N^{28}} \right)^{1/2} \quad \sigma^H = 20$
6	$I^{25} = \min \left[ 9 \left( \frac{N^H \sigma^H}{N^{25}} \right)^{1/2}, 169 \right] \quad \alpha^{25} = 0.9$ $I^{28} = 1.3 \left( \frac{N^H \sigma^H}{N^{28}} \right)^{1/2}$
7	$k\infty_7 = k_7 = 2.05$

NOTE. The symbol  $\min [x, y]$  signifies the smaller of the quantities  $x$  and  $y$ .

TABLE VI

VALUES OF THE RADIUS, THE MULTIPLICATION FACTOR  $k$ , THE DERIVATIVE OF  $k$  WITH RESPECT TO SMALL HYDROGEN ADDITION, AND OF THE ABSORPTION FRACTION  $A$ , THE FRACTION OF NEUTRONS BORN THAT ARE ABSORBED

$c = \frac{N^{28}}{N^{26}} \rightarrow$	0	1	2	4	7	10	13
Radius (cm) $\frac{N^H}{N^U}$ $r = N^H/N^U$	$\frac{7.9}{\rho}$	$\frac{11.5}{\rho}$	$\frac{14.4}{\rho}$	$\frac{19.8}{\rho}$	$\frac{28.6}{\rho}$	$\frac{41.3}{\rho}$	$\frac{69.4}{\rho}$
0 $k$ A $\left(\frac{dk}{dr}\right)_{r=0}$	1 (0.44)	1 (0.48)	1 (0.52)	1 (0.60)	1 (0.71)	1 (0.81)	1 (0.92)
0.1 $k$ A	1.03 (0.47)	1.04 (0.53)	1.05 (0.58)	1.05 (0.67)	1.04 (0.78)	1.02 (0.87)	1.006 (0.95)
0.2 $k$ A	1.06 (0.49)	1.09 (0.56)	1.09 (0.63)	1.09 (0.72)	1.08 (0.82)	1.06 (0.90)	1.05 (0.96)
0.5 $k$ A	1.14 (0.55)	1.17 (0.65)	1.18 (0.71)	1.18 (0.80)	1.17 (0.88)	1.14 (0.94)	1.12 (0.98)
1.2 $k$ A	1.27 (0.65)	1.29 (0.76)	1.29 (0.82)	1.27 (0.88)	1.24 (0.94)	1.23 (0.97)	1.22 (0.99)
3 $k$ A	1.45 (0.80)	1.42 (0.88)	1.40 (0.91)	1.39 (0.95)	1.40 (0.97)	1.42 (0.99)	1.44 (0.995)
7 $k$ A	1.59 (0.91)	1.54 (0.95)	1.55 (0.97)	1.56 (0.98)	1.60 (0.99)	1.62 (0.995)	1.64 (0.998)

Notes. The quantity  $\rho$  is the total uranium density divided by 18.6 g/cm<sup>3</sup>. The function of the parentheses around the  $A$  values is to help distinguish them from the  $k$  values.

root dependence is assumed only until the calculated resonance integral becomes equal to the infinite dilution value, at which point the resonance integral is assumed to remain constant at the infinite dilution value.

### Results and discussion

The results of the reactivity calculations are presented in Table VI which lists the radii, the  $k$ -values, the values of

$$\left(\frac{dk}{dr}\right)_{r=0}$$

where  $r = N^H/N^U$ , and the values of the fraction of neutrons born that are absorbed.

The interplay between the leakage and  $k_\infty$  effects of hydrogen addition may be traced by use of Table VI. Consider, for example, the addition of  $r = 0.1$  into the

TABLE VII

VALUES OF  $k_{\infty g}$  AND  $k_g$  IN GROUPS 1-4 FOR REACTORS WITH NO HYDROGEN

$c = \frac{N^{28}}{N^{25}}$	0	1	2	4	7	10	13
$k_{\infty 1}$ $k_1$	2.79 (0.95)	2.79 (1.10)	2.79 (1.25)	2.79 (1.53)	2.79 (1.90)	2.79 (2.23)	2.79 (2.54)
$k_{\infty 2}$ $k_2$	2.50 (0.87)	2.41 (0.90)	2.35 (0.96)	2.27 (1.11)	2.21 (1.35)	2.17 (1.61)	2.15 (1.89)
$k_{\infty 3}$ $k_3$	2.02 (1.09)	1.83 (1.00)	1.66 (0.94)	1.41 (0.875)	1.15 (0.82)	0.97 (0.79)	0.84 (0.77)
$k_{\infty 4}$ $k_4$	1.67 (1.54)	1.47 (1.36)	1.31 (1.22)	1.08 (1.01)	0.85 (0.82)	0.70 (0.69)	0.60 (0.59)

Notes. The  $k_{\infty g}$  values change by negligible amounts when hydrogen is added. The  $k_g$  values increase somewhat due to the direct effect of hydrogen scattering on leakage. The function of the parentheses around the  $k$  values is to help distinguish them from the  $k_{\infty}$  values.

TABLE VIII

VALUES OF  $k_{\infty g} = k_g$  IN GROUPS 5-7

	$N^{28}/N^{25}$	0	1	2	4	7	10	13
	$N^H/N^U$							
$k_5$	0.1	1.65	1.55	1.50	1.44	1.40	1.36	1.32
	0.2	1.65	1.54	1.50	1.55	1.40	1.36	1.32
	0.5	1.65	1.54	1.50	1.45	1.38	1.30	1.23
	1.2	1.65	1.54	1.50	1.41	1.27	1.15	1.07
	3	1.65	1.52	1.44	1.30	1.10	1.00	0.89
	7	1.65	1.46	1.34	1.13	0.95	0.81	0.71
$k_6$	0.1	1.30	1.13	1.07	0.94	0.94	0.89	0.85
	0.2	1.30	1.13	1.07	1.01	0.94	0.89	0.85
	0.5	1.30	1.13	1.07	1.01	0.94	0.89	0.85
	1.2	1.30	1.13	1.07	1.01	0.94	0.89	0.85
	3	1.30	1.13	1.07	1.01	0.89	0.81	0.72
	7	1.30	1.13	1.07	0.92	0.78	0.68	0.60
$k_7$				2.05				

pure U<sup>235</sup> reactor where  $r=0$ ,  $c=0$ . As a result of the increase in the absorption factor  $A$ , from 0.44 to 0.47, the  $k$ -value is expected to increase from 1 to  $1/0.44 = 1.07$ . The actual increase is 1.03. Thus, the leakage effect is 7% positive, the  $k_{\infty}$  effect is 4% negative, and the net effect is 3% positive.

The interplay for small hydrogen-additions may be traced by use of Table VIII which lists the values of  $k_{\infty g} = k_g$  in groups 5-7. The perturbation calculations show that the main effects of small hydrogen-addition are the transfer of neutrons from group 3 to 4 and 5 and from group 4 to 5 in all cases, except  $c=0$ . As a result, the value of  $dk/dr$  may be obtained by the use of Eq. (16). The fact that the neutron population of group 3 increases with increasing  $c$ -value explains the initial increase of  $dk/dr$  with  $c$ . It is seen from Table VII that, although  $k_{\infty 4}$

TABLE IX

**VALUES OF g, THE NUMBER OF NEUTRONS SLOWING DOWN TO BELOW GROUP 4 DUE TO ONE NEUTRON BORN IN FISSION**

$N^{28}/N^{25}$	0	1	2	4	7	10	13
$NH/NU$	0	0.005	0.014	0.025	0.047	0.077	0.103
0	0	0	0	0	0	0	0
0.1	0.005	0.014	0.025	0.047	0.077	0.103	0.126
0.2	0.014	0.038	0.064	0.111	0.166	0.211	0.245
0.5	0.054	0.127	0.189	0.281	0.369	0.247	0.467
1.2	0.168	0.312	0.404	0.513	0.598	0.647	0.678
3	0.405	0.575	0.657	0.738	0.792	0.820	0.837
7	0.657	0.781	0.830	0.874	0.900	0.914	0.921

is less than  $k_{\infty,3}$  for all  $c$ -values,  $k_4$  is less than  $k_3$  only for  $c > 7$ . This is the reason for the change-over from positive to negative values of  $dk/dr$ .

For somewhat larger amounts of hydrogen-addition, the fact that  $k_5$  is larger than  $k_3$  and  $k_4$  causes the hydrogen effect to become positive for the reactors with large  $c$ . This is the case at  $r=0.1$ .

An interesting feature of the results of Table VI is the comparatively slight variation of  $k$  with  $c$  for a given large value of  $r$ . This effect may be traced by considering the cases  $r=3$ ,  $c=0$  and  $r=3$ ,  $c=13$ . In the first case, a comparison with  $r=0$ ,  $c=0$  shows that the leakage effect would increase  $k$  from 1 to 1.8. In this case, therefore, there is a large positive leakage effect and a negative  $k_{\infty}$  effect about half as large. In the second case, the leakage effect is small and positive, and the  $k_{\infty}$  effect is large and positive, arising from neutrons entering group 7.

The number of neutrons absorbed in the low-energy groups may be calculated by use of Tables IX and X. Table IX lists the values of the number of neutrons slowing into the low-energy region, and Table X lists the fractions absorbed in groups 5, 6 and 7.

### A remark on flooding

The tables may be used to illustrate the problems involved in the analysis of the effects of flooding in a steam-cooled fast reactor. Consider, for example, a reactor with  $c=7$  and in the normal state with  $r=0.2$  at a steam density 1/15 that of water. The completely flooded state then corresponds to  $r=3$ . (Reactivity changes are to be measured from the base value of 1.08.) As the steam density increases from standard to full, the reactor passes through the  $r$ -values between 0.2 and 3. Table XI illustrates the situation that arises out of an attempt to suppress the flooding reactivity by incorporating into the reactor a resonance-poison. It lists the  $k$ -values and the contribution to the  $k$ -value due to fissions in groups 5, 6 and 7. As a simple example, consider a resonance-poison which absorbs all neutrons slowing down below group 6 and only those neutrons. The completely flooded reactor as well as the  $r=1.2$  case have reactivities well below the base value of 1.08. The reactor does, however, pass through supercritical states, one

TABLE X  
**VALUES OF  $\frac{N^{28}}{N^{25}}$ , THE NUMBER OF NEUTRONS ABSORBED IN GROUP g PER NEUTRON SLOWING DOWN TO BELOW GROUP 4 (g = 5, 6, 7)**

		$N^{28}/N^{25}$	0	1	2	4	7	10	13
		$N^H/N^U$	0	1	2	4	7	10	13
$A_5$	0.1	1	1	1	0.99	0.98	0.97	0.95	
	0.2	1	0.99	0.98	0.96	0.93	0.91	0.89	
	0.5	0.98	0.96	0.93	0.88	0.81	0.72	0.65	
	1.2	0.93	0.87	0.81	0.66	0.52	0.45	0.40	
	3	0.81	0.63	0.50	0.37	0.28	0.24	0.21	
	7	0.55	0.36	0.27	0.21	0.16	0.13	0.12	
$A_6$	0.1	0	0	0	0.01	0.02	0.03	0.05	
	0.2	0	0.01	0.02	0.04	0.06	0.08	0.09	
	0.5	0.02	0.04	0.06	0.10	0.14	0.20	0.24	
	1.2	0.06	0.10	0.14	0.22	0.29	0.30	0.31	
	3	0.13	0.23	0.28	0.31	0.29	0.26	0.24	
	7	0.24	0.29	0.28	0.23	0.19	0.17	0.16	
$A_7$	0.1	0	0	0	0	0	0	0	
	0.2	0	0	0	0	0.01	0.01	0.02	
	0.5	0	0	0.01	0.02	0.05	0.08	0.11	
	1.2	0.01	0.03	0.05	0.12	0.19	0.25	0.29	
	3	0.06	0.14	0.22	0.32	0.43	0.50	0.55	
	7	0.21	0.35	0.45	0.56	0.65	0.70	0.73	

TABLE XI  
**THE k VALUES AND THE CONTRIBUTIONS FROM GROUPS 5, 6, AND 7 FOR THE REACTORS WITH  $c=7$  AND  $r=0.2$  TO 3**

Reactor	k value	Contribution to k value due to fissions in group			
		5	6	7	
$c = 7$	$r = 0.2$	1.08	0.216	0.011	0
$c = 7$	$r = 0.5$	1.17	0.413	0.049	0.037
$c = 7$	$r = 1.2$	1.24	0.395	0.163	0.234
$c = 7$	$r = 3$	1.40	0.244	0.205	0.697

of which is the  $r=0.5$  state. To reduce the reactivity in the  $r=0.5$  state to the base value and at the same time to minimize the poison-effect in the base case, the poison-absorption must predominate over the  $U^{235}$ -absorption in groups 6 and 7 and be comparatively weak in group 5.

### Comparison with Godiva

The critical radius of a full density sphere of uranium enriched to 94%, or  $c=6/94$ , is 8.13 cm as obtained by linear interpolation between the  $c=0$  and  $c=1$  values of Table VI. The measured value [4] is 8.73 cm, the radius of Godiva. The value of 0.26 for

$$\left(\frac{dk}{dr}\right)_{r=0}$$

is to be compared with the measured value of 0.2 in Godiva. The latter value is obtained by averaging the Godiva results [4] for the reactivity as a function of hydrogen-position. The resulting value of 14 c/g at. H is converted to \$31 per  $r$  unit by using the critical mass value [4] of 224 mole, and then to  $\delta k=0.2$  per  $r$  unit.

### ACKNOWLEDGEMENT

The author is pleased to thank Mr. Martin Shapiro for expediting the Datatron calculations.

### REFERENCES

- [1] SOFER, G., HANKEL, R., GOLDSTEIN, L. and BIRMAN, G., NDA 2148-4 (1961).
- [2] REYNOLDS, A. B. and WOLFE, B., *Trans. Amer. nucl. Soc.* **4** (1961) 19—20.
- [3] JENS, W. H., Summary of APDA fast reactor safety studies, RHM-4, US-UK Meeting on Reactor Hazards (June 1956).
- [4] ENGLE, L. B., HANSEN, G. E. and PAXTON, H. C., *Nucl. Sci. Engng* **8** (1960) 546, 549.
- [5] KIEHN, R. M., *Nucl. Sci. Engng* **4** (1958) 166—170.
- [6] YIFTAH, S., OKRENT, D and MOLDAUER, P. A., Fast Reactor Cross Sections, Pergamon Press, New York (1960).
- [7] ROÄCH, W. H., *Nucl. Sci. Engng* **8** (1960) 621—630.
- [8] BROOKS, W. L. and SOODAK, H., NDA 2131-19 (1960) 15—23.
- [9] MAROTTA, C. R. and TRALLI, N., Multigroup Cross Sections for the Doppler Calculations, internal NDA memorandum (May 1961).

# REACTIVITY COEFFICIENTS OF SODIUM IN SOME LARGE FAST REACTORS\*

M. G. BHIDE

ATOMIC ENERGY ESTABLISHMENT, TROMBAY, BOMBAY,

INDIA

and

H. H. HUMMEL

ARGONNE NATIONAL LABORATORY, ARGONNE, ILL.,

UNITED STATES OF AMERICA

**Abstract — Résumé — Аннотация — Resumen**

**Reactivity coefficients of sodium in some large fast reactors.** Several studies have been made regarding the change of reactivity in fast reactors with the temperature of sodium or with the loss of coolant. In this paper, the effect on the sodium void-coefficient of taking into account more accurately the effect of elastic resonance scattering by light and medium atomic-weight materials is studied for some large fast systems. Fundamental-mode calculations were performed for the different sodium concentrations in the systems using 574 energy groups from 3.7 MeV to 25 keV. The elastic removal cross-sections and transport cross-sections were re-evaluated for a 16-group cross-section set and the reactivity coefficients were calculated using a one-dimensional diffusion-theory code for the idealized spherical systems. A more accurate calculation of the very-low-energy flux is provided by this method. This flux has been found to be very important for calculation of the Doppler effect in large reactors.

**Coefficients de réactivité du sodium dans certains grands réacteurs à neutrons rapides.** Les variations de réactivité provoquées dans les réacteurs à neutrons rapides par les variations de la température du sodium ou par la perte de fluide de refroidissement ont fait l'objet de plusieurs études. Les auteurs étudient, pour quelques grands réacteurs à neutrons rapides, ce que devient le coefficient cavitaire du sodium lorsqu'on serre de plus près l'effet de diffusion élastique par résonance dans les matériaux de masse atomique faible ou intermédiaire. On a calculé les modes fondamentaux pour les différentes concentrations de sodium dans les systèmes, en utilisant 574 groupes d'énergie allant de 25 keV à 3,7 MeV. On a procédé à une nouvelle évaluation des sections efficaces de déplacement élastique et des sections efficaces de transport pour un ensemble de 16 groupes de sections efficaces et au calcul des coefficients de réactivité à partir d'un programme de diffusion à une dimension dans le cas de systèmes sphériques idéaux. Il est ainsi possible de calculer avec plus de précision le flux des neutrons de très faible énergie. On a constaté que ce flux joue un rôle très important dans le calcul de l'effet Doppler dans les grands réacteurs.

**Коэффициенты реактивности натрия в некоторых больших реакторах на быстрых нейтронах.** Были проведены некоторые работы, изучающие изменение реактивности в реакторах на быстрых нейтронах с температурой натрия или с потерей охладителя. В этой работе изучается эффект пустотного коэффициента натрия с более тщательным применением эффекта упругого резонансного рассеяния материалами с легкими и средними атомными весами для некоторых больших систем на быстрых нейтронах. Расчеты основного состояния были проведены для различных концентраций натрия в системах, используя

\* Work done at the Argonne National Laboratory.

574 энергетические группы от 3,7 мегаэлектронвольт до 25 килоэлектронвольт. Сечения упругого процесса выведения и транспортное сечение были переоценены для набора 16-групповых поперечных сечений и коэффициенты реактивности были рассчитаны с использованием одноразмерного кода теории диффузии для идеальных сферических систем. Этот метод предусматривает более точный расчет потока нейтронов самых малых энергий. Этот поток оказался очень важным для расчета эффекта Доплера в больших реакторах.

**Coefficientes de reactividad del sodio en algunos reactores rápidos de gran tamaño.**  
En el caso de los reactores rápidos, se han efectuado diversos estudios acerca de la variación de la reactividad en función de la temperatura del sodio o de la pérdida de refrigerante. En el presente trabajo, los autores estudian las consecuencias que se derivan del hecho de evaluar con mayor precisión el efecto que la dispersión elástica por resonancia ejerce, en los materiales de peso atómico bajo y mediano, sobre el coeficiente de vacío del sodio, en el caso de algunos reactores rápidos de gran tamaño. Calcularon los modos fundamentales para las diferentes concentraciones del sodio en los sistemas, utilizando 574 grupos de energías, que abarcan desde 25 keV hasta 3,7 MeV. Procedieron a una nueva evaluación de las secciones eficaces de eliminación elástica y de las secciones eficaces de transporte para un conjunto de secciones eficaces de 16 grupos y calcularon los coeficientes de reactividad usando una clave unidimensional de difusión para sistemas esféricos ideales. Con este método, es posible calcular con mayor precisión flujos neutrónicos de energías muy bajas. Se ha comprobado que el conocimiento de estos flujos reviste mucha importancia para el cálculo del efecto Doppler en los reactores de gran tamaño.

## Introduction

In recent years, several studies have been made regarding the change of reactivity in fast reactors with temperature change of sodium coolant or with the loss of coolant. Since the reactor-power and coolant-temperature are closely coupled (with a response-time, associated, of the order of 1 s or less) the sodium temperature-coefficient of reactivity is essentially prompt. There is a possibility of having voids occur in the coolant because of boiling caused by local hot spots or because of the presence of blanket gas-bubbles in the coolant. A positive sodium void-coefficient (i.e., the reactivity increases as sodium density decreases) under such conditions could lead to over-heating or even melt-down of the core. The reactivity effects having a faster time-response to reactor-power are axial fuel-expansion and Doppler broadening, and the associated reactivity coefficients are generally of the same magnitude as or less than those of sodium.

The fact that the sodium void-coefficient can be positive in large Pu-fuelled reactors was first pointed out by NIMS and ZWEIFEL [1]. YIFTAH and OKRENT [2] studied the transition of the coefficient from negative at small reactor size to positive at large size in spherical geometry as a function of the nature of the materials used for fuel, structure and fertile material. At present, design studies for fast reactors avoid any known prompt-positive coefficient. Studies of advanced reactors for the future have contemplated the possibility of a positive sodium void-coefficient over-ridden by a larger negative Doppler coefficient. In any case, an accurate knowledge of the sign and magnitude of the coefficient for large reactors is important. In order to improve the accuracy of the calculations, some of the cases considered in [2] have been recomputed, taking more detailed account of the effect of elastic resonance scattering by light and medium atomic-weight materials. In addition, calculations have been made for Pu-Th systems.

There are three components of the sodium void-coefficient of reactivity.

1. *Effect of  $(n, \gamma)$  capture by Na.* This effect is positive, but usually comparatively insignificant. This effect was taken to be the same as in the previous work by Yiftah and Okrent [2], and the same capture cross-sections were used for all the materials.

2. *Leakage component.* This effect is negative. The magnitude of the effect decreases as the core-size increases since the amount of leakage from the core becomes an insignificant part of the overall neutron balance with the larger core-size. The magnitude of this effect depends on the transport cross-section of the core; the transport cross-sections of sodium, stainless steel (type 304) and oxygen were changed from those of [2] to account more accurately for elastic-scattering resonances from 3.7 MeV to 25 keV.

3. *Spectral shift.* This effect can be positive or negative depending on the reactor composition. Sodium degrades the neutron spectrum at the high end as a result of inelastic and elastic scattering and builds up the low end of the spectrum. Thus, a decrease in the sodium density tends to harden the spectrum and to increase the fissions in materials (e.g.,  $U^{238}$ ) having a threshold slightly above the peak in the core spectrum. Similarly, the fission cross-sections of the normal fissile material (e.g.,  $Pu^{239}$ ) can decrease slower than the total absorption cross-section of the core at higher energies. The inelastic and fission cross-sections were assumed to be the same as given by YIFTAH *et al.* [4]. The elastic removal cross-sections were re-evaluated for Na, stainless steel, and O.

## 1. Description of the systems studied

All the calculations were made in spherical geometry by means of the diffusion-theory code RE-122 on an IBM-704. Each reactor was assumed to consist of three regions: core, blanket, and external reflector. The core size and composition were varied while keeping the same thickness and compositions of blankets and reflectors. Only a small fraction of possible permutations of systems were calculated as only a comparison with the previous results was sought.

The specifications of the systems studied were as follows:

*Core volumes:* 800, 1 500, 2 500 l

*Core volume fractions:* Fuel and fertile material—0.25

Structural material—0.25 (stainless steel)

Sodium coolant—0.5, 0.45, 0.4, 0.3, 0.2

*Fuel and fertile material:* U, Pu metals with density 19 g/cm<sup>3</sup>

Th metal with density 11.58 g/cm<sup>3</sup>

$UO_2$ ,  $PuO_2$ ,  $ThO_2$  with density 8.4 g/cm<sup>3</sup>

*Isotopic composition of Pu in at. %:*

Type	$Pu^{239}$	$Pu^{240}$	$Pu^{241}$	$Pu^{242}$
$Pu^A$	100	0	0	0
$Pu^B$	74.7	10.2	12.4	2.7

*Blanket:*

*Thickness:* 45 cm for systems having  $U^{238}$  as fertile material in core

54 cm for systems having  $Th^{232}$  as fertile material in core

$U^{238}$  or Th—0.6 (Same as the fertile material in core)

Na—0.2

Stainless steel—0.2

*Reflector:*

Thickness: 30 cm  
 Composition: Stainless steel—0.6  
 Sodium—0.4

**2. ELMOE code calculations**

Fundamental mode calculations were performed for a 800-l core, using the ELMOE code RE-196 [3, 5]. The volume fractions of Pu<sup>239</sup> and U<sup>238</sup> were kept constant in a series of calculations with the sodium volume fraction equal to 0.5, 0.4, 0.3, 0.2 and 0 and the stainless steel volume fraction equal to 0.25 and 0.125. A similar series of calculations was done for oxide core containing Pu<sup>A</sup> and U<sup>238</sup> fuel with the appropriate volume fractions.

The code library contains cross-sections and anisotropic components for Na, stainless steel, O, etc., tabulated at small energy intervals. The total cross-section data used for Na were those in [6] rather than the higher resolution data given in [7]. The code solves the following equation in the ordinary  $P_1$  approximation by the iterative process.

$$\varphi_k^{(i)} = \frac{\beta_k + \psi_k^{(i)}}{\frac{B^2(i)}{3 \Sigma_{tr,k}} + \Sigma_{a,k} + \Sigma_{elr,k}}$$

where

$\varphi_k^{(i)}$ =total flux in  $k$ th group in  $i$ th iteration

$\beta_k$ =fraction of fission neutrons born in group  $k$

$\Sigma_{tr,k} = \Sigma_{sc,k} (1 - \mu_k) + \Sigma_{a,k}$ =transport cross-section in group  $k$

$\Sigma_{a,k}$ =total removal cross-section from group  $k$  (except removal by elastic scattering)

$\psi_k^{(i)} = \sum_{j=1}^{k-1} \Sigma_{j \rightarrow k} \varphi_j^{(i)}$     [inelastic component of  $\Sigma_{j \rightarrow k}$  is assumed constant in the coarse groups as defined in [4]]

The value of  $B^2$  is changed until  $\left| \sum_{k=1}^N \nu_k \Sigma_{f,k} \varphi_k^{(i)} - 1 \right| < \varepsilon$  where  $\varepsilon$  is a small

number determining the convergence.

The whole energy range from 3.65 MeV to 25 keV was divided into finer groups having an equal lethargy width of 0.0087. The group boundaries defined in the cross-section set by Yiftah *et al.* [4] were adjusted slightly to coincide with some of these group boundaries. The correspondence of groups is given in Table I. All the cross-sections, except for elastic-scattering cross-sections in the above energy range, were taken from the 16-group set mentioned above. In the above calculations U and Pu were considered as "heavy" elements and the refined study of the elastic-scattering effect by U, Pu and Th was not carried out. The spectra obtained for the metallic core and oxide core, with varying sodium volume fractions, are given in Figs. 1 and 2, respectively.

The code prints out an elastic removal cross-section for every element. These cross-sections for the ten coarse groups are given in Table II. The code prints out  $3 \Sigma_{tr}$  for the ten coarse groups for the mixture of core materials. The transport cross-sections for Pu and U were taken from the 16-group set [4], the cross-sections for stainless steel and sodium were deduced successively from the different

TABLE I  
CORRESPONDENCE OF FINE AND COARSE GROUPS

Coarse group	Energy range (MeV)	Fine groups		
		Metal core		Oxide core
		First pass	Second pass	
1	$\infty$ — 3.65	—	—	—
2	3.65 — 2.22	1 — 58	—	1 — 58
3	2.22 — 1.35	59 — 115	—	59 — 115
4	1.35 — 0.82	116 — 172	—	116 — 172
5	0.82 — 0.50	173 — 329	1 — 57	173 — 229
6	0.50 — 0.300	230 — 288	58 — 116	230 — 288
7	0.300 — 0.180	289 — 347	117 — 175	289 — 347
8	0.180 — 0.109	348 — 404	176 — 232	348 — 404
9	0.109 — 0.067	—	233 — 289	405 — 461
10	0.067 — 0.041	—	290 — 346	462 — 519
11	0.041 — 0.025	—	347 — 402	520 — 547
12	0.025 — 0.015	—	—	—
13	0.015 — 0.0091	—	—	—
14	0.0091 — 0.0055	—	—	—
15	0.0055 — 0.0021	—	—	—
16	0.0021 — 0.0005	—	—	—

NOTE. When the calculations were performed for metal core, only 450 fine groups could be handled at a time. The calculations were done in two passes, and in the second pass the transport cross-sections for the higher groups were adjusted to agree with the output of the first pass. The overlap of four coarse groups was found to be sufficient to produce the correct slowing-down source for the coarse groups 9, 10, and 11. The results obtained in the second pass for the coarse groups 5 to 8 were neglected.

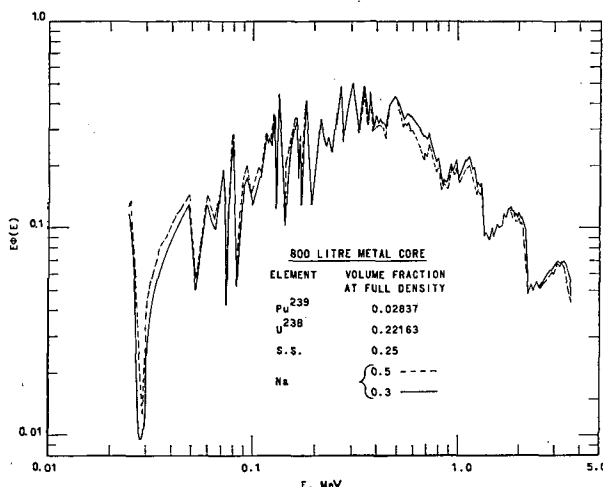


Fig. 1  
The spectrum at the centre of  $800\text{-l}$   $\text{Pu}^A + \text{U}^{238}$  metal core.

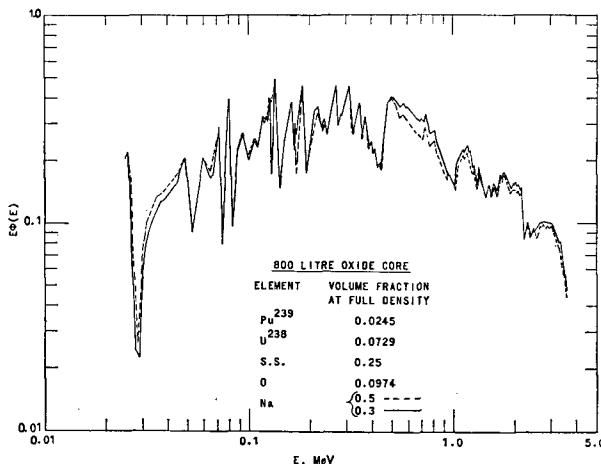


Fig. 2  
The spectrum at the centre of 800-l Pu<sup>A</sup> + U<sup>238</sup> oxide core.

variations of core compositions. In the case of the oxide core, the cross-section for oxygen was deduced before stainless steel and sodium. Since these cross-sections depend on the amounts of the various materials present, the values of cross-sections deduced from the compositions nearest to the above systems were used in the successive work. These transport cross-sections are given in Table III.

A similar calculation was made for the oxide core composition for the core-size of 2,500 l. This case is expected to give the largest differences in the cross-sections derived. However, the differences in cross-sections seem to be negligible in comparison to the changes obtained when the volume fractions of light and medium elements are changed. Thus, the cross-sections derived are not sensitive to the enrichment of the fuel or to the nature of fuel and fertile materials, and the cross-sections are valid for any core spectrum in a large reactor, if the volume fractions of lighter elements are within the range of these calculations. The cross-sections evaluated from the fundamental-mode spectrum are not necessarily valid in blanket, reflector, and coolant header regions, or at the edge of the core, because of the change in light-element composition. Any error caused for this reason is probably not important in a large reactor, except possibly in the case of "pancake" reactors with a very low  $L/D$  ratio.

### 3. Diffusion theory calculations

These new cross-sections were included in the libraries of the code RE-122. Two separate sets were made for the oxide and metal cores. In general, the elastic removal cross-sections were higher than the previous set of Yiftah *et al.* [4] by about 10 to 50% in the metal cores, and the cross-sections were usually higher for the oxide cores than the corresponding values for metal cores. The transport cross-sections were generally smaller than the previous set for the metal assemblies. The cross-sections for oxide systems were generally smaller than those for metal systems. Thus, the new sets are less reactive than the set used in the previous work

TABLE II  
EFFECTIVE ELASTIC REMOVAL CROSS-SECTIONS  
(barns)

Coarse group	Metal core		Oxide core		Standard [4]
	Range	Values used	Range	Values used	
<b>Sodium</b>					
2	0.211—0.207	0.210	0.245—0.218	0.245	0.164
3	0.240—0.239	0.239	0.264—0.250	0.264	0.215
4	0.435—0.417	0.429	0.514—0.500	0.505	0.374
5	0.659—0.600	0.639	0.668—0.568	0.594	0.594
6	0.605—0.595	0.603	0.691—0.614	0.683	0.500
7	0.641—0.627	0.635	0.714—0.623	0.708	0.518
8	0.545—0.532	0.541	0.550—0.550	0.551	0.458
9	0.623—0.600	0.612	0.655—0.632	0.650	0.468
10	0.700—0.659	0.686	0.645—0.595	0.622	0.619
11	0.927—0.868	0.897	0.995—0.936	0.968	0.518
<b>Stainless steel (type 304)</b>					
2	0.064—0.060	0.062	0.073—0.068	0.072	0.079
3	0.090—0.090	0.090	0.102—0.100	0.101	0.086
4	0.139—0.118	0.135	0.183—0.176	0.178	0.120
5	0.248—0.153	0.229	0.222—0.165	0.208	0.157
6	0.140—0.132	0.136	0.166—0.153	0.157	0.193
7	0.176—0.172	0.175	0.190—0.188	0.190	0.164
8	0.215—0.203	0.211	0.228—0.217	0.225	0.225
9	0.229—0.216	0.220	0.236—0.234	0.234	0.326
10	0.349—0.286	0.337	0.263—0.275	0.314	0.244
11	0.416—0.352	0.369	0.430—0.379	0.391	0.572
<b>Oxygen</b>					
2	—	—	0.211—0.209	0.210	0.430
3	—	—	0.546—0.546	0.546	0.559
4	—	—	1.125—1.115	1.121	0.793
5	—	—	0.823—0.754	0.790	0.797
6	—	—	1.365—1.344	1.357	0.914
7	—	—	0.876—0.861	0.868	0.715
8	—	—	0.872—0.870	0.871	0.710
9	—	—	0.841—0.828	0.834	0.651
10	—	—	0.863—0.820	0.842	0.626
11	—	—	0.979—0.949	0.963	0.643

[2]. The values of  $k$  calculated for some of the assemblies are given in Tables IV and V. Table IV shows that the reactivity coefficient of Na is not linear and rises sharply as the density decreases. In the other systems, the effect was investigated for the decrease in Na density by 40%. The values of  $k$  and  $\Delta k$  are given in Table V.

Table V (p. 186) shows that the  $\text{Pu}^4\text{U}^{238}$  system has the most positive coefficient, since the fission threshold of  $\text{U}^{238}$  is above the peak of the spectrum and the harder spectrum caused by the lower Na density increases the fission-neutron contribution from  $\text{U}^{238}$ , and it appears that  $\text{U}^{238}$ -fission is the major contribution to the positive coefficient of reactivity. The fission contribution from  $\text{Pu}^{240}$  and  $\text{Pu}^{242}$  is not

TABLE III  
EFFECTIVE TRANSPORT CROSS-SECTIONS  
(barns)

Coarse group	Values used		Standard [4]
	Metal	Oxide	
<b>Sodium</b>			
2	1.426	1.333	1.47
3	1.658	1.625	1.96
4	2.684	2.512	2.89
5	4.178	4.152	3.93
6	3.319	3.300	3.22
7	3.733	3.484	3.49
8	3.752	3.500	3.10
9	4.017	3.866	3.46
10	4.689	4.562	4.77
11	5.683	5.291	3.88
<b>Stainless steel</b>			
2	1.939	1.967	2.244
3	2.063	2.068	2.125
4	1.980	2.031	2.125
5	2.356	2.332	2.371
6	2.728	2.686	3.000
7	2.635	2.635	2.666
8	3.293	3.267	3.649
9	4.088	3.996	5.828
10	4.406	4.392	4.536
11	5.870	5.674	10.426
<b>Oxygen</b>			
2		1.416	1.72
3		1.843	2.56
4		3.881	3.51
5		2.555	3.47
6		5.240	4.09
7		4.313	3.35
8		3.765	3.35
9		3.661	3.35
10		3.552	3.35
11		4.273	3.35

changed appreciably by the harder spectrum and, hence, the coefficient for  $\text{Pu}^B \text{ U}^{238}$  (with less  $\text{U}^{238}$  in core) is more negative than that of  $\text{Pu}^A \text{ U}^{238}$ . The fission threshold for Th is very high, and the fission-neutron contribution from Th is very small. Also, the total increase in the flux above the threshold for  $\text{Th}^{232}(n, f)$  due to the harder spectrum is small. Thus, the magnitude of the spectral effect in  $\text{Pu}^B \text{ Th}$  systems is much smaller than the others. The presence of oxygen in oxide cores reduces the effect of the lower Na density and the spectral shift is reduced. The coefficients for oxide cores are more negative than those of corresponding metal cores.

TABLE IV  
 $k_{\text{eff}}$  FOR 800-l METAL CORES WITH VARIOUS SODIUM DENSITIES

System		Sodium density				
		100 %	90 %	80 %	60 %	40 %
$\text{Pu}^B + \text{U}^{238}$	$k$	0.99999	0.99955	0.99902	0.99768	0.99597
	$\Delta k \times 10^5$ for 1% decrease	—	-4.38	-4.84	-5.75	-6.70
$\text{Pu}^B + \text{Th}^{232}$	$k$	0.99997	0.99633	0.99253	0.98456	0.97608
	$\Delta k \times 10^5$ for 1% decrease	—	-36.44	-37.18	-38.53	-39.82

NOTE. A 10 % decrease in sodium density corresponds to about a 350°C rise at the operating temperatures.

#### 4. Conclusions

As mentioned above, the elastic removal cross-sections for sodium are higher in this work than those used in the previous work by Yiftah *et al.* [2]. This enhances the spectral-shift effect by the decrease in sodium density and makes the reactivity coefficients more positive than those calculated before, as is shown in the comparison in Table V. For example, for the  $\text{Pu}^A \text{U}^{238}$  oxide system, the coefficient became positive in the previous results for the core-size of 3 500 l, while in the new results it is positive at the core-size of 2 500 l. Thus, the threshold for the positive coefficients seems to be lower than previously predicted.

Of all the systems studied, the  $\text{Pu}^B \text{Th}$  system (in metal or oxide form) seems to be the safest from the viewpoint of the prompt reactivity coefficient due to any decrease in the sodium density from a rise in temperature of sodium or from some gas bubbles in sodium flow. Design studies can be usefully made for large core-sizes for a fast breeder from the viewpoint of utilizing the "dirty" plutonium (such as  $\text{Pu}^B$ ) obtained from the spent fuel elements of large thermal reactors and the vast reserves of thorium in India.

#### ACKNOWLEDGEMENTS

The authors wish to thank Mr. A. L. Rago of the Argonne National Laboratory for carrying out the ELMOE code calculations during the code development. One of the authors (M. G. Bhide) wishes to thank the United States Atomic Energy Commission and its Argonne National Laboratory for providing the facilities for this work during his stay at Argonne.

#### REFERENCES

- [1] NIMS, J. B. and ZWEIFEL, P. F., APDA-135 (1959).
- [2] YIFTAH, S. and OKRENT, D., ANL-6212 (1960).
- [3] HUMMEL, H. H. and RAGO, A. L., *Trans. Amer. nucl. Soc.* **3** (1960).
- [4] YIFTAH, S., OKRENT, D. and MOLDAUER, P. A., *Fast Reactor Cross Sections —A Study Leading to a 16-Group Set*. Pergamon Press (1960).
- [5] HUMMEL, H. H. and RAGO, A. L., *These proceedings*, Vol. 1, p. 231.
- [6] HUGHES, D. J., MAGURNO, B. A. and BRUSSEL, M. K., BNL-325, Suppl. No. 1 (1960).
- [7] HIBDON, C. T., *Phys. Rev.* **118** (1960) 514—532.

TABLE V  
*k* FOR THE VARIOUS SYSTEMS

System	800-l core			1500-l core			2500-l core		
	<i>k</i> with Na		$\Delta k \times 10^5$ for 1% decrease	<i>k</i> with Na		$\Delta k \times 10^5$ for 1% decrease	<i>k</i> with Na		$\Delta k \times 10^5$ for 1% decrease
	100 %	60 %		100 %	60 %		100 %	60 %	
<i>Metal</i>									
Pu <sup>A</sup> + U <sup>238</sup>	0.99473*	0.99360	-2.81	0.99037*	0.99475	+10.96	0.99177*	1.00098	+23.03
Pu <sup>B</sup> + Th <sup>232</sup>	0.99997	0.98456	-38.53	0.99998	0.98933	-26.62	0.99998	0.99456	-13.54
Pu <sup>B</sup> + U <sup>238</sup>	0.99999	0.99768	-5.75	—	—	—	—	—	—
<i>Oxide</i>									
Pu <sup>A</sup> + U <sup>238</sup>	0.98840*	0.97901	-23.47	0.98182*	0.97783	-9.97	0.97624*	0.97780	+3.90
Pu <sup>B</sup> + Th <sup>232</sup>	1.00001	0.97800	-55.03	1.00000	0.98275	-43.12	1.00001	0.98869	-28.28
Pu <sup>B</sup> + U <sup>238</sup>	0.99042*	0.97970	-26.80	—	—	—	—	—	—

\* The compositions were taken from [2]. They were calculated as critical with  $|k-1| < 5 \times 10^{-5}$ . The new values of *k* are higher by about 0.2%, since these calculations used stainless steel (type 304) as structural material instead of the iron used in [2]. The departure of these new values from 1 indicates the effect of the new cross-section sets reduced by the use of stainless steel cross-sections instead of Fe cross-sections.

# МЕТОДЫ РАСЧЕТА ВЫГОРАНИЯ ПОГЛОТИТЕЛЕЙ В РЕАКТОРАХ НА ПРОМЕЖУТОЧНЫХ НЕЙТРОНАХ

Г. И. Тошинский и А. Г. Калашников  
АКАДЕМИЯ НАУК СССР, МОСКВА,  
СССР

**Abstract — Résumé — Аннотация — Resumen**

**Methods for calculating burn-up of absorbers in intermediate reactors.** This paper describes techniques of calculating the burn-up of absorbers used to compensate excess reactivity in intermediate reactors. The equations arrived at here require, in general, a numerical solution; but for certain simplifying assumptions, problems can be solved analytically. The paper likewise arrives at approximate formulae which are useful in certain particular cases.

When the absorber is distributed homogeneously (i.e. when the self-shielding factor approaches unity) a solution is obtained which accounts for the neutron spectrum change in the reactor during its run (in the case of a reflectorless reactor).

The paper suggests criteria for homogeneous absorber distribution which make it possible to select the optimum properties of the absorber.

**Méthodes de calcul du taux de consommation des absorbants dans les réacteurs à neutrons intermédiaires.** Les auteurs décrivent les méthodes de calcul du taux de consommation des absorbants utilisés pour compenser la réactivité en excès dans les réacteurs à neutrons intermédiaires. Les équations auxquelles on parvient dans ce cas exigent en général une solution par une méthode numérique; mais en faisant certaines hypothèses simplificatrices, on peut résoudre analytiquement les problèmes. Les auteurs établissent également des formules approchées, utiles dans certains cas particuliers.

Lorsque l'absorbant est réparti de façon homogène (c'est-à-dire quand le facteur d'autoprotection approche de l'unité), on obtient une solution qui tient compte des changements du spectre neutronique au moment où le réacteur fonctionne (pour un réacteur sans réflecteur).

Les auteurs proposent, pour parvenir à une répartition homogène des absorbants, certains critères qui permettent de choisir les propriétés optima de l'absorbant.

**Методы расчета выгорающих поглотителей в реакторах на промежуточных нейтронах.** В докладе изложена методика расчета выгорания поглотителей, применяющихся для компенсации избыточной реактивности в реакторах на промежуточных нейтронах. Полученные уравнения требуют в общем случае численного решения. При некоторых упрощающих предположениях задача решена аналитически. В докладе получены также приближенные формулы, полезные в некоторых частных случаях.

В случае, когда поглотитель размещён гомогенно (т.е. фактор самозкранирования близок к единице), получено решение, учитывающее изменение спектра нейронов в реакторе в течение кампании (для реактора без отражателя).

Для гетерогенного размещения поглотителя приводятся критерии, позволяющие выбрать оптимальные характеристики поглотителя.

**Métodos para calcular la combustión de absorbentes en los reactores intermedios.** Los autores describen un conjunto de métodos para calcular el grado de combustión de los elementos absorbentes que se utilizan para compensar el exceso de reactividad en los reactores de neutrones intermedios.

En el caso general, las ecuaciones obtenidas exigen una solución numérica. Partiendo de ciertas suposiciones que simplifican el problema éste puede resolverse también analíticamente.

Los autores deducen asimismo ciertas fórmulas aproximadas que pueden aplicarse en casos particulares.

Cuando la distribución del absorbente es homogénea (o sea, cuando el factor de autoblindaje es próximo a la unidad), se obtiene una solución que tiene en cuenta la modificación del espectro neutrónico en el reactor durante el ciclo de funcionamiento (para un reactor desprovisto de reflector).

Asimismo, se indican criterios que permiten elegir las características óptimas del absorbente cuando su distribución es heterogénea.

## 1. Введение

Применение выгорающих поглотителей в реакторах для компенсации эффектов, медленно меняющих реактивность (выгорание горючего, защелковывание и т.п.), в последние годы получило значительное распространение.

Выгорающие поглотители позволяют сократить количество подвижных органов регулирования и упростить конструкцию реактора или при заданной системе регулирования увеличить длительность кампании реактора, компенсируя увеличение начальной избыточной реактивности от дополнительного введения в реактор горючего. Вместе с тем применение выгорающих поглотителей создает более благоприятные условия с точки зрения выравнивания поля энерговыделения в реакторе в течение кампании.

Ряд вопросов теории расчета и применения выгорающих поглотителей изложен в работах [1], [2], [3]. Однако в [1] и [2] эти вопросы рассмотрены применительно только к реакторам на тепловых нейтронах, а в [3] изложены лишь некоторые частные случаи для реактора на промежуточных нейтронах.

В настоящей работе изложена методика расчета выгорания поглотителей для реактора на промежуточных нейтронах в более общем случае. Полученные результаты применимы также и для реакторов на тепловых нейтронах.

При применении выгорающих поглотителей представляют интерес такие характеристики, как максимальная величина разбаланса реактивности, обусловленного несоответствием законов выгорания поглотителя и горючего, которая определяет необходимое количество подвижных органов регулирования, и величина остаточной реактивности от невыгоревшего к концу кампании поглотителя, которая определяет уменьшение продолжительности кампании или величину дополнительного количества горючего для компенсации этой потери реактивности.

Наилучшим является такой поглотитель, для которого как величина максимального разбаланса реактивности, так и остаточная реактивность являются минимальными. Однако эти требования являются взаимно противоречивыми. Поэтому оптимальные характеристики поглотителя находятся путем компромисса.

Если для рассматриваемого реактора можно подобрать поглотитель, скорость выгорания которого значительно больше скорости выгорания горючего, то более эффективным оказывается гетерогенное размещение поглотителя, тогда как для поглотителя с умеренной скоростью выгорания

гетерогенное размещение дает очень большую потерю реактивности из-за невыгоревшего к концу кампании поглотителя. Это связано с тем, что эффект самоэкранирования уменьшает скорость выгорания поглотителя из-за депрессии потока нейтронов в области его расположения.

## 2. Решение уравнения выгорания поглотителя

Уравнение выгорания поглотителя имеет вид:

$$\frac{dN_{\pi}(r,t)}{dt} = -\lambda_{\pi}(r,t) \cdot N_{\pi}(r,t) \quad (1)$$

где:  $N_{\pi}(r, t)$  — число ядер поглотителя в единице объема в точке реактора с координатой  $r$  в момент времени  $t$ ,  
 $t$  — эффективное время работы реактора

$$t = \int_0^{t'} P(t'') dt''$$

$t'$  — действительное время работы реактора,  
 $P$  — относительный уровень мощности реактора.

$$\lambda_{\pi}(r, t) = \int f_{\pi}(r, u, t) \sigma_c^{\pi}(u) \Phi(r, u, t) du$$

$f_{\pi}$  — фактор самоэкранирования поглотителя,  
 $\sigma_c^{\pi}$  — сечение захвата поглотителя,  
 $\Phi$  — поток нейтронов при номинальном уровне мощности реактора.

Решение уравнения (1) может быть получено в виде:\*

$$\frac{N_{\pi}}{N_{\pi}^0} = e^{- \int_0^t \lambda_{\pi}(r, t') dt'} \quad (2)$$

Здесь  $N_{\pi}^0$  — концентрация поглотителя в начале кампании.

Из выражения (2) можно получить зависимость  $N_{\pi}/N_{\pi}^0$ , используя метод итераций, так как фактор самоэкранирования  $f_{\pi}$ , входящий в функцию  $\lambda_{\pi}(r, t)$ , зависит от  $N_{\pi}$ . Кроме того поток нейтронов  $\Phi$  также неявно зависит от  $N_{\pi}$ .

Однако практически в связи с большим объемом вычислительной работы выражение (2) является полезным лишь при использовании быстродействующих электронно-счетных машин.

При некоторых допущениях можно получить уравнение выгорания поглотителя, допускающее решение более простыми средствами.

Предположим, что спектр нейтронов в реакторе не меняется на протяжении кампании, т.е.

$$\Phi(r, u, t) = \Phi_0(r, u) S(t) \quad (3)$$

\* Здесь и далее предполагается, что сечение захвата ядра, образующегося при захвате нейтрона ядром поглотителя, равно нулю. Случай цепочки из двух поглощающих изотопов в простейшем приближении рассмотрен в работе [3].

Множитель  $S(t)$  определяется из условия сохранения мощности реактора в течение кампании:

$$\int N_r^0(\mathbf{r}) dv \int f_r^0(\mathbf{r}, u) \sigma_f(u) \Phi_0(\mathbf{r}, u) du = S(t) \int N_r(\mathbf{r}, t) dv \int f_r(\mathbf{r}, u, t) \sigma_f(u) \Phi_0(\mathbf{r}, u) du \quad (4)$$

где:  $f_r(\mathbf{r}, u, t)$  — фактор самоэкранирования горючего.

Будем считать, что  $f_r$  линейно зависит от концентрации горючего. Такое предположение является достаточно справедливым, так как выгорание горючего за кампанию обычно невелико.

Тогда

$$f_r(\mathbf{r}, u, t) = f_r^0(\mathbf{r}, u) \left\{ 1 + A(\mathbf{r}, u) \left[ 1 - \frac{N_r(\mathbf{r}, t)}{N_r(\mathbf{r}, 0)} \right] \right\}.$$

Здесь

$$A(\mathbf{r}, u) = N_r(\mathbf{r}, 0) \frac{d}{dN_r} \left[ \ln f_r(u, N_r) \right]_{N_r = N_r^0}.$$

Как будет показано ниже:

$$N_r(\mathbf{r}, t)/N_r(\mathbf{r}, 0) = 1 - \lambda_r^{0,c}(\mathbf{r}) t.$$

Где:

$$\lambda_r^{0,c}(\mathbf{r}) = \int f_r^0(\mathbf{r}, u) \sigma_c^r(u) \Phi_0(\mathbf{r}, u) du.$$

Следовательно

$$f_r(\mathbf{r}, u, t) = f_r^0(\mathbf{r}, u) \left[ 1 + A(\mathbf{r}, u) \lambda_r^{0,c}(\mathbf{r}) t \right].$$

Теперь, воспользовавшись условием (4), получим:

$$S(t) = \left[ \frac{\langle N_r(t) \rangle_{av}}{\langle N_r(0) \rangle_{av}} (1 - B t) \right]^{-1}. \quad (5)$$

Здесь:

$$\langle N_r(t) \rangle_{av} = \frac{\int N_r(\mathbf{r}, t) \lambda_r^{0,f}(\mathbf{r}) dv}{\int \lambda_r^{0,f}(\mathbf{r}) dv}$$

$$\lambda_r^{0,f}(\mathbf{r}) = \int f_r^0(\mathbf{r}, u) \sigma_f(u) \Phi_0(\mathbf{r}, u) du.$$

$$B(t) = \frac{\int \bar{A}(\mathbf{r}) \lambda_r^{0,c}(\mathbf{r}) N_r(\mathbf{r}, t) \lambda_r^{0,f}(\mathbf{r}) dv}{\int N_r(\mathbf{r}, t) \lambda_r^{0,f}(\mathbf{r}) dv}$$

$$\bar{A}(\mathbf{r}) = \frac{\int A(\mathbf{r}, u) f_r^0(\mathbf{r}, u) \sigma_f(u) \Phi_0(\mathbf{r}, u) du}{\int f_r^0(\mathbf{r}, u) \sigma_f(u) \Phi_0(\mathbf{r}, u) du}.$$

Функция  $B(t)$  слабо зависит от времени, поэтому для простоты в дальнейшем будем считать  $B(t) = B(0) = \text{const}$ .

Для определения зависимости  $\langle N_r(t) \rangle_{av}$  необходимо определить функцию  $N_r(\mathbf{r}, t)$ .

Уравнение выгорания горючего имеет вид:

$$\frac{dN_r(r, t)}{dt} = -\lambda_r^c(r, t) \cdot N_r(r, t), \quad (6)$$

$$\lambda_r^c(r, t) = \int f_r(r, u, t) \sigma_r^c(u) \Phi(r, u, t) du.$$

Предполагая, что число делений в единицу времени в каждой точке реактора не зависит от времени, т.е.

$$N_r(r, 0) \int f_r^0(r, u) \sigma_r^f(u) \Phi_0(r, u) du =$$

$$N_r(r, t) \int f_r(r, u, t) \sigma_r^f(u) \Phi(r, u, t) du$$

уравнение (6) можно привести к виду:

$$\frac{(dN_r(r, t))}{dt} = -N_r(r, 0) \lambda_r^{0,c}(r) \frac{b_r(r, t)}{b_r(r, 0)}. \quad (7)$$

Здесь

$$b_r(r, t) = \frac{\lambda_r^c(r, t)}{\lambda_r^f(r, t)}; b_r(r, 0) = \frac{\lambda_r^{0,c}(r)}{\lambda_r^{0,f}(r)}$$

С хорошей точностью можно считать, что  $b_r(r, t)/b_r(r, 0) \approx 1$ , так как отношение усредненных сечений захвата к делению для горючего очень слабо меняется в течение кампании.

Тогда решение уравнения (7) очевидно примет вид:

$$\frac{N_r(r, t)}{N_r(r, 0)} = 1 - \lambda_r^{0,c}(r) \cdot t. \quad (8)$$

Теперь можно определить зависимость  $\langle N_r(t) \rangle_{av} / \langle N_r(0) \rangle_{av}$ , входящую в выражение для  $S(t)$ :

$$\frac{\langle N_r(t) \rangle_{av}}{\langle N_r(0) \rangle_{av}} = 1 - \langle \tilde{\lambda}_r^{0,c} \rangle_{av} \cdot t$$

Здесь

$$\langle \tilde{\lambda}_r^{0,c} \rangle_{av} = \frac{\int \lambda_r^{0,c}(r) N_r(r, 0) \lambda_r^{0,f}(r) dv}{\int N_r(r, 0) \lambda_r^{0,f}(r) dv}.$$

Заметим, что если начальное распределение горючего не зависит от координат, то

$$\langle \tilde{\lambda}_r^{0,c} \rangle_{av} = \langle \lambda_r^{0,c} \rangle_{av}.$$

Таким образом выражение для  $S(t)$ , пренебрегая квадратичным членом, можно записать в следующем виде:

$$S(t) = \frac{1}{1 - Ct}. \quad (9)$$

где  $C = B + \langle \tilde{\lambda}_r^{0,c} \rangle_{av}$ .

Используя теперь соотношение (3), получим уравнение (1) в виде:

$$\frac{1}{N_n(r, t)} \frac{dN_n(r, t)}{dt} = -\frac{1}{1 - Ct} \int f_n(r, u, t) \sigma_c^n(u) \Phi_0(r, u) du. \quad (10)$$

Но, следовательно, разделив переменные, уравнение можно проинтегрировать:

$$\int_z^1 \frac{dz'}{z' \lambda_{\pi}(\mathbf{r}, z')} = -\frac{1}{C} \ln(1 - Ct) \quad (11)$$

Здесь

$$z = \frac{N_{\pi}(\mathbf{r}, t)}{N_{\pi}(\mathbf{r}, 0)}; \lambda_{\pi}(\mathbf{r}, z) = \int f_{\pi}(\mathbf{r}, u, z) \sigma_c^{\pi}(u) \Phi_0(\mathbf{r}, u) du.$$

Решение уравнения (11) может быть найдено численно. Используя решение уравнения (11) в качестве первого приближения, в котором не учитывается влияние изменения спектра нейтронов в реакторе на процесс выгорания поглотителя, можно методом итераций решить уравнение (2) и получить точное решение. В тех случаях, когда влияние изменения спектра нейтронов на процесс выгорания поглотителя невелико, например, в тепловых и эпитеческих реакторах, решение уравнения (11) является достаточно точным.

Решение уравнения (10) может быть получено также и в аналитическом виде при использовании разложения фактора самоэкранирования поглотителя в степенной ряд по времени в начале кампании.

$$f = f_0 + \sum_{n=1}^{\infty} \frac{y^n}{n!} f_0^{(n)}. \quad (12)$$

Здесь

$$f_0 = f_{\pi}(\mathbf{r}, u, 0),$$

$$f_0^{(n)} = \left. \frac{d^n f(\mathbf{r}, u, y)}{dy^n} \right|_{y=0}$$

$$y = t/T \text{ — безразмерное время} \\ T \text{ — длительность кампании}$$

Используя (12), получим решение уравнения (10) в виде:

$$\frac{N_{\pi}(\mathbf{r}, y)}{N_{\pi}(\mathbf{r}, 0)} = \left(1 - \frac{y}{x_r}\right)^{\Omega(\mathbf{r})} - \frac{T \sum_{n=1}^{\infty} \frac{1}{n!} \left[ \int_0^y \frac{y^n dy}{1 - (y/x_r)} \right] \left[ f_0^{(n)} \sigma_c^{\pi}(u) \Phi_0(\mathbf{r}, u) du \right]}{\ln[1 - (y/x_r)]}$$

Здесь  $\Omega(\mathbf{r}) = x_r / x_{\pi}^0(\mathbf{r})$

$x_r = 1/cT$  — безразмерное время жизни горючего,  
 $x_{\pi}^0(\mathbf{r}) = 1/\lambda_{\pi}^0(\mathbf{r})T$  — безразмерное время жизни поглотителя в точке  $\mathbf{r}$  в момент времени  $t=0$ .

$$\lambda_{\pi}^0(\mathbf{r}) = \int f(\mathbf{r}, u, 0) \sigma_c^{\pi}(u) \Phi_0(\mathbf{r}, u) du$$

Преобразуем выражение (13) к более удобному виду, разложив  $\ln[1 - (y/x_r)]$  и  $1/[1 - (y/x_r)]$  под интегралом по степеням  $y/x_r$ . При этом в разложении  $\ln[1 - (y/x_r)]$  возможно ограничиться первыми двумя членами ряда, так как  $y/x_r$  обычно меньше 0,2. В результате получим следующее выражение для

$$\frac{N_{\pi}(\mathbf{r}, y)}{N_{\pi}(\mathbf{r}, o)} = \left(1 - \frac{y}{x_r}\right)^{\omega(\mathbf{r}) + \frac{x_r T}{y[1 + (y/2)x_r]}} \sum_{n=1}^{\infty} \left[ \int_0^{(n)} f_0^{(n)} \sigma_c^{\pi} \Phi_0 du \right] \frac{y^{n+1}}{n!} \sum_{m=0}^{\infty} \frac{y^m}{(n+m+1)x_r^m} \quad (13)$$

Так как  $f_0^{(n)}$  зависит от вида функции  $N_{\pi}(\mathbf{r}, y)$ , то выражение (13) не дает возможности определить  $N_{\pi}(\mathbf{r}, y)/N_{\pi}(\mathbf{r}, 0)$ .

Запишем производные от функции  $f$  следующим образом:

$$\begin{aligned} \frac{df}{dy} &= \frac{df}{d\beta} \cdot \frac{d\beta}{dy} \\ \frac{d^a f}{dy^a} &= \frac{d^a f}{d\beta^a} \left( \frac{d\beta}{dy} \right)^a + \frac{df}{d\beta} \cdot \frac{d^a \beta}{dy^a} \end{aligned}$$

и т.д.

Здесь  $\beta$  — оптическая толщина образца поглотителя.

$$\beta = R \sigma_c^{\pi} (u) N_{\pi} (\mathbf{r}, y)$$

$R$  — характерный размер образца.

В тех случаях, когда фактор самоэкранирования  $f$  может быть получен в виде явной функции  $\beta$ , вычисление производных  $d^n f/d\beta^n$  не представляет труда. Следовательно, для знания  $f^{(n)}$  требуется лишь знание  $\beta^{(n)}$ .

Так как  $\beta = \beta_0 N_{\pi}/N_{\pi}^0$ , то очевидно

$$\beta^{(n)} = \beta_0 \frac{d^n}{dy^n} \left( \frac{N_{\pi}}{N_{\pi}^0} \right) \quad (14)$$

где  $\beta_0 = \beta(\mathbf{r}, u, 0)$

Дифференцируя обе части уравнения (13) последовательно „ $n$ “ раз ( $n = 1, 2, 3 \dots$ ) и подставляя  $y=0$ , получим

$$\begin{aligned} (N_{\pi}/N_{\pi}^0)' &= -\omega/x_r, \\ (N_{\pi}/N_{\pi}^0)'' &= [\omega(\omega-1)/x_r^2] - T \int f'_0 \sigma_c^{\pi} \Phi_0 du \\ (N_{\pi}/N_{\pi}^0)''' &= [\omega(\omega-1)(\omega-2)/x_r^3] + [(3\omega-2)T/X_r] \int f'_0 \sigma_c^{\pi} \Phi_0 du \\ &\quad - T \int f'_0 \sigma_c^{\pi} \Phi_0 du. \end{aligned}$$

и т.д.

Из приведенных выражений видно, что, зная все производные от  $(N_{\pi}/N_{\pi}^0)_0$  до „ $n$ “-го порядка включительно, можно найти „ $(n+1)$ “-ую производную, т.е. в показателе правой части уравнения (10) или (10<sup>1</sup>) может быть взято сколь угодно много членов.

### 3. Приближенные выражения для закона выгорания поглотителя

В некоторых частных случаях могут оказаться полезными приближенные более простые способы расчета изменения концентрации поглотителя в процессе выгорания, основанные на использовании приближенных выражений для фактора самоэкранирования поглотителя.

### АППРОКСИМИРОВАНИЕ ЗАВИСИМОСТИ $f(\beta)$ ФУНКЦИЕЙ ВИДА $1/(1+\gamma\beta)$

Заменим точную зависимость  $f(\beta)$  функцией вида  $1/(1+\gamma\beta)$ , где  $\gamma$  — некоторая постоянная, которая подбирается так, чтобы ошибка в определении  $f(\beta)$  в интервале от 0 до  $\beta_0^{\max}$  была наименьшей.

В этом предположении функция  $\lambda_n(r, z)$  из уравнения (11) примет вид:

$$\lambda_n(r, z) = \int \frac{\sigma_c^\pi(u) \Phi_0(r, u) du}{1 + \gamma \beta_0(r, u) z}$$

Или, воспользовавшись теоремой о среднем, получим:

$$\lambda_n(r, z) = \frac{[\lambda_n^0(r)]}{1 + \gamma \bar{\beta}(r, z) \cdot z}$$

где

$$[\lambda_n^0(r)]_{\text{гом}} = \int \sigma_c^\pi(u) \Phi_0(r, u) du$$

Очевидно  $\bar{\beta}$  будет зависеть от  $z$  как от параметра.

При  $z=1$  и  $z < < 1$  можно получить следующие формулы усреднения  $\beta_0(r, u)$ :

$$\bar{\beta}_n(r) = \frac{1}{\gamma} \left[ \frac{\int \sigma_c^\pi(u) \Phi_0(r, u) du}{\int [\sigma_c^\pi(u) \Phi_0(r, u) / (1 + \gamma \beta_0(r, u))] du} - 1 \right]_{z=1}$$

$$\bar{\beta}_k(r) = \frac{\int \beta_0(r, u) \sigma_c^\pi(u) \Phi_0(r, u) du}{\int \sigma_c^\pi(u) \Phi_0(r, u) du},$$

Очевидно случай  $z=1$  соответствует началу кампании, а случай  $z < < 1$  — концу кампании.

Если во всем интервале изменения  $z$  от 1 до 0 величина  $\beta(r, z)$  меняется слабо, что соответствует слабой зависимости сечения захвата поглотителя от летаргии в области его эффективного действия, то зависимость  $\bar{\beta}(r, z)$  можно представить линейной функцией  $z$ :

$$\bar{\beta}(r, z) = \bar{\beta}_k(r) + [\bar{\beta}_n(r) - \bar{\beta}_k(r)]z,$$

и  $\lambda_n(r, z)$  окончательно примет вид:

$$\lambda_n(r, z) = \frac{[\lambda_n^0(r)]}{1 + \gamma Z [\bar{\beta}_k + (\bar{\beta}_n - \bar{\beta}_k) Z]} \quad (15)$$

Уравнение (11) с учетом (15) после интегрирования сводится к следующему трансцендентному уравнению.

$$z e^{\epsilon - (\delta - \theta z)^2} = \left(1 - \frac{y}{X_r}\right)^{\omega_{\text{гом}}} \quad (16)$$

$$\epsilon = \gamma (\bar{\beta}_n)^\alpha / \alpha (\bar{\beta}_k - \bar{\beta}_n), \quad \omega_{\text{гом}} = X_r / (X_n^0)_{\text{гом}},$$

$$\delta = \bar{\beta}_k \sqrt{\gamma / \alpha (\bar{\beta}_k - \bar{\beta}_n)}, \quad (X_n^0)_{\text{гом}} = 1 / [\lambda_n^0(r)]_{\text{гом}} \cdot T,$$

$$\theta = \sqrt{\gamma (\bar{\beta}_k - \bar{\beta}_n) / \alpha}.$$

Если  $\sigma_c^n = \begin{cases} \text{const.} \\ 0 \end{cases}$  при  $u \geq u_0$   
то уравнение (16) перейдет в уравнение при  $u < u_0$

$$z = [1 - (y/x_r)]^{\omega_{\text{гом}}} e^{\gamma \beta_0 (1 - z)}$$

### АППРОКСИМИРОВАНИЕ ФУНКЦИИ $f(\beta)$ ПОЛИНОМОМ

Аппроксимируем  $f(\beta)$  в практически интересном интервале изменения  $\beta$  полиномом степени „ $n$ “

$$f(\beta) = \sum_{l=0}^n a_l \beta^l \quad (17)$$

Подставив (17) в уравнение (11) и вводя обозначение

$$A_l(r) = a_l T \int \beta_l^0(r, u) \sigma_c^n(u) \Phi_0(r, u) du$$

получим уравнение для  $N_n(r, y)/N_n(r, 0)$ :

$$\int_{N_n/N_n^0}^1 \frac{dz}{\sum_{l=0}^n A_l(r) z^{l+1}} = -x_r \ln \left( 1 - \frac{y}{x_r} \right) \quad (18)$$

#### СЛУЧАЙ МАЛЫХ $\beta$

В случае малых  $\beta$ , когда  $f(\beta)$  может быть аппроксимирована с достаточной точностью линейной функцией  $\beta$

$$f(\beta) = 1 - \alpha \beta,$$

решение уравнения (18) можно получить в виде:

$$(N_n/N_n^0)^{\text{ ret}} = (N_n/N_n^0)^{\text{гом}} / [(1 - \mu) + \mu (N_n/N_n^0)^{\text{гом}}] \quad (19)$$

Параметр  $\mu$  характеризует степень гетерогенности поглотителя

$$\mu = a \frac{\int \beta_0 \sigma_n c \Phi_0 d\mu}{\int \sigma_n c \Phi_0 d\mu}$$

$(N_n/N_n^0)^{\text{гом}} = [1 - (y/x_r)]^{\omega_{\text{гом}}}$  — есть закон выгорания гомогенно расположенного поглотителя (см. 5).

На рис. 1 приведены графики  $(N_n/N_n^0)^{\text{гом}}$  как функции  $\omega$  и  $x_r^{\text{гом}}/y$ .

На рис. 2 —  $(N_n/N_n^0)^{\text{ret}}$  как функции  $(N_n/N_n^0)^{\text{гом}}$  и  $\mu$ .

#### 4. Оптимальные условия гетерогенного размещения поглотителя

Зная зависимость изменения концентрации поглотителя в течение кампаний, можно найти величину реактивности, вносимой поглотителем в реактор в любой момент времени. Пользуясь теорией возмущений [4], [5] будем иметь:

$$\varrho_n(t) = -\frac{1}{\Pi. H. D.} \int \int N_n(r, t) f_n(r, u, t) \sigma_c^n(u) \Phi(r, u, t) \quad (20)$$

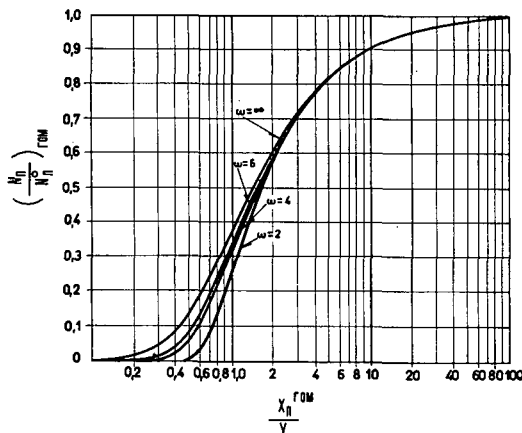


Рис. 1  
Зависимость  $\left(\frac{N_n}{N_n^0}\right)_{ROM}$  от  $\omega_{ROM}$  и  $\frac{x_n}{x_n^0}$

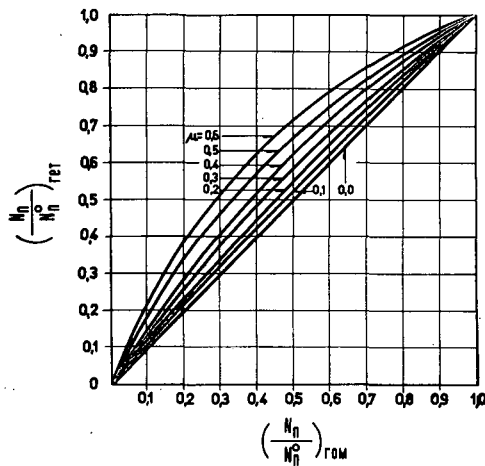


Рис. 2  
Зависимость  $\left(\frac{N_n}{N_n^0}\right)_{RET}$  от  $\left(\frac{N_n}{N_n^0}\right)_{ROM}$  и  $\mu$

$$\times \Phi^*(r, u, t) du dv.$$

Здесь

$\varrho_n(t)$  — реактивность, вносимая поглотителем в реактор в момент времени  $t$ ,

$\Phi(r, u, t)$  — поток нейтронов в реакторе с поглотителем,

$\Phi^*(r, u, t)$  — ценность нейтронов в реакторе без поглотителя,

Ц. Н. Д. — ценность нейтронов деления, рождающихся за одну секунду в реакторе.

Получим приближенное выражение для относительного изменения реактивности, полезное для ориентировочных расчетов.

Будем считать, что энергетические распределения потока и ценности нейтронов не зависят от времени. Предположим также, что поток и ценность нейтронов не зависят от координат и равны средним значениям по объему реактора.

Тогда, аппроксимируя зависимость фактора самоэкранирования поглотителя  $f(\beta)$  функцией вида  $(1/(1+\gamma\beta))$  (см. п. 3) и используя соотношение (9), получим, переходя к безразмерным параметрам:

$$\frac{\varrho_n(y)}{\varrho_n(0)} = \frac{1}{1 - (y/x_r)} \cdot \frac{(1 + \gamma \bar{\beta}_H^*) z(y)}{1 + \sigma \bar{\beta}_K^* z(y) + \gamma (\bar{\beta}_H^* - \bar{\beta}_K^*) \cdot z^0(y)} \quad (21)$$

где  $z(y) = N_n(y)/N_n(0)$  определяется из уравнения (16)

$$\bar{\beta}_n^* = \frac{1}{\gamma} \left( \frac{\int \sigma_n^c(u) \Phi_0(u) \Phi_0^*(u) du}{\int [\sigma_c^n(u) \Phi_0(u) \Phi_0^*(u)] / (1 - \gamma \beta_0(u)) du} - 1 \right)$$

$$\bar{\beta}_K^* = \frac{\int \beta_0(u) \sigma_n^c(u) \Phi_0(u) \Phi_0^*(u) du}{\int \sigma_c^n(u) \Phi_0(u) \Phi_0^*(u) du}$$

Здесь, также как и при выводе (16), приближенно считалось, что  $\bar{\beta}^*(z)$  меняется линейно между  $\bar{\beta}_H^*(z=1)$  и  $\bar{\beta}_K^*(z \ll 1)$ .

Для определения оптимальных условий гетерогенного размещения поглотителя проанализируем зависимость относительной реактивности, которая освобождается в результате выгорания поглотителя  $[\varrho_r(0) - \varrho_n(y)]/\varrho_{r,\text{шл}}^0$  и реактивности, расходующейся на компенсацию процессов выгорания горючего и зашлаковывания

$$\varrho_{r,\text{шл}}(y)/\varrho_{r,\text{шл}}^0$$

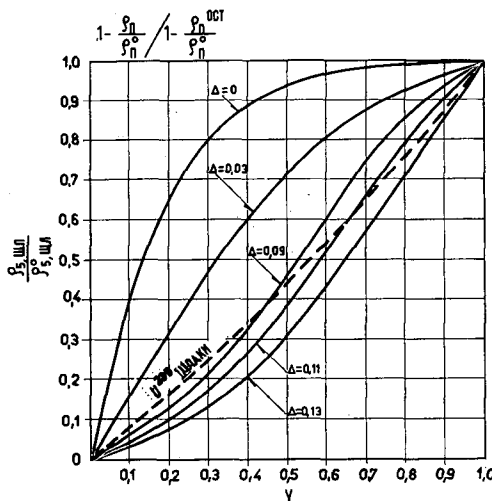


Рис. 3  
Зависимость  $\frac{\varrho_n(0) - \varrho_n(y)}{\varrho_{r,\text{шл}}^0}$  и  $\frac{\varrho_{r,\text{шл}}(y)}{y}$

Здесь  $\varrho_{r, \text{шл}}^0$  — начальный запас реактивности на выгорание горючего и зашлаковывание

$$\varrho_{r, \text{шл}}^0 = \varrho_{r, \text{шл}}(y) \text{ при } y = 1.$$

Так как в конце кампании должно выполняться условие

$$\varrho_n(0) - \varrho_n^{\text{oct}} = \varrho_{r, \text{шл}}^0$$

где  $\varrho_n^{\text{oct}} = \varrho_n(1)$  — остаточная реактивность от невыгоревшего к концу кампании поглотителя, то

$$\frac{\varrho_n(0) - \varrho_n(y)}{\varrho_{r, \text{шл}}^0} = \frac{1 - \frac{\varrho_n(y)}{\varrho_n(0)}}{1 - \frac{\varrho_n^{\text{oct}}}{\varrho_n(0)}}$$

Эта зависимость представлена сплошными кривыми на рис. 3 для поглотителя из кадмиевых пластинок различной толщины (толщина указана в мм).  $\varrho_n(y)/\varrho_n(0)$  рассчитывалось из уравнения (21) с использованием уравнения (16) для реактора с  $\xi \Sigma_r / N_r = 500$  барн.

Зависимость

$$\frac{\varrho_{r, \text{шл}}(y)}{\varrho_{r, \text{шл}}^0} = \frac{y [1 - (1/x_r)]}{1 - (y/x_r)}$$

(вывод этого выражения приведен в следующем параграфе) представлена на рис. 3 штриховой кривой.

Обозначим через

$$m = \frac{\varrho_n(0) - \varrho_n^{\text{oct}}}{\varrho_{r, \text{шл}}^0}$$

отношение реактивности, освобождающейся к концу кампании выгорающим поглотителем, к начальному запасу реактивности на выгорание и зашлаковывание.

Как видно из рис. 3, кривые освобождающейся реактивности (построенные для  $m=1$ ) в общем случае пересекают кривую реактивности, расходящейся на компенсацию выгорания и зашлаковывания, образуя сначала область отрицательного, а затем положительного разбалансов реактивности. Из дальнейшего будет ясно, что случаи очень слабой гетерогенности (область отрицательного разбаланса при  $m=1$  отсутствует) и очень сильной (область положительного разбаланса при  $m=1$  отсутствует) не представляют практического интереса.

Наличие области отрицательного разбаланса реактивности указывает на то, что при использовании поглотителя, расположенного гетерогенно, реализовать условие  $m=1$  невозможно, так как в этом случае цепная реакция прекратится вскоре после пуска реактора.

Поэтому в начале кампании при использовании гетерогенного поглотителя часть начального запаса реактивности на выгорание и зашлаковывание ( $1-m$ ) должна быть скомпенсирована подвижными органами регулирования для прохождения области отрицательного разбаланса.

Наличие положительного разбаланса реактивности в свою очередь требует для его компенсации размещения дополнительного количества под-

важных органов регулирования (или увеличения их компенсационной способности), так как в противном случае реактор выйдет из-под контроля.

Следовательно, общая компенсационная способность подвижных органов регулирования, требующихся в начале кампании для компенсации разбаланса реактивности от несоответствия законов выгорания горючего и поглотителя, должна составлять (в долях начального запаса реактивности на выгорание и зашлаковывание):

$$\text{где } \left( \frac{\varrho_p}{\varrho_{r, \text{шл}}} \right)_{\max}^+ + \left( \frac{\varrho_p}{\varrho_{r, \text{шл}}} \right)_{\max}^-,$$

где  $(\varrho_p / \varrho_{r, \text{шл}})_{\max}^+$  и  $(\varrho_p / \varrho_{r, \text{шл}})_{\max}^-$  — соответственно максимальные значения положительного и отрицательного разбалансов реактивности. Относительный разбаланс реактивности определяется соотношением:

$$\frac{\varrho_p(y)}{\varrho_{r, \text{шл}}(0)} = \frac{1 - [\varrho_n(y) / \varrho_n(0)]}{1 - [\varrho_n^{\text{ост}} / \varrho_n(0)]} m - \frac{\varrho_{r, \text{шл}}(y)}{\varrho_{r, \text{шл}}^0} \quad (22)$$

Так как одной из целей применения выгорающих поглотителей является сокращение числа регулирующих органов, необходимо установить условия, при которых количество подвижных органов регулирования, необходимое для нормальной работы реактора, является минимальным.

Выше было показано, что для обеспечения компенсации отрицательного разбаланса реактивности величина  $m$  должна быть меньше единицы. Следовательно кривая освобождающейся от выгорания поглотителя реактивности при  $m < 1$  пойдет ниже исходной кривой ( $m = 1$ ). При этом очевидно значение максимального отрицательного разбаланса возрастет, а положительного уменьшится.

Можно показать (см. приложение), что при этом сумма максимальных положительного и отрицательного разбалансов, а, следовательно, и необходимое количество органов регулирования, будет уменьшаться.

При уменьшении  $m$  наступит такой момент, когда область положительного разбаланса будет вовсе отсутствовать, а кривая освобождающейся реактивности будет касаться кривой расходящейся реактивности только в одной точке. Каждому значению толщины поглотителя соответствует своя величина  $m_k$ , при которой осуществляется касание кривых. Этому значению  $m = m_k$  соответствует минимальная величина суммы положительного и отрицательного максимальных разбалансов реактивности. Очевидно дальнейшее уменьшение  $m$  нецелесообразно.

Точка касания кривых  $y = y_k$  определяется условием:

$$\frac{d}{dy} \ln \left[ \frac{\varrho_{r, \text{шл}}(y)}{\varrho_{r, \text{шл}}^0} \right]_{y=y_k} = \frac{d}{dy} \ln \left[ 1 - \frac{\varrho_n(y)}{\varrho_n(0)} \right]_{y=y_k}$$

а величина  $m_k$ , обеспечивающая касание кривых, удовлетворяет соотношению:

$$m_k = \frac{\varrho_{r, \text{шл}}(y_k) / \varrho_{r, \text{шл}}^0}{1 - [\varrho_n(y_k) / \varrho_n(0)]} \left( 1 - \frac{\varrho_n^{\text{ост}}}{\varrho_n(0)} \right) \quad (23)$$

На рис. 4 представлены кривые освобождающейся реактивности, построенные при  $m = m_k$ .

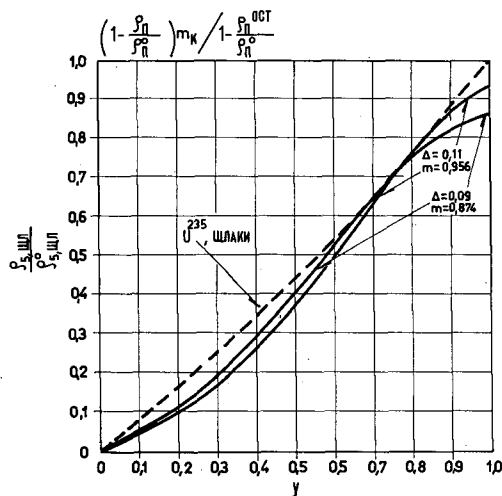


Рис. 4  
Зависимость  $\frac{\varrho_{\text{п}}(0) - \varrho_{\text{п}}(y)}{\varrho_{\text{г, шл}}^0}$  и  $\frac{\varrho_{\text{г}}(y)}{\varrho_{\text{г, шл}}^0}$  при  $m = m_k$

При касании кривых освобождающейся реактивности с кривой расходующейся реактивности могут представаться три случая

- 1)  $1 - m_k > (\varrho_{\text{п}}/\varrho_{\text{г, шл}}^0)_{\text{макс}}$
- 2)  $1 - m_k < (\varrho_{\text{п}}/\varrho_{\text{г, шл}}^0)_{\text{макс}}$
- 3)  $1 - m_k = (\varrho_{\text{п}}/\varrho_{\text{г, шл}}^0)_{\text{макс}}$

Нетрудно видеть, что первый случай не является оптимальным, так как запас реактивности, скомпенсированный органами регулирования в начале кампании, используется не полностью для компенсации максимального отрицательного разбаланса реактивности. Второй случай является нереализуемым, т.к. запас реактивности, скомпенсированный органами регулирования в начале кампании, недостаточен для прохождения максимального отрицательного разбаланса.

Следовательно, оптимальная величина  $m_k$  должна удовлетворять условию:

$$1 - m_k^{\text{опт}} = (\varrho_{\text{п}}/\varrho_{\text{г, шл}}^0)_{\text{макс}}$$

Толщина поглотителя, которой соответствует такая кривая освобождающейся реактивности, является оптимальной толщиной для данного поглотителя в данном реакторе.

Кривые разбаланса реактивности от несоответствия законов выгорания горючего и поглотителя для различных толщин пластинок поглотителя представлены на рис. 5.

Для рассмотренного случая оптимальной является толщина поглотителя  $(Cd)\Delta_{\text{опт}} \approx 0,1$  мм, а необходимая компенсирующая способность подвижных

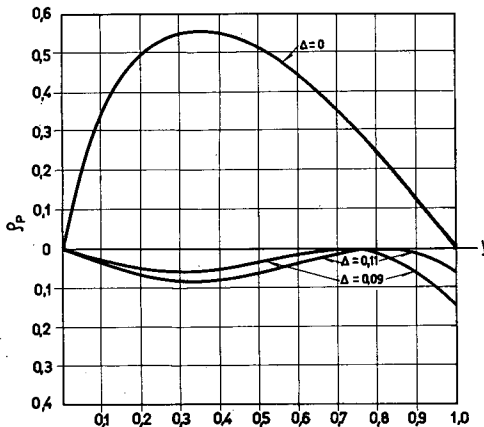


Рис. 5  
Кривые разбаланса реактивности.

органов регулирования составляет  $(1 - m_k^{\text{опт}}) \approx 0,1$ , т.е. 10 % от начального запаса реактивности на выгорание горючего и защлаковывание.

Относительная величина реактивности, компенсируемая выгорающим поглотителем в начале кампании, для оптимального случая равна

$$\frac{\rho_n(0)}{\rho_{\text{г, шл}}} = \frac{m_k^{\text{опт}}}{1 - [\rho_n^{\text{ост}}(0)]}$$

Дополнительное количество горючего, которое необходимо ввести в реактор для компенсации потери реактивности от невыгоревшего к концу кампании поглотителя, определяется величиной потери реактивности:

$$\frac{\rho_n^{\text{ост}}}{\rho_{\text{г, шл}}} = m_k^{\text{опт}} \frac{\rho_n^{\text{ост}}/\rho_n(0)}{1 - [\rho_n^{\text{ост}}/\rho_n(0)]}$$

Для рассмотренного примера в оптимальном случае  $\rho_n^{\text{ост}}/\rho_{\text{г, шл}} = 0,02$ .

Из рис. 5 видно, что гетерогенное размещение поглотителя оказывается значительно более эффективным, чем гомогенное размещение (кривая  $\Delta=0$ ), если для данного реактора можно подобрать быстровыгорающий поглотитель ( $x_n^{\text{гом}} \ll 1$ ). В противном случае, если для рассматриваемого реактора удается подобрать поглотитель лишь с  $x_n^{\text{гом}} \gtrsim 1$ , его гетерогенное размещение приведет к очень большим потерям реактивности от невыгоревшего к концу кампании поглотителя.

## 5. Гомогенное расположение поглотителя

Если поглотитель и горючее расположены гомогенно, т.е. при условии  $f_n(\mathbf{r}, u, t) = f_g(\mathbf{r}, u, t) = 1$ , то, решая совместно уравнения (1) и (6), получим:\*

\* Тот же самый результат получается в случае, если поглотитель и горючее расположены гетерогенно, но факторы самоэкранирования  $f_g$  и  $f_n$  считаются независящими от времени (что приближенно справедливо для небольших отрезков кампаний).

$$\frac{N_{\text{n}}(\mathbf{r}, t)}{N_{\text{n}}(\mathbf{r}, 0)} = \left( \frac{N_{\text{r}}(\mathbf{r}, t)}{N_{\text{r}}(\mathbf{r}, 0)} \right)^{\omega(\mathbf{r})} \frac{D_{\text{n}}(\mathbf{r}, t)}{D_{\text{r}}(\mathbf{r}, t)} \quad (24)$$

где

$$\omega(\mathbf{r}) = \lambda_{\text{n}}^0(\mathbf{r}) / \lambda_{\text{r}}^0(\mathbf{r})$$

$$D_{\text{i}} = \frac{\int \sigma_{\text{i}}(u) \Phi_0(\mathbf{r}, u) du \int_0^t [\Phi(\mathbf{r}, u, t) / \Phi(\mathbf{r}, u)] t dt}{\int \sigma_{\text{i}}(u) \Phi_0(\mathbf{r}, u) du}$$

Приближенно будем считать, что  $D_{\text{n}}(\mathbf{r}, t)/D_{\text{n}}(\mathbf{r}, 0) = 1$ . В некоторых практических важных случаях такое предположение является совершенно строгим: например, если сечения захвата горючего и поглотителя имеют одинаковую энергетическую зависимость, или если реактор является тепловым.

С учетом этого предположения, используя выражение (8), получим (24) в виде:

$$\frac{N_{\text{n}}(\mathbf{r}, t)}{N_{\text{n}}(\mathbf{r}, 0)} = (1 - \lambda_{\text{r}}^{0, c}(\mathbf{r}))^{\omega(\mathbf{r})} \quad (25)$$

Если выгорающий поглотитель расположен гомогенно, а горючее гетерогенно, то в предположении о неизменности спектра нейтронов из уравнения (10) получим:\*

$$\frac{N_{\text{n}}(\mathbf{r}, t)}{N_{\text{n}}(\mathbf{r}, 0)} = (1 - Ct)^{\lambda_{\text{n}}^0(\mathbf{r})/c} \quad (26)$$

Заметим, что выражение (26) не переходит точно в (25), если в коэффициенте  $C = B + \langle \lambda_{\text{r}}^{0, c} \rangle_{\text{av}}$  положить  $B=0$  (что соответствует гомогенному распределению горючего). Это является следствием того, что при получении (26) пренебрегалось изменением спектра нейтронов в течение кампании, в то время как при получении выражения (25) использовалось менее сильное предположение  $(D_{\text{n}}(\mathbf{r}, t)/D_{\text{r}}(\mathbf{r}, t)=1)$ .

Используя выражение (20) в предположении о независимости спектра и ценности нейтронов в реакторе от времени, найдем относительное изменение во времени реактивности, вносимой в реактор поглотителем.

$$\frac{\varrho_{\text{n}}(t)}{\varrho_{\text{n}}(0)} = S(t) \frac{\langle N_{\text{n}}(t) \rangle_{\text{av}}^*}{\langle N_{\text{n}}(0) \rangle_{\text{av}}^*} \quad (27)$$

или в безразмерных параметрах

$$\frac{\varrho_{\text{n}}(y)}{\varrho_{\text{n}}(0)} = \left( 1 - \frac{y}{\chi_{\text{r}}} \right)^{\tilde{\omega}} - 1 \quad (28)$$

\* Аналогичным образом из уравнения (10) может быть получено выражение, справедливое для случая, когда поглотитель размещен непосредственно в горючем, и фактор самоэкранирования поглотителя можно положить равным фактору самоэкранирования горючего. Обычно такое предположение оправдано, так как макроскопическое сечение поглотителя, добавленного в горючее, значительно меньше макроскопического сечения горючего. В этом случае выгорающее поглотителя описывается формулой:

$$\frac{N_{\text{n}}(\mathbf{r}, t)}{N_{\text{n}}(\mathbf{r}, 0)} = (1 - Ct) \frac{\lambda_{\text{r}}^0(\mathbf{r})}{c} \left[ 1 + \frac{\lambda_{\text{r}}^0(\mathbf{r})}{c} \bar{A}_{\text{n}}(\mathbf{r}) \right] \cdot e^{\lambda_{\text{r}}^0(\mathbf{r}) \bar{A}_{\text{n}}(\mathbf{r})},$$

где

$$\bar{A}_{\text{n}}(\mathbf{r}) = \frac{\int A(\mathbf{r}, u) f_{\text{r}}^0(\mathbf{r}, u) \sigma_{\text{c}\text{n}}(u) \Phi_0(\mathbf{r}, u) du}{\int f_{\text{r}}^0(\mathbf{r}, u) \sigma_{\text{c}\text{n}}(u) \Phi_0(\mathbf{r}, u) du}$$

Для определения величины разбаланса реактивности от несоответствия законов выгорания поглотителя и горючего найдем, используя теорию возмущений, зависимость изменения реактивности, израсходованной на компенсацию выгорания горючего и зашлаковывания:

$$\varrho_{\text{ршл}}(t) = \frac{S(t)}{\Pi. \text{Н. д.}} \int [N_r(r, 0) - N_r(r, t)] \lambda_{r, \text{шл}}^*(r) dv$$

Здесь:

$$\lambda_{r, \text{шл}}^*(r) = \int \left[ [\sigma_{\text{шл}}^c - \sigma_r^c + D_f \sigma_s f \frac{\Phi^*(r, 0)}{\Phi^*(r, u)}] \Phi_0(r, u) \Phi_0^*(r, u) du \right]$$

$\Phi_0^*(r, u)$  — ценность одного нейтрона деления,

$\sigma_{\text{шл}}^c$  — сечение поглощения шлаков (вместе с U-236), нормированное на одно выгоревшее ядро горючего.

Относительное изменение реактивности, расходующейся на компенсацию процессов выгорания горючего и зашлаковывания, можно представить тогда в виде:

$$\frac{\varrho_{r, \text{шл}}(t)}{\varrho_{r, \text{шл}}^0} = \frac{S(t)}{S(T)} \cdot \frac{1 - \frac{\langle N_r(t) \rangle_{\text{av}}^*}{\langle N_r(0) \rangle_{\text{ав}}^*}}{1 - \frac{\langle N_r(T) \rangle_{\text{ав}}^*}{\langle N_r(0) \rangle_{\text{ав}}^*}} \quad (30)$$

где  $\varrho$  — начальный запас реактивности на выгорание горючего и зашлаковывание,

$$\langle N_r(t) \rangle_{\text{ав}}^* = \frac{\int N_r(r, t) \lambda_{r, \text{шл}}^*(r) dv}{\int \lambda_{r, \text{шл}}^*(r) dv}$$

Усредненное соотношение (8) с весом  $\varrho_{r, \text{шл}}^*(r)$ , найдем что

$$\frac{\langle N_r(t) \rangle_{\text{ав}}^*}{\langle N_r(0) \rangle_{\text{ав}}^*} = 1 - \langle \lambda_{r, 0,c} \rangle_{\text{ав}}^* \quad (31)$$

$$\langle \lambda_{r, 0,c} \rangle_{\text{ав}}^* = \frac{\int \lambda_{r, 0,c}(r) \lambda_{r, \text{шл}}^*(r) dv}{\int \lambda_{r, \text{шл}}^*(r) dv}$$

При усреднении использовалось приближенное соотношение:

$$\langle N_r(0) \lambda_{r, 0,c} \rangle_{\text{ав}}^* = \langle N_r(0) \rangle_{\text{ав}}^* \cdot \langle \lambda_{r, 0,c} \rangle_{\text{ав}}^*$$

Теперь, имея в виду (31) и (9), можно записать зависимость (30) как явную функцию времени:

$$\frac{\varphi_{r, \text{шл}}(t)}{\varphi_{r, \text{шл}}^0} = \frac{1 - C T}{1 - C t} \cdot \frac{t}{T}$$

или в безразмерных параметрах

$$\frac{\varrho_{r, \text{шл}}(y)}{\varrho_{r, \text{шл}}^0} = \frac{y \left( 1 - \frac{1}{x_r} \right)}{1 - (y/x_r)} \quad (32)$$

Величину относительного разбаланса реактивности, определенную соотношением (22), учитывая (29) и (32), можно представить в следующем виде (при  $m=1$ ):

$$\frac{\varrho_p(y)}{\varrho_{r, \text{шл}}^0} = \frac{1 - \left(1 - \frac{y}{x_r}\right)^{\tilde{\omega}-1}}{1 - \left(1 - \frac{1}{x_r}\right)^{\tilde{\omega}-1}} - \frac{y \left(1 - \frac{1}{x_r}\right)}{1 - (y/x_r)} \quad (33)$$

Время максимального разбаланса реактивности находим из условия:

$$\frac{d}{dy} \left( \frac{\varrho_p(y)}{\varrho_{r, \text{шл}}^0} \right)_{y=y_{\max}} = 0$$

$$\text{где } \langle N_n(t) \rangle_{av}^* = \frac{\int N_n(r, t) \lambda_n^*(r) dv}{\int \lambda_n^*(r) dv}$$

$$\lambda_n^*(r) = \int \sigma_c^u(u) \Phi_0(r, u) \Phi_0^*(r, u) du$$

Для определения зависимости  $\langle N_n(t) \rangle_{av}^*/\langle N_n(0) \rangle_{av}^*$  усредним с весом  $\lambda_n^*(r)$  уравнение (10), имея в виду, что  $f_n = 1$ .

Тогда получим:

$$\frac{d \langle N_n(t) \rangle_{av}^*}{dt} = -\frac{1}{1 - Ct} \langle \lambda_n N_n(t) \rangle_{av}^* \quad (28)$$

Будем приближенно считать, что

$$\langle \lambda_n \cdot N_n(t) \rangle_{av}^* \approx \langle \lambda_n \rangle_{av}^* \langle N_n(t) \rangle_{av}^*$$

где

$$\langle \lambda_n \rangle_{av}^* = \frac{\int \lambda_n(r) \lambda_n^*(r) dv}{\int \lambda_n^*(r) dv}$$

Теперь, интегрируя (28), получим:

$$\frac{\langle N_n(t) \rangle_{av}^*}{\langle N_n(0) \rangle_{av}^*} = (1 - Ct)^{\tilde{\omega}}$$

где

$$\tilde{\omega} = \langle \lambda_n \rangle_{av}^* / C$$

Подставляя это выражение в (27) и используя (9), найдем, что

$$\begin{aligned} \varrho_p(y)/\varrho_p(0) &= (1 - Ct)^{\tilde{\omega}-1} \\ y_m &= x_r \left\{ 1 - \left( \frac{x_r - 1}{\tilde{\omega} - 1} \right)^{1/\tilde{\omega}} \left[ 1 - \left( 1 - \frac{1}{x_r} \right)^{\tilde{\omega}-1} \right]^{1/\tilde{\omega}} \right\} \end{aligned} \quad (34)$$

Подставляя (34) и (33), можно найти величину максимального разбаланса реактивности в течение кампании от несоответствия законов выгорания горючего и поглотителя.

Выражение для потери реактивности от невыгоревшего к концу кампании поглотителя в долях начального запаса реактивности на выгорание и зашлакование получим из (29)

$$\frac{\varrho_{\text{ост}}}{\varrho_{r, \text{шл}}^0} = \frac{[1 - (1/x_r)]^{\tilde{\omega}-1}}{1 - [1 - (1/x_r)]^{\tilde{\omega}-1}} \quad (35)$$

При этом считалось, что  $\varrho_p(0) = \varrho_{\text{ост}} = \varrho_{r, \text{шл}}^0$

В случае очень малого выгорания горючего за кампанию, т.е.  $x_r \gg 1$ , вместо соотношений (33), (34), (35) будем иметь:

$$\varrho_p(y) = \frac{1 - e^{-y/x_n}}{1 - e^{-1/x_n}} - y,$$

$$y_m = -x_n \ln x_n (1 - e^{-1/x_n})$$

$$\varrho_{\text{ост}}/\varrho_{r, \text{шл}}^0 = \frac{e^{-1/x_n}}{1 - e^{-1/x_n}}$$

Здесь

$$x_n = 1/\langle \lambda_n \rangle_{\text{av}}^* \cdot T$$

На рис. 6 представлены зависимости  $[\varrho_p(y)/\varrho_{r, \text{шл}}^0]_y = y_m$ ,  $y_m$  и  $\varrho_{\text{ост}}/\varrho_{r, \text{шл}}^0$  как функции  $x_r$  и  $x_n$ .

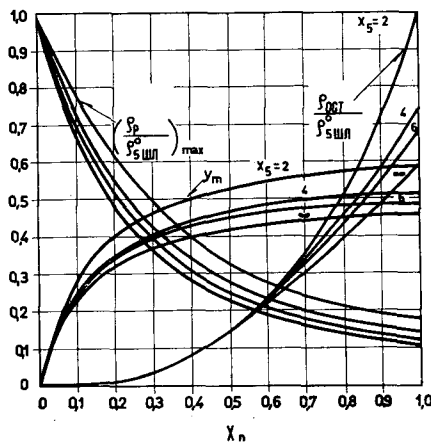


Рис. 6  
Зависимость  $\varrho_p(y_m)/\varrho_{r, \text{шл}}^0$ ,  $y_m$  и  $\varrho_{\text{ост}}/\varrho_{r, \text{шл}}^0$  в случае гомогенного размещения поглотителя.

Из рис. 6 видно, что в случае гомогенного расположения поглотителя требование минимального разбаланса реактивности приводит к большому значению остаточной реактивности, а следовательно и к большой дополнительной загрузке горючего для ее компенсации.

Наборот, при малых значениях остаточной реактивности получается большой разбаланс, а следовательно уменьшаются преимущества от применения выгорающего поглотителя. Оптимальные характеристики выгорающего поглотителя выбираются поэтому путем компромисса.

Следует заметить, что применение смеси двух различных гомогенных поглотителей может дать более оптимальные характеристики выгорания, чем каждый из поглотителей в отдельности. Может также оказаться полезным для уменьшения величины остаточной реактивности скомпенсировать часть начального запаса реактивности на выгорание горючего и зашлаковывание подвижными органами регулирования (при этом  $m < 1$ ). Соответствующие выражения для этих случаев легко могут быть получены аналогичным образом.

## 6. Учет влияния изменения спектра нейтронов в течение кампании на процесс выгорания поглотителя при гомогенном размещении поглотителя и горючего

Спектр нейтронов в реакторе в общем случае можно представить в виде

$$\Phi(\mathbf{r}, u, t) = \Phi_0(\mathbf{r}, u) e^{F(\mathbf{r}, u, t)} \quad (36)$$

где  $F(\mathbf{r}, u, t)$  — функция, учитывающая изменение спектра нейтронов в реакторе в течение кампании, обусловленное изменением изотопного состава и перемещением регулирующих органов, компенсирующих разбаланс реактивности.

В возрастном приближении для реактора без отражателя в предположении, что выгорание горючего и поглотителя происходит равномерно по объему реактора, функция  $F(u, t)$  имеет вид:

$$F(u, t) = \int_0^u \frac{1}{\xi \Sigma_r} [(N_r(0) - N_r(t)) (\sigma_c^r - \sigma_c^{cpl}) + (N_n(0) - N_n(t)) \sigma_c^n] du - \delta \chi^2(t) \tau(u). \quad (37)$$

Здесь

$\delta \chi^2(t)$  — изменение геометрического параметра реактора, связанное с перемещением регулирующих органов, компенсирующих разбаланс реактивности,

$\tau(u)$  — возраст нейтронов,

$$\sigma_c^{shp} = \frac{\bar{\alpha}}{1 + \bar{\alpha}} \sigma_c^{236} + \frac{1}{1 + \bar{\alpha}} \sigma_c^{osc}$$

$$\bar{\alpha} = \int \Phi_0 \sigma_\gamma^r du / \int \Phi_0 \sigma_f^r du.$$

Рассмотрение для простоты проводится без учета спектра деления, т.е. предполагается  $\chi(u) = \delta(u)$

Кроме того, вместо введения отдельной группы тепловых нейтронов замедление распространяется до  $u=\infty$ , причем сечения в области  $u_{rp} \div \infty$  считаются постоянными и равными усредненным сечениям в этой области.

В дальнейшем будем считать, что  $F(u, t) < 0.2$ . Если это условие не выполняется, то кампанию можно разбить на несколько участков так, чтобы на каждом из них это неравенство удовлетворялось.

Тогда можно  $e^{F(u,t)}$  разложить в ряд и ограничиться линейной частью:  $e^F = 1 + F$ . Из условия сохранения мощности реактора

$$N_r(0) \int \sigma_f \Phi_0 du = N_r(t) \int \sigma_f \Phi_0 [1 + F(u, t)] du,$$

используя соотношение (8) и выражение для  $F(u, t)$  (37), можно получить уравнение, связывающее  $N_n(t)/N_n(0)$  и  $\delta \chi^2(t)$ :

$$\frac{N_n(\eta)}{N_n(0)} = 1 - \delta \chi^\sigma(\eta) \frac{\bar{\tau}_f}{\alpha_n f} - \frac{\eta}{\alpha_n f (1 - \eta)} \cdot [1 - (\alpha_f^r - \alpha_{shp}^r) (1 - \eta)], \quad (38)$$

где  $\eta = \lambda_c^r t$

$$\tau_k = \int \tau(u) \sigma_k \Phi_0 du / \int \sigma_k \Phi_0 du,$$

$$A_i^K = \int \sigma_k \Phi_0 du \int_0^u \frac{\Sigma_c^i}{\xi \Sigma_s} du / \sigma_K \Phi_0 du,$$

$$\Sigma_c^i = \sigma_c^i N_i(0),$$

Второе уравнение, связывающее  $N_n t)/N_n(0)$  и  $\delta \chi^2(t)$  получается из уравнения (1) с учетом соотношений (36), (37) и сделанных выше упрощающих предположений:

$$\frac{d}{d\eta} \left[ \frac{N_n(\eta)}{N_n(0)} \right] = -\omega_{rom} \frac{N_n(\eta)}{N_n(0)} \left[ 1 - \delta \chi^2(\eta) \tau_n + \eta (a_n^r - a_n^n) \right. \\ \left. + \left( 1 - \frac{N_n(\eta)}{N_n(0)} \right) a_n^n \right] \quad (39)$$

Вводя обозначения:

$$\psi(\eta) = \omega_{rom} \left( K + \eta L + \frac{\eta}{1-\eta} M \right),$$

где

$$K = 1 - a_n^f \frac{\bar{\tau}_n}{\bar{\tau}_f} + a_n^n \\ L = a_n^n - a_{nl}^n - (a_n^f - a_{nl}^f) \frac{\bar{\tau}_n}{\bar{\tau}_f} \\ M = \frac{\bar{\tau}_n}{\bar{\tau}_f}$$

и, подставляя в (39) выражение для  $\delta \chi^2(\eta)$  из (38), получим:

$$\frac{1}{z^2} \frac{dz}{d\eta} + \frac{\psi(\eta)}{z} = -\Delta \quad (40)$$

где

$$z = N_n / N_n^0; \quad \Delta = \omega_{rom} \left( \frac{\bar{\tau}_n}{\bar{\tau}_f} a_n^f - a_n^n \right)$$

Уравнение (40) является уравнением Бернулли. Его решение имеет вид:

$$\frac{N_n(\eta)}{N_n(0)} = \frac{e^{-\psi(\eta)}}{1 + \int_0^\eta e^{-\psi(\eta')} d\eta'} \quad (41)$$

где

$$\psi(\eta) = \int_0^\eta \psi'(\eta') d\eta' = \omega_{rom} \left\{ \eta K + \frac{\eta^2}{2} L - [\eta + \ln(1-\eta)] M \right\}$$

Так как на практике  $\eta_{max}$  обычно меньше 0,25, то в разложении

$$\ln(1-\eta) = -\eta - \frac{\eta^2}{2} - \dots$$

можно ограничиться первыми двумя членами. В этом случае

$$\int_0^\eta e^{-\psi(\eta')} d\eta' = \begin{cases} \frac{\sqrt{\pi}}{2\sqrt{P}} e^{pq^2} \left\{ \operatorname{erf} \left[ (q+\eta)\sqrt{P} \right] - \operatorname{erf}(q\sqrt{P}) \right\} & \text{если } P > 0, \\ \frac{e^{-|P|q}}{\sqrt{|P|}} \left\{ \int_0^q e^{t^2} dt - \int_0^q e^{t^2} dt \right\} & \text{если } P < 0 \end{cases}$$

Здесь  $q = K/(L + M)$

$$P = \frac{\omega_{\text{том}}}{2} (L + M), \quad \text{erf}(x) = \frac{2}{\sqrt{\pi}} \int_0^x e^{-t^2} dt$$

Выражение (41) представляет собой закон выгорания поглотителя с учетом изменения спектра нейтронов на протяжении кампании в возрастном приближении. Зная  $N_p(\eta)$   $N_p(0)$  можно из уравнения (38) определить  $\delta\chi^2(\eta)$  и рассчитать временную зависимость разбаланса реактивности от несоответствия законов выгорания горючего и поглотителя, которая связана с  $\delta\chi^2$  следующим соотношением:

$$\varrho_P(t) = \frac{\delta\chi^2(t)}{\text{П.Н.Д.}} \int \int D \Phi_0(r, u) \Phi_0^*(r, u) du dv,$$

где — коэффициент диффузии нейтронов.

Из условия сохранения критичности реактора в течение кампании

$$N_r(t) \int \sigma_f(u) \Phi_0(u) [1 + F(u, t)] du = \text{const.}$$

следует, что  $\int F(u, t) du < 0$ , то есть спектр нейтронов в реакторе в течение кампании смягчается. Это приводит к увеличению скорости выгорания поглотителя с течением времени, а следовательно к уменьшению потери реактивности от невыгоревшего к концу кампании поглотителя, по сравнению с величиной потери реактивности, даваемой формулой (35), не учитывающей изменение спектра нейтронов в течение кампании.

В заключение авторы благодарят А. И. Лейпунского, Г. И. Марчука, Л. Н. Усачева за интерес к работе и обсуждение полученных результатов.

Авторы также благодарят В. Н. Петрова, принимавшего участие в начальной стадии работы.

## ПРИЛОЖЕНИЕ

### Зависимость величин разбаланса реактивности от $m$

Пусть  $y'$  и  $y''$  (см. рис. 7) моменты времени (волях кампании), при которых имеют место соответственно максимальный отрицательный и положительный разбалансы для случая  $m=1$  (кривая II).

$$\begin{aligned} \text{Тогда } & \left( \frac{\varrho_p}{\varrho_{\text{р, шл}}} \right)^{-}_{\max} = A - a = \alpha \\ \text{и } & \left( \frac{\varrho_p}{\varrho_{\text{р, шл}}} \right)^{+}_{\max} = b - B = \beta \end{aligned}$$

При  $m < 1$  кривая II перейдет в кривую III. Пусть теперь значения максимального отрицательного и максимального положительного разбалансов будут достигаться в точках  $y'(m)$  и  $y''(m)^*$

\* Можно показать, что при уменьшении  $m$  должны выполняться неравенства:

$$y'(m) > y' \text{ и } y''(m) < y'' \quad (\text{a})$$

Это следует из того, что в точках экстремума разбаланса

$$\frac{d}{dy} \left[ \frac{\varrho_{\text{р, шл}}(y)}{\varrho_{\text{р, шл}}(0)} \right] = m \cdot \frac{d}{dy} \left[ \frac{1 - \frac{\varrho_{\text{п}}(y)}{\varrho_{\text{п}}(0)}}{1 - \frac{\varrho_{\text{п ост}}}{\varrho_{\text{п}}(0)}} \right] \quad (6)$$

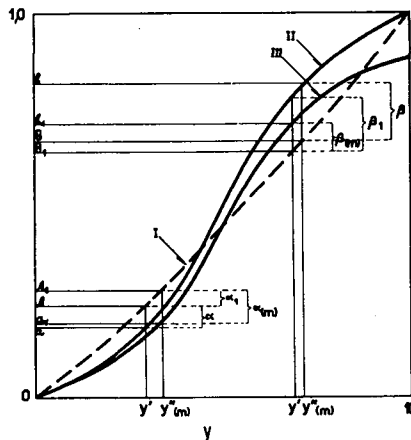


Рис. 7

Зависимость величины разбаланса реактивности от  $m$ ,  
где  $m = (\varrho_n(0) - \varrho_n^{oct}) / \varrho_{r, \text{шл}}^0$

Из формы кривой освобождающейся реактивности видно, что для удовлетворения соотношения (б) при уменьшении  $m$  требуется выполнение неравенств (а).

Тогда новые значения максимального отрицательного и положительного разбалансов запишутся следующим образом:

$$\alpha(m) = A_1 - a_1 m$$

$$\beta(m) = b_1 m - B_1$$

Требуется показать, что  $\alpha + \beta > \alpha(m) + \beta(m)$   
 $\alpha(m)$  и  $\beta(m)$  можно переписать в виде:

$$\alpha(m) = \alpha_1 + a_1(1 - m)$$

$$\beta(m) = \beta_1 - b_1(1 - m)$$

Следовательно:

$$(\alpha - \alpha_1) + (\beta - \beta_1) + (1 - m)(b_1 - a_1) > 0$$

Это неравенство является очевидным, так как все члены левой части положительны.

Таким образом, действительно, сумма максимального отрицательного и положительного разбалансов будет уменьшаться с уменьшением  $m$ .

## ЛИТЕРАТУРА

- [1] RADKOWSKY, A., Theory and Application of Burnable Poisons.  
(Доклад № 1900 на Международной конференции по мирному использованию атомной энергии, 1958 г.)
- [2] SMITH, A. M. and JEFFREY, J., Burnable Poisons in Small Power Reactors.  
(Доклад № 86 на Международной конференции по мирному использованию атомной энергии, 1958 г.)
- [3] The Physics of Intermediate Spectrum Reactors. USAEC. 1858 г.
- [4] Усачев, Л. Н., „Уравнение для ценности нейтронов, кинетика реактора и теория возмущений.“ Сб. „Реакторостроение и теория реакторов“ (1955).
- [5] МАРЧУК, Г. И., „Численные методы расчета реакторов.“ Атомиздат, 1958 г.



### **III. 4. LONG-TERM EFFECTS**



# LONG-TIME BEHAVIOUR OF FAST BREEDERS

K. OTT AND A. JANSEN

KERNFORSCHUNGSZENTRUM, KARLSRUHE,  
FEDERAL REPUBLIC OF GERMANY

**Abstract — Résumé — Аннотация — Resumen**

**Long-time behaviour of fast breeders.** For studying the long-time behaviour of fast breeders, a suitable O-dimensional model of fissile (plutonium), fertile ( $U^{238}$ ) and absorbing material (structural material and coolant) is investigated. Charging, discharging and re-charging of fissile and fertile material are idealized as continuous processes. Criticality requires continuous discharge of each specific Pu-composition. The time behaviour of the isotope composition is described by a first-order-differential-equation system whose solution was determined numerically for different initial conditions. Calculating the stationary isotope composition (stationary after a long time) leads to an eigenvalue problem with the plutonium current to be discharged as eigenvalue and the Pu-isotope concentrations as eigenvector components. Generally, this eigenvalue problem has but one physically reasonable solution with the so-called  $Pu^\infty$  as eigenvector. The eigenvalue determines the breeding rate. The principal structure of fuel recycling is investigated.

**Comportement à long terme des réacteurs surgénérateurs à neutrons rapides.** Pour étudier le comportement à long terme des réacteurs surgénérateurs à neutrons rapides, les auteurs ont considéré un modèle ponctuel approprié composé de matières fissile (plutonium), fertile ( $^{238}U$ ) et absorbante (matériau de construction et fluide de refroidissement). Le chargement, le déchargement et le rechargeement des matières fissile et fertile sont idéalisés en opérations continues. L'état critique exige un déchargement continu de chaque composition spécifique de plutonium. Le comportement en fonction du temps de la composition isotopique est décrit par un système d'équations différentielles du premier ordre dont la solution numérique a été faite pour des conditions initiales différentes. Le calcul de la composition isotopique stationnaire (stationnaire après une longue période) conduit à un problème de valeur propre, où le flux de plutonium à décharger est la valeur propre et les concentrations isotopiques de plutonium les composantes du vecteur propre. D'une manière générale, ce problème de valeur propre n'a, du point de vue physique, qu'une seule solution raisonnable où  $Pu^\infty$  est le vecteur propre. La valeur propre détermine le taux de surgénération. Les auteurs examinent la structure principale du retraitement du combustible.

**Временной режим реакторов-размножителей на быстрых нейтронах.** Для изучения временного режима реакторов-размножителей на быстрых нейтронах исследуется подходящая О-размерная модель расщепляющегося (плутоний), производящего (уран-238) и поглощающего материала. Загрузка, разгрузка и перегрузка расщепляющегося и производящего материала идеализированы как непрерывный процесс. Критичность требует непрерывной разгрузки каждого конкретного состава плутония. Поведение изотопного состава описывается с помощью дифференциальной системы уравнений первого порядка, решение которой производится численным методом для различных начальных условий. Подсчет стационарного изотопного состава (стационарность после длительного времени) приводит к проблеме собственного значения, где поток разгружаемого плутония является собственным значением, а концентрация изотопов плутония — компонентами собственного вектора. Обычно эта проблема собственного значения имеет лишь одно физически разумное решение с т.н.  $Pu^\infty$  в качестве собственного вектора. Собственное значение определяет скорость размножения. Исследуется принципиальная структура повторного использования топлива.

**Comportamiento a largo plazo de los reactores reproductores rápidos.** Para estudiar el comportamiento a largo plazo de los reactores reproductores rápidos, los autores consideran un modelo puntual adecuado compuesto por materiales fisionables (plutonio), fértiles ( $^{238}\text{U}$ ), y absorbentes (materiales estructurales y refrigerantes). Se supone que la carga, la descarga y el reemplazo de los materiales fisionables y fértiles se realizan de manera continua. El estado crítico exige la descarga continua del plutonio para cada una de las composiciones isotópicas. La ley de variación de la composición isotópica del plutonio en función del tiempo viene dada por un sistema de ecuaciones diferenciales de primer orden, cuya solución ha sido determinada numéricamente para diferentes condiciones iniciales. El cálculo de la composición isotópica estacionaria (al cabo de un largo período) exige la solución de un problema de valor propio en el que la corriente del plutonio que se ha de descargar constituye el valor propio y las concentraciones de los isótopos del plutonio, los componentes del vector propio. En general, desde el punto de vista físico sólo existe para este problema de valor propio una solución única en que el así llamado  $\text{Pu}^\infty$  representa el vector propio. El valor propio determina el índice de reproducción. Los autores examinan la estructura principal del reciclado del combustible.

## Introduction

Two questions must be answered by investigations on the long-time behaviour of fast-breeder reactors: (a) How does a reactor system behave between two interventions from the outside, i.e. what is the time behaviour of neutron flux, of reactivity, and of the fuel-isotope mixture between two charging events? (b) How does a reactor system behave over long periods of time, taking into account reprocessing and refabricating plants?

When looking into the second question, to which we are going to restrict ourselves here, one is permitted by the type of question to make some simplifications, which make it possible to arrive at general interrelationships. Especially the influence of the principal structure of the fuel cycle between blanket, core, and reprocessing plant is to be investigated.

In general, fuel recycling is made in batches which are small compared to the volume of the core, and for this reason it may be replaced by a continuous stream of matter. Moreover, some other simplifications will be introduced which are permissible for the purposes of the investigation, and thus do not alter the main features of the results. First we regard the two media (core and blanket) as homogeneous ones. This has the consequence that the fuel stream drawn off from the core at the time  $t$  is of the same isotope composition present in the core at that time  $t$ . Secondly, the time required for reprocessing and refabrication may be neglected because in general it is small compared to the time it takes for the isotope composition to be changed essentially.

For this reason we do not have to take into account the streams of fissile and fertile material which only pass reprocessing and refabricating plants and are fed back into the core unchanged. This also applies to trivial inflow and outflow of structural material. Also that part of the fuel produced by breeding in the blanket which reaches the core via reprocessing and fuel-element-fabrication plants may be regarded as an immediate stream from the blanket to the core.

Fig. 1 schematically shows the non-trivial streams of fissile and fertile material for a reactor system consisting of two zones. The scheme is restricted to the case where the breeder is able to satisfy its fuel needs by itself. For the sake of simplicity, we also neglected the  $\text{U}^{235}$ -content of the fertile material.  $g_8$  and  $U_8$

are the streams of  $U^{238}$  into the core or the blanket, respectively.  $\gamma_B$  and  $\gamma_C$  designate the fuel streams which are not recycled into the system and thus can be sold. There are two extreme cases of the fuel cycle.

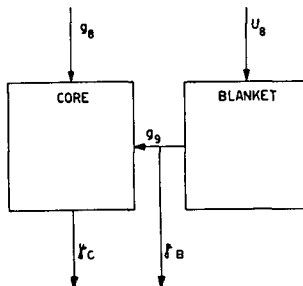


Fig. 1  
Scheme of the fertile- and fissile-material streams in a two-zone system.

*Case B.*  $\gamma_B \neq 0$ , and  $\gamma_C = 0$ , i.e. plutonium produced by breeding is only sold from the blanket. No plutonium is ever drawn off from the core.

*Case C.*  $\gamma_C \neq 0$ , and  $\gamma_B = 0$ , i.e. all plutonium produced by breeding in the blanket is fed into the core, from where a stream  $\gamma_C$  of the isotope mixture present there at the moment must be drawn off continuously for criticality reasons if the system works with a breeding gain  $> 0$ .

In the following sections, the long-term change of the isotope mixture in the core is first calculated in a general way. Another section gives numerical results for the two extreme cases B and C.

### The time differential equations of the two-media problem

Fundamentally, neutron flux is a function of space, energy, and time.

The dependence on time, however, is very weak, if one idealizes the recharging batch process to appear as a continuous stream, as is done here, and, moreover, it demands that the volume of the core be not changed in time (see below). At least the flux may be taken as being constant over relatively large time intervals. Within such an interval of time, the quantities appearing in the reaction rates may be replaced by average values or integrated quantities in the following way:

$$\bar{\varphi}(\mathbf{r}) = \int \varphi(\mathbf{r}, E) dE \quad (1)$$

$$\bar{\varphi} = \int \bar{\varphi}(\mathbf{r}) d\mathbf{r} \quad (2)$$

where volume integration is over the core or over the blanket.

The average values of the cross-sections are given by the following term:

$$\bar{\sigma} = \frac{\int \sigma(E) \varphi(\mathbf{r}, E) dE d\mathbf{r}}{\int \varphi(\mathbf{r}, E) dE d\mathbf{r}} = \frac{1}{\bar{\varphi}} \int \sigma(E) \varphi(\mathbf{r}, E) dE d\mathbf{r}. \quad (3)$$

For the differential equations describing the change of the isotope mixture in the core, this results in

$$\left. \begin{aligned} V_C \frac{dN_8}{dt} &= -\bar{\sigma}_8 N_8 \bar{\varphi}_C + \bar{g}_8 \\ V_C \frac{dN_9}{dt} &= -\bar{\sigma}_9^a N_9 \bar{\varphi}_C + \bar{\sigma}_9^c N_8 \bar{\varphi}_C + \bar{g}_9 - \bar{\gamma}_C N_9 \\ V_C \frac{dN_0}{dt} &= -\bar{\sigma}_0^a N_0 \bar{\varphi}_C + \bar{\sigma}_0^c N_9 \bar{\varphi}_C + (\bar{g}_0) - \bar{\gamma}_C N_0 \\ V_C \frac{dN_1}{dt} &= -\bar{\sigma}_1^a N_1 \bar{\varphi}_C + \bar{\sigma}_1^c N_0 \bar{\varphi}_C + (\bar{g}_1) - \bar{\gamma}_C N_1 \\ V_C \frac{dN_2}{dt} &= -\bar{\sigma}_2 N_2 \bar{\varphi}_C + \bar{\sigma}_1 N_1 \bar{\varphi}_C + (\bar{g}_2) - \bar{\gamma}_C N_2 \\ 0 &= -\bar{\gamma}_3 + \bar{\sigma}_2 N_2 \bar{\varphi}_C \end{aligned} \right\} \quad (4)$$

where  $N_8, N_9, N_0 \dots$  are the numbers of  $\text{U}^{238}, \text{Pu}^{239}, \text{Pu}^{240} \dots$  nuclei per cubic-centimeter of core volume ( $V_C$ ),  $\bar{\varphi}_C$  is the volume integral of neutron flux in the core,  $\bar{g}_1$  the total stream of particles of sort  $N_1$  into the core.  $\bar{g}_0, \bar{g}_1$  and  $\bar{g}_2$  are put in brackets, because in the following part we are going to assume that no remarkable concentration of higher Pu-isotopes builds up in the blanket. This assumption is unimportant for the fundamental results, but it will be improved upon continuation of this work. In the last equation, it is assumed that  $\text{Am}^{243}$  is removed from the core so quickly that its concentration can be neglected or else has such a low constant value that it is of no interest for the criticality of the system.

Eqs. (4) are altered in such a way as to contain only quantities without dimensions. Instead of time, a quantity

$$\tau = t \frac{\bar{\varphi}_C}{V_C} \times 10^{-24} \text{ cm}^2 \quad (5)$$

proportional to the flux-time is introduced. The average values of the effective cross-sections are replaced by their (dimensionless) measured figures in barns.

$$\bar{\sigma} = \sigma \times 10^{-24} \text{ cm}^2. \quad (6)$$

The particle concentrations are changed into pure numbers by multiplication with a "unit volume" where the unit volume  $V$  has been selected so as to render

$$\sum n_i = 1 \quad (7)$$

$$n_i = N_i / V. \quad (8)$$

In this case the streams change to

$$\gamma_C = \frac{\bar{\varphi}_C}{\bar{\varphi}_B} \times 10^{24} \text{ cm}^{-3} \quad (9)$$

$$g_i = \frac{g_i \cdot V}{\bar{\varphi}_B} \times 10^{24} \text{ cm}^{-2}. \quad (10)$$

Plutonium production in the blanket per unit time is given by this expression:

$$\bar{\sigma}_{8B}^c N_{8B} \int \bar{\varphi}_B(r) dr = \bar{\sigma}_{8B}^c N_{8B} \bar{\varphi}_B. \quad (11)$$

Out of this, the fraction  $\gamma_B$  (stream directed toward the outside) is available for sale, and the fraction  $1 - \gamma_B$  is fed into the core. For the  $Pu^{239}$ -stream within the core we then have:

$$\bar{g}_8 = \bar{\sigma}_{8B}^c N_{8B} \bar{\varphi}_B (1 - \gamma_B) \quad (12)$$

or, after introducing quantities without dimensions,

$$g_8 = \sigma_{8B}^c V N_{8B} \frac{\bar{\varphi}_B}{\varphi_C} (1 - \gamma_B) = \sigma_{8B}^c \bar{n}_{8B} (1 - \gamma_B) \quad (13)$$

where

$$\bar{n}_{8B} = N_{8B} \frac{\bar{\varphi}_{B'}}{\varphi_C} V \quad (14)$$

is the number of nuclei in the fertile material, reduced to core conditions with the rate of reaction maintained:

$$\bar{\sigma}_{B'} \int_B N_{8B}(\mathbf{r}) \bar{\varphi}_{B'}(\mathbf{r}) d\mathbf{r} = \bar{\sigma}_B N_{8B} \bar{\varphi}_{B'} = \bar{\sigma}_B \bar{N}_{8B} \bar{\varphi}_C. \quad (15)$$

From the reduced concentration  $\bar{N}_{8B}$  we obtain the reduced number of particles by multiplication with the unit volume:

$$\bar{n}_{8B} = \bar{N}_{8B} V. \quad (16)$$

Thus, out of (4) comes

$$\left. \begin{aligned} \frac{dn_8}{d\tau} &= -\sigma_a^a n_8 + g_8 \\ \frac{dn_9}{d\tau} &= -\sigma_a^a n_9 + \sigma_c^c n_8 + g_9 - \gamma_C n_9 \\ \frac{dn_0}{d\tau} &= -\sigma_a^a n_0 + \sigma_c^c n_9 - \gamma_C n_0 \\ \frac{dn_1}{d\tau} &= -\sigma_a^a n_1 + \sigma_c^c n_0 - \gamma_C n_1 \\ \frac{dn_2}{d\tau} &= -\sigma_a^a n_2 + \sigma_c^c n_1 - \gamma_C n_2 \\ 0 &= -\gamma_3 + \sigma_c^c n_2. \end{aligned} \right\} \quad (17)$$

The system of equations (17) is to be solved under the secondary condition of normalization, which corresponds to the postulation of a particle-density constant with regard to time, and under the secondary condition of criticality, i.e. all neutrons produced in the reactor either are also absorbed in it or get out of the system:

$$\sum_{i=8}^2 n_i(\tau) = 1 \quad (18)$$

$$\sum_{i=8}^2 a_i n_i(\tau) + a_{8B} \bar{n}_{8B} + \pi' + \lambda' = 0 \quad (19)$$

with

$$a_i = \sigma_a^a - \nu_i \sigma_f^f, \quad i = 8 \dots 2 \text{ and } 8B \quad (20)$$

where  $\lambda'$  is the number of leakage neutrons for the unit volume  $V$ , and  $\pi'$  is the number of neutrons absorbed by parasitic capture in the unit volume. In one

special case, calculation of the place and energy-dependent neutron flux leads to  $\lambda'$ . As we do not aim at a special case, we treat  $\lambda'$  and  $\pi'$  as free parameters with a scope of quantities:

$$\begin{aligned} 0 &\leq \lambda' \leq \lambda'^* \\ 0 &\leq \pi' \leq \pi'^* \end{aligned} \quad (21)$$

where  $\lambda'^*$  and  $\pi'^*$  may, e.g., limit the scope of positive breeding gain.

The system of equations (17) to (19) first contains ten unknown time functions, the six particle numbers  $n_8$  to  $n_2$  and  $\bar{n}_{8B}$ , and the four streams  $g_8$ ,  $\gamma_B$ ,  $\gamma_C$  and  $\gamma_3$  flowing in or out. For their determination there are five differential equations and three algebraic equations, so that two remaining time functions may be presupposed at random from the mathematical point of view.

The five initial values of the particle numbers to be presupposed according to the five first-order differential equations must satisfy the secondary condition (18) and, inserted in (19), furnish a value for  $\bar{n}_{8B} > 0$ .

The fact that two of the time functions contained in the system of equations (17) to (19) may be freely presupposed within certain limits reflects the freedom in operating a reactor system consisting of core and blanket. For this reason, one is going to use this freedom in order to lay down regulations for operating the system fixed by the initial conditions. The first freedom will be disposed of by the postulation that the reactor, with the size of core and blanket dimensioned in the beginning, remains critical at all times. This leads to the consequence that within the periods of time quoted above, where the flux may be regarded as independent of time, the same number of neutrons streams from the core into the blanket at any moment, so that

$$\bar{n}_{8B}(\tau) \equiv \bar{n}_{8B}(0). \quad (22)$$

There is genuine freedom in selecting the second free time function, not only from the mathematical point of view, but also from that of the physics of the reactor system. According to the statements made above, this freedom is used for laying down an exact regulation for the fuel cycle. Mathematically, this regulation consists in presupposing  $\gamma_B(\tau)$  or  $\gamma_C(\tau)$  as time functions within the permissible limits. In case  $\gamma_B(\tau)$  is presupposed, this decides what share of the plutonium produced in the blanket by breeding will be fed into the core. One may freely choose the curve of a function between a minimal function  $\text{Min}(1 - \gamma_B(\tau))$  and the maximum value 1 (i.e. all blanket plutonium will be fed into the core). The corresponding fact is true of  $\gamma_C(\tau)$  between the minimum value  $\gamma_C = 0$  and a maximum function  $\text{Max}(\gamma_C(\tau))$ , which results if all plutonium produced by breeding in the blanket is fed into the core ( $\gamma_B = 0$ ).

The structure of the differential equation system (17) is very different in both extreme cases. In case B,  $\gamma_C = 0$  and (17) is a linear differential equation system with constant coefficients. Even if  $\gamma_B(\tau) > 0$  is presupposed, the system remains linear. In case C, however, the system of differential equations (17) becomes non-linear, because the unknown functions  $\gamma_C(\tau)$  and  $n_i(\tau)$  appear as a product. The same thing holds true if  $\gamma_B(\tau) > 0$  is presupposed. Thus we have to calculate in the following section the solution of the systems (17) to (19) in both the linear and non-linear cases.

The initial conditions will be presupposed in this form:

$$\frac{n_0(0)}{n_8(0)}, \quad \frac{n_1(0)}{n_8(0)}, \quad \frac{n_2(0)}{n_8(0)}, \quad y(0) = y_0 \quad (23)$$

with

$$y(\tau) = \frac{n_9(\tau)}{\sum_9^2 n_i(\tau)} \quad (24)$$

as quantities which may be chosen freely. Then

$$n_9(0) = \left[ \left( 1 + \frac{n_0(0)}{n_9(0)} + \frac{n_1(0)}{n_9(0)} + \frac{n_2(0)}{n_9(0)} \right) (1 + y_0) \right]^{-1} \quad (25)$$

is calculated from the normalization condition. The criticality postulation then determines  $\bar{n}_{8B}(0)$  and thus, lastly, the size of the reactor.

### Solution of system (17) to (19)

First, the system (17) to (19), consisting of differential and algebraic equations, was to be changed into a pure system of differential equations for the particle numbers of the plutonium isotopes. For the sake of simplicity, we restrict ourselves in this section to the situation where  $\gamma_B$ , or  $\gamma_C$ , respectively, are presumed not to be time functions, but constant quantities, as this takes care of the extreme cases B and C which are investigated here numerically. Depending upon whether the linear or the non-linear problem is treated, it is useful to apply different eliminations, because in the latter case  $g_9$  is presupposed, whereas it is wanted in the first one.

#### SOLUTION OF THE LINEAR PROBLEM

Normalization condition and criticality should be met any time. Apart from (18) and (19), it should therefore also apply that

$$\sum_8^2 \dot{n}_i(\tau) = 0 \quad (26)$$

$$\sum_8^2 a_i \dot{n}_i(\tau) = 0 \quad (27)$$

If one inserts Eqs. (17) into (26), one obtains the general balance equation of the fissile and fertile material nuclei:

$$-\sum_8^2 \sigma_i^f n_i + g_8 + g_9 - \gamma_3 = 0 \quad (28)$$

i.e., all nuclei introduced into the core as  $U^{238}$  or  $Pu^{239}$  are either fissioned or drawn off as  $Am^{243}$ . Elimination of  $\gamma_3$  by using Eqs. (17) gives

$$g_8 + g_9 = \sum_8^2 \sigma_i^f n_i + \sigma_2^c n_2. \quad (29)$$

Another relation between  $g_8$  and  $g_9$  is obtained by inserting (17) into (27):

$$a_8 g_8 + a_9 g_9 = n_8(a_8 \sigma^a_8 - a_9 \sigma^c_8) + n_9(a_9 \sigma^a_9 - a_0 \sigma^c_9) + n_0(a_0 \sigma^a_0 - a_1 \sigma^c_0) \\ + n_1(a_1 \sigma^a_1 - a_2 \sigma^c_1) + n_2 a_2 \sigma^a_2. \quad (30)$$

It is possible, by using (29) and (30), to express  $g_8$  and  $g_9$  in terms of  $n_i$ :

$$g_8 = \frac{1}{a_9 - a_8} \left[ n_8 \sigma^a_8 (a_9 - a_8) + n_9 \sigma^c_9 (a_0 - a_9) + n_0 \sigma^a_0 (a_9 - a_0) + n_0 \sigma^c_0 (a_1 - a_9) \right. \\ \left. + n_1 \sigma^a_1 (a_9 - a_1) + n_1 \sigma^c_1 (a_2 - a_9) + n_2 \sigma^a_2 (a_9 - a_2) \right] \quad (31)$$

$$g_9 = \frac{-1}{a_9 - a_8} \left[ n_8 \sigma^c_8 (a_9 - a_8) + n_9 \sigma^c_9 (a_0 - a_8) + n_9 \sigma^a_9 (a_8 - a_9) + n_0 \sigma^c_0 (a_1 - a_8) \right. \\ \left. + n_0 \sigma^a_0 (a_8 - a_0) + n_1 \sigma^c_1 (a_2 - a_8) + n_1 \sigma^a_1 (a_8 - a_1) + n_2 \sigma^a_2 (a_8 - a_2) \right]. \quad (32)$$

If one inserts (32) into Eqs. (17), the terms with  $n_8$  cancel out and the four central equations in (17) become a homogeneous linear system of differential equations for determining the numbers of plutonium particles. One may considerably abbreviate this notation by regarding the quantities  $n_9$  to  $n_2$  as components of one vector:

$$\mathbf{n} = \begin{pmatrix} n_9 \\ n_0 \\ n_1 \\ n_2 \end{pmatrix} \quad (33)$$

and writing the core of the equation system (17) in this way:

$$\frac{d\mathbf{n}}{d\tau} = \mathbf{B}\mathbf{n} \quad (34)$$

where

$$\mathbf{B} = \begin{pmatrix} \sigma^c_9 \alpha_0 & \sigma^c_0 \alpha_1 - \sigma^a_0 \alpha_0 & \sigma^c_1 \alpha_2 - \sigma^a_1 \alpha_1 - \sigma^a_2 \alpha_2 \\ \sigma^c_9 & -\sigma^a_0 & 0 & 0 \\ 0 & \sigma^c_0 & -\sigma^a_1 & 0 \\ 0 & 0 & \sigma^c_1 & -\sigma^a_2 \end{pmatrix} \quad (35)$$

with  $\alpha_i$  given by the following quotients:

$$\alpha_i = \frac{a_i - a_8}{a_8 - a_9}. \quad (36)$$

With the eigenvalues of the matrix  $\mathbf{B}$  to be determined from the determinant

$$|\mathbf{B} - r \mathbf{E}| = 0 \quad (37)$$

and the relevant eigenvectors  $\mathbf{x}_k$ , one obtains the solution of the time-dependent linear problem in this shape:

$$\mathbf{n}(\tau) = \sum_{k=1}^4 \zeta_k \mathbf{x}_k e^{-r_k \tau}. \quad (38)$$

The quantities  $\zeta_k$  must be calculated from the initial conditions, where the interrelations between the Pu-isotopes could be chosen freely and parasitic absorption ( $\pi'$ ), leakage ( $\lambda'$ ), and distribution of the fertile material in core and blanket ( $y_0$ ) only appear in one common factor. As the matrix  $\mathbf{B}$  and thus

also the eigenvalues  $r_k$  and the eigenvectors do not depend upon  $\pi' + \lambda'$  and  $y_0$ ,  $y_0$  and the neutron loss influence the total solution (38) only through a factor common to all terms. Thus, if one does not take into account spectral shifts, the following facts apply:

In the extreme case B, where no plutonium for sale is taken out of the core, the relative concentration of the plutonium isotopes at any time is independent of parasitic absorption, leakage, and initial distribution of fertile material in the core and blanket.

Especially for  $Pu^\infty$ , if one introduces the normalization (without  $n_8$ )

$$\sum_9^2 n'_i = 1 \quad (39)$$

which is much more illustrative for regarding the relative plutonium concentrations (the superscript is to denote the quantities normalized according to (39) instead of (18)), — the following terms result from (35):

$$\left. \begin{aligned} n'_9 &= \frac{\sigma_0^a \sigma_1^a \sigma_2^a}{\sigma_9^c \sigma_0^c \sigma_1^c} n'_2 \\ n'_0 &= \frac{\sigma_1^a \sigma_2^a}{\sigma_0^2 \sigma_1^2} n'_2 \\ n'_1 &= \frac{\sigma_2^a}{\sigma_1^c} n'_2 \\ n'_2 &= \left[ 1 + \frac{\sigma_2^a}{\sigma_1^c} + \frac{\sigma_2^a \sigma_1^a}{\sigma_1^c \sigma_0^c} + \frac{\sigma_2^a \sigma_1^a \sigma_0^a}{\sigma_1^c \sigma_0^c \sigma_9^c} \right]^{-1} \end{aligned} \right\} \quad (40)$$

All other quantities may be directly determined from  $n_9$  to  $n_2$ :  $n_8$  from (18),  $g_8$  from (31),  $g_9$  from (32), and  $\gamma_3$  from (17).

#### SOLUTION OF THE NON-LINEAR PROBLEM

In the extreme case C, where plutonium for sale is only drawn from the core,  $g_9$  is presupposed. We therefore change the mixed system of Eqs. (17) to (19) in the following way so as to form a pure system of differential equations.

First we regard the term  $g_9$  in the second of Eqs. (17) as being equipped with a factor  $\sum_8^2 n_i = 1$  and also in the criticality condition the terms  $a_{8B} \bar{n}_{8B} + \pi' + \lambda'$ .

This latter fact, physically speaking means that net absorption of uranium-238 in the blanket, parasitic absorption, and leakage are taken into account in the core as increased absorption:

$$\frac{dn_9}{d\tau} = -\sigma_9^a n_9 + \sigma_8^c n_8 + g_9 \sum_8^2 n_i - \gamma_c n_9 \quad (41)$$

$$0 = \sum_8^2 (\sigma_i^a (-\nu_i \sigma_i^t + a_{8B} \bar{n}_{8B} + \pi' + \lambda') n_i). \quad (42)$$

The parentheses in (42) we denote by  $b_i$ :

$$b_i = (\sigma_i^a - \nu_i \sigma_i^t + a_{8B} \bar{n}_{8B} + \pi' + \lambda'). \quad (43)$$

We resolve (42) for  $n_8$  and insert into (41):

$$\frac{dn_9}{d\tau} = -\sigma_9^a n_9 + \sum_9^2 C_i n_i - \gamma_C n_9 \quad (44)$$

with

$$C_i = g_9 - (\sigma_8 + g_9) \frac{b_i}{b_8}. \quad (45)$$

As in the treatment of linear problems we introduce the plutonium vector (33). Instead of (34) we now obtain:

$$\frac{d\mathbf{n}}{d\tau} = \mathbf{C}\mathbf{n} - \gamma_C(\tau)\mathbf{n} \quad (46)$$

with

$$\mathbf{C} = \left\{ \begin{array}{cccc} -\sigma_9^a + C_9 & C_0 & C_1 & C_2 \\ \sigma_9^C & -\sigma_0^a & 0 & 0 \\ 0 & \sigma_0^C & -\sigma_1^a & 0 \\ 0 & 0 & \sigma_1^C & -\sigma_2^a \end{array} \right\} \quad (47)$$

where the quantities  $C_i$  are dependent upon  $\pi'$ ,  $\lambda'$ , and  $y_0$ . In contrast to the extreme case B, the following statement holds, even if one does not take into account spectral shifts:

In the extreme case C and in every other fuel recycling with  $\gamma_C(\tau)$  not presupposed, the whole time plot of the relative plutonium concentrations and especially  $Pu^\infty$  depends upon parasitic absorption, leakage, and the distribution of fertile material in the core and in the blanket.

Corresponding to (40) one obtains this term in the specific normalization (39) for the components of the  $Pu^\infty$ -mixture in case C:

$$\left. \begin{aligned} n_9' &= \frac{(\sigma_2^a + \gamma_C)(\sigma_1^a + \gamma_C)(\sigma_0^a + \gamma_C)}{\sigma_1^c \sigma_0^c \sigma_9^c} n_2' \\ n_0' &= \frac{(\sigma_2^a + \gamma_C)(\sigma_1^a + \gamma_C)}{\sigma_1^c \sigma_0^c} n_2' \\ n_1' &= \frac{\sigma_2^a + \gamma_C}{\sigma_1^c} n_2' \\ n_2' &= \left[ 1 + \frac{\sigma_2^a + \gamma_C}{\sigma_1^c} + \frac{(\sigma_2^a + \gamma_C)(\sigma_1^a + \gamma_C)}{\sigma_1^c \sigma_0^c} + \frac{(\sigma_2^a + \gamma_C)(\sigma_1^a + \gamma_C)(\sigma_0^a + \gamma_C)}{\sigma_1^c \sigma_0^c \sigma_9^c} \right]^{-1} \end{aligned} \right\} \quad (48)$$

Thus the stationary plutonium concentrations depend upon  $\gamma_C(\infty)$ , which (together with the  $n_i(\infty)$ ) results from the solution of the eigenvalue problem:

$$\mathbf{C}\mathbf{n} = \gamma_C \mathbf{n}. \quad (49)$$

As the matrix  $\mathbf{C}$  is not a symmetrical one, not necessarily all four eigenvalues are real. Moreover, negative real eigenvalues have no practical meaning as they describe a plutonium stream into the core which has the same composition as the plutonium already present in the core. Such a fuel charge is not possible in general. Negative values of  $\gamma_C$ , which lead to negative particle numbers according to (49) or (48), must be excluded because they are physically impossible.

The average cross-sections typical for a reactor fuelled with fuel oxide or carbide were taken as a basis of this work (*cf.* Table I). They furnished one positive and three negative eigenvalues. The positive eigenvalue has been realized physically.

The solution of the non-linear differential equation system (46) can be calculated in the following way in the form of a Taylor series: with  $n(0)$  presupposed by the initial condition,  $\gamma_C(0)$  appears in (46) only as a product with the known vector  $n(0)$ .

At  $\tau=0$ , (46) together with (26) and (27) form an inhomogeneous, linear system of equations for determining the six unknown quantities  $n_i(0)$  ( $i=8$  to 2) and  $\gamma_C(0)$ . By differentiating (46), (26) and (27), one obtains a corresponding system of equations for calculating  $\dot{n}_i(0)$  ( $i=8$  to 2) and  $\dot{\gamma}_C(0)$ , and by continuing these processes the whole Taylor development of the functions  $\gamma_C(\tau)$  and  $n_i(\tau)$  at  $\tau=0$  is obtained.  $g_8(\tau)$  and  $\gamma_8(\tau)$  thus may be calculated immediately from (17). In the numerical evaluation, the Taylor development was used only in such a small interval  $\Delta\tau$  that at the end of the interval the quantities  $n_i(\tau + \Delta\tau)$  described by ten-series terms had an error of less than  $10^{-10}$ . These particle numbers were taken as initial conditions for the next  $\Delta\tau$ -interval, etc.

#### NUMERICAL RESULTS

Table I gives the average values typical of a reactor fuelled with oxide or carbide fuel used for the capture and fission cross-sections.

TABLE I  
AVERAGE CROSS-SECTIONS  
(barns)

	$U^{238}$	$Pu^{239}$	$Pu^{240}$	$Pu^{241}$	$Pu^{242}$
$\sigma^c$	0.16	0.29	0.29	0.20	0.29
$\sigma^f$	0.01	1.70	0.03	2.05	0.05
$\nu$	2.5	2.9	3.1	3.0	3.1

For  $U^{238}$ , identical cross-sections were used for core and blanket in the first informative results quoted here.

The two stationary Pu-isotope mixtures calculated with these cross-sections for the two extreme cases B and C are quoted in Table II in normalization (39). In case B, the relative concentrations are independent of the amount of neutron losses as well as of  $y_0$ . In case C, the relative Pu-concentrations at constant  $\pi' + \lambda'$  depend upon  $y_0$ . However, if one relates the neutron losses not to the nuclei present in the core ( $\sum n_i = 1$ ) but to  $1 + \bar{n}_{8B}$ , i.e. if instead of  $\pi' + \lambda'$  the quantity

$$\pi + \lambda = \frac{\pi' + \lambda'}{1 + \bar{n}_{8B}} \quad (50)$$

is kept constant, also in case C the relative plutonium concentrations are independent of  $y_0$ , the initial distribution of fertile material in core and blanket.  $\pi + \lambda$  is quoted as a parameter in Table II.

TABLE II

Extreme case	B	C				
		0	0.01	0.02	0.03	0.0946
$\pi + \lambda$						
$100 \cdot n'_9$	47.76	83.41	81.18	78.70	76.03	47.76
$100 \cdot n'$	43.28	15.19	17.10	19.21	21.46	43.28
$100 \cdot n'_1$	5.58	1.25	1.50	1.79	2.11	5.58
$100 \cdot n_2$	3.38	0.16	0.22	0.30	0.41	3.38
$\gamma_C$	0	1.273	1.057	0.868	0.707	0
BR-1	<i>cf.</i> Table III	0.733	0.620	0.520	0.434	0

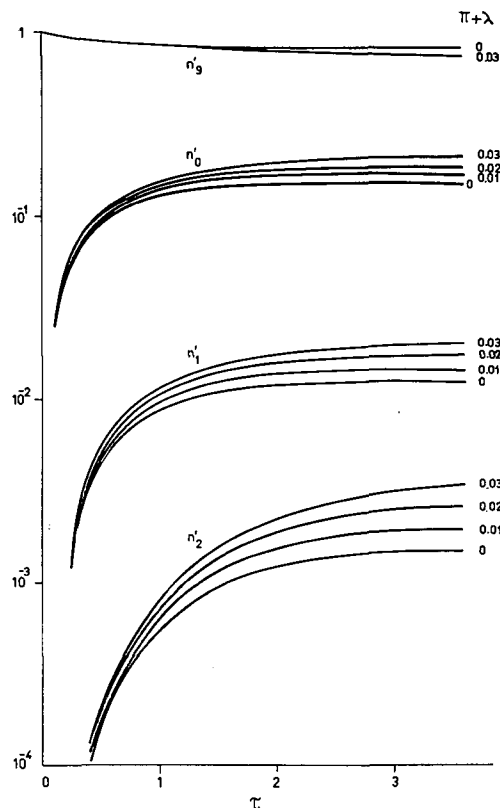


Fig. 2  
Time variation of relative concentrations of Pu-isotopes with neutron losses as parameter in case C for clean  $Pu^{239}$  at  $\tau = 0$ .

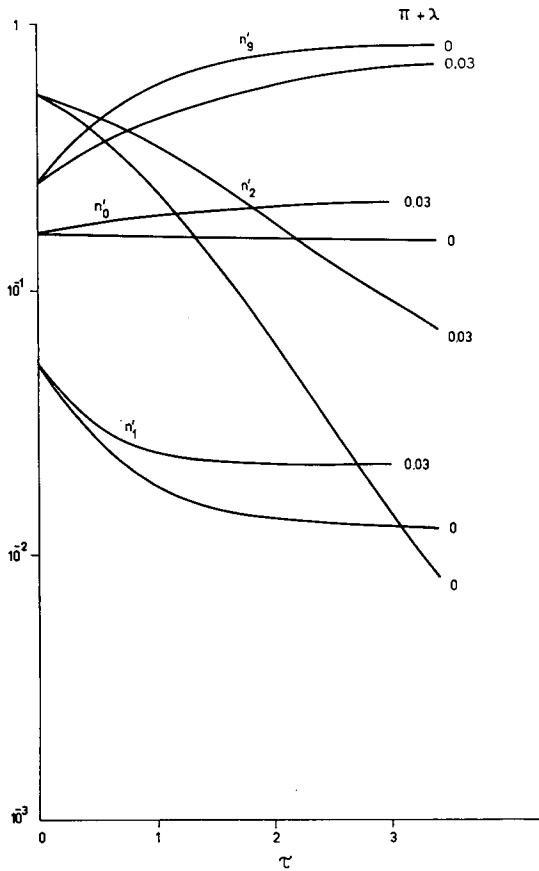


Fig. 3

Time variation of relative concentrations of Pu-isotopes with neutron losses as parameter in case C for thermal Pu at  $\tau=0$ .

Obviously, the breeding rate must be defined differently for cases B and C. In case B, pure  $\text{Pu}^{239}$  is produced in the blanket by breeding and then sold. The core is kept critical by addition of  $\text{Pu}^{239}$ . The higher plutonium isotopes cannot be included in the definition of the breeding gain, because they have effects similar to those of catalysts unchanged by time.

$$(BR - 1)_B = \frac{\bar{n}_{8B} \sigma_{8B}^c \gamma_B}{\bar{n}_{8B} \sigma_{8B} (1 - \gamma_B) + n_8 \sigma_8} . \quad (51)$$

In case C, however, only the plutonium mixture as a whole taken out of the core for sale may be termed fuel produced by breeding. Therefore in this case the breeding gain must not be defined by (51), but by an expression containing for the fuel gain the output of stationary isotope mixture and for the fuel consumption the amount of this mixture turned over in the core per unit time:

$$(BR - 1)_C = \gamma_C \frac{\sum_{i=1}^2 n_i}{\sum_{i=1}^9 \sigma_i^a n_i} . \quad (52)$$

For discussing Table II, we will use the following terminology for the sake of brevity. A plutonium-isotope mixture is to be termed the better, the higher is its share of  $Pu^{239} + Pu^{241}$ , relative to the share of  $Pu^{240} + Pu^{242}$ . The essentials of Table II can be summarized in this terminology in the following way:

In charging regulation C, the  $Pu^\infty$  mixture is very good for  $\pi + \lambda = 0$ . With increasing neutron losses, on the one hand the breeding gain decreases, on the other Pu-isotope mixture deteriorates. High neutron losses thus create a twofold disadvantage. In cases of vanishing breeding gain ( $\gamma_C = 0$ ) the  $Pu^\infty$  mixture deteriorates to the same extent as in charging regulation B. The higher quality of the isotope mixture in case C is achieved at the expense of the inferior quality of plutonium available for sale.

Table III shows the breeding gain in case B for the same values of neutron loss ( $\pi + \lambda$ ) as in Table II.

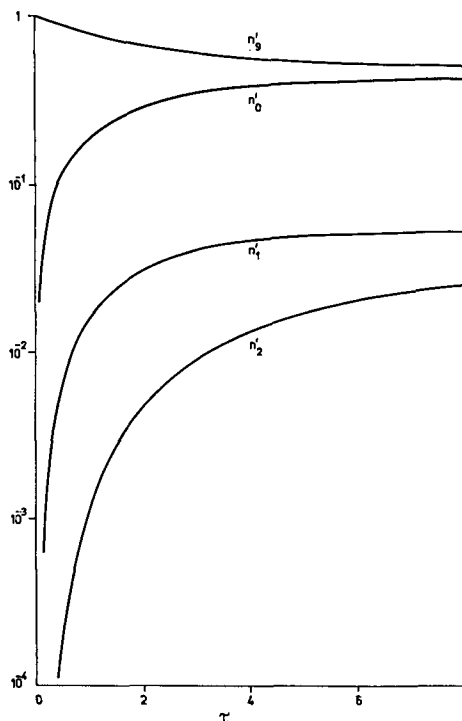


Fig. 4  
Time variation of relative concentrations of Pu-isotopes in case B for clean  $Pu^{239}$  at  $\tau = 0$ .

TABLE III  
BREEDING GAIN IN CASE B

$\pi + \lambda$	0	0.01	0.02	0.03	0.0946
BR—1	0.762	0.634	0.526	0.435	0

Tables II and III show that the breeding gain at equal neutron loss is practically independent of the type of fuel recycling. All values are somewhat higher in case B than in case C, which might be due to the higher Pu<sup>241</sup>-content in case B. However, an accurate discussion of small differences does not seem feasible, because the breeding ratios refer to the increase of the different isotope mixtures.

In Figs. 2 and 3 the relative concentrations of Pu-isotopes in case C are plotted as a function of time, with  $\pi + \lambda$  as a parameter. Pure Pu<sup>239</sup> has been assumed as the initial fuel in Fig. 2, and Pu<sup>∞</sup> of thermal reactors in Fig. 3.

At a specific power of 0.2 MW/kg, a period of 23 years corresponds to the quantity of  $\tau = 1$ . Fig. 3 shows how Pu<sup>∞</sup>, because of the necessary extensive changes in concentration, is decreased only slowly and then changed into the mixture corresponding to the fast reactor.

Fig. 4 shows the relative Pu-concentrations of case B (the initial conditions are the same as in Fig. 2); they are independent of neutron loss. The stationary

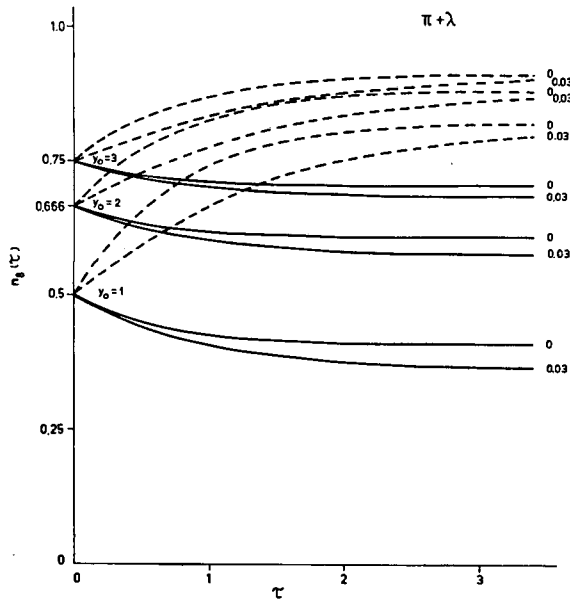


Fig. 5

Time variation of relative content of U<sup>238</sup> with its initial content and neutron losses as parameter in case C.

— clean Pu<sup>239</sup> at  $\tau = 0$   
 - - - Pu<sup>∞</sup> thermal at  $\tau = 0$

isotope mixture is only established after a longer period of time, because  $\text{Pu}^{240}$ ,  $\text{Pu}^{241}$ , and  $\text{Pu}^{242}$  must increase to higher concentrations than in case C. Figs. 5 and 6 show the  $\text{U}^{238}$  concentrations for cases C (Fig. 5) and B (Fig. 6). With pure  $\text{Pu}^{239}$  as the initial fuel (solid lines in Fig. 5 and 6) the  $\text{U}^{238}$  concentrations

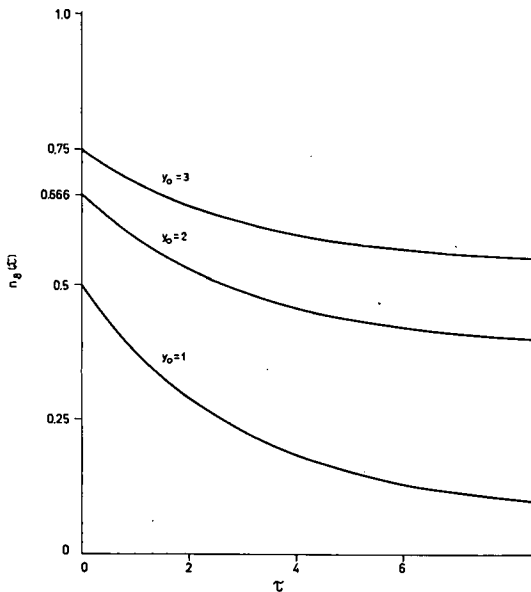


Fig. 6  
Time variation of relative content of  $\text{U}^{238}$  with its initial content in case B for clean  $\text{Pu}^{239}$  at  $\tau = 0$ .

decrease with increasing time, corresponding to the build-up of  $\text{Pu}^{240}$  and  $\text{Pu}^{242}$ . In case  $\text{Pu}^\infty$  of thermal reactors is taken as an initial fuel (dotted line in Fig. 5),  $n_8(\tau)$  increases, because the initially high concentration of  $\text{Pu}^{242}$  decreases. For all changes of time of the  $\text{U}^{238}$ -Pu mixtures approximately the following fact holds, if one postulates the invariability of the core volume:

The  $\text{Pu}^{239}$ -share decreases in proportion with the build-up of  $\text{Pu}^{241}$ . The  $\text{U}^{238}$ -share is reduced with increasing concentration of  $\text{Pu}^{240}$  and  $\text{Pu}^{242}$ , so that this approximation holds:

$$\begin{aligned} n_9 + n_1 &\approx \text{const.} \\ n_8 + n_0 + n_2 &\approx \text{const.} \end{aligned}$$

The physical reason for this is that the cross-sections of odd or even nuclei, respectively, differ only slightly. As a consequence, the neutron flux is nearly constant in time.

# FISSION GAS PRESSURE BUILD-UP AND FAST BREEDER ECONOMY

P. ENGELMANN

KERNFORSCHUNGSZENTRUM, KARLSRUHE,  
FEDERAL REPUBLIC OF GERMANY

Abstract — Résumé — Аннотация — Resumen

**Fission gas pressure build-up and fast-breeder economy.** Fuel-cycle costs and doubling time of fast-breeder reactors are strongly affected by the fuel-burn-up obtainable. Use of oxide or carbide fuel offers the possibility of reaching a burn-up of 100 000 MWd/t. In fuel-clad elements, a limiting factor is the fission-gas-pressure build-up. At the high burn-up considered, an appreciable fraction of the fission gases gets into the pores and thus contributes to the pressure on the can.

Starting from the known fission-product yields and decay chains, gas production and pressure build-up have been calculated. Three physical models have been employed in calculating the pressure acting upon the can: the gas is contained either in interconnected pores, in separate pores, or in a central hole.

The pressure-dependence upon free volume (fuel density) and temperature will be discussed. Cans made of high-strength materials as Inconel-X and molybdenum could stand the fission-gas pressure at operating temperatures. Unfortunately, these materials have higher absorption cross-sections than stainless steel. Results of a multi-group calculation are given, showing the effect of using these can materials and of decreasing the fuel density on critical mass and breeding ratio in small and medium-size breeders.

**Accumulation de la pression des gaz de fission et économie des réacteurs surgénérateurs à neutrons rapides.** Le coût du cycle de combustible et la période de doublement des réacteurs surgénérateurs à neutrons rapides dépendent étroitement du taux de combustion. En utilisant pour combustible un oxyde ou un carbone, on peut atteindre un taux de combustion de 100 000 MW j/t. Avec des combustibles gainés, l'accumulation de la pression des gaz de fission est un facteur limitatif. Pour le fort taux de combustion envisagé, une fraction non négligeable des gaz de fission pénètre dans les interstices et contribue ainsi à la pression sur la gaine.

A partir des rendements en produits de fission et des chaînes de désintégration connus, l'auteur a calculé la production de gaz et l'accumulation de pression. Pour calculer la pression exercée sur la gaine, il a utilisé trois modèles où le gaz était contenu dans des interstices reliés entre eux, dans des interstices séparés ou dans un orifice central.

Le mémoire traite de la variation de la pression en fonction du volume libre (densité du combustible) et de la température. Des gaines en matériaux très résistants, comme l'Inconel-X et le molybdène, ont pu supporter la pression des gaz de fission aux températures de fonctionnement. Malheureusement, les sections efficaces d'absorption de ces matériaux sont plus élevées que celle de l'aluminium. Les résultats de calculs multigroupes sont présentés, pour montrer comment ces matériaux de gainage et la diminution de la densité du combustible influent sur la masse critique et le rapport de surgénération dans les réacteurs surgénérateurs de petites ou moyennes dimensions.

**Накопление давления газов продуктов деления и экономика реакторов-размножителей на быстрых нейтронах.** На стоимость топливного цикла и на время удвоения реакторов-бридеров на быстрых нейтронах сильно влияет степень достигаемого выгорания топлива. Использование оксидного или карбидного топлива дает возможность достигнуть выгорания порядка 100 000 мвт·н/т. В топливных элементах с покрытием ограничивающим фактором является рост газов продуктов деления. При рассматриваемом высоком выгорании поддающаяся оценке фракция газов, образуемых при делении, попадает в поры и тем самым увеличивает давление на оболочку.

Исходя из известных выходов продуктов деления и цепочек распада было вычислено количество образующегося газа и создаваемое им давление. При расчете давления, действующего на оболочку, были использованы три физических модели: i) газ содержался в связанных между собой порах, ii) в отдельных порах и iii) в центральном отверстии.

Будет рассмотрена зависимость давления от свободного объема (плотность топлива) и температуры. Оболочки, изготовленные из высокопрочных материалов, например, из инконеля-Х и молибдена, могли бы выдержать при рабочих температурах давление газов, выделяющихся в результате деления. К сожалению, эти материалы обладают более высокими поперечными сечениями поглощения, чем нержавеющая сталь. Будут даны результаты многогруппового расчета, показывающие влияние использования этих материалов для оболочки и уменьшения плотности топлива на критическую массу, а также коэффициент размножения в малых и средних бридерах.

**Aumento de la presión de los gases de fisión y economía de los reactores reproductores rápidos.** El costo del ciclo de combustible y el período de duplicación en los reactores reproductores de neutrones rápidos dependen en gran medida del grado de combustión que pueda alcanzarse. La utilización de combustible en forma de óxido o de carburo permite obtener un grado de combustión de 100 000 MWd/t. Cuando se emplean elementos combustibles con revestimiento, el aumento de presión de los gases de fisión constituye un factor limitativo. En el caso del elevado grado de combustión previsto, una fracción considerable de los gases de fisión penetra en los poros del material, contribuyendo así a aumentar la presión en el interior de la envoltura.

Sobre la base de los rendimientos de fisión y de las cadenas de desintegración conocidas, el autor ha evaluado la producción de gas y el aumento de presión. Para calcular la presión ejercida sobre la envoltura, ha empleado tres modelos físicos en que el gas estaba contenido en poros conectados entre sí, en poros separados, o en un orificio central.

El autor analiza la variación de la presión, en función del volumen libre (densidad del combustible) y de la temperatura. Las envolturas de materiales de alta resistencia, tales como el Inconel-X y el molibdeno pueden soportar la presión de los gases de fisión a las temperaturas de funcionamiento corrientes. Desgraciadamente, la sección eficaz de absorción de estos materiales es superior a la del acero inoxidable. El autor presenta los resultados de cálculos, realizados según una teoría de varios grupos, que permite conocer el efecto de la utilización de estos materiales y de la disminución de la densidad del combustible, sobre la masa crítica y sobre la razón de reproducción en los reactores reproductores de pequeñas y medianas dimensiones.

## Introduction

The economy of fast-breeding reactors is strongly dependent on the attainable fuel burn-up for the following reasons: (a) low burn-up leads to frequent changes of fuel and thus to disturbances in the operation of the power plant; (b) cost of reprocessing and re-fabricating fuel elements as well as losses in fissile material

decreases with higher burn-up; (c) the external inventory decreases with higher burn-up, which reduces capital costs for the fuel inventory and shortens doubling time.

In the fast reactors, burn-up is limited not by fission-product poisoning but by the mechanical stability of the fuel elements. Essentially this is determined by the fission-gas pressure causing "swelling" in metallic fuel and can ruptures in ceramic fuel.

In ceramic fuel, the burn-up may be increased by using a very sturdy can and/or by reducing the fission-gas pressure. This is effected through working at low operating temperatures and thus keeping fission-gas diffusion at a minimum. However, this procedure is unreliable: the fission gases may be released in a power excursion and tear up the can. Moreover, it is costly: the fuel elements must be of very small dimensions in order to keep temperatures low at this high-power density.

It seems more favourable to permit a release of the fission gases from the lattice and reduce the pressure by a pore volume in the fuel and/or by a storage volume for the fission gases.

This work calculates the pressure of the fission gas for various reactor systems in porous oxide fuels ( $\text{UO}_2\text{-PuO}_2$ ). This then leads to the establishment of conditions permitting a burn-up of 65—100 MWd/kg fuel. The various possibilities are compared with each other.

### Calculation of fission-gas pressure

The following elements contribute to the gas pressure when  $\text{Pu}^{239}\text{O}_2$  is used as a fuel:

(a) The inert gases xenon and krypton; they make up the major portion with some 90% of the fission-gas pressure.

(b) The fission products: iodine, rubidium, caesium, cadmium, bromine and selenium, which are vaporous at operating temperature.

TABLE I  
FISSION YIELDS AND PRESSURE CONTRIBUTION

Element	Isotopes	Fission yield (atoms per 100 fissions)	Boiling point at atmospheric pressure (°C)	Contribution of pressure
Selenium .....	77, 78, 79, 80, 82	0.008	680	Negligible
Bromine .....	79, 81, 83, 84, 85	< 0.001	58	Negligible
Krypton .....	83, 84, 85, 86, 87, 88	0.894	-152	Some 4%
Rubidium .....	85, 87, 88, 89	1.074	680	< 4%
Cadmium .....	111, 112, 113, 114, 115, 116	0.901	765	< 3%
Iodine .....	127, 129, 131, 132, 133, 134, 135	3.011	183	< 10%
Xenon .....	129, 131, 132, 133, 134, 135, 136, 138	23.270	-108	Some 90%
Caesium .....	133, 135, 137, 138, 139	16.464	690	< 10%

(c) The oxygen of  $\text{PuO}_2$  released during the fission. However, it is quantitatively bound by addition to the lattices of  $\text{PuO}_2$  or  $\text{UO}_2$ , respectively, which are stable at high temperatures up to  $\text{UO}_{2.14}$ . Part of it also forms compounds with the fission products Mo, Nb, Cs, Zr, etc.

The fission yields were calculated for fast fission of  $\text{Pu}^{239}$  and a burn-up period of some 100—1000 days according to statements made by DILLON *et al.* [1]. The results have been compiled in Table I.

The pressure contributed by the vapours of selenium and bromine is negligible because of the low fission yield (less than 1%). The largest pressure contribution at high operating temperatures is made by caesium, but according to the vapour-pressure equation (2) this pressure stays below 10% of the gas pressure of the inert gases xenon and krypton in the temperature range that is of interest here. Rubidium and caesium have low fission yields and high boiling points, and for this reason their contribution to the fission-gas pressure is only a few per cent. Iodine could make a pressure contribution up to 10%, but it is expected that this element forms compounds not easily volatile with other fission products, as e.g., caesium, and thus cannot contribute towards the fission-gas pressure. Under this assumption, the fission-gas pressure  $p$  results in

$$p = p(\text{Xe}) + p(\text{Kr}) + p(\text{Cs}) + p(\text{Rb}) + p(\text{Cd})$$

$p(\text{Xe})$  and  $p(\text{Kr})$  being calculated from concentration and temperature on the basis of the ideal gas equation. For  $p(\text{Cs})$ ,  $p(\text{Rb})$ ,  $p(\text{Cd})$ , the saturation vapour pressure according to (2) is inserted in those cases where there is a saturation. Otherwise, the pressure of unsaturated vapour is calculated by the ideal gas equation (conservative assumption). The mean gas concentration  $\bar{n}$  in the pore volume can be calculated from the fission yield, the burn-up  $b$ , and the relative pore volume  $\alpha$  of the fuel:

$$\alpha = \frac{\text{pore volume}}{\text{volume of porous fuel}}$$

For a burn-up of 100 kg  $\text{Pu}^{239}$  per metric ton of fuel, i.e. about 100 MWd/kg fuel, the figures resulting for complete release of the fission-gas atoms from the lattice into the porous volume are given in Table II.

TABLE II  
INERT GAS CONCENTRATION IN THE PORE VOLUME  
at a burn-up of 100 MWd/kg fuel

$\alpha$ (%)	Fuel density $e_f$ (g/cm <sup>3</sup> )	Specific pore volume (l/kg fuel)	$\bar{n}$ (Xe + Kr) (Mol/l pore volume)
0	11.0	0	$\infty$
10	9.9	0.010	10.1
20	8.8	0.022	4.6
30	7.7	0.039	2.6

The pressure upon the can depends on the qualities of the fuel. The gases have a nearly homogeneous source distribution in the fuel element; because of the large

differences in temperature, high pressure gradients are formed. An equalization of pressure may take place either by diffusion of gases between the pores or by displacement of fuel. Under certain operating conditions, a central cavity collecting all fission gases may be formed in the fuel rods. These three possibilities were examined more closely as models No. 1, 2, and 3 for fuel rods.

#### MODEL NO. 1: PRESSURE EQUALIZATION BY DIFFUSION

Radial equalization is highly probable because of the high pressure gradient. Formation of cracks in starting up and cooling the reactor favours the pressure equalization. For the pressure of the inert gases, it follows, at a fixed height  $z$  of the fuel rod, that

$$p_{11}(r) = n(r) RT(r) = \text{const.} = p_{11} \quad (1)$$

$$n(r) = \frac{p_{11}}{RT(r)} = \frac{n(r_0) T(r_0)}{T(r)}. \quad (2)$$

where  $T$ =the absolute temperature at an axial distance  $r$ , measured in degrees Kelvin,

$R$ =the universal gas constant,

$r_0$ =the radius of the rod, measured in centimeters.

With homogeneous power distribution over the cross-section of the rod, the temperature curve is parabolic.

$$T(r) = T(r_0) + \Delta T \left\{ 1 - \left( \frac{r}{r_0} \right)^2 \right\} \quad (3)$$

where  $\Delta T = T(0) - T(r_0)$ .

From the known mean fission-gas concentration  $\bar{n}$  and the distribution according to equation (2),  $n(r_0)$  and thus  $p_{11}$  may be calculated:

$$\bar{n} = \frac{\int_0^{r_0} n(r) r dr}{\int_0^{r_0} r dr}. \quad (4)$$

From (2), (3), and (4) it results that

$$p_{11} = \bar{n} R \frac{\Delta T}{\ln \left\{ \frac{T(r_0) + \Delta T}{T(r_0)} \right\}}. \quad (5)$$

Added to this pressure of the inert gases Xe + Kr is the pressure of the vapours, which according to this model is the saturation vapour pressure at  $T(r_0)$ .

In case there is an axial equalization of pressure, the following equation holds true for the inert gases:

$$p_{12}(r, z) = n(r, z) R T(r, z) = \text{const.} = p_{12}. \quad (6)$$

For the measurement of  $z$ , cf. Fig. 1.

$$n(r, z) = \frac{p_{12}}{RT(r, z)} = \frac{n(r_0, O) T(r_0, O)}{T(r, z)} \quad (7)$$

$$\bar{n} = \frac{\int_{-h'/2}^{h'/2} dz \int_0^{r_0} n(r, z) r dr}{\int_{-h'/2}^{h'/2} dz \int_0^{r_0} r dr}. \quad (8)$$

Let  $\Delta\vartheta$  be the temperature increase of the coolant inside the core, and let the core be cylindrical. Then for the temperature distribution it holds that

$$T(r, z) = T(r_0, z) + \Delta T(z) \left\{ 1 - \left( \frac{r}{r_0} \right)^2 \right\} \quad (9)$$

$$T(r_0, z) = T(r_0, O) \cos \frac{\pi z}{h} + \Delta \vartheta \frac{\pi}{2h} \frac{1}{\sin \frac{\pi}{2} \frac{h'}{h}} \int_0^z \cos \frac{\pi z}{h} dz - \frac{h'}{2} \leq z \leq \frac{h'}{2}. \quad (10)$$

In this case, a distribution of flux or power is assumed proportional to  $\cos \pi z/h$ , with  $h > h'$ , that is to say, at the edge of the core the power level does not decrease to zero. The second summand on the right side of (10) gives the coolant temperature  $\vartheta(z)$ , the first summand furnishes the temperature jump between wall of the rod and temperature of the coolant; it is proportional to the power. Finally, the temperature drop in the fuel is

$$\Delta T(z) = \Delta T(O) \cos \frac{\pi z}{h}. \quad (11)$$

If  $\bar{n}$  is known, the pressure  $p_{12}$  may be calculated from Eqs. (7), (8), (9), and (10). Whereas closed integration over  $dr$  is possible in (8), one has to integrate numerically over  $dz$ .

A decrease in the fission-gas pressure can be obtained by storage volumes at the ends of the rod. These volumes, for instance, may be filled with a highly porous fertile material ( $U^{238}O_2$ ). Let the storage volumes be situated between  $z = (+/-) \frac{h'}{2}$  and  $z = (+/-) \frac{h''}{2}$  and have the identical radius  $r_0$  (cf. Fig. 1). The temperature behaviour in the fuel section again is given by (9), (10), and (11); in the upper fertile section (=storage volume) it shall hold that

$$T(r, z) = \frac{T\left(r_0, \frac{h'}{2}\right) + \vartheta_2}{2} \quad \frac{h'}{2} < z \leq \frac{h''}{2} \quad (12)$$

and in the lower fertile section

$$T(r, z) = \frac{T\left(r_0, -\frac{h'}{2}\right) + \vartheta_1}{2} \quad -\frac{h''}{2} \leq z < -\frac{h'}{2} \quad (13)$$

Thus, a constant temperature is assumed at the end pieces resulting as a mean value of each coolant temperature ( $\vartheta_1$  or  $\vartheta_2$ , and of the border temperature of the fuel at the end of the rod  $\left(T(r_0, \pm \frac{h'}{2})\right)$ ).

As no gases are formed in the end pieces, the mean fission-gas density at complete pressure equalization decreases to a value of

$$\bar{n}' = \bar{n} \frac{h'}{h''} \quad (14)$$

if the relative pore volume is the same in the fuel as in the fertile sections. In the case of unequal pore portions,  $\alpha$  in the fuel section, and  $\beta$  in the fertile section, it is

$$\bar{n}' = \bar{n} \frac{h' \alpha}{h' \alpha + (h'' - h') \beta}. \quad (15)$$

The fission-gas pressure  $p_{13}$  can be calculated again on the basis of Eqs. (7), (9), (10), (11), (12), (13), if the mean gas density  $\bar{n}$  is known, in which case  $n(r_0, 0)$  is determined from

$$\begin{aligned} \bar{n}' = & \frac{1}{\int_{-h''/2}^{h''/2} dz \int_0^{r_0} r dr} \left\{ \int_{z=-h''/2}^{-h'/2} dz \int_{r=0}^{r_0} \frac{n(r_0, O) T(r_0, O) r dr}{\frac{1}{2} \left\{ T\left(r_0, -\frac{h'}{2}\right) + \theta_1 \right\}} + \right. \\ & + \int_{-h'/2}^{h'/2} dz \int_0^{r_0} \frac{n(r_0, O) T(r_0, O) r dr}{T(r_0, z) + \Delta T(z) \left\{ 1 - \left( \frac{r}{r_0} \right)^2 \right\}} + \\ & \left. + \int_{+h'/2}^{h''/2} dz \int_0^{r_0} \frac{n(r_0, O) T(r_0, O) r dr}{\frac{1}{2} \left\{ T\left(r_0, +\frac{h'}{2}\right) + \theta_1 + \Delta \theta \right\}} \right\} \end{aligned} \quad (16)$$

Again, it is closed integration over  $dr$ , numerical integration over  $dz$  in the fuel section.

The contribution of vapours to the fission-gas pressure is still more reduced by storage volumes because the vapours diffuse at the relatively cold ends and condensate there. The results will be given after discussion of the other two models.

#### MODEL NO. 2: SEPARATE PORES, PRESSURE EQUALIZATION BY DISPLACEMENT

If there is no fission-gas diffusion between the pores, the high pressure gradient causes the inner pores to inflate under the compression caused by the outer ones, until there has been a pressure equalization. For the pressure of the inert gases, this results in the same value as was found according to model No. 1, but the pressure of the vapours increases, because now it must be calculated not for the cold wall temperature but for a higher mean temperature. As the total pressure determined according to model No. 2 is only by a maximum of 10% higher than that determined according to model No. 1, no special values were quoted in the results.

The essential difference is that according to model No. 2, a reduction in pressure by external pore volumes is not possible without displacement of fuel from the core area. Such a displacement of fuel, however, must be prevented in all fuel elements for reasons of reactivity.

## MODEL No. 3: FISSION GASES IN CENTRAL CAVITY

ROBERTSON [3] reports that a central cavity is formed in the course of burn-up in fuel rods with porous oxide fuel at high central temperatures; this cavity collects fission gases. The cause for this phenomenon is a recrystallization in such a way that the oxide crystals grow towards the interior from the colder region of the wall. Porous inclusions and empty spots are pushed into the interior. At the same time, the thermal conductivity in the recrystallized area improves and the temperature drop in the fuel is reduced.

In case the central cavity contains the whole pore volume, the temperature drop in the full rod

$$\Delta T_1 = \frac{\bar{q}_1 r_0^2}{4 k_1} \quad (17)$$

is replaced by the temperature drop in the "cavity rod" with outside cooling

$$\Delta T_2 = \frac{\bar{q}_2 r_0^2}{4 k_2} \left\{ 1 - \left( \frac{r_i}{r_0} \right)^2 \left( 1 + 2 \ln \frac{r_0}{r_i} \right) \right\} \quad (18)$$

with  $r_0$  radius of the rod,

$r_i$  radius of the central cavity,

$\bar{q}$  power density,

$k$  thermal conductivity.

In model No. 3, the fission-gas pressure is composed of the pressure of the inert gases at the temperature of the central cavity

$$p(\text{Xe} + \text{Kr}) = \bar{n} R (T(r_0) + \Delta T_2) \quad (19)$$

and the pressure of the vapours

$$p(\text{Rb} + \text{Cs} + \text{Cd}) = \sum_i p_i (T(r_0) + \Delta T_2) \quad (20)$$

with  $p_i$  mostly being the saturation vapour pressure at  $T(r_0) + \Delta T_2$ .

For relative pore volumes  $\alpha \geq 20\%$ , the temperature drop is

$$\Delta T_2 < 0.5 \Delta T_1$$

and the fission-gas pressure remains below the value calculated by model No. 1, which may be written in an approximation for the inert gases as

$$p_{11} = \bar{n} R \frac{\Delta T_1}{\ln \left\{ \frac{T(r_0) + \Delta T_1}{T(r_0)} \right\}} \approx \bar{n} R (T(r_0) + 0.5 \Delta T_1) \quad \left. \begin{array}{l} (21) \\ (5') \end{array} \right\}$$

The central cavity makes it possible to derivate the fission gases into a storage volume, which may result in a considerable reduction of pressure.

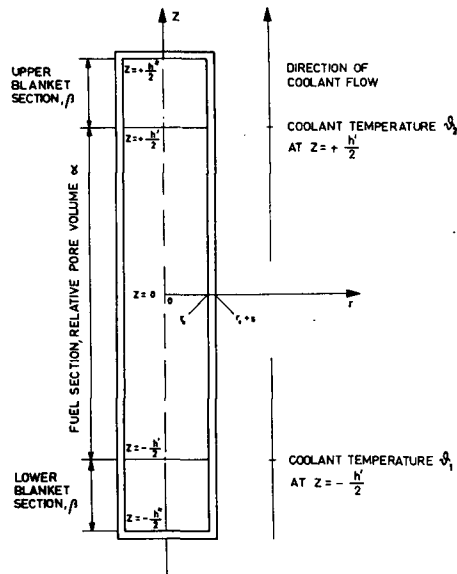


Fig. 1  
Scheme of fuel rod.

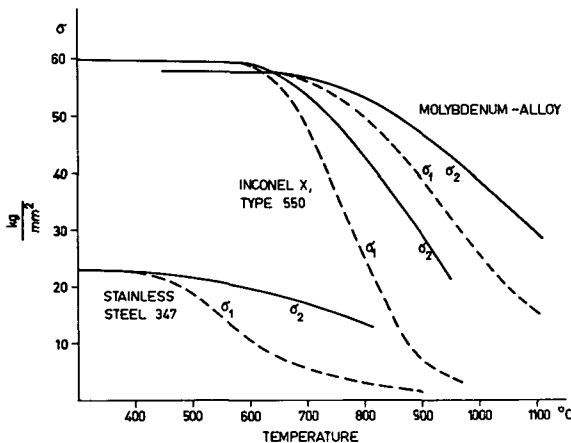


Fig. 2  
Creep strength and yield strength of cladding materials *vs.* temperature.  
 $\sigma_1$  = creep strength ( $10^{-5}/h$ );  $\sigma_2$  = yield strength

### Stability of can

The fission-gas pressure  $p$  causes a hoop-stress  $\sigma$  in the can of the fuel rod which may be described, for low wall thicknesses  $s$ , by the relation

$$\sigma = p \frac{d}{2s}. \quad (22)$$

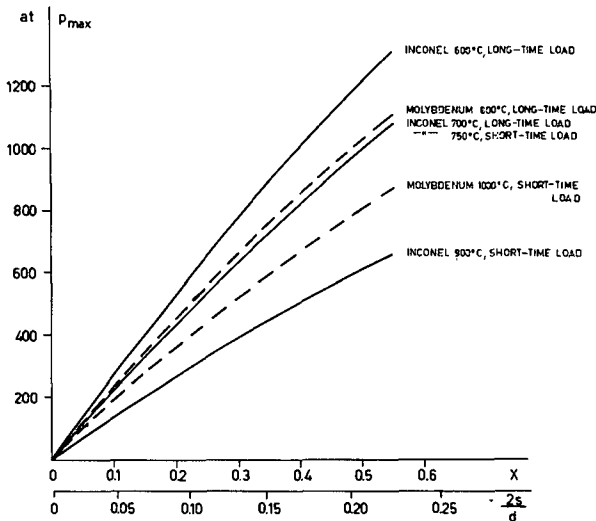


Fig. 3  
Maximum permissible pressure on can at various operating conditions vs. relative can thickness.

It is connected with  $2s/d$  by the relation

$$x = \frac{(d+s)^2 - (d-s)^2}{(d-s)^2} \approx 2 \frac{2s}{d} \left\{ 1 + \frac{2s}{d} \right\}. \quad (24)$$

In this connection,  $d=2r+s$  is the mean tube diameter (*cf.* Fig. 1). Thermal stresses which additionally arise in the can are negligible as against the pressure stress, because of the low wall thickness and of the relatively good thermal conductivity. For this reason, the pressure resistance of the can may be calculated from

$$p = \sigma' \frac{2s}{d}. \quad (23)$$

In case of a long-time load, the creep strength has to be inserted for  $\sigma'$ . In case of a short-time load, the yield strength must be inserted: it is somewhat higher at higher temperatures.

Fig. 2 shows the creep strength  $\sigma_1$  for 1% elongation within 1000 hours and the yield strength for heat-resistant steel, Inconel X Type 550, and a low molybdenum alloy as a function of temperature.

Fig. 3 gives the pressure stability as a function of the relative amount of material,  $x$ , for the materials regarded and for several operating temperatures, where  $x$  is defined as

$$x = \frac{\text{can volume}}{\text{fuel volume}}.$$

### Results: fission-gas pressure and attainable burn-up

The fission-gas pressure was calculated according to the equations for model No. 1. The value for this pressure is about the same as that determined according to model No. 3 and only lower by 10% than that of model No. 2. With a corresponding safety factor, these values may therefore be looked upon as upper limits for all fuel models discussed.

The pressure was calculated for a burn-up of 100 kg Pu<sup>239</sup> per metric ton of fuel (i.e. for about 100 MWd/t fuel). From this the attainable burn-up was determined by comparison with the pressure stability of the can. In this connection, the well-sustained presumption was made that the fission-gas pressure increases as a proportion of the burn-up. A precondition for all calculations is the complete release of the fission gases from the lattice into the pore volume.

The following safety factors were included in calculating the attainable burn-up:

1. The can should withstand short-time operation at 50% overload without damage. Because of the higher can temperature, the yield strength is lower in that case. At the same time, the higher operating temperatures make the fission-gas pressure rise. For simplicity, as maximum pressure the value was taken which is produced if there is no equalization of pressure during the excursion (this is an overestimate):

$$p_{\max} = p_0 \frac{T_{\text{ex}}(r_0, O) + \Delta T_{\text{ex}}(O)}{T_0(r_0, O) + \Delta T_0(O)}. \quad (25)$$

The values indexed 0 refer to normal operation, those marked with an index "ex" denote excursion (overload by 50%).

2. Because of several uncertainties in the calculation, as for instance the pressure contributed by the vapours and the stability of the can materials under irradiation, another safety factor of 1.5 was included, that is to say, the attainable burn-up is defined as the burn-up calculated for 50% overload, divided by 1.5.

Three reactor systems were investigated:

- (a) Fast breeder with Na-cooling and Inconel X, type 550 can.
- (b) Fast breeder with He-cooling and Inconel X, type 550 can.
- (c) Fast breeder with He-cooling and molybdenum (0.5% Ti) can.

The fuel elements are presumed to be rods of some 0.5 cm diameter, and the operating conditions were always adapted to each system.

The fuel is made up of a mixture of porous Pu<sup>239</sup>O<sub>2</sub> and U<sup>238</sup>O<sub>2</sub> in a 1/2 ratio. This ratio results from the requirement of a critical mass as small as possible at a negative Doppler reactivity coefficient\*. This type of fuel will be referred to as oxide fuel.

The thermal conductivity of the oxide fuel can probably be doubled by adding 20% metal (Ni or Mo) (oxide-metal fuel mixture).

Pore component ( $\alpha$ ), storage volumes ( $h''/h'$ ,  $\beta$ ), and can material component ( $x$ ) were varied.

The results of the calculations are given for a small parameter area in Table III.

The burn-up values included in Table III do not yet contain the safety factor of 1.5.

---

\* According to more recent calculations, the 1:2 ratio will lead to a positive Doppler reactivity coefficient. The ratio, therefore, should be changed for future considerations into about 1:4.

TABLE III  
FISSION-GAS PRESSURE AND OBTAINABLE FUEL BURN-UP

System specific power	Cladding temperature (°K)	$T(r_0, O)$ (°K)	$\Delta T(O)$ (°K)	Fuel type	Can/fuel volume ratio	Maximum permissible pressure (atm)	Fission-gas pressure $p$ (atm) at burn-up 100 MWd/kg fuel, and obtainable burn-up $b$ (MWd/kg)								Operating conditions
							Model	$\alpha = 0.1$	$\alpha = 0.2$	$\alpha = 0.3$	$\alpha = 0.1$	$\alpha = 0.2$	$\alpha = 0.3$	$\beta = 0.5$	$h''/h' = 1.5$
Na-Inconel $P_{\text{spec}} = 0.8 \frac{\text{MW}}{\text{kg Pu}}$	873	900	1600	Oxide	0.5	1200	Pressure equalization	$p = 1210$	$p = 550$	$p = 310$	$p = 220$	$p = 400$	$p = 160$	$p = 250$	Full power 50% overload
	1023	1050	(2400)	Oxide	0.5	980		$p = 1750$	$p = 800$	$p = 450$	$p = 320$	$p = 580$	$p = 230$	$p = 360$	
					0.5	980		$b = 56$	$b = 120$	$b = 220$	$b = 300$	$b = 170$	$b = 425$	$b = 270$	
					0.25	530		$b = 30$	$b = 66$	$b = 118$	$b = 165$	$b = 90$	$b = 230$	$b = 145$	
He-Inconel $P_{\text{spec}} = 0.4 \frac{\text{MW}}{\text{kg Pu}}$	873	900	800	Oxide-Metal	0.5	1200	Pressure equalization	$p = 970$	$p = 440$	$p = 250$	$p = 200$	$p = 340$	$p = 140$	$p = 220$	Full power 50% overload at 50% overload at 50% overload
	1023	1050	1200	Oxide-Metal	0.5	980		$p = 1350$	$p = 610$	$p = 350$	$p = 280$	$p = 470$	$p = 195$	$p = 305$	
					0.5	980		$b = 72$	$b = 160$	$b = 280$	$b = 350$	$b = 210$	$b = 500$	$b = 320$	
					0.25	530		$b = 39$	$b = 87$	$b = 150$	$b = 190$	$b = 110$	$b = 270$	$b = 175$	
He-Mo $P_{\text{spec}} = 0.6 \frac{\text{MW}}{\text{kg Pu}}$	973	1000	800	Oxide	0.5	980	Pressure equalization	$p = 1050$	$p = 480$	$p = 270$	$p = 210$	$p = 370$	$p = 150$	$p = 230$	Full power 50% overload at 50% overload at 50% overload
	1173	1200	1200	Oxide	0.5	605		$p = 1400$	$p = 640$	$p = 360$	$p = 280$	$p = 495$	$p = 200$	$p = 310$	
					0.5	605		$b = 43$	$b = 95$	$b = 168$	$b = 216$	$b = 122$	$b = 300$	$b = 195$	
					0.25	330		$b = 23$	$b = 51$	$b = 90$	$b = 118$	$b = 66$	$b = 165$	$b = 106$	
	973	1000	400	Oxide-Metal	0.5	980	Pressure equalization	$p = 900$	$p = 420$	$p = 240$	$p = 190$	$p = 340$	$p = 110$	$p = 210$	Full power 50% overload at 50% overload at 50% overload
	1173	1200	600	Oxide-Metal	0.5	605		$p = 1160$	$p = 540$	$p = 310$	$p = 245$	$p = 440$	$p = 180$	$p = 270$	
					0.5	605		$b = 52$	$b = 112$	$b = 195$	$b = 245$	$b = 137$	$b = 335$	$b = 225$	
					0.25	330		$b = 28$	$b = 61$	$b = 105$	$b = 135$	$b = 75$	$b = 180$	$b = 120$	
	1073	1100	1200	Oxide	0.5	1015	Pressure equalization	$p = 1240$	$p = 580$	$p = 330$	$p = 230$	$p = 420$	$p = 170$	$p = 270$	Full power 50% overload at 50% overload at 50% overload
	1273	1300	1600	Oxide	0.5	800		$p = 1570$	$p = 740$	$p = 420$	$p = 290$	$p = 530$	$p = 215$	$p = 345$	
					0.5	800		$b = 52$	$b = 108$	$b = 190$	$b = 275$	$b = 148$	$b = 370$	$b = 230$	
					0.25	440		$b = 28$	$b = 59$	$b = 105$	$b = 152$	$b = 83$	$b = 205$	$b = 127$	
	1073	1100	600	Oxide-Metal	0.5	1015	Pressure equalization	$p = 1050$	$p = 500$	$p = 280$	$p = 210$	$p = 380$	$p = 160$	$p = 240$	Full power 50% overload at 50% overload at 50% overload
	1273	1300	900	Oxide-Metal	0.5	800		$p = 1360$	$p = 650$	$p = 365$	$p = 275$	$p = 500$	$p = 210$	$p = 310$	
					0.5	800		$b = 59$	$b = 123$	$b = 220$	$b = 290$	$b = 160$	$b = 380$	$b = 258$	
					0.25	440		$b = 32$	$b = 67$	$b = 120$	$b = 160$	$b = 88$	$b = 210$	$b = 142$	

$T(r_0, O)$  = surface temperature of fuel rod at core centre;

$\Delta T(O)$  = temperature drop in fuel rod at core centre;

$\alpha$  = void fraction in fuel section;

$\beta$  = void fraction in breeding section;

$h'$  = length of fuel section;

$h''$  = length of fuel + breeding section.

The investigation has this result: with oxide fuel permitting the fission gas to escape into the pore volume, it is possible to obtain a very high burn-up if suitable canning material is used and the pore volume is made sufficiently large.

For a burn-up of some 100 MWd/kg fuel, corresponding to a burn-up of some 30% of the fissile  $\text{Pu}^{239}$  nuclei at the enrichment of 33% quoted, one needs the components of pore and canning material, given in Table IV, where the safety factor of 1.5 has been taken into account\*.

From Table IV the value of the storage volumes may be seen. They make it possible to reduce at equal burn-up the pore component in the fuel and the canning material component, which in turn is of advantage for critical mass and breeding ratio.

According to Table IV, the pure oxide fuel is more advantageous than the oxide-metal fuel mixture. This is because the operating data were adapted to the oxide fuel. The fuel mixture, however, delays melting of the fuel during powerex cursons and permits larger fuel-element dimensions, thus reducing fabricating costs.

#### Discussion of results and optimization

In order to achieve high burn-up, one has to put up with either a large pore volume, i.e. low fuel density, or a high percentage of canning material. This adversely influences the critical mass and breeding ratio. It still remains open to debate which combination of parameters,  $(x; \alpha)$  or  $(x; \alpha, \beta, h''/h')$ , is best suited for the desired burn-up of 100 kg Pu per ton of fuel.

TABLE IV  
CAN/FUEL VOLUME RATIO ( $x$ ) AND PORE/FUEL VOLUME RATIO ( $\alpha$ )  
NECESSARY TO OBTAIN A BURN-UP OF 100 MWd/kg FUEL, AND EFFECT OF  
STORAGE VOLUME

System	$x$	$\alpha$ or $\alpha'; \beta; h''/h'$	Fuel
Na-Inconel (specific power 0.8 MW/kg Pu)	0.5	0.23 or 0.1; 0.5; 1.20	Oxide
	0.25	0.34 or 0.1; 0.5; 1.45	Oxide
	0.5*	0.30 or 0.1; 0.5; 1.38	Oxide-metal
He-Inconel (specific power 0.4 MW/kg Pu)	0.5	0.275 or 0.1; 0.5; 1.35	Oxide
	0.25	0.40 or 0.1; 0.5; 1.70	Oxide
	0.5*	0.37 or 0.1; 0.5; 1.60	Oxide-metal
He-Mo (specific power 0.6 MW/kg Pu)	0.5	0.25 or 0.1; 0.5; 1.26	Oxide
	0.25	0.38 or 0.1; 0.5; 1.50	Oxide
	0.5*	0.34 or 0.1; 0.5; 1.45	Oxide-metal

\* The value of  $x = 0.5$  in the oxide-metal fuel mixture includes the metal portion of the fuel; only  $x' = 0.25$  is due to the can. Identical values of  $x$  furnish identical critical masses and breeding ratios.

\* These pore components must be present after a burn-up of 100 MWd/t. Correspondingly, the original pore volume must be larger than the volume of the original fissionable material by the volume the solid fission products take up. At 100 MWd/t, this may amount to 10%.

For the combination of parameters ( $x; \alpha$ ) this question could be decided by a one-dimensional multi-group calculation in an IBM-704 computer. The effect of storage volumes on critical mass ( $M_c$ ) and breeding ratio ( $R_b$ ) could not be determined by the one-dimensional calculation.

Fixed values in this calculation were

Percentage of coolant in the core	40 vol. %
Percentage of structural material in the core	15 vol. % (identical materials for structure and can)
Fuel composition	$\text{Pu}^{239}\text{O}_2/\text{U}^{238}\text{O}_2 = 1/2$
Composition of blanket:	
Steel	20 vol. %
$\text{U}^{238}$	80 vol. %
Steel	20 vol. %
$\text{U}^{238}$	64 vol. %
Na	16 vol. %
Blanket thickness	about 80 cm

Varied were the relative volumes of can

$$x = \frac{\text{volume of canning material}}{\text{volume of } \text{UO}_2 + \text{PuO}_2}$$

and the fuel density or relative pore volume  $\alpha \dots$

Table V shows results of this calculation for a pore volume of 25%.

Figs. 4 and 5 show the dependence on the pore volume of critical mass and breeding ratio for the helium-Inconel reactor with  $x=0.5$ . As a rule of thumb one may take it from these calculations that

an increase in the pore volume by 1%  $\left\{ \begin{array}{l} \text{increases } M_c \text{ by about 1.2\%* or 1.6\%**} \\ \text{decreases } R_b \text{ by about 0.0012* or 0.0025**.} \end{array} \right.$

TABLE V  
RESULTS OF MULTI-GROUP CALCULATION

System	$x = 0$	$x = 0.25$	$x = 0.5$	$x = 1$
Na-Inconel	$M_c$ 132 kg	169 kg	206 kg	284 kg
	$R_{bi}$ 0.189	0.203	0.216	0.239
	$R_{be}$ 1.518	1.367	1.242	1.046
	$R_{bt}$ 1.707	1.570	1.458	1.285
He-Inconel	$M_c$ 150 kg	190 kg	233 kg	333 kg
	$R_{bi}$ —	—	0.202	0.222
	$R_{be}$ —	—	1.333	1.137
	$R_{bt}$ 1.780	1.648	1.535	1.359
He-Mo	$M_c$ 162 kg	258 kg	420 kg	1595 kg
	$R_{bi}$ 0.181	0.190	0.197	0.209
	$R_{be}$ 1.486	1.223	0.978	0.497
	$R_{bt}$ 1.667	1.413	1.175	0.706

$M_c$  = critical mass;  $R_b$  = breeding ratio; i = internal; e = external; t = total.

\* Inconel systems.

\*\* Molybdenum systems.

A better measure of the qualities of a breeding reactor than the breeding ratio is the doubling time. Doubling time  $T_D$  for internal plus external inventory form a relation with the breeding ratio  $R_b$ , the specific power  $P_{\text{spec}}$  (MW/kg Pu), the burn-up  $b'$  (MWd/kg Pu), and the reprocessing time  $T_R$ :

$$T_D = \frac{1}{R_b - 1} \left\{ \frac{A}{P_{\text{spec}}} + \frac{A - b'}{b'} T_R \right\}. \quad (26)$$

$A$  is the fission energy released per kg of Pu<sup>239</sup> at complete burn-up:

$$A \approx 1000 \text{ MWd/kg Pu}. \quad (27)$$

For the burn-up, we use the terms  $b$  and  $b'$ , where  $b$  is burn-up in megawatt-days per kilogram of fuel, the fuel being a UO<sub>2</sub>—PuO<sub>2</sub> mixture, and  $b'$  is the burn-up in megawatt-days per kilogram of plutonium.  $T_R$  will be assumed to be 200 d.

Table VI gives a survey of nuclear data (breeding ratio and critical mass) and operational data (doubling time and burn-up period) for the reactor systems included in Table IV. In the calculation, the reduction in the pore volume by the volume of the solid fission products was not taken into account. At an initial

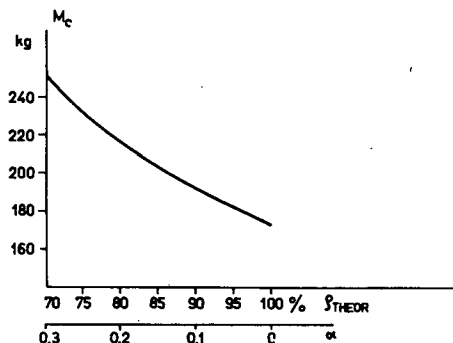


Fig. 4  
Critical mass  $M_c$  vs. relative fuel density and/or relative volume of pores in fuel.

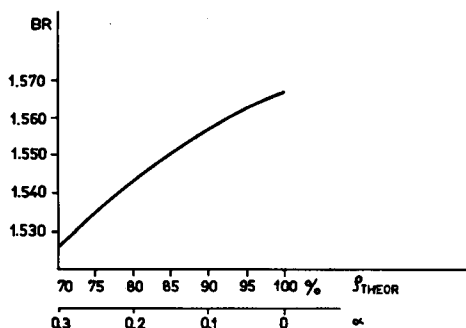


Fig. 5  
Breeding ratio  $R_b$  vs. relative fuel density and/or relative volume of pores in fuel.

TABLE VI  
COMPARISON AMONG DIFFERENT REACTOR SYSTEMS

System	$P_{\text{spec}}$ MW/kg Pu	$x$ Can/fuel volume ratio	$\alpha$	$BR$	$T_D^*$ (Years)	$M_c$ (kg Pu <sup>239</sup> )	Burn-up period (Years)
Na-Inconel	0.8	0.5	0.23	1.458	15	202	0.85
	0.8	0.25	0.34	1.554	13	204	0.85
He-Inconel	0.4	0.5	0.28	1.513	21	240	1.70
	0.4	0.25	0.40	1.622	18	225	1.70
He-Mo	0.6	0.5	0.25	1.175	48	420	1.30
	0.6	0.25	0.38	1.381	21	308	1.30

\* 80 % load factor assumed.

pore volume of  $\alpha \times$  volume-of-fuel there is only a pore volume of  $\alpha' \times$  volume-of-fuel at the end of the burn-up period for taking up the fission gases, with

$$\alpha' = \alpha - \Delta\alpha(b) \quad (28)$$

$$\Delta\alpha(b) \leq 1\% \text{ per MWd/kg fuel.} \quad (29)$$

Part of the reduction in volume is compensated by the elongation of the fuel element can.

If one regards the values  $\alpha$  as portions of the pores in the new fuel element, the attainable burn-up of  $b = 100$  MWd/kg fuel will be reduced to about  $b = 65$  MWd/kg fuel because of  $\alpha' < \alpha$ . At 33% enrichment, this means a burn-up of some 20% of the Pu<sup>239</sup> nuclei, or  $b' \approx 200$  MWd/kg Pu.

The following facts may be gathered from Table VI:

1. In general, it is more favourable to use a relatively high pore component and low can thickness, because the materials Inconel and molybdenum are neutron absorbers. Especially with molybdenum, the can thickness is critical, as can be seen from a comparison between the two values for  $x = 0.25$  and  $x = 0.5$ . The possible pore content of the fuel is determined by the manufacturing processes and by safety considerations.

2. Because of the high burn-up, the fuel elements stay in the reactor for about one year. Thus the operation of the power plant is not impeded by frequent exchange of fuel elements\*.

3. Doubling times of 15 to 20 years can be attained. The plutonium credit and the low number of reprocessing operations lead to low fuel-cycle costs.

4. Despite the use of porous oxide fuel at an enrichment of 33%, the fuel inventory may be kept below 300 kg of Pu<sup>239</sup>. This enables the design of small and medium-sized plants. In order to assure a negative Doppler reactivity coefficient, the fuel enrichment probably has to be lowered to about 20—25%. This might change the situation to some extent.

The systems having an additional storage volume for the fission gases could not be investigated in the one-dimensional calculation. However, it is to be expected

\* The low internal breeding ratio may, however, necessitate reloading operations for reactivity reasons.

that, because of their lower portions of canning material and pore volume in the core, they will lead to more favourable critical masses and breeding ratios.

We plan to investigate the properties of special oxide and oxide-metal fuels under irradiation. We shall attempt to measure the pressure build-up during irradiation and to determine the composition of the gaseous or vaporous fission products.

#### REFERENCES

- [1] DILLON, I. G. and BURRIS, L. Jr., *Nucl. Sci. Engng* **2** (1957) 567.
- [2] LANDOLT and BOERNSTEIN, Zahlenwerte und Funktionen, Springer, vol. **2** (1960) Pt. 2, pp. 3f.
- [3] ROBERTSON, J. A. L. *et al.*, Proc. 2nd. UN Int. Conf. PUAE **6** (1958) 655.



# FISSION-PRODUCT BURN-UP IN FAST REACTORS

M. M. LEVINE

BROOKHAVEN NATIONAL LABORATORY, UPTON, N.Y.,  
UNITED STATES OF AMERICA

## Abstract — Résumé — Аннотация — Resumen

**Fission-product burn-up in fast reactors.** In fast reactors where breeding is emphasized the burn-up of fission products can be of considerable importance. Statistical estimates of fission-product cross-sections are combined with recent yield data for the various fissionable species to estimate the gross fission-product cross-section as a function of irradiation time in a number of fast reactor spectra with various fuels.

Because of gaps in yield data for some of the fuel species, it is necessary to interpolate on the yield curves in some cases. The chain yield for a given mass is then apportioned among the chain members through use of the equal charge displacement recipe. The cross-sections estimated for  $U^{235}$  fission products by previous authors are supplemented by estimates for fission products important for other fuels.

A range of such spectra is considered. These spectra are characterized by the index  $\langle \text{average } (E^{-1/2}) \rangle$  in the spectra. The sensitivity of the gross poisoning and its burn-up with respect to spectrum variations are considered.

The results are also expressed in terms of a few pseudo-fission products, so that changes in effective cross-section of fission products with irradiation can be taken into account in a simple computational fashion.

**Combustion des produits de fission dans les réacteurs à neutrons rapides.** La combustion des produits de fission peut présenter une grande importance dans les réacteurs à neutrons rapides où la surgénération est primordiale. L'auteur associe des estimations statistiques relatives aux sections efficaces des produits de fission aux données récentes relatives au rendement de fission de diverses matières fissiles, afin d'évaluer la section efficace globale des produits de fission en fonction du temps d'irradiation dans un certain nombre de spectres neutroniques de réacteurs à neutrons rapides avec divers combustibles.

Du fait des lacunes des données numériques relatives à certains combustibles, il faut parfois procéder à des interpolations dans les courbes de rendement. Le rendement de la réaction en chaîne est réparti parmi les différents produits de la réaction en se basant sur la méthode du déplacement de charge identique. Les sections efficaces évaluées par d'autres auteurs pour les produits de fission de  $^{235}\text{U}$  sont complétées par des estimations relatives à des produits de fission d'autres combustibles.

L'auteur étudie certaines zones de ces spectres, qui sont caractérisés par l'indice  $\langle (E^{-1/2}) \text{ moyen} \rangle$  dans les spectres. Il étudie, en fonction des variations du spectre, la sensibilité de l'empoisonnement global et la combustion qui s'ensuit.

Les résultats sont également exprimés en termes de quelques produits de pseudo-fission, de sorte qu'il peut être tenu compte des variations de la section efficace effective des produits de fission avec l'irradiation au moyen d'une méthode de calcul simple.

**Выгорание продуктов деления в реакторах на быстрых нейтронах.** В реакторах на быстрых нейтронах, где упор делается на расширенное воспроизведение ядерного топлива, большое значение имеет выгорание продуктов деления. Статистические оценки сечения продуктов деления объединяются с недавно полученными данными для различных делящихся изотопов, чтобы оценить полное сечение продуктов деления, как функции времени облучения в ряде спектров быстрых реакторов с различным топливом.

Вследствие недостатка в имеющихся данных для некоторых видов топлива необходимо в некоторых случаях интерполировать кривые выхода. Выход изобарной цепочки при делении для данной массы распределяется затем среди членов цепочки путем использования метода равного смещения заряда. Поперечное сечение, определенное предыдущими авторами для продуктов деления урана-235, дополняется оценками для продуктов деления важных для других видов топлива.

Учитывается диапазон такого спектра. Эти спектры характеризуются индексом  $\langle$ среднее значение ( $E^{-1/2}$ ) $\rangle$  в спектре. Рассматривается чувствительность полного отравления и выгорания по отношению к вариациям спектра.

Результаты выражены также в членах нескольких псевдоделящихся продуктов так, что изменения в эффективном поперечном сечении продуктов деления с облучением могут быть учтены при помощи простого вычисления.

**Combustible de los productos de fisión en los reactores rápidos.** La combustión de los productos de fisión puede presentar una importancia considerable en los reactores rápidos en que la reproducción desempeña un papel primordial. El autor combina las evaluaciones estadísticas de las secciones eficaces de los productos de fisión con los datos más recientes sobre rendimientos de fisión para las diversas especies fisionables, con el fin de calcular la sección eficaz global de los productos de fisión en función del tiempo de irradiación en cierto número de espectros neutrónicos de reactores rápidos alimentados con distintos combustibles.

En algunos casos, debido a la falta de datos numéricos sobre el rendimiento para algunas de las especies combustibles, es preciso proceder a interpolaciones en las curvas respectivas. En estas condiciones, el rendimiento de la reacción en cadena, para una masa dada, se prorrata entre los eslabones de la cadena, aplicando el procedimiento del desplazamiento de cargas iguales. Las secciones eficaces evaluadas por otros autores para los productos de fisión del  $^{235}\text{U}$  se complementan con estimaciones relativas a los productos de fisión correspondientes a otros combustibles.

El autor examina una serie de tales espectros, que se caracterizan por el índice  $\langle(E^{-1/2}) \text{ medio} \rangle$  en los espectros. Estudia, en función de las variaciones del espectro, la sensibilidad del envenenamiento global y de la combustión consiguiente.

Los resultados se expresan también con referencia a unos pocos productos de pseudofisión, de modo que, mediante un simple cálculo, se pueden tomar en cuenta las variaciones de la sección eficaz efectiva de los productos de fisión a medida que la radiación progresá.

## Introduction

The character of fission-product poisoning in a fast reactor differs considerably from that in a thermal reactor. In the thermal system, the fission-product cross-sections go over a total range from zero to many thousands of times the fuel atom cross-sections; and in a thermal reactor, even aside from the very quickly saturating poisons there are a considerable number of poisons with cross-sections comparable to and somewhat larger than the fuel cross-section. This broad range of thermal cross-sections is due to the fact that in such a large ensemble of nuclear species as the group of fission products, there will be many members with lowest resonances quite close to thermal energy. In a fast-reactor spectrum, on the other hand, the cross-sections of importance are at such high energies and averaged over such large ranges of energies that the accidents of the exact locations of the resonances become of practically no importance, and most of the poisoning comes from fission products with a much narrower range of cross-sections. Thus the behaviour in time of fission-product poisoning in a fast reactor should show a much simpler behaviour than that in a thermal reactor as given in detail by WALKER [1].

The gross fission-product poisoning in a fast reactor does, however, change its character slowly as the irradiation proceeds. There are two main reasons for this—first the preferential burn-up of the higher cross-section poisons brings about a decreasing poison increment per fission, and secondly the change in the reactor spectrum as a function of burn-up causes the effective average cross-section of the individual fission products to change. The latter effect is probably important only for those reactors initially charged with one species of fuel and breeding substantial amounts of another (e.g. a U<sup>235</sup>-loaded plutonium breeder).

### Gross fission-product cross-sections

To find the effective poisoning as a function of irradiation time, it is necessary to have information both on cross-section of fission products as functions of energy and on the spectra in which the irradiation takes place. A number of authors [2, 3, 4, 5, 10] have estimated the cross-sections of fission products at high energy. These estimates are to a large extent indirect, having been based on statistical models for resonance parameter distribution and on nuclear systematics for the estimates of the average resonance parameters themselves. It is not surprising therefore that there is appreciable disagreement among the results obtained by the various authors. The present work used the cross-section estimates of GREEBLER, HURWITZ and STORM [2]. The later work of Roos and GARRISON [5] and of BENZI and SARUIS [10] has exploited much new information on strength functions and appears to be a more accurate estimate. These results will be used in subsequent work.

The effects of the radioactive decay of the fission products were taken into account only approximately. That is, fission products with half-lives of the order of a year and up were treated as stable, and the rest were assumed to decay immediately.

Taking as the independent variable the fuel burn-up  $F$  defined by

$$F = \int_0^t \sigma_F \varphi dt \quad (1)$$

the equations for the concentrations  $N$  and  $M$  of a direct fission product (first generation) and its direct descendent through neutron capture (second generation) are

$$\left. \begin{aligned} \frac{dN}{dF} &= y N_f - N\sigma/\sigma_F \\ \frac{dM}{dF} &= N\sigma/\sigma_F - M s/\sigma_F \end{aligned} \right\} \quad (2)$$

where  $y$  is the yield of the fission product;  $\sigma$  and  $s$  are the cross-sections of the fission product and its descendent; and  $N_f$  and  $\sigma_F$  are the concentration and fission cross-section of the fuel.

The quantity of barns per fission, denoted by  $\gamma$ , is defined here as

$$\left. \begin{aligned} \gamma &= d(N\sigma + Ms)/d(N_f\sigma_F\varphi t) \\ &= (\sigma dN/dF + s dM/dF)/N_f. \end{aligned} \right\} \quad (3)$$

Making use of the solution of Eqs. 2 gives

$$\gamma = y\sigma e^{-\frac{\sigma}{\sigma_F} F} \left[ 1 + \frac{s}{\sigma - s} \left( e^{\frac{\sigma-s}{\sigma_F} F} - 1 \right) \right]. \quad (4)$$

The term in square brackets gives the correction due to the second generation.

It is useful to evaluate Eq. (4) approximately. To lowest order in  $F$  it is

$$\gamma \approx y\sigma - (y\sigma^2 - y\sigma s) F/\sigma_F. \quad (5)$$

If we sum over all fission-product species  $i$ , then it is clear that (to first order) the ratio of the positive contribution by the second-generation poison to the negative contribution caused by burn-up of the first-generation poisons is

$$r = \sum_i y_i \sigma_i s_i / \sum_i y_i \sigma_i^2. \quad (6)$$

Because of the small degree of correlation to be expected between the cross-sections of the first and second generations (more accurately, one expects an anti-correlation), it is clear that this ratio  $r$  should be small. For typical cases in the range of spectra considered here, this ratio varied approximately from 0.25 to 0.35. Therefore, for the purpose of simplifying the calculation, it will be assumed that the effect of the second generation can be described adequately by considering only first-generation burn-up but decreasing the burn-up rate by 30%, the approximate average value of  $r$ . This approximation, although somewhat rough, ought to be all right in view of the uncertainties in the cross-sections themselves.

Hence the gross barns-per-fission value will be taken as

$$\gamma = \sum_i y_i \sigma_i e^{-\frac{\sigma_i}{\sigma_F} F} \quad (7)$$

and the appropriate corrections for second-generation effects will be performed on the results.

### Spectrum effects

Eq. (7) requires knowledge of the fission-product cross-sections averaged over the reactor spectrum. A range of reactor spectra were considered. They were drawn from several sources [6, 7, 8] and are listed in Table I. They were chosen to give a range of representative spectra rather than for the significance of the particular reactor systems from which they were drawn. It is necessary to find some way of characterizing the spectrum shape with regard to hardness and other characteristics. Use of the average fission cross-section, the median fission energy, or other indices which depend on the shape of the fuel cross-section *vs.* energy are probably not so useful for this purpose as some index which depends rather on the shape of the cross-fission-products cross-section *vs.* energy. Since the latter changes with fuel and with burn-up, however, the simple expedient of quoting the average value (in the spectrum) of  $E^{-1/2}$  is taken. This is not too far different from the behaviour of most cross-sections at high energy; however, the best indication of the usefulness of this index is that the results show a fairly smooth behaviour when plotted against it, despite the fact that the spectra were drawn from several quite different sources. Further work on just how to characterize the spectrum might, however, be useful.

TABLE I  
SOURCES FOR SPECTRA

Spectrum No.	Ref.	Description	$\langle E^{-1/2} \rangle \text{ MeV}^{-1/2}$
1	[6]	PuA oxide, 2500 l	7.42
2	—	Interpolated between 1 and 3	6.45
3	[7]	Fast oxide breeder	5.70
4	—	Interpolated between 3 and 5	4.96
5	[6]	PuA oxide, 800 l	4.14
6	[6]	PuA metal, 2500 l	3.60
7	[6]	PuA metal, 800 l	2.71
8	[8]	Pu Bi breeder	2.41
9	[8]	Pu Bi breeder	1.93
10	—	Fission spectrum	0.73

The weighting of the cross-sections of the fission products and the fissile atoms were carried out in a simple scheme which is a variation of the multi-group treatment. The cross-sections at energies of  $10^2$ ,  $10^3$ ,  $10^4$ ,  $10^5$  and  $10^6$  eV were taken from the sources quoted and assumed to vary linearly in lethargy between these points. (Cross-section vs. lethargy was extrapolated up to  $10^7$  eV according to the straight line in the preceding lower energy range. However, this high-energy cross-section has little influence on the results in the spectra investigated here.) Then it is possible to define weights  $w_n$  for any given spectrum such that

$$\bar{\sigma} = \sum_n w_n \sigma(E_n) \quad (8)$$

making it a simple task to obtain average cross-sections for any spectrum and any fission product once the weighting functions are established for that spectrum.

The  $w_n$  values are obtained from the spectrum by

$$w_n = X_n - X_{n-1} + I_n \quad (9)$$

where

$$X_n \equiv \left[ n \int_{n \ln 10}^{(n+1) \ln 10} \varphi(u) du - \frac{1}{\ln 10} \int_{n \ln 10}^{(n+1) \ln 10} u \varphi(u) du \right] / \int_0^\infty \varphi(u) du \quad (10)$$

$$I_n \equiv \int_{n \ln 10}^{(n+1) \ln 10} \varphi(u) du / \int_0^\infty \varphi(u) du .$$

The very large number of fission products makes an evaluation of Eq. (7) a rather formidable task when non-zero values of  $F$  are involved. Hence the evaluation was carried out by means of a digital computer.

One effect not taken into account is the increasing amount of resonance self-shielding as the fission products build up. The amount of self-shielding cannot be estimated from the averaged cross-sections as used here, but rather it must be computed from the peak cross-sections of the individual resonances making up these cross-sections. This correction will be investigated in subsequent work.

Because the effective cross-section of the fuel varies so strongly with spectrum, a simple statement of the value of  $\gamma$  is not nearly so informative here as it is in

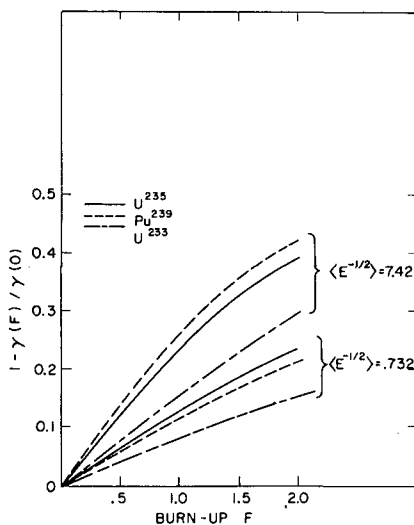


Fig. 1  
Effect of burn-up fission poisoning  $1 - \gamma(F)/\gamma(0)$  vs. burn-up  $F$ .

the case of a thermal reactor, where the average fuel cross-section is predominantly that in the thermal group and is not particularly sensitive to changes in epithermal spectrum. Therefore, instead of quoting barns/fission values, Fig. 1 shows the ratio of absorptions in fission products at burn-up  $F$  to the initial value  $(\gamma(0) - \gamma(F))/\gamma(0)$  as a function of burn-up for two different values of the spectral index. This gives a qualitative picture of how important the burn-up of the fission products is.

For the purpose of including these results in actual reactor calculations, another approach is more useful. For each fissile material it is possible to find a pseudo fission product having such values of yield and cross-section that it matches the

TABLE II  
PSEUDO-FISSION-PRODUCT  
YIELDS AND CROSS-SECTIONS

Spec- trum No.	$\langle E^{-1/2} \rangle$ MeV $^{-1/2}$	U-233			U-235			Pu-239		
		$\bar{\gamma}$	$\bar{\sigma}$	$\sigma_F$	$\bar{\gamma}$	$\bar{\sigma}$	$\sigma_F$	$\bar{\gamma}$	$\bar{\sigma}$	$\sigma_F$
1	7.42	1.25	0.473	4.00	1.36	0.500	2.77	1.55	0.536	2.70
2	6.45	1.21	0.383	3.74	1.31	0.404	2.56	1.48	0.442	2.47
3	5.70	1.16	0.316	3.54	1.25	0.335	2.40	1.42	0.369	2.31
4	4.96	1.13	0.270	3.29	1.22	0.286	2.22	1.37	0.321	2.21
5	4.14	1.08	0.225	3.02	1.17	0.238	2.02	1.81	0.270	2.10
6	3.60	0.99	0.176	2.94	1.07	0.187	1.91	1.19	0.220	1.98
7	2.71	0.88	0.137	2.58	0.96	0.145	1.68	1.05	0.178	1.89
8	2.41	0.81	0.133	2.45	0.90	0.139	1.61	0.99	0.171	1.88
9	1.93	0.79	0.119	2.28	0.86	0.127	1.50	0.94	0.158	1.86
10	0.73	0.70	0.109	1.87	0.74	0.120	1.25	0.84	0.144	1.86

gross fission-product-poisoning behaviour. That is, it is possible to find yield  $\bar{y}$  and cross-section  $\bar{\sigma}$  such that

$$\bar{y}\sigma e^{-\frac{\sigma}{\sigma_F}} \approx \gamma \quad (11)$$

to good accuracy over a range of burn-up to  $F=2$ . These values are presented in Table II and plotted in Figs. 2 and 3 vs. the spectrum index.  $\bar{y}$  and  $\bar{\sigma}$  were

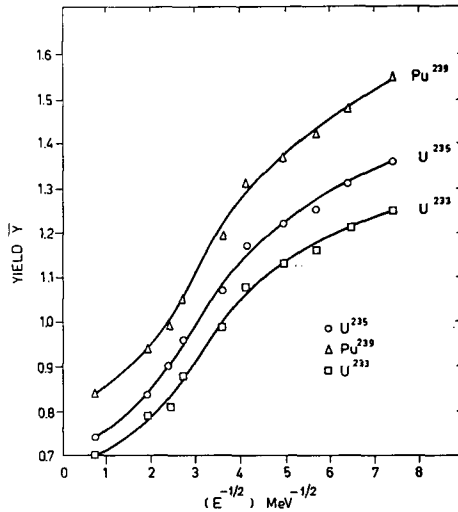


Fig. 2  
Yield of pseudo fission product *vs.* spectrum index  $\langle E^{-1/2} \rangle$ .

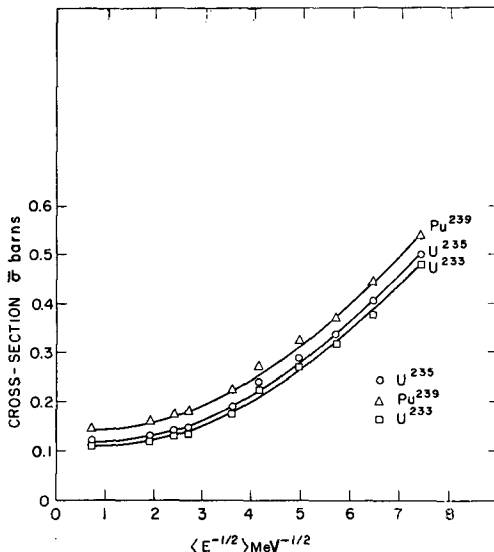


Fig. 3  
Cross-section of pseudo fission product *vs.* spectrum index  $\langle E^{-1/2} \rangle$ .

TABLE III  
FISSION CROSS-SECTIONS OF FUELS

$E$ (MeV)	$\sigma_F$ ( $U^{233}$ )	$\sigma_F$ ( $U^{235}$ )	$\sigma_F$ ( $Pu^{239}$ )
$10^0$	1.95	1.3	1.85
$10^{-1}$	2.65	1.7	1.8
$10^{-2}$	6.0	3.7	2.4
$10^{-3}$	10.0	8.5	6.0
$10^{-4}$	30.0	23.0	24.0

chosen to make the pseudo fission-product poisoning agree exactly with the gross fission-product poisoning at  $F=0$ , and even for large values of  $F$  the error in  $\gamma(0) - \gamma(F)$  is not more than about 10%, which is much more than adequate in view of the uncertainties in the cross-sections of the fission products themselves.

Fission-product cross-sections and  $U^{235}$ -yields on which these results were based are those of Greebler, Hurwitz and Storm [2]. The  $U^{233}$ - and  $Pu^{239}$ -yields are from the compilation by HYDE [9]. Many of the cross-sections given by Garrison and Roos [5] and by Benzi and Saruis [10] are considerably higher in the important  $10^4$ - to  $10^5$ -eV range than those of Greebler, Hurwitz and Storm. This will cause a corresponding difference in the  $\sigma$ -values of the pseudo fission products, but probably much less difference in the yields of the pseudo fission products. Hence, until this work is extended to the cross-sections of Garrison and Roos, it appears to be reasonable approximation to use the  $\bar{y}$  values developed here and to obtain the  $\bar{\sigma}$ -values from the Garrison and Roos data by defining

$$\bar{\sigma} = \left( \sum_i y_i \sigma_i \right) / \bar{y}. \quad (12)$$

The values in Table II and Fig. 2 are not the direct results of the matching between Eq. (11) and Eq. (7). In accordance with the earlier discussion about second-generation fission-products, the  $\bar{\sigma}$  has been lowered by 30% and  $\bar{y}$  has been raised correspondingly in order to keep  $\gamma(0) = \bar{y}\bar{\sigma}$  correct but to decrease the rate at which  $\gamma$  falls off as the burn-up proceeds.

It should be observed that these results do not depend on the accuracy of the values of the fission cross-sections of the fuel atoms in Table III. As Eqs. (7) and (11) show, the fission cross-section enters only in the combination  $F/\sigma_f$ , so that changes in  $\sigma_f$  can be likened to changes in  $F$ , thereby modifying the range of the fit between Eqs. (11) and (7).

Because of the way the fitting of the pseudo fission products was done, it is possible to rewrite (Eq. 11) in the form

$$\gamma(F) = \sum_i y_i \sigma_i e^{-\frac{\sum_i y_i \sigma_i}{\bar{y} \sigma_F}} \quad (13)$$

and therefore

$$\frac{\delta \gamma}{\gamma} = \frac{\sum_i y_i \sigma_i}{\bar{y} \sigma_F} F \frac{\delta \bar{y}}{\bar{y}} = \frac{\bar{\sigma}}{\sigma_F} F \frac{\delta \bar{y}}{\bar{y}}. \quad (14)$$

Since  $\sigma/\sigma_F$  as shown in Table I is never more than 0.2, it is clear that the percentage error in  $\gamma$  is considerably less than in  $\bar{\gamma}$  even for the largest value of  $F$  considered here, and is of course proportional to  $F$ . The contribution of fission products which result from symmetric and near symmetric fission—omitted by Greebler, Hurwitz and Storm because of their small effect—is of little importance even in the hard spectra considered here. For  $\text{Pu}^{239}$  this contribution was less than 2% of the burn-up effect, and it was smaller for  $\text{U}^{233}$  and  $\text{U}^{235}$ . The error in matching the pseudo fission products to the gross fission products is negligible, but the error in the quantity  $\sum_i y_i \sigma_i$ , i.e. in the original data, is likely to be quite large and probably cannot be assessed properly until the basic cross-section information is more firmly established.

#### REFERENCES

- [1] WALKER, W. H., CRRP-634 (1956).
- [2] GREEBLER, P., HURWITZ, H. and STORM, M. L., *Nucl. Sci. and Engng* **2** (1957) 334.
- [3] BUSINARO, U. L., GALLONE, S. and MORGAN, D., *J. nucl. Energy* **4** (1957) 319.
- [4] GORDEEV, I. V. and PUPKO, V. Y., Proc. 2nd UN Int. Conf. PUAE **16** (1958) 141.
- [5] GARRISON, J. D. and ROOS, B. W., GA-2112 (1961).
- [6] YIFTAH, S. and OKRENT, D., ANL-6212.
- [7] GREEBLER, P., ALINE, P. and SUEOKA, J., GFAP-3287 (1959).
- [8] ARONSON, A., BNL Memo (June 1961).
- [9] HYDE, F. K., UCRL-9036 (1960).
- [10] BENZI, V. and SARUIS, A. M., *These proceedings*, Vol. I, p. 179.



# EFFECT OF THE PLUTONIUM ISOTOPIC COMPOSITION ON THE PERFORMANCE OF FAST REACTORS

S. YIFTAH

ISRAEL ATOMIC ENERGY COMMISSION,  
ISRAEL

**Abstract — Résumé — Аннотация — Resumen**

**Effect of the plutonium isotopic composition on the performance of fast reactors.** The isotopic composition of plutonium to be used as fuel for fast reactors will depend on the source of plutonium. In principle three different sources are possible: (a) production reactors; (b) thermal power reactors (using natural uranium or enriched uranium as fuel); (c) fast reactor blankets.

In general, source (a) and to some extent source (c) will provide relatively "clean" plutonium, that is mostly  $\text{Pu}^{239}$ , while plutonium from source (b) will be "dirty" plutonium, that is plutonium rich in  $\text{Pu}^{240}$ ,  $\text{Pu}^{241}$ , and  $\text{Pu}^{242}$ . The degree of "dirtiness" will depend on the kind of reactor, amount of burn-up and in general on the irradiation history of the fuel.

The question then arises, can one use as fuel for fast reactors any kind of plutonium?

To investigate the effect of different isotopic composition of the plutonium fuel, in the metallic, oxide and carbide form, on the performance of fast reactors, a limited series of spherical geometry 16-group diffusion theory calculations were performed, using the 16-group cross-section set developed recently by Yiftah, Okrent and Moldauer and taking three different kinds of plutonium, starting with pure  $\text{Pu}^{239}$  and increasing the amount of higher isotopes.

For the systems studied—800, 1500 and 2500-l core-volumes, which are typical for large fast power reactors—the result is, when one takes into account only the thermally fissionable isotopes  $\text{Pu}^{239}$  and  $\text{Pu}^{241}$ , that the "dirtier" the plutonium, the smaller the critical mass and the higher the breeding ratio.

For the 1500-l reactor, taken as an example, it is further found that in the metallic, oxide and carbide plutonium fuels the reactivity change upon removal of 40% of the sodium initially present in the core is made more negative (or less positive) when the plutonium is richer in higher isotopes.

**Effet de la composition isotopique du plutonium sur le rendement de réacteurs à neutrons rapides.** La composition isotopique du plutonium qui doit être utilisé comme combustible dans des réacteurs à neutrons rapides dépend de son origine. En principe, ce plutonium peut provenir de trois sources différentes; a) réacteurs plutonigènes; b) réacteurs de puissance à neutrons thermiques, utilisant l'uranium naturel ou l'uranium enrichi comme combustible; c) couches fertiles de réacteurs à neutrons rapides.

En général, la source a) et, à un degré moindre, la source c) fourniront du plutonium relativement « propre », c'est-à-dire composé en majeure partie de  $\text{Pu}^{239}$ , tandis que le plutonium provenant de la source b) sera un plutonium « sale », c'est-à-dire un plutonium contenant une forte proportion de  $\text{Pu}^{240}$ ,  $\text{Pu}^{241}$  et  $\text{Pu}^{242}$ . Ce plutonium sera plus ou moins « sale » suivant le type du réacteur, le taux de combustion et, de manière générale, suivant l'irradiation subie par le combustible.

La question qui se pose est alors la suivante: peut-on utiliser comme combustible, dans les réacteurs à neutrons rapides, n'importe quelle sorte de plutonium?

Pour étudier l'effet des différentes compositions isotopiques de plutonium utilisé comme combustible sous forme de métal, d'oxyde ou de carbone, sur le rendement

de réacteurs à neutrons rapides, les auteurs ont procédé à une série de calculs dans une théorie de la diffusion à 16 groupes en géométrie sphérique; ils ont utilisé à cet effet l'ensemble de sections efficaces à 16 groupes, récemment mis au point par Yiftah, Okrent et Moldauer, et ont étudié trois types différents de plutonium en prenant d'abord le  $^{239}\text{Pu}$  à l'état pur et en augmentant ensuite la quantité des isotopes supérieurs.

Pour les systèmes étudiés — cœurs d'un volume de 800, 500 et 2500 l, qui sont courants pour les grands réacteurs de puissance à neutrons rapides — on constate, en ne tenant compte que des isotopes  $^{239}\text{Pu}$  et  $^{241}\text{Pu}$ , fissiles sous l'action de neutrons thermiques, que plus le plutonium est «sale», plus la masse critique est faible et plus le rapport de conversion est élevé.

Dans le cas d'un réacteur dont le cœur a un volume de 1500 l, on constate également que dans le plutonium utilisé comme combustible sous forme de métal, d'oxyde ou de carbure, les variations de la réactivité, après enlèvement de 40% du sodium initialement présent dans le cœur, sont plus négatives (ou moins positives) si le plutonium a une plus forte teneur en isotopes supérieurs.

**Влияние изотопного состава плутония на работу реакторов на быстрых нейтронах.** Изотопный состав плутония, который должен использоваться в качестве горючего для реакторов на быстрых нейтронах, будет зависеть от источника получения плутония. В принципе возможны три различных источника: a) производящие реакторы; b) тепловые энергетические реакторы (использующие в качестве топлива естественный или обогащенный уран); c) зоны воспроизведения реактора на быстрых нейтронах.

В основном источник (a) и в некотором отношении источник (c) будут давать сравнительно „чистый“ плутоний, т.е. главным образом плутоний-239, тогда как плутоний из источника (b) будет „грязным“, т.е. плутонием, богатым изотопами плутония-240, плутония-241 и плутония-242. Степень „загрязнения“ будет зависеть от типа реактора, величины выгорания и вообще от истории облучения топлива.

В таком случае возникает вопрос, можно ли использовать в качестве горючего для реакторов на быстрых нейтронах любые виды плутония?

Для изучения влияния различного изотопного состава плутониевого топлива в металлическом, оксидном и карбидном виде на работу реакторов на быстрых нейтронах были осуществлены ограниченные серии подсчетов по 16-групповой диффузационной теории сферической геометрии с помощью 16-группового комплекта поперечных сечений, разработанного недавно Ифтахом, Окрентом и Мольдауером с использованием трех различных видов плутония, начиная с чистого плутония-239 и повышая количество более высоких изотопов.

Для изучаемых систем (объем активной зоны в 800, 1.500 и 2.500 литров, которые являются типичными для крупных энергетических реакторов на быстрых нейтронах) результат сводился к тому (если учесть лишь расщепляющиеся от тепловых нейтронов изотопы плутония-239 и плутония-241), что чем „грязнее“ плутоний, тем меньше критическая масса и выше коэффициент размножения.

Для реактора с объемом активной зоны в 1.500 л, который был взят в качестве примера, было также найдено, что в металлическом, оксидном и карбидном плутониевом топливе изменение реактивности по удалению 40% натрия, который первоначально присутствует в активной зоне, носит более отрицательный характер (или менее положительный), когда плутоний более богат высокими изотопами.

**Efectos de la composición isotópica del plutonio sobre el funcionamiento de los reactores rápidos.** La composición isotópica del plutonio empleado como combustible en los reactores de neutrones rápidos depende de su procedencia. En principio, existen tres fuentes posibles, a saber: a) los reactores generadores de plutonio; b) los reactores de potencia térmicos (alimentados con uranio natural o enriquecido); c) las envolturas fértiles de los reactores de neutrones rápidos.

La fuente a), y hasta cierto punto la fuente c), proporcionan plutonio-239 relativamente puro, mientras que el plutonio de la fuente b) es rico en  $^{240}\text{Pu}$ ,  $^{241}\text{Pu}$  y  $^{242}\text{Pu}$ .

La cantidad de impurezas depende del tipo de reactor empleado, del grado de combustión y, en general, de las condiciones de irradiación del combustible.

Cabe preguntarse, entonces, si es posible emplear cualquier clase de plutonio como combustible en los reactores de neutrones rápidos.

Con el propósito de estudiar los efectos que ejerce sobre el funcionamiento de los reactores la composición isotópica del combustible de plutonio, en forma de metal, óxido o carburo, se realizó una serie de cálculos de geometría según una teoría de difusión de 16 grupos, utilizando el conjunto de secciones eficaces de 16 grupos recientemente establecido por Yiftah, Okrent y Moldauer; esos cálculos se aplicaron a plutonio de tres composiciones isotópicas diferentes, empezando por  $^{239}\text{Pu}$  puro y aumentando la concentración de los isótopos de número másico más elevado.

Se han estudiado sistemas con cuerpos de 800, 1500 y 2500 litros de volumen, que son los típicos de los reactores generadores rápidos de grandes dimensiones. Se llega a la conclusión de que, si sólo se tienen en cuenta los isótopos fisionables por neutrones térmicos ( $^{239}\text{Pu}$  y  $^{241}\text{Pu}$ ), cuanto más impuro sea el plutonio, tanto menor será la masa crítica y mayor la razón de reproducción. Tomando como ejemplo el reactor de 1500 l, se comprobó además que al eliminar un 40 por ciento del sodio inicialmente presente en el cuerpo, la variación de reactividad tiende a ser negativa a medida que aumenta la proporción de isótopos superiores contenidos en el combustible de plutonio (en forma de metal, óxido o carburo).

## Introduction

It has been often mentioned that, although the biggest plutonium critical assemblies to date have not exceeded critical masses of up to 50 kg of plutonium in any form, the fast power breeders of the future will be Pu-fuelled reactors requiring ten to twenty times as much plutonium, that is, 500—1000 kg. The core volumes of these reactors will probably be of 800—3000 l.

Such reactors have special physics problems of their own, which are and should be investigated.

The present report deals with one of these problems, connected with the source or sources of the big amounts of plutonium needed. It mentions very briefly a second problem, namely the sodium reactivity coefficient, only to the extent that it is affected by the first.

The isotopic composition of plutonium to be used as fuel for fast reactors will depend on the source of the plutonium. In principle, three different sources are possible:

(a) So-called *production reactors*, that is, thermal reactors whose natural uranium fuel elements are run to relatively small burn-ups before reprocessing and separation of built-in plutonium from the uranium.

(b) *Thermal power reactors* fuelled with either natural or enriched uranium, in which plutonium is produced as a by-product of the electrical power. This should provide in the future a considerable source whose size is proportional to the number of thermal power reactors. The bigger the volume of a nuclear-power industry based on thermal reactors, the larger will become the quantities of plutonium produced.

(c) In the future, if many fast breeders are in operation, a third source will become the *blankets of the fast reactors* themselves.

In general, production reactors and to some extent blankets of fast reactors will provide relatively "clean" plutonium, that is mostly  $^{239}\text{Pu}$ , while plutonium from thermal power reactors will have an isotopic composition depending on the

kind of reactor, amount of burn-up and, in general, on the irradiation history of the fuel. Varying compositions of "dirty" plutonium, that is, plutonium rich in the higher isotopes  $\text{Pu}^{240}$ ,  $\text{Pu}^{241}$  and  $\text{Pu}^{242}$ , are possible from this latter source.

The questions then arise, what effect does a differing isotopic composition of plutonium have on the performance of the reactor for which it is used as fuel. Can one use any kind of plutonium? What penalty does one have to pay, if at all, for using plutonium from high-burn-up reactors, and therefore, presumably, rich in higher isotopes?

Of course, once plutonium-fuelled big critical assemblies—the necessity of which is emphasized by LOEWENSTEIN and MENEGHETTI [1]—are operated, and if plutonium of different isotopic content is available for experimentation, at least part of these questions can be answered experimentally. Until such time, however, one has to rely on provisional answers which can be arrived at by performing theoretical calculations.

Any calculations of this nature, performed by multi-group techniques, depend on the reliability of the various cross-sections of  $\text{Pu}^{239}$ ,  $\text{Pu}^{240}$ ,  $\text{Pu}^{241}$  and  $\text{Pu}^{242}$ , at least part of which are inadequately known. The results are therefore provisional because of the state of knowledge or state of ignorance of the nuclear cross-sections, and also because no experimental checking is as yet possible.

With the above remarks in mind, a limited series of comparative calculations have been performed [2], using spherical geometry 16-group diffusion theory and the recent 16-group fast-reactor cross-sections set of YIFTAH, OKRENT and MOLDAUER [3]. Plutonium fuel in the metallic, oxide and carbide form was investigated. Three representative isotopic compositions of plutonium were chosen, so as to bracket the range of interest. The effects on critical mass, breeding ratios, neutron-energy spectra and neutron balance were examined for systems of 800, 1500 and 2500 l core volumes, which are typical for large fast-power reactors. An example of the effect of the plutonium isotopic composition on the sodium reactivity coefficient is given for the 1500-l system.

### Three isotopic compositions of plutonium

The three representative isotopic compositions of plutonium chosen for this study are given in Table I.

TABLE I  
PLUTONIUM COMPOSITION  
(Atom %)

Type	$\text{Pu}^{239}$	$\text{Pu}^{240}$	$\text{Pu}^{241}$	$\text{Pu}^{242}$
Pu A	100	0	0	0
Pu B	74.7	10.2	12.4	2.7
Pu C	40	10	25	25

*Plutonium A* is pure  $\text{Pu}^{239}$ .

*Plutonium B* corresponds to the composition of the recycled plutonium extracted from a thermal reactor fuelled with enriched uranium, in this case the

pressurized-water, oxide-fuelled Yankee reactor\*, as calculated by JAYE, BENNETT and LIETZKE [4].

*Plutonium C* corresponds to the plutonium which might result from not one, but several recycles in a thermal reactor with large burn-up, and provides some sort of extreme condition of potential feed material.

It is seen that the 39 and 41 fraction in plutonium B is 87.1% and that in spite of the relatively low percentage of  $\text{Pu}^{239}$  in plutonium C we still have a two-to-one ratio of  $\text{Pu}^{239}$  and  $\text{Pu}^{241}$  to  $\text{Pu}^{240}$  and  $\text{Pu}^{242}$ .

The three different compositions can be considered as plutonium from different sources, or as different stages resulting from the recycling of core plutonium. This recycling results in changing isotopic concentrations approaching an equilibrium condition (approximated by plutonium C), which is a function of core design, feed material and fuel-cycle characteristics.

### Specifications of the systems studied

The specifications of the system studied are given in Table II.

TABLE II  
SPECIFICATIONS OF THE SYSTEMS

Core volume	800, 1500 and 2500 l*
Core volume fractions	Fuel and fertile material 0.25 Structural material 0.25 Coolant 0.50
Fuels	Metallic : { $\text{Pu-U}^{238}$ , density 19 g/cm <sup>3</sup> PuO <sub>2</sub> -UO <sub>2</sub> density 8.4 g/cm <sup>3</sup> — 77% of theoretical density (10.9 g/cm <sup>3</sup> ) Ceramic : { PuC-UC density 11.39 g/cm <sup>3</sup> — 84% of theoretical density (13.63 g/cm <sup>3</sup> ), PuC — 13.99 g/cm <sup>3</sup> )
Coolant	Liquid sodium, density 0.84 g/cm <sup>3</sup>
Structure	Stainless steel
Blanket	45 cm uranium
Blanket volume fractions	U <sup>238</sup> 0.6 Na 0.2 Fe 0.2
Reflector	30 cm steel
Reflector volume fractions	Fe 0.6 Na 0.4

\* These volumes correspond to core radii of 57, 59, 71 and 84 cm.

\* The Yankee reactor is a 136-MWe (485-MWt), PWR-type reactor fuelled with 3.4% enriched UOr pellets in stainless-steel tubes (core loading: 25 t).

It is seen that everything in the system is kept constant except the core. The changes made in the core are of three types: (a) size, (b) fuel type and (c) isotopic composition of Pu. We shall display our results, accordingly, in terms of three effects, namely the size effect, the fuel-type effect and the isotopic-composition effect.

### Results: critical masses, breeding ratios, neutron energy spectra, neutron balances

The following definitions are used.

The breeding ratio is the rate at which  $\text{Pu}^{239}$  and  $\text{Pu}^{241}$  are being formed to the rate at which they are being destroyed, that is,

$$\text{Breeding ratio (BR)} = \frac{\text{U}^{238} \text{ and } \text{Pu}^{240} \text{ captures in reactor}}{(\text{Pu}^{239} \text{ and } \text{Pu}^{241}) \text{ captures + fissions in reactor}} \quad (1)$$

$$\text{Internal breeding ratio (IBR)} = \frac{\text{Production of thermally fissionable isotopes in core}}{\text{Destruction of thermally fissionable isotopes in entire reactor}}$$

The rate at which reactor fuel is "wasted" by neutron capture,  $\bar{\alpha}$ , is given by:

$$\bar{\alpha} = \frac{\text{Pu}^{239} \text{ and } \text{Pu}^{241} \text{ captures}}{\text{Pu}^{239} \text{ and } \text{Pu}^{241} \text{ fissions}}$$

The comparative calculated results of critical masses, breeding ratios and  $\bar{\alpha}$ 's for the 800, 1500 and 2500 l reactors are given respectively in Tables III, IV and V and Figs. 1—4, while the detailed neutron energy spectra and neutron balances are displayed in the corresponding Tables III-A, IV-A and V-A.

Tables III, IV and V combine the isotopic-composition effect (horizontal) with the fuel-type effect (vertical) for the same sizes of respectively 800, 1500 and 2500 l.

TABLE III  
EFFECT OF ISOTOPIC COMPOSITION OF PLUTONIUM IN 800-l REACTOR  
FUELLED WITH METAL, OXIDE AND CARBIDE FUEL

	Fuel type	Pu A	Pu B		Pu C	
			Total Pu	$\frac{\text{Pu}^{239}}{+ \text{Pu}^{241}}$	Total Pu	$\frac{\text{Pu}^{239}}{+ \text{Pu}^{241}}$
Critical mass (kg)	Metal Oxide Carbide	431 372 396	458 392 417	399 341 363	533 452 480	346 294 312
Breeding ratio	Metal	IBR BR	0.73 1.82	0.79 1.93		0.86 2.12
	Oxide	IBR BR	0.31 1.55	0.35 1.65		0.37 1.81
	Carbide	IBR BR	0.46 1.62	0.51 1.73		0.55 1.90
	Metal Oxide Carbide	0.188 0.230 0.224		0.173 0.209 0.204		0.150 0.178 0.174

TABLE IV  
EFFECT OF ISOTOPIC COMPOSITION OF PLUTONIUM IN 1500-1 REACTOR  
FUELLED WITH METAL, OXIDE AND CARBIDE FUEL

	Fuel type	Pu A	Pu B		Pu C	
			Total Pu	Pu <sup>239</sup> + Pu <sup>241</sup>	Total Pu	Pu <sup>239</sup> + Pu <sup>241</sup>
Critical mass (kg)	Metal Oxide Carbide	686 562 613	729 590 645	635 514 562	849 680 743	552 442 483
Breeding ratio	Metal      IBR      BR Oxide    IBR    0.44 BR     1.47 Carbide   IBR    0.61 BR     1.56	0.91 1.79 0.44 1.47 0.61 1.56		0.97 1.90 0.48 1.57 0.66 1.67		1.05 2.08 0.51 1.72 0.71 1.82
$\bar{\alpha}$	Metal Oxide Carbide	0.198 0.251 0.241		0.182 0.228 0.218		0.156 0.192 0.185

TABLE V  
EFFECT OF ISOTOPIC COMPOSITION OF PLUTONIUM IN 2500-1 REACTOR  
FUELLED WITH METAL, OXIDE AND CARBIDE FUEL

	Fuel type	Pu A	Pu B		Pu C	
			Total Pu	Pu <sup>239</sup> + Pu <sup>241</sup>	Total Pu	Pu <sup>239</sup> + Pu <sup>241</sup>
Critical mass (kg)	Metal Oxide Carbide	1025 806 897	1089 845 943	949 736 821	1269 973 1086	825 632 706
Breeding ratio	Metal      IBR      BR Oxide    IBR    0.54 BR     1.42 Carbide   IBR    0.73 BR     1.52	1.04 1.76 0.54 1.42 0.73 1.52		1.11 1.87 0.59 1.52 0.79 1.62		1.21 2.05 0.64 1.65 0.85 1.77
$\bar{\alpha}$	Metal Oxide Carbide	0.205 0.267 0.253		0.187 0.240 0.229		0.161 0.203 0.192

**TABLE III A**  
**STUDY OF 800-LITER SPHERICAL REACTORS FUELLED WITH METAL, OXIDE AND CARBIDE PLUTONIUM FUELS  
 WITH DIFFERENT ISOTOPIC COMPOSITIONS OF PLUTONIUM**

Fuel		Pu A						Pu B						Pu C							
		Metal		Oxide		Carbide		Metal		Oxide		Carbide		Metal		Oxide		Carbide			
Ratio of fuel atoms to diluent atoms ( $\text{Pu}/\text{U}^{238}$ )	Critical mass of fuel (kg)	0.128		0.336		0.222		0.137		0.360		0.237		0.163		0.439		0.283			
		431	372	399 (458)*	396	341 (392)*	363 (417)*	346 (533)*	341 (392)*	294 (452)*	312 (480)*	294 (452)*	312 (480)*	346 (533)*	341 (392)*	294 (452)*	312 (480)*	346 (533)*	341 (392)*		
<b>Flux integrals</b>																					
Group	Energy interval (MeV)	Core	Blanket	Core	Blanket	Core	Blanket	Core	Blanket	Core	Blanket	Core	Blanket	Core	Blanket	Core	Blanket	Core	Blanket		
1	3.668	—	10.00	1.62	0.21	2.13	0.30	1.92	0.26	1.62	0.21	2.13	0.30	1.92	0.26	1.62	0.21	2.13	0.29	1.92	0.26
2	2.225	—	3.668	3.16	0.38	4.37	0.56	3.90	0.49	3.16	0.38	4.37	0.56	3.90	0.49	3.16	0.38	4.38	0.56	3.91	0.49
3	1.35	—	2.225	5.66	0.80	8.00	1.18	7.14	1.05	5.66	0.80	8.00	1.18	7.15	1.05	5.67	0.80	8.02	1.18	7.16	1.05
4	0.825	—	1.35	9.51	2.22	11.02	2.86	10.58	2.69	9.50	2.22	11.03	2.86	10.58	2.69	9.47	2.21	11.00	2.85	10.55	2.68
5	0.5	—	0.825	16.18	5.72	16.30	6.83	15.75	6.41	16.16	5.72	16.31	6.84	15.75	6.41	16.08	5.70	16.24	6.81	15.69	6.39
6	0.3	—	0.5	20.15	8.60	18.93	9.75	18.63	9.24	20.19	8.61	18.99	9.76	18.68	9.25	20.17	8.59	18.98	9.74	18.68	9.24
7	0.18	—	0.3	18.22	8.94	19.80	10.43	17.62	9.56	18.34	8.96	19.95	10.47	17.74	9.59	18.46	8.96	20.07	10.47	17.85	9.59
8	0.11	—	0.18	14.80	8.23	17.17	9.87	15.09	8.88	14.94	8.26	17.34	9.91	15.23	8.91	15.11	8.28	17.53	9.94	15.40	8.94
9	0.067	—	0.11	8.10	4.53	11.73	5.77	10.28	5.14	8.17	4.55	11.86	5.81	10.38	5.17	8.28	4.57	12.02	5.83	10.52	5.19
10	0.0407	—	0.067	7.40	5.76	10.26	7.35	9.10	6.54	7.46	5.79	10.34	7.40	9.20	6.58	7.54	8.81	10.47	7.43	9.33	6.61
11	0.025	—	0.0407	3.24	2.33	5.53	3.12	5.02	2.78	3.26	2.34	5.60	3.14	5.08	2.80	3.30	2.35	5.68	3.16	5.15	2.81
12	0.015	—	0.025	3.73	2.80	6.79	4.00	5.88	3.50	3.75	2.81	6.86	4.03	5.94	3.52	3.77	2.82	6.94	4.06	6.01	3.55
13	0.0091	—	0.015	1.42	1.05	3.50	1.65	3.10	1.44	1.41	1.05	3.52	1.66	3.12	1.45	1.41	1.06	3.53	1.67	3.13	1.45
14	0.0055	—	0.0091	0.61	0.40	1.93	0.70	1.73	0.61	0.60	0.40	1.93	0.71	1.73	0.62	0.59	0.40	1.91	0.71	1.72	0.62
15	0.0021	—	0.0055	0.26	0.18	1.12	0.34	0.96	0.30	0.26	0.18	1.12	0.34	0.96	0.30	0.25	0.18	1.11	0.34	0.95	0.30
16	0.0005	—	0.0021	0.20	0.070	1.54	0.19	1.21	0.16	0.20	0.070	1.55	0.19	1.22	0.16	0.19	0.070	1.56	0.19	1.22	0.16
<b>Neutron balance</b>																					
$\text{Pu}^{239}$	Fissions	0.282	—	0.313	—	0.301	—	0.224	—	0.247	—	0.238	—	0.140	—	0.153	—	0.148	—	0.0333	—
$\text{Pu}^{239}$	Captures	0.0532	—	0.0720	—	0.0676	—	0.0424	—	0.0570	—	0.0536	—	0.0266	—	0.0355	—	0.00782	—	0.00822	—
$\text{Pu}^{240}$	Fissions	—	—	—	—	—	—	—	—	—	—	—	—	—	—	—	—	—	—	—	—
$\text{Pu}^{240}$	Captures	—	—	—	—	—	—	—	—	—	—	—	—	—	—	—	—	—	—	—	—
$\text{Pu}^{241}$	Fissions	—	—	—	—	—	—	—	—	—	—	—	—	—	—	—	—	—	—	—	—
$\text{Pu}^{241}$	Captures	—	—	—	—	—	—	—	—	—	—	—	—	—	—	—	—	—	—	—	—
$\text{Pu}^{242}$	Fissions	—	—	—	—	—	—	—	—	—	—	—	—	—	—	—	—	—	—	—	—
$\text{Pu}^{242}$	Captures	—	—	—	—	—	—	—	—	—	—	—	—	—	—	—	—	—	—	—	—
$\text{U}^{238}$	Fissions	0.0583	0.0214	0.0264	0.0311	0.0379	0.0277	0.0578	0.0214	0.0259	0.0311	0.0375	0.0276	0.0366	0.0214	0.0245	0.0310	0.0362	0.0276	0.0427	0.000556
$\text{U}^{238}$	Captures	0.245	0.364	0.120	0.476	0.171	0.427	0.244	0.366	0.119	0.479	0.170	0.429	0.240	0.366	0.113	0.480	0.165	0.430	0.182	0.0933
Coolant (Na) captures	—	0.00144	0.000353	0.00502	0.000635	0.00433	0.000555	0.00142	0.000353	0.00500	0.000637	0.00431	0.000556	0.00139	0.000353	0.00495	0.000637	0.00427	0.000556	0.00427	0.000556
Structural captures	—	0.0149	0.00637	0.0179	0.00805	0.0179	0.00728	0.0150	0.00639	0.0200	0.00810	0.0180	0.00731	0.0150	0.00641	0.0202	0.00813	0.0182	0.00933	0.0182	0.00933
Internal breeding ratio	—	0.73	—	0.31	—	0.46	—	0.79	—	0.35	—	0.51	—	0.86	—	0.37	—	0.55	—	—	—
Breeding ratio	—	1.82	—	1.55	—	1.62	—	1.93	—	1.65	—	1.73	—	2.12	—	1.81	—	1.90	—	—	—
Ratio captures to fissions in $\text{Pu}^{239} + \text{Pu}^{241}$	—	0.188	—	0.230	—	0.224	—	0.173	—	0.209	—	0.204	—	0.150	—	0.178	—	0.174	—	—	—
Escape from blanket	—	0.0118	—	0.0143	—	0.0135	—	0.0118	—	0.0144	—	0.0133	—	0.0118	—	0.0143	—	0.0134	—	—	—

\* The figures of critical mass represent the critical mass of the two fissionable isotopes  $\text{Pu}^{239}$  and  $\text{Pu}^{241}$ . The values in parentheses give the total mass of all four plutonium isotopes,  $\text{Pu}^{239}$ ,  $\text{Pu}^{240}$ ,  $\text{Pu}^{241}$  and  $\text{Pu}^{242}$ .

TABLE IV A  
STUDY OF 1500-LITER SPHERICAL REACTORS FUELLED WITH METAL, OXIDE, AND CARBIDE PLUTONIUM FUELS  
WITH DIFFERENT ISOTOPIC COMPOSITIONS OF PLUTONIUM

Fuel		Pu A						Pu B						Pu C							
		Metal		Oxide		Carbide		Metal		Oxide		Carbide		Metal		Oxide		Carbide			
Ratio of fuel atoms to diluent atoms (Pu/U <sup>238</sup> )		0.106		0.253		0.176		0.113		0.269		0.187		0.135		0.323		0.222			
Critical mass of fuel (kg)		686		562		613		635 (729)*		514 (590)*		562 (645)*		552 (849)*		442 (680)*		483 (743)*			
Flux integrals																					
Group	Energy interval (MeV)	Core	Blanket	Core	Blanket	Core	Blanket	Core	Blanket	Core	Blanket	Core	Blanket	Core	Blanket	Core	Blanket	Core	Blanket		
1	3.668	-10.00	1.68	0.15	2.24	0.22	2.00	0.19	1.68	0.15	2.24	0.22	2.00	0.19	1.68	0.15	2.24	0.22	2.01	0.19	
2	2.225	-	3.668	3.28	0.28	4.62	0.42	4.10	0.37	3.28	0.28	4.62	0.42	4.10	0.37	3.28	0.28	4.63	0.42	4.10	0.37
3	1.35	-	2.225	5.95	0.60	8.61	0.90	7.63	0.79	5.96	0.60	8.62	0.90	7.64	0.79	5.96	0.60	8.63	0.90	7.65	0.79
4	0.825	-	1.35	10.23	1.67	12.06	2.20	11.52	2.05	10.22	1.67	12.07	2.20	11.52	2.05	10.19	11.67	12.04	2.19	11.50	2.05
5	0.5	-	0.825	17.84	4.38	18.19	5.31	17.47	4.95	17.83	4.38	18.21	5.31	17.48	4.96	17.74	4.37	18.15	5.30	17.43	4.94
6	0.3	-	0.5	22.85	6.70	21.63	7.67	21.15	7.24	22.90	6.70	21.69	7.68	21.22	7.25	22.88	6.69	21.69	7.67	21.22	7.24
7	0.18	-	0.3	21.21	7.07	23.38	8.38	20.52	7.60	21.35	7.09	23.54	8.41	20.65	7.62	21.47	7.09	23.66	8.42	20.77	7.63
8	0.11	-	0.18	17.66	6.60	20.90	8.08	18.00	7.16	17.81	6.63	21.10	8.12	18.16	7.19	18.00	6.65	21.31	8.14	18.34	7.21
9	0.067	-	0.11	7.84	3.68	14.69	4.82	12.55	4.21	9.93	3.69	14.85	4.85	12.68	4.24	10.05	3.71	15.03	4.87	12.83	4.25
10	0.0407	-	0.067	9.23	4.72	13.22	6.21	11.43	5.42	9.31	4.74	13.37	6.25	11.55	5.45	9.41	4.76	13.53	6.29	11.69	5.47
11	0.025	-	0.0407	4.13	1.92	7.38	2.68	6.47	2.33	4.17	1.94	7.46	2.70	6.54	2.35	4.21	1.94	7.56	2.72	6.62	2.36
12	0.015	-	0.025	4.96	2.36	9.54	3.57	7.91	3.02	4.99	2.37	9.65	3.59	7.99	3.04	5.02	2.38	9.76	3.62	8.08	3.06
13	0.0091	-	0.015	1.94	0.90	5.14	1.52	4.33	1.28	1.94	0.90	5.17	1.53	4.36	1.28	1.94	0.90	5.20	1.53	4.38	1.29
14	0.0055	-	0.0091	0.86	0.35	2.94	0.67	2.50	0.56	0.85	0.35	2.94	0.67	2.50	0.56	0.83	0.35	2.93	0.67	2.49	0.56
15	0.0021	-	0.0055	0.39	0.16	1.77	0.33	1.43	0.28	0.37	0.16	1.76	0.33	1.42	0.28	0.37	0.16	1.75	0.34	1.41	0.28
16	0.0005	-	0.0021	0.31	0.062	2.76	0.21	1.98	0.16	0.31	0.061	2.79	0.21	2.00	0.16	0.30	0.061	2.82	0.21	2.01	0.16
Neutron balance																					
Pu <sup>239</sup>	Fissions	0.278	—	0.310	—	0.299	—	0.222	—	0.244	—	0.236	—	0.139	—	0.151	—	0.146	—		
Pu <sup>239</sup>	Captures	0.0553	—	0.0780	—	0.072	—	0.0441	—	0.0616	—	0.0569	—	0.0276	—	0.0383	—	0.0354	—		
Pu <sup>240</sup>	Fissions	—	—	—	—	—	—	—	—	—	—	—	—	—	—	—	—	—	—		
Pu <sup>240</sup>	Captures	—	—	—	—	—	—	—	—	—	—	—	—	—	—	—	—	—	—		
Pu <sup>241</sup>	Fissions	—	—	—	—	—	—	—	—	—	—	—	—	—	—	—	—	—	—		
Pu <sup>241</sup>	Captures	—	—	—	—	—	—	—	—	—	—	—	—	—	—	—	—	—	—		
Pu <sup>242</sup>	Fissions	—	—	—	—	—	—	—	—	—	—	—	—	—	—	—	—	—	—		
Pu <sup>242</sup>	Captures	—	—	—	—	—	—	—	—	—	—	—	—	—	—	—	—	—	—		
U <sup>238</sup>	Fissions	0.0621	0.0159	0.0300	0.0235	0.0417	0.0208	0.0617	0.0159	0.0296	0.0235	0.0413	0.0208	0.0606	0.0159	0.0284	0.0235	0.0402	0.0208		
U <sup>238</sup>	Captures	0.302	0.295	0.169	0.404	0.226	0.354	0.302	0.297	0.168	0.406	0.225	0.355	0.297	0.297	0.162	0.407	0.220	0.357		
Coolant (Na) captures	—	0.00192	0.000303	0.00774	0.000606	0.00629	0.000507	0.00194	0.000303	0.00772	0.000608	0.00628	0.000509	0.00171	0.000303	0.00767	0.000609	0.00623	0.000509		
Structural captures	—	0.0178	0.00513	0.0251	0.00673	0.0220	0.00595	0.0179	0.00515	0.0253	0.00676	0.0221	0.00598	0.0180	0.00516	0.0255	0.00678	0.0223	0.00599		
Internal breeding ratio	—	0.91	—	0.44	—	0.61	—	0.97	—	0.48	—	0.66	—	1.05	—	0.51	—	0.71	—		
Breeding ratio	—	1.79	—	1.47	—	1.56	—	1.90	—	1.57	—	1.67	—	2.08	—	1.72	—	1.82	—		
Ratio captures to fissions in Pu <sup>239</sup> -Pu <sup>241</sup>	—	0.198	—	0.251	—	0.241	—	0.182	—	0.228	—	0.218	—	0.156	—	0.192	—	0.185	—		
Escape from blanket	—	0.00865	—	0.0104	—	0.00972	—	0.00866	—	0.0104	—	0.00974	—	0.00865	—	0.0104	—	0.00971	—		

\* The figures of critical mass represent the critical mass of the two fissionable isotopes Pu<sup>239</sup> and Pu<sup>241</sup>. The values in parentheses give the total mass of all four plutonium isotopes, Pu<sup>239</sup>, Pu<sup>240</sup>, Pu<sup>241</sup> and Pu<sup>242</sup>.

TABLE V A  
STUDY OF 2500-LITER SPHERICAL REACTORS FUELLED WITH METAL, OXIDE AND CARBIDE PLUTONIUM FUELS  
WITH DIFFERENT ISOTOPIC COMPOSITIONS OF PLUTONIUM

Fuel	Pu A						Pu B						Pu C						
	Metal		Oxide		Carbide		Metal		Oxide		Carbide		Metal		Oxide		Carbide		
	0.0945	1026	0.210	806	0.152	897	0.100	949 (1089)*	0.223	736 (845)*	0.161	821 (943)*	0.119	825 (1269)*	0.265	632 (973)*	0.190	706 (1086)*	
Ratio fuel atoms to diluent atoms (Pu/U <sup>238</sup> )																			
Critical mass of fuel (kg)																			
Flux integrals																			
Group	Energy interval (MeV)	Core	Blanket	Core	Blanket	Core	Blanket	Core	Blanket	Core	Blanket	Core	Blanket	Core	Blanket	Core	Blanket	Core	Blanket
1	3.668 — 10.00	1.72	0.12	2.31	0.17	2.06	0.15	1.72	0.12	2.31	0.17	2.06	0.15	1.72	0.12	2.31	0.17	2.06	0.15
2	2.225 — 3.668	3.36	0.22	4.79	0.33	4.22	0.29	3.36	0.22	4.79	0.33	4.23	0.29	3.36	0.22	4.80	0.33	4.23	0.29
3	1.35 — 2.225	6.15	0.46	9.02	0.70	7.96	0.62	6.15	0.46	9.03	0.70	7.96	0.62	6.15	0.46	9.04	0.70	7.97	0.62
4	0.825 — 1.35	10.71	1.31	12.78	1.74	12.16	1.62	10.70	1.31	12.79	1.73	12.18	1.62	10.67	1.30	12.76	1.73	12.14	1.61
5	0.5 — 0.825	18.98	3.45	19.53	4.22	18.68	3.93	18.97	3.45	19.54	4.22	18.69	3.93	18.89	3.44	19.49	4.21	18.63	3.92
6	0.3 — 0.5	24.77	5.33	23.58	6.16	22.96	5.79	24.82	5.34	23.64	6.16	23.03	5.80	24.81	5.33	23.64	6.15	23.03	5.79
7	0.18 — 0.3	23.41	5.69	26.05	6.82	22.65	6.14	23.55	5.71	26.21	6.84	22.78	6.16	23.68	5.71	26.35	6.85	22.90	6.16
8	0.11 — 0.18	19.81	5.37	23.78	6.67	20.19	5.85	19.98	5.39	23.99	6.69	20.36	5.87	20.17	5.41	24.21	6.71	20.54	5.89
9	0.067 — 0.11	11.18	3.01	17.03	4.03	14.30	3.48	11.27	3.03	17.20	4.05	14.44	3.49	11.40	3.04	17.40	4.07	14.59	3.51
10	0.0407 — 0.067	10.67	3.89	15.65	5.24	13.25	4.50	10.77	3.91	15.82	5.27	13.39	4.52	10.87	3.92	16.00	5.30	13.53	4.54
11	0.025 — 0.0407	4.85	1.60	8.90	2.29	7.63	1.96	4.89	1.61	9.00	2.30	7.71	1.97	4.94	1.61	9.11	2.32	7.80	1.98
12	0.015 — 0.025	5.98	1.99	11.92	3.12	9.59	2.59	6.02	2.00	12.06	3.15	9.69	2.60	6.05	2.00	12.18	3.17	9.78	2.62
13	0.0091 — 0.015	2.39	0.76	6.61	1.36	5.38	1.11	2.39	0.76	6.66	1.37	5.42	1.12	2.38	0.77	6.70	1.37	5.44	1.12
14	0.0055 — 0.0091	1.07	0.30	3.87	0.61	3.17	0.50	1.06	0.30	3.88	0.62	3.17	0.50	1.05	0.30	3.87	0.62	3.16	0.50
15	0.0021 — 0.0055	0.48	0.13	2.37	0.31	1.83	0.25	0.48	0.13	2.37	0.31	1.83	0.25	0.47	0.13	2.36	0.31	1.82	0.25
16	0.0005 — 0.0021	0.41	0.054	4.03	0.21	2.72	0.15	0.40	0.054	4.08	0.21	2.75	0.15	0.40	0.053	4.13	0.21	2.77	0.15
Neutron balance																			
Pu <sup>239</sup>	Fissions	0.276	—	0.308	—	0.296	—	0.220	—	0.243	—	0.234	—	0.138	—	0.150	—	0.145	—
Pu <sup>239</sup>	Captures	0.0568	—	0.0823	—	0.0750	—	0.0452	—	0.0650	—	0.0593	—	0.0283	—	0.0404	—	0.0368	—
Pu <sup>240</sup>	Fissions	—	—	—	—	—	—	—	—	0.00593	—	0.00560	—	0.00575	—	0.00677	—	0.00628	—
Pu <sup>240</sup>	Captures	—	—	—	—	—	—	—	—	0.00625	—	0.00851	—	0.00782	—	0.00718	—	0.00962	—
Pu <sup>241</sup>	Fissions	—	—	—	—	—	—	—	—	0.0473	—	0.0564	—	0.0534	—	0.111	—	0.131	—
Pu <sup>241</sup>	Captures	—	—	—	—	—	—	—	—	0.00501	—	0.00715	—	0.00653	—	0.0118	—	0.0167	—
Pu <sup>242</sup>	Fissions	—	—	—	—	—	—	—	—	0.00153	—	0.00142	—	0.00150	—	0.0165	—	0.0153	—
Pu <sup>242</sup>	Captures	—	—	—	—	—	—	—	—	—	—	0.00221	—	0.00208	—	0.0179	—	0.0240	—
U <sup>238</sup>	Fissions	0.0646	0.0122	0.0323	0.0184	0.0442	0.0162	0.0642	0.0122	0.0320	0.0184	0.0439	0.0162	0.0632	0.0122	0.0310	0.0184	0.0428	0.0162
U <sup>238</sup>	Captures	0.347	0.242	0.212	0.342	0.271	0.295	0.347	0.243	0.212	0.344	0.271	0.296	0.342	0.244	0.206	0.345	0.266	0.297
Coolant (Na) captures	0.00242	0.000259	0.0102	0.000558	0.00802	0.000452	0.00240	0.000259	0.0102	0.000560	0.00801	0.000454	0.00236	0.000258	0.0102	0.000561	0.00796	0.000454	
Structural captures	0.0200	0.00419	0.0298	0.00563	0.0252	0.00491	0.0201	0.00421	0.0297	0.00565	0.0254	0.00493	0.0202	0.00421	0.0299	0.00567	0.0255	0.00494	
Internal breeding ratio	1.04	—	0.54	—	0.73	—	1.11	—	0.59	—	0.79	—	1.21	—	0.64	—	0.85	—	
Total breeding ratio	1.76	—	1.42	—	1.52	—	1.87	—	1.52	—	1.62	—	2.05	—	1.65	—	1.77	—	
Ratio captures to fissions in Pu <sup>239</sup> + Pu <sup>241</sup>	0.205	—	0.267	—	0.253	—	0.187	—	0.240	—	0.229	—	0.161	—	0.203	—	0.192	—	
Escape from blanket	0.00620	—	0.00811	—	0.00718	—	0.00623	—	0.00812	—	0.00720	—	0.00620	—	0.00811	—	0.00718	—	

\* The figures of critical mass represent the critical mass of the two fissionable isotopes Pu<sup>239</sup> and Pu<sup>241</sup>. The values in parentheses give the total mass of all four plutonium isotopes, Pu<sup>239</sup>, Pu<sup>240</sup>, Pu<sup>241</sup> and Pu<sup>242</sup>.

Figs. 1—3 show the combination of the size effect with the isotopic composition effect for the same fuel types, namely, respectively, metal, oxide and carbide plutonium fuels.

Fig. 4 combines all three effects—size, fuel type and isotopic composition—on breeding ratios, but shows the isotopic-composition effect only for the metallic case in order not to complicate the figure.

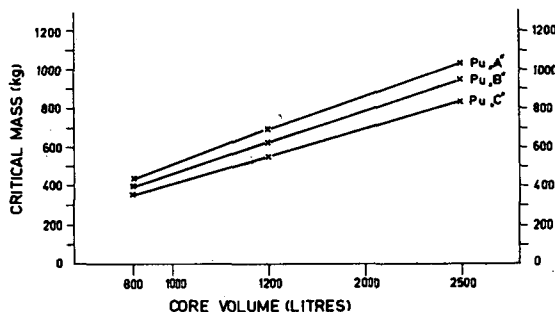


Fig. 1

Plutonium metallic fuel: critical mass as function of core size and plutonium isotopic composition.

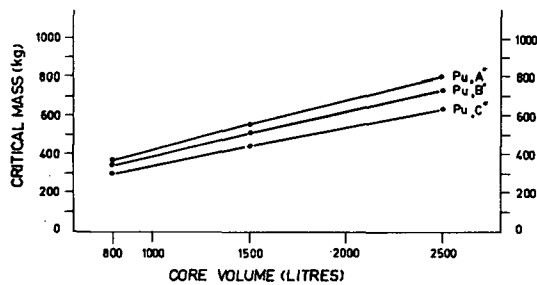


Fig. 2

Plutonium oxide fuel: critical mass as function of core size and plutonium isotopic composition.

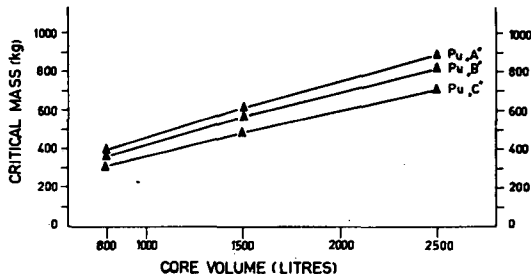


Fig. 3

Plutonium oxide fuel: critical mass as function of core size and plutonium isotopic composition.

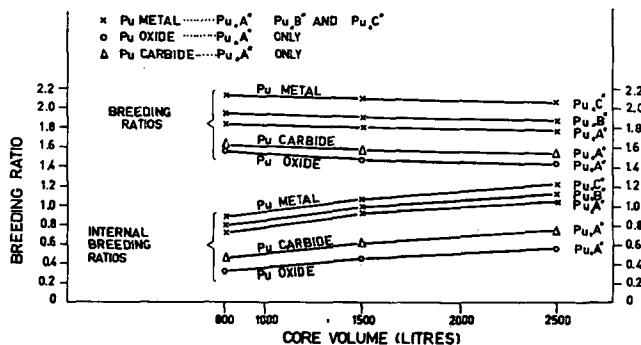


Fig. 4  
Plutonium metallic and ceramic fuels: breeding ratios.

× Pu metal                      Pu A, Pu B and Pu C  
 ○ Pu oxide                      Pu A only  
 △ Pu carbide                    Pu A only

The following observations arise from these results:

(a) When one takes into account only the thermally fissionable isotopes  $\text{Pu}^{239}$  and  $\text{Pu}^{241}$ , one finds that the "dirtier" the plutonium, the smaller the critical mass and the higher the breeding ratio. These results are both a direct consequence of the fact that  $\text{Pu}^{240}$  is preferable to  $\text{U}^{238}$  as a fertile material, due to its larger fission cross-section, and that  $\text{Pu}^{241}$  is preferable to  $\text{Pu}^{239}$ .

(b) The critical masses which are about 300—400 kg for the 800-l cores, about 450—700 for the 1500-l cores and about 650—1000 for the 2500-l cores are diminished by typically 20% when one passes from pure  $\text{Pu}^{239}$  to  $\text{Pu C}$ , which contains 40%  $\text{Pu}^{239}$ .

(c) The total breeding ratios decrease slightly with increasing size (they are almost independent of core size) and also decrease when one passes from metallic to carbide to oxide fuel, in that order. On the other hand, the internal breeding ratios increase with increasing core size. Internal breeding ratios have some economic importance because of the possibility of burning the plutonium produced in the core *in situ*, without reprocessing and fabrication, as is the case for plutonium formed in the blanket.

(d) Again, replacing  $\text{Pu A}$  by  $\text{Pu C}$ , the breeding ratios increase from 1.76—1.82 to 2.05—2.12 in the metallic fuel, from 1.52—1.62 to 1.77—1.90 in the carbide fuel and from 1.42—1.55 to 1.65—1.81 in the oxide fuel.

It is of importance to note that for  $\text{Pu C}$  and metallic fuel, the breeding ratio is calculated to be above 2 for the three reactor sizes, 800, 1500 and 2500 l.

It is here interesting to mention without details a somewhat similar provisional result obtained at Hanford [4] for *large thermal reactors*, namely, that plutonium with a high  $\text{Pu}^{240}$  and  $\text{Pu}^{241}$  content was calculated to be a better enrichment material than either plutonium-239 or uranium-235, in that order.

Combined with our results, this provisionally seems to indicate that *the "dirtier" the plutonium the better it is as fuel for both fast and thermal reactors*.

### Example of effect on sodium reactivity coefficients

If some of the sodium coolant in the core of a fast reactor were removed, representing either a change in density due to heating or some accidental condition, it would be desirable, of course, to lose reactivity, that is to have a negative sodium reactivity coefficient.

*Positive* sodium reactivity coefficients for some large fast reactor designs were first reported by NIMS and ZWEIFEL [5] and have since been calculated by others [6].

A rough calculation of the effect for the systems considered in this study has been performed by removing uniformly 40% of the core sodium. The reactivity change is reported in terms of  $\delta M_c/M_c$ , the fractional increment in critical mass which would produce the same reactivity effect as the removal of the sodium. (The constant of proportionality,  $(k/\delta k)/(\delta M_c/M_c)$ , was observed to be between 0.5 and 0.7 for these reactors.)

The resulting positive sodium coefficient was found to be a function of size, structural material and type of fuel as reported by Yiftah and Okrent [2], who calculate, for instance, that the threshold size for the positive effect for a metal-fuelled system with niobium structure is about 400 l.

It should be noted that since these calculations were performed about a year ago, some of them have been repeated with two refinements: (a) the effect of elastic resonance scattering of light and medium elements, and (b) the use of the lower  $\alpha$ -values of Pu<sup>239</sup> measured by Hopkins and Diven.

According to BHIDE and HUMMEL [10], who did the first refinement in general, since the elastic removal cross-sections of Na are higher than those used in [2], the spectral shift effect is enhanced by the decrease in sodium density, and the reactivity coefficients become more positive than we calculated. Thus the threshold sizes for the positive coefficients seem to be lower than previously predicted.

The second refinement also tends to make the sodium coefficients for the oxide and carbide cases less negative (or more positive), as shown by Okrent [9].

It can be concluded, therefore, that the positive sodium coefficient is more positive today than it used to be a year ago. This is what happens when one refines one's calculations.

The effect of the isotopic composition of plutonium on the sodium reactivity coefficient was calculated for the 1500-l reactor fuelled with metallic, oxide and carbide fuels and having a steel structure. The results are summarized in Table VI.

It is seen that, in all cases calculated, the "dirtier" the plutonium, the less positive (or more negative) is the sodium removal reactivity coefficient.

TABLE VI  
REACTIVITY CHANGE UPON REMOVING 40% OF SODIUM FROM 1500-l STEEL  
STRUCTURE REACTORS FUELLED WITH METAL, OXIDE OR CARBIDE  
PLUTONIUM FUELS OF TWO ISOTOPIC COMPOSITIONS

$\delta M_c/M_c$ to produce same reactivity change			
Fuel type	Metal	Oxide	Carbide
Pu A	+0.0041	-0.0140	-0.0058
Pu C	+0.0014	-0.0162	-0.0076

### Remarks on cross-sections

The dependence of the above results on the reliability of the various cross-sections of  $\text{Pu}^{239}$ ,  $\text{Pu}^{240}$ ,  $\text{Pu}^{241}$  and  $\text{Pu}^{242}$  has been emphasized in the Introduction. The present study uses the recent 16-group cross-section set of Yiftah, Okrent and Moldauer [3], to which we refer for an analysis of the available experimental data as well as the methods, assumptions and theoretical calculations on which the set is based.

It should be mentioned, however, that the recent Los Alamos measurements of the ratio of capture to fission cross-sections of  $\text{Pu}^{239}$  [8] would imply somewhat lower  $\text{Pu}^{239}$  capture cross-sections than used in the 16-group set. Previous calculations with low alphas for  $\text{Pu}^{239}$  [7] seem to indicate that the new lower  $\text{Pu}^{239}$  capture cross-sections will probably decrease slightly the critical masses and increase slightly the breeding ratios.

The sensitivity of the calculated results to neutron cross-section data, considering the above alpha measurements and also making arbitrary changes in the least-certain multi-group cross-sections, is treated by Okrent [9].

### Conclusions

The two main conclusions of this report can be summarized as follows.

1. For typical large fast-power plutonium reactors, exemplified by 800, 1500 and 2500 l core volumes, it is found that when one takes into account only the thermally fissionable  $\text{Pu}^{239}$  and  $\text{Pu}^{241}$ , the "dirtier" the plutonium, the smaller the critical mass and the higher the breeding ratio.
2. For the 1500-l reactor, taken as an example, it is found that in the metallic, oxide and carbide plutonium fuels, the "dirtier" the plutonium, the less positive (or more negative) the sodium removal reactivity coefficient. It is emphasized, however, that this statement is only applicable to the example calculated, and further calculations should be performed before one can generalize for all cases.

### REFERENCES

- [1] LOEWENSTEIN, W. B. and MENEGHETTI, D., *These proceedings*, Vol. I p. 415.
- [2] YIFTAH, S. and OKRENT, D., ANL-6212 (1960).
- [3] YIFTAH, S., OKRENT, D. and MOLDAUER, P. A., *Fast Reactor Cross Sections, A Study Leading to a 16 Group Set*, Pergamon Press (1960).
- [4] JAYE, S., BENNETT, L. L. and LIETZKE, M. P., ORNL-60-2-34, (1960) 49.
- [5] Plutonium Recycle Program Annual Report, HW-62000, 21 (1959).
- [6] NIMS, I. B. and ZWEIFEL, P. F., *Trans. Amer. nucl. Soc.* 2 (1959). See also APDA-135.
- [7] OKRENT, D., Proc. Conf. Physics of Breeding, ANC-6122 (1959).
- [8] DIVEN, B. C. and HOPKINS, J. C., *Bull. Amer. phys. Soc.*, Ser. II, 5 (1960) 494. Also, *These proceedings*, Vol. I, p. 149.
- [9] OKRENT, D., *These proceedings*, Vol. II, p. 271.
- [10] BHIDE, M. G. and HUMMEL, H. H., *These proceedings*, Vol. II, p. 177.

# PERFORMANCE OF LARGE FAST POWER REACTORS INCLUDING EFFECTS OF HIGHER ISOTOPES, RECYCLING AND FISSION PRODUCTS\*

D. OKRENT

ARGONNE NATIONAL LABORATORY, ARGONNE, ILL.,  
UNITED STATES OF AMERICA

Abstract — Résumé — Аннотация — Resumen

Performance of large fast power reactors, including effects of higher isotopes, recycling and fission products. Using a new sixteen-group cross-section set, the initial and long-term performance of a representative group of large fast power reactors will be examined. The build-up of higher isotopes of plutonium as a function of core-fuel material and reactor design will be analysed, and the influence of changing plutonium isotopic composition on critical mass, breeding ratio, reactivity, coolant void coefficient, and delayed-neutron fraction will be treated. The sensitivity of these results to neutron-cross-section data will be discussed (*a*) in the light of recent measurements of  $\alpha = \sigma_c/\sigma_f$  of  $\text{Pu}^{239}$  and (*b*) by making arbitrary changes in the least-certain multi-group cross-sections.

The effects of fission-product build-up on critical mass, breeding ratio and reactivity will be calculated. Measurements with mock fission products at ZPR-III will be correlated and compared with predictions based on the estimates of theoretical nuclear physics.

Other effects to be treated include the reactivity growth associated with blanket plutonium build-up, the sensitivity of sodium void coefficient to reactor-core composition and the high-energy spectrum ( $> 1.4 \text{ MeV}$ ) of such reactor systems.

**Fonctionnement des grands réacteurs à neutrons rapides: effets des isotopes lourds, recyclage et produits de fission.** L'auteur étudie le fonctionnement initial et à long terme d'un groupe représentatif de grands réacteurs à neutrons rapides, en utilisant un nouvel ensemble de sections efficaces de seize groupes. Il analyse l'accumulation des isotopes lourds du plutonium en fonction du combustible initial et du type du réacteur, ainsi que l'influence de la composition en isotopes du plutonium sur la masse critique, le taux de surgénération, la réactivité, le coefficient cavitaire du fluide de refroidissement et la fraction des neutrons retardés. Il étudie également l'influence sur ces résultats des données relatives aux sections efficaces neutroniques: *a*) en tenant compte des mesures récentes de  $\alpha = \sigma_c/\sigma_f$  de  $\text{Pu}^{239}$ , et *b*) en modifiant arbitrairement les sections efficaces multigroupes les moins sûres.

L'auteur calcule les effets de l'accumulation des produits de fission sur la masse critique, le taux de surgénération et la réactivité. Il fait une corrélation et une comparaison entre les mesures avec des produits de fission simulée dans le ZPR-III et les estimations fondées sur la physique nucléaire théorique.

L'auteur examine également l'accroissement de réactivité associé à l'accumulation de la couche fertile de plutonium, l'influence de la composition du cœur sur le coefficient cavitaire du sodium, et le spectre de haute énergie ( $> 1,4 \text{ MeV}$ ) des réacteurs de ce type.

**Характеристика крупных энергетических реакторов на быстрых нейтронах, включая действие тяжелых изотопов, продуктов повторного использования и продуктов деления.** В докладе будут рассмотрены характеристики типичной группы крупных энергетических реакторов на быстрых нейтронах в пусковые периоды и при установленных режимах с

\* Work done under the auspices of the United States Atomic Energy Commission.

применением нового набора шестигрупповых поперечных сечений. Будет изучено накопление тяжелых изотопов плутония, как функции ядерного топлива и конструкции реактора, а также будет определено влияние изменения изотопического состава плутония на критическую массу, коэффициент воспроизводства, реактивность, пустотный коэффициент теплосителя и на долю запаздывающих нейтронов. В докладе будет рассмотрено влияние этих результатов на данные по нейтронным сечениям *a)* в свете последних измерений  $\alpha = \sigma_c/\sigma_f$  Pu<sup>239</sup>, *b)* путем внесения произвольных изменений в наименее точные многогрупповые сечения.

Будет подсчитан эффект накопления продуктов деления на критическую массу, коэффициент воспроизводства и реактивность. Измерения, произведенныес ложными продуктами деления на ZPR-III будут откоррелированы и сравнены с предположениями, основанными на оценках теоретической ядерной физики.

К другим эффектам, которые будут рассмотрены, относятся увеличение реактивности, связанное с накоплением плутония в зоне воспроизводства, чувствительность пустотного коэффициента натрия к составу активной зоны реактора и спектру высоких энергий ( $> 1,4$  МэВ) таких реакторных систем.

**Funcionamiento de los grandes reactores de potencia rápidos: efectos de los isótopos superiores, del reciclado y de los productos de fisión.** Utilizando un nuevo conjunto de secciones eficaces para una teoría de 16 grupos, el autor examina el funcionamiento inicial y a largo plazo de un grupo representativo de reactores rápidos de potencia de grandes dimensiones. Analiza la acumulación de isótopos superiores del plutonio en función de la composición inicial del combustible del tipo de reactor, y estudia la influencia de modificaciones de la composición isotópica del plutonio sobre la masa crítica, la razón de reproducción, la reactividad, el coeficiente de vacío del refrigerante y la fracción de neutrones retardados. Estudia igualmente la influencia ejercida sobre estos resultados por los datos relativos a las secciones eficaces neutrónicas: *a)* teniendo en cuenta las mediciones más recientes de  $\alpha = \sigma_c/\sigma_f$  del <sup>239</sup>Pu, y *b)* modificando arbitrariamente las secciones eficaces multigrupales más inciertas.

El autor calcula los efectos de la acumulación de productos de fisión sobre la masa crítica, la razón de reproducción y la reactividad. Establece una correlación y comparación entre las mediciones efectuadas con productos de fisión simulados en el ZPR-III y las predicciones basadas en los cálculos de la física nuclear teórica.

Además, el autor examina el aumento de reactividad asociado a la acumulación de plutonio en la envoltura fértil, la influencia de la composición del cuerpo del reactor sobre el coeficiente de vacío del sodio y el espectro de elevada energía ( $> 1,4$  MeV) de los reactores de este tipo.

## Introduction

In the past, performance calculations for large, fast power reactors have frequently been concentrated on initial conditions of operation [1, 2]. Only a single fissionable isotope, not representative of recycled fuel, was usually considered. The results were intended to provide general background information.

As the design of such reactors approaches closer to reality, and as cross-section information on the higher isotopes of plutonium becomes more available, the long-term physics characteristics warrant attention. Some preliminary calculations aimed in this direction provide the central theme of this paper.

YIFTAH and OKRENT [3] have recently reported the initial performance characteristics of a series of large, fast reactors, using the new 16-group cross-section set they developed jointly with MOLDAUER [4]. By choosing as a possible plutonium supply the material resulting from thermal-reactor recycle, the effects of higher

plutonium isotopes on breeding ratio and critical mass [5], and to some extent on sodium-coolant reactivity coefficient, were examined. These calculations are used, herein, as a starting point from which to examine the effects of fuel recycling. Specifically, the difference between initial and equilibrium isotopic composition is compared for metal-, oxide- and carbide-fuelled reactors assuming different types of plutonium-feed material. For some of these systems, furthermore, the change from initial to equilibrium composition is followed in a step-wise fashion. The effects of specific cross-section uncertainties on these results are computed, as well as the influence of reprocessing losses.

The change in performance characteristics such as critical mass, breeding ratio, sodium reactivity coefficient and delayed-neutron fraction are reported, as well as the reactivity changes associated with build-up of fission products and the burn-out and build-up of fuel during a single cycle.

In addition, certain other phenomena of interest in fast-reactor analysis, such as the high-energy end of the neutron spectrum, are treated.

All criticality calculations have been made in spherical geometry by means of diffusion theory. Each reactor was assumed to consist of three regions, namely, core, blanket and external reflector. The specifications of the systems studied were as follows, except where noted otherwise.

*Core volume:* 800 or 1500 l

*Core volume fractions:*

Fuel and fertile material	0.25
Structural material (usually steel)	0.25
Coolant	0.50

<i>Fuels:</i>	<i>Density (g/cm<sup>3</sup>)</i>
Pu-U <sup>238</sup>	19
PuO <sub>2</sub> -UO <sub>2</sub>	8.4
PuC-UC	11.39

*Plutonium composition:*

Type	Pu <sup>239</sup>	Pu <sup>240</sup>	Atom %	Pu <sup>241</sup>	Pu <sup>242</sup>
A	100	0	0	0	0
AB	90	10	0	0	0
B	74.7	10.2	12.4	2.7	
C	40	10	25	25	

*Blanket thickness:* 45 cm

*Blanket volume fractions:*

U <sup>238</sup>	0.6
Na	0.2 (0.84 g/cm <sup>3</sup> )
Fe	0.2

*Reflector thickness:* 30 cm

*Reflector volume fraction:* Fe 0.6  
Na 0.4

### Isotopic composition changes with recycle

#### THE CONSTANT REACTIVITY APPROACH TO EQUILIBRIUM

The change in isotopic composition of plutonium on recycle was computed with two different methods developed primarily by H. J. Wheeler of Argonne. In the so-called "constant reactivity" or "infinitesimal burn-up" method, the differential equations describing burn-up, build-up and make-up of each isotope were constrained to maintain continuously both reactivity and total combined

fissile and fertile atoms. Thus, the equations to be solved simultaneously were as follows:

$$\begin{aligned}\frac{dN^{238}}{dt} &= -N^{238} \sigma_a U^{238} + f^{U^{238}} \\ \frac{dN^{Pu^{239}}}{dt} &= N^{238} \sigma_c U^{238} \varphi - N^{Pu^{239}} \sigma_a Pu^{239} \varphi + f^{Pu^{239}} \\ \frac{dN^{Pu^{240}}}{dt} &= N^{Pu^{239}} \sigma_c Pu^{239} \varphi - N^{240} \sigma_a Pu^{240} \varphi + f^{Pu^{240}} \\ \frac{dN^{Pu^{241}}}{dt} &= N^{Pu^{240}} \sigma_c Pu^{240} \varphi - N^{Pu^{241}} \sigma_a Pu^{241} \varphi + f^{Pu^{241}} \\ \frac{dN^{Pu^{242}}}{dt} &= N^{Pu^{241}} \sigma_c Pu^{241} \varphi - N^{Pu^{242}} \sigma_a Pu^{242} \varphi + f^{Pu^{242}}\end{aligned}$$

where

$\sigma_c$  is the radiative capture cross-section

$\sigma_a$  includes capture and fission

$\varphi$  is the flux

$N$  is the atoms/cm<sup>3</sup>

$f^x$  is the feed of isotope "x" from an external source.

Since the ratio of  $f^{Pu^{239}}$  to  $f^{Pu^{240}}$  to  $f^{Pu^{241}}$  to  $f^{Pu^{242}}$  is originally specified, there remain seven unknowns in the form of the  $N$ 's and two  $f$ 's. Maintaining the total number of atoms constant provides one equation:

$$\sum_x N^x = \text{constant.}$$

Maintaining the reactivity constant in the form of a figure of merit ( $\nu \sigma_f - \sigma_c - \sigma_f$ ) summed over all fissionable and fertile isotopes provided the final equation:

$$\sum_x N^x (\nu \sigma_f - \sigma_c - \sigma_f)^x = \text{constant.}$$

TABLE I  
EQUILIBRIUM COMPOSITION FOR 800-1 REACTORS

Reactor type	Comp. of feed Pu	Equilibrium Pu composition				Atoms Pu atoms U <sup>238</sup> at equil.	Atoms Pu atoms U <sup>238</sup> initially
		Pu <sup>239</sup>	Pu <sup>240</sup>	Pu <sup>241</sup>	Pu <sup>242</sup>		
Metal	Pu A	0.653	0.293	0.041	0.013	0.172	0.128
	Pu B	0.613	0.307	0.055	0.025	0.176	0.137
	Pu C	0.544	0.281	0.066	0.109	0.189	0.163
Oxide	Pu A	0.609	0.324	0.049	0.018	0.510	0.336
	Pu B	0.474	0.366	0.096	0.064	0.571	0.360
	Pu C	0.288	0.266	0.121	0.325	0.795	0.439
Carbide	Pu A	0.618	0.318	0.048	0.017	0.319	0.222
	Pu B	0.517	0.350	0.082	0.051	0.344	0.237
	Pu C	0.367	0.276	0.104	0.253	0.420	0.283

The figure of merit was computed for each isotope in each reactor from a multi-group solution for the initial reactor composition and assumed not to vary with burn-up and recycle.

The initial and equilibrium compositions for a group of reactors having a core volume of 800 l are presented in Table I. For metal, oxide and carbide fuels, calculations have been made assuming that the initial plutonium composition and associated feed material were either plutonium A, B or C. (The equilibrium composition, of course, depends only on the composition of the feed material.) The results show the fraction of  $\text{Pu}^{242}$  present at equilibrium to be particularly sensitive to the feed material.

The results of similar calculations for a group of 1500-l reactors are given in Table II. The oxide and carbide reactors exhibit a behaviour similar to that of their 800-l counterparts. The build-up of  $\text{Pu}^{242}$  is reduced, since greater

TABLE II  
EQUILIBRIUM COMPOSITION FOR 1500-l REACTORS

Reactor type	Comp. of feed Pu	Equilibrium Pu composition				Atoms Pu atoms $\text{U}^{238}$ at equil.	Atoms Pu atoms $\text{U}^{238}$ initially
		$\text{Pu}^{239}$	$\text{Pu}^{240}$	$\text{Pu}^{241}$	$\text{Pu}^{242}$		
Metal	Pu A	0.656	0.291	0.041	0.012	0.143	0.106
	Pu B	0.665	0.284	0.039	0.011	0.139	0.113
	Pu C	0.654	0.293	0.041	0.012	0.144	0.135
Oxide	Pu A	0.582	0.343	0.054	0.021	0.391	0.253
	Pu B	0.481	0.372	0.088	0.059	0.425	0.269
	Pu C	0.329	0.287	0.109	0.275	0.542	0.323
Carbide	Pu A	0.594	0.334	0.052	0.020	0.259	0.176
	Pu B	0.532	0.353	0.073	0.042	0.271	0.187
	Pu C	0.430	0.302	0.088	0.180	0.309	0.222

internal breeding requires less  $\text{Pu}^{242}$ -bearing feed material. The metal-fuelled reactors are distinctly different, however. These reactors gained reactivity with burn-out and build-up. At equilibrium, it was necessary to remove some core plutonium, replacing it with  $\text{U}^{238}$  to maintain reactivity. Hence, the results are independent of the composition of the plutonium feed.

#### STEP-WISE APPROACH TO EQUILIBRIUM

The so-called "infinitesimal burn-up" or "constant local reactivity" approach to equilibrium is an approximation of the actual "step-wise" approach in the reactor. The real fuel elements undergo an appreciable burn-up before reprocessing and reconstitution with the addition of feed material. To test the error introduced by the "infinitesimal burn-up" approximation, five of the reactors listed in Tables I and II were rerun, using a computing programme for the step-wise approach devised by WHEELER [6]. In this programme, the average reactivity (in the form of the figure of merit described earlier) during a cycle is maintained at the prescribed value automatically. For a given burn-up of combined fissionable and fertile

atoms, assuming a plutonium-feed composition and knowing the composition of irradiated element sent to the reprocessing stage, the initial, final and average compositions of the next cycle are computed. Other reactivity effects, such as fuel growth under irradiation and neutron capture by fission products are ignored.

Major results of the step-wise calculation for 1500-l oxide reactors fed with Pu A, B and C, a 1500-l carbide reactor fed with Pu C, and an 800-l metal reactor fed with Pu A are listed respectively in Tables III—VII. The total number of fissionable and fertile atoms has been normalized to unity at the beginning of each cycle. Ten per cent burn-up is used for the oxide and carbide, five per cent for the metal. No reprocessing loss is assumed herein. In all cases the initial plutonium composition is that of the feed material.

The composition was always very close to the equilibrium value by twenty cycles. To attain 80% of equilibrium, usually measured by the change in relative

TABLE III  
STEP-WISE APPROACH TO EQUILIBRIUM  
1500-l oxide, Pu A feed

Cycle No.	Stage	$U^{238}$	$Pu^{239}$	$Pu^{240}$	$Pu^{241}$	$Pu^{242}$
1	initial	0.767	0.233	0	0	0
	final	0.712	0.167	0.021	0.001	0.000
	average	0.739	0.197	0.012	0.0004	0.000
2	initial	0.752	0.227	0.021	0.001	0.000
	final	0.697	0.163	0.037	0.003	0.000
	average	0.724	0.192	0.030	0.002	0.000
4	initial	0.731	0.214	0.050	0.005	0.000
	final	0.678	0.154	0.060	0.007	0.001
	average	0.704	0.182	0.056	0.006	0.001
7	initial	0.713	0.201	0.074	0.010	0.002
	final	0.662	0.146	0.079	0.011	0.002
	average	0.687	0.171	0.077	0.010	0.002
12	initial	0.702	0.192	0.089	0.014	0.004
	final	0.651	0.141	0.090	0.014	0.004
	average	0.676	0.164	0.090	0.014	0.004
20	initial	0.696	0.189	0.094	0.015	0.005
	final	0.647	0.139	0.094	0.015	0.005
	average	0.672	0.162	0.095	0.015	0.005
30	initial	0.696	0.188	0.095	0.015	0.006
	final	0.646	0.138	0.095	0.015	0.006
	average	0.671	0.161	0.095	0.015	0.006
40	initial	0.696	0.188	0.095	0.015	0.006
	final	0.646	0.138	0.095	0.015	0.006
	average	0.671	0.161	0.095	0.015	0.006

TABLE IV  
STEP-WISE APPROACH TO EQUILIBRIUM  
1500-l oxide Pu B feed

Cycle No.	Stage	$U^{238}$	$Pu^{239}$	$Pu^{240}$	$Pu^{241}$	$Pu^{242}$
1	initial	0.754	0.183	0.025	0.030	0.007
	final	0.700	0.138	0.037	0.018	0.007
	average	0.727	0.159	0.032	0.023	0.007
2	initial	0.736	0.186	0.044	0.025	0.009
	final	0.683	0.139	0.053	0.016	0.009
	average	0.710	0.160	0.049	0.020	0.009
4	initial	0.713	0.181	0.071	0.024	0.011
	final	0.662	0.135	0.075	0.018	0.011
	average	0.687	0.156	0.073	0.020	0.011
7	initial	0.695	0.172	0.094	0.026	0.014
	final	0.645	0.129	0.092	0.020	0.013
	average	0.669	0.148	0.093	0.023	0.013
12	initial	0.683	0.164	0.108	0.029	0.016
	final	0.634	0.124	0.103	0.023	0.015
	average	0.658	0.142	0.106	0.026	0.016
20	initial	0.678	0.162	0.112	0.030	0.018
	final	0.630	0.123	0.107	0.024	0.017
	average	0.654	0.140	0.110	0.026	0.017
26	initial	0.678	0.161	0.112	0.030	0.018
	final	0.630	0.123	0.107	0.024	0.017
	average	0.653	0.140	0.110	0.026	0.018

TABLE V  
STEP-WISE APPROACH TO EQUILIBRIUM  
1500-l oxide Pu C feed

Cycle No.	Stage	$U^{238}$	$Pu^{239}$	$Pu^{240}$	$Pu^{241}$	$Pu^{242}$
1	initial	0.716	0.114	0.028	0.071	0.071
	final	0.666	0.098	0.034	0.039	0.063
	average	0.691	0.105	0.032	0.053	0.067
2	initial	0.691	0.128	0.042	0.058	0.081
	final	0.644	0.105	0.046	0.033	0.071
	average	0.668	0.116	0.044	0.044	0.076
4	initial	0.661	0.135	0.063	0.047	0.093
	final	0.617	0.109	0.064	0.030	0.081
	average	0.638	0.121	0.064	0.038	0.087

*Cont. following page.*

TABLE V, cont.

Cycle Nr.	Stage	$U^{238}$	$Pu^{239}$	$Pu^{240}$	$Pu^{241}$	$Pu^{242}$
7	initial	0.638	0.132	0.083	0.045	0.102
	final	0.596	0.106	0.080	0.030	0.088
	average	0.616	0.118	0.082	0.037	0.094
12	initial	0.624	0.127	0.096	0.046	0.106
	final	0.583	0.102	0.092	0.031	0.091
	average	0.603	0.114	0.094	0.038	0.099
20	initial	0.619	0.125	0.102	0.047	0.107
	final	0.578	0.101	0.096	0.032	0.093
	average	0.598	0.112	0.099	0.039	0.100
30	initial	0.618	0.124	0.103	0.047	0.108
	final	0.578	0.101	0.097	0.032	0.093
	average	0.598	0.112	0.100	0.039	0.100
40	initial	0.618	0.124	0.103	0.047	0.108
	final	0.578	0.101	0.097	0.032	0.093
	average	0.598	0.112	0.100	0.039	0.100

TABLE VI  
STEP-WISE APPROACH TO EQUILIBRIUM  
1500-1 carbide, Pu C feed

Cycle No.	Stage	$U^{238}$	$Pu^{239}$	$Pu^{240}$	$Pu^{241}$	$Pu^{242}$
1	initial	0.792	0.083	0.021	0.052	0.052
	final	0.723	0.082	0.026	0.024	0.044
	average	0.757	0.083	0.024	0.036	0.048
2	initial	0.775	0.102	0.031	0.036	0.056
	final	0.709	0.091	0.036	0.018	0.046
	average	0.741	0.096	0.034	0.026	0.051
4	initial	0.758	0.110	0.048	0.027	0.057
	final	0.693	0.094	0.050	0.016	0.047
	average	0.725	0.102	0.049	0.020	0.052
7	initial	0.749	0.108	0.062	0.026	0.055
	final	0.685	0.093	0.061	0.016	0.045
	average	0.716	0.100	0.062	0.020	0.050
12	initial	0.746	0.106	0.070	0.026	0.052
	final	0.682	0.092	0.067	0.017	0.043
	average	0.714	0.098	0.068	0.021	0.047
20	initial	0.746	0.105	0.072	0.026	0.051
	final	0.682	0.091	0.068	0.017	0.042
	average	0.713	0.098	0.070	0.021	0.046
23	initial	0.746	0.105	0.072	0.026	0.050
	final	0.682	0.091	0.068	0.017	0.041
	average	0.713	0.098	0.070	0.021	0.046

TABLE VII  
STEP-WISE APPROACH TO EQUILIBRIUM,  
800-l metal Pu A feed

Cycle No.	Stage	$U^{238}$	$Pu^{239}$	$Pu^{240}$	$Pu^{241}$	$Pu^{242}$
1	initial	0.881	0.119	0	0	0
	final	0.837	0.105	0.007	0.000	0.000
	average	0.859	0.112	0.004	0.000	0.000
2	initial	0.876	0.117	0.007	0.000	0.000
	final	0.832	0.104	0.013	0.000	0.000
	average	0.854	0.110	0.010	0.000	0.000
4	initial	0.868	0.112	0.018	0.001	0.000
	final	0.825	0.100	0.022	0.002	0.000
	average	0.846	0.106	0.020	0.001	0.000
7	initial	0.861	0.107	0.030	0.003	0.000
	final	0.818	0.097	0.031	0.004	0.000
	average	0.839	0.101	0.030	0.003	0.000
12	initial	0.855	0.102	0.037	0.005	0.001
	final	0.812	0.094	0.038	0.005	0.001
	average	0.832	0.098	0.038	0.005	0.001
20	initial	0.851	0.100	0.042	0.006	0.001
	final	0.809	0.092	0.042	0.006	0.002
	average	0.830	0.096	0.042	0.006	0.001
30	initial	0.851	0.099	0.042	0.006	0.002
	final	0.808	0.091	0.043	0.006	0.002
	average	0.829	0.095	0.043	0.006	0.002

concentration of  $Pu^{239}$  in the plutonium from the beginning of the initial cycle, it was found to take the following times:

Reactor	Cycles to 80% equil.	% Burn-up/cycle
1500-l oxide, Pu-A	7—8	10
1500-l oxide, Pu-B	8	10
1500-l oxide, Pu-C	10	10
1500-l carbide, Pu-C	8	10
800-l metal, Pu-A	10	5

The equilibrium composition obtained by the step-wise procedure was nearly identical to that derived from "the infinitesimal burn-up" method. The results obtained by the two methods are compared for five different reactors in Table VIII. For the step-wise calculation the average composition during an equilibrium cycle is tabulated. The volume fractions are normalized to unity.

As described earlier, a "figure of merit" was used to "maintain" criticality throughout the many cycles needed to approach equilibrium. The validity of this approach was checked by calculating the actual deviation from criticality of the

TABLE VIII  
EQUILIBRIUM COMPOSITION BY STEP-WISE AND INFINITESIMAL BURN-UP METHODS

Reactor type	Feed material	Method of calculation	Relative volume fractions				
			U <sup>238</sup>	Pu <sup>239</sup>	Pu <sup>240</sup>	Pu <sup>241</sup>	Pu <sup>242</sup>
1500-l oxide	Pu A	Step-wise Inf. burn-up	0.708	0.170	0.100	0.016	0.006
			0.719	0.164	0.096	0.015	0.006
1500-l oxide	Pu B	Step-wise Inf. burn-up	0.689	0.148	0.116	0.028	0.019
			0.702	0.143	0.111	0.026	0.018
1500-l oxide	Pu C	Step-wise Inf. burn-up	0.630	0.118	0.105	0.041	0.105
			0.648	0.116	0.101	0.038	0.097
1500-l carbide	Pu C	Step-wise Inf. burn-up	0.752	0.103	0.074	0.023	0.048
			0.764	0.102	0.071	0.021	0.043
800-l metal	Pu A	Step-wise Inf. burn-up	0.850	0.098	0.044	0.006	0.002
			0.853	0.096	0.043	0.006	0.002

nominally critical systems. The oxide reactors fed with Pu A, B and C were all tested at various cycles between the initial and equilibrium point. The deviation of the average composition from a  $k_{eff}$  of 1.0 was always less than 0.01.

#### EFFECT OF REPROCESSING LOSSES ON EQUILIBRIUM COMPOSITION

To investigate the effect of reprocessing losses on equilibrium composition, in each of two reactors 2% of the fuel alloy was assumed to be lost in processing at the end of each burn-up cycle. The results are presented in Table IX for the 1500-l oxide reactor, fuelled and fed with either Pu A or Pu C. Comparison with the case of no reprocessing loss shows the difference to be slight.

TABLE IX  
EQUILIBRIUM COMPOSITION WITH REPROCESSING LOSS

Reactor type	Feed material	% Loss per cycle	Relative volume fractions				
			U <sup>238</sup>	Pu <sup>239</sup>	Pu <sup>240</sup>	Pu <sup>241</sup>	Pu <sup>242</sup>
1500-l oxide	Pu A	0	0.708	0.170	0.100	0.016	0.006
		2	0.714	0.174	0.093	0.014	0.005
1500-l oxide	Pu C	0	0.631	0.118	0.105	0.041	0.105
		2	0.638	0.119	0.099	0.041	0.103

#### SENSITIVITY OF EQUILIBRIUM COMPOSITION TO $\sigma_n, \gamma$ FOR PLUTONIUM ISOTOPES

Since the cross-section for radiative capture is poorly known or unknown for all the plutonium isotopes, it is of interest to study the sensitivity of various performance parameters to changes in these cross-sections. In this section the change in equilibrium composition with certain specific cross-section variation is reported.

Some data for neutron capture by Pu<sup>239</sup> existed at the time of formulation of the 16-group used herein. However, recent measurements of the capture-to-fission ratio of fast neutrons for this isotope [7] are appreciably lower than earlier experiments. A set of 16-group capture cross-sections for Pu<sup>239</sup> utilizing the new data in the energy range measured is compared with those of Ref. [4] in Table X. These cross-sections represent an obvious variation with which to study performance sensitivity.

TABLE X  
NEW 16-GROUP  $\sigma_{n,\gamma}$  FOR Pu<sup>239</sup>

Group	Energy interval (MeV)	$\sigma_{n,\gamma}$ of Ref. [4]	New $\sigma_{n,\gamma}$
1	10 — 3.668	0.054	0
2	3.668 — 2.225	0.0798	0
3	2.225 — 1.35	0.0965	0.020
4	1.35 — 0.825	0.104	0.050
5	0.825 — 0.5	0.129	0.096
6	0.5 — 0.3	0.182	0.153
7	0.3 — 0.18	0.290	0.204
8	0.18 — 0.11	0.409	0.240
9	0.11 — 0.067	0.534	0.265
10	0.067 — 0.0407	0.686	0.315
11	0.0407 — 0.025	0.892	0.675
12	0.025 — 0.015	1.084	1.056
13	0.015 — 0.0091	1.211	1.211
14	0.0091 — 0.0055	1.280	1.280
15	0.0055 — 0.0021	1.891	1.891
16	0.0021 — 0.0005	4.020	4.020

For each of the three higher plutonium isotopes, the variation assumed was to double the capture cross-section of Ref. [4] uniformly as a function of energy, maintaining the original fission and scattering cross-sections.

These four variations have been applied individually and as a group to the calculation of equilibrium mixture of a series of reactors. In Table XI the equilibrium mixture for each variation separately and for the group simultaneously is compared with that calculated with the reference cross-sections for six metal- and oxide-fuelled, 800-l reactors. In addition, the equilibrium mixture for all variations simultaneously is compared with reference cross-section results for three 800-l carbide-fuelled reactors and three 1500-l oxide-fuelled reactors.

The changes in equilibrium composition are measurable but not huge. Major design decisions are not likely to be delayed by these composition uncertainties. However, the effects on reactivity of such cross-section variations may be of some significance.

### Critical mass and breeding ratios

#### DIFFERENCES BETWEEN INITIAL AND EQUILIBRIUM COMPOSITION

Earlier calculations [3, 5] have already provided a measure of how breeding ratio rises and critical mass, measured in terms of thermally fissionable plutonium isotopes, falls with increases in the proportion of higher isotopes. This results

TABLE XI

SENSITIVITY OF EQUILIBRIUM COMPOSITION TO VARIATIONS IN THE CAPTURE CROSS-SECTION ( $\sigma_{n,\gamma}$ ) OF PLUTONIUM ISOTOPES

Reactor type	Change in Pu cross-sections	Equilibrium Pu composition				Atoms Pu atoms $U^{238}$ at equilibrium
		$Pu^{239}$	$Pu^{240}$	$Pu^{241}$	$Pu^{242}$	
800-l metal Pu A feed	None	0.653	0.293	0.041	0.013	0.172
	Lower $\sigma_{n,\gamma}$ ( $Pu^{239}$ )	0.732	0.226	0.032	0.010	0.160
	Double $\sigma_{n,\gamma}$ ( $Pu^{240}$ )	0.705	0.216	0.061	0.019	0.162
	Double $\sigma_{n,\gamma}$ ( $Pu^{241}$ )	0.649	0.291	0.038	0.023	0.175
	Double $\sigma_{n,\gamma}$ ( $Pu^{242}$ )	0.656	0.294	0.041	0.009	0.171
	Change all together	0.776	0.164	0.042	0.018	0.155
800-l metal Pu B feed	None	0.613	0.307	0.055	0.025	0.176
	Lower $\sigma_{n,\gamma}$ ( $Pu^{239}$ )	0.688	0.244	0.046	0.022	0.164
	Double $\sigma_{n,\gamma}$ ( $Pu^{240}$ )	0.663	0.227	0.077	0.033	0.164
	Double $\sigma_{n,\gamma}$ ( $Pu^{241}$ )	0.606	0.305	0.050	0.039	0.179
	Double $\sigma_{n,\gamma}$ ( $Pu^{242}$ )	0.618	0.310	0.055	0.017	0.175
	Change all together	0.734	0.178	0.058	0.030	0.155
800-l metal Pu C feed	None	0.544	0.281	0.066	0.109	0.189
	Lower $\sigma_{n,\gamma}$ ( $Pu^{239}$ )	0.618	0.225	0.057	0.100	0.173
	Double $\sigma_{n,\gamma}$ ( $Pu^{240}$ )	0.585	0.206	0.087	0.123	0.176
	Double $\sigma_{n,\gamma}$ ( $Pu^{241}$ )	0.543	0.278	0.059	0.120	0.189
	Double $\sigma_{n,\gamma}$ ( $Pu^{242}$ )	0.574	0.291	0.065	0.069	0.178
	Change all together	0.697	0.166	0.063	0.074	0.151
800-l oxide Pu A feed	None	0.609	0.324	0.049	0.018	0.510
	Lower $\sigma_{n,\gamma}$ ( $Pu^{239}$ )	0.677	0.268	0.041	0.014	0.470
	Double $\sigma_{n,\gamma}$ ( $Pu^{240}$ )	0.670	0.234	0.071	0.025	0.464
	Double $\sigma_{n,\gamma}$ ( $Pu^{241}$ )	0.604	0.321	0.044	0.031	0.527
	Double $\sigma_{n,\gamma}$ ( $Pu^{242}$ )	0.613	0.326	0.049	0.012	0.508
	Change all together	0.733	0.190	0.052	0.025	0.447
800-l oxide Pu B feed	None	0.474	0.366	0.096	0.064	0.571
	Lower $\sigma_{n,\gamma}$ ( $Pu^{239}$ )	0.522	0.324	0.090	0.064	0.533
	Double $\sigma_{n,\gamma}$ ( $Pu^{240}$ )	0.529	0.267	0.125	0.078	0.504
	Double $\sigma_{n,\gamma}$ ( $Pu^{241}$ )	0.464	0.359	0.086	0.091	0.602
	Double $\sigma_{n,\gamma}$ ( $Pu^{242}$ )	0.485	0.374	0.098	0.043	0.560
	Change all together	0.581	0.238	0.107	0.073	0.488
800-l oxide Pu C feed	None	0.288	0.266	0.121	0.325	0.795
	Lower $\sigma_{n,\gamma}$ ( $Pu^{239}$ )	0.314	0.238	0.118	0.329	0.752
	Double $\sigma_{n,\gamma}$ ( $Pu^{240}$ )	0.314	0.189	0.144	0.353	0.715
	Double $\sigma_{n,\gamma}$ ( $Pu^{241}$ )	0.278	0.259	0.108	0.356	0.852
	Double $\sigma_{n,\gamma}$ ( $Pu^{242}$ )	0.326	0.299	0.136	0.238	0.698
	Change all together	0.376	0.188	0.142	0.293	0.637
800-l carbide Pu A feed	None	0.618	0.318	0.048	0.017	0.319
	Change all together	0.739	0.187	0.051	0.023	0.286

Cont. following page

TABLE XI, *cont.*

Reactor type	Change in Pu cross-sections	Equilibrium Pu composition				Atoms Pu atoms U <sup>238</sup> at equilibrium
		Pu <sup>239</sup>	Pu <sup>240</sup>	Pu <sup>241</sup>	Pu <sup>242</sup>	
800-1 carbide Pu B feed	None	0.517	0.350	0.082	0.051	0.344
	Change all together	0.626	0.222	0.092	0.059	0.299
800-1 carbide Pu C feed	None	0.367	0.276	0.104	0.253	0.420
	Change all together	0.470	0.187	0.119	0.224	0.340
1500-1 oxide Pu A feed	None	0.582	0.343	0.054	0.021	0.391
	Change all together	0.709	0.204	0.058	0.029	0.342
1500-1 oxide Pu B feed	None	0.481	0.372	0.088	0.059	0.425
	Change all together	0.595	0.238	0.099	0.068	0.360
1500-1 oxide Pu C feed	None	0.329	0.287	0.109	0.275	0.542
	Change all together	0.434	0.200	0.126	0.243	0.427

because Pu<sup>241</sup> is more reactive than Pu<sup>239</sup> and because Pu<sup>240</sup> provides a greater fast-fission bonus than U<sup>238</sup>.

The change in performance from initial to equilibrium composition has been computed herein for the three oxide reactors whose step-wise approach to equilibrium was reported above. The critical mass and breeding ratio are compared in Table XII. The considerable increases in breeding ratio in each case are attributed primarily to a net build-up of Pu<sup>240</sup> in the equilibrium mixture, and the consequent increased fast-fission bonus.

TABLE XII  
COMPARISON OF INITIAL AND EQUILIBRIUM CRITICAL MASS AND BREEDING RATIO FOR 1500-1 OXIDE REACTORS

Feed	Critical mass*		Breeding ratio**	
	Initial	Equil.	Initial	Equil.
Pu A	562	496	1.47	1.67
Pu B	514	468	1.57	1.80
Pu C	442	421	1.72	1.96

\* Kilograms of (Pu<sup>239</sup> + Pu<sup>241</sup>).

\*\* (Pu<sup>239</sup> + Pu<sup>241</sup> produced) / (Pu<sup>239</sup> + Pu<sup>241</sup> consumed).

#### EFFECT OF CAPTURE CROSS-SECTION OF PLUTONIUM ISOTOPES ON BREEDING AND CRITICAL MASS

The changes in breeding ratio and critical mass occasioned by the use of recent data on  $\alpha$  ( $=\sigma_n, \gamma/\sigma_f$ ) for Pu<sup>239</sup> [7] are illustrated in Table XIII. The performances

for an 800-l metal-fuelled reactor and for 1500-l metal-, oxide- and carbide-fuelled reactors are compared, using the  $\alpha_{\text{Pu}^{239}}$  cross-sections of YIFTAH *et al.* [4] and the altered multi-group cross-sections listed in Table X.

TABLE XIII  
CHANGE IN BREEDING RATIO AND CRITICAL MASS WITH NEW DATA FOR  
 $\sigma_{n,\gamma}$   $\text{Pu}^{239}$

Reactor type*	Old data (Ref. [4])			New data (Ref. [7])		
	Critical mass (kg)	Breeding ratio	$\gamma - \text{Pu}^{239}$	Critical mass (kg)	Breeding ratio	$\gamma - \text{Pu}^{239}$
800-l metal fuel	431	1.82	0.188	422	1.96	0.132
1500-l metal fuel	686	1.79	0.198	672	1.93	0.140
1500-l oxide fuel	567	1.47	0.251	562	1.55	0.190
1500-l carbide fuel	613	1.56	0.241	601	1.68	0.183

\* All use Pu A fuel and steel structure.

The critical mass is seen to drop slightly, while the breeding ratio rises by 0.08 to 0.14. The metal-fuelled reactors show greater gains. They have a harder spectrum and take greater advantage of the reductions in  $\alpha$  above 100 kV.

The effect of possibly higher capture cross-sections in the higher plutonium isotopes was also investigated. Metal-, oxide- and carbide-fuelled reactors using Pu C with doubled capture cross-sections for the higher isotopes were calculated. Their performance is compared against that predicted by the original 16-group cross-section set in Table XIV. The critical mass rises 5 to 10%, while the breeding ratio drops by about 0.15 for this fairly extreme mixture of plutonium isotopes.

TABLE XIV  
CHANGE IN BREEDING RATIO AND CRITICAL MASS UPON DOUBLING  $\sigma_{n,\gamma}$   
FOR  $\text{Pu}^{240}$ ,  $\text{Pu}^{241}$ ,  $\text{Pu}^{242}$

Reactor type*	Old data (Ref. [4])		Doubled $\sigma_c$	
	Critical mass **(kg)	Breeding ratio	Critical mass (kg)	Breeding ratio
Metal fuel	552	2.08	579	1.94
Oxide fuel	442	1.72	486	1.55
Carbide fuel	483	1.82	514	1.68

\* All reactors have 1500-l core, use Pu C and steel structure.

\*\* Critical mass in terms of thermally fissionable isotopes.

#### EFFECT OF STRUCTURAL MATERIAL ON PERFORMANCE

The effect of substituting other structural materials for the 25% by volume of steel (iron) used in the usual calculations is illustrated in Table XV, which is reproduced from Ref. [3]. Titanium and zirconium perform similarly to steel, while vanadium is slightly worse because of a large inelastic-scattering cross-section. Appreciable capture in molybdenum and niobium reduces the breeding considerably in these 800-l metal-fuelled reactors, while tantalum drops the breeding ratio nearly to unity.

TABLE XV

**EFFECT OF VARIOUS STRUCTURAL MATERIALS ON 800-l PLUTONIUM-METAL-FUELLED REACTORS**

Structural material	Critical mass (kg)	Breeding ratio	Alpha
Fe (stainless steel)	431	1.82	0.188
Ti	425	1.92	0.180
V	456	1.68	0.222
Zr	415	1.89	0.181
Nb	494	1.51	0.169
Mo	502	1.46	0.185
Ta	716	1.02	0.170

**Sodium coefficients**
**INFLUENCE OF HIGHER ISOTOPES OF PLUTONIUM**

A cursory look at the influence of higher plutonium isotopes on the sodium reactivity coefficient was taken in Ref. [3]. For 1500-l metal-, oxide- and carbide-fuelled reactors, using Pu A or Pu C, the sodium coefficients were compared and found to be more negative in each case with Pu C. However, Pu C contains a very large proportion of  $Pu^{241}$ , an isotope which has been assumed to exhibit a flatter dependence with energy of  $\eta$ , the neutrons emitted per absorption. It was believed that this might have overridden anticipated positive contributions from the threshold-fissionable isotopes,  $Pu^{240}$  and  $Pu^{242}$ . Hence, a sodium-reactivity-coefficient calculation has been made for a 1500-l metal-fuelled reactor, using Pu AB, which contains 90%  $Pu^{239}$  and 10%  $Pu^{240}$ . In this case the sodium coefficient was calculated to be more positive than for the same reactor fuelled with Pu A. For a 40% reduction in core sodium, the  $\delta M/M_c$  which produced the same reactivity change was +0.004 with Pu A and +0.006 with Pu AB.

**VARIATION OF SODIUM COEFFICIENT WITH RECYCLE**

The change in plutonium isotopic composition with recycle can be expected to produce some change in the sodium reactivity coefficient. Actually, the change can be appreciable, as is shown in Table XVI. Sodium coefficients for 1500-l oxide reactors fed with Pu A, B and C respectively have been followed from the initial to the equilibrium cycle. The numbers reported are in terms of the fractional change in critical mass producing the same reactivity change as a 40% reduction in core sodium. In these three cases, the sodium coefficient became less negative as the equilibrium composition built up.

**SENSITIVITY TO CROSS-SECTION UNCERTAINTIES**

The sensitivity of the sodium reactivity coefficient to uncertainties in capture cross-sections for the plutonium isotopes was examined briefly. For an 800-l metal and for 1500-l metal, oxide and carbide reactors using Pu A, the sodium coefficient was compared, using the cross-sections of Ref. [3] and the new data for  $Pu^{239}$ . The results given in Table XVII show practically no effect for the

TABLE XVI  
VARIATION IN SODIUM COEFFICIENT WITH RECYCLE IN OXIDE REACTORS

Feed material*	Cycle No.	$\Delta M_c/M_c$
Pu A	1	-0.0115
	3	-0.0091
	6	-0.0077
	9	-0.0069
	12	-0.0064
	Equil.	-0.0061
Pu B	1	-0.0131
	3	-0.0094
	7	-0.0071
	Equil.	-0.0058
Pu C	1	-0.0130
	3	-0.0074
	6	-0.0041
	8	-0.0032
	10	-0.0028
	Equil.	-0.0021

\* Initial Pu composition same as feed. 1500-l reactors.

metal-fuelled reactors with this specific cross-section change. The oxide and carbide, with many more neutrons at low energies, apparently have a spectral shift carrying over into the energy region of large deviation in the cross-section, and show a less negative sodium coefficient, on the other hand.

TABLE XVII  
SENSITIVITY OF SODIUM REACTIVITY COEFFICIENT TO ALPHA OF  $Pu^{239}$

Reactor type	Sodium coefficient in $\delta M/M_c$ required to provide same reactivity effect as 40% removal of Na in core	
	Data of Ref. [4]	New data
800-l metal	-0.0047	-0.0048
1500-l metal	+0.0041	+0.0043
1500-l oxide	-0.0140	-0.0107
1500-l carbide	-0.0058	-0.0033

Sodium-coefficient calculations were also made maintaining the original  $\sigma_{n,\gamma}$  in  $Pu^{239}$  and doubling capture in all groups for  $Pu^{240}$ ,  $Pu^{241}$  and  $Pu^{242}$ . For 1500-l reactors fuelled with Pu C, the sodium coefficient became appreciably more positive in all cases, as expected. The results are presented in Table XVIII.

It must be cautioned that the two effects studied are not additive in linear fashion.

TABLE XVIII

**SENSITIVITY OF SODIUM REACTIVITY COEFFICIENT TO CAPTURE IN  $\text{Pu}^{240}$ ,  
 $\text{Pu}^{241}$  AND  $\text{Pu}^{242}$** 

Reactor type*	Sodium coef. in $\delta M/M_c$ required to provide same reactivity effect as 40 % removal of Na in core	
	Data of Ref. [4]	Double capture in $\text{Pu}^{240}$ , $\text{Pu}^{241}$ and $\text{Pu}^{242}$
Metal	+0.0014	+0.0035
Oxide	-0.0162	-0.0113
Carbide	-0.0076	-0.0039

\* All reactors have 1500-l core volume, used Pu C and steel structure.

**SENSITIVITY TO CORE COMPOSITION**

The competing reactivity effects of neutron scattering and neutron moderation by sodium [8] will depend on the composition of the core. In the large metal-fuelled reactors, it may be possible to change the sign of the net sodium coefficient by reducing the volume fractions of  $\text{U}^{238}$  and steel appreciably, so that sodium scattering becomes a greater fraction of the total. The results from some 1500-l metal-fuelled reactors in Table XIX confirm this effect to be significant, with the  $\text{U}^{238}$  being of greater importance.

TABLE XIX

**VARIATION OF SODIUM COEFFICIENT WITH CORE COMPOSITION**

Reactor type*				Sodium coefficient, in terms of $\delta M/M$ to produce same reactivity effect as removal of 40 % Na
Vol % $\text{U}^{238}$	Vol % structure	Vol % Na	Type structure	
25	25	50	Steel	+0.0043
15	25	60	Steel	-0.0093
15	15	70	Steel	-0.0116
15	15	70	Nb	+0.0067

\* 1500-l, metal-fuelled reactors. The new  $\text{Pu}^{239}$  cross-sections for  $\sigma_{\gamma\gamma}$  were used.

A calculation where niobium has been substituted for steel in the "reduced scattering" composition core reconfirms an effect demonstrated earlier [3], namely, that strongly capturing structural materials can make the sodium coefficient more positive. This follows from a reduction in core leakage as well as an increase in the slope of  $d\bar{\eta}/dE$  for the mixture. Such calculations suggest strongly that the future of very large fast reactors may require the use of structural and cladding materials with small capture cross-sections, like titanium or zirconium.

### Delayed-neutron characteristics

Another reactor characteristic affected by changes in plutonium isotopic composition is the delayed-neutron fraction. Simple estimates of this quantity are presented for a series of reactors in Table XX. Criticality calculations were used to determine the relative number of fissions by each isotope in the core, using the 16-group set of Ref. [4]. The delayed-neutron fractions for the pure isotopes were taken as follows:

Material	$\bar{\beta}^*$
$U^{238}$	0.0157
$Pu^{239}$	0.0021
$Pu^{240}$	0.00267
$Pu^{241}$	0.00534
$Pu^{242}$	0.0080

No allowance was made for spatial variation of fission in the various isotopes, and contributions from the blanket were not included.

The reactors fuelled with Pu A exhibit the expected increase in  $\bar{\beta}$  above that for pure  $Pu^{239}$  which is due to contributions from  $U^{238}$ . As a large fraction of higher plutonium isotopes is added,  $\bar{\beta}$  is found to increase appreciably. For the oxide fuel a 50% increase in the delayed neutrons from the core is experienced on going from Pu A to Pu C.

TABLE XX  
DELAYED-NEUTRON FRACTION FOR CORE OF REACTORS FUELLED WITH  
Pu A, B, AND C

Reactor type	$\bar{\beta}$ core	$\bar{v}$
Pu A Metal	0.00454	2.932
	0.00326	2.939
	0.00372	2.936
Pu B Metal	0.00501	2.950
	0.00384	2.958
	0.00427	2.955
Pu C Metal	0.00596	2.984
	0.00491	2.993
	0.00530	2.989

Within any given composition, much smaller changes in  $\bar{\beta}$  were calculated upon changing reactor size. Of course, the relative number of different delay groups will also be altered, resulting in further changes in the kinetic behaviour of the reactor, as evidenced by the zero power transfer function, for example.

\* Data for all isotopes but  $Pu^{242}$  taken from ANL-6300, Reactor Physics Constants (to be published) or S. A. Cox (submitted to *Phys. Rev.*, April 1961). Value for  $Pu^{242}$  estimated by A. B. Smith empirically from systematics.

The delayed-neutron fraction for a given reactor will also change measurably with burn-up and recycle. Assuming 10% burn-up of combined fissile and fertile isotopes, the change in delay fraction during a single cycle was computed for the 1500-l oxide reactors fuelled with Pu A, B and C respectively. The calculation was repeated for the same reactors fuelled with the equilibrium composition resulting from feeds of Pu A, B and C respectively. The results given in Table XXI indicate the effect to be minor from safety considerations. However, if routine transfer measurements are to be made during the lifetime of a reactor, measurable shifts in the zero-power results can be anticipated, even during a single burn-up cycle. Actually, the results of Table XXI indicate that the change over the reactor lifetime with recycle may not be very much greater than that in a single cycle.

TABLE XXI  
CHANGE IN DELAYED-NEUTRON FRACTION DURING A SINGLE CYCLE OF  
10% BURN-UP

Reactor type*	Beginning of cycle		End of cycle	
	$\bar{\beta}$	$\bar{\nu}$	$\bar{\beta}$	$\bar{\nu}$
Pu A fuel	0.003 079	2.940	0.003 415	2.946
Pu B fuel	0.003 669	2.960	0.003 794	2.962
Pu C fuel	0.004 747	2.996	0.004 702	2.994
Equil. comp. for Pu A feed	0.003 385	2.973	0.003 635	2.980
Equil. comp. for Pu B feed	0.003 731	2.988	0.003 901	2.992
Equil. comp. for Pu C feed	0.004 509	3.018	0.004 580	3.021

\* 1500-l oxide reactors.

## Fission products and long-term reactivity effects

### FISSION PRODUCTS

Measurements of the fast-neutron cross-sections for most fission products are very sparse. Theoretical estimates have been made of their average capture cross-section as a function of energy, however, and the most recent of these [9] has been adopted herein. For simplicity, the inelastic- and elastic-scattering cross-sections have been assumed to be the same as those of molybdenum, and the 16-group representation of Yiftah *et al.* [4] was used. The 16-group capture cross-sections adopted for fission products are given in Table XXII.

This cross-section set was used to analyse a series of central reactivity measurements made upon Physicium I and II, a pair of non-radioactive mixtures of natural elements which are nuclear mock-ups [10, 11] of the fission products. Similar measurements made on samples of molybdenum, niobium and tantalum were also calculated. A comparison of theory and experiment is presented in Table XXIII. The agreement is about the same for all materials analysed, not perfect but much better than a factor of 2 on the average. The measurements for Physicium on Assembly No. 32 were subject to some uncertainty, hence have a question mark attached. The composition and geometry of the various ZPR-III assemblies can be found in Ref. [4], [11] and [12]. The relation between inhours

TABLE XXII  
CAPTURE CROSS-SECTIONS FOR FISSION PRODUCT

Group	$\sigma_{n,\gamma}$
1	0.020
2	0.040
3	0.063
4	0.090
5	0.092
6	0.095
7	0.110
8	0.125
9	0.140
10	0.165
11	0.200
12	0.250
13	0.330
14	0.450
15	0.690
16	1.54

TABLE XXIII  
CENTRAL REACTIVITY EFFECTS FOR PHYSICUM, Mo, Nb AND Ta IN VARIOUS  
ZPR-III ASSEMBLIES  
Measured and calculated

Assembly No.	Inhours per % $\delta k/k$	Loss in $\delta k/k$ per gram atom					
			Ph I	Ph II	Mo	Nb	Ta
8	430	Meas.	0.000053	0.000063	0.000030	0.000047	0.000123
		Calc.	0.000081	0.000081	0.000042	0.000053	0.000153
20	444	Meas.	0.000063	—	0.000023	—	0.000101
		Calc.	0.000060	—	0.000043	—	0.000113
24	475	Meas.	0.000048	0.000063	0.000032	0.000040	0.000124
		Calc.	0.000048	0.000048	0.000035	0.000037	0.000095
25	478	Meas.	0.000052	0.000050	0.000025	0.000031	0.000098
		Calc.	0.000036	0.000036	0.000025	0.000025	0.000073
29	437	Meas.	0.000076	0.000058	0.000026	0.000041	0.000134
		Calc.	0.000049	0.000049	0.000030	0.000045	0.000123
30	433	Meas.	0.000049	0.000052	—	—	—
		Calc.	0.000044	0.000044	—	—	—
31	434	Meas.	0.000031	0.000028	—	—	—
		Calc.	0.000034	0.000034	—	—	—
32	422	Meas.	0.000100	0.000069	0.000014	—	—
		Calc.	0.000066	0.000066	0.000029	—	—
33	422	Meas.	0.000092	0.000073	0.000014	0.000026	0.000131
		Calc.	0.000055	0.000055	0.000024	0.000038	0.000121

and %  $\delta k/k$  used to convert experimental measurements was crudely estimated and does not represent a sophisticated calculation.

Of course, Physicum itself represents only a simple approximation of fission products. And the central reactivity measurements are sensitive to both capture and energy degradation, but not elastic transport. Hence, the validity of performance calculations on the effect of fission products in large reactor systems is by no means assured.

TABLE XXIV  
INFLUENCE OF FISSION PRODUCTS\* ON BREEDING RATIO, CRITICAL MASS AND REACTIVITY

Reactor type**	Critical mass (kg)		Breeding ratio		Loss in reactivity
	New reactor	With fission products*	New reactor	With fission products**	
Metal	686	700	1.79	1.74	0.0115
Oxide	562	592	1.47	1.39	0.0312
Carbide	613	630	1.56	1.47	0.0165

\*  $0.0008 \times 10^{24}$  atoms per cubic centimeter of fission product.

\*\* 1500-l, fuelled with Pu A.

The effect of fission products on critical mass, breeding ratio and reactivity is given in Table XXIV for 1500-l reactors using metal, oxide and carbide fuels respectively. To the original reactor,  $0.0008 \times 10^{24}$  atoms per cubic centimeter of fission product have been added uniformly to the core and the ratio of Pu A to U<sup>238</sup> adjusted slightly for criticality. This many atoms of fission products would accumulate if 3½% of the combined Pu and U<sup>238</sup> fissioned in the metal reactor, for an average of 33,000 MWD per ton. The corresponding burn-up is 8.55% for the oxide, 5.8% for the carbide.

The method of calculation introduces small side-effects, since a spectral change occurs and the U<sup>238</sup>-fission bonus is influenced. Cross-section uncertainties represent a greater potential error, however. The drop of 0.05 to 0.09 in breeding ratio can only be considered semi-quantitative.

The loss in reactivity for each reactor was computed by finding the change in  $k_{\text{eff}}$  upon addition of  $0.0008 \times 10^{24}$  atoms per cubic centimeter of fission product, other things remaining undisturbed.

#### BUILD-UP OF PLUTONIUM IN BLANKET

The reactivity gain accompanying the build-up of plutonium in the blanket was calculated, neglecting second-order effects such as burn-out of bred plutonium. For 800-, 1500- and 2500-l metal-fuelled reactors, the plutonium build-up corresponding to the fissioning of 5% of the combined uranium and plutonium atoms in the core was inserted into the blanket. For 1500-l oxide and carbide reactors, the identical blanket-plutonium build-up was used as in the 1500-l metal case. The reactivity gains are listed in Table XXV.

The reactivity gain decreases with increasing size, even though the amount of plutonium bred in the blanket for the 2500-l reactor doubles that at 800 l. This must be due to the reduced reactivity value of plutonium at greater radii.

TABLE XXV  
REACTIVITY EFFECT OF BLANKET PLUTONIUM

Reactor type	$\Delta k/k^*$
800-l metal	0.026
1500-l metal	0.021
1500-l oxide	0.027
1500-l carbide	0.025
2500-l metal	0.017

\* Corresponding to 5% burn-up for metal-fuelled reactors, and exactly the same plutonium build-up for oxide and carbide as in the 1500-l metal reactor.

In the oxide and carbide, the reduced core density makes for a greater reactivity worth of plutonium near the core boundary, hence a greater reactivity gain.

Other studies [13] have indicated that the shape of the plutonium production in the blanket is relatively insensitive to the core composition. Hence, the calculations reported herein for the oxide and carbide can be applied directly to reactors of this size with a correction for differences in external breeding relative to core burn-up.

#### REACTIVITY EFFECT OF BURN-OUT AND BUILD-UP IN CORE

The change in reactivity due to burn-out and/or build-up of core plutonium and uranium has been computed for five reactors, as follows.

1500-l oxide, fuelled and fed with Pu A, B and C respectively;

1500-l carbide, fuelled and fed with Pu C;

800-l metal, fuelled and fed with Pu A.

TABLE XXVI  
REACTIVITY LOSS FROM BURN-OUT AND BUILD-UP IN CORE OF Pu AND U<sup>238</sup>

Reactor type	Cycle	$\Delta k/k$
1500-l oxide Pu A 10% burn-up	Initial	0.169
	Equil.	0.137
1500-l oxide Pu B 10% burn-up	Initial	0.171
	Equil.	0.178
1500-l oxide Pu C 10% burn-up	Initial	0.136
	Equil.	0.154
1500-l carbide Pu C 10% burn-up	Initial	0.147
	Equil.	0.105
800-l metal Pu A 5% burn-up	Initial	0.054
	Equil.	0.034

In each case the reactivity change has been computed for the first cycle of the reactor, and for a cycle at equilibrium composition. Ten per cent of the combined uranium and plutonium atoms fission in an oxide or carbide cycle, five per cent in the metal case. The results are listed in Table XXVI. The reactivity change is moderately sensitive to the plutonium isotopic composition, but by far the biggest effect occurs with change in internal breeding ratio. For the 800-l metal reactor the internal breeding ratio is 0.7—0.8. For the oxide this parameter is only half as great.

#### COMBINED FISSION-PRODUCT, BLANKET-BUILD-UP AND CORE-BURN-OUT REACTIVITY EFFECTS

The combined reactivity effects of fission products, blanket build-up and core burn-out are listed in Table XXVII for a metal-, oxide- and carbide-fuelled reactor respectively. The burn-ups chosen are arbitrary; the numbers can quickly be scaled for other conditions. The initial, rather than equilibrium, condition, using Pu A, is represented.

TABLE XXVII  
COMBINED REACTIVITY EFFECTS

Reactor type*	Atoms/cm <sup>3</sup> Pu plus U ( $\times 10^{-24}$ )	Burn-up, % of Pu + U fissioned	$\delta k/k$			Total
			Burn-out in core	Build-up in blanket	Fission product build-up	
800-l metal	0.012	5	—0.054	+0.026	—0.017**	—0.045
1500-l oxide	0.00467	10	—0.169	+0.025	—0.037	—0.181
1500-l carbide	0.0069	10	—0.147	+0.031	—0.028	—0.144

\* All use Pu A.

\*\* Actually computed for 1500-l reactor.

The reactivity loss is seen to be very large for the oxide and carbide. Frequent, partial reloading will be needed for such reactors, unless the internal breeding ratio can be raised. Unfortunately, increased internal breeding can be expected to lead to a more positive sodium coefficient.

#### High-energy spectrum

It had been the practice in the past to assume that the high-energy spectrum of fast reactors had the shape of the fission spectrum. For multi-group cross-section sets with only one group above the U<sup>238</sup> fission threshold ( $\sim 1.4$  MeV), this assumption was usually applied to group 1. In the recent 16-group set [4], where three groups were used above 1.4 MeV, a fission spectrum was assumed for the first two groups.

The existence of this latter cross-section set, with some degree of meaning to the inelastic cross-sections for most materials at high energies, makes it of interest to examine the calculated high-energy spectra of various reactors, comparing them with the fission spectrum.

First, the series of ZPR-III and Los Alamos criticals calculated to test the 16-group set of Yiftah *et al.* [4] are treated. The ratio of the flux in group 1 to

that in group 2, and the ratios of the fluxes in groups 1 and 2 respectively to that in group 3 are tabulated and compared to similar ratios for fission spectrum neutrons in Tables XXVIII and XXIX. Since the overall spectrum may change appreciably in traversing these fairly small cores, the ratios are listed for three core positions, centre, half-way out and near the core boundary. Table XXVIII shows that the high-energy spectrum is essentially constant in the bare reactors GODIVA and JEZEBEL, and does not deviate greatly from the fission spectrum.

TABLE XXVIII  
RATIO OF CORE FLUXES IN HIGH ENERGY-GROUPS FOR LOS ALAMOS CRITICALS

Assembly	Group 1/Group 2			Group 1/Group 3			Group 2/Group 3		
	Centre	Midway	Near edge	Centre	Midway	Near edge	Centre	Midway	Near edge
GODIVA	0.60	0.60	0.61	0.48	0.49	0.49	0.81	0.81	0.81
TOPSY	0.59	0.62	0.66	0.48	0.36	0.35	0.81	0.57	0.53
JEZEBEL	0.59	0.60	0.61	0.51	0.51	0.52	0.86	0.86	0.86
POPSY	0.59	0.63	0.66	0.50	0.35	0.35	0.85	0.56	0.53
U <sup>233</sup> with U <sup>235</sup> reflector	0.59	0.60	0.61	0.51	0.51	0.52	0.86	0.86	0.86
Fission spectrum	0.62			0.57			0.92		

Group 1: 3.668 to 10 MeV. Group 2: 2.225 to 3.668 MeV. Group 3: 1.35 to 2.225 MeV.

TABLE XXIX  
RATIO OF CORE FLUXES IN HIGH-ENERGY GROUPS FOR ZPR-III CRITICALS

Assembly No.	Group 1/Group 2			Group 1/Group 3			Group 2/Group 3		
	Centre	Midway	Near edge	Centre	Midway	Near edge	Centre	Midway	Near edge
2A	0.49	0.54	0.63	0.31	0.28	0.30	0.63	0.52	0.48
6F	0.54	0.55	0.57	0.36	0.30	0.26	0.67	0.54	0.45
9A	0.55	0.58	0.65	0.35	0.31	0.32	0.64	0.54	0.49
10	0.56	0.57	0.65	0.36	0.36	0.32	0.64	0.64	0.49
11	0.58	0.59	0.65	0.37	0.34	0.32	0.64	0.58	0.49
12	0.58	0.60	0.58	0.38	0.34	0.27	0.66	0.57	0.45
14	0.55	0.62	0.67	0.35	0.34	0.33	0.66	0.56	0.48
15	0.55	0.56	0.65	0.35	0.33	0.31	0.64	0.58	0.49
16	0.58	0.60	0.66	0.37	0.34	0.32	0.65	0.57	0.49
17	0.56	0.61	0.67	0.37	0.34	0.33	0.65	0.56	0.49
20	0.51	0.51	0.56	0.30	0.26	0.24	0.59	0.50	0.44
24	0.59	0.59	0.65	0.37	0.37	0.32	0.63	0.64	0.50
25	0.59	0.59	0.59	0.37	0.37	0.36	0.63	0.63	0.61
Fission spectrum	0.62			0.57			0.92		

Group 1: 3.668 to 10 MeV. Group 2: 2.225 to 3.668 MeV. Group 3: 1.35 to 2.225 MeV.

However, the small reflected assemblies TOPSY and POPSY show a considerable change in the ratio of groups 1 or 2 to group 3 on traversing the core. Closer examination of the calculations showed that this change was not gradual but took place rather abruptly on traversing 10 cm radially in the inner half of the core.

Since the statistical model was used to describe the energy loss upon inelastic scattering in groups 1 and 2 for essentially all materials in the 16-group set [4], it is not surprising that the ratio of the fluxes in these two groups remains relatively constant.

In Table XXIX, considerably more deviation from the fission spectrum is demonstrated for the series of moderate-sized critical assemblies performed in the ZPR-III facility.

The calculated spectra for a series of large, fast power reactors [3] provide the basis for comparing the high-energy flux in more dilute assemblies with the fission spectrum. The results for average core flux of Table XXX show the high-energy spectra to be further degraded from fission spectrum than was calculated for the intermediate-sized ZPR-III assemblies. However, for any particular reactor type, little change in the high-energy spectrum was found on going from 800 to 2500 l core volume. The substitution of Pb-Bi for the sodium coolant reduced the relative amount of group 1 flux, as would be expected from an

TABLE XXX  
RATIO OF AVERAGE CORE FLUXES IN HIGH-ENERGY GROUPS FOR LARGE POWER REACTORS

Reactor type				Group 1 Group 2	Group 1 Group 3	Group 2 Group 3
Core volume (l)	Fuel alloy	Coolant	Structure			
800	Pu-U <sup>238</sup>	Na	SS*	0.51	0.29	0.56
1500	Pu-U <sup>238</sup>	Na	SS	0.51	0.28	0.55
2500	Pu-U <sup>238</sup>	Na	SS	0.51	0.28	0.55
800	Pu-U <sup>238</sup>	Na	Ta	0.60	0.40	0.66
800	Pu-U <sup>238</sup>	Na	Mo	0.55	0.34	0.61
800	Pu-U <sup>238</sup>	Na	Zr	0.54	0.30	0.56
800	Pu-U <sup>238</sup>	Na	Nb	0.60	0.36	0.60
800	Pu-U <sup>238</sup>	Na	Ti	0.51	0.30	0.58
800	Pu-U <sup>238</sup>	Na	V	0.56	0.34	0.61
1500	PuO <sub>2</sub> -U <sup>238</sup> O <sub>2</sub>	Na	SS	0.49	0.26	0.54
1500	PuC-U <sup>238</sup> C	Na	SS	0.49	0.26	0.54
800	Pu-U <sup>238</sup>	Pb-Bi	SS	0.44	0.22	0.51
800	PuO <sub>2</sub> -U <sup>238</sup> O <sub>2</sub>	Pb-Bi	SS	0.41	0.20	0.49
800	Pu C-U <sup>238</sup> C	Pb-Bi	SS	0.41	0.20	0.49
800	U <sup>233</sup> -Th	Na	SS	0.50	0.28	0.56
800	U <sup>233</sup> O <sub>2</sub> -Th O <sub>2</sub>	Na	SS	0.48	0.27	0.55
Fission spectrum				0.62	0.57	0.92

Group 1: 3.668 to 10 MeV. Group 2: 2.225 to 3.668 MeV. Group 3: 1.35 to 2.225 MeV.

\* SS = stainless steel.

examination of the inelastic cross-sections. In a similar vein, there was some effect due to a change in structural material or a change from metal to ceramic fuel. The latter was effective primarily as a reduction in  $U^{238}$  concentration.

From a practical point of view, these variations from fission spectrum are important in how they affect multi-group cross-sections. A simple but indicative test was made by forming flux-weighted cross-sections for  $Pu^{239}$  and graphite in groups 1 and 2, using the fission spectrum on the one hand, and a smooth curve, drawn through the block diagram of the spectrum calculated for the 1500-l oxide-fuelled reactor of Table XXX. The percentage differences for groups 1 and 2 are shown in Table XXXI.

TABLE XXXI  
PERCENTAGE DIFFERENCE IN CROSS-SECTIONS FOR  $Pu^{239}$  AND GRAPHITE  
upon averaging with fission spectrum or reactor spectrum

	$\sigma_{tot}$	$\sigma_{tr}$	$\sigma_{es}^*$	$\bar{\mu}$	$\sigma_{er}^{**}$	$\sigma_{inel}$	$\sigma_c$	$\sigma_f$
<b>Pu 239</b>								
Group 1	2.1	3.4	3.4	1.0	17.5	10.3	3.6	0.2
Group 2	0.8	1.6	1.6	0.9	53.2	0	1.2	0.1
<b>Carbon</b>								
Group 1	3.7	9.3	3.7	6.7	22.6	—	—	—
Group 2	3.3	1.4	3.3	7.8	50.9	—	—	—

\*  $\sigma_{es}$  = elastic-scattering cross-section.

\*\*  $\sigma_{er}$  = elastic-removal cross-section.

It is immediately obvious that the major error will arise from the elastic removal cross-section for reactors containing light elements. Significant changes also appeared in other cross-sections, however, e.g., transport in graphite in group 1, also inelastic scattering in plutonium. Of course, the "reactor spectrum" chosen for flux-weighting here is only approximate, and merely is used to provide trends.

#### ACKNOWLEDGEMENTS

H. J. Wheeler provided considerable assistance in the equilibrium composition calculations, particularly in the devising of actual computing techniques. G. Main performed the bulk of the numerical analysis, with some help from D. O'Shea and L. Kvitek. Completion of this paper in time would have been impossible without these combined efforts.

#### REFERENCES

- [1] OKRENT, D., AVERY, R. and HUMMEL, H., Proc. UN Int. Conf. PUAE 5 (1956) 347.
- [2] LOEWENSTEIN, W. and OKRENT, D., Proc. 2nd UN Int. Conf. PUAE 12 (1958) 16.
- [3] YIFTAH, S. and OKRENT, D., ANL-6212 (1960).
- [4] YIFTAH, S., OKRENT, D. and MOLDAUER, P. A., Fast Reactor Cross Sections, Pergamon Press (1960).

- [5] YIFTAH, S., *These proceedings*, Vol. II, p. 257.
- [6] WHEELER, H. J., Unpublished.
- [7] DIVEN, B. C. and HOPKINS, J. C., *Bull. Amer. phys. Soc.* **5**, Ser. III (1960) 494.
- [8] NIMS, J. B. and ZWEIFEL, P. F., *Trans. Amer. nucl. Soc.* **2** (1959). See also APDA-135.
- [9] MOLDAUER, P. A., Proc. Conf. Physics of Breeding, ANL-6122 (1959).
- [10] OKRENT, D., Proc. Conf. Physics of Breeding, ANL-6122 (1959).
- [11] LONG, J. K. *et al.*, Proc. 2nd UN Int. Conf. PUAE **12** (1958) 119.
- [12] LONG, J. K. *et al.*, *These proceedings*, Vol. I, p. 271.
- [13] KVITEK, L. and OKRENT, D., Unpublished.



### **III. 5. REACTOR CONCEPT STUDIES**



# QUELQUES ÉTUDES DE PILES RAPIDES DE PUISSEANCE

A. KANIA, P. MOINEREAU, G. VENDRYÈS ET C. P. ZALESKI

CENTRE D'ÉTUDES NUCLÉAIRES DE SACLAY,

FRANCE

**Abstract — Résumé — Аннотация — Resumen**

**Some studies of fast power reactors.** After some neutron studies with fast reactors of 800 MW thermal, in which changes were made in the type of fuel (metal, carbide, oxide, different cermets) and in the shape and dimensions of the core, an attempt has been made to determine the factors affecting the price per kilowatt of power produced under these conditions. The paper emphasizes the part played by the breeding ratio, the permissible irradiation rate and the specific power, and gives optimum values of the latter for adoption in fast power reactors.

**Quelques études de piles rapides de puissance.** Après des études neutroniques concernant des piles rapides de 800 MW thermiques, dans lesquelles on a fait varier la nature du combustible (métal, carbone, oxyde, cermets divers), la forme et les dimensions du cœur, on a voulu déterminer les facteurs influençant le prix du kilowatt électrique produit par cette filière. On met ainsi en évidence le rôle joué par le taux de régénération, le taux d'irradiation admissible et la puissance spécifique, et on donne les valeurs optima de cette dernière à adopter pour les réacteurs rapides de puissance.

**Некоторые исследования энергетических реакторов на быстрых нейтронах.** После нейтронных исследований, касающихся реакторов на быстрых нейтронах мощностью 800 тепловых мегаватт, в которых изменяли вид топлива (металл, карбид, окисел, различные керметы), форму и размер активной зоны, авторы пытались установить факторы, влияющие на стоимость электрического киловатта, произведенного этими видами топлива. Таким образом, стала известна роль, которую играет степень воспроизведения, допустимая интенсивность облучения и удельная мощность топлива, а также выявлены оптимальные значения этого вида топлива для энергетических реакторов на быстрых нейтронах.

**Estudios sobre reactores de potencia rápidos.** Después de efectuar algunos estudios neutrónicos relativos a los reactores rápidos de 800 MW, en los que se modificó la naturaleza del combustible (metal, carburo, óxido, cermets de varios tipos), así como la forma y las dimensiones del cuerpo, los autores de la presente memoria han tratado de determinar los factores que influyen sobre el precio del kilovatio eléctrico producido con esas variantes. De esta manera ponen de manifiesto el papel que desempeña el índice de regeneración, el grado de irradiación admisible y la potencia específica; presentan los valores óptimos correspondientes a esta última que conviene adoptar para los reactores de potencia rápidos.

## Introduction

Malgré les incertitudes des évaluations économiques à long terme, en particulier de celles concernant les réalisations qui, techniquement, ne sont pas encore au point, il nous a semblé utile de faire une étude paramétrique des piles rapides de puissance, avec, comme critère de qualité, le prix du kilowattheure.

Nous espérons que ce travail pourra contribuer à orienter les efforts consacrés à l'étude des piles rapides.

Nous nous sommes limités à l'étude de combustibles solides et à l'utilisation du plutonium comme matière fissile. Par contre, nous envisageons l'emploi comme matière fertile du thorium-232 et de l'uranium-238.

Nous avons étudié les types de combustibles suivants:

- Alliage Pu—U—Mo,
- Céramique PuO<sub>2</sub>—UO<sub>2</sub>,
- Céramique PuC—UC,
- Cermet PuO<sub>2</sub> — dans UMo,
- Cermet PuO<sub>2</sub> — dans Th,
- Cermet PuO<sub>2</sub> — dans l'acier.

Pour aborder cette étude paramétrique, nous avons été amenés à distinguer d'une part les paramètres dont nous désirons voir l'influence sur le prix du kilowattheure, et que nous appellerons par la suite les *variables*, et d'autre part le cadre fixe de l'étude, c'est-à-dire les *équations*, qui relient entre elles les variables et les paramètres fixes et donnent le prix du kilowattheure.

Deux séries de calculs ont été faits, la première supposant un retraitement par cycle court (tel que la pyrométallurgie), la seconde utilisant le retraitement par voie aqueuse.

Pour chaque type de combustible traité indépendamment, nous avons choisi comme variables:

- Le taux de régénération de matière fissile, *x*;
- La puissance spécifique par kilogramme de matière fissile (Pu-239), *y*;
- Le taux de combustion admissible exprimé en MWj par tonne de combustible, *z*.

Les paramètres fixes communs à tous les combustibles sont les suivants:

- La puissance totale produite, 800 MWt;
- La forme géométrique du combustible (aiguilles assemblées dans des faisceaux);
- Le prix du kilowatt installé (1300 NF/kW);
- La durée d'amortissement (15 ans) des installations fixes et le taux d'intérêt (7%);
- Le prix du plutonium-239 (60 NF/g);
- Le prix du retraitement défini par unité de poids de combustible ou de matière fertile traités;
- Le prix de refabrication du combustible fonction du nombre d'aiguilles et de la masse traitées.

Notre étude comporte trois parties: l'étude neutronique, l'étude économique et la conclusion.

L'étude neutronique a pour objet essentiel de déterminer le pourcentage de plutonium dans le cœur, la masse critique et le taux de régénération pour les combustibles cités plus haut, et d'étudier la variation de ces valeurs en fonction du volume du cœur, ou de la puissance spécifique, la puissance totale restant constante. Pour tenir compte de la variation possible en fonction du dessin exact de la pile du facteur de régénération, nous avons étudié de façon assez complète l'influence de la géométrie dans le cas des combustibles cermets surtout à matrice inerte, et nous avons, sur quelques exemples, évalué l'effet de la variation de l'épaisseur des couvertures axiales et de leur teneur en fertile, ainsi que l'effet de la teneur volumétrique du cœur en combustible. En plus, nous avons évalué les effets des moyens de contrôle sur le gain de régénération et la masse critique, la répartition des taux de combustion dans le cœur et les couvertures et l'évolution

de la réactivité. Ces évaluations permettent d'indiquer les fréquences de retraitemt pour un taux de combustion admissible donné.

A partir de ces résultats, il a été possible, dans la deuxième partie, de tracer les courbes donnant le prix du kilowattheure pour divers combustibles et en fonction des variables que nous avons définies plus haut. Pour cela, nous avons été amenés à fixer un certain nombre d'hypothèses et de paramètres dont l'essentiel est exposé plus haut, et dont certains détails sont donnés en particulier dans la partie économique de cet article. De plus, nous avons jugé intéressant de voir dans quelques cas types ( $x$ ,  $y$  et  $z$  étant donnés) l'influence sur le prix du kilowattheure de la variation de certains paramètres dits fixes, tels que: le prix du kilowatt installé, le prix du traitement de combustible par kilogramme, le prix de refabrication des aiguilles et le prix du plutonium-239.

Finalement, dans la conclusion, nous essayons d'interpréter les courbes obtenues dans la deuxième partie en précisant les domaines possibles et intéressants des valeurs de  $x$ ,  $y$  et  $z$  pour les divers combustibles, et en insistant sur certains arrangements particuliers possibles comme ceux comportant des assemblages de cermets avec matrice d'acier inoxydable et des assemblages fertiles disposés de façon homogène dans le cœur.

## 1. Etude neutronique

### GÉNÉRALITÉS

Cette première partie est consacrée à la détermination des caractéristiques neutroniques des combustibles solides déjà signalés.

On trouvera d'abord une comparaison de ces divers types de combustible placés dans des conditions identiques, puis une étude particulière des cermets: effets de la forme du cœur, de la composition et de l'épaisseur des couvertures axiales, emploi du thorium comme matériau fertile.

Les calculs correspondants ont été faits dans les hypothèses suivantes:

Volume du cœur: 1000 l

Composition volumétrique du cœur constante: 30% combustible, 20% d'acier de structure, 50% de sodium

Puissance du réacteur: 800 MWt.

Ceci conduit, comme on le verra, à une puissance moyenne par litre de cœur assez élevée — de l'ordre de 0,7 MW — et à des taux de combustion du plutonium parfois très importants. Ces hypothèses faites dans un but de simplification ne sauraient être considérées comme les meilleures, et ceci dans tous les cas. C'est pourquoi nous avons ensuite, par des calculs où le volume du cœur a été porté à 3000 l et sa composition changée sur un exemple, étudié la variation des masses critiques et du taux de régénération en fonction du volume du cœur.

En dernier lieu, nous avons étudié l'effet du système de contrôle sur les caractéristiques neutroniques, ainsi que l'évolution de la réactivité et des taux de combustion pendant la marche du réacteur dans les principaux cas envisagés.

Nos calculs ont été faits en géométrie ( $r$ ,  $z$ ) avec le code «PDQ» sur ordinateur IBM-7090, avec des sections efficaces à 3 groupes qui ont été obtenues à partir des sections efficaces d'Argonne.

Des calculs à 8 groupes (d'après ANL-5800) et une dimension ont également été faits pour la détermination des spectres neutroniques et des constantes à 3 groupes.

### PILES DE 1000 LITRES -- COMPARAISON DE DIVERS TYPES DE COMBUSTIBLES

Nous avons étudié, dans les mêmes conditions, les combustibles suivants:

- Alliage U—Pu—Mo à 10% en poids de molybdène (A),
- Carbures PuC—UC (B),
- Oxydes PuO<sub>2</sub>—UO<sub>2</sub> (C1),
- Cermét constitué par une dispersion de PuO<sub>2</sub> dans l'acier (D),
- Cermét constitué par une dispersion de PuO<sub>2</sub> dans une matrice U—Mo à 10% en poids de Mo (D<sup>1</sup>).

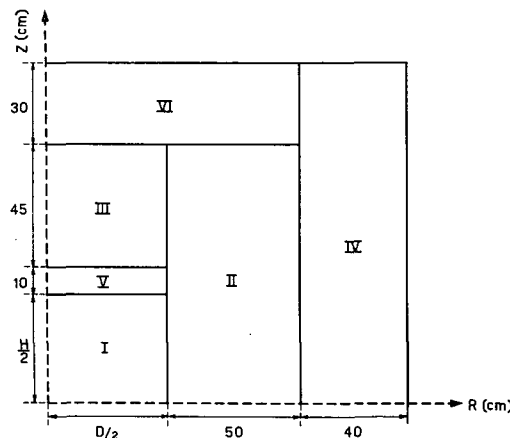


Figure 1  
Coupe axiale de la pile — Cœur cylindrique.

Le réacteur calculé est schématisé sur la figure 1. Le cœur est un orthocylindre ( $H/D=1$ ), ce qui, pour un volume de 1000 l conduit aux dimensions suivantes:

$$H=D=108,4 \text{ cm.}$$

Les compositions volumétriques des divers milieux (numérotés de I à VI) sont indiquées sur le tableau I.

TABLEAU I  
COMPOSITIONS VOLUMÉTRIQUES  
(%)

Milieux	Combustible	Fertile U-Mo à 3% de Mo en poids*	Acier	Sodium
I Cœur . . . . .	30	—	20	50
II Couv. rad. . . . .	—	60	15	25
III Couv. ax. . . . .	—	35	15	50
IV Réfl. acier . . . . .	—	—	80	20
V Zone de trans. interne . . . . .	—	—	40	60
VI Zone de trans. externe . . . . .	—	—	40	60

\* Pour atteindre des taux de combustion de l'ordre de 1% dans les couvertures il est probablement nécessaire de porter la teneur en molybdène des fertiles à 10%. Les taux de régénération externes seront de ce fait légèrement diminués.

Nous avons supposé que le plutonium était du  $^{239}\text{Pu}$ , ce qui n'est pas très réaliste dans la mesure où l'on s'intéresse à une filière existante et où le plutonium provient de l'usine de retraitement. Cependant la présence des deux isotopes 240 et 241 n'est pas gênante, le 241 est un excellent combustible et le 240 contribue de façon importante aux fissions rapides. Nous montrerons sur un exemple l'influence que l'on peut attendre d'une forte teneur du plutonium en 240 sur les caractéristiques neutroniques du réacteur.

Nous avons supposé aussi que l'uranium, qu'il s'agisse de celui se trouvant dans le cœur ou du matériau fertile, était de l'uranium naturel — allié à 3% en poids de molybdène pour le fertile — il est à noter qu'alors les fissions du 235 ne sont pas négligeables.

Pour les calculs nous avons adopté les densités suivantes:

U—Pu—Mo:	16,8
PuC:	12,24
UC:	12,27
PuO <sub>2</sub> :	10,31
UO <sub>2</sub> :	9,86
Acier:	7,8
Thorium:	11,5

soit 90% de la densité théorique pour ce qui est des carbures et des oxydes. Pour les combustibles céramiques ou cermets, nous avons supposé que la densité variait linéairement en fonction de la composition.

La puissance spécifique maximale atteinte dans le cœur est importante, et son évacuation peut être difficile dans le cas des oxydes, combustible dont la conductibilité thermique est faible. C'est pourquoi nous avons envisagé un deuxième cœur à oxydes dont le volume serait porté à 1200 l (C2) pour produire la même puissance totale de 800 MW. On a conservé la même hauteur du cœur (108,4 cm), et on a porté le diamètre à 118,7 cm, ce qui donne  $H/D=0,913$ .

Le tableau II rassemble les principaux résultats de calcul; compositions, masses critiques, taux de régénération, puissances spécifiques et taux de combustion au bout de 30 jours (pour 800 MW thermiques). Toutes ces valeurs se rapportent au schéma idéalisé de la figure I; il n'est pas tenu compte, en particulier, de la présence des canaux du système de contrôle et des barres de contrôle elles-mêmes. Les masses critiques sont donc sous -évaluées, les taux de régénération surévalués. Nous verrons plus loin quel est l'ordre de grandeur des corrections à apporter.

A volume de cœur égal, ce sont les combustibles A et D' qui nécessitent le plus grand investissement en  $^{239}\text{Pu}$ , tandis que le cermet D paraît particulièrement avantageux à cause du rôle modérateur et peu capturant de l'acier.

Nous avons défini le taux de régénération comme étant le rapport du nombre d'atomes de  $^{239}\text{Pu}$  formés par captures de  $^{238}\text{U}$  au nombre d'atomes de  $^{239}\text{Pu}$  détruits par captures ou fissions. On constate qu'il est particulièrement bon pour le combustible A et conserve une valeur intéressante pour les combustibles B, C1 et D'. Il y a à cela deux raisons: la conversion interne est importante et le pourcentage des fissions du cœur qui se produisent dans l'uranium est important (de 28,7% pour A à 13,6% pour C1). Pour le cermet D, bien qu'il n'y ait pas de conversion interne, le taux de régénération reste très nettement supérieur à l'unité.

Près de 90% de la puissance se dégage dans le cœur pour les combustibles A, B, C1 et D', 84% pour D. Toutefois, du fait de sa masse critique plus faible, c'est ce combustible qui conduit à la plus grande puissance moyenne par kilogramme de matière fissile.

TABLEAU II  
COMPARAISON DE DIVERS TYPES DE COMBUSTIBLES  
Volume du cœur: 1000 l —  $H/D = 1$  (sauf pour C2) — Puissance: 800 MWt

Combustible	U-Pu 239-Mo (A)	PuC-UC (B)	PuO <sub>2</sub> -UO <sub>2</sub> (C1)	PuO <sub>2</sub> -UO <sub>2</sub> (C2)	Cermet (D)	Cermet (D <sup>1</sup> )
<i>Composition</i>						
nombre d'atomes Pu	10,3% en poids de Pu	14,06% en vol. de PuC	16,39% en vol. de PuO <sub>2</sub>	15,46% en vol. de PuO <sub>2</sub>	12,75% en vol. de PuO <sub>2</sub>	19% en vol. de PuO <sub>2</sub>
nombre d'atomes U	0,129	0,1625	0,204	0,1905	$\infty$	0,1228
<i>Masses critiques (kg)</i>						
Total	5040	3679	2982	3577	2436	4792
<sup>239</sup> Pu	519	492	447	507	348	518
U naturel	4017	3011	2182	2647	0	3784
$\alpha = \frac{\text{captures } {}^{239}\text{Pu}}{\text{fissions } {}^{239}\text{Pu}}$	0,235	0,261	0,263	0,265	0,266	0,238
% des fissions dans le cœur dues à l'uranium	28,7	16,6	13,6	14,5	0	20
<i>Taux de régénération</i>						
Cœur	0,81	0,72	0,56	0,63	0	0,80
Couverture radiale	0,82	0,80	0,86	0,81	1,12	0,74
Couvertures axiales	0,14	0,14	0,15	0,17	0,20	0,14
Total	1,77	1,66	1,57	1,61	1,32	1,68
<i>Puissances (MW)</i>						
Cœur	716	712	702	707	671	723
Couverture radiale	74	77	86	79	112	67
Couvertures axiales	10	11	12	14	17	10
Puissance moyenne (MW/l cœur)	0,716	0,712	0,702	0,589	0,671	0,723
MW/kg <sup>239</sup> Pu	1,541	1,626	1,790	1,578	2,299	1,544
Puissance max. cœur (MW/l cœur)	1,425	1,405	1,375	1,173	1,294	1,466
P max./P moy.(cœur)	1,99	1,97	1,96	1,99	1,93	2,03
<i>Taux de combustion (%) (800 MW) (1 mois)</i>						
1. Combustible	0,418	0,345	0,301	0,253	0,236	0,360
2. MWj/t de combustible	4,260	5,810	7,060	5,930	8,260	4,530
3. <sup>239</sup> Pu / Combustion Disparition	3,72	4,09	4,60	4,05	6,57	3,79
	4,60	5,16	5,82	5,13	8,31	4,69

Un autre fait nous paraît important à signaler: c'est que le rapport  $P_{\max}/P_{\text{moy}}$  est particulièrement élevé dans le cœur (voisin de 2); l'évacuation de la puissance maximale peut poser de sérieux problèmes, et il pourrait être intéressant d'«aplatisir» le flux neutronique en disposant par exemple du fertile au centre du cœur.

Notons qu'avec les configurations A, B, C1 étudiées, le flux total au centre du cœur est de l'ordre de  $1,5 \text{ à } 1,6 \cdot 10^{16} \text{ cm}^2/\text{s}$ .

Pour chiffrer le taux de combustion nous avons adopté plusieurs définitions:

1. Taux de combustion du combustible, défini comme le rapport du nombre d'atomes détruits par fission (plutonium et uranium) au nombre total d'atomes de combustible présents initialement, y compris les éléments non fissiles tels que molybdène, oxygène, carbone et fer dans le cas des cermets.

2. Taux d'irradiation en MWj par tonne de combustible avec la même définition que ci-dessus pour le combustible (seule est comptée la puissance développée dans le cœur).

3. Nous avons traité à part le plutonium-239, considéré comme le seul élément précieux, en distinguant le taux de combustion qui ne tient compte que des fissions de cet élément et le taux de disparition qui tient compte des fissions et des captures, étant entendu que ces taux sont définis comme le rapport du nombre d'atomes de  $^{239}\text{Pu}$  ainsi disparus au nombre d'atomes initial de  $^{239}\text{Pu}$ .

Ces différents taux ont été calculés après une marche du réacteur de trente jours à la puissance constante de 800 MW. Ils sont donnés dans le tableau II en pourcentage.

On notera que le taux brut de disparition du plutonium est particulièrement élevé. Toutefois, pour les combustibles A, B, C1 et D', pour lesquels la régénération interne est importante, le taux net de disparition est bien plus faible: 0,85% seulement pour A, 1,55% pour B, 2,55% pour C1, 0,94% pour D'. C'est de ce taux net que va dépendre essentiellement l'évolution de la réactivité (voir tableau XII). Pour les cermets à matrice inerte, par contre, le taux de disparition de  $^{239}\text{Pu}$  est si élevé que l'on peut s'attendre à une baisse très rapide de la réactivité.

*Remarque.* Un taux d'irradiation de 10 000 j par tonne du combustible correspond à un taux de combustion des atomes lourds (plutonium et uranium) qui est sensiblement de 1% pour le métal, 1,2% pour les carbures et 1,3% pour les oxydes.

### *Comparaison des deux coeurs à oxydes C1 et C2*

L'accroissement du volume du cœur a pour effet d'augmenter de 12% environ l'investissement en plutonium et de diminuer les puissances spécifiques qui restent cependant élevées. Les taux de combustion sont évidemment diminués, et ceci permettra un plus long séjour en pile; le taux de régénération est accru, mais dans des proportions modestes.

### *Evolution de la teneur en plutonium dans le cœur et les couvertures*

A partir des résultats du tableau II, nous avons évalué les masses de  $^{239}\text{Pu}$  et  $^{240}\text{Pu}$  détruites ou formées après un mois à 800 MW, dans le cœur et les couvertures. On les trouvera dans le tableau III.

Ces évaluations supposent les phénomènes linéaires et ne tiennent pas compte des événements qui interviennent au «deuxième ordre», tels que production de  $^{241}\text{Pu}$  à partir du  $^{240}\text{Pu}$  dans le cœur, de  $^{240}\text{Pu}$  à partir de  $^{239}\text{Pu}$  dans les couvertures.

Les temps de doublement théoriques que nous en avons déduits (rapport de la masse critique de  $^{239}\text{Pu}$  à la production nette par mois) sont évidemment beaucoup plus optimistes que les temps de doublement réels. Ils seraient à peu près vrais pour des coeurs dont on effectuerait le déchargeement tous les mois — ou mieux à des intervalles encore plus courts — sans que le temps de déchargement soit pris en compte (facteur de charge égal à 1); ils sont à considérer seulement en valeurs

TABLEAU III  
MASSES DU  $^{239}\text{Pu}$  ET  $^{240}\text{Pu}$  FORMÉES OU DÉTRUITES APRÈS 30 JOURS DE  
FONCTIONNEMENT A 800 MW  
(Kilogrammes)

Combustible	A	B	C1	C2	D	D'
<i>Cœur</i>						
$^{239}\text{Pu}$ détruit	23,87	25,34	26,01	25,98	28,82	24,30
$^{239}\text{Pu}$ formé	19,45	18,31	14,60	16,29	0	19,48
$^{240}\text{Pu}$ formé	4,46	5,26	5,42	5,45	6,06	4,67
<i>Couverture radiale</i>						
$^{239}\text{Pu}$ formé	19,60	20,22	22,35	21,02	33,08	17,85
<i>Couvertures axiales</i>						
$^{239}\text{Pu}$ formé	3,42	3,54	3,92	4,40	5,89	3,13
<i>Production nette de <math>^{239}\text{Pu}</math> dans le réacteur</i>	18,60	16,74	14,86	15,73	10,15	16,15
<i>Temps de doublement théorique</i>	2 ans 4 mois	2 ans 5 mois 11 jours	2 ans 6 mois	2 ans 8 mois 8 jours	2 ans 10 mois 10 jours	2 ans 8 mois

relatives: le temps de doublement du plutonium, à facteur d'utilisation égal, est de 22% plus grand pour le cermet D que pour le combustible métallique A, bien que la masse critique soit de 33% plus faible. On constate d'autre part qu'un accroissement du volume du cœur conduit à un accroissement du temps de doublement.

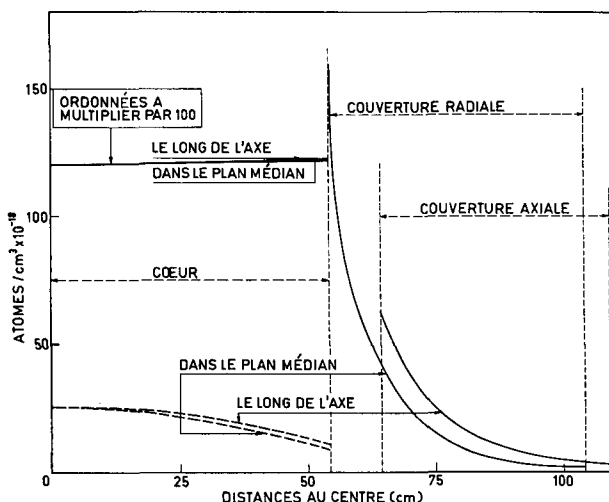


Figure 2  
Combustible PuC—UC. Teneur en  $^{239}\text{Pu}$  (—) et  $^{240}\text{Pu}$  (— —) après un mois de fonctionnement continu du réacteur à 800 MW.

Les courbes de la figure 2 représentent la teneur en  $^{239}\text{Pu}$  en nombre d'atomes par centimètre cube dans le plan médian de la couverture radiale et le long de l'axe de la couverture axiale dans le cas du combustible carbures B, au bout d'une marche d'un mois à 800 MW. Nous avons également porté la teneur en 239 et 240 le long des mêmes directions dans le cœur. On voit que le  $^{239}\text{Pu}$  se forme surtout dans les couches de couvertures adjacentes au cœur.

Les teneurs initiales avec B (combustible et fertile neufs) sont:

	<i>Noyaux/cm<sup>3</sup></i>
$^{239}\text{Pu}$ dans le cœur	$0,001\ 239 \cdot 10^{24}$
$^{239}\text{Pu}$ dans les couvertures	0
$^{240}\text{Pu}$ dans le cœur et les couvertures	0
$^{238}\text{U}$ dans le cœur	$0,007\ 567 \cdot 10^{24}$
$^{238}\text{U}$ dans la couverture radiale	$0,027\ 066 \cdot 10^{24}$
$^{238}\text{U}$ dans les couvertures axiales	$0,015\ 788 \cdot 10^{24}$

#### *Effets de la densité dans le cas des combustibles PuO<sub>2</sub> — UO<sub>2</sub>*

On sait que la densité pratique des oxydes varie dans d'assez larges proportions, selon le procédé de fabrication. Pour les coeurs C1 et C2, nous avons supposé qu'elle était 90 % de la densité théorique, soit presque le maximum réalisable. Nous avons comparé C1 à un combustible à oxydes C3 ayant la densité minimale actuellement admise, soit 65 % de la densité théorique (tableau IV). La masse critique est légèrement diminuée, et le taux de régénération est pratiquement inchangé: la diminution de la conversion interne consécutive à l'abaissement de la teneur du cœur en  $^{238}\text{U}$  est compensée par un accroissement dans la couverture.

TABLEAU IV  
EFFETS DE DENSITÉ DES OXYDES

Combustible	C1	C3
Densité	$0,9\ d_{th}$	$0,65d_{th}$
<i>Masses critiques</i>		
$^{239}\text{Pu}$	447	428
Totale	2982	2160
<i>Taux de régénération</i>		
Interne	0,56	0,39
Externe	1,01	1,17
Total	1,57	1,56

Note. Les réacteurs ayant pour combustibles C1 et C3 ont exactement les mêmes caractéristiques, densité des oxydes exceptée.

Il semble donc que le choix d'une densité plutôt que l'autre ne doive pas dépendre de considérations telles qu'investissement en plutonium et régénération totale.

#### *Effets de la teneur du plutonium en 240.*

Nous avons envisagé une variante du combustible métallique A, A1, dans lequel un tiers du plutonium serait du  $^{240}\text{Pu}$ . On trouvera dans le tableau V les

comparaisons des masses critiques et du taux de régénération. Pour A1 nous avons donné deux définitions du taux de régénération:

1. Rapport du nombre d'atomes de  $^{239}\text{Pu}$  formés au nombre d'atomes de  $^{239}\text{Pu}$  détruits.

2. Rapport du nombre d'atomes de  $^{239}\text{Pu}$  et  $^{241}\text{Pu}$  formés au nombre d'atomes de  $^{239}\text{Pu}$  détruits, le  $^{241}\text{Pu}$  étant un excellent combustible.

Par rapport à A, A1 conduit à une masse critique de  $^{239}\text{Pu}$  plus faible et à un taux de régénération nettement supérieur, surtout si l'on tient compte du  $^{241}\text{Pu}$ .

TABLEAU V  
EFFETS DU  $^{240}\text{Pu}$  DANS LE COMBUSTIBLE U — Pu — Mo

Combustible	A	A1
$^{240}\text{Pu}/^{239}\text{Pu}$	0	0,5
<i>Masses critiques (kg)</i>		
$^{239}\text{Pu}$	519	486
$^{240}\text{Pu}$	0	243
<i>Taux de régénération</i>		
Interne	0,81	(a) 0,82
Externe	0,96	(b) 0,99
Total	1,77	1,83 2,00

TABLEAU VI  
SPECTRES NEUTRONIQUES AVEC DIFFÉRENTS TYPES DE COMBUSTIBLES  
(Volume du cœur: 1000 l)

N° de groupe	$E_{\text{inf.}}$ (MeV)	U — $^{239}\text{Pu}$	U — Pu $^{240}\text{Pu}/$ $^{239}\text{Pu} = 1/2$	U — Pu — Mo*	UO <sub>2</sub> (d = PuO <sub>2</sub> — 0,9 d <sub>th</sub> )	PuO <sub>2</sub> —UO <sub>2</sub> (d = 0,65 d <sub>th</sub> )	PuC — UC
<i>Cœur</i>							
1	1,35	0,0824	0,0835	0,0808	0,0936	0,0968	0,0933
2	0,825	0,0748	0,0747	0,0741	0,0696	0,0733	0,0800
3	0,5	0,1374	0,1353	0,1276	0,1114	0,1118	0,1165
4	0,3	0,1786	0,1769	0,1674	0,1675	0,1629	0,1469
5	0,18	0,1525	0,1520	0,1460	0,1203	0,1206	0,1304
6	0,0674	0,2328	0,2344	0,2340	0,1662	0,1724	0,1715
7	0,0091	0,1322	0,1331	0,1551	0,1884	0,1868	0,1851
8	0	0,0097	0,0103	0,0148	0,0828	0,0756	0,0763
<i>Couverture radiale</i>							
1	1,35	0,0125	0,0124	0,0122	0,0138	0,0155	0,0137
2	0,825	0,0163	0,0161	0,0160	0,0159	0,0181	0,0175
3	0,5	0,0543	0,0533	0,0515	0,0496	0,0548	0,0517
4	0,3	0,0805	0,0792	0,0765	0,0753	0,0823	0,0745
5	0,18	0,0778	0,0768	0,0744	0,0699	0,0767	0,0720
6	0,0674	0,1311	0,1302	0,1283	0,1122	0,1242	0,1148
7	0,0091	0,0804	0,0801	0,0832	0,0851	0,0926	0,0849
8	0	0,0043	0,0043	0,0047	0,0098	0,0099	0,0093

\* Le réacteur à combustible U — Pu — Mo dont on donne ici le spectre diffère de A par la composition du cœur: combustible: 25 % — acier: 25 % — sodium: 50 %.

formé. Ceci est dû au fait que dans Al une partie du  $^{238}\text{U}$  est remplacée par du  $^{240}\text{Pu}$ , qui est plus fissile: seuil de fission plus bas, sections efficaces de fission et nombre de neutrons émis par fission plus grands. Une fraction importante des fissions est due au  $^{240}\text{Pu}$ .

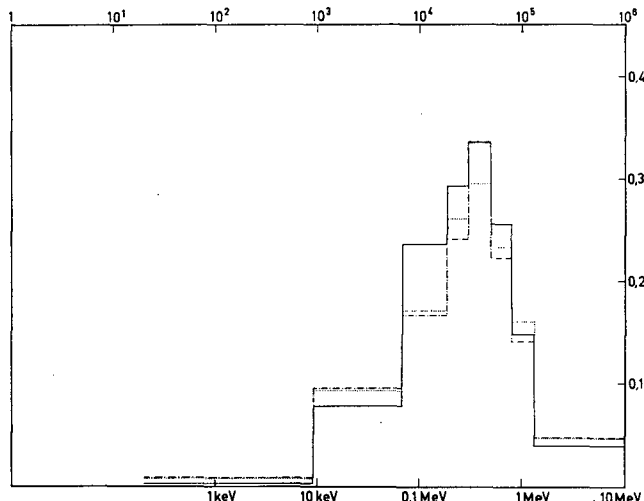


Figure 3  
Spectres moyens dans le cœur. Flux par unité de léthargie.

— PuMo  
- - -  $\text{PuO}_2\text{-UO}_2$   
....  $\text{PuC-UC}$

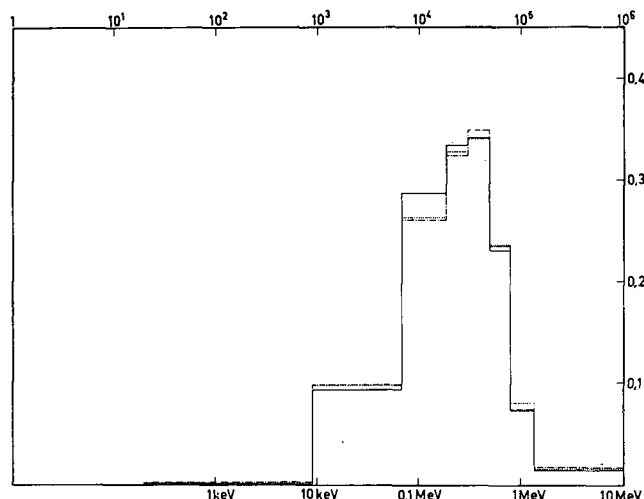


Figure 4  
Spectres moyens dans la couverture radiale. Flux par unité de léthargie.

— PuMo  
- - -  $\text{PuO}_2\text{-UO}_2$   
....  $\text{PuC-UC}$

*Spectres des neutrons*

A titre indicatif, nous donnons dans le tableau VI les spectres neutroniques calculés dans le cœur et la couverture radiale en géométrie sphérique à 8 groupes pour plusieurs types de combustible identiques ou très voisins de ceux étudiés dans ce paragraphe (volume de cœur : 1000 l). Les valeurs données sont les intégrales de flux dans chaque région, normalisées de façon que leur somme pour tous les groupes soit égale à 1000.

Les figures 3 et 4 représentent ces mêmes spectres en flux par unité de léthargie, dans le cœur et dans la couverture radiale, avec les combustibles U—Pu—Mo (A), PuC—UC (B) et PuO<sub>2</sub>—UO<sub>2</sub> (C1).

TABLEAU VII  
CERMETS AVEC CŒURS CYLINDRIQUES  
Influence de H/D et de l'épaisseur de la couverture axiale  
(Volume du cœur: 1000 l — Puissance: 800 MWt)

Combustible	D1	D2	D3	D4	D5	D6
H/D	1	0,8	0,6	0,4	0,4	0,4
Epaisseur couv. axiale (cm)	50	50	50	50	40	60
Composition (vol. % de PuO <sub>2</sub> )	12,8	12,85	13,1	14,2	14,2	14,2
<i>Masses critiques (kg)</i>						
PuO <sub>2</sub> et matrice	2437	2438	2439	2448	2448	2448
PuO <sub>2</sub>	396	398	405	439	439	439
Pu	350	351	358	388	388	388
$\alpha = \frac{\text{captures } ^{239}\text{Pu}}{\text{fissions } ^{239}\text{Pu}}$	0,265	0,265	0,264	0,262	0,262	0,262
<i>Taux de régénération</i>						
Couverture radiale	1,11	1,00	0,884	0,723	0,715	0,728
Couvertures axiales	0,24	0,34	0,454	0,629	0,606	0,643
Total	1,35	1,34	1,338	1,352	1,321	1,371
<i>Puissances (MW)</i>						
Cœur	665	668	672	670	673	669
Couverture radiale	109	99	86	71	70	71
Couvertures axiales (MW/kg Pu)	26	33	42	59	57	60
Puiss. max. cœur (MW/1)	2,286	2,279	2,235	2,062	2,062	2,062
$P_{\text{max.}}/P_{\text{moy.}}(\text{cœur})$	1,296	1,298	1,301	1,291	1,295	1,289
1,95	1,94	1,94	1,93	1,92	1,92	1,93
<i>Taux de combustion (%) (800 MW—1 mois)</i>						
1. Combustible	0,23	0,23	0,24	0,23	0,23	0,23
2. MWj/t combustible	8190	8220	8270	8210	8250	8200
3. $^{239}\text{Pu}$ { combustion disparition	6,46	6,44	6,38	5,87	5,89	5,86
	8,17	8,14	8,07	7,41	7,44	7,40

### PILES DE 1000 LITRES — ÉTUDE PARTICULIÈRE DES CERMETS

Les cermets dont la matrice est inerte ayant une régénération interne nulle, on peut chercher à accroître la régénération externe en favorisant la fuite des neutrons hors du cœur par accroissement du rapport surface/volume.

Un premier moyen est d'aplatir le cœur en diminuant  $H/D$ , un autre de placer du fertile au centre du cœur, ce qui présente en outre l'avantage d'aplatir le flux. Nous avons également envisagé le cas où un assemblage cœur sur deux serait un assemblage fertile. Enfin, nous avons, à des fins de comparaison, envisagé des cermets à matrice fertile, le matériau fertile étant du  $^{232}\text{Th}$ , élément dont on peut espérer une tenue sous irradiation meilleure que celle de l'uranium.

#### *Cermets à matrice inerte — coeurs cylindriques*

Nous avons conservé le schéma de principe de la figure 1 et les compositions volumétriques du tableau I, avec cependant deux modifications de la couverture axiale destinées à augmenter la régénération externe :

a) Un accroissement de la hauteur, portée de 45 à 50 cm, au détriment de l'espace de transition interne ramené de 10 à 5 cm.

b) Une nouvelle composition volumétrique :

fertile	45%
acier	15%
sodium	40%

Nous avons successivement donné à  $H/D$  les valeurs : 1, 0,8, 0,6, 0,4 (cermets D1, D2, D3, D4), et avec  $H/D=0,4$  nous avons étudié l'effet de l'épaisseur de la couverture axiale en lui donnant les valeurs 40 puis 60 cm (cermets D5 et D6). On trouvera les résultats des calculs dans le tableau VII.

*Influence de  $H/D$ .* La masse critique augmente lorsque  $H/D$  diminue, un plus grand nombre de neutrons quittant le cœur. Mais cet accroissement n'est pas très important, du moins tant que  $H/D$  reste dans la gamme étudiée.

Le taux de régénération total reste à peu près constant. En effet, l'aplatissement du cœur favorise la fuite des neutrons dans les couvertures axiales qui, ayant une teneur en fertile plus faible, du fait du volume de sodium de refroidissement nécessaire, sont moins efficaces que la couverture radiale du point de vue production de  $^{239}\text{Pu}$ . Pour qu'un aplatissement du cœur conduise à un accroissement du taux de régénération, il faudrait accroître la teneur en fertile des couvertures axiales ou leur épaisseur. Remarquons que ceci est théoriquement réalisable : la diminution de la hauteur du cœur conduit à une diminution de la puissance à évacuer par unité de surface (de section droite) du cœur et, par conséquent, à une diminution du débit de sodium nécessaire.

Les puissances maximales dans le cœur varient peu avec  $H/D$ .

*Influence de l'épaisseur des couvertures axiales.* A la précision du calcul près, les masses critiques sont inchangées.

Le taux de régénération augmente avec l'épaisseur de la couverture axiale, mais on peut penser qu'au-delà de 60 cm le gain est faible.

*Influence de la teneur en fertile des couvertures axiales.* Les réacteurs D et D1 ne diffèrent que par l'épaisseur de l'espace de transition (5 cm pour D1 contre 10 cm pour D) et par la composition de la couverture axiale (45% de fertile avec D1, 35% avec D). Ces modifications conduisent à un taux de régénération légèrement meilleur pour D1 : 1,35 contre 1,32 pour D.

*Evolution de la teneur en plutonium dans le cœur et les couvertures.* Des résultats du tableau VII on peut déduire que, au bout de 30 jours de marche à 800 MW, la masse de  $^{239}\text{Pu}$  détruite dans le cœur est de l'ordre de 29 kg, dont 6 kg sont transformés en  $^{240}\text{Pu}$ , et la masse de  $^{239}\text{Pu}$  formée dans les couvertures varie entre 30 et 40 kg selon le cas.

On a donc une production nette de  $^{239}\text{Pu}$  de 9 à 11 kg, et les temps de doublement théoriques vont de 31 mois (D1) à 42 mois (D5). Les temps de doublement réels seront beaucoup plus longs, d'autant plus que la vitesse de combustion du  $^{239}\text{Pu}$  du cœur obligera à des déchargements, donc à des arrêts du réacteur très fréquents.

#### *Autres exemples de cermets avec matrice inerte*

*Cœurs annulaires.* Le schéma de principe du réacteur est indiqué sur la figure 5. Le cœur a la forme d'un cylindre creux, le centre étant occupé par une région de même composition que la couverture radiale, de 30 cm de rayon. Les régions numérotées de I à VI ont les compositions du tableau I, sauf pour les couvertures axiales (III), qui contiennent 45% en volume de fertile. Le volume du cœur est de 1000 l.

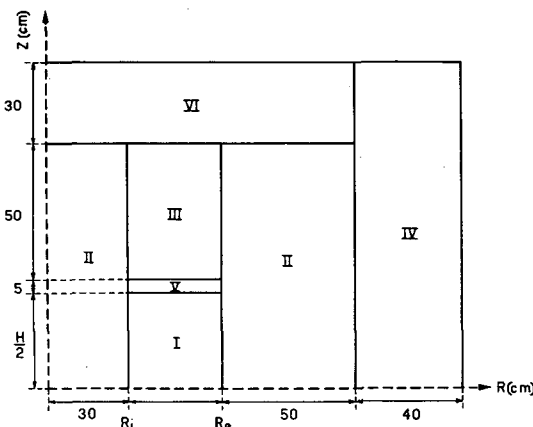


Figure 5  
Coupe axiale de la pile. Cœur annulaire.  
 $E_1: H = 67,45 \text{ cm} \quad R_e = 74,97 \text{ cm}$   
 $E_2: H = 41,63 \text{ cm} \quad R_e = 92,45 \text{ cm}$

Nous avons étudié deux exemples caractérisés par  $H/(R_e - R_i) = 1,5$  (E1) et  $2/3$  (E2),  $H$  étant la hauteur du cœur,  $R_i (= 30 \text{ cm})$  le rayon intérieur, et  $R_e$  le rayon extérieur.

*Cœur « mixte » combustible-fertile.* Afin d'éviter l'inconvénient majeur — du point de vue régénération — des cermets à matrice inerte, nous avons imaginé un modèle de réacteur (F) dans lequel le chargement serait réalisé de façon qu'un assemblage cœur sur deux soit un assemblage de la même nature que ceux de la couverture radiale. Nous avons conservé un volume de combustible de 1000 l, ce qui conduit pour le cœur « mixte » à un volume de 2000 l, que nous avons choisi tel que  $H/D = 0,6$ , soit  $H = 97,1 \text{ cm}$  et  $D = 161,9 \text{ cm}$ . Les

autres dimensions et les compositions des zones du réacteur sont les mêmes que pour les autres types de cermets.

*Résultats.* Les caractéristiques calculées des trois réacteurs ainsi définis sont indiquées par le tableau VIII. Par rapport aux cermets à cœur cylindrique, on notera l'accroissement du taux de régénération, mais surtout de la masse critique. Ceci est particulièrement net avec le « cœur mixte » : le taux de régénération devient meilleur qu'avec le combustible U—Pu—Mo (A), mais la masse de  $^{239}\text{Pu}$  investie est presque doublée.

TABLEAU VIII  
CERMETS A CŒUR ANNULAIRE ET A «CŒUR MIXTE» —  
PRINCIPALES CARACTÉRISTIQUES

Type	E 1 (annulaire)	E 2 (annulaire)	F (mixte)
% en volume de $\text{PuO}_2$ dans le combustible	19,8	21,5	36
<i>Masses critiques (kg)</i>			
$\text{PuO}_2$ et matrice (total)	2490	2502	2612
$\text{PuO}_2$	613	665	1114
Pu	540	587	982
$\alpha = \frac{\text{captures } ^{239}\text{Pu}}{\text{fissions } ^{239}\text{Pu}}$	0,250	0,250	0,239
Taux de régénération total	1,47	1,47	1,80*
<i>Puissances (MW)</i>			
Cœur	648	650	743**
Couverture radiale	119	85	33
Couvertures axiales	33	65	24
MW/kg $^{239}\text{Pu}$	1,481	1,363	0,815
Puiss. max. cœur (MW/1)	0,920	0,914	—
$P_{\text{max.}}/P_{\text{moy.}}$ (cœur)	1,420	1,406	—
<i>Taux de combustion % (800 MW—1 mois)</i>			
1. Combustible	0,23	0,23	0,20
2. MWj/t combustible	7810	7790	6450
3. $^{239}\text{Pu}$ { combustion	4,07	3,76	1,92
disparition	5,09	4,70	2,39

\* Le taux de régénération dans le fertile présent dans le « cœur mixte » est 1,15.

\*\* La puissance dans le cœur donnée pour F concerne le cœur mixte ; elle se répartit ainsi : 560 MW pour le combustible et 183 MW pour le fertile présent dans le cœur.

Le fait de placer du fertile au centre du cœur (E1 et E2) présente l'avantage de diminuer la puissance maximale dans le cœur de façon appréciable ainsi que le rapport  $P_{\text{max.}}/P_{\text{moy.}}$ . Le flux total est plus plat qu'avec un cœur cylindrique de même volume, comme le montre la figure 6, où sont tracés les flux dans le plan médian pour les réacteurs E2 et D1.

Remarquons que la teneur volumétrique en  $\text{PuO}_2$  de la matrice devient importante avec ces structures. Il se peut même que le cermet F ne soit pas réalisable ; il ne semble pas que l'on ait jusqu'ici dépassé les 25%.

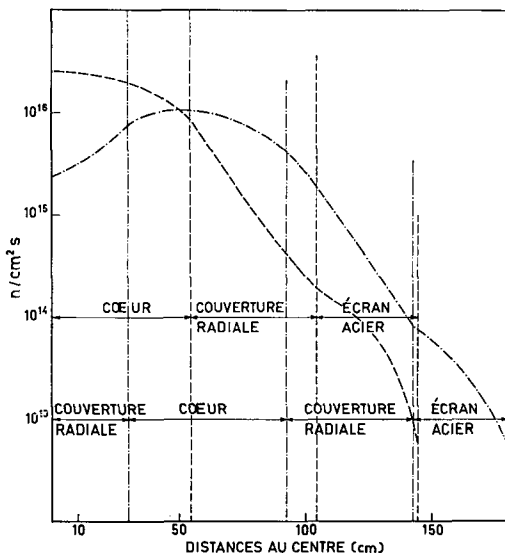


Figure 6  
Flux total dans le plan médian.  
 ——— Cermet plat ( $D_1$ )  
 ····· Cermet annulaire ( $E_2$ )

#### Cermets avec matrice fertile et couvertures en thorium

Trois exemples ont été étudiés: deux avec cœur cylindrique caractérisés par  $H/D=1$  (T1) et  $H/D=0,6$  (T2), et un avec cœur « mixte » (T3) comme précédemment, un assemblage du cœur sur deux étant fertile (avec thorium), le combustible étant constitué par une dispersion de  $\text{PuO}_2$  dans le thorium.

Pour ce qui est des dimensions et des compositions volumétriques, T1, T2 et T3 ont les mêmes caractéristiques, respectivement, que D1, D3 et F, mais l'uranium naturel allié à 3 % de molybdène a été remplacé par du thorium pur comme matériau fertile\*.

Les principales caractéristiques correspondant à ces trois exemples de réacteurs sont données dans le tableau IX.

Le taux de régénération total, défini ici comme le rapport du nombre d'atomes de  $^{233}\text{U}$  formés au nombre d'atomes de  $^{239}\text{Pu}$  détruits est toujours supérieur à 1,30, presque aussi bon que celui obtenu avec les cermets à matrice inerte et à fertile U—Mo, et en tous cas très nettement supérieur à ce qu'il est possible d'obtenir avec des réacteurs régénérateurs thermiques utilisant le thorium comme matériau fertile.

Cependant, il n'est peut-être pas très justifié d'accorder la même valeur au  $^{233}\text{U}$  qu'au  $^{239}\text{Pu}$ .

\* Signalons, d'une part, que nous avons pris des couvertures de même épaisseur que dans le cas du fertile U—Mo, ce qui n'est pas très justifié car en prenant des épaisseurs plus grandes on peut espérer augmenter le taux de régénération, et d'autre part qu'il n'est peut-être pas sûr que le thorium ait une tenue sous irradiation suffisante pour pouvoir être utilisé sans stabilisant — mais dans ce cas les performances neutroniques ne seraient que légèrement diminuées.

TABLEAU IX  
CERMETS AVEC MATRICE ET COUVERTURES EN THORIUM — PRINCIPALES CARACTÉRISTIQUES

Type	T 1	T 2	T 3
% en volume de PuO <sub>2</sub> dans le combustible	22,55	22,75	41,50
<i>Masses critiques (kg)</i>			
PuO <sub>2</sub> et matrice	3370	3369	2653
PuO <sub>2</sub>	698	704	1284
Pu	615	621	1132
$\alpha = \frac{\text{captures } ^{239}\text{Pu}}{\text{fissions } ^{239}\text{Pu}}$	0,240	0,240	0,235
% des fissions dans le cœur dues au thorium	2,84	2,81	—
<i>Taux de régénération</i>			
Interne	0,54	0,54	0,76
Externe	0,80	0,79	0,56
Total	1,34	1,33	1,32
<i>Puissances (MW)</i>			
Cœur	791,9	792,3	795*
Couverture radiale	6,7	5,3	2,9
Couvertures axiales	1,4	2,4	2,1
MW/kg <sup>239</sup> Pu	1,301	1,288	0,707
Puissance max. cœur (MW/l)	1,576	1,567	—
$P$ max./ $P$ moy. (cœur)	1,99	1,98	—
<i>Taux de combustion % (800 MW—1 mois)</i>			
1. Combustible	0,584	0,583	0,257
2. MWj/t combustible	7050	7050	8990
3. $^{239}$ Pu { combustion	4,24	4,21	2,27
{ disparition	5,26	5,22	2,81

\* Cette valeur concerne le cœur mixte. 4,49 % de cette puissance est due aux fissions du thorium.

Il est à noter que la solution « cœur mixte » n'améliore pas le taux de régénération.

#### INFLUENCE DU VOLUME DU COEUR ET DE LA TENEUR EN COMBUSTIBLE

Nous avons déjà signalé le caractère arbitraire des hypothèses faites lors des calculs précédents: même volume de cœur (1000 l) et mêmes compositions volumétriques pour tous les combustibles pour une puissance de 800 MWt. Gardant inchangée cette puissance, nous avons donc étudié l'influence du volume du cœur et de la teneur en combustible sur les masses critiques et le taux de régénération en nous appuyant sur quelques exemples, des cermets et un alliage métallique: H1 dispersion de PuO<sub>2</sub> dans le thorium avec couvertures en thorium;

H2 dispersion de PuO<sub>2</sub> dans une matrice en uranium-molybdène à 10% de molybdène en poids avec couvertures en U-Mo à 3% de molybdène;

H3 même combustible que H2, mais avec un « cœur mixte », un assemblage cœur sur deux étant du type couverture radiale;

H4 dispersion de PuO<sub>2</sub> dans une matrice en acier inoxydable avec couvertures en U—Mo;

H5 même combustible que H4, mais avec « cœur mixte »;

H6 alliage U—Pu—Mo à 10% en poids de molybdène, couvertures en U—Mo.

TABLEAU X  
CŒURS DE 3000 LITRES — PRINCIPALES CARACTÉRISTIQUES

Type	H1	H2	H3	H4	H5	H6
% en vol. de PuO <sub>2</sub> dans le combustible	17,15	15,45	34,40	7,63	30,0	6,40% Pu en pds
<i>Masses critiques (kg)</i>						
Combustible (total)	10167	14600	13407	7193	7700	22680
PuO <sub>2</sub>	1592	1437	3193	708	2785	
Pu	1404	1267	2816	625	2456	1452
$\alpha = \frac{\text{captures } ^{239}\text{Pu}}{\text{fissions } ^{239}\text{Pu}}$	0,245	0,241	0,237	0,284	0,241	0,222
% de fissions dans le cœur dues à l'uranium ou au thorium	3,3	23	29,4*	0	26,25**	27,8
<i>Taux de régénération:</i>						
Interne	0,78	1,10	1,47*	0	1,37**	1,32
Externe	0,57	0,61	0,33	1,16	0,42	0,50
Total	1,35	1,71	1,80	1,16	1,79	1,82
<i>Puissances (MW)</i>						
Cœur	795	751	773*	695	765**	760
Couverture radiale	4	42	15	83	19	33
Couvertures axiales	1	7	12	22	16	7
MW/kg <sup>239</sup> Pu	0,570	0,631	0,284	1,280	0,326	0,551
Puiss. max. cœur (MW/l)	0,586	0,575	—	0,510	—	0,590
$P_{\text{max.}}/P_{\text{moy.}}(\text{cœur})$	2,211	2,300	—	2,198	—	2,332
<i>Taux de combustion (%)</i>						
(800 MW—1mois)						
1. Combustible	0,21	0,13	0,10	0,08	0,07	0,10
2. MWj/t combustible	2350	1550	1350	2900	2200	1000
3. <sup>239</sup> Pu {combustion disparition}	1,86	1,55	0,63	3,77	0,78	1,28
	2,31	1,92	0,78	4,84	0,97	1,57

\* Ces valeurs se rapportent au « cœur mixte ». Le pourcentage des fissions dues à l'uranium dans le combustible est 9,1 %, la puissance dégagée dans le combustible est 600 MW.

\*\* Même remarque: 26,25 % des fissions se produisent dans les assemblages fertiles du cœur mixte. La puissance dégagée dans le combustible est 564 MW.

Dans tous les cas le volume du cœur a été pris égal à 3000 l. Pour H1, H2, H4 et H6, les dimensions du cœur sont  $H=D=156,32$  cm. H3 et H5 sont définis par le rapport:  $H/D=0,6$ , ce qui conduit à:  $H=140,1$  cm et  $D=233,5$  cm.

Les compositions volumétriques du cœur sont les mêmes que pour les études précédentes pour H1, H2, H3, H4 et H5, à savoir:

combustible	30%
acier	20%
sodium	50%

Par contre, avec H6, nous avons adopté la composition volumétrique suivante:

combustible	45%
acier	15%
sodium	40%

Les compositions de toutes les autres régions sont inchangées. Nous avons adopté en particulier la même couverture axiale qu'avec les cermets: 45% en volume de fertile.

On trouvera dans le tableau X les caractéristiques neutroniques se rapportant à ces divers exemples.

Une étude particulière de la variation en fonction du volume du cœur de la teneur pondérale en  $^{239}\text{Pu}$  du combustible  $\mu$ , du taux de régénération  $\alpha$  et de la puissance  $y$  par kilogramme de  $^{239}\text{Pu}$  a été faite avec le combustible métallique U—Pu—Mo (fig. 7). Nous avons utilisé pour cela d'autres résultats de calculs internes, dont il n'est pas fait mention dans ce rapport. Les courbes de la figure 7 se rapportent à une composition volumétrique constante du cœur qui est celle adoptée tout au long de cette étude, les points isolés à la composition de H6.

On peut aisément étendre cette étude en fonction du volume à quelques autres types de combustibles en comparant D' à H2 (cermets PuO<sub>2</sub> dans U—Mo), T1 à H1 (PuO<sub>2</sub> dans Th), D1 à H4 (PuO<sub>2</sub> dans acier) et F à H5 (PuO<sub>2</sub> dans acier avec cœur mixte).

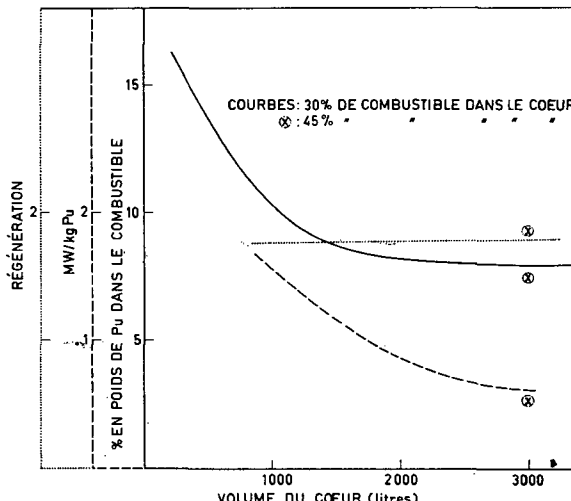


Figure 7  
Combustible U-Pu-Mo. Variation de quelques caractéristiques en fonction du volume du cœur.

Les conclusions à retenir sont les suivantes:

1. Le taux de régénération reste pratiquement constant entre 1000 l et 3000 l. Il augmente cependant légèrement pour H6, cœur pour lequel la teneur en combustible est portée à 45 %, et diminue dans le cas du cermet à PuO<sub>2</sub> dans l'acier H4. Dans ce dernier cas, la teneur en acier dans le cœur devient si importante que les captures parasites favorisées par la dégradation du spectre (le rapport  $\alpha$  du <sup>239</sup>Pu est plus grand qu'avec les autres types de piles) sont accrues de façon sensible.

2. Les masses critiques sont 2,3 à 2,5 fois plus grandes pour 3000 l que pour 1000 l, sauf pour le cermet PuO<sub>2</sub> dans l'acier, pour lequel elle n'est accrue que d'un facteur 1,8 à cause de l'adoucissement du spectre. Le paramètre  $y$  varie en raison inverse. Le paramètre  $\mu$  diminue évidemment lorsque le volume du cœur augmente, mais de plus en plus lentement (fig. 7).

3. Le taux d'irradiation en MWj par tonne de combustible est inversement proportionnel au volume du combustible.

4. Avec les cermets mixtes, la teneur volumétrique du combustible en PuO<sub>2</sub> reste très importante, même avec un cœur de 3000 l: 30% dans le cas d'une matrice acier.

5. Les temps de doublement théoriques sont beaucoup plus longs qu'avec un volume de cœur de 1000 l.

H2: 6 ans 6 mois

H3: 12 ans 9 mois

H4: 10 ans 11 mois

H5: 10 ans 11 mois

H6: 6 ans 6 mois.

#### ÉVOLUTION DANS LE TEMPS ET CORRECTIONS A APPORTER AUX RÉSULTATS PRÉCÉDENTS

La combustion des isotopes lourds, particulièrement le <sup>239</sup>Pu, lors du fonctionnement du réacteur à un niveau élevé de puissance, se traduit — si le taux de régénération interne est inférieur à 1 — par une diminution de la réactivité qu'il faut compenser par le retrait progressif de barres de contrôle du type « poison » par exemple. Nous avons fixé la compensation maximale — c'est-à-dire la diminution de réactivité que l'on peut admettre sans avoir à recharger le combustible — à 3000 pcm (3%)\*.

#### *Masses critiques réelles*

Lors de la mise en route du réacteur, il est nécessaire de disposer dans le cœur d'une masse de matière fissile nettement supérieure à la masse critique calculée, pour apporter le complément de réactivité de 3000 pcm. Pour le combustible (B), l'excès de masse de <sup>239</sup>Pu doit être de 103 kg, soit à peu près 20% de la masse critique calculée sans tenir compte du système de contrôle. Nous avons admis qu'il est du même ordre pour tous les autres combustibles. Les masses de <sup>239</sup>Pu notées dans les tableaux II, VII, VIII, IX et X sont donc à majorer de 20%.

\* Dans le cas du combustible carbures (B) par exemple, on a calculé que le contrôle peut être réalisé au moyen de barres au carbure de bore très enrichi en B 10 (90 %) placées à 23 cm de l'axe du réacteur et contenant sensiblement 4000 g au total de B 10: l'antiréactivité totale disponible est alors de l'ordre de 7000 pcm.

### *Incertitude sur le taux de régénération*

Le taux de régénération est un facteur économique important. Celui que nous avons indiqué pour chaque combustible correspond à des conditions bien déterminées, mais dans la pratique il sera probablement plus faible, et ceci pour deux raisons surtout :

1° La présence de barres de contrôle et les captures parasites du B 10 qu'elles entraînent;

2° Le fait qu'il faudra probablement porter la teneur du fertile des couvertures en molybdène de 3 à 10% pour atteindre des taux de combustion de l'ordre de 1%. Nous avons estimé que l'on obtiendrait ainsi un taux de régénération  $x'$  inférieur de 10% à celui calculé  $x$ . Compte tenu des incertitudes de calcul, en particulier des sections efficaces, nous avons pensé qu'il était raisonnable de prévoir une marge d'incertitude de l'ordre de  $\pm 10\%$  sur  $x'$ . En définitive, ceci revient à attribuer à chaque combustible un taux de régénération se situant entre la valeur calculée, portée dans les différents tableaux, et une valeur inférieure de 20%.

### *Taux de combustion dans les couvertures*

Les figures 8 et 9 représentent, dans le plan médian du réacteur et le long de l'axe, les taux de combustion des isotopes lourds (Pu et U) après un mois de fonctionnement du réacteur à la puissance constante de 800 MW dans le cas des combustibles B et D respectivement. A noter que dans les couvertures il n'est pas tenu compte

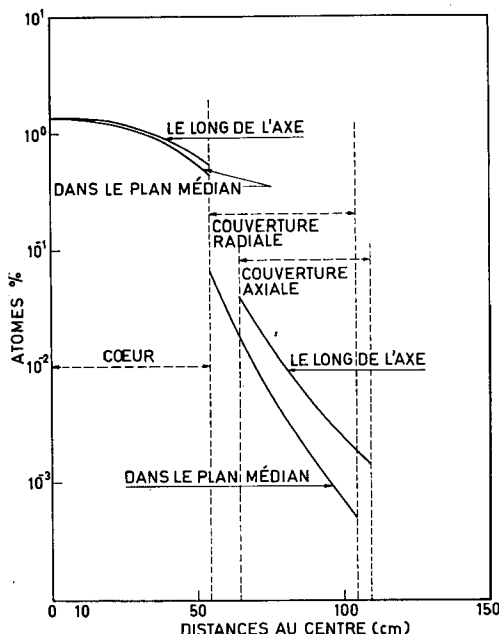


Figure 8

Combustible PuC—UC (B). Taux de combustion des isotopes lourds après un mois de fonctionnement continu du réacteur à 800 MW.

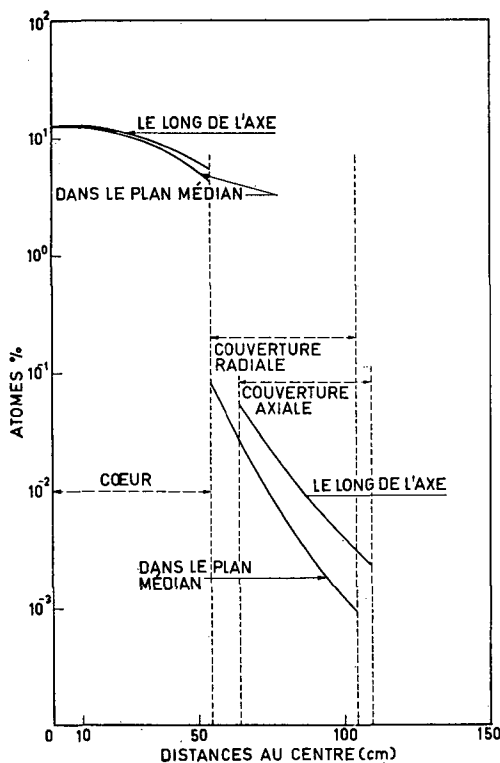


Figure 9

Combustible cermet (D). Taux de combustion des isotopes lourds après un mois de fonctionnement continu du réacteur à 800 MW.

TABLEAU XI  
TAUX DE COMBUSTION DANS LES COUVERTURES AVEC DIFFÉRENTS  
COMBUSTIBLES  
(Après 30 jours à 800 MW)

Volume de cœur	Type de combustible	Couverture radiale		Couvertures axiales	
		Taux max.	Taux moy.	Taux max.	Taux moy.
1000 l	A	0,067	0,0043	0,038	0,0069
	B	0,073	0,0044	0,042	0,0071
	C1	0,082	0,0049	0,047	0,0080
	C2	0,069	0,0043	0,043	0,0073
	D—D1	0,096	0,0065	0,059	0,0108
	D'	0,058	0,0036	0,033	0,0058
3000 l	H2	0,019	0,0014	0,012	0,0022
	H4	0,034	0,0028	0,031	0,0045
	H5	0,0064	0,0005	0,018	0,0011
	H6	0,015	0,0011	0,010	0,0015

des fissions du  $^{239}\text{Pu}$  formé au cours de la marche, mais que ces fissions peuvent devenir importantes si les assemblages de la couverture restent longtemps en pile.

Avec les mêmes hypothèses, le tableau XI indique les taux de combustion maximal (dans le plan médian) et moyen (intégrale sur le volume) dans la couverture radiale avec plusieurs combustibles.

Les courbes 8 et 9 et les résultats du tableau XI serviront dans la deuxième partie de ce rapport à déterminer la fréquence de déchargement des éléments de la couverture radiale.

*Cas des cœurs annulaires et mixtes.* Des assemblages fertiles sont placés dans des zones à flux élevé, au centre du réacteur (cœurs annulaires) ou à l'intérieur du cœur mixte. On peut s'attendre pour eux à des taux de combustion importants qui nécessitent des décharges fréquentes.

La figure 6 montre que le taux de combustion maximal des éléments fertiles placés au centre de (E 2) est — si l'on suppose les spectres peu différents — légèrement inférieur au taux de combustion maximal dans la couverture radiale de D1 soit 0,096% en un mois à 800 MW. On pourra donc appliquer à ces éléments centraux le même rythme de déchargement qu'aux éléments fertiles placés à la périphérie du cœur dans la plupart des cas étudiés à 1000 l (B, C1, D1...).

Dans le cas du cermet mixte F, le taux de combustion en un mois à 800 MW des assemblages fertiles placés dans le cœur varie de 0,13% au centre du cœur à 0,02% à la périphérie.

### *Evolution de la réactivité*

Elle dépend essentiellement de trois facteurs:

a) Le taux net de disparition du  $^{239}\text{Pu}$  dans le cœur, c'est-à-dire la différence entre le taux brut de disparition de cet isotope (par fissions et captures) et son taux de formation par captures de  $^{238}\text{U}$ . Ce taux net peut être positif si le taux de régénération interne est inférieur à 1, mais aussi négatif si le taux de régénération interne est supérieur à 1. Dans le premier cas, il s'ensuit un effet négatif sur la réactivité, dans le second cas, un effet positif. C'est le facteur le plus important.

b) Le taux de régénération externe, qui a un effet positif sur la réactivité, d'autant plus que le plutonium se forme surtout dans les assemblages fertiles contigus au cœur.

c) L'accumulation des produits de fission, qui accroît les captures parasites; cet effet peut devenir très important si l'on atteint des taux de combustion élevés.

L'étude de l'évolution de la réactivité — différente avec chaque type de cœur et de combustible — est complexe; les phénomènes ne sont pas linéaires, et les sections efficaces de capture des produits de fission sont mal connues.

Nous avons cependant évalué grossièrement le temps de séjour en pile de chaque cœur compatible avec une baisse de réactivité de 3%, le réacteur fonctionnant à 800 MW, en négligeant l'effet des produits de fission.

*Cas des piles de 1000 l.* Le taux de régénération interne, dans tous les exemples étudiés sauf un, est assez nettement inférieur à l'unité. On peut donc s'attendre à une diminution de la réactivité. Dans le cas des cœurs B (carbures) et D (cermet à matrice inox), cette diminution, calculée après 30 jours de fonctionnement continu à 800 MW, est respectivement de 640 et de 4400 pcm, ce qui autorise des séjours en pile de 140 et 20 jours. Nous basant sur ces chiffres et sur les taux de disparition du plutonium et de régénération calculés, nous avons estimé le temps de séjour en pile possible avec les autres cœurs (tableau XII).

TABLEAU XII

**TEMPS DE SÉJOUR DU CŒUR EN PILE (A 800 MW)**  
**compatibles avec une baisse de réactivité maximale de 3% et un taux de disparition**  
**du plutonium inférieur à 30%**

Volume du cœur	Type de combustible	Nombre de jours possibles imposés par		Irradiation correspondante (MWj/t combustible)
		la réactivité	la disparition du $^{239}\text{Pu}$	
1000 l	A U—Pu—Mo	230	—	32 700
	B PuC—UC	140	—	27 300
	C1 PuO <sub>2</sub> —UO <sub>2</sub>	85	—	20 000
	C2 PuO <sub>2</sub> —UO <sub>2</sub>	110	—	21 600
	D cermet à matrice inerte	20	—	5 500
	D' cermet à matrice U—Mo	210	—	32 000
	D6 cermet à matrice inerte	23	—	6 300
	E2 cermet annulaire, matrice inerte	45	—	11 700
	F cermet mixte, matrice inerte	—	375	80 000
	T1 cermet à matrice Th	75	—	17 600
	T3 cermet mixte, matrice Th	180	—	54 000
3000 l	H1 cermet à matrice en Th	270	—	21 000
	H2 cermet à matrice U—Mo	—	—	sans limite
	H3 cermet mixte, matrice U—Mo	—	—	sans limite
	H4 cermet à matrice inox	35	—	3 400
	H5 cermet mixte, matrice inox	—	930	68 000
	H6 U—Pu—Mo	—	—	sans limite

L'exception est constituée par le cermet « mixte » F, pour lequel le taux de régénération interne est 1,15, mais il faut noter que dans ce cas la production de plutonium se fait dans les assemblages fertiles dans le cœur, donc d'une façon non homogène, et que la valeur calculée en supposant une composition homogène est peut-être optimiste. Il est donc difficile de prévoir comment va évoluer la réactivité, mais, étant donnée la valeur assez nettement supérieure à 1 du taux de régénération calculé, on peut penser quand même qu'elle n'est pas une limitation sérieuse pour le séjour en pile du cœur.

*Cas des piles de 3000 l.* Le taux de régénération interne est toujours très nettement supérieur à 1, sauf pour H1 et H4. Il se peut donc que la réactivité augmente pendant la marche du réacteur, et qu'il soit nécessaire de la compenser par une insertion des barres. Quoi qu'il en soit, et les taux de régénération étant probablement un peu surévalués, on peut penser que le problème de la réactivité est secondaire avec les cœurs H2, H3, H5 et H6, et que la limitation du temps de séjour en pile dépendra d'autres facteurs.

#### *Temps de séjour en pile et irradiations correspondantes*

Le rythme de chargement-décharge du cœur sera imposé selon le combustible, par l'un des facteurs suivants : la réactivité, que nous venons d'étudier ;

la diminution du nombre d'atomes fissiles ( $^{239}\text{Pu}$ ) dans le combustible, qui entraîne une diminution des sources de chaleur et une distortion importante du flux, et le taux d'irradiation que peut supporter le combustible, et que l'on peut exprimer en mégawattjours par tonne. Les deux premiers facteurs sont d'ordre physique, et nous nous sommes fixés comme critères une baisse de réactivité admissible de 3% ainsi que nous l'avons déjà signalé, et un taux de disparition maximal du  $^{239}\text{Pu}$  égal à 30% des atomes initiaux. Le troisième facteur, d'ordre métallurgique, est assez mal connu; nous avons adopté les valeurs généralement admises (voir deuxième partie).

Dans le tableau XII nous avons porté les temps de séjour en pile compatibles avec celui des deux premiers facteurs qui est limitatif pour le cœur considéré; en regard, nous avons indiqué le taux d'irradiation correspondant en mégawatt-jours par tonne de combustible, que ce taux soit ou non supportable par le combustible.

Dans le cas où le volume du cœur est 1000 l, le facteur limitatif est presque toujours la réactivité, sauf pour les coeurs A, D' et F (pour A et D' les deux critères sont d'ailleurs pratiquement équivalents). Avec le combustible métallique A, on arrive sensiblement au taux d'irradiation maximal qui puisse être envisagé; par contre, les combustibles carbures et oxydes peuvent certainement accepter des irradiations supérieures à 27 000 ou 20 000 MWj/t. Enfin, les cermets à matrice inerte qui, théoriquement, peuvent supporter des irradiations très importantes, ne sont intéressants qu'avec une solution du type « cœur mixte ».

Dans le cas où le volume du cœur est 3000 l, c'est la disparition de l'élément fissile qui devient limitative, sauf pour les cermets à matrice en thorium ou en acier inox. Les temps de séjour en pile peuvent être beaucoup plus longs et on aboutit — en se fixant pour critère la disparition de 30% des atomes de plutonium — à des taux d'irradiation qui sont vraisemblablement, pour chaque exemple envisagé, supportables par le combustible ou la matrice, sauf peut-être pour les cermets mixtes.

#### *Remarques générales*

a) Nous avons étudié des exemples de piles dont la réalisation technique ne semble pas, à priori, poser des problèmes insolubles. Toutefois, il peut quand même subsister quelques difficultés dans certains cas: avec les cermets pour ce qui est de la teneur en matière fissile dans la matrice, avec quelques piles de 3000 l en ce qui concerne la hauteur du cœur.

b) Il convient de faire quelques réserves sur les calculs intéressant les « cermets mixtes »: leur structure très hétérogène, surtout si les assemblages sont de grandes dimensions, s'adapte mal à des calculs qui supposent essentiellement les milieux homogènes.

c) Nous n'avons pas étudié les coefficients de réactivité. Les coefficients dus à la dilatation du combustible sont toujours négatifs, par contre la dilatation du sodium peut conduire à un effet positif dans le cas de grosses piles à forte teneur en  $^{238}\text{U}$  dans le cœur. De même, le coefficient Doppler sera certainement positif dans le cas des cermets à matrice inerte, mais l'introduction de grandes quantités de fertile dans le cœur avec la solution « cœur mixte » permettra de diminuer fortement ce coefficient Doppler ou même de le rendre négatif.

d) Les limitations que nous avons adoptées (indépendamment de la tenue sous irradiation du combustible) pour déterminer le temps de séjour en pile de chaque cœur — baisse de réactivité de 3% et disparition nette de 30% des atomes

de  $^{239}\text{Pu}$  — sont évidemment un peu arbitraires, mais elles nous paraissent raisonnables. Nous avons vu que, pour des coeurs de 1000 l, l'évolution de la réactivité est un facteur particulièrement restrictif pouvant conduire à des déchargements très fréquents. Cette limitation peut être rendue un peu moins sévère en adoptant des coeurs de volume plus grand ou partiellement empoisonnés par déchargements partiels (ce qui revient à accroître la masse critique), mais la meilleure solution pour permettre des taux d'irradiation importants est d'introduire du fertile dans le cœur.

### Etude économique

Après avoir effectué des calculs neutroniques de quelques piles rapides, nous voudrions voir l'influence de la nature du combustible, de la forme et des dimensions du cœur, sur l'économie du réacteur. Plus précisément, et ainsi qu'il a été dit plus haut, nous voudrions mettre en évidence le rôle:

- a) Du taux de régénération  $x$  (rapport du poids de matière fissile précieuse telle que le  $^{239}\text{Pu}$  formée dans la pile, au poids de même matière détruite dans le cœur);
- b) De la puissance spécifique  $y$  (exprimée en mégawatts par unité de poids de matière fissile précieuse telle que le  $^{239}\text{Pu}$ );
- c) Du taux de combustion  $z$  des combustibles (évalué le plus commodément dans cette partie en mégawattjouls par tonne de combustible).

### GÉNÉRALITÉS

Nous nous sommes fixé comme cadre des piles d'une puissance thermique constante et égale à 800 MW. Cette hypothèse vient de ce que le coût du kilowatt diminue quand la taille de la pile et de la centrale électrique associée augmente, et de ce que des centrales de 300 MW électriques peuvent être considérées comme réalisables dans les prochaines années.

En ce qui concerne le retraitement du combustible, nous avons étudié les cas d'un cycle court (pyrométallurgie) et le cas du retraitement classique par voie aqueuse. D'une façon générale, nous pensons qu'à l'époque où on construira des réacteurs rapides industriels et à laquelle cette étude s'applique (1970—1980), les usines de retraitement seront, quel que soit le procédé adopté, suffisamment nombreuses pour qu'on puisse définir un prix  $\gamma$  par unité de poids de combustible irradié retraité. Nous prenons pour  $\gamma$  les évaluations:

$\gamma_1 = 250$  NF par kilogramme de combustible retraité dans le cas du cycle court,  
 $\gamma_2 = 600$  NF par kilogramme de combustible retraité par voie aqueuse.

Nous précisons que la valeur de 250 NF/kg correspond à des études sur des opérations effectuées dans des usines d'une capacité de 100 kilogrammes de combustible par jour\*.

Le prix  $P$  du kilowatt produit est évidemment directement influencé par le prix du retraitement (nous faisons d'ailleurs, dans le cas du cycle court, une étude de  $P$  en fonction des variations de  $\gamma_1$  — cf. fig. 27 à 29). Mais, de plus, le procédé de retraitement adopté influe directement sur  $P$  par l'immobilisation du plutonium qu'il entraîne.

---

\* Une telle usine nécessite un investissement de 30 000 000 NF, des frais d'exploitation annuels de 1 400 000 NF et des frais variables évalués à 50 NF par kilogramme de combustible traité [1].

En effet, dans le cas du cycle court, dont la durée exacte est à déterminer mais qui pourrait être de l'ordre de deux mois, on peut imaginer qu'on immobilise deux masses critiques dans le réacteur et les usines de retraitement et de refabrication, tout au moins lorsque le taux d'irradiation admissible se trouve dans les zones étudiées, c'est-à-dire au-dessus de 5000 MWj/t.

Au contraire, dans le retraitement par voie aqueuse, il peut s'écouler près d'une année entre deux mises en piles successives d'un même cœur. Le temps d'immobilisation hors pile d'un cœur peut se décomposer en :

Refroidissement .....	3 mois
Stockage avant envoi au traitement .....	1 mois
Transport site-traitement .....	0,5 mois
Stockage avant traitement .....	1 mois
Traitements .....	1 mois
Transport traitement-fabrication .....	0,5 mois
Stockage avant fabrication .....	1,5 mois
Fabrication .....	1,5 mois
Stockage après fabrication .....	0,5 mois
Transport fabrication-site .....	0,5 mois
Stockage avant mise en pile .....	<u>1 mois</u>
	<u>12 mois</u>

Il s'en suit, dans ce dernier cas, il devient difficile de considérer comme fixe le nombre de coeurs immobilisés. Il faut l'évaluer comme une fonction de la puissance spécifique  $y$  et du taux d'irradiation admissible  $z$ .

Notre étude paramétrique comprendra donc deux parties : celle du cycle court, où on admet un prix de retraitement de 250 NF par kilogramme de combustible et où on immobilise au total deux coeurs, et celle du retraitement par voie aqueuse, où le prix de retraitement est de 600 NF/kg et où le nombre de coeurs immobilisés est calculé suivant les formules données à l'annexe 1.

Comme autre hypothèse, nous postulons l'existence d'un marché de plutonium dans lequel un prix  $s$  pourra être affecté au gramme de plutonium et qui pourra être une valeur d'équilibre dans le cadre d'une production de plutonium faite par un ensemble de réacteurs rapides et thermiques [2]\*.

#### DÉFINITION DU PRIX DU KILOWATTHEURE

Dans ces conditions, le prix de revient du kilowatt électrique produit par l'ensemble réacteur rapide-usines de retraitement et refabrication est donné par la relation :

$$P = \frac{\text{Coût annuel de fonctionnement d'un réacteur de } 800 \text{ MWt} + \text{Coût annuel du cycle de combustible correspondant}}{\text{Quantité d'énergie électrique produite}} - \text{Recette due à la vente de la production de plutonium}$$

L'emploi de cette formule implique que nous voulons déterminer le prix du kilowattheure dans un régime permanent où le réacteur est supposé construit, où tous les coeurs immobilisés ont été fabriqués et où on paie annuellement les intérêts des capitaux investis. Cette situation est un peu différente de la réalité, où on doit dépenser à un moment initial bien précis les capitaux de construction

\* Nous prenons pour  $s$  la valeur de \$12 = 60 NF/g, chiffre susceptible de représenter le prix d'équilibre du marché de plutonium vers 1970—1980 [3].

TABLEAU XIII

**ESTIMATION DU PRIX DE REVIENT DU KILOWATTHEURE**  
**produit par l'ensemble réacteur rapide—usines de retraitement par cycle court et de**  
**refabrication**

**I. Coût du fonctionnement du réacteur***A. Dépenses de capital*

Amortissement du capital  $I_1$  investi dans  
la construction du réacteur

$$\alpha I_1$$

*B. Dépenses de fonctionnement du réacteur*

$$\text{TOTAL } \frac{f}{\alpha I_1 + f}$$

**II. Coût du cycle de combustible***A. Frais de location du combustible*

$$(cf. Annexe 1) \quad \frac{2 \times 8 \cdot 10^5 rs}{y}$$

*B. Coût de retraitement du cœur*

Frais de retraitement du cœur  
(cf. Annexe 1)

$$\frac{288 \cdot 10^6 d \gamma_1}{z}$$

*C. Coût de refabrication du cœur*

Frais de refabrication des aiguilles  
(cf. Annexe 2)

$$k_1 MN = \frac{36 \cdot 10^4 \mu y k_1 M d}{z}$$

*D. Coût de retraitement et refabrication des couvertures supérieure et inférieure et de refabrication des gaines*

$$(cf. Annexe 3) \quad \frac{288 \cdot 10^6 \frac{2 d w'_1 d'_1 H' (c_1 + c_2)}{z w_1 d_1 H}}$$

*E. Coût de retraitement et refabrication des couvertures radiales*

$$\begin{aligned} 1. & \text{ Retraitement annuel} & 0,3 q c_1 \\ 2. & \text{ Refabrication annuelle} & 0,3 q c_2 \end{aligned}$$

*F. Frais de location de l'uranium des couvertures*

$$1,6 q s' r$$

$$\begin{aligned} \text{TOTAL } \frac{2 \times 8 \cdot 10^5 rs}{y} &+ \frac{288 \cdot 10^6 d \gamma_1}{z} + \frac{36 \cdot 10^4 \mu y k_1 M d}{z} + \\ &+ \frac{288 \cdot 10^6 2 d w'_1 d'_1 H' (c_1 + c_2)}{z w_1 d_1 H} + 0,3 q (c_1 + c_2) + 1,6 q s' r \end{aligned}$$

**III. Crédit provenant de la vente du plutonium**

$$(cf. Annexe 4) \quad 800 d \delta \delta' (x - 1) (1 + \alpha) 370 s$$

**IV. Production annuelle d'électricité**

$$8 \cdot 10^5 d \varrho \times 360 \times 24 \text{ kWh}$$

$$\text{Prix du kilowattheure} \quad P = \frac{(I) + (II) - (III)}{(IV)}$$

du réacteur et où on ne fabrique pas à la même époque tous les coeurs. Il s'agit dans ce cas d'un régime transitoire tendant à l'établissement d'un état permanent. Si nous avons étudié ce dernier, c'est parce qu'une étude complète avec capitalisation initiale eût été trop lourde et que ce à quoi nous nous attachions était moins une évolution précise de la valeur absolue du kilowattheure, que la comparaison de diverses solutions techniques permettant de définir dans quelle voie les recherches doivent être poussées. Nous pensons néanmoins que les résultats auxquels nous aboutissons, malgré l'hypothèse du régime permanent établi, représentent assez bien la réalité, car les diverses solutions techniques envisageables impliquent toutes les mêmes et gros investissements initiaux

TABLEAU XIV

**ESTIMATION DU PRIX DE REVIENT DU KILOWATTHEURE**  
**produit par l'ensemble réacteur rapide — usines de traitement par voie aqueuse et de refabrication**

**I. Coût du fonctionnement du réacteur**A. *Dépenses de capital*

Amortissement du capital  $I_1$  investi dans la construction du réacteur  $a I_1$

B. *Dépenses de fonctionnement du réacteur*

$$\text{TOTAL} \quad \frac{f}{a I_1 + f}$$

**II. Coût du cycle de combustible**A. *Frais de location du combustible*

$$(cf. Annexe 1) \quad \frac{8 \cdot 10^5 rs}{y} + \frac{288 \cdot 10^6 d \mu rs}{z}$$

B. *Coût de retraitement du cœur*

Frais de retraitement du cœur  
 $(cf. Annexe 1)$   $\frac{288 \cdot 10^6 d \gamma_2}{z}$

C. *Coût de refabrication du cœur*

Frais de refabrication des aiguilles  
 $(cf. Annexe 2)$   $k_1 MN = \frac{36 \cdot 10^4 d \mu y k_1 M}{z}$

D. *Coût de retraitement et refabrication des couvertures supérieure et inférieure et de refabrication des gaines*

$$(cf. Annexe 3) \quad 288 \cdot 10^6 \frac{2 d w'_1 d'_1 H' (c_1 + c_2)}{z w_1 d_1 H}$$

E. *Coût de retraitement et refabrication des couvertures radiales*

1. Retraitement annuel  $0.3 q c_1$
2. Refabrication annuelle  $0.3 q c_2$

F. *Frais de location de l'uranium naturel des couvertures*

$$1.6 q s' r$$

$$\text{TOTAL} \quad \frac{8 \cdot 10^5 rs}{y} + \frac{288 \cdot 10^6 d \mu rs}{z} + \frac{288 \cdot 10^6 d \gamma_2}{z} + \frac{36 \cdot 10^4 d \mu y k_1 M}{z} + \\ + 288 \cdot 10^6 \frac{2 d w'_1 d'_1 H' (c_1 + c_2)}{z w_1 d_1 H} + 0.3 q (c_1 + c_2) + 1.6 q s' r$$

**III. Crédit provenant de la vente du plutonium**

$$(cf. Annexe 4) \quad 800 d \delta \delta' (x - 1) (1 + \alpha) 370 s$$

**IV. Production annuelle d'électricité**

$$8 \cdot 10^5 d \varrho 360 \times 24 \text{ kWh}$$

$$\text{Prix du kilowattheure}$$

$$P = \frac{(I) + (II) - (III)}{(IV)}$$

de construction de réacteur et ne diffèrent que par le cycle de combustible, et que le prix du réacteur représente, ainsi qu'on le verra plus loin, près de 70% du coût du kilowattheure produit.

Les tableaux XIII et XIV donnent les éléments qui permettent de définir  $P$  respectivement dans le cas du cycle court et du retraitement par voie aqueuse.

On y voit en premier lieu que le coût de fonctionnement du réacteur (tableaux XIII et XIV, § 1) se compose de deux postes fixes: l'amortissement du capital investi  $I_1$ , calculé sur la base de 1300 NF par kilowattheure électrique installé [4]

(tableaux XIII et XIV, § I-A), et les frais de fonctionnement  $f$  (tableaux XIII et XIV, § I-B).

Le taux d'amortissement a été pris égal à  $\alpha = 0,11$ , ce qui correspond au taux d'intérêt pratiqué en France ( $r = 7\%$ ) et à un amortissement des installations en quinze ans [5].

Le cycle de combustible se compose de plusieurs parties. On doit en premier lieu payer les frais de location du matériau fertile (uranium naturel ou thorium) et du plutonium, puis le retraitement et la refabrication de ce dernier (tableaux XIII et XIV, § II-A).

En ce qui concerne les couvertures, nous avons admis que pour tous les types de réacteurs nous immobilisions une quantité de matériau fertile dans la pile de  $q = 65\,000$  kg. Il est certain qu'il s'agit là d'une hypothèse simplificatrice adoptée pour la commodité des calculs et parce que le prix de retraitement  $c_1$  et de refabrication  $c_2$  du kilogramme de matière fertile influe assez peu sur le prix du kilowattheure, mais qui rend d'autant moins compte de la réalité que les dimensions de la pile augmentent, c'est-à-dire que la puissance spécifique y diminue. Pour des études ultérieures plus précises, il serait nécessaire de revoir l'évaluation de ce poste. De même, nous avons, d'une façon relativement arbitraire, supposé pour l'évaluation de frais de location de l'uranium naturel ou du thorium

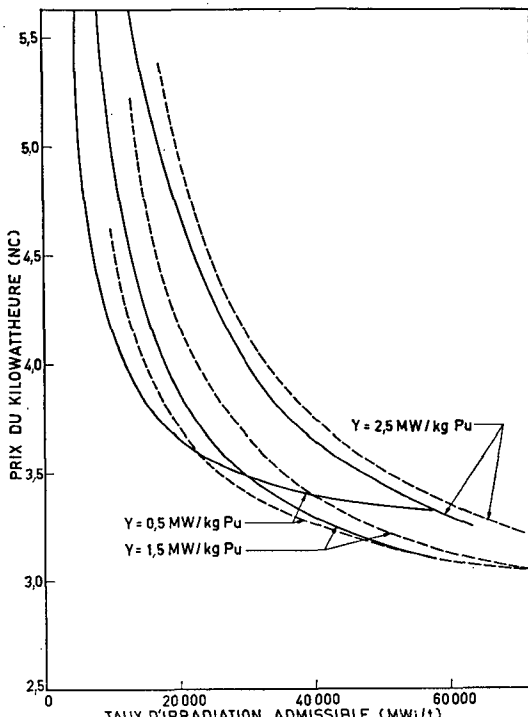


Figure 10  
Combustible UPuMo.  
— Retraitement court  
- - - - Retraitement aqueux

des couvertures, une immobilisation égale à  $1,6 q$ , donc un coût annuel (tableaux XIII et XIV, § II-F) de  $1,6 q s' r$  ( $s'$ : prix du kilogramme de matériau fertile,  $s'=150$  NF par kilogramme d'uranium naturel et  $s'=200$  NF par kilogramme de thorium).

Dans la refabrication des assemblages du cœur, nous avons distingué deux parties :

a) Pour le cœur lui-même, nous avons admis que le prix de refabrication était proportionnel au nombre d'aiguilles  $M$  (nous avons évalué  $M$  pour chaque type de combustible — cf. Annexe 2). Le prix de refabrication  $k_1$  d'une aiguille est, en effet, en première approximation, indépendant de ses dimensions. Le coût annuel de refabrication des aiguilles du cœur est donc  $k_1 MN$  (tableaux XIII et XIV, § II-C), relation où  $N$  représente le nombre de coeurs à mettre en pile par an et dépend à la fois de la puissance spécifique  $y$  et du taux d'irradiation admissible  $z$ . L'évaluation de  $N$  est donnée à l'Annexe 1. On a pris pour  $k$  la valeur de 350 NF par aiguille.

b) Pour les couvertures supérieure et inférieure (tableaux XIII et XIV, § II-D), nous avons postulé que le prix de retraitement et de refabrication s'évaluait en fonction de leur poids et pouvait être ramené au poids de combustible traité par an (cf. Annexe 3). On remarquera que l'on inclut dans cette évaluation le prix de refabrication des gaines des assemblages.

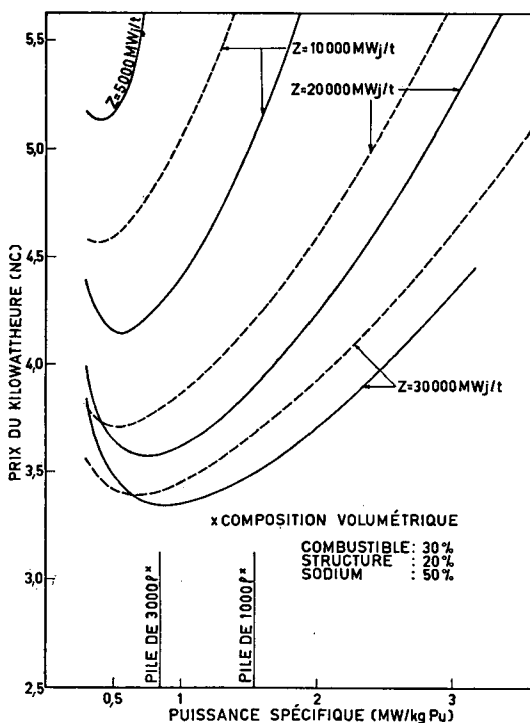


Figure 11  
Combustible U-Pu-Mo.  
— Retraitements courts  
- - - - - Retraitements aqueux

Pour les couvertures latérales, nous avons supposé que nous retraitions par an  $0,3 q = 0,3 \times 65\,000 = 19\,500$  kg de matériau fertile. La justification de cette hypothèse est discutée à l'Annexe 5.

Le détail de la recette due à la vente du plutonium (tableaux XIII et XIV, § III) est donné à l'Annexe 4.

#### RÉSULTATS OBTENUS

A partir de ces données, il a été possible de tracer, pour divers combustibles, les variations du prix du kilowattheure en fonction des variables  $x$ ,  $y$  et  $z$ . Les courbes des figures 10 et suivantes présentent pour chaque combustible les variations de  $P$  en fonction du taux d'irradiation  $z$  pour diverses valeurs fixes de la puissance spécifique  $y$ , et de la puissance spécifique  $y$  en fonction de valeurs fixes du taux d'irradiation admissible  $z$ . On tient compte, d'une façon implicite, dans la plupart des cas, des valeurs du taux de régénération  $x$ . Ce dernier, pour un combustible donné, varie très peu en fonction de la puissance spécifique. On donne initialement à  $x$  les valeurs trouvées dans les études neutroniques (plus exactement, on a diminué de 10% les valeurs données par les calculs neutroniques pour tenir compte des barres de contrôle dont la présence fait décroître  $x$ ), et on réserve à plus loin la discussion du rôle du taux de régénération.

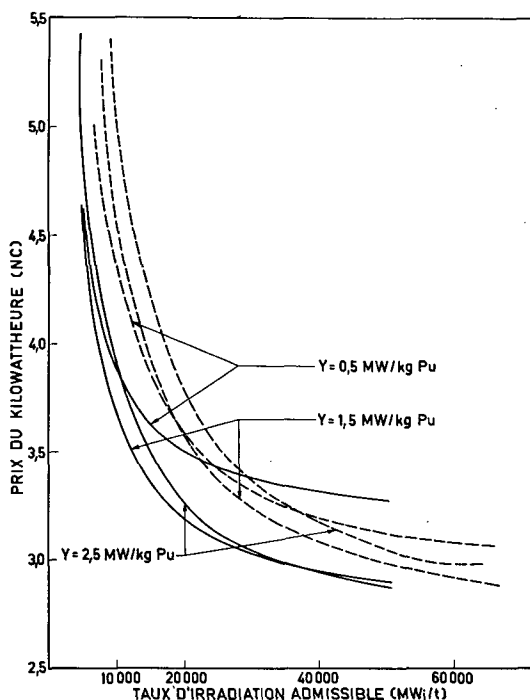


Figure 12  
Combustible PuC—UC.  
— Retraitement court  
- - - Retraitement aqueux

### Rôle du cycle de combustible

On remarquera l'importance du cycle de combustible qui se traduit par le fait que  $P$  décroît lorsque  $z$  augmente. Cette variation de  $P$  avec  $z$  est d'autant plus rapide que l'on se trouve dans les zones de faible  $z$ . Par contre, dès que l'on dépasse les taux de l'ordre de 30 000 MWj/t, on ne gagne plus beaucoup sur la diminution de  $P$ . On peut penser pouvoir atteindre et même dépasser techniquement ce chiffre de 30 000 MWj/t pour certains combustibles (PuO<sub>2</sub>—UO<sub>2</sub>, UC—PuC) alors que pour d'autres, comme le U—Pu—Mo, ce semble être une limite qu'il sera peut-être très difficile d'atteindre.

La comparaison entre le cycle court et le procédé de retraitement aqueux montre le net avantage du premier, sensible surtout pour les faibles valeurs de  $z$ . Ceci provient d'une part de ce que les prix de retraitement ne sont pas les mêmes (le retraitement aqueux a été pris par unité de poids, 2,4 fois plus cher que celui du cycle court), mais surtout de ce que ce dernier immobilise moins de plutonium. C'est donc pour les combustibles qui nécessitent la plus grande masse de plutonium dans le cœur (tels que U—Pu—Mo, PuO<sub>2</sub>—UMo, PuC—UC, cermets mixtes) que la différence est la plus sensible.

Par contre, dès que le taux d'irradiation augmente beaucoup, la différence entre les deux cycles est moins sensible. En effet, le prix de retraitement joue

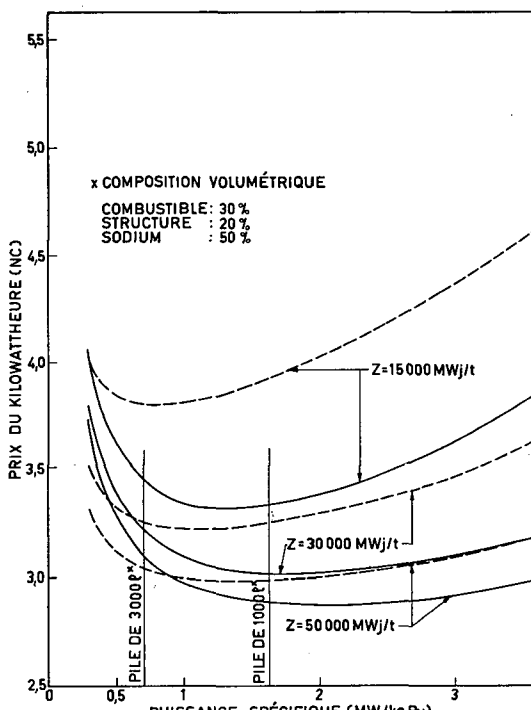
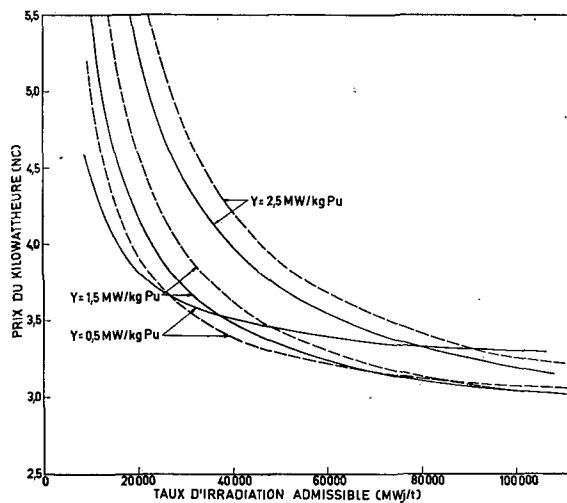
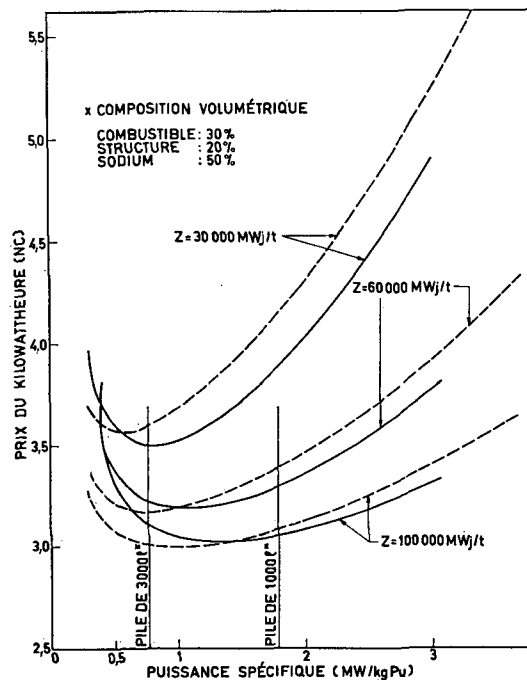


Figure 13  
Combustible PuC—UC.  
— Retraitemen court  
- - - - Retraitemen aqueux



**Figure 14**  
**Combustible  $\text{UO}_2-\text{PuO}_2$  ( $d_1 = 0,9 d_{\text{th}}$ ).**  
 Retraitemen court  
 Retraitemen aqueux



**Figure 15**  
**Combustible  $\text{UO}_2-\text{PuO}_2$  ( $d_1 = 0,9 d_{\text{th}}$ ).**  
 Retraitemen court  
 Retraitemen aqueux

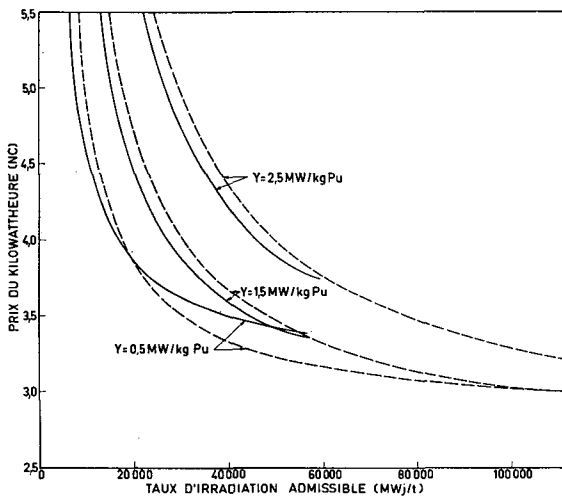


Figure 16  
Cermet  $\text{PuO}_2$  dans matrice UMo.  
 — Retraitement court  
 - - - - Retraitement aqueux

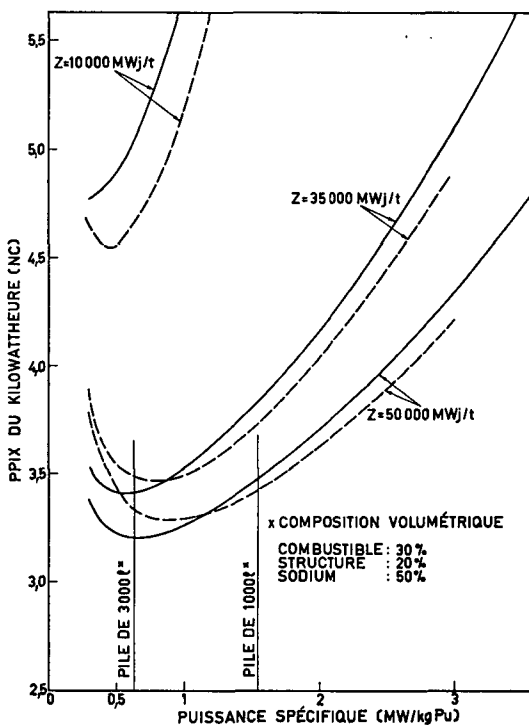


Figure 17  
Cermet  $\text{PuO}_2$  dans matrice UMo.  
 — Retraitement court  
 - - - - Retraitement aqueux

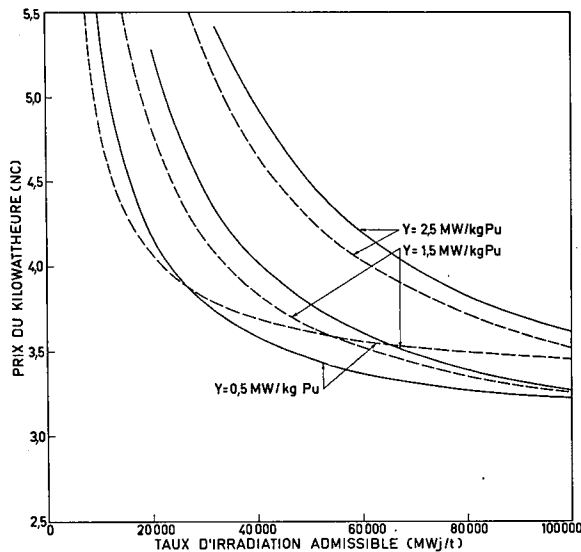


Figure 18  
Cermét  $\text{PuO}_2$  dans matrice Th.  
— Retraitemen court — - - - Retraitemen aqueux

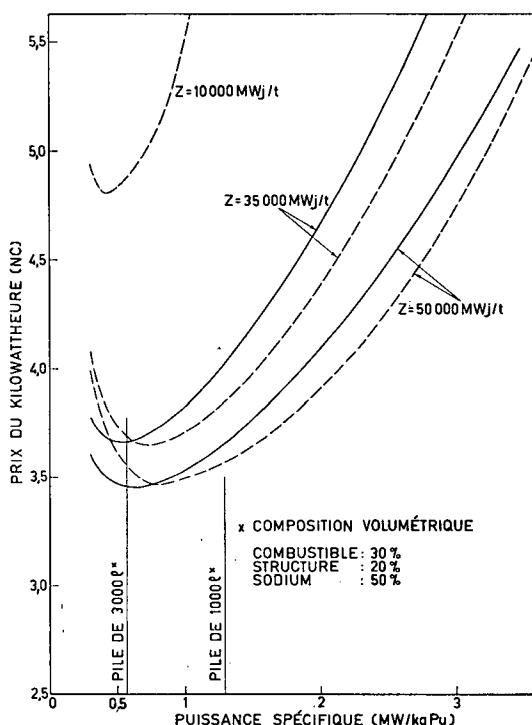


Figure 19  
Cermét  $\text{PuO}_2$  dans matrice Th.  
— Retraitemen court — - - - Retraitemen aqueux

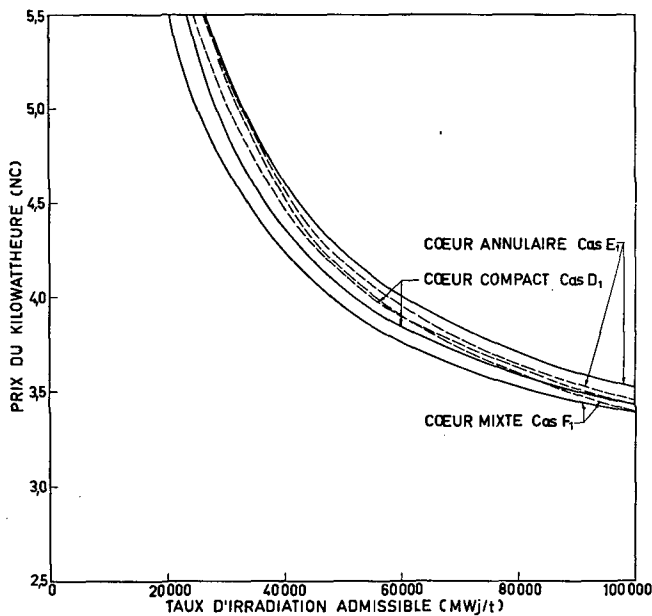


Figure 20  
Cermet inerte ( $\text{PuO}_2$  dans acier inoxydable). Pile de 1000 l.  
— Retraitemet court    - - - - Retraitemet aqueux

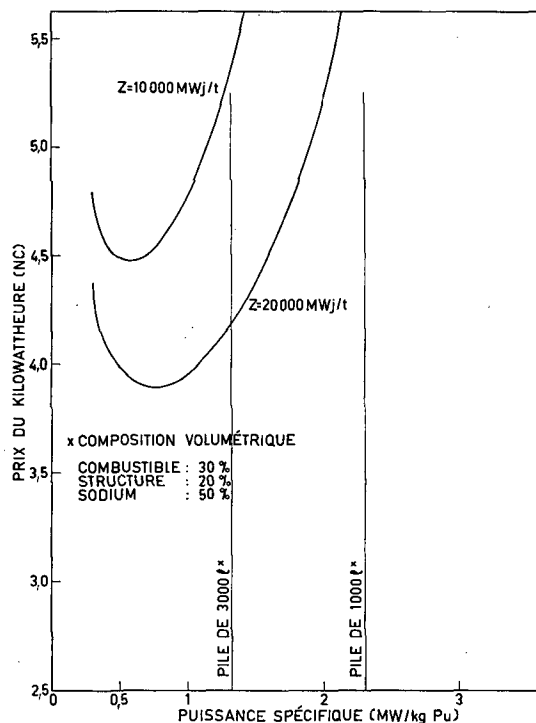


Figure 20 bis  
Cermet inerte ( $\text{PuO}_2$  dans acier inoxydable). Cœur compact  $H/D = 1$ . Retraitemet court.

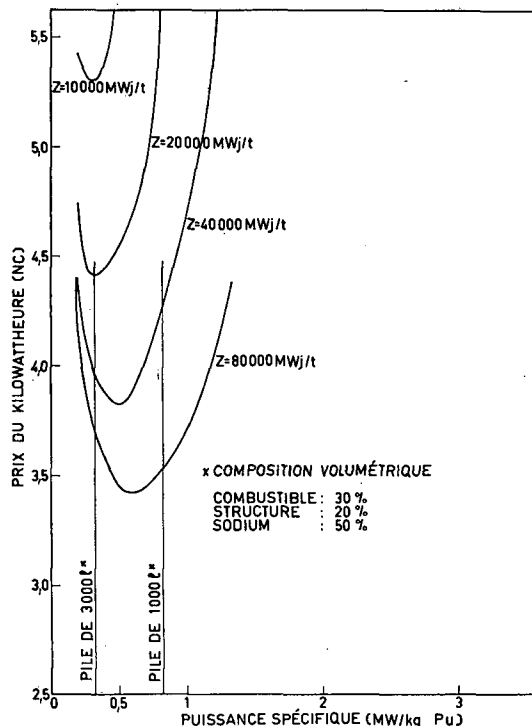


Figure 20 ter

Cermet inerte ( $\text{PuO}_2$  dans acier inoxydable). Configuration mixte. Retraitements court.

un rôle relativement faible, ainsi qu'il sera montré plus loin, et le nombre de cœurs immobilisés, lorsque  $z$  devient grand, décroît dans le retraitement aqueux, et arrive à être, avec les hypothèses faites, inférieur à 2, valeur fixe prise pour l'étude du cycle court.

Il s'ensuit que les deux cycles arrivent pour de grandes valeurs de  $z$  à donner la même valeur de  $P$ .

#### *Rôle de la puissance spécifique*

Pour chaque taux d'irradiation donné, la variation de  $P$  en fonction de la puissance spécifique  $y$  montre qu'il existe un minimum qui correspond (les formules des tableaux XIII et XIV permettent de le voir) à un optimum tenant compte de ce que  $P$  comprend dans le § II-C des tableaux XIII et XIV un poste de refabrication du cœur proportionnel à  $y$  et des frais de location de plutonium (tableaux XIII et XIV, § II-A) inversement proportionnels à  $y$ .

L'ordonnée de ce minimum est d'autant plus faible que le taux d'irradiation  $z$  auquel il s'applique est plus grand, mais la valeur de  $y$  correspondante est plus forte. On en déduit qu'en général, si on n'est pas sûr de pouvoir atteindre des taux  $z$  très élevés, il vaudrait mieux construire des piles de grand volume (1800 l environ) plutôt que des piles de 1000 l. Cette tendance est d'autant plus nette si on ne peut utiliser que le retraitement par voie aqueuse. En tout état de cause,

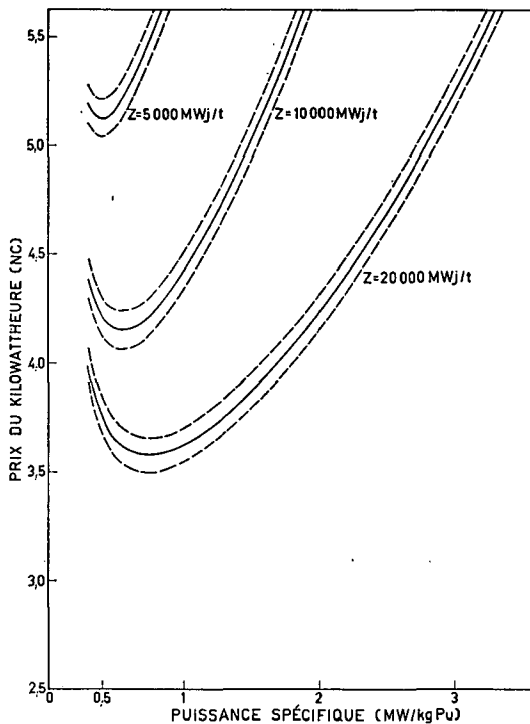


Figure 21  
Combustible U—Pu—Mo. Retraitemen court. Influence du taux de régénération  $x$ .

—  $x$  calculé  
- - -  $x \pm 10\%$

les valeurs optimales sont aux alentours de 0,6 à 1 MW par kilogramme de plutonium et correspondent à environ 0,45 MW par litre de cœur (cf. tableau XVIII).

#### Rôle du facteur de régénération

Nous avons, dans le cas du cycle court, étudié l'influence du taux de régénération  $x$ . Les études neutroniques montrent, comme il a déjà été indiqué plus haut, que, sauf dans le cas des cermets, il varie très peu, pour une composition volumétrique donnée, avec le volume du cœur. Néanmoins, on peut imaginer qu'en faisant varier la forme des assemblages, donc la composition volumétrique, on puisse l'augmenter de 10% environ. Les courbes des figures 21 à 25 mettent en évidence la variation de  $P$  qui en résulte. Elle n'est pas négligeable, mais elle demeure faible. On ne peut pas espérer rendre compétitif  $P$ , dans les zones où il ne l'est pas, en essayant d'augmenter  $x$ , alors que des progrès technologiques sur la tenue des combustibles autorisant une plus longue tenue en pile font décroître sensiblement  $P$ .

#### Rôle des paramètres fixes

*Influence du capital investi.* Après avoir examiné l'influence des variables  $x$ ,  $y$  et  $z$ , considérons celle des paramètres dits fixes. Les tableaux XV et XVI,

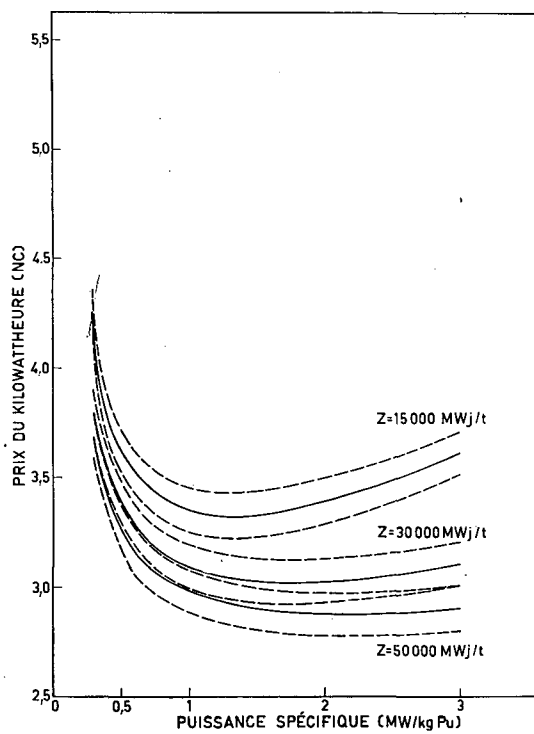


Figure 22  
Combustible PuC—UC. Retraitemen court. Influence du taux de régénération  $x$ .

—  $x$  calculé  
— — —  $x \pm 10\%$

qui donnent la décomposition de  $P$  pour des valeurs que l'on peut espérer atteindre pour  $z$  et correspondant au voisinage de l'optimum de  $y$ , montrent que le prix du réacteur intervient pour 70% environ dans la valeur du kilowattheure. On voit donc l'importance que joue la valeur du capital investi  $I_1$  dans la construction du réacteur et calculé sur la base de 1300 NF/kWh. L'expérience que l'on tirera des premiers réacteurs rapides expérimentaux devrait permettre de réduire ce chiffre. Si on pouvait l'amener à 1000 NF/kW, il en résulterait une baisse de  $P$  de 0,5 NC/kWh.

*Influence du prix du plutonium.* Les courbes de la figure 26 montrent le rôle du prix  $s$  du gramme de plutonium. Lorsque  $s$  passe de 60 à 150 NF/g (12 à 30 \$/g), les variations de  $P$  résultantes ne sont pas grandes aussi longtemps que les puissances spécifiques ne sont pas trop faibles. Ceci tient à ce que l'immobilisation de la matière fissile est alors compensée par la recette provenant de la vente du plutonium. On remarque que lorsque  $s$  augmente, les minima de  $P$  en fonction de  $y$  sont légèrement déplacés vers les zones de hautes puissances spécifiques.

*Influence de la refabrication et du retraitement.* Dans le cas du cycle court, on a étudié l'influence du prix de retraitement  $\gamma_1$  (figures 27, 28 et 29) et du prix de refabrication  $k_1$  des aiguilles (fig. 30). C'est ce dernier qui introduit les

TABLEAU XV

**ÉVALUATION DANS QUELQUES CAS TYPES DU PRIX DE REVIENT  
DU KILOWATTHEURE ÉLECTRIQUE**
**Cas du cycle court de retraitement**

Poste	U-Pu-Mo $x = 1,6$ $y = 0,8$ MW/kg $z = 20\ 000$ MWj/t	PuC-UC $x = 1,5$ $y = 1,63$ MW/kg $z = 30\ 000$ MWj/t	PuO <sub>2</sub> -UO <sub>2</sub> $x = 1,43$ $y = 1,15$ MW/kg $z = 60\ 000$ MWj/t	PuO <sub>2</sub> -UMo $x = 1,53$ $y = 0,8$ MW/kg $z = 35\ 000$ MWj/t	PuO <sub>2</sub> -Th $x = 1,20$ $y = 0,75$ MW/kg $z = 35\ 000$ MWj/t
<i>I. Coût de fonctionnement du réacteur</i>					
A. Dépenses de capital	2,0689	2,0689	2,0689	2,0689	2,0689
B. Dépenses de fonctionnement	0,4759	0,4759	0,4759	0,4759	0,4759
<i>II. Coût du cycle du combustible</i>					
A. Frais de location du combustible	0,3998	0,1962	0,2781	0,3998	0,4264
B. Coût du retraitement du cœur	0,1368	0,0912	0,0456	0,1173	0,1173
C. Coût de refabrication des aiguilles du cœur	0,3971	0,1139	0,2422	0,3579	0,3296
D. Coût de refabrication des couvertures supérieure et inférieure	0,1419	0,1297	0,0800	0,0850	0,1209
E. Coût de refabrication des couvertures radiales	0,2227	0,2227	0,2227	0,2227	0,2227
F. Coût de location de l'uranium naturel (ou thorium) des couvertures	0,0520	0,0520	0,0520	0,0520	0,0693
<i>III. Crédit provenant de la vente du plutonium</i>	-0,3197	-0,3278	-0,2700	-0,3183	-0,1697
<b>Prix du kilowatt électrique produit (NC/kWh)</b>	<b>3,5754</b>	<b>3,0227</b>	<b>3,1954</b>	<b>3,4612</b>	<b>3,6613</b>

plus grandes variations de  $P$ . Par contre, le prix du retraitement  $\gamma_1$  a une influence d'autant moins grande que  $z$  est plus grand, c'est-à-dire que l'on retraite moins souvent. On notera que dans le cas du carbure PuC-UC le prix de refabrication joue un rôle faible. Ceci tient à ce que la conductibilité des carbures étant très bonne, le nombre  $M$  d'aiguilles à utiliser est faible et l'importance de leur refabrication est petite.

*Influence de la composition volumétrique.* Nous avons voulu, dans un cas donné, voir l'influence des proportions volumétriques du combustible, des structures et du sodium. La figure 31 montre les variations de  $P$  pour deux piles de 3000 l ayant un combustible PuO<sub>2</sub> dans une matrice UMo, et dont la composition en volume est :

*Combustible*  
30%  
45%

*Structures*  
20%  
15%

*Sodium*  
50%  
40%

**TABLEAU XVI**  
**ÉVALUATION DANS QUELQUES CAS TYPES DU PRIX DE REVIENT**  
**KILOWATTHEURE**  
**Cas du cycle aqueux de retraitement**

Poste	U-Pu-Mo $x = 1,6$ $y = 0,8$ MW/kg $z = 20\ 000$ MWj/t	PuC-UC $x = 1,5$ $y = 1,63$ MW/kg $z = 30\ 000$ MWj/t	PuO <sub>2</sub> -UO <sub>2</sub> $x = 1,43$ $y = 1,15$ MW/kg $z = 60\ 000$ MWj/t	PuO <sub>2</sub> -UMo $x = 1,53$ $y = 0,8$ MW/kg $z = 35\ 000$ MWj/t	PuO <sub>2</sub> -Th $x = 1,20$ $y = 0,75$ MW/kg $z = 35\ 000$ MWj/t
<i>I. Coût du réacteur</i>					
A. Dépense de capital	2,0689	0,2689	2,0689	2,0689	2,0689
B. Dépense de fonctionnement	0,4759	0,4759	0,4759	0,4759	0,4759
<i>II. Coût du cycle du combustible</i>					
A. Frais de location du combustible	0,4002	0,3040	0,2355	0,2131	0,2727
B. Coût de retraitement du cœur	0,3283	0,2189	0,1094	0,2815	0,2815
C. Coût de refabrication des aiguilles du cœur	0,3971	0,1139	0,2422	0,3579	0,3296
D. Coût de refabrication des couvertures supérieure et inférieure	0,1419	0,1297	0,0800	0,0850	0,1209
E. Coût de refabrication des couvertures radiales	0,2227	0,2227	0,2227	0,2227	0,2227
F. Coût de location de l'uranium naturel (ou thorium) des couvertures	0,0520	0,0520	0,0520	0,0520	0,0693
<i>III. Crédit provenant de la vente du plutonium</i>	—0,3197	—0,3278	—0,2700	—0,3183	—0,1697
<b>Prix du kilowattheure produit (NC/kWh)</b>	<b>3,7673</b>	<b>3,2573</b>	<b>3,2166</b>	<b>3,4387</b>	<b>3,6718</b>

La proximité des deux courbes montre que le prix  $P$  est assez peu sensible aux proportions volumétriques dès que le taux d'irradiation atteint 20000 MWj/t.

*Influence de la nature du combustible.* D'une façon générale, on remarquera l'intérêt que présentent les carbures, intérêt dû à leur grande conductibilité et à leur tenue sous irradiation supposée bonne. Dans la mesure où on pourra les fabriquer, ils seront un combustible de choix. Quant aux cermets inertes (tels que ceux contenant du PuO<sub>2</sub> dans une matrice d'acier inoxydable), ils ont la caractéristique de ne pas avoir de régénération inerte. Par contre, il semble qu'ils aient été déjà fabriqués et qu'ils puissent subir de très fortes irradiations sans être détruits (80000 MWj/t).

Nous avons, pour les cermets inertes, étudié le cas de trois piles de 1000 l (cf. fig 20): une pile compacte (D1) où la hauteur est égale au diamètre ( $H/D = 1$ ), une pile à cœur annulaire (E1), et une pile mixte (F) où des assemblages fertiles sont disposés d'une façon homogène à l'intérieur du cœur.

On remarquera que pour un taux d'irradiation donné le prix  $P$  varie assez peu quand on passe d'un des trois types cités à un autre. Ceci vient (cf. tableau

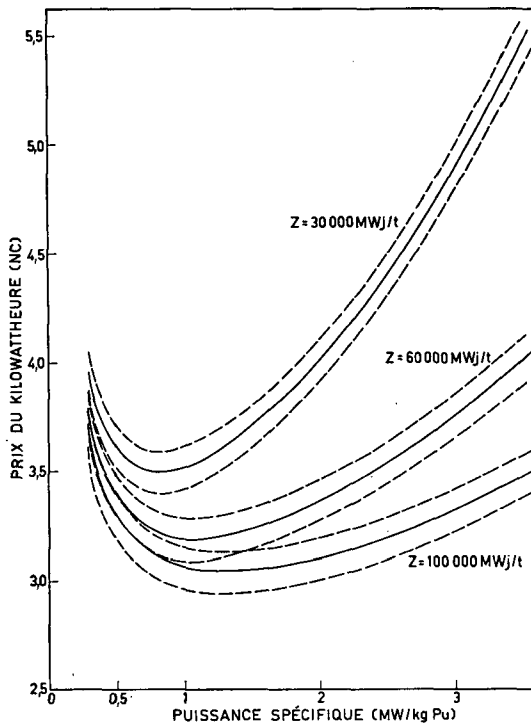


Figure 23

Combustible  $\text{UO}_2-\text{PuO}_2$ . Retraitements court. Influence du taux de régénération  $x$ .

$x$  calculé  
 $x \pm 10\%$

XVII, colonnes 3 et 4) de ce que le coût de l'immobilisation de matière fissile est compensé par la recette provenant de la vente du plutonium.

Le séjour en pile peut cependant ne pas être uniquement déterminé par la tenue sous irradiation du combustible, mais par la variation de réactivité ou le changement des sources de chaleur qui résultent du fonctionnement de la pile. Dans les cermets inertes sans régénération interne, c'est précisément ce qui se produit. Les études neutroniques (cf. tableau XII) montrent l'intérêt d'un cermet mixte que l'on peut irradier à 80 000 MWj/t sans que la réactivité varie de plus de 3000 pcm ni que les sources de chaleur soient modifiées de plus de 30%, alors que le cermet D1 doit être déchargé à 5500 MWj/t.

Il s'en suit que dans le cas de piles de 1000 l seuls les cermets mixtes à matrice inerte (cf. tableaux XVII et XVIII) peuvent arriver à être économiquement intéressants.

Pour des volumes plus grands (cf. fig. 20 bis), les cermets inertes, que l'on ne peut guère espérer pouvoir irradier à plus de 6000 MWj/t, ne peuvent pas être compétitifs. Par contre, pour les dispositifs mixtes (cf. fig. 20 ter), une variation de volume entre 1000 et 3000 l lorsque le taux d'irradiation est de 80 000 MWj/t ne change pas beaucoup le prix du kilowattheure, qui est alors comparable à celui que fourniraient des combustibles  $\text{U}-\text{Pu}-\text{Mo}$  ou  $\text{UO}_2-\text{PuO}_2$  irradiés respectivement à 20 000 ou 25 000 MWj/t.

TABLEAU XVII  
ÉVALUATION DU PRIX DE REVIENT DU KILOWATTHEURE  
Cas des cermets inertes — pile de 1000 l — cycle court de retraitement

Poste	Cermet D* $z =$ 5500 MWj/t	Cermet F** $z =$ 80 000 MWj/t	Cermet D* $z =$ 40 000 MWj/t	Cermet F** $z =$ 40 000 MWj/t
<i>I. Coût de fonctionnement</i>				
A. Dépenses de capital	2,0689	2,0689	2,0689	2,0689
B. Dépenses de fonctionnement	0,4759	0,4759	0,4759	0,4759
<i>II. Coût du cycle du combustible</i>				
A. Frais de location du combustible	0,1390	0,3929	0,1390	0,3929
B. Coût de retraitement du cœur	0,7476	0,0514	0,1028	0,1028
C. Coût de refabrication des aiguilles du cœur	9,3278	0,5738	1,2826	1,1475
D. Coût de refabrication des couvertures supérieure et inférieure	1,0673	0,0765	0,1468	0,1529
E. Coût de refabrication des couvertures radiales	0,2227	0,2227	0,2227	0,2227
F. Coût de location de l'uranium naturel (ou thorium) des couvertures	0,0520	0,0520	0,0520	0,0520
<i>III. Crédit provenant de la vente du plutonium</i>	—0,1365	—0,3871	—0,1365	—0,3871
<b>Prix du kilowattheure (NC/kWh)</b>	<b>18,9647</b>	<b>3,5270</b>	<b>4,3542</b>	<b>4,2285</b>

\* Configuration compacte ( $H/D = 1$ ).

\*\* Configuration mixte.

TABLEAU XVIII  
CORRESPONDANCE ENTRE LES PUSSANCES SPÉCIFIQUES  
par litre et par kilogramme de plutonium

Type de combustible	Valeurs optimales de $y$ (MW/kg de Pu)	$\mu$	$w_1$	$d_1$	Valeurs optimales de $y'$ MW/cœur
U—Pu—Mo	0,8 (cf. fig. 10)	0,0865	0,3	16,8	0,436
UC—PuC	1,2 (cf. fig. 12)	0,1186	0,3	12,26	0,436
UO <sub>2</sub> —PuO <sub>2</sub>	1 (cf. fig. 14)	0,1199	0,3	9,93	0,357
PuO <sub>2</sub> —UMo	0,7 (cf. fig. 16)	0,0887	0,3	16,7	0,444
PuO <sub>2</sub> —Th	0,65 (cf. fig. 18)	0,143	0,3	11,23	0,482
PuO <sub>2</sub> —Acier «mixte»	0,6 (cf. fig. 20 ter)	—	—	—	0,400

$\mu$  = enrichissement en poids du combustible en <sup>239</sup>Pu

$w_1$  = pourcentage du volume du combustible dans le cœur

$d_1$  = densité du combustible

$y$  = puissance spécifique par unité de poids de Pu (MW/kg)

$y'$  = puissance spécifique par litre (MW/litre)

$y$  et  $y'$  sont liés par la relation  $y' = y \mu w_1 d_1$

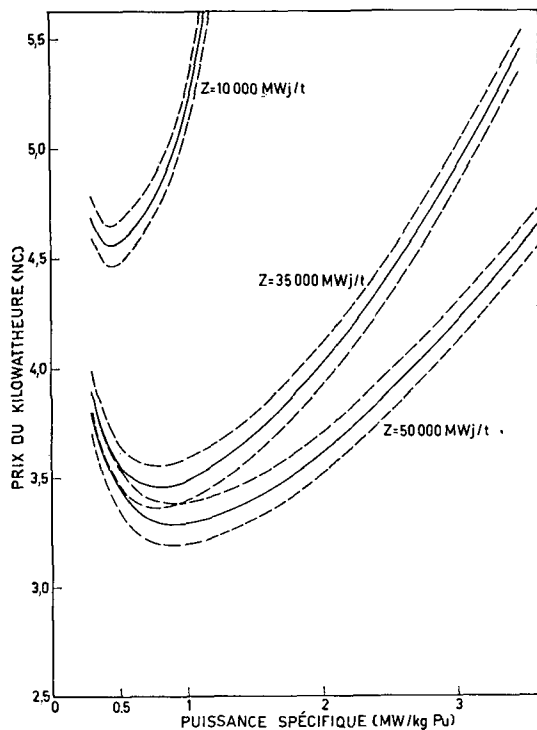


Figure 24  
Cermet PuO<sub>2</sub> dans matrice UMo. Retraitements court. Influence du taux de régénération  $x$ .

—  $x$  calculé  
- - - -  $x \pm 10\%$

TABLEAU XIX  
CALCUL DE  $M$  DANS QUELQUES CAS TYPES

Combustible	U—Pu —Mo	UC— PuC	UO <sub>2</sub> — PuO <sub>2</sub>	PuO <sub>2</sub> — UMo	PuO <sub>2</sub> — Th	PuO <sub>2</sub> — acier D <sub>1</sub>	PuO <sub>2</sub> — acier E <sub>1</sub>	PuO <sub>2</sub> — acier mixte F
$\delta'$	0,895	0,895	0,895	0,895	0,895	0,831	0,81	0,700
$j$	2	2	2	2	2	1,95	1,42	2
$H$ (cm)	108,4*	108,4*	108,4*	108,4*	108,4*	108,4*	67,2	97,1
$\lambda$ (cal/cm s°)	0,07	0,07	—	0,07	0,07	0,07	0,07	0,07
$\theta_{mm}$	700°	1650°	2500°	700°	800°	700°	700°	700°
$\Delta\theta$	150°	1100°	Intégrale de con- ductibili- té 12 cal/ cm s	150°	250°	150°	150°	150°
$M$	23 964	3267	20 968	14 738	14 378	21 680	24 840	20 900

\* Piles de 1000 l ( $H/D = 1$ ).

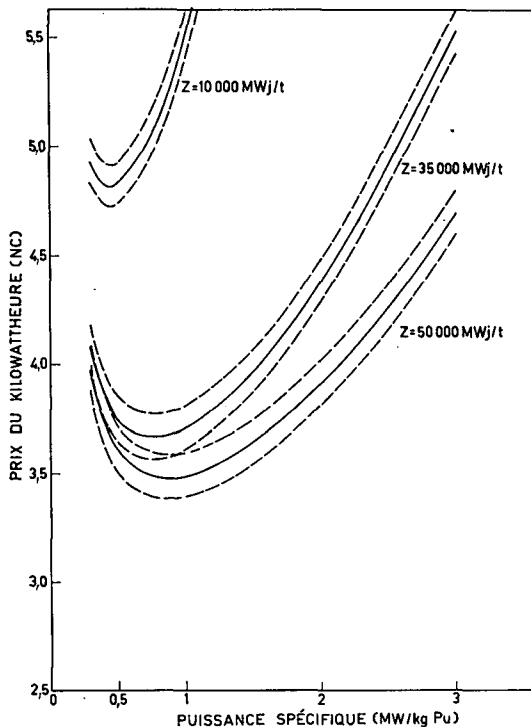


Figure 25

Cermet  $\text{PuO}_2$  dans matrice Th. Retraitements courts. Influence du taux de régénération  $z$ .

—  $z$  calculé  
— - -  $z \pm 10\%$

## Conclusion

### *Existence d'un optimum de puissance spécifique*

Pour tout combustible donné, il existe, pour chaque taux d'irradiation admissible  $z$  (exprimé en mégawattjours par tonne de combustible) une puissance spécifique  $y_m$  optimale qui donne un prix minimal du kilowattheure. Ces puissances  $y_m$  augmentent légèrement avec le taux d'irradiation admissible, mais demeurent faibles (0,45 MW par litre de cœur — cf. tableau XVIII) et ne dépassent pas les valeurs utilisées jusqu'à présent dans les piles rapides surrégénératrices en projet. Pour les piles d'avenir, il semble qu'il n'y ait pas intérêt à les augmenter.

### *Rôle du taux d'irradiation*

Pour une pile donnée, c'est-à-dire pour une valeur fixée de la puissance spécifique, le prix du kilowattheure décroît lorsque le taux d'irradiation admissible augmente, soit d'une façon très rapide pour les faibles valeurs de  $z$  ( $z < 30\,000 \text{ MWj/t}$  environ), soit d'une manière beaucoup plus lente dès que  $z$  est grand. Les courbes qui traduisent ces variations (fig. 10, 12, 14, 16 et 18) présentent deux zones aux pentes très différentes et, si on se trouve dans le domaine des grandes valeurs de  $z$  (partie peu inclinée des courbes), le prix du kilowattheure ne décroît pas sensiblement lorsque  $z$  augmente.

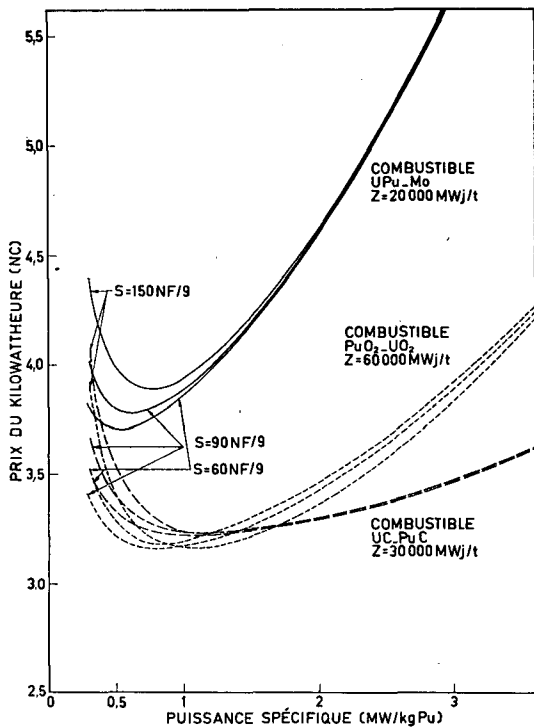


Figure 26

Influence du prix du kilowattheure sur le prix du plutonium. Retraitements aqueux.

#### *Charges de capital*

Dès que l'on considère des taux d'irradiation pas trop bas ( $z > 10\,000 \text{ MWj/t}$ ), les charges de capital investi dans le réacteur représentent près de 70 % du coût du kilowattheure. Une diminution du capital investi permettrait de faire décroître le coût du kilowattheure d'une manière sensible. On peut espérer que ce sera possible du fait qu'on n'aura pas tendance à augmenter les puissances spécifiques et qu'on ne créera pas ainsi de problèmes technologiques nouveaux par rapport à ceux que l'on est en train de résoudre actuellement et qui ont servi à définir le capital investi.

#### *Comparaison avec les procédés conventionnels*

Le prix du kilowattheure nucléaire, produit par les réacteurs rapides se situe, pour des valeurs convenables des puissances spécifiques et des taux d'irradiation admissibles aux alentours de 3 à 4 NC, alors que le prix du kilowattheure conventionnel en France est estimé à 3,50 NC\* environ pour les années à venir. On peut donc penser qu'avec l'avènement des grandes piles rapides, l'énergie électrique d'origine nucléaire sera compétitive.

\* Soit 0,007 dollar des Etats-Unis (7 mills).

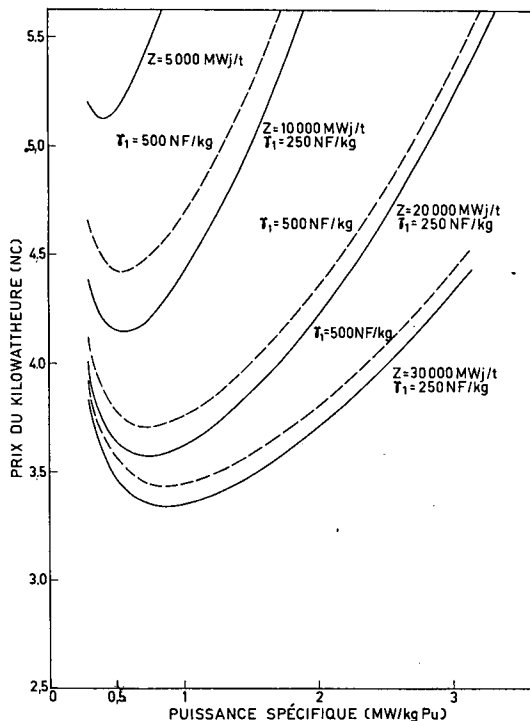


Figure 27  
Combustible UO<sub>2</sub>—PuO<sub>2</sub>. Influence du prix de retraitement court  $\gamma_1$ .

#### *Nature des combustibles à employer*

Parmi tous les combustibles étudiés, ce sont les carbures UC—PuC qui semblent les plus avantageux, car ils permettent d'espérer le prix de revient le plus bas du kilowattheure (inférieur à 3 NC). Leur fabrication n'est cependant encore qu'au stade du laboratoire. S'il se révélait que leurs propriétés réelles étaient moins bonnes que ce que l'on escomptait, les autres combustibles étudiés pourraient fort bien être utilisés, à condition qu'ils puissent subir des irradiations assez élevées dont la limite inférieure, correspondant à un prix de revient de 3,60 NC/kWh, peut être de l'ordre de :

- 20 000 MWj/t pour l'U—Pu—Mo,
- 25 000 MWj/t pour l'UO<sub>2</sub>—PuO<sub>2</sub>,
- 30 000 MWj/t pour les cermets PuO<sub>2</sub> dans une matrice U—Mo,
- 35 000 MWj/t pour les cermets PuO<sub>2</sub> dans une matrice Th.

Ces valeurs montrent tout l'intérêt des combustibles oxydes, qui semblent devoir supporter facilement des irradiations de 50 000 MWj/t et qui de ce fait peuvent être considérés presque aussi intéressants que les carbures.

Quant aux cermets inertes (PuO<sub>2</sub> dans une matrice d'acier), leur emploi ne peut être envisagé, à cause de conditions d'évolution du combustible, que sous

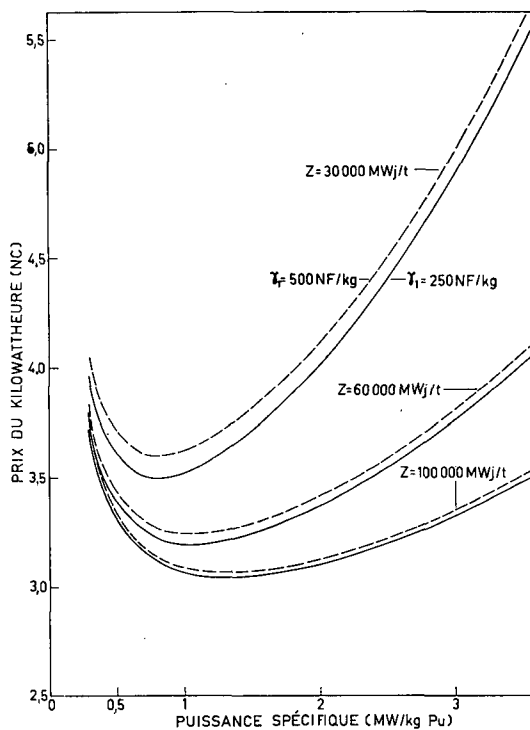


Figure 28  
Combustible UO<sub>2</sub>—PuO<sub>2</sub>. Influence du prix de retraitement court  $\gamma_1$ .

forme de configurations mixtes où des assemblages fertiles seraient présents dans le cœur. Dans ce cas, avec des irradiations de 80 000 MWj/t, ils donnent un prix de revient du kilowattheure comparable à celui de l'U—Pu—Mo irradié à 20 000 MWj/t.

#### ANNEXE 1

##### Evaluation du nombre de cœurs immobilisés dans l'ensemble réacteur—usine de retraitement et refabrication et du coût annuel de retraitement

- Soient :
- $p'$  la masse de <sup>239</sup>Pu contenu dans la masse critique,
  - $s$  le prix du gramme de plutonium ( $s = 60 \text{ NF/g}$ ),
  - $r$  le taux d'intérêt ( $r = 0,07$ ),
  - $y$  la puissance spécifique par unité de poids de <sup>239</sup>Pu investi (MW/kg),
  - $z$  le taux de combustion admissible (MWj/t ou kWj/kg),
  - $d$  le facteur de charge ( $d = 0,8$ ),
  - $\mu$  l'enrichissement du combustible en <sup>239</sup>Pu ( $p'/\mu$  = masse critique),
  - $\gamma_1$  et  $\gamma_2$  les coûts de retraitement dans le cycle court et par voie aqueuse du kilogramme de combustible,
  - $N$  le nombre de cœurs à mettre en pile par an,
  - $T'$  le temps de séjour en pile (exprimé en années) d'un cœur ( $T' = 1/N$ ),
  - $T$  le temps de séjour en pile (exprimé en jours) d'un cœur.

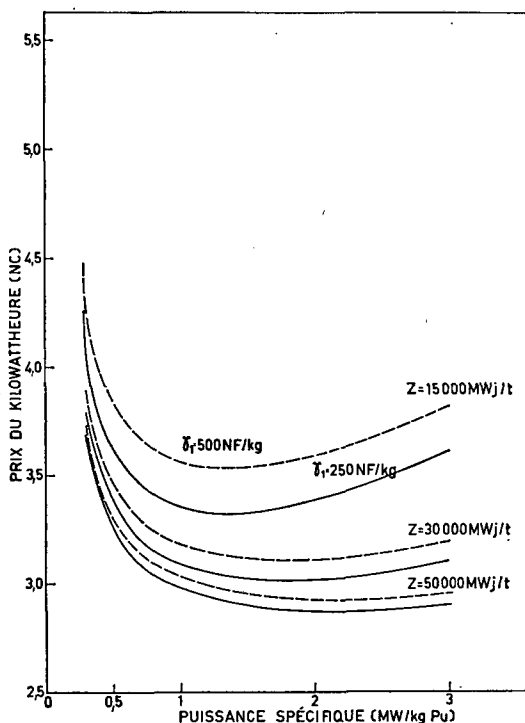


Figure 29  
Combustible PuC—UC. Influence du prix de retraitement court  $\gamma_1$ .

#### Calcul de l'immobilisation

a) Dans le cas où on emploie le cycle court de retraitement, on immobilise deux coeurs dans l'ensemble réacteur—usine de retraitement. Le coût de l'immobilisation est:

$$2 p' r s = \frac{2 \times 800\,000 r s}{y}$$

b) Dans le cas du retraitement par voie aqueuse, le temps de retraitement et de refabrication est d'un an. La période pendant laquelle un cœur fait un cycle complet est:  $t = T' + 1$ . Sa fréquence d'utilisation est:  $n = 1/t = 1/(T' + 1)$ ; or on a besoin de  $N = 1/T'$  coeurs par an; on doit donc immobiliser:  $(T' + 1)/T' = (1/T') + 1 = (1 + N)$  coeurs.

Le coût annuel est:

$$(1 + N) p' r s = (1 + N) \frac{800\,000}{y} r s.$$

Or  $N$  est lié au taux de combustion qu'un combustible peut supporter par la relation:

$$\begin{aligned} z_{\text{MWj/t}} \text{ de combustible} &= z_{\text{kWj/kg}} \text{ de combustible} = d \mu y \text{ MW/kg de matière fissile} \times 1000 \quad T = \\ &= 1000 \quad d y \mu \frac{360}{N} \end{aligned}$$

d'où:

$$N = 360\,000 \frac{d \mu y}{z}.$$

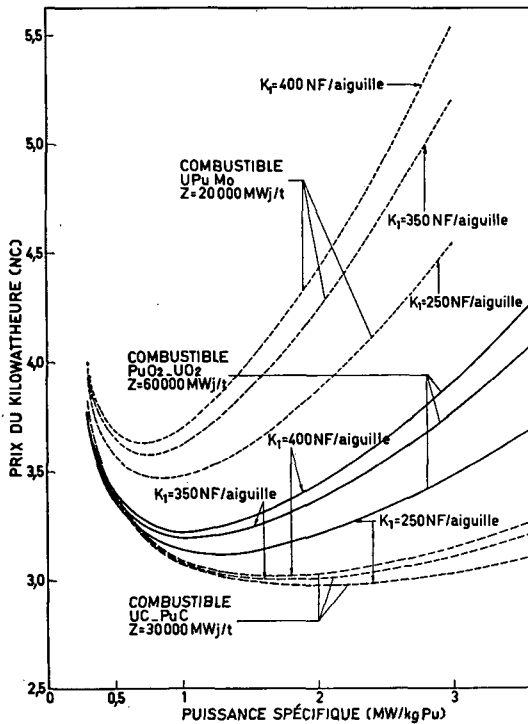


Figure 30  
Influence du prix de refabrication  $k$  des aiguilles. Retraitemen court.

Le coût de l'immobilisation s'écrira donc :

$$(1 + N) \frac{800000 rs}{y} = \left(1 + 360000 \frac{d\mu y}{z}\right) \frac{800000 rs}{y}$$

$$= \frac{800000 rs}{y} + \frac{288000000000 d rs \mu}{z}.$$

#### *Calcul du retraitement*

Le coût annuel de retraitement par cycle court est  $[(y_1 p')/\mu] N$ , soit, compte tenu de la valeur de  $N$  et de  $p'$  :

$$\frac{y_1 p'}{\mu} N = \frac{y_1}{\mu} \frac{800}{y} 360000 \frac{d\mu y}{z} = 288000000 \frac{d y_1}{z}$$

De même, le coût du retraitement par voie aqueuse est :

$$288000000 \frac{d y_2}{z}$$

#### ANNEXE 2

##### Détermination du nombre d'aiguilles d'un combustible donné

Le nombre d'aiguilles  $M$  à adopter dépend de la conductibilité thermique  $\lambda$  du combustible et de la température maximale  $\theta_m$  à laquelle on peut le porter.

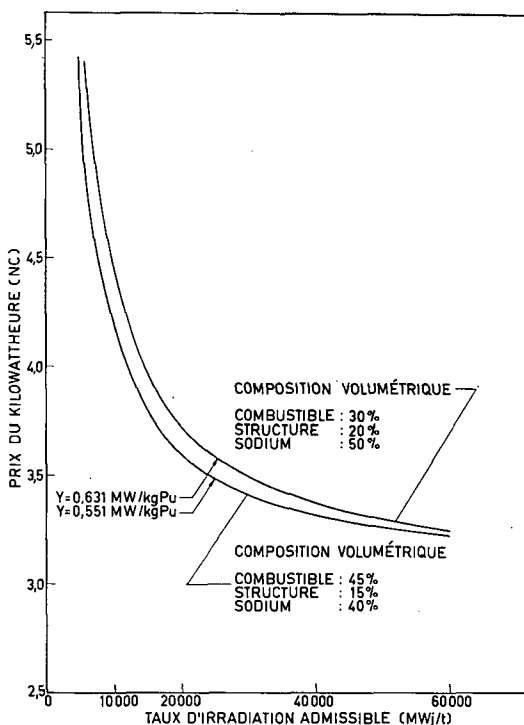


Figure 31  
Combustible PuO<sub>2</sub> dans matrice UMo. Retraitemen court. Piles de 3000 l.

L'intégration de l'équation de conductibilité thermique de Fourier à un cylindre permet d'écrire :

$$\Delta \theta = \frac{b^2}{4 \lambda w_1} y_1 \max = \frac{b^2}{4 \lambda w_1} j y_1 \quad (1)$$

relation dans laquelle :

$\Delta \theta = \theta_m - \theta_g$  est la chute de température maximale entre le centre de l'aiguille et la gaine (on fait l'hypothèse simplificatrice que la température de gaine  $\theta_g$  est égale à la température de sortie du sodium de la pile, soit 550°C),

$w_1$  est le pourcentage en volume du combustible dans le cœur,

$b$  est le rayon de l'aiguille,

$y_1$  est la puissance spécifique moyenne par unité de volume de cœur (MW/l),  
 $j$  est le rapport de la puissance spécifique maximale au centre du réacteur à la puissance spécifique moyenne.

Par ailleurs, le nombre d'aiguilles  $M$  est déterminé par la relation :

$$M = \frac{w_1 V}{v} \quad (2)$$

où :

$V$  est le volume critique,

$v$  est le volume du combustible contenu dans une aiguille,

$\delta'$  est le rapport de la puissance dégagée dans le cœur à la puissance totale de la pile,

$H$  est la hauteur du cœur,

et où :  $V = 800 \delta' / y_1$  et  $v = \pi H b^2$  (800 représente la puissance du réacteur en mégawatts).

$M$  est donc déterminé par :

$$M = \frac{800 \delta' w_1}{y_1 \pi H b^2} \quad (2')$$

qui devient, compte tenu de (1) :

$$M = \frac{800 \delta' j}{\pi H 4 \lambda \Delta \theta} \quad (2'')$$

soit, si  $\lambda$  est exprimé en calories par centimètre par seconde par degré, et  $H$  en centimètres :

$$M = \frac{800 000 000 \delta' j}{4,18 \times 4 \pi H \text{cm} \lambda_{\text{cal/cm s degré}} \Delta \theta \text{degrés}} \quad (2''')$$

La formule (2''') montre que, pour une hauteur du cœur donnée, le nombre  $M$  d'aiguilles est fixé si  $\lambda$  et  $\Delta \theta$  sont donnés, c'est-à-dire pour un combustible donné.  $M$  se trouve être indépendant de la puissance spécifique. Pour les combustibles UO<sub>2</sub>—PuO<sub>2</sub> où  $\lambda$  varie en fonction de la température, nous remplaçons  $\lambda \Delta \theta$  par l'intégrale de conductibilité dont la valeur sera prise égale à 12 cal cm s [6].

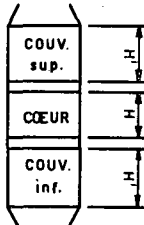
On remarque que le nombre  $M$  dépend sensiblement de  $\lambda \Delta \theta$  (ou de l'intégrale de conductibilité). Certains des résultats numériques de cette étude devront donc être revus lorsque des informations technologiques nouvelles concernant  $\lambda$ ,  $\theta_m$  seront connues.

### ANNEXE 3

#### Cout de retraitement et de refabrication des couvertures supérieure et inférieure

Nous avons supposé que le cout de retraitement et de refabrication des couvertures supérieure et inférieure pouvait être pris proportionnel à leur poids.

Soient :



- $H$  la hauteur du cœur,
- $H'$  la hauteur des couvertures axiales supérieure et inférieure,
- $w_1$  le pourcentage en volume de combustible dans le cœur ( $w_1 = 0,3$  dans la plupart des cas),
- $w'_1$  le pourcentage en volume de matériau fertile dans les couvertures axiales ( $w'_1 = 0,35$ ),
- $S$  la section droite d'un assemblage du cœur,
- $c_1$  le prix de retraitement d'un kilogramme de matériau fertile,
- $c_2$  le prix de refabrication d'un kilogramme de matériau fertile,
- $d_1$  et  $d'_1$  les densités respectives du combustible et du matériau fertile.

La fréquence de retraitement des couvertures est imposée par celle du cœur.

Chaque fois que l'on traite un cœur contenant  $p'/\mu$  kilogrammes de combustible, on doit traiter :

$$\frac{p'}{\mu} \times \frac{2 S H' w'_1 d_1}{S H w_1 d_1} = \frac{p'}{\mu} \times \frac{2 w'_1 d'_1 H'}{w_1 d_1 H} \text{ kilogrammes de matériau fertile.}$$

Or on traite  $N$  coeurs par an, avec  $N = 360 000 d (\mu y/z)$  (cf. Annexe 1). Il s'ensuit que le cout annuel de réfabriqueation et de retraitement des couvertures axiales est :

$$(c_1 + c_2) \frac{p'}{\mu} \times \frac{2 w'_1 d'_1 H'}{w_1 d_1 H} \times 360 000 d \frac{\mu y}{z} = 288 000 000 \frac{d}{z} \times \frac{2 w'_1 d'_1 H'}{w_1 d_1 H} (c_1 + c_2)$$

car  $p' y = 800$ .

On a adopté pour  $c_1$  la valeur de 140 NF/kg, qui comprend: d'une part, pour 100 NF/kg environ, toutes les opérations qui ont lieu depuis la sortie des couvertures de la pile jusqu'à la fin de leur traitement par voie aqueuse et qui permettent d'obtenir des sels d'uranium débarrassés de plutonium et des produits de fission, et d'autre part, pour une valeur de 40 NF/kg environ, la refabrication d'uranium appauvri métallique à partir des sels d'uranium.

Pour  $c_2$ , on a pris la valeur  $c_2 = 100$  NF/kg, qui comprend le façonnage de l'uranium naturel métallique, la fourniture de l'acier et la refabrication des aiguilles et des assemblages du cœur.

La valeur de  $c_1 + c_2$  représente donc le coût du cycle complet des couvertures, évalué par kilogramme de matière fertile traitée.

#### ANNEXE 4

##### Evaluation de la recette provenant de la vente de plutonium

La quantité de plutonium produite par an et disponible pour la vente est donnée par la relation:

$$u = 800 d \delta \delta' (x - 1) (1 + \alpha) 370$$

où:

$\delta$  = fraction de la puissance produite dans le cœur par les fissions dues au  $^{239}\text{Pu}$ ,  
 $\delta'$  = fraction de la puissance dégagée dans le cœur,

$\alpha$  = quotient de la section moyenne de capture et de la section moyenne de fission dans le cœur pour le  $^{239}\text{Pu}$  ( $\alpha = \sigma_c/\sigma_f$ ).

Cette relation s'établit facilement si on considère qu'un mégawattjour d'énergie est produit par la fission de 1,03 gramme de plutonium. Or, la puissance moyenne du cœur est  $800 d \delta \delta'$  MW, et seule la fraction  $800 d \delta \delta'$  est due à la fission du  $^{239}\text{Pu}$ . Il s'ensuit que pour produire  $800 d \delta \delta'$  MW-an, il a fallu fissionner:

$$800 d \delta \delta' \times 1,03 \times 360 = 800 d \delta \delta' \times 370 \text{ grammes de } ^{239}\text{Pu}.$$

Or le coefficient de régénération étant défini comme:

$$x = \frac{\text{Poids de Pu formé}}{\text{Poids de Pu fissionné} + \text{Poids de Pu détruit par captures parasites}}$$

$$x = \frac{\text{Poids de Pu formé}}{\text{Poids de Pu fissionné} (1 + \alpha)}$$

on en déduit le poids de plutonium formé, égal à:

$$\text{Poids de Pu formé} = x (1 + \alpha) \times \text{poids de Pu fissionné} = x (1 + \alpha) 800 d \delta \delta' \times 370.$$

L'augmentation annuelle de stock est donc:

$$u = 800 d \delta \delta' (x - 1) (1 + \alpha) 370$$

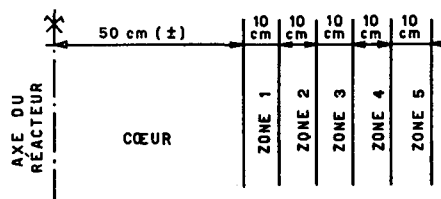
et la recette annuelle est donc:

$$800 d \delta \delta' (x - 1) (1 + \alpha) 370 s \text{ NF}.$$

#### ANNEXE 5

##### Détermination de la fréquence de déchargement des couvertures

Dans le cas des configurations « compactes », c'est-à-dire autres que celles des cermet mixtes ou annulaires, on peut imaginer un déchargement de couvertures par zone. Une zone donnée serait déchargée lorsqu'en un de ses points le taux d'irradiation aurait atteint une valeur donnée à priori et qui peut être fixée à 1% des atomes fissionnés.



Considérons dans le cas des *piles de 1000 l* les couvertures radiales de 50 cm, que nous divisons en cinq zones. Les calculs neutroniques montrent que dans le plan médian du cœur le taux d'irradiation maximal ne dépasse pas  $9,5 \cdot 10^{-2} \%$  au bout d'un mois de fonctionnement à pleine puissance, et que le taux décroît de  $10^2$  en 50 cm, cette décroissance étant en première approximation exponentielle.

Soient :

- $d$  le facteur de charge,
- $\theta_i$  le temps de séjour (en mois) dans la zone  $i$  ( $1 < i < 5$ ) pour que le taux d'irradiation atteigne 1 %,
- $\beta$  le taux de décroissance de l'irradiation avec la distance, tel que  $e^{-5\beta} = 10^{-2}$ ,
- $e_i$  le pourcentage en poids de la couverture de la zone  $i$ ,
- $\theta$  le temps moyen de séjour en pile de la couverture.

$t$  est donné par :

$$\frac{1}{\theta} = \frac{e_1}{\theta_1} + \frac{e_2}{\theta_2} + \cdots + \frac{e_5}{\theta_5}$$

et les  $t_i$  sont fournis par :

$$1\% = 9,5\% \cdot 10^{-2} e^{-(i-1)\beta} \theta_i.$$

On trouve ainsi  $\theta = 49,3$  mois = 4,1 ans.

Etant donné que pratiquement ce sont des assemblages (et non des couronnes circulaires) que l'on décharge, on sera amené à un rythme de déchargement plus rapide. Nous supposerons un temps de séjour moyen de 3,3 années, ce qui veut dire que l'on doit traiter par an :

$0,3 q = 0,3 \times 65\,000 = 19\,500$  kilogrammes de matériau fertile.

Dans le cas du *cermet annulaire* à matrice inoxydable (combustible E1), on traitera, pour le cas de la *pile de 1000 l*, le noyau central dès que le taux d'irradiation en un de ses points aura atteint 1 %. Le calcul montre que ceci se produit en dix mois. La quantité à traiter par an est :

$$d'_1 \frac{12}{10} b_1^2 \pi H w'_1 = 2556 \text{ kg}$$

où :

$d'_1$  = densité de l'uranium naturel,

$b_1$  = rayon de la couverture centrale (= 30 cm),

$H$  = hauteur du cœur (= 67,2 cm),

$w'$  = pourcentage en volume de matériau fertile dans la couverture considérée (= 0,6).

A ce chiffre de 2556 kg, il convient d'ajouter les couvertures externes, où le taux d'irradiation est un peu moins fort que dans le cas des configurations compactes. On prendra donc en première approximation  $0,3 q = 19\,500$  kilogrammes de matière fertile à traiter par an comme pour les configurations compactes.

Dans le cas des *cermets mixtes de 1000 l* (cas F), le taux d'irradiation varie rapidement du centre de la pile vers les bords, où il est quatre fois plus faible que dans une configuration compacte. A l'intérieur du cœur mixte, il atteint 1 % en un an (valeur moyenne sur le cœur). On doit donc traiter par an :

$$1000 \text{ l} \times w'_1 \times d'_1 = 1000 \text{ l} \times 0,6 \times 18,7 = 11\,220 \text{ kilogrammes d'uranium}$$

à quoi il convient d'ajouter les couvertures externes, qui donnent une contribution quatre fois plus petite que les configurations compactes. On adoptera comme traitement annuel la valeur  $0,3 q = 19\,500$  kg.

Ainsi, aussi longtemps que le volume du cœur reste constant, la quantité de couvertures à traiter par an ne varie pas en première approximation malgré les variations que l'on peut imaginer dans les configurations ou les combustibles. Nous insistons néanmoins sur le fait que ces hypothèses seraient à reprendre pour des études plus précises.

## GLOSSAIRE GÉNÉRAL DE L'ÉTUDE ÉCONOMIQUE

comportant les valeurs numériques de certains paramètres

$a$  taux d'amortissement des capitaux investis (= 0,11),

$b$  rayon des aiguilles,

$b_1$  rayon de la couverture centrale (dans le cas des configurations annulaires),

$c_1$  prix de retraitement des couvertures (= 140 NF par kilogramme de matériau fertile) (cf. Annexe 3),

- $c_2$  prix de refabrication des couvertures (= 100 NF par kilogramme de matériau fertile refabriqué) (cf. Annexe 3),  
 $d$  facteur de charge du réacteur (= 0,80),  
 $d_1$  densité du combustible,  
 $d'_1$  densité de matériau fertile (= 18,7 pour U naturel et 11,3 pour Th),  
 $e_i$  pourcentage en poids de la couverture de la zone  $i$  (cf. Annexe 5),  
 $f$  dépenses annuelles de fonctionnement du réacteur (= 10 000 000 NF/an),  
 $H$  hauteur du cœur (cm) (cf. Annexe 3),  
 $H'$  hauteur des couvertures supérieure et inférieure (cm) (cf. Annexe 3),  
 $I_1$  capital investi dans la construction du réacteur (NF),  
 $j$  rapport de la puissance spécifique maximale au centre du cœur à la puissance spécifique moyenne,  
 $k$  prix du kilowatt électrique produit par des moyens conventionnels (= 0,035 NF = 3,5 NC),  
 $k_1$  prix de refabrication de l'aiguille de combustible (NF par aiguille),  
 $n$  fréquence d'utilisation d'un cœur,  
 $N$  nombre de cœurs à mettre en pile par an ( $N$  est lié à  $y$  et  $z$ ) (cf. Annexe 1),  
 $P$  coût du kilowatt électrique produit par l'ensemble réacteur-usine (NC),  
 $p'$  poids de matériau fissile immobilisé dans le cœur du réacteur (kg),  
 $q$  poids de matériau fertile immobilisé dans les couvertures (= 65 000 kg),  
 $r$  taux d'intérêt (= 0,07),  
 $s$  prix d'équilibre du plutonium métal (= 60 NF/g = 12 \$/g),  
 $S$  section droite d'un assemblage,  
 $s'$  prix de l'uranium naturel (= 150 NF/kg) ou du thorium (= 200 NF/kg),  
 $t$  période d'un cœur (années) = temps s'écoulant entre deux retraitements,  
 $T$  temps de séjour en pile d'un cœur (jours),  
 $T'$  temps de séjour en pile d'un cœur (années),  
 $u$  quantité de plutonium produite par an et disponible à la vente (g),  
 $w_1$  pourcentage en volume du combustible dans le cœur,  
 $w'$  pourcentage en volume du fertile dans les couvertures,  
 $w'_1$  pourcentage en volume du fertile dans les couvertures axiales,  
 $x$  taux de régénération = poids de Pu formé/poids de Pu détruit,  
 $y$  puissance spécifique par unité de poids de matière fissile investie (MW/par kilogrammes de plutonium investi dans le réacteur),  
 $y_1$  puissance spécifique moyenne par unité de volume de cœur (MW/l),  
 $z$  taux d'irradiation admissible (MWj par tonne de combustible ou kWj/kg),  
 $\alpha$  quotient de la section moyenne de capture et de la section moyenne de fission dans le cœur pour le  $^{239}\text{Pu}$  ( $\alpha = \sigma_c/\sigma_f$ ),  
 $\beta$  taux de décroissance de l'irradiation dans les couvertures,  
 $\gamma_1$  coût du retraitement du cœur par cycle court (= 250 NF par kilogramme de combustible),  
 $\gamma_2$  coût de retraitement du cœur par voie aqueuse (= 600 NF par kilogramme de combustible),  
 $\delta$  fraction de la puissance produite dans le cœur par les fissions dues au  $^{239}\text{Pu}$ ,  
 $\delta'$  rapport de la puissance produite dans le cœur à la puissance totale du réacteur,  $\delta = \delta'/d$ ,  
 $\varrho$  rendement de séchangeurs et alternateurs (= 0,38),  
 $\theta_i$  temps de séjour en pile de la zone  $i$  de couverture (mois) (cf. Annexe 5),  
 $\theta$  temps moyen des éjour en pile de la couverture (mois),  
 $\mu$  taux d'enrichissement du combustible en matière fissile telle que le  $^{239}\text{Pu}$ .

## RÉFÉRENCES

- [1] PETIT, J. Communication privée (CEA).
- [2] ANDRIOT, J. et GAUSSENS, J., Programme de centrales à réacteurs thermiques et réacteurs rapides: économie de combustible, problème de stockage, prix du plutonium. SP/F 60/1285 (1960).
- [3] GAUSSENS, J., Communication privée (1961).
- [4] YEVICK, J. G. et AMOROSI, A., *Nucleonics* (février 1961).
- [5] GAUSSENS, J., Communication privée.
- [6] RUNNALS, O. J. C., *Nucleonics* (mai 1959).

## SOME PHYSICS ASPECTS OF CERMET AND CERAMIC FAST SYSTEMS

J. CODD, M. F. JAMES AND J. E. MANN

UNITED KINGDOM ATOMIC ENERGY AUTHORITY

REACTOR GROUP,  
UNITED KINGDOM

**Abstract — Résumé — Аннотация — Resumen**

**Some physics aspects of cermet and ceramic fast systems.** The characteristics of a system using an iron-based oxide cermet as fuel material are discussed. A transport theory investigation to develop methods of predicting the effect of core heterogeneity on reactivity and flux distribution is described. Some preliminary calculations are also given of resonance self-shielding and Doppler temperature effects in a cermet system.

**Quelques aspects de la physique des réacteurs à neutrons rapides utilisant des cermets et des céramiques comme combustibles.** Les auteurs étudient les caractéristiques d'un réacteur utilisant comme combustible un cermet d'oxydes à armature de fer.

Ils exposent une application de la théorie du transport à la mise au point des méthodes permettant de prévoir l'effet de l'hétérogénéité du cœur sur la réactivité et sur la distribution du flux.

Ils donnent également quelques calculs préliminaires d'effets d'autoprotection due à la résonance et d'effet Doppler dû à la chaleur dans un réacteur utilisant un cermet.

**Некоторые физические аспекты керметных и керамических систем на быстрых нейтронах.** Обсуждаются характеристики системы, использующей в качестве топливного материала оксидные керметы, разработанные на основе железа. Описывается исследование теории переноса, чтобы развить методы предсказания влияния гетерогенности активной зоны на реактивность и распределение потока. Даются также некоторые предварительные расчеты эффектов резонансной самозащиты и температурного эффекта Допплера в керметной системе.

**Algunos aspectos físicos de los sistemas rápidos a base de combustibles cermet y cerámicos.** La memoria discute las características de un sistema que emplea como combustible un óxido tipo cermet a base de hierro. Describe una investigación de la teoría de transporte con miras a desarrollar métodos para evaluar el efecto de la heterogeneidad del cuerpo sobre la reactividad y la distribución de flujo. También da algunos cálculos preliminares de los efectos del autoblindaje por resonancia y de la temperatura de Doppler en un sistema de tipo cermet.

### General introduction

This paper falls into three Sections. In the first Section, consideration is given to the characteristics of a fast reactor fuelled with an iron-based oxide cermet.

Section 2 contains a description of an investigation into methods of predicting the effects of heterogeneity on reactivity and flux distribution.

Finally, in Section 3, some preliminary calculations are reported of resonance self-shielding and Doppler temperature effects for an oxide cermet core.

### 1. Some characteristics of a cermet-fuelled fast system

A prerequisite of a fast breeder-reactor is that it should breed more fuel than it consumes. Equally, however, it is necessary that, as a power producer, it should have an acceptably low electrical generation cost. This requirement implies, among other things, that the fuel should be capable of achieving high burn-up to reduce recycling losses and out-of-pile inventory and to minimize the effects of fabrication and chemical reprocessing charges.

There are a number of fuel materials which potentially are capable of achieving high burn-up, among them being the ceramics and cermets. The latter fuels may either contain a dispersion of fissionable material in ceramic form in a fertile matrix, or a dispersion of fissile and fertile ceramic material in a non-fertile matrix.

The second of these alternatives is the one considered here. Inherently, this type of fuel possesses the disadvantage of reduced breeding, and while the system breeding ratio, depending on the matrix volume-fraction in the fuel, may be greater than unity, core reactivity will tend to decrease with time. This effect implies that either a more frequent loading schedule is required for a fixed amount of excess reactivity held for operational control, or that, for a stipulated shutdown cycle, more control reactivity must be provided than might be required for other fuel types.

The system considered is described in Table IA.

TABLE IA  
REACTOR DIMENSIONS AND COMPOSITION

Core length, 3.7 ft — Overall core diameter, 5.6 ft — Inner core diameter, 3.9 ft  
Axial blanket thickness, 1.5 ft — Overall radial blanket thickness, 2.0 ft.

Volume composition	Core and axial blankets	Radial blankets		
		Inner	Middle	Outer
Fuel	0.372	0.40	0.55	0.70
Can and structure	0.268	0.30	0.22	0.15
Coolant	0.360	0.30	0.23	0.15

The core fuel material is a cermet of 50 vol. % plutonium and uranium dioxides and 50 vol. % matrix material, assumed to be iron for calculational purposes. The axial blankets are of the same volume composition as the core with a fertile cermet containing no plutonium initially. The radial reflector contains uranium metal as the fertile "fuel" material and is divided into three annuli, of equal thickness, the uranium volume density increasing with distance from the core. The core itself is divided radially into two regions of approximately equal cross-sectional areas. The plutonium content of the fuel within each region was adjusted for criticality so that the maximum fuel rating was the same in each region. In practice this would result in some degree of flux and power flattening.

The coolant is assumed to be sodium, and the canning material and structure are assumed to be iron. All feed uranium was assumed to be material depleted in U<sup>235</sup> content. The feed-plutonium isotopic composition was assumed to be

$\text{Pu}^{239}:\text{Pu}^{240}:\text{Pu}^{241}:\text{Pu}^{242}=76:18:5:1$ . This composition is one which might arise in material produced from thermal reactors.

The pertinent results are listed in Table IB. The calculations were performed using the 11-group cross-section set of reference [1] and the TDC computational code.

TABLE IB  
CRITICAL MASS, BREEDING RATIO AND NEUTRON BALANCE

	Total	Core		Axial blanket	Radial blanket		
		Inner	Outer		Inner	Middle	Outer
Critical mass of plutonium (kg)	1123	434	689	—	—	—	—
Initial breeding ratio	1.153	0.350	0.184	0.139	0.362	0.103	0.015
<b>Neutron balance normalized to total fission source = 1000</b>							
<i>Production</i>							
$\text{Pu}^{239}$ and $\text{Pu}^{241}$ fissions	875.9	452.9	423.0	—	—	—	—
$\text{Pu}^{240}$ and $\text{Pu}^{242}$ fissions	21.8	10.3	11.5	—	—	—	—
$\text{U}^{235}$ fissions	33.3	9.9	5.0	4.2	10.8	3.0	0.4
$\text{U}^{238}$ fissions	69.0	28.4	19.2	3.0	16.6	1.6	0.2
<i>Absorption</i>							
$\text{Pu}^{239}$ and $\text{Pu}^{241}$ captures	298.0	154.2	143.8	—	—	—	—
$\text{Pu}^{240}$ and $\text{Pu}^{242}$ captures	8.7	4.1	4.6	—	—	—	—
$\text{U}^{235}$ captures	13.4	4.0	2.0	1.7	4.3	1.2	0.2
$\text{U}^{238}$ captures	26.5	10.9	7.4	1.1	6.4	0.6	0.1
$\text{Pu}^{239}$ and $\text{Pu}^{241}$ captures	96.4	52.2	44.2	—	—	—	—
$\text{Pu}^{240}$ and $\text{Pu}^{242}$ captures	18.8	10.1	8.7	—	—	—	—
$\text{U}^{235}$ captures	4.1	1.2	0.6	0.6	1.3	0.3	0.1
$\text{U}^{238}$ captures	435.9	127.9	64.0	55.0	142.4	40.6	6.0
Na captures	3.1	1.5	0.9	0.5	0.2	—	—
Fe captures	87.7	42.0	25.5	12.6	6.4	1.1	0.1
Net leakage	7.4	—	—	—	—	—	—
<b>Regional normalized flux integrals</b>							
Group 1	2.36	2.65	1.63	1.03	0.33	0.31	0.31
Group 2	3.59	4.30	1.30	1.82	0.57	0.43	0.43
Group 3	5.03	5.82	2.20	3.54	1.68	1.86	1.86
Group 4	9.07	10.03	5.52	9.42	7.86	6.71	6.71
Group 5	8.93	9.82	6.06	11.79	12.72	12.30	12.30
Group 6	11.02	11.70	8.60	12.78	13.91	14.09	14.09
Group 7	10.17	10.54	8.77	12.04	13.41	13.96	13.96
Group 8	9.10	9.26	8.51	11.53	13.80	15.10	15.10
Group 9	12.31	12.06	13.00	15.16	18.97	21.90	21.90
Group 10	11.07	10.23	13.70	10.91	10.81	10.23	10.23
Group 11	17.35	13.26	31.70	9.97	5.94	3.92	3.92

The plutonium-to-uranium ratios in the inner and outer core regions are 0.244 and 0.428 respectively for the cold, clean critical condition. The corresponding critical mass of plutonium (all isotopes) is 1123 kg. The breeding characteristics are not good, a result which is to be expected. The overall breeding ratio, defined as the ratio of the rate of production to the rate of destruction of thermally fissile isotopes of plutonium, is only 1.15. The net gain would be even less than this in a practical system when recycling losses are taken into

consideration. About 46% of the breeding takes place in core regions. Of the total blanket breeding,  $22\frac{1}{2}\%$  is in the axial blanket,  $58\frac{1}{2}\%$  in the inner radial blanket, and a further  $16\frac{1}{2}\%$  in the middle radial blanket.

About 90% of the total neutrons from fission arise from plutonium. Of the remaining 10% one-third arise from  $U^{235}$  and two-thirds from  $U^{238}$ . Within the core only, 93% of fissions occur in plutonium and only 5% occur in  $U^{238}$ .

Considering the power distribution, 95% of the power is generated in the core regions (50% in the inner region and 45% in the outer region), 1% in the axial blankets and 4% in the radial blankets. The axial form factor is about 1.25 (maximum/average). The radial form factors are 1.17 and 1.34 respectively for the inner and outer core regions, giving an overall radial power form-factor across the core of 1.25 also.

Despite the large volume of the core (approximately 2500 l) there is considerable leakage over the core reflector boundary. This effect is contributed in part by the low uranium volume-density in the core and the two-zone enrichment scheme adopted. The reflector dimensions considered could probably be reduced without incurring a serious penalty. It is apparent that the outer radial reflector could be dispensed with, for little loss in breeding, especially if the uranium volume-density were increased in the inner regions. Similarly, the axial blanket thickness could be reduced if the cermet fertile material were replaced by oxide.

Despite the high iron-content of the core (about 45 vol. %) capture in iron accounts for less than 10% of total neutron absorptions. The presence of the diluent is felt more through its effect on the neutron-energy level through scattering processes than by its direct effect on neutron absorption. Neutron losses to coolant are small, as is to be expected, the parasitic loss being only 0.3% of total absorption.

The flux spectra for the two core regions show considerable similarity, with a slight hardening in the outer region. The spectrum for the axial reflectors is very soft, the already degraded core leakage spectrum being further degraded through scattering by iron and oxygen. The radial blanket spectra show a progressive change with increasing radial distance from the core, the flux tending to concentrate in the middle range of energy groups due, on the one hand, to preferential capture of low-energy neutrons by  $U^{238}$  and, on the other hand, to reduced production of fission-spectrum neutrons by  $U^{238}$  fission. The spectra indicate that the group structure of the cross-section set used is barely adequate for the representation of this type of system. Additionally, a large number of reactions are occurring in the lower energy ranges where uncertainties in cross-section data exist.

The effective delayed-neutron fraction has been calculated by a method suggested by PALMER [2] in which the effective delayed-neutron fraction is determined from the difference in  $k_{eff}$  between two multi-group calculations, one being the usual delayed critical calculation and the other a calculation in which prompt neutrons only are considered. In the latter calculation, if the delayed neutrons from fission of an isotope are emitted in groups  $i, j, \dots$ , then the group values for the fission neutron-energy distribution,  $\chi$ , are modified to  $(\chi_i - \alpha_i \beta), (\chi_j - \alpha_j \beta), \dots$ , where  $\alpha_i, \alpha_j, \dots$  are the relative abundances of delayed neutrons in groups  $i, j, \dots$ , and  $\beta$  is the total delayed-neutron fraction for the isotope. If the multi-group code requires  $\chi$  to be normalized to unity then the sets of  $\chi$  should be normalized to unity and all the group  $v$ -values multiplied by  $(1-\beta)$  for each isotope. The prompt  $\chi$  distribution is of course different

for each isotope. The method may be used to determine the effectiveness of the individual delayed-neutron groups, or the effect of a particular reactor region on the overall  $\beta_{\text{eff}}$ , and is a quick method, although it may not give the same insight into the neutronics of the system as is given by the more usual method, using adjoint calculations, of determining the relative worths, dependent on energy and spatial position, of prompt and delayed fission-neutrons.

A five-group diffusion theory calculation, using the flux spectra from the 11-group TDC calculation to weight cross-sections within the reduced groups for the different reactor regions, resulted in values of  $k_{\text{eff}}$  for the prompt and delayed calculations differing by 0.0030. This low value of  $\beta$  is mainly a consequence of the use of plutonium as the fissile material, but is also a reflection of the low  $U^{238}$  content of the core.

## 2. Heterogeneity in fast reactors — preliminary calculations

### 2.1. INTRODUCTION

Most calculations on a fast reactor assume a model that is constructed of several homogeneous regions (e.g. the core and reflectors) of sizes that are large compared with a neutron mean free path. However, in the real reactor, each of these regions will be of heterogeneous construction, with alternating regions of, say, coolant, canning and fuel or fertile material. Usually this heterogeneity will be of a periodic nature, and, in a fast reactor, the size of a lattice cell will be not much larger than a mean free path. The error in the calculated properties, such as  $k_{\text{eff}}$  and breeding ratio, due to the assumption of homogeneity, will therefore be small: in the system discussed below, the error in  $k_{\text{eff}}$  is  $\sim 1\%$ .

However, as data and methods of calculation improve, such an error will become larger than the errors due to remaining imperfections in them. Secondly, for a large dilute fast reactor, an error of 1% in  $k_{\text{eff}}$  may mean an error of  $\sim 10\%$  in the critical volume of the core, and hence perhaps about 100 kg of fuel. Thirdly, it may be possible to bunch materials in such a way as to improve slightly some of the properties of a reactor. For all these reasons, it has become important to be able to estimate the effect of fine structure.

A method has been described by LONG *et al.* [3] and by MENEGHETTI and LOOMIS [4] for converting the calculation of the  $k_{\text{eff}}$  and flux distribution of a finite core with a periodic structure to the calculation of  $k_{\text{eff}}$  and flux distribution of an infinite lattice with the same structure. The first aim of the work described here has been to test this method for a bare core in the shape of an infinite slab, with the pieces of the different materials arranged with their faces parallel to the faces of the slab, so that the core had a periodic structure in one dimension, and was infinite in the other two. The second aim was to investigate the best method of carrying out the cell calculation. Since the difference in  $k_{\text{eff}}$  of the heterogeneous core and of the equivalent homogeneous core is small, it is necessary to calculate  $k_{\text{eff}}$  to a high degree of accuracy. This requirement, coupled with the fact that the size of some of the regions within the cell may be small compared with a mean free path, implies that an approximation to the neutron transport equation of high order must be used. It has been shown that, for the system considered, the double-Gauss discrete-ordinates method ([5] p. 180) converges more quickly (and hence gives an answer of required accuracy in less computing time) than a method similar to CARLSON's  $S_n$  method [6]. An alternative method, based on the integral transport equation, appears to be promising.

In the next two sections, the method of Long *et al.* and Meneghetti is described, and the methods used to solve the Boltzmann equation are discussed. Following that, the reactor composition is described, and the results reviewed.

## 2.2. CONVERSION TO AN INFINITE LATTICE

The method used is as follows. A multi-group calculation is first performed for the homogenized core. This can either be a fundamental-mode calculation, yielding the critical buckling  $B^2$  or the  $k_{\text{eff}}$  corresponding to a specified buckling, or a more detailed calculation giving  $k_{\text{eff}}$  and the leakage of neutrons from the core for each group. In the former case, the estimated probability of a neutron in group  $g$  leaking out is  $\bar{D}_g B^2$ , where  $\bar{D}_g$  is the diffusion coefficient of the homogenized core, in group  $g$ .

It is then assumed that the probability of a neutron in one of the lattice cells escaping from the core without making a collision is the same as the corresponding probability for a neutron in the corresponding volume of the homogeneous core. This is a reasonable assumption, physically, if the size of the lattice cell is small compared with the core dimensions. It is not known to the author whether the assumption can be justified from rigorous mathematical arguments.

If this assumption is made, the calculations can then be performed on a lattice cell of the same size and composition as a lattice cell of the finite reactor, but with the total transport cross-section for each material in each group increased by a fictitious absorption term that gives the probability of escape. If  $\sigma'_{tg}(X)$  is the transport cross-section in group  $g$  for material  $X$ , then the cross-section actually used is:

$$\sigma'_{tg}(X) = \sigma_{tg}(X) + L_g$$

where  $L_g = \frac{\text{number of neutrons in group } g \text{ escaping from the homogeneous core per second}}{\text{total flux in group } g \text{ integrated over the whole homogeneous core}}$   
 $= \bar{D}_g B^2$  if a fundamental-mode calculation has been carried out.

All the other cross-sections are unchanged. The calculations are performed using boundary conditions that are appropriate for a typical cell in an infinite lattice. There are two possible boundary conditions. First, if the structure of the lattice cell to the right of a cell boundary is the mirror image, with respect to the boundary, of the structure of the cell to the left of the boundary, there will be complete reflection of neutrons at each boundary. Secondly, if the lattice structure is merely periodic, without such mirror planes, the neutron flux leaving the right-hand boundary in a particular direction must be equal to that entering the left-hand boundary in the same direction, and *vice-versa*. Although all the calculations so far performed have used the first boundary condition, the discrete ordinates programme that has been written can solve the second type, if required. It should be noted that the second type can only apply to systems with plane geometry.

## 2.3. METHODS OF SOLVING THE TRANSPORT EQUATION

The method used at first was based on the SNG programme [6] for the IBM-704. However, it was known that this gave unsymmetric fluxes for a symmetric reactor in plane geometry, owing to the basic assumptions of the method. To overcome this, the programme was modified to solve the equations of the "double  $S_n$ "

method. If  $\mu$  is the direction-cosine of a neutron relative to the  $x$ -axis,  $\mu$  can have any value in the range  $-1$  to  $+1$ , negative values representing neutrons moving to the left, and positive values neutrons moving to the right. The  $S_n$  method starts from  $\mu = -1$ , and, assuming that the angular flux is a linear function of  $\mu$  in each of  $n$  equal intervals, proceeds to calculate the fluxes at the edge of each interval until the  $\mu = +1$  direction is reached. In the double- $S_n$  programme (SND), on the other hand, the  $S_n$  method is applied separately to positive and to negative  $\mu$  values, starting with the fluxes for  $\mu = +1$  and  $\mu = -1$  respectively. This may give a discontinuity in angular flux at  $\mu = 0$ , and as it is known that such discontinuities will actually occur at interfaces between different materials, this should give better accuracy.

A second programme, still based on SNG and using many of the routines of that code, was written to solve the discrete ordinate equations, with arbitrary weights and ordinates, in plane geometry. This has been used with Gaussian weights and ordinates applied separately to positive and to negative values of  $\mu$ . An improved version of this programme has also been written but has not yet been fully tested. This improves the spatial finite difference approximations used for the smaller discrete angles  $\mu_j$ , and solves the boundary conditions (of either of the types discussed in the previous section) exactly, instead of iteratively.

A third method, that of "collision probabilities", has so far only been used in one simple desk-calculation. This is based on the integral transport equation. The cell is sub-divided into regions, and a constant flux assumed in each. The integral transport equation is then integrated over all space, yielding a set of simultaneous linear equations for the group fluxes in each region.

#### 2.4. REACTOR COMPOSITION

All the calculations were performed for an unreflected core of one basic composition. This was intended to represent a mock-up in ZEBRA of a typical uranium carbide cermet reactor. ZEBRA will contain stainless-steel tubes, 2 in<sup>2</sup> in cross-sections, holding pieces of different materials. These pieces will be  $1/8$  in thick, except for some enriched-uranium pieces which will be only  $1/16$  in thick, and all the pieces considered in these calculations were assumed not to be canned. It was assumed that each tube throughout the core would, at any given position along its length, contain the same type of piece. Probably without much loss of accuracy, the stainless steel in each tray (assumed to be 0.03 in thick) was smeared uniformly over the whole core, so that the core could be thought of as containing uniform layers of different materials.

The core consisted of pieces of enriched uranium (with an assumed enrichment of 93%) natural uranium, graphite, stainless steel, and aluminium of 45% normal density; this last material may be used in ZEBRA to simulate sodium. The proportions of the different constituents were chosen so that their relative volumes were in simple proportion, so that a basic lattice cell could be designed with as few pieces as possible. The relative amounts of uranium and graphite were also chosen so that there were approximately equal numbers of uranium and of carbon atom, so that uranium monocarbide (UC) could be simulated. Table II gives the number of pieces of the different materials in a cell, together with their composition. The total cell length was 1.4375 in, and the core was assumed to be an infinite slab of thickness 28.75 in, so that it contained 20 cells with boundaries parallel to the faces of the slab.

TABLE II  
COMPOSITION OF A LATTICE CELL

Material	No. of pieces	Number of atoms/cm <sup>3</sup> ( $\times 10^{-24}$ )				
		U <sup>235</sup>	U <sup>238</sup>	C	Fe	Al
Enriched U	$\frac{1}{2}^*$	0.041786	0.003145	0	0.005088	0
Natural U	3	0.0003190	0.044613	0	0.005088	0
Graphite	2	0	0	0.078304	0.005088	0
Steel	2	0	0	0	0.0848025	0
Aluminium	4	0	0	0	0.005088	0.025474

\* 1 piece of 1/16-in thickness

It should be pointed out that no calculations were carried out for cells at right angles to the core faces: it may be necessary, for the highest accuracy, to take different diffusion coefficients for directions parallel to and perpendicular to the cells.

## 2.5. RESULTS

All the calculations used three energy groups of neutrons, the three-group constants for which were obtained from an 11-group calculation using the constants of LOEWENSTEIN and OKRENT [1]. The boundaries between the groups were at 1.35 MeV and 0.11 MeV.

### (a) Homogeneous core

The base homogeneous core was found, by an  $S_8$  calculation, to have a  $k_{\text{eff}}$  of 1.0091. The neutron-leakage in each group was used to alter the transport cross-sections of the different materials in the heterogeneous cell calculations, in accordance with the prescription of section 2.2.

### (b) Test of the method of section 2.2

Three calculations were carried out on finite heterogeneous cores, using the double- $S_8$  approximation. Each core contained 20 basic cells, and the three cases were for cores with the following structures:

Case 1.	U <sub>E</sub> U <sub>N</sub> C Fe Al	Al Fe C U <sub>N</sub> U <sub>E</sub>	U <sub>E</sub> ... ;	$k_{\text{eff}} = 1.0175$ $\frac{\Delta k}{k_{\text{hom}}} = +0.83\%$
Free boundary	Cell boundary	Cell boundary		
Case 2.	Al Fe C U <sub>N</sub> U <sub>E</sub>	U <sub>E</sub> U <sub>N</sub> C Fe Al	Al ... ;	$k_{\text{eff}} = 1.01895$ $\frac{\Delta k}{k_{\text{hom}}} = +0.98\%$
Free boundary	Cell boundary	Cell boundary		
Case 3.	U <sub>E</sub> C U <sub>N</sub> Fe Al	Al Fe U <sub>N</sub> C U <sub>E</sub>	U <sub>E</sub> ... ;	$k_{\text{eff}} = 1.0154$ $\frac{\Delta k}{k_{\text{hom}}} = +0.62\%$
Free boundary	Cell boundary	Cell boundary		

In these diagrams, U<sub>E</sub> represents 90% enriched uranium, and U<sub>N</sub> natural uranium. In each case, the material at the left-hand free boundary was the same as that at the right-hand free boundary. It will be seen that cases 1 and 2 have the same basic cell structure, so that a cell calculation must give the same value of  $k_{\text{eff}}$  for each. However, the exact calculations give a difference of 0.15% in  $k_{\text{eff}}$  between them. The difference might not be so great if the core were reflected,

say, with a natural-uranium blanket, but it will always represent a contribution to  $k_{\text{eff}}$  that cannot be deduced from a cell calculation.

The third case differs from case 1 in that the natural uranium is separated from the enriched uranium by a region of graphite: all this makes the spectrum of neutrons in the natural uranium softer, and hence decreases the number of  $\text{U}^{238}$  fissions. Case 3 is therefore less reactive than either of the other cases.

Cell calculations, using the method outlined in section 2.2, were also made for these three cases. Some of the results, for the double- $S_8$  method, are shown in Table III. In this table,

$$\frac{\delta k}{K} = \frac{k_{\text{eff}} - k_{\text{eff}} (\text{homogeneous core})}{k_{\text{eff}} (\text{homogeneous core})}$$

is the fractional difference between the calculated  $k_{\text{eff}}$  for the heterogeneous core and  $k_{\text{eff}}$  for the homogeneous core. The quantity  $R_g$  is meant to give some indication of the flux-peaking or depression in each group  $g$ ; it is defined as:

$$R_g = \frac{\text{Mean flux in group } g \text{ in enriched uranium}}{\text{Mean flux in group } g \text{ in the whole core}}$$

TABLE III  
COMPARISON OF EXACT AND CELL CALCULATIONS

Case	Cell	$k_{\text{eff}}$		$\frac{\delta k}{K} \times 100 \%$		$R_1$		$R_2$		$R_3$	
		Exact	Cell calc.	Exact	Cell calc.	Exact	Cell calc.	Exact	Cell calc.	Exact	Cell calc.
1	$\text{U}_E \text{ U}_N \text{ C Fe Al}$	1.0175	1.0189	0.83%	0.97%	1.421	1.434	1.038	1.054	0.885	0.898
2	$\text{Al Fe C U}_N \text{ U}_E$	1.0189	1.0189	0.97%	0.97%	1.438	1.434	1.054	1.054	0.901	0.898
3	$\text{U}_N \text{ CU}_E \text{ Fe Al}$	1.0154	1.0165	0.62%	0.73%	—	—	—	—	—	—

It will be seen that agreement between the cell calculation and the exact calculation for case 2 is very good, but for the other two cases it is less good. It should be pointed out that double- $S_8$  approximations may not be sufficiently accurate for these calculations, and consequently there is a certain amount of error in the figures quoted. The cell calculations for cases 1 and 2 have been repeated with higher orders of approximation to the Boltzmann equation, but such a computation for the exact calculation (which requires a large number of spatial mesh-points) would require a great deal of machine time.

To sum up, it seems that the method used to obtain the cell constants can predict  $k_{\text{eff}}$  to within about 0.1%, and fluxes to within 2%.

#### (c) Convergence of results with increasing order of approximation

Meneghetti [4] has found that the value of  $k_{\text{eff}}$  found from a cell calculation with the DSN programme [7] does not converge very rapidly with increasing  $n$ , the order of the  $S_n$  approximation.

Experience with the double- $S_n$  method has been similar. For this reason it was decided to try the double-discrete-ordinates method, using Gaussian weights and ordinates for the two ranges  $(-1, 0)$  and  $0, +1$  of  $\mu$ . It was found that convergence was greatly improved, as may be seen from Table IV. This

gives  $k_{\text{eff}}$  for the cell of cases 1 and 2, for various orders of approximation. In this table, "double- $S_n$ " means an approximation in which the whole range of  $\mu$  is sub-divided into  $n$  equal intervals, while " $m$ -ordinates" means a discrete ordinates method in which ordinates were used in each of the two ranges ( $-1, 0$ ) and  $(0, +1)$ . A double- $S_n$  calculation has  $(n+2)$  different angular fluxes, while an  $m$ -ordinate calculation has  $m$  angular fluxes, so that the work involved is of similar complexity (and will take a similar amount of computing time) for a double- $S_n$  and an  $(n+2)$ -ordinate calculation.

TABLE IV  
CONVERGENCE OF THE DOUBLE- $S_n$  AND DOUBLE-GAUSS METHODS

Method	No. of angular fluxes	$k_{\text{eff}}$	$\frac{\delta k}{k} \times 100\%$
Double- $S_8$	10	1.0189	+ 0.97%
$S_{12}$	14	1.0192	+ 1.00%
$S_{16}$	18	1.0196	+ 1.04%
10-ordinates (DP <sub>4</sub> )	10	1.0196	+ 1.04%
14-ordinates (DP <sub>6</sub> )	14	1.0201	+ 1.09%
18-ordinates (DP <sub>8</sub> )	18	1.0201	+ 1.09%
30-ordinates (DP <sub>14</sub> )	30	1.0201	+ 1.09%

The double-Gauss method is equivalent to the double- $P_n$  method of Yvon; the brackets in the first column of the table above give the equivalent double- $P_n$  approximation.

It will be seen that the double-Gauss method converges much more quickly than the double- $S_n$  approximation, although even with the former, about 14 ordinates are necessary if a very accurate result (correct to 0.01%) is required.

#### (d) Collision-probability method

As was stated in section 2.3, one desk-calculation was carried out using a collision-probability method, based on the integral transport equation. This calculation was for a two-region cell, in which all the materials other than the enriched uranium were smeared together. The results were then compared with a 10-point double-Gauss discrete-ordinate calculation for the same cell. The values of  $k_{\text{eff}}$  and of  $R_g$ , the ratio of the average flux in the enriched uranium to the average flux in the whole core, for group  $g$ , are compared in Table V.

TABLE V  
COMPARISON OF THE COLLISION PROBABILITY AND DOUBLE-GAUSS METHODS.

Method	$k_{\text{eff}}$	$\frac{\delta k}{k} \times 100\%$	$R_1$	$R_2$	$R_3$
Collision probability	1.0139	+ 0.48%	1.428	1.034	0.944
10-ordinates	1.0130	+ 0.39%	1.434	1.041	0.933

Considering that the collision-probability calculation assumed constant fluxes in each region, and was sufficiently simple to be able to be made on a desk-machine in a reasonable time, the agreement is very gratifying, and further investigation of this method is planned. It should be pointed out that whereas it will be very difficult to extend the discrete-ordinates method to cylindrical geometry, the collision-probability method can be so extended without a great increase of complexity.

## 2.6. CONCLUSION

The work outlined here has shown that cell calculations can be used with some confidence for systems with lattice cells small compared with the core dimensions, in the simple case of a one-dimensional slab lattice, and that the double-Gauss discrete-ordinates method and possibly the collision-probability method seem the most suitable and the most accurate for this geometry.

The extension of the theory to deal with cylindrical cells, and with the rectangular cells that will actually exist in ZEBRA, can only be checked by experiment.

Further work will attempt to investigate the most suitable number of groups to use, and the detailed physical effects of fine structure. Cylindrical cells will also be studied.

## 3. Resonance absorption and Doppler effects

### 3.1. INTRODUCTION

The use of diluent materials in the fuel elements of future power-breeder reactors may result in a degraded neutron spectrum which extends well into the resonance energy region of the fissile and fertile materials, say below 10 keV. It is therefore important to investigate the effect of resonance self-shielding on reactivity and critical size, as well as the magnitude and sign of the temperature coefficient of reactivity associated with Doppler broadening of the resonances. Some preliminary approximate calculations concerning these phenomena are described in this part of the paper, with reference to the core of a simple spherical model of a typical fast breeder reactor.

### 3.2. REACTOR INVESTIGATED

The reactor selected for investigation was a typical plutonium oxide breeder with  $U^{238}$ , sodium and iron as the fertile, coolant and diluent materials, respectively. For the idealized spherically symmetric model assumed in the calculations, the core radius and reflector thickness were taken to be 78 cm and 61 cm, respectively. The material compositions of the core and reflector, assumed to be homogeneous, are given in Table VI.

The basic criticality calculation for this system was carried out in another connexion using multi-group diffusion theory with the 16-group constants of ROACH [11]. The reactor was slightly sub-critical ( $k_{\text{eff}} = 0.96$ ), but this should not affect the present work significantly.

The calculated group fluxes and adjoint functions (neutron importance) at the core centre are given in Table VII, where each is normalized to have a maximum value of unity.

An inspection of the radial plots of  $\varphi$  and  $\varphi^*$  shows that the spectrum is fairly constant out to a radius of about 65 cm.

TABLE VI  
REACTOR SPECIFICATION  
(Atoms per  $\text{cm}^3 \times 10^{-24}$ )

Material	Core	Reflector
$\text{U}^{235}$	$1.6 \times 10^{-5}$	$1.3 \times 10^{-4}$
$\text{U}^{238}$	$3.8 \times 10^{-3}$	$3.1 \times 10^{-2}$
$\text{Pu}^{239}$	$8.8 \times 10^{-4}$	—
$\text{Pu}^{240}$	$2.1 \times 10^{-4}$	—
Fe	$4.1 \times 10^{-2}$	$1.3 \times 10^{-2}$
Na	$6.0 \times 10^{-3}$	$4.0 \times 10^{-3}$
O	$9.8 \times 10^{-3}$	—

TABLE VII  
GROUP FLUXES AND ADJOINTS AT CORE CENTRE

Group <i>i</i>	Energy range	$\varphi_i$	$\varphi_i^*$
1	3 — 10 MeV	0.075	1.000
2	1.4 — 3 MeV	0.188	0.909
3	0.9 — 1.4 MeV	0.160	0.825
4	0.4 — 0.9 MeV	0.483	0.807
5	0.1 — 0.4 MeV	1.000	0.772
6	17 — 100 keV	0.722	0.717
7	3 — 17 keV	0.253	0.688
8	0.55 — 3 keV	0.093	0.600
9	0.1 — 0.55 keV	0.012	0.532
10	30 — 100 eV	0.0005	0.362

### 3.3. RESONANCE SELF-SHIELDING EFFECTS

The multi-group constants used in the basic criticality calculation were those given in Table 1 of ref. [11], and are uncorrected for resonance self-shielding. By 'self-shielding' is meant the effect of the sharp dips in the neutron energy spectrum at resonance positions. The  $\text{U}^{238}$  group capture cross-sections, and the  $\text{Pu}^{239}$  group capture and fission cross-sections corrected for self-shielding can be obtained for the low-energy groups from the graphs in Roach's paper. Knowing the changes in the group cross-section due to self-shielding, one can estimate the associated reactivity change to a first approximation by multi-group perturbation theory. Roach gives no data which would allow scattering cross-sections to be corrected for self-shielding but the effect on reactivity is expected to be relatively small.

The numerical results for  $\text{U}^{238}$  in the reactor core, with respect to groups 8—10, are given in Table VIII. From the run of the figures one would expect a small reactivity contribution from group 7, but no cross-section data is given by Roach for estimating this. On the other hand, the contributions from groups 11 onwards will be negligible since these groups contain very few neutrons.

TABLE VIII

REACTIVITY CHANGE  $\Delta R$  WHEN THE  $U^{238}$  GROUP CROSS-SECTIONS IN THE CORE ARE CHANGED FROM UNSHIELDED TO SHIELDED VALUES  
(Energy range: 0.03 — 3 keV)

Group	$\sigma_c$ (unsh.) (barn)	$\sigma_c$ (sh.) (barn)	$\Delta\sigma_c$	$\Delta R$ (%)
8	2	1.3*	— 0.7	+1.0
9	11	3	— 8.0	+1.3
10	50	8	—42.0	+0.2

\* Graphical value uncertain.

The results imply that allowance for  $U^{238}$  resonance self-shielding in the reactor core, for neutron energies between 30 eV and 3 keV, would increase reactivity by 2.5%. This is equivalent to a decrease in critical mass of  $Pu^{239}$  by about 4.4%, made uniformly over the core. The corresponding decrease would probably be appreciably larger, perhaps 10—20%, if the core-size were allowed to change, keeping the  $Pu^{239}$  concentration fixed.

A reactivity effect worth 2.5% appears to be a rather large contribution from an energy region containing only 3.5% of the total flux (from Table VII). However, the  $U^{238}$  capture cross-section increases strongly with decreasing energy, and it is estimated that about 30% of all  $U^{238}$  capture in the core occurs in the energy region concerned, below 3 keV.

A precise calculation of the reactivity effect of  $Pu^{239}$  self-shielding was not feasible, owing to difficulty in reading the relevant graphs in Roach's paper to the necessary accuracy. For groups 9—11 the result is estimated to lie within—0.1 and —0.3%, in reactivity. Roach gives no data for higher energy groups, and the self-shielding effect is evidently small. The sign of the reactivity change is opposite to that for  $U^{238}$ , since  $Pu^{239}$  is multiplying but  $U^{238}$  is non-multiplying at the energies concerned. To follow up this work a full multi-group diffusion-theory calculation was performed for the same reactor using "shielded"  $U^{238}$  constants in both core and reflector, and "shielded"  $Pu^{239}$  constants in the core. One found an increase of 3.4% in reactivity over the original calculation, in which "unshielded" constants were used. This figure is consistent with the above results, but is not directly comparable since it will include the contribution from the reflector, as well as taking up any errors due to the use of perturbation theory.

It is concluded that resonance self-shielding may be very significant in dilute fast reactors, and should be taken into account in calculations where high accuracy in predicting critical size is attempted.

### 3.4. DOPPLER TEMPERATURE COEFFICIENTS

Early work [8, 9] on the calculation of Doppler effects in fast reactors was mainly concerned with neutron energies of 100 keV and above. In the case of dilute fast breeder reactors, however, there is reason to expect the major Doppler effect to come from the low-energy part of the spectrum [10], where the fissile and fertile materials have strong resonances.

In this section a brief account is given of approximate calculations of the  $U^{238}$  and  $Pu^{239}$  Doppler temperature coefficients for the reactor described in

section 3.2. The energy range covered by groups 7—10 was considered, namely 0.03—17 keV. The resonances of both materials were treated as *s*-wave, discrete, and unresolved, i.e. mean values of the resonance widths are assumed, together with some law for the statistical distribution about the mean values. The correction due to overlapping of the Pu<sup>239</sup> resonances, especially at the higher energies, is not discussed.

A first approximation to the temperature-dependent group cross-sections can be obtained by averaging over many resonances in the neighbourhood of some representative energy for each group,  $\bar{E}$  say. For the numerical calculations  $\bar{E}$  has been chosen arbitrarily to be the median energy of a group. Following the discussion of ref. [8] we obtain the following approximate expression for the temperature-dependent group capture cross-section:

$$\Sigma_c(T) = \frac{\Sigma_{tN} \Gamma_c}{S} J(\xi, \beta), \quad (4.1)$$

with  $J(\xi, \beta) = \int_0^\infty \Psi / (\Psi + \beta) dx.$

$\Psi$ =the standard Doppler-broadened Breit-Wigner resonance profile.

$\Sigma_{tN}$ =total non-resonant core cross-section.

$\Gamma_c$ =resonance capture width.

$\Gamma$ =resonance total width.

$S$ =mean spacing of resonances.

$\xi = \Gamma/\Delta$ .

$\Delta = 2(\bar{E}kT/A)^{1/2}$ , the Doppler width,

where  $T$ =absolute temperature;

$k$ =the Boltzmann constant;

$A$ =mass number of absorber nucleus.

$\beta = \Sigma_{tN}/N\sigma_0$ ,

where  $N$ =number of absorbing nuclei per cm<sup>3</sup>;

$\sigma_0$ =peak total resonance cross-section.

A similar expression for the group fission cross-section for Pu<sup>239</sup>,  $\Sigma_f(T)$  is obtained by replacing  $\Gamma_c$  by  $\Gamma_f$  in (4.1).

The expression (4.1) has been derived by assuming that all resonances in the neighbourhood of the energy point concerned,  $E=\bar{E}$ , have the same widths  $\Gamma_c$  and  $\Gamma_n$ . If one assumes  $\Gamma_c$  constant, as is usually done, but allows  $\Gamma_n$  to have a statistical distribution about its mean, then  $J(\xi, \beta)$  should be averaged over this distribution. Likewise, in evaluating  $\Sigma_f(T)$  the term  $\Gamma_f J(\xi, \beta)$  should be averaged with respect to the distributions for  $\Gamma_f$  and  $\Gamma_n$ .

Finally, when  $\Sigma_c(T)$  and  $\Sigma_f(T)$  (for Pu<sup>239</sup>) have been evaluated at two selected temperatures  $T_1$  and  $T_2$ , the mean Doppler temperature coefficient over this temperature range can be estimated from multi-group perturbation theory. In the case of U<sup>238</sup>, for example, the contribution to the Doppler coefficient from group  $i$ , a mean value over the range  $T_1$  and  $T_2$ , will be of the form

$$di = \varphi_i \varphi_i^* \cdot \frac{\Sigma_{tN} \Gamma_c}{S} \left[ \frac{\langle J(\xi_2, \beta) \rangle - \langle J(\xi_1, \beta) \rangle}{T_2 - T_1} \right]. \quad (4.2)$$

Here  $\varphi_i$  and  $\varphi_i^*$  are suitably normalized and averaged values of the neutron flux and adjoint functions for group  $i$  in the reactor core.  $\xi_1$  and  $\xi_2$  are the values

of  $\xi$  at  $T_1$  and  $T_2$ ;  $di$  has to be evaluated and summed over all energy groups  $i$  of interest. In the case of Pu<sup>239</sup> the equation for  $di$  will have another term representing the contribution of resonance fission. The brackets  $\langle \rangle$  denote an average over the distribution of resonance widths.

Preliminary numerical results for U<sup>238</sup> in the temperature range 300—1800 °K can be fitted approximately by the formula

$$d = -2.6 (T_0/T) \times 10^{-5}/^{\circ}\text{C},$$

where  $d$  is the Doppler temperature coefficient and  $T_0 = 300$  °K. This result is based upon mean resonance parameters and includes contributions from groups 7—10, i.e. 0.03—17 keV. About 85% of the coefficient comes from below 3 keV. A rough calculation based on the Porter-Thomas distribution suggests that allowance for the fluctuation of the neutron width about its mean value would reduce the coefficient by some 25%, giving

$$d = -2.0 \times (T_0/T) \times 10^{-5}/^{\circ}\text{C}.$$

Using data from [10], which includes  $p$ -wave as well as  $s$ -wave effects, the contribution to the coefficient from groups 5 and 6, (17—400 keV), is estimated crudely to be an order of magnitude less than the contribution from below 17 keV.

Preliminary estimates suggest that the positive Pu<sup>239</sup> Doppler coefficient is approximately  $10^{-5}/^{\circ}\text{C}$ . The result depends sensitively on the assumed values of the unresolved resonance parameters, which are not known accurately, and accordingly the estimate is not to be considered very reliable.

In conclusion, the work done so far indicates the possibility that very dilute fast reactors may have Doppler temperature coefficients of the order of  $10^{-5}/^{\circ}\text{C}$ , which would be important from the point of view of stability and control. It is considered, however, unlikely that present nuclear data and mathematical techniques are adequate to enable these coefficients to be estimated reliably. Their magnitude will depend strongly on the very-low-energy part of the neutron spectrum in the reactor, and refinements of existing multi-group methods and constants will probably be necessary to predict this spectrum accurately.

## REFERENCES

- [1] LOEWENSTEIN, W. B. and OKRENT, D., Proc. 2nd UN Int. Conf. PUAE **12** (1958) 16.
- [2] PALMER, R. G., private communication.
- [3] LONG, J. K. *et al.*, Proc. 2nd UN Int. Conf. PUAE **12** (1958) 119.
- [4] MENEGHETTI, D. and LOOMIS, M. F., ANL-6218.
- [5] DAVIDSON, B., Neutron Transport Theory, Oxford University Press (1957).
- [6] CARLSON, B. G., LAMS-2201 (1958).
- [7] CARLSON, B. G. *et al.*, LAMS-2346.
- [8] GOERTZEL, G., Proc. UN Int. Conf. PUAE **5** (1956) 472.
- [9] LANE, A. M., LYNN, J. E. and STORY, J. S., AERE T/M 137 (1956).
- [10] NICHOLSON, R. B., APDA 139 (1960).
- [11] ROACH, W. H., *Nucl. Sci. Engng* **8** (1960) 621.



# THE PHYSICS ASPECTS OF A COUPLED FAST-THERMAL STEAM SUPERHEATING REACTOR\*

B. J. TOPPEL AND R. AVERY

ARGONNE NATIONAL LABORATORY, ARGONNE, ILL.,  
UNITED STATES OF AMERICA

Abstract — Résumé — Аннотация — Resumen

**The physics aspects of a coupled fast-thermal steam superheating reactor.** Physics calculations were performed on a light-water version of the coupled steam superheater using 13-group, one-dimensional and 4-group, two-dimensional diffusion theory in cylindrical geometry. The 13-group cross-sections were obtained using an iterative procedure employing fundamental mode flux results. The 4-group cross-sections were obtained by collapsing the 13-group set using the appropriate spectra from the results of a 13-group, one-dimensional calculation.

In the steam-cooled zones, the regional cross-sections were obtained by simple homogenization. In the water zones, special attention was given to heterogeneity when obtaining appropriate regional cross-sections.

A comparison of the 4-group and 13-group results is presented. The agreement is in general good, although there is some indication that the resonance capture considerations in the 4-group calculations need to be refined.

The calculated initial breeding ratio is 1.4, a value typical of previously studied fast and coupled systems, and comparable with the value obtained for the heavy-water version of the system. This large breeding ratio is realized because of the small water density and large power fraction in the fast core, and because of the large fuel density in the thermal zones.

Calculations of the prompt-neutron lifetime, division of reactivity, and coupling parameters are discussed. In addition, reactivity coefficients for water addition in the fast and thermal regions are presented. These coefficients are of particular significance to the safety of the concept.

**Physique d'un réacteur à couplage neutrons rapides neutrons thermiques et à vapeur surchauffée.** Les calculs de physique effectués sur une variante à eau ordinaire du réacteur couplé à vapeur surchauffée utilisaient une théorie de la diffusion à 13 groupes et une dimension et une théorie à 4 groupes et deux dimensions, en géométrie cylindrique. Les sections efficaces pour 13 groupes ont été obtenues par itération à partir des résultats des flux de modes fondamentaux. Les sections efficaces pour 4 groupes ont été obtenues par réduction du système à 13 groupes en utilisant le spectre approprié, à partir des résultats du calcul à 13 groupes et à une dimension.

Dans les zones refroidies par la vapeur, les sections efficaces régionales ont été obtenues par simple homogénéisation. Dans les zones à eau, les auteurs ont avant tout tenu compte de l'hétérogénéité dans la détermination des sections efficaces régionales convenables.

On présente la comparaison entre les résultats des calculs à 4 groupes et ceux des calculs à 13 groupes. Ils concordent en général assez bien, mais il faudrait, semble-t-il, dans les calculs à 4 groupes, étudier la capture de résonance de façon plus approfondie.

Le taux initial de régénération donné par le calcul est de 1,4, ce qui est une valeur typique pour les réacteurs à neutrons rapides et les réacteurs couplés précédemment

---

\* Work performed under the auspices of the United States Atomic Energy Commission.

étudiés; elle se rapproche de la valeur obtenue pour la variante à eau lourde du réacteur. Ce taux élevé est dû à la faible densité de l'eau et à l'importante fraction de la puissance dans le cœur à neutrons rapides et à la densité élevée du combustible dans les zones thermiques.

Les auteurs examinent les calculs portant sur le temps de vie des neutrons instantanés, sur le partage de la réactivité et sur les paramètres de couplage. Ils présentent également les coefficients de réactivité obtenus lorsque l'on introduit de l'eau dans la région des neutrons rapides et dans la région thermique. Ces coefficients jouent un rôle très important dans les études théoriques de la sécurité.

**Физические аспекты быстротеплового реактора с перегревом пара.** Физические расчеты производились на легководном варианте быстротеплового реактора с перегревом пара с использованием 13-групповой одноразмерной и 4-групповой двухразмерной диффузионной теории в цилиндрической геометрии. Сечения для 13 групп были получены, используя итерацию с применением фундаментальных результатов распределения потока. Сечения для 4 групп получались путем разложения 13-групповой системы, используя соответствующие спектры от результатов 13-группового одноразмерного вычисления.

В зонах охлаждения пара региональные сечения получались посредством простой гомогенизации. В водных зонах особое внимание обращалось на гетерогенность для получения соответствующих региональных сечений.

В докладе будет дано сравнение 4-групповых и 13-групповых результатов. Они, как правило, хорошо согласуются друг с другом, хотя, как кажется, необходимо уточнить соображения по резонансному захвату в 4-групповых вычислениях.

Вычисленный начальный коэффициент воспроизводства равняется 1,4, что является значением, точным для ранее изучавшихся быстрых и быстротепловых систем и сравнимым с тяжеловодным вариантом этой системы. Этот высокий коэффициент воспроизводства достигается благодаря низкой плотности воды и большой доле энергии, выделяемой в „быстрой“ активной зоне, и благодаря высокой плотности топлива в тепловых зонах.

В докладе будут обсуждаться вычисления времени жизни мгновенных нейтронов, распределение реактивности и других параметров этого быстротеплового реактора. Кроме того, будет сообщено о влиянии на коэффициенты реактивности добавления воды в областях быстрых и тепловых нейтронов. Эти коэффициенты имеют особое значение для безопасности системы.

**Física de un reactor con acoplamiento rápido-térmico para la producción de vapor sobre calentado.** Los autores han efectuado un estudio de la física de una variante, que funciona con agua ligera, del reactor con acoplamiento rápido-térmico para la la producción de vapor sobrecalentado; para ello han utilizado una teoría de difusión unidimensional de 13 grupos y una teoría bidimensional de 4 grupos en geometría cilíndrica. Las secciones eficaces para los 13 grupos se calcularon por iteración a partir de los resultados de los flujos de los modos fundamentales. Las secciones eficaces para los 4 grupos se obtuvieron por reducción del conjunto de 13 grupos, para lo que se emplearon los espectros apropiados, obtenidos para los cálculos según la teoría unidimensional de 13 grupos.

En las zonas refrigeradas por vapor, los autores calcularon las secciones eficaces regionales por simple homogeneización. En las zonas refrigeradas por agua, tuvieron debidamente en cuenta la heterogeneidad para determinar las secciones eficaces regionales.

Los autores comparan los resultados del método de los 4 grupos con los del método de los 13 grupos. Por lo general, dichos resultados concuerdan satisfactoriamente, aunque parece que para los cálculos de 4 grupos convendría estudiar en forma minuciosa la captura por resonancia.

La razón inicial de reproducción calculada es igual a 1,4, valor típico para los reactores de neutrones rápidos y acoplados, anteriormente estudiados; este valor es comparable al obtenido para la variante que funciona con agua pesada. Esta

elevada razón de reproducción se debe a la escasa densidad del agua y a la gran concentración de potencia en la zona de neutrones rápidos, así como a la elevada densidad del combustible en las zonas térmicas.

Los autores discuten el cálculo de la vida de los neutrones inmediatos, de la distribución de la reactividad y de los parámetros de acoplamiento. Asimismo, calculan los coeficientes de reactividad de las regiones rápida y térmica cuando aumenta la cantidad de agua. Estos coeficientes son de especial importancia para la seguridad del sistema.

## Introduction

The coupled fast-thermal reactor concept involves coupling neutronically a fast assembly and a thermal assembly to each other. Various such systems have been studied in the past [1, 2]. The primary purpose of these studies has been to determine the extent to which the coupled system may possess favourable characteristics for various reactor applications. The major application considered has been with respect to a power-breeder system. The primary potential advantages offered by a fast-thermal power breeder are the possibilities of attaining the high breeding gain of a fast assembly and the long neutron lifetime of a thermal assembly.

In a system where there is a small fraction of the neutrons that have very much longer prompt lifetimes than the others, the overall prompt-neutron lifetime will be largely determined by these slowest neutrons as long as they are still needed to maintain the chain reaction. This is analogous to the delayed-neutron effect, where the neutron generation time is primarily determined by the delayed neutrons as long as the system is below prompt critical. For this reason, the neutron lifetime in the coupled fast-thermal system is in the range characteristic of thermal reactors.

To obtain a breeding gain characteristic of fast assemblies, the power must be generated primarily in the fast part. In addition, it is necessary to shield the fast region as much as possible from the low-energy neutron spectrum in the thermal region. The reason for this is twofold: (a) to maintain the energy of neutrons causing fissions in  $\text{Pu}^{239}$  high so as to attain a low value for the capture-to-fission ratio (alpha), and (b) to prevent a hot spot at the edge of the fast assembly.

The essential problem in the design of the system is to obtain sufficient coupling between the systems while at the same time introducing a barrier between the systems which sufficiently isolates the fast system from low-energy neutrons.

The coupled fast-thermal systems that have been studied have had cylindrical symmetry, with one of the assemblies forming an annulus surrounding the other. Because of the high critical mass usually associated with a fast assembly, it has usually been on the inside. The earlier investigations have been on liquid-metal-cooled systems. The system reported on here retains the usual geometry, but uses both water and steam as coolants. The fast core acts as a superheater and is steam-cooled, while the thermal part is cooled by water of approximately normal density.

The primary consideration of a large breeding ratio originally led to consideration of a system having  $\text{D}_2\text{O}$  for the coolant [3] because of the lower parasitic capture as compared with  $\text{H}_2\text{O}$ . The results presented in Section 1, however, indicate that an  $\text{H}_2\text{O}$  system can be devised which has a substantial breeding ratio. Owing to this fact, and to the greater technological problems which would

be encountered using  $D_2O$ , the concept has turned from the original  $D_2O$  system to the present  $H_2O$  system.

The calculations reported on in Section 1 are of a preliminary survey nature. The systems were selected on the basis of rather preliminary engineering considerations. From the results of Section 1 a specific system was selected for a rather thorough engineering conceptual design. The physics calculations reported on in Section 2 are based on this system.

### 1. Preliminary survey calculations

This section describes the exploratory physics calculations, which have preceded and lead to the concept as presented in Section 2. All of the early systems used metal fuels. The original concept assumed that all of the steam would be produced in the thermal region of the reactor, which would, therefore, be a more or less conventional boiling system. Because of the thermodynamics of steam, if the thermal region were the sole source of saturated steam, it would be difficult to achieve a system having more than about 25% of the power in the fast superheater. This is illustrated by a specific numerical example in Fig. 1, where the characteristics of a boiling-superheating system are given. The breeding ratio attainable with such a system would not be expected to approach the values common for all-fast-reactor systems. On the other hand, depending upon the extent to which auxiliary superheated steam-powered boilers were employed, the thermal regions could be used to produce only part of the saturated steam which is to be superheated. In particular, if the thermal region were used only as a non-boiling pressurized water-preheater for the auxiliary boilers so that the fast part of the system contained most of the power, breeding ratios comparable with those of the fast liquid-metal systems might be attainable.

#### REFERENCE SYSTEMS

The systems examined are examples of the coupled-superheater concept which represent the extremes discussed above. The first is one in which all the steam to be superheated is produced in the boiling, thermal portion of the reactor. Since for this system only about 25% of the power will be produced in the fast parts of the reactor, this system will be designated the thermal-fast system. The second system is one in which none of the steam is generated in the reactor. In this case, the thermal portion of the coupled reactor will act as a pressurized water-preheater for external boilers, and about 80% of the power will be generated in the fast portion of the reactor. This system will be designated the fast-thermal system.

Figs. 2 and 3 show schematic drawings indicating the relative dimensions of the thermal-fast and fast-thermal coupled steam superheaters, respectively. Only heavy water for the coolant has been examined for the case of the thermal-fast system. The fast-thermal concept, on the other hand, has been investigated both for heavy-water and light-water coolants. In the light-water case, the radial thickness of region 4 in Fig. 3 is only about half as great as in the heavy-water case. The relative dimensions shown in Fig. 3 are as used in the heavy-water studies. For purposes of comparison, a prototype, all-fast sodium-cooled reference system has also been examined. This system is shown schematically in Fig. 4.

In the thermal-fast concept, since only about 25% of the power will be generated in the fast part of the system, the thermal portion must be highly reactive; one requires a large  $k_\infty$  for the thermal system. For this reason, regions 4 and 5 (Fig. 2)

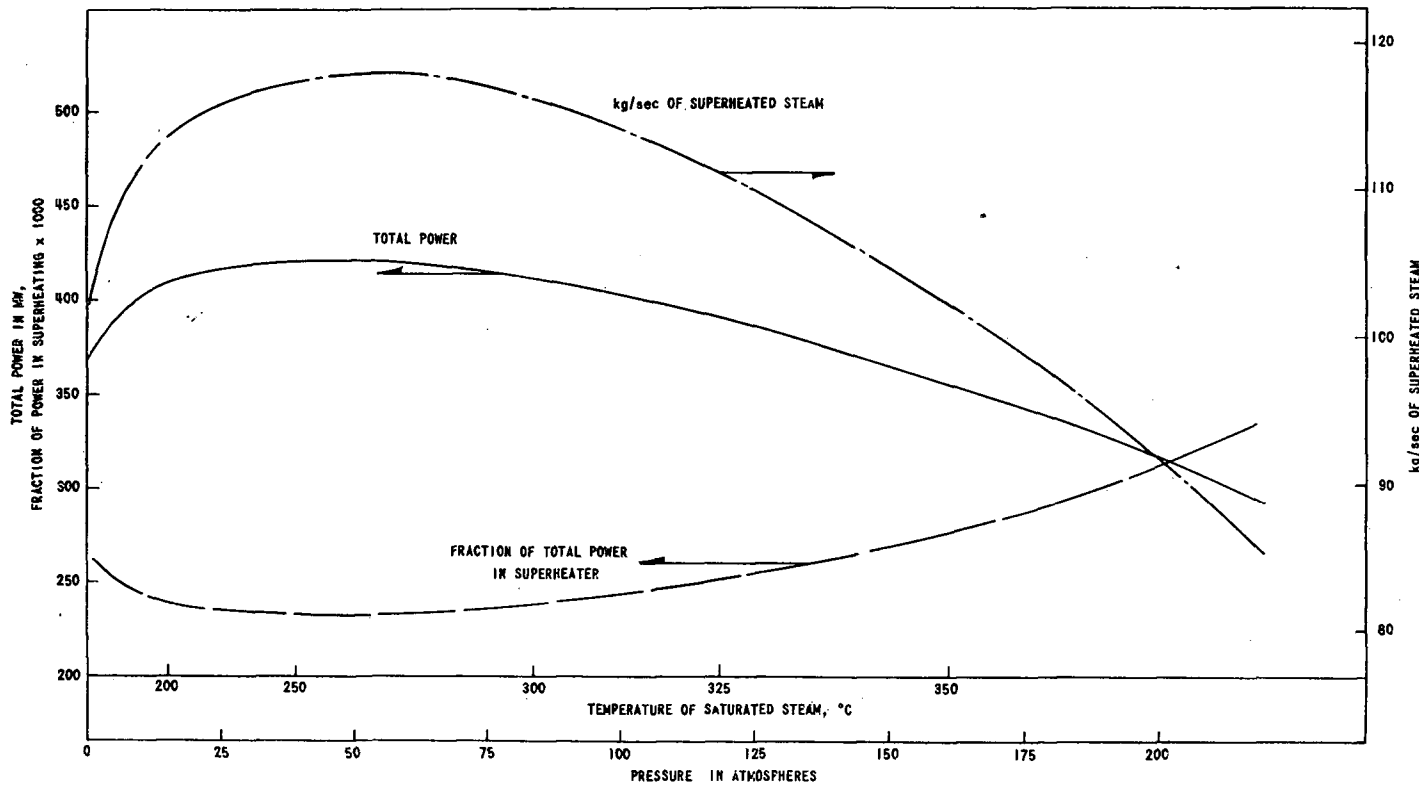


Fig. 1  
Characteristics of a boiling-superheating system assuming 100-MW in the superheater  
and 593 °C superheated steam.

contain clusters of fuel. This clustering increases the resonance-escape probability as compared with a non-clustered fuel arrangement. In the case of the fast-thermal system, on the other hand, since the thermal part of the system need not be highly reactive, non-clustered fuel arrangements may be used. The fuel cluster arrange-

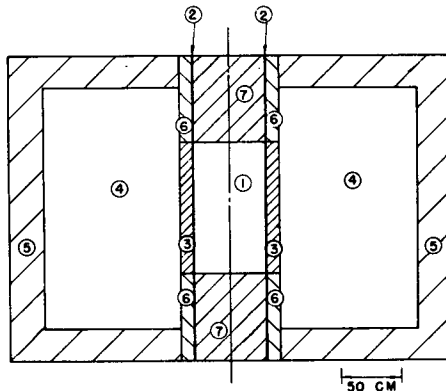


Fig. 2  
Schematic drawing of thermal-fast coupled steam superheater.

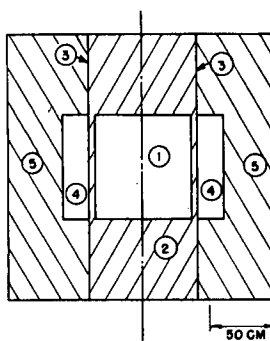


Fig. 3  
Schematic drawing of fast-thermal coupled steam superheater.

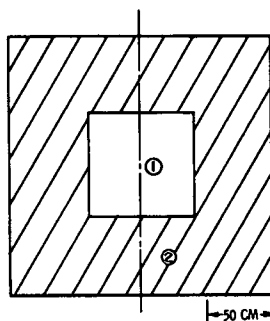


Fig. 4  
Schematic drawing of all-fast reference system.

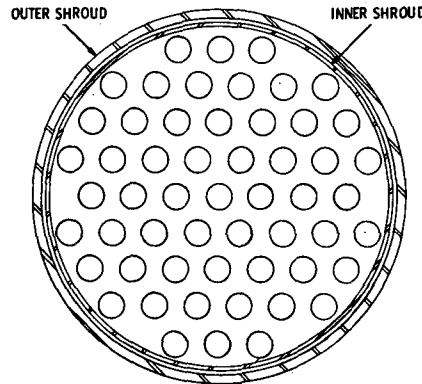


Fig. 5  
Fuel cluster used in thermal-fast steam superheater.

ment assumed for the thermal-fast concept is shown in Fig. 5. The cluster consists of 55 zirconium-clad uranium pins located within a double zirconium shroud. The dimensions of the cluster are given in Table I. The clusters contain natural uranium

TABLE I  
FUEL CLUSTER USED IN THE THERMAL-FAST STEAM SUPERHEATER  
(centimeters)

Radius of natural- uranium pin	0.1588
Thickness of zirconium clad	0.0254
Triangular pitch of pins	0.6223
Inner shroud, ID	4.953
Inner shroud, OD	5.055
Outer shroud, ID	5.258
Outer shroud, OD	5.461

TABLE II  
COMPOSITION OF VARIOUS REGIONS OF THERMAL-FAST D<sub>2</sub>O COUPLED STEAM  
SUPERHEATER

Region	Volume fractions					
	Pu <sup>239</sup>	U <sup>238</sup>	U <sup>235</sup>	Fe	Zr	D <sub>2</sub> O*
Core	0.0447	0.4553	0	0.15	0	0.0084
Inner blanket	0	0.4966	0.0036	0	0.1729	0.1559
Water annulus	0	0.0461	0.0003	0	0.0427	0.8362
Water blanket	0	0.0463	0.0001	0	0.0427	0.8362
Inner blanket reflector	0	0.4990	0.0010	0	0.1729	0.1559
Core blanket	0	0.4990	0.0010	0.15	0	0.0084

\* Equivalent amount of D<sub>2</sub>O at 100° C.

TABLE III  
COMPOSITION OF VARIOUS REGIONS OF FAST-THERMAL D<sub>2</sub>O COUPLED  
STEAM SUPERHEATER

Region	Volume fractions					
	Pu <sup>239</sup>	U <sup>238</sup>	U <sup>235</sup>	Fe	Zr	D <sub>2</sub> O*
Core	0.0531	0.4469	0	0.15	0	0.0114
Core blanket	0	0.4990	0.0010	0.15	0	0.0114
Water annulus	0	0.0993	0.0007	0	0.0102	0.8898
Water blanket	0	0.0998	0.0002	0	0.0102	0.8898

\* Equivalent amount of D<sub>2</sub>O at 300 °C.

TABLE IV  
COMPOSITION OF VARIOUS REGIONS OF FAST-THERMAL H<sub>2</sub>O COUPLED  
STEAM SUPERHEATER

Region	Volume fractions					
	Pu <sup>239</sup>	U <sup>238</sup>	U <sup>235</sup>	Fe	Zr	H <sub>2</sub> O*
Core	0.0487	0.4513	0	0.15	0	0.0114
Core blanket	0	0.4990	0.0010	0.15	0	0.0114
Water annulus	0	0.19856	0.00144	0	0.02048	0.77952
Water blanket	0	0.7984	0.0016	0	0.08192	0.11808

\* Equivalent amount of H<sub>2</sub>O at 300 °C.

TABLE V  
COMPOSITION OF REGIONS OF ALL-FAST REFERENCE SYSTEM

Region	Volume fractions				
	Pu <sup>239</sup>	U <sup>238</sup>	U <sup>235</sup>	Fe	Na*
Core	0.0460	0.4540	0	0.15	0.35
Blanket	0	0.4990	0.0010	0.15	0.35

\* At 480 °C.

in region 4 and depleted uranium in region 5 (Fig. 2). The uranium, zirconium clad, and boiling D<sub>2</sub>O are at a temperature of 300°C. The non-boiling D<sub>2</sub>O and zirconium shrouds are at a temperature of 100°C. (The region between the shrouds contains non-boiling D<sub>2</sub>O.) In the case of the boiling D<sub>2</sub>O, steam voids were taken into account by assuming the density to be 0.65 times that of non-boiling D<sub>2</sub>O at 300 °C.

The compositions of the various regions for the reference systems are given in Tables II through V. Tables III and IV correspond, respectively, to heavy- and light-water versions for the fast-thermal concept. Table II corresponds to Fig. 2, Tables III and IV to Fig. 3, and Table V to Fig. 4.

## CALCULATIONAL PROCEDURES

*General*

Calculations were made using 4-group diffusion theory, both in one- and two-dimensional ( $r-z$ ) geometry. The one-dimensional (1D) calculations [4] assumed a bare axial height which includes a reflector savings of 15 cm on each end. The two-dimensional (2D) problems were studied using the PDQ code [5].

In the fast parts of the system (in general the steam-cooled regions), the regional cross-sections were obtained by a simple homogenization of the basic cross-section set (Table VI). This procedure is valid because of the hardness of the spectrum in the steam-cooled zones. In the water zones, special attention was given to calculation of the resonance-escape probability and, in the case of clustered elements, to calculation of fast-effect and thermal-disadvantage factors. In the case of the non-clustered lattices in the water regions of the fast-thermal systems, thermal cross-sections were obtained by simple homogenization.

The 4-group equations which are solved are written as:

$$\begin{aligned} D_1 \nabla^2 \varphi_1 - \Sigma_{s1} \varphi_1 + \beta_1 S &= 0 \\ D_2 \nabla^2 \varphi_2 - \Sigma_{a2} \varphi_2 + \Sigma_{1 \rightarrow 2} \varphi_1 + \beta_2 S &= 0 \\ D_3 \nabla^2 \varphi_3 - \Sigma_{a3} \varphi_3 + \Sigma_{2 \rightarrow 3} \varphi_2 &= 0 \\ D_4 \nabla^2 \varphi_4 - \Sigma_{a4} \varphi_4 + \Sigma_{3 \rightarrow 4} \varphi_3 &= 0 \end{aligned} \quad (1)$$

where

$$S = \sum_{j=1}^4 \nu_j \Sigma_{fj} \varphi_j. \quad (2)$$

The  $D_i$  are the group diffusion coefficients and are given by  $(3\Sigma_{\text{tri}})^{-1}$  where the  $\Sigma_{\text{tri}}$  are the group transport cross-sections. The  $\Sigma_{a_i}$  are the total group removal cross-sections and the  $\Sigma_{i \rightarrow i+1}$  are the group transfer cross-sections. The  $\beta_i$  give the fraction of the fission neutrons born into group  $i$ . We note that neutrons are assumed to be born only in groups 1 and 2 ( $\beta_1 + \beta_2 = 1$ ).

In the water regions, the resonance-escape probability,  $p$ , is taken into account by assuming  $p\Sigma_{a3} = \Sigma_{3 \rightarrow 4}$ , so that in the fourth equation  $\Sigma_{3 \rightarrow 4}$  is replaced by the value of  $p\Sigma_{a3}$ .

In the case of the clustered elements, all the thermal cross-sections were obtained by a spatial-flux weighting. A diffusion-theory cell calculation was used for evaluating the thermal-disadvantage factors. As usual, the gradient of the flux was set equal to zero at the outer boundary of the cell moderator region. The sources in fuel and moderator regions of the cell were assumed to be proportional to the amount of  $D_2O$  present in each region. The compositions of the fuel and moderator zones for the cell calculations used in the clustered geometries are given in Table VII.

*Resonance-escape probability*

The resonance-escape probability was calculated using the expression:

$$p = \exp \left\{ -\frac{N}{\xi \Sigma_s} \right\} I_{\text{eff}} \quad (3)$$

TABLE VI  
4-GROUP MICROSCOPIC CROSS-SECTIONS  
(barns)

j	Lower energy $E_L$	Fission spectrum	Pu <sup>239</sup>					U <sup>238</sup> *					U <sup>235</sup>					Fe		
			$\sigma_{tr}$	$\sigma_f$	$\nu$	$\sigma_c$	$\frac{1+f}{\sigma_c}$	$\sigma_{tr}$	$\sigma_f$	$\nu$	$\sigma_c$	$\sigma_{j \rightarrow j+1}$	$\sigma_{tr}$	$\sigma_f$	$\nu$	$\sigma_c$	$\sigma_{j \rightarrow j+1}$	$\sigma_{tr}$	$\sigma_c$	$\sigma_{j \rightarrow j+1}$
1	1.353 MeV	0.575	4.8	2.00	3.07	0.06	0.9	4.70	0.53	2.65	0.04	2.10	4.70	1.30	2.65	0.100	1.40	2.14	0.00249	0.7372
2	9.12 keV	0.425	7.0	1.80	2.96	0.450		7.00	0	0	0.18	0	7.00	1.40	2.55	0.300	0	2.93	0.00570	0.0025
3	0.4 eV	0	74.0	41.00	2.90	23.0	0.01	11.01	0	0	1.037	0.0085	56.21	25.94	2.55	20.3	0.0085	9.62	0.127	0.0331
4	thermal	0	1055.3	687.40	2.90	358.3	0	10.18	0	0	1.738	0	444.17	365.83	2.50	68.40	0	11.22	1.800	0

j	H <sub>2</sub> O			D <sub>2</sub> O			Zr			B <sup>10</sup>			Na**			$10^7 / \nu$		
	$\sigma_{tr}$	$\sigma_c$	$\sigma_{j \rightarrow j+1}$	$\sigma_{tr}$	$\sigma_c$	$\sigma_{j \rightarrow j+1}$	$\sigma_{tr}$	$\sigma_c$	$\sigma_{j \rightarrow j+1}$	$\sigma_{tr}$	$\sigma_c$	$\sigma_{j \rightarrow j+1}$	$\sigma_{tr}$	$\sigma_c$	$\sigma_{j \rightarrow j+1}$	$\sigma_{tr}$	$\sigma_c$	$\sigma_{j \rightarrow j+1}$
1	3.08	0	2.81	4.413	0		5.393	3.00	0.020	0.800	1.600	0.282	0.188	2.00	0.0005	0.300	0.00412	
2	10.52	0	4.04	7.864	0		1.140	7.395	0.020	0.0738	4.839	1.714	0.131	3.885	0.00045	0.0676	0.0204	
3	16.55	0.035	4.14	8.129	0		0.537	7.395	0.020	0.0369	194.52	190.25	0.0747	8.988	0.0550	0.0773	2.267	
4	48.95	0.403	0	11.329	0.00132	0	6.139	0.1146	0	1971.20	1967.51	0	3.532	0.279	0	28.97		

\* U<sup>238</sup> as given was used for the all-fast reference problems. For the various superheater calculations, the group-3 values were adjusted for each problem for the various water zones. In the steam-cooled regions, the values given in the table were used in the case of the D<sub>2</sub>O studies. For the H<sub>2</sub>O cases, group 3 for U<sup>238</sup> had  $\sigma_{tr} = 11.23$  and  $\sigma_c = 1.257$  b.

\*\* The sodium is at 480 °C. All other materials are at 300 °C.

Material	Atomic density (atoms/cm <sup>3</sup> )
Pu <sup>239</sup>	$0.040 \times 10^{24}$
U <sup>238</sup>	0.048
U <sup>235</sup>	0.048
Fe	0.0848
H <sub>2</sub> O	0.02375
D <sub>2</sub> O	0.0234
Zr	0.0425
B <sup>10</sup>	0.1499
Na	0.0220

where

$$\bar{\xi} = \frac{\sum_i \xi_i \Sigma_{si}}{\sum_i \Sigma_{si}} = \frac{\sum_i \xi_i \Sigma_{si}}{\Sigma_s} \quad (4)$$

and the summation extends over all materials of the mixture.  $N$  is the number of absorber atoms per cubic centimeter;  $\xi_i$  is the average logarithmic energy loss suffered by a neutron per collision with material  $i$  and  $\Sigma_{si}$  is the resonance group scattering cross-section of the material  $i$ . The same expression was used both for the clustered and non-clustered geometries so that resonance-disadvantage factors are being ignored in the clustered case.

For the  $U^{238}$ , the effective resonance integral,  $I_{\text{eff}}$ , was evaluated using the formula given by HELLSTRAND [6]:

$$I_{\text{eff}}^{28} = \frac{7.8}{F} + 30.2 \frac{S_{\text{eff}}}{M}. \quad (5)$$

$F$  [7] is the ratio of resonance energy flux at the rod surface to average resonance energy flux in the rod interior.  $F$  is evaluated using constants appropriate to the resonance energy group. A 1.4-barn  $1/v$  correction has been added to the values obtained using Eq. (5) before inserting in Eq. (3).

For the non-clustered lattices,  $S_{\text{eff}}$  has been evaluated following the method of DANCOFF and GINSBURG [8, 9]. The actual values for the Dancoff correction factor,  $1 - C$ , for two rods of radius  $\rho$  and separation  $d$  immersed in a medium of mean free path  $\lambda$ , were obtained using an approximate formula similar to that given by THIE [10], namely

$$1 - C = 1 - \frac{4}{\pi^2} \sin^{-1} \frac{\rho}{d} Ki_3 \left[ \left( \frac{d}{\rho} - 1.78 \right) \frac{\rho}{\lambda} \right]. \quad (6)$$

The  $Ki_3$  function was evaluated using recently tabulated values [11].

For the clustered geometries, the empirical method of CARLVIK and PERSHAGEN [6, 12] was used to obtain the value of  $S_{\text{eff}}$  for use in Eq. (5). In this case, the interaction between the various clusters has been ignored.

TABLE VII  
COMPOSITION OF FUEL AND MODERATOR REGIONS FOR CELL CALCULATIONS  
IN CLUSTERED FUEL ZONES\*

Fuel region		Moderator region	
Material	Volume fraction	Material	Volume fraction
Uranium**	0.2360	Boiling D <sub>2</sub> O	0.0372
Zirconium	0.0816	Non-boiling D <sub>2</sub> O	0.9305
Boiling D <sub>2</sub> O	0.6824***	Zirconium	0.0323

\* Cluster pitch = 10.414 cm.

\*\* Natural uranium in region 4; depleted uranium in region 5 (Fig. 2).

\*\*\* 0.65 times this value used for homogenizing cross-sections.

In both the non-clustered and clustered geometries, the resonance-escape probabilities for the U<sup>235</sup> and Zr were evaluated using the infinite dilution values of the resonance integrals [13]. For U<sup>235</sup>, the total  $I_{\text{eff}}$  was obtained from the fission  $I_{\text{eff}}$  by multiplying by  $1 + \alpha$ , where  $\alpha (= 0.783)$  is the assumed capture-to-fission ratio for the U<sup>235</sup> in group 3.

The total resonance-escape probability was taken as

$$p = p^{28} \times p^{25} \times p^{\text{Zr}}. \quad (7)$$

The individual materials were assumed to have group-3 capture-plus-fission cross-sections given by  $(N_i I_{\text{eff}i})/\Delta_u$ , where  $\Delta_u$  is the lethargy width of group 3.  $N_i$  is the number of atoms per cubic centimeter for the isotope under consideration, and  $I_{\text{eff}i}$  is the corresponding effective resonance integral. Then, the group-3-to-4 transfer cross-section is taken to be

$$\Sigma_{3 \rightarrow 4} = \frac{p}{1-p} \sum \frac{N_i I_{\text{eff}i}}{\Delta_u}. \quad (8)$$

The transport cross-section was taken to be

$$\Sigma_{\text{tri}} = \frac{N_i I_{\text{eff}i}}{\Delta_u} + (1 - \bar{\mu}_i) \Sigma_{\text{si}}. \quad (9)$$

For the light-water lattices, an effective resonance integral for H<sub>2</sub>O of 0.35 barn was used. As in the clustered arrangement, the total resonance-escape probability to be used in Eq. (8) was taken as the product of the individual escape probabilities.

#### *Fast effect*

In a homogeneous system, the fast-fission bonus will be automatically accounted for in a multi-group calculation if values for the U<sup>238</sup> fission cross-section are included in the multi-group cross-sections. In the case of a one-group calculation, on the other hand, the fast-fission factor  $\varepsilon$  may be accounted for by using a homogeneous formula such as [14]:

$$\varepsilon = 1 + \frac{\frac{\bar{\Sigma}_{\text{f}}^{28}}{\Sigma_{\text{r}}} (\nu^{28} - 1 - \alpha^{28})}{1 - \nu^{28} \frac{\bar{\Sigma}_{\text{f}}^{28}}{\Sigma_{\text{r}}}} \quad (10)$$

and including the value of  $\varepsilon$  in the four-factor formula ( $k_{\infty} = \varepsilon p / \eta$ ). In Eq. (10),  $\bar{\Sigma}_{\text{f}}^{28}$  is the U<sup>238</sup> fission cross-section averaged over the fission spectrum,  $\Sigma_{\text{r}}$  is the total cross-section for removing neutrons from above the U<sup>238</sup> fission threshold,  $\nu^{28}$  is the average number of fission neutrons released per U<sup>238</sup> fission, and  $\alpha^{28}$  is the ratio of U<sup>238</sup> captures to U<sup>238</sup> fissions in the region above the U<sup>238</sup> threshold.

In the case of a heterogeneous system, the geometric enhancement of  $\varepsilon$  must be considered separately since, even though the calculations may be of a multi-group type, it is still a homogeneous calculation in each region.

The fast-fission factor is commonly calculated for a heterogeneous system using the formula [15]

$$\varepsilon = 1 + \frac{(\nu^{28} - 1 - \alpha^{28}) \left( \frac{\bar{\Sigma}_{\text{f}}^{28}}{\Sigma_{\text{tr}}} \right) P_1}{1 - (\nu^{28} \bar{\Sigma}_{\text{f}}^{28} + \Sigma_e) \frac{P_2}{\Sigma_{\text{tr}}}}. \quad (11)$$

In Eq. (11),  $\Sigma_{tr}$  is the transport cross-section for the fuel element,  $\Sigma_e$  is the elastic-scattering cross-section and is taken to be the transport cross-section minus the sum of the capture-plus-fission-plus-inelastic cross-sections. The  $P_1$  and  $P_2$  are first- and second-generation collision probabilities [16].

Eq. (11) was used to evaluate  $\varepsilon$  for the various clustered zones of the thermal-fast D<sub>2</sub>O system. The procedure used was to homogenize the material inside the shrouds (Fig. 5) and consider the resulting mixture as constituting a large "fuel rod".  $P_1$  and  $P_2$  were taken to be equal and to have the value 0.28 [17]. The cross-sections varied slightly according to the region considered, but the resulting values of  $\varepsilon$  were sufficiently constant so that for all clustered zones  $\varepsilon$  may be taken to be 1.013. The value of  $\varepsilon$  deduced from a 2D calculation (which was homogeneous within each region) for region 4 (Fig. 2) was 1.007. The neutron inventory and breeding ratio given in Tables IX and XIII are based on the homogeneous value and hence the quoted breeding ratio slightly underestimates the correct value.

### Xenon poison effects

In the portions of the system which have an appreciable thermal flux, it is necessary to examine the effects due to the xenon poisoning. The ratio of the average equilibrium xenon absorption cross-section was calculated using the expression [18]:

$$\frac{\Sigma_{Xe}}{\Sigma_f} = \frac{y \tau_{Xe} \sigma_{Xe} \bar{\varphi}}{1 + \tau_{Xe} \sigma_{Xe} \bar{\varphi}}. \quad (12)$$

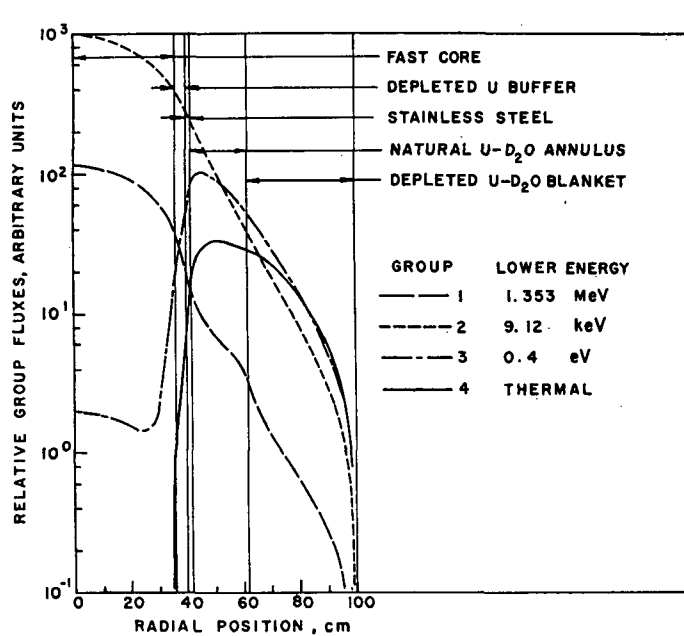
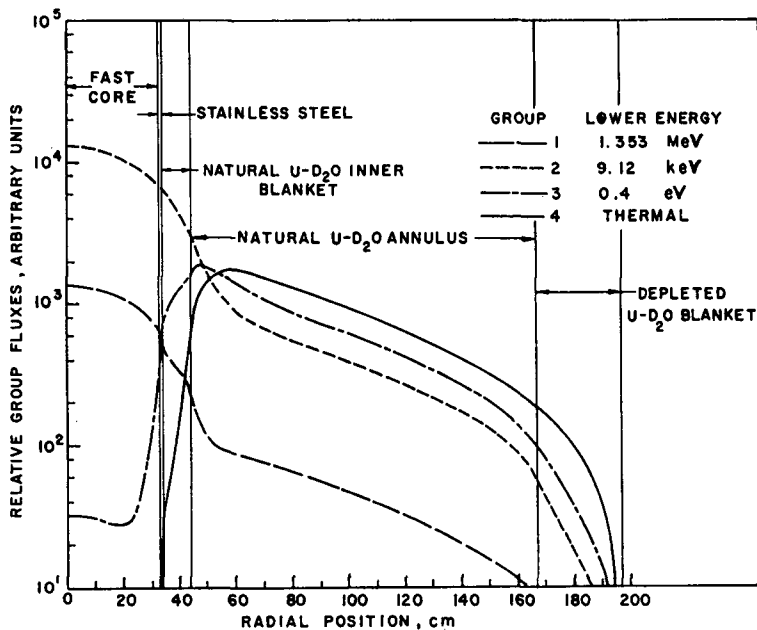
$y$  is the fission yield of Xe<sup>135</sup>,  $\tau_{Xe}$  is the mean lifetime of Xe<sup>135</sup>,  $\sigma_{Xe}$  the microscopic thermal absorption cross-section of the Xe<sup>135</sup>, and  $\bar{\varphi}$  is the volume average value of the thermal flux for the region under consideration. For the thermal-fast superheater concept,  $\bar{\varphi}$  was calculated assuming a power of 314 MW in the boiling zone (region 4 of Fig. 2). For the fast-thermal concept, a power of 40 MW was assumed for region 4 of Fig. 3. In the first case,  $\bar{\varphi}$  was calculated to be  $8.5 \times 10^{13}$  n/cm<sup>2</sup> s; for the fast-thermal system,  $\bar{\varphi}$  was found to be  $2.0 \times 10^{14}$  n/cm<sup>2</sup> s. Fluxes in the other thermal regions were calculated as above using a suitable two-dimensional problem to determine the relative thermal fluxes in the various regions.

The influence of the xenon poisoning on the breeding ratio was found to be small. In particular, the xenon captures were generally less than 4% of the U<sup>238</sup> captures in the same region. The change in breeding ratio expected would be only about 0.02 for the cases examined.

## RESULTS

### Flux and power distributions

The calculated radial flux distributions are shown in Figs. 6 through 9 for the thermal-fast and fast-thermal D<sub>2</sub>O systems, the fast-thermal H<sub>2</sub>O system, and the all-fast reference system. The corresponding power distributions are given in Figs. 10 through 13. The power flattening in the fast core typical of coupled as opposed to all-fast systems can be seen from the power distributions. The size of the power spike at the outer edge of the fast core for the coupled systems depends strongly upon the value of the thermal flux at that point. In practice, the thickness of the buffer zone would be varied to limit the size of the spike.



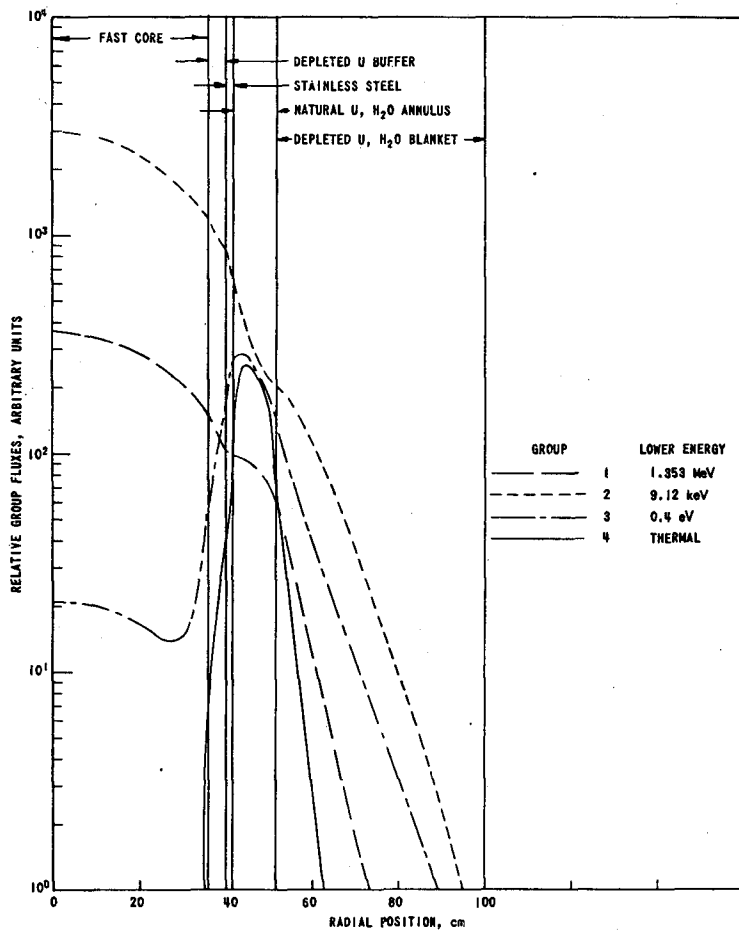


Fig. 8  
Radial flux distribution for fast-thermal  $\text{H}_2\text{O}$ -coupled steam superheater at midplane.

#### *Reactivity effects*

The magnitude of the prompt-neutron lifetime and of the coefficients of reactivity for water addition in the fast core and thermal regions are of direct interest with regard to the kinetic behaviour and safety of the coupled steam superheater concept. In addition, knowledge of the fraction of reactivity contributed by the fast part of the system is important since it determines how far the system is from being critical on the fast neutrons alone. An indication of the reactivity due to only the fast part of the system can be obtained by calculating the  $k_{\text{eff}}$  of the system when no thermal fissions are permitted. (Actually the calculated  $k_{\text{eff}}$  will be greater than the true value owing to distortion in the flux distribution due to the method of calculation [2]. The correct value may, of course, be obtained from the coupling parameters [1] of the system.)

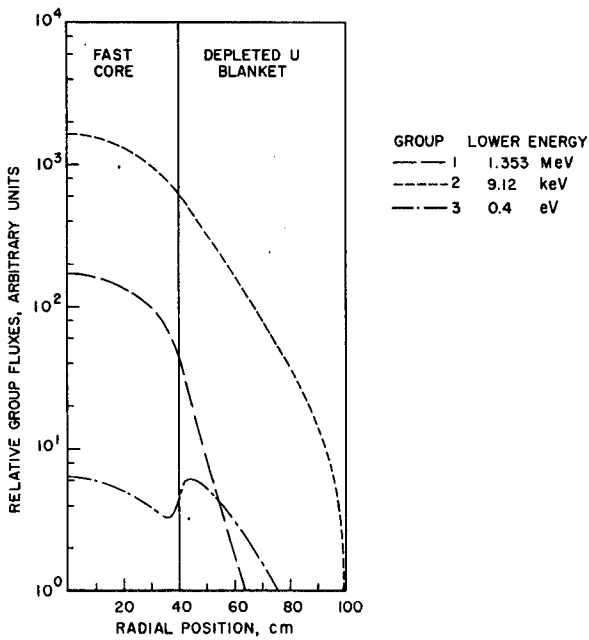


Fig. 9

Radial flux distribution for all-fast sodium-cooled reference system at midplane.

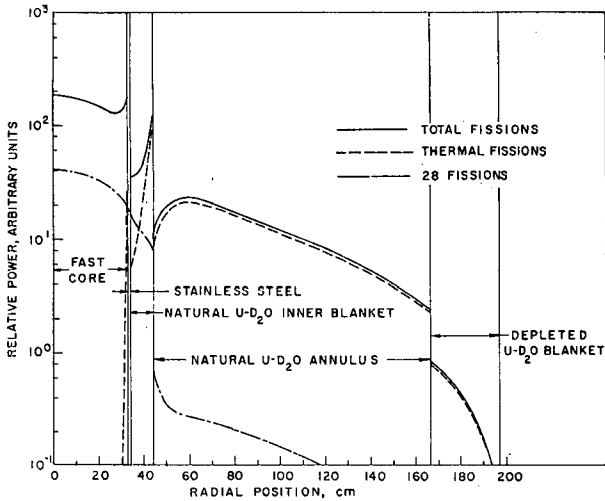


Fig. 10

Radial power distribution for thermal-fast  $D_2O$ -coupled steam superheater at midplane.

Table VIII lists the prompt-neutron lifetime, water-reactivity coefficient for fast core and thermal annulus, and  $k_{eff}$  for the case of no thermal fissions for the three-superheater reference systems. (The prompt lifetime was calculated

TABLE VIII  
REACTIVITY CHARACTERISTICS OF REFERENCE SYSTEMS

System	Prompt neutron lifetime $\mu\text{s}$	$\frac{\delta k}{k} / \left( \frac{\delta M}{M} \right)$ fast core water	$\frac{\delta k}{k} / \left( \frac{\delta M}{M} \right)$ thermal annulus water	$(k_{\text{eff}})_{\nu_{\text{thermal}} = 0}$
Thermal-fast $\text{D}_2\text{O}$	400*	0.009	—	—
Fast-thermal $\text{D}_2\text{O}$	4	0.011	0.032	0.978
Fast-thermal $\text{H}_2\text{O}$	4	0.036**	0.022	0.961

\* Obtained from system similar to thermal-fast  $\text{D}_2\text{O}$  reference system but utilizing  $\text{U}^{235}$  rather than  $\text{Pu}^{239}$  in the fast core.

\*\* Obtained from system similar to fast-thermal  $\text{H}_2\text{O}$  reference system but having the following composition in region 4 (Fig. 3): natural uranium, 45%; zirconium, 4.608%; water, 50.392%.

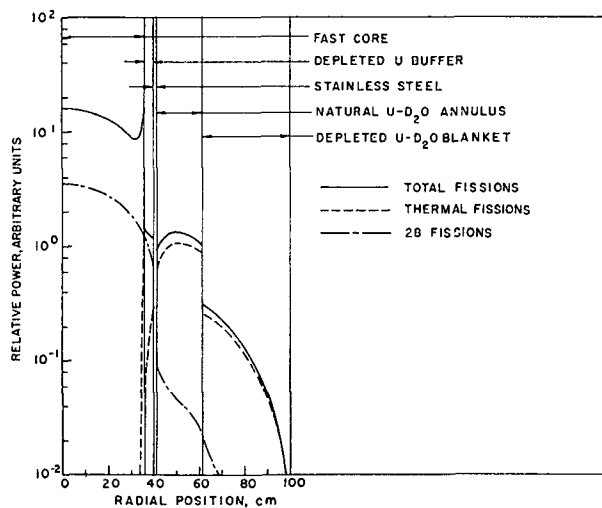


Fig. 11  
Radial power distribution for fast-thermal  $\text{D}_2\text{O}$ -coupled steam superheater at midplane.

by uniform insertion of  $1/v$  poison.) The long lifetime for the thermal-fast system is due to the large power fraction in the thermal regions and to the fact that the moderator is  $\text{D}_2\text{O}$ . The water reactivity coefficients can be used to deduce temperature coefficients of reactivity for the various systems. For example, if one assumes a constant pressure of 95 atm, for a core temperature of  $448.9^\circ\text{C}$  one obtains fast core  $(\delta k/k)/^\circ\text{C}$  (due only to water density changes) values of  $-1.8 \times 10^{-5}$ ,  $-2.2 \times 10^{-5}$ , and  $-7.2 \times 10^{-5}$  for the thermal-fast  $\text{D}_2\text{O}$ , fast-thermal  $\text{D}_2\text{O}$ , and fast-thermal  $\text{H}_2\text{O}$  systems respectively.

#### *Neutron inventories and breeding ratios*

Tables IX through XII list the neutron inventories for the three coupled systems and for the all-fast reference system. As indicated on the tables, all

TABLE IX  
NEUTRON INVENTORY FOR THERMAL-FAST D<sub>2</sub>O COUPLED STEAM SUPERHEATER

Event*	Region					
	Core	Stainless-steel tank	Inner blanket	Water annulus	Water blanket	Remaining blanket
Pu <sup>239</sup> fissions	0.271	—	—	—	—	—
Pu <sup>239</sup> captures	0.075	—	—	—	—	—
U <sup>235</sup> fissions	—	—	0.100	0.965	0.028	0.011
U <sup>235</sup> captures	—	—	0.036	0.222	0.006	0.003
U <sup>238</sup> fissions	0.076	—	0.022	0.011	0.0004	0.005
U <sup>238</sup> captures	0.269	—	0.240	1.090	0.095	0.095
D <sub>2</sub> O captures	0	—	0	0.008	0.0008	0
Zr captures	—	—	0.017	0.134	0.009	0.004
Fe captures	0.006	0.011	—	—	—	0.001

Neutrons leaking = 0.060.

\* All numbers normalized to one fission neutron in the core.

TABLE X  
NEUTRON INVENTORY FOR FAST-THERMAL D<sub>2</sub>O COUPLED STEAM SUPERHEATER

Event*	Region				
	Core	Core blanket	Stainless-steel tank	Water annulus	Annulus blanket
Pu <sup>239</sup> fissions	0.277	—	—	—	—
Pu <sup>239</sup> captures	0.073	—	—	—	—
U <sup>235</sup> fissions	—	0.005	—	0.066	0.036
U <sup>235</sup> captures	—	0.002	—	0.019	0.009
U <sup>238</sup> fissions	0.074	0.013	—	0.002	0.001
U <sup>238</sup> captures	0.238	0.132	—	0.126	0.169
D <sub>2</sub> O captures	0	0	—	0.0001	0.0003
Zr captures	—	—	—	0.0004	0.0007
Fe captures	0.005	0.006	0.031	—	—

Neutrons leaking = 0.044.

\* All numbers normalized to one fission neutron in the core.

numbers are normalized to one fission neutron in the fast core. It can be seen that the zirconium captures for the case of the thermal-fast D<sub>2</sub>O system represent a serious parasitic loss. For the fast-thermal systems, the zirconium is not an important parasitic agent, although for these cases the stainless-steel separator is seen to have a more serious effect on the inventory than on the boiling reference system. In all cases, the number of neutrons leaking from the system could be reduced by increasing blanket thicknesses.

Table XIII compares the various references systems. The fast-thermal D<sub>2</sub>O and H<sub>2</sub>O systems are seen to have similar breeding ratios; the greater parasitic

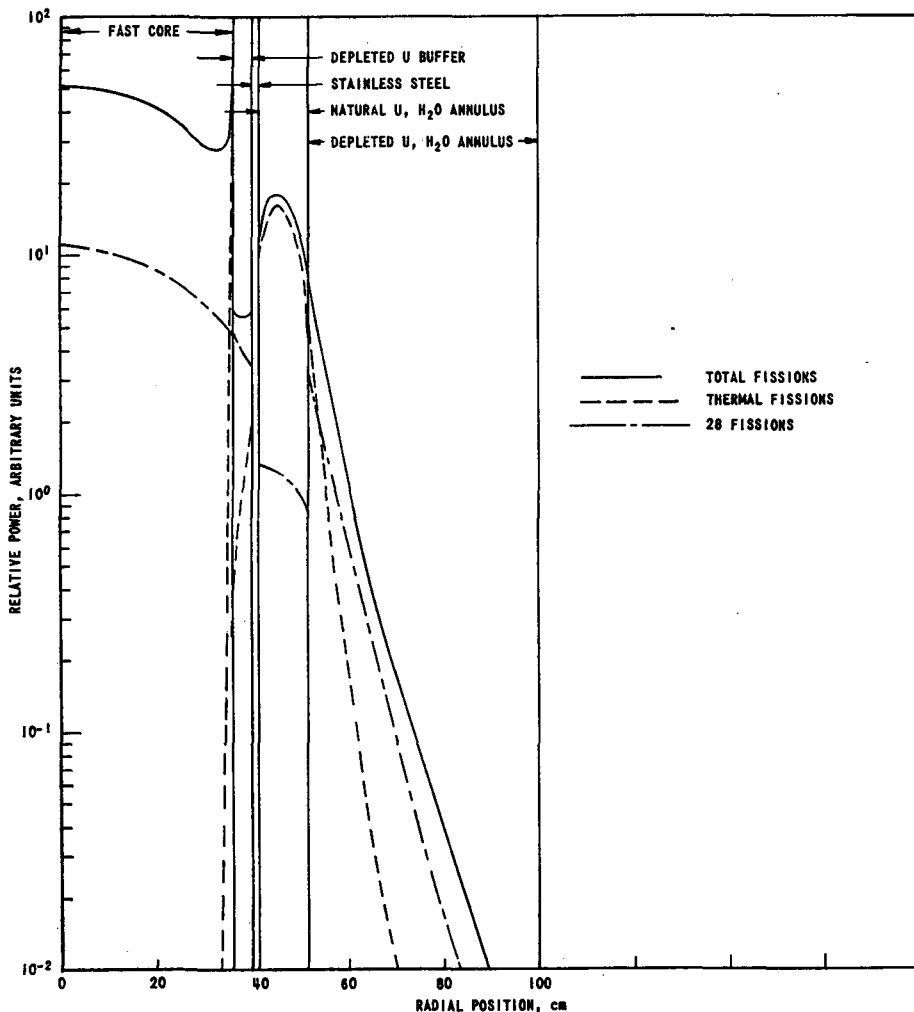


Fig. 12  
Radial power distribution for fast-thermal  $H_2O$ -coupled steam superheater at midplane.

loss of the  $H_2O$  as compared with the  $D_2O$  is compensated by the smaller leakage in the  $H_2O$  system.

#### CONCLUSIONS ON PRELIMINARY CALCULATIONS

Although the systems considered in these survey studies have not been optimized, the results obtained indicate that it should be possible to achieve a large breeding ratio for a coupled fast-thermal reactor using as coolants either light or heavy water in the thermal regions and light or heavy water steam in the fast regions. The large breeding ratio can be realized because of the small water density in the fast core and large fast-power fraction.

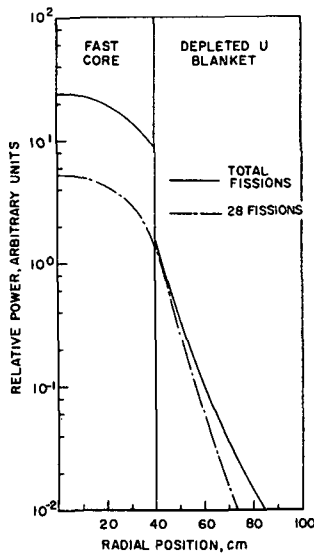


Fig. 13

Radial power distribution for all-fast sodium-cooled reference system at midplane.

TABLE XI  
NEUTRON INVENTORY FOR FAST-THERMAL H<sub>2</sub>O REFERENCE SYSTEM

Event*	Region				
	Core	Core blanket	Stainless-steel tank	Water annulus	Annulus blanket
Pu <sup>239</sup> fissions	0.269	—	—	—	—
Pu <sup>239</sup> captures	0.077	—	—	—	—
U <sup>235</sup> fissions	—	0.006	—	0.107	0.022
U <sup>235</sup> captures	—	0.002	—	0.025	0.008
U <sup>238</sup> fissions	0.076	0.016	—	0.008	0.019
U <sup>238</sup> captures	0.234	0.123	—	0.137	0.231
H <sub>2</sub> O captures	0	0	—	0.032	0.0009
Zr captures	—	—	—	0.0006	0.001
Fe captures	0.005	0.007	0.038	—	—

Neutrons leaking = 0.004.

\* All numbers normalized to one fission neutron in the core.

The breeding ratio in the light-water system is not appreciably different from that of a corresponding heavy-water system, because the smaller neutron leakage in the light-water system compensates for the greater parasitic loss. The parasitic loss in the external region of the light-water system is minimized by the use of a high fuel density.

TABLE XII  
NEUTRON INVENTORY FOR ALL-FAST REFERENCE SYSTEM

Event*	Region		Event*	Region	
	Core	Blanket		Core	Blanket
Pu <sup>239</sup> fissions	0.273	—	U <sup>238</sup> fissions	0.077	0.018
Pu <sup>239</sup> captures	0.070	—	U <sup>238</sup> captures	0.281	0.305
U <sup>235</sup> fissions	—	0.006	Na captures	0.0004	0.0007
U <sup>235</sup> captures	—	0.002	Fe captures	0.006	0.007

Neutrons leaking = 0.030.

\* All numbers normalized to one fission neutron in the core.

TABLE XIII  
COMPARISON OF SUPERHEATERS AND THE FAST REFERENCE SYSTEM

System	Core volume (l)	Critical mass (kg)	Fraction of power in thermal fissions	Neutrons leaking*	Initial breeding ratio**
Thermal-fast D <sub>2</sub> O superheater	402	285	0.669	0.060	1.07
Fast-thermal D <sub>2</sub> O superheater	326	275	0.200	0.044	1.53
Fast-thermal H <sub>2</sub> O superheater	326	251	0.230	0.004	1.52
All-fast reference	402	293	0	0.030	1.71

\* Normalized to one fission neutron in the core.

\*\* Not counting U<sup>235</sup> burned in depleted uranium.

## 2. Physics analysis of a conceptual design

### REFERENCE SYSTEM

Fig. 14 shows a schematic drawing of a system based on engineering considerations so that the dimensions and compositions of the various regions correspond to a possible practical concept. In particular, oxide fuel is used except in the outer thermal reflectors in contrast to the assumption of metal fuel in the previous survey studies.

The regional compositions are given in Table XIV in terms of the volume fractions of the various constituents. The thermal-zone fuel is assumed to be contained in a hexagonal array of zirconium pressure tubes having an inside diameter of 8.38 cm and an outside diameter of 9.65 cm. The interstices formed by the tubes are filled with zirconium filler rods. The details of the thermal-region fuel in the zirconium pressure tubes are given in Table XV.

A realistic system would presumably have a physical divider between the steam zones and water zones (e.g. at a radial position of 40 cm in Fig. 14). For the present physics calculations, such a divider has been ignored although later

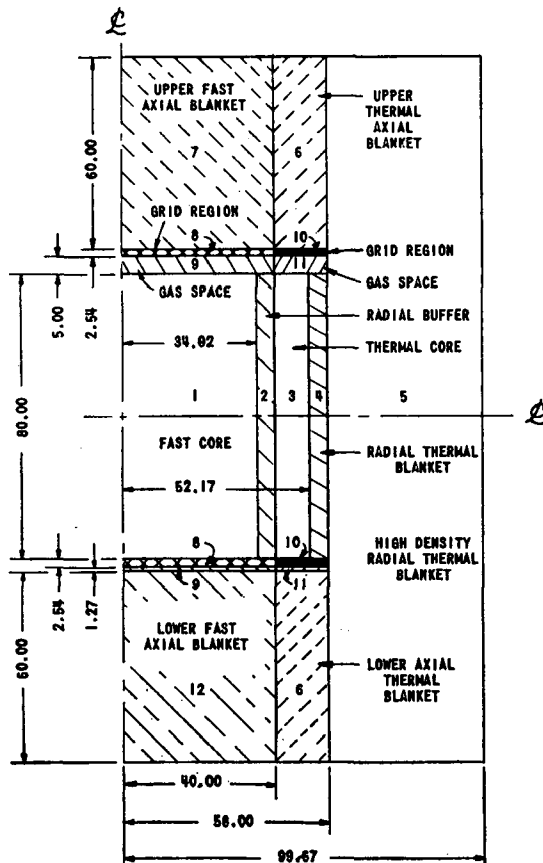


Fig. 14  
Schematic drawing of conceptual design.

(e.g. in Tables XVIII and XIX) the estimated influence of an assumed 0.635-cm stainless-steel divider on the breeding ratio and neutron inventory has been included.

#### CALCULATIONAL PROCEDURES AND CROSS-SECTIONS

The system was examined in cylindrical geometry using 13-group, one-dimensional diffusion theory and 4-group, two-dimensional diffusion theory. Previous calculations [2] have indicated that at the axial midplane, 4-group calculations of flux and power distributions in one and two-dimensions were in excellent agreement for liquid-metal-cooled coupled systems. If we assume such agreement to carry over to the present concept, the 13-group, 1D and 4-group, 2D results may be compared to indicate the extent to which the few-group calculation can reproduce the many-group results.

Table XVI gives the 13-group macroscopic cross-sections. The Pu, Fe, H<sub>2</sub>O and O cross-sections were obtained using the spectrum appropriate to the steam-cooled oxide fast core. The U<sup>238</sup>, U<sup>235</sup> and zirconium cross-sections were obtained

TABLE XIV  
REGIONAL COMPOSITIONS FOR CONCEPTUAL DESIGN

Region	Volume fraction						
	PuO <sub>2</sub>	U <sup>238</sup> O <sub>2</sub>	U <sup>235</sup> O <sub>2</sub>	Depleted U*	Fe	Zr	H <sub>2</sub> O**
1	0.08556	0.37369	0.00075	—	0.156	—	0.014131
2	—	0.42016	0.00084	—	0.157	—	0.01553
3	—	0.29456	0.00214	—	—	0.4151†	0.2087
4	—	0.29611	0.00059	—	—	0.4151†	0.2087
5	—	—	—	0.3715	—	0.4372††	0.1350
6	—	—	—	0.2967	—	0.4151†	0.2087
7	—	0.42016	0.00084	—	0.157	—	0.02245
8	—	—	—	—	0.616	—	0.014131
9	—	—	—	—	0.156	—	0.014131
10	—	—	—	—	—	0.7118	0.2087
11	—	—	—	—	—	0.4151	0.2087
12	—	0.42016	0.00084	—	0.157	—	0.01084

\* 99.8 % U<sup>238</sup>.

\*\* Equivalent water of normal density.

† Volume fraction of Zr in clad is 0.0878.

†† Volume fraction of Zr in clad is 0.1098.

TABLE XV  
THERMAL REGION FUEL DATA FOR CONCEPTUAL DESIGN

	Region			
	3	4	5	6
Fuel	Natural UO <sub>2</sub>	Depleted UO <sub>2</sub>	Depleted U metal	Depleted UO <sub>2</sub>
Rod outer diameter (cm)	0.544	0.544	2.710	0.544
Clad	Zirconium	Zirconium	Zirconium	Zirconium
Clad thickness (cm)	0.033	0.033	0.165	0.033
Rod pitch (hexagonal)	0.645	0.645	2.774	0.645
Number of rods per pressure tube	139	139	7	139
Water volume fraction inside pressure tubes*	0.2079	0.2079	0.1342	0.2079

\* Equivalent normal density water.

using 1/E weighting. The same H<sub>2</sub>O cross-sections were used for the steam-cooled regions and for the water zones since the "age" to 0.4 eV calculated using these cross-sections (34.1 cm<sup>2</sup>) is in close enough agreement with experiment for the present conceptual study. The UO<sub>2</sub> density has been taken to be 10.2 g/cm<sup>3</sup>; the PuO<sub>2</sub> density is taken to be 10.5 g/cm<sup>3</sup>.

TABLE XVI  
13-GROUP MACROSCOPIC CROSS-SECTIONS  
(cm<sup>-1</sup>)

<i>j</i>	Lower energy, <i>E<sub>L</sub></i>	Fission spectrum	Pu <sup>239</sup> O <sub>2</sub>								U <sup>238</sup> O <sub>2</sub>								
			$\Sigma_f$	$\nu$	$\Sigma_c$	$3\Sigma_{tr}$	$\Sigma_{j \rightarrow j+1}$	$\Sigma_{j \rightarrow j+2}$	$\Sigma_{j \rightarrow j+3}$	$\Sigma_{j \rightarrow j+4}$	$\Sigma_f$	$\nu$	$\Sigma_c$	$3\Sigma_{tr}$	$\Sigma_{j \rightarrow j+1}$	$\Sigma_{j \rightarrow j+2}$	$\Sigma_{j \rightarrow j+3}$	$\Sigma_{j \rightarrow j+4}$	
1	1.353 MeV	0.575	0.0466	3.2	0.0028	0.5365	0.0206	0.0045	0.0012	0.0004	0.0121	2.8	0.0023	0.5113	0.0395	0.0102	0.0028	0.0009	
2	0.4979 MeV	0.301	0.0405	2.99	0.0023	0.8896	0.0348	0.0038	0.0009	0.0003	0	0	0.0027	0.8294	0.0408	0.0056	0.0014	0.0004	
3	0.1832 MeV	0.091	0.0384	2.93	0.0047	1.2737	0.0383	0.0026	0.0008	0	0	0	0.0036	1.1301	0.0376	0.0025	0.0008	0	
4	0.0674 MeV	0.025	0.0401	2.91	0.0105	1.2308	0.0216	0.0011	0	0	0	0	0.0057	1.0744	0.0214	0.0010	0	0	
5	0.0248 MeV	0.006	0.0480	2.9	0.0179	1.4125	0.0164	0	0	0	0	0	0.0080	1.2796	0.0167	0	0	0	
6	0.00912 MeV	0.002	0.0559	2.9	0.0261	1.5523	0.0168	0	0	0	0	0	0.0114	1.3480	0.0171	0	0	0	
7	0.00335 MeV	0	0.0596	2.9	0.0326	1.7114	0.0174	0	0	0	0	0	0.0125	1.3874	0.0176	0	0	0	
8	1234 eV	0	0.0785	2.9	0.0480	1.7603	0.0193	0	0	0	0	0	0.0137	1.4558	0.0195	0	0	0	
9	454 eV	0	0.1153	2.9	0.0774	1.2431	0.0141	0	0	0	0	0	0.0148	1.4558	0.0161	0	0	0	
10	200 eV	0	0.1890	2.9	0.1417	2.3824	0.0155	0	0	0	0	0	0.0160	1.5242	0.0170	0	0	0	
11	6 eV	0	0.4380	2.9	0.3504	3.9901	0.0014	0	0	0	0	0	0	0.0342	1.2848	0.0017	0	0	0
12	0.4 eV	0	0.5275	2.9	0.3430	3.7874	0.0009	0	0	0	0	0	0	0.0087	1.1138	0.0014	0	0	0
13	thermal (273.89 °C)	0	15.6652	2.9	7.9428	72.054	0	0	0	0	0	0	0	0.0401	1.2310	0	0	0	0

$n = 0.0233 \times 10^{24}$  mol./cm<sup>3</sup>

$n = 0.0228 \times 10^{24}$  mol./cm<sup>3</sup>

<i>j</i>	Fe				H <sub>2</sub> O*								Zr						
	$\Sigma_c$	$3\Sigma_{tr}$	$\Sigma_{j \rightarrow j+1}$	$\Sigma_{j \rightarrow j+2}$	$\Sigma_c$	$3\Sigma_{tr}$	$\Sigma_{j \rightarrow j+1}$	$\Sigma_{j \rightarrow j+2}$	$\Sigma_{j \rightarrow j+3}$	$\Sigma_{j \rightarrow j+4}$	$\Sigma_{j \rightarrow j+5}$	$\Sigma_{j \rightarrow j+6}$	$\Sigma_c$	$3\Sigma_{tr}$	$\Sigma_{j \rightarrow j+1}$	$\Sigma_{j \rightarrow j+2}$	$\Sigma_{j \rightarrow j+3}$	$\Sigma_{j \rightarrow j+4}$	
1	0.0002	0.5436	0.0594	0.0023	0.0008	0.0010	0.3085	0.0665	0.0230	0.0084	0.0031	0.0011	0.0008	0.0008	0.3825	0.0241	0.0072	0.0020	0.0006
2	0.0003	0.5269	0.0158	0.0027	0.0016	0	0.6887	0.1586	0.0528	0.0194	0.0071	0.0026	0.0017	0.0008	0.6375	0.0137	0.0026	0.0006	0.0002
3	0.0004	0.8011	0.0082	0	0	0	1.0271	0.2343	0.0793	0.0292	0.0108	0.0039	0.0027	0.0008	1.0200	0.0106	0.0008	0.0002	0
4	0.0007	0.8755	0.0096	0	0	0	1.1389	0.3375	0.1198	0.0441	0.0162	0.0059	0.0035	0.0008	1.0840	0.0080	0	0	0
5	0.0009	1.1194	0.0131	0	0	0	1.4150	0.4279	0.1536	0.0563	0.0208	0.0067	0.0053	0.0008	1.0200	0.0075	0	0	0

6	0.0011	0.8802	0.0103	0	0	0	1.5686	0.4886	0.1752	0.0646	0.0210	0.0160	0.0005	0.0008	0.8925	0.0065	0	0	
7	0.0005	1.8869	0.0165	0	0	0.0001	1.6742	0.5110	0.1843	0.0600	0.0458	0.0014	0.0001	0.0008	0.8925	0.0065	0	0	
8	0.0008	1.6366	0.0160	0	0	0.0001	1.7009	0.5405	0.1719	0.1313	0.0038	0.0004	0	0.0008	0.8288	0.0061	0	0	
9	0.0014	2.3171	0.0182	0	0	0.0001	1.7009	0.4524	0.3379	0.0098	0.0008	0	0	0.0008	0.7650	0.0056	0	0	
10	0.0022	2.6536	0.0209	0	0	0.0002	1.7009	0.8396	0.0239	0.0018	0	0	0	0.0008	0.8925	0.0080	0	0	
11	0.0049	2.6618	0.0018	0	0	0.0005	1.7343	0.1727	0.0122	0	0	0	0	0.0008	0.7778	0.0017	0	0	
12	0.0243	2.7200	0.0013	0	0	0.0023	1.7677	0.2624	0	0	0	0	0	0.0010	0.7778	0.0013	0	0	
13	0.1556	3.1138	0	0	0	0.0140	4.8148	0	0	0	0	0	0	0.0050	0.7828	0	0	0	
	$n = 0.0848 \times 10^{24} \text{ atoms/cm}^3$				$n = 0.0334 \times 10^{24} \text{ mol./cm}^3$				$n = 0.0425 \times 10^{24} \text{ atoms/cm}^3$										

<i>j</i>	$\text{U}^{235}\text{O}_2$						Depleted U						$\frac{10^7}{\nu}$				
	$\Sigma_f$	$\nu$	$\Sigma_e$	$3\Sigma_{tr}$	$\Sigma_f$	$\nu$	$\Sigma_e$	$3\Sigma_{tr}$	$\Sigma_f$	$\nu$	$\Sigma_e$	$3\Sigma_{tr}$					
1	0.0299	2.8	0.0038	0.5296	0.0317	0.0078	0.0022	0.0007	0.0255	2.8	0.0019	0.6625	0.0715	0.0214	0.0060	0.0019	0.0045
2	0.0276	2.54	0.0033	0.8712	0.0411	0.0056	0.0014	0.0004	0.0001	2.54	0.0058	0.7201	0.0437	0.0117	0.0028	0.0008	0.0081
3	0.0322	2.46	0.0124	1.1745	0.0377	0.0025	0.0008	0	0.0001	2.46	0.0077	0.9361	0.0242	0.0053	0.0016	0	0.0133
4	0.0391	2.44	0.0094	1.1835	0.0214	0.0010	0	0	0.0002	2.44	0.0120	1.2961	0.0108	0.0022	0	0	0.0219
5	0.0506	2.43	0.0152	1.2908	0.0164	0	0	0	0.0002	2.43	0.0168	1.7280	0.0047	0	0	0	0.0361
6	0.0690	2.42	0.0242	1.4288	0.0168	0	0	0	0.0003	2.42	0.0240	1.8723	0.0050	0	0	0	0.0596
7	0.1035	2.42	0.0414	1.6066	0.0172	0	0	0	0.0004	2.42	0.0265	1.8729	0.0050	0	0	0	0.0982
8	0.1495	2.42	0.0673	1.8136	0.0190	0	0	0	0.0006	2.42	0.0290	2.0174	0.0054	0	0	0	0.1620
9	0.1955	2.42	0.0880	2.4346	0.0167	0	0	0	0.0008	2.42	0.0315	2.0200	0.0054	0	0	0	0.2670
10	0.3220	2.42	0.1610	3.1246	0.0178	0	0	0	0.0013	2.42	0.0342	2.1667	0.0070	0	0	0	0.4200
11	0.9200	2.42	0.4600	5.3326	0.0018	0	0	0	0.0038	2.42	0.0738	1.6728	0.0012	0	0	0	1.3900
12	0.9200	2.42	0.4600	5.3326	0.0015	0	0	0	0.0058	2.42	0.0211	1.3222	0.0013	0	0	0	4.8320
13	8.1073	2.42	1.5017	30.0703	0	0	0	0	0.0338	2.42	0.0906	1.5533	0	0	0	0	29.4920
	$n = 0.0230 \times 10^{24} \text{ mol./cm}^3$						$n = 0.048 \times 10^{24} \text{ atoms/cm}$										

\* The calculated age to 0.4 eV is 34.1 cm<sup>2</sup>.

TABLE XVII  
4-GROUP MACROSCOPIC CROSS-SECTIONS  
(cm<sup>-1</sup>)

<i>j</i>	Lower energy, <i>E<sub>L</sub></i>	Fission spectrum	Pu <sup>239</sup> O <sub>2</sub>					U <sup>238</sup> O <sub>2</sub>						
			$\Sigma_f$	$\nu$	$\Sigma_c$	$3\Sigma_{tr}$	$\Sigma_{j \rightarrow j+1}$	$\Sigma_f$	$\nu$	$\Sigma_c$	$3\Sigma_{tr}$	$\Sigma_{j \rightarrow j+1}$		
1	1.353 MeV	0.575	0.0466	3.2	0.0028	0.5365	0.0267	0.0121	2.8	0.0023	0.5113	0.0535		
2	9.12 keV	0.425	0.0425	2.93	0.0095	1.2088	0.0016	0	0	0.0056	1.0938	0.0023		
3	0.4 eV	0	0.1154	2.9	0.0772	1.8645	0.00002	0	0	0.0182	1.3194	0.0004		
4	thermal (273.89 °C)	0	15.6652	2.9	7.9428	72.054	0	0	0	0.0401	1.2310	0		
$n = 0.0233 \times 10^{24} \text{ mol./cm}^3$														
<i>j</i>	U <sup>235</sup> O <sub>2</sub>					Fe			H <sub>2</sub> O*			H <sub>2</sub> O**		
	$\Sigma_f$	$\nu$	$\Sigma_c$	$3\Sigma_{tr}$	$\Sigma_{j \rightarrow j+1}$	$\Sigma_e$	$3\Sigma_{tr}$	$\Sigma_{j \rightarrow j+1}$	$\Sigma_c$	$3\Sigma_{tr}$	$\Sigma_{j \rightarrow j+1}$	$\Sigma_e$	$3\Sigma_{tr}$	$\Sigma_{j \rightarrow j+1}$
1	0.0299	2.8	0.0038	0.5296	0.0424	0.0002	0.5436	0.0625	0.0010	0.3085	0.1021	0.0010	0.3085	0.1021
2	0.0404	2.45	0.0114	1.1503	0.0023	0.0006	0.8019	0.0010	0	1.0740	0.1317	0	1.0902	0.1572
3	0.5710	2.42	0.2820	3.8393	0.0004	0.0016	2.0202	0.00003	0.0002	1.6932	0.0067	0.0009	1.7276	0.0839
4	8.1073	2.42	1.5017	30.0703	0	0.1556	3.1138	0	0.0140	4.8148	0	0.0140	4.8148	0
$n = 0.0230 \times 10^{24} \text{ mol./cm}^3$					$n = 0.0848 \times 10^{24} \text{ atoms/cm}^3$			$n = 0.0334 \times 10^{24} \text{ mol./cm}^3$			$n = 0.0334 \times 10^{24} \text{ mol./cm}^3$			
<i>j</i>	Zr				Depleted U									
	$\Sigma_c$	$3\Sigma_{tr}$		$\Sigma_{j \rightarrow j+1}$	$\Sigma_f$	$\nu$	$\Sigma_c$	$3\Sigma_{tr}$	$\Sigma_{j \rightarrow j+1}$	$\Sigma_c$	$3\Sigma_{tr}$	$\Sigma_{j \rightarrow j+1}$		
1	0.0008	0.3825		0.0340	0.0255	2.8	0.0019	0.6625		0.6625		0.1008		
2	0.0008	0.9152		0.0009	0.0002	2.46	0.0116	1.1954		1.1954		0.0007		
3	0.0009	0.8088		0.0003	0.0032	2.42	0.0396	1.7049		1.7049		0.0004		
4	0.0050	0.7828		0	0.0338	2.42	0.0906	1.5533		1.5533		0		
$n = 0.0425 \times 10^{24} \text{ atoms/cm}^3$					$n = 0.048 \times 10^{24} \text{ atoms/cm}^3$									

\* For use in steam regions. The calculated age to 0.4 eV is 110.4 cm<sup>2</sup>.

\*\* For use in water regions. The calculated age to 0.4 eV is 30.7 cm<sup>2</sup>.

An iterative procedure was used for the cross-sections appropriate to the steam-cooled oxide fast core. The assumed cross-sections were used to generate fundamental mode fluxes which were then used to modify the original cross-sections. The cross-sections presented in Table XVI are the result of two such iterations.

The 4-group set given in Table XVII was obtained by collapsing the 13-group set using the spectra given by the 13-group, 1D calculation. The spectrum in the fast core (region 1, Fig. 14) was used to collapse the  $\text{PuO}_2$  and  $\text{H}_2\text{O}$  cross-sections. The 4-group depleted-U values were obtained using the spectrum of the high-density, radial-thermal blanket (region 5). In the 4-group case, two water sets were required, since the "age" to 0.4 eV calculated for the  $\text{H}_2\text{O}$  cross-sections to be used in the steam zones ( $110.4 \text{ cm}^2$ ) is unrealistically large for  $\text{H}_2\text{O}$  to be used in the thermal zones. The thermal-core (region 3) spectrum was used to obtain the  $\text{H}_2\text{O}$  cross-sections for use in the thermal zones. These cross-sections yield a calculated "age" to 0.4 eV of  $30.7 \text{ cm}^2$ .

The  $\text{U}^{238}$  effective resonance integrals in the water regions were obtained using Eq. (5) in the case of the high-density, radial thermal blanket (region 5) and using the equation:

$$I_{\text{eff}}^{28} = 11.6 + 22.8 \frac{S_{\text{eff}}}{M} \quad (13)$$

for the water-cooled oxide regions 3, 4, and 6. A Dancoff-Ginsburg calculation [8, 9] was used in determining  $S_{\text{eff}}$ . In the steam zones, the homogeneous formula

$$I_{\text{eff}}^{28} = 3.8 \left( \frac{10^{24} \Sigma_s}{N_U} \right)^{0.42} \quad (14)$$

was used, where  $\Sigma_s$  is the homogenized resonance-group-scattering cross-section, and  $N_U$  is the number of  $\text{U}^{238}$  nuclei per cubic centimeter.

In the 13-group set, group 11 was taken to be the resonance group so that

$$\Sigma_{11}^{\text{removal}} = p_{11} \Sigma_{a11} \quad (15)$$

in analogy with the 4-group equivalent  $p \Sigma_{a3} = \Sigma_{3 \rightarrow 4}$  given in Section 1. The resonance-group-capture cross-sections ( $\sigma_{c11}$  or  $\sigma_{c3}$  in the 13- and 4-group cases) were adjusted for each region so that when combined with the other group capture cross-sections as

$$\sum_{j=1}^{k-1} \Delta_{uj} \sigma_{cj},$$

the total effective resonance integral was obtained ( $k$  is the number of groups and  $\Delta_{uj}$  the group lethargy widths). For materials other than  $\text{U}^{238}$ , infinite dilution resonance integrals were assumed [13]. The resonance-escape probability was calculated using Eq. (3) and the appropriate part of the total effective resonance integral corresponding to the resonance group ( $\Delta_{u11} \sigma_{c11}$  or  $\Delta_{u3} \sigma_{c3}$  in the 13- and 4-group cases). The total  $p$  was taken, as in Section 1, to be the product of the escape probabilities for the various materials in the region.

Diffusion-theory cell calculations in the water regions indicate a thermal-disadvantage factor within 2% of unity. In addition, it was found that the disadvantage factor is insensitive to the value of the cell "fuel zone" absorption cross-section. Variations of the absorption cross-section by a factor of 2 resulted

TABLE XVIII  
SUMMARY OF CONCEPTUAL DESIGN CHARACTERISTICS

Core volume	Critical mass $\text{PuO}_2$	Fraction of power in thermal fissions	Neutron leakage*	Initial breeding ratio**
306.5 l	275.0 kg	0.213	0.006	1.44

\* Normalized to one fission neutron in the fast core.  
 \*\* Not counting  $\text{U}^{235}$  burned in depleted uranium and including the estimated effect of the stainless-steel separator and the Xe-poisoning in the thermal core.

TABLE XIX  
NEUTRON INVENTORY FOR CONCEPTUAL DESIGN

Event *	Region							
	Fast core	Radial buffer	Fast axial blankets	Stainless separator	Thermal core	Radial thermal blankets	High den- sity radial thermal blankets	Thermal axial blankets
$\text{Pu}^{239}$ fissions ..	0.292	—	—	—	—	—	—	—
$\text{Pu}^{239}$ captures ..	0.086	—	—	—	—	—	—	—
$\text{U}^{235}$ fissions ..	0.004	0.003	0.002	—	0.067	0.007	0.024	0.010
$\text{U}^{235}$ captures ..	0.002	0.001	0.0008	—	0.015	0.002	0.006	0.002
$\text{U}^{238}$ fissions ..	0.045	0.006	0.003	—	0.008	0.002	0.008	0.002
$\text{U}^{238}$ captures ..	0.200	0.055	0.056	—	0.128	0.042	0.131	0.054
Fe captures ..	0.007	0.008	0.003	~0.019	—	—	—	—
Zr captures ..	—	—	—	—	0.013	0.004	0.007	0.003
$\text{H}_2\text{O}$ captures ..	0.0002	0.0001	0	—	0.011	0.005	0.003	0.003

Event *	Region			
	Fast grid regions	Fast gas spaces	Thermal grid regions	Thermal gas spaces
$\text{Pu}^{239}$ fissions ..	—	—	—	—
$\text{Pu}^{239}$ captures ..	—	—	—	—
$\text{U}^{235}$ fissions ..	—	—	—	—
$\text{U}^{235}$ captures ..	—	—	—	—
$\text{U}^{238}$ fissions ..	—	—	—	—
$\text{U}^{238}$ captures ..	—	—	—	—
Fe captures ..	0.003	0.001	—	—
Zr captures ..	—	—	0.001	0.0009
$\text{H}_2\text{O}$ captures ..	0	0	0.0007	0.0009

Neutrons leaking = 0.006

\* All numbers normalized to one fission neutron in the fast core.

in less than 0.1% change in the thermal-disadvantage factor. The thermal cross-sections were therefore obtained by simple homogenizing assuming a unit disadvantage factor.

The calculated ratio of xenon- to  $U^{238}$ -captures in region 3 was less than 0.03. The initial breeding ratio quoted in Table XVIII includes the estimated effect of the parasitic xenon captures.

The fast effect due to the geometric clustering of the pressure tubes is expected to be small, since the region between the tubes is almost all zirconium. Eq. (10)

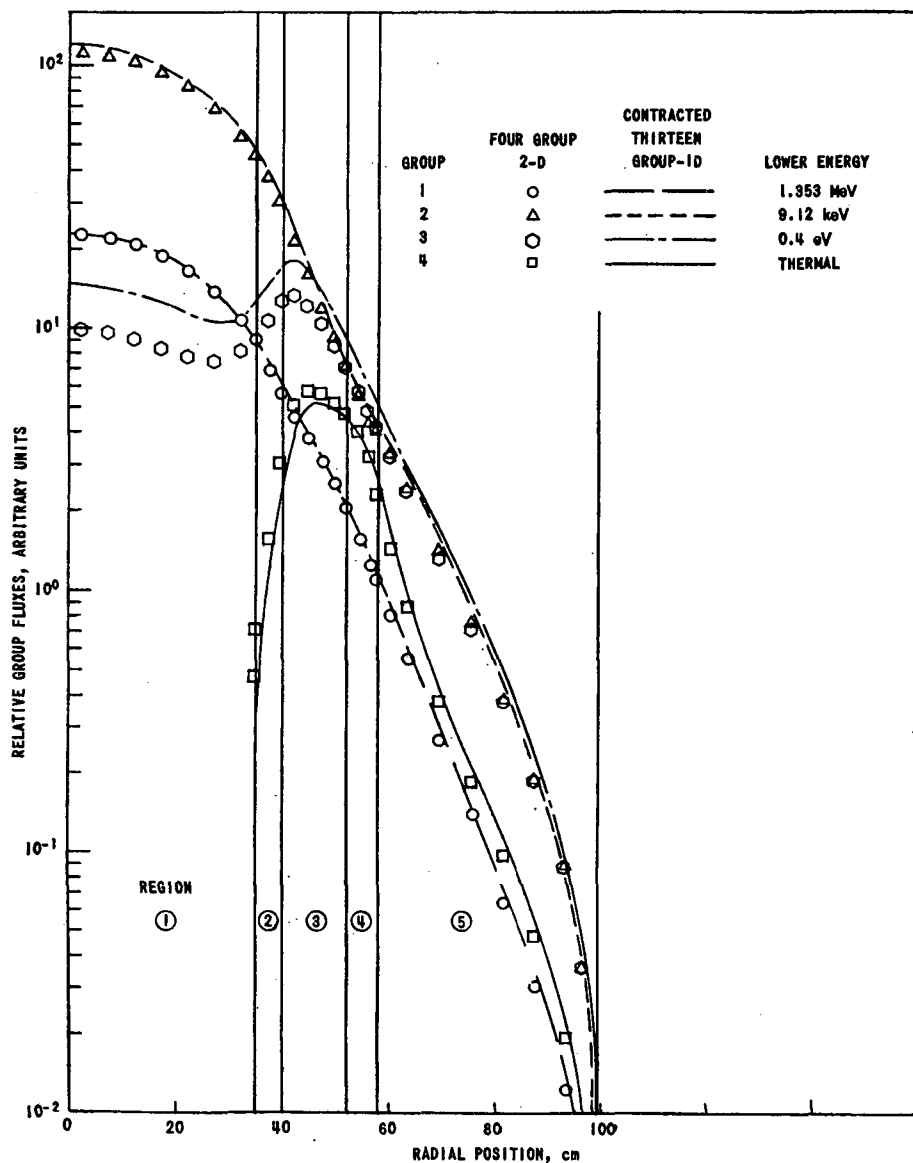


Fig. 15  
4-group, 2D, and contracted 13-group, 1D radial flux distributions at midplane.

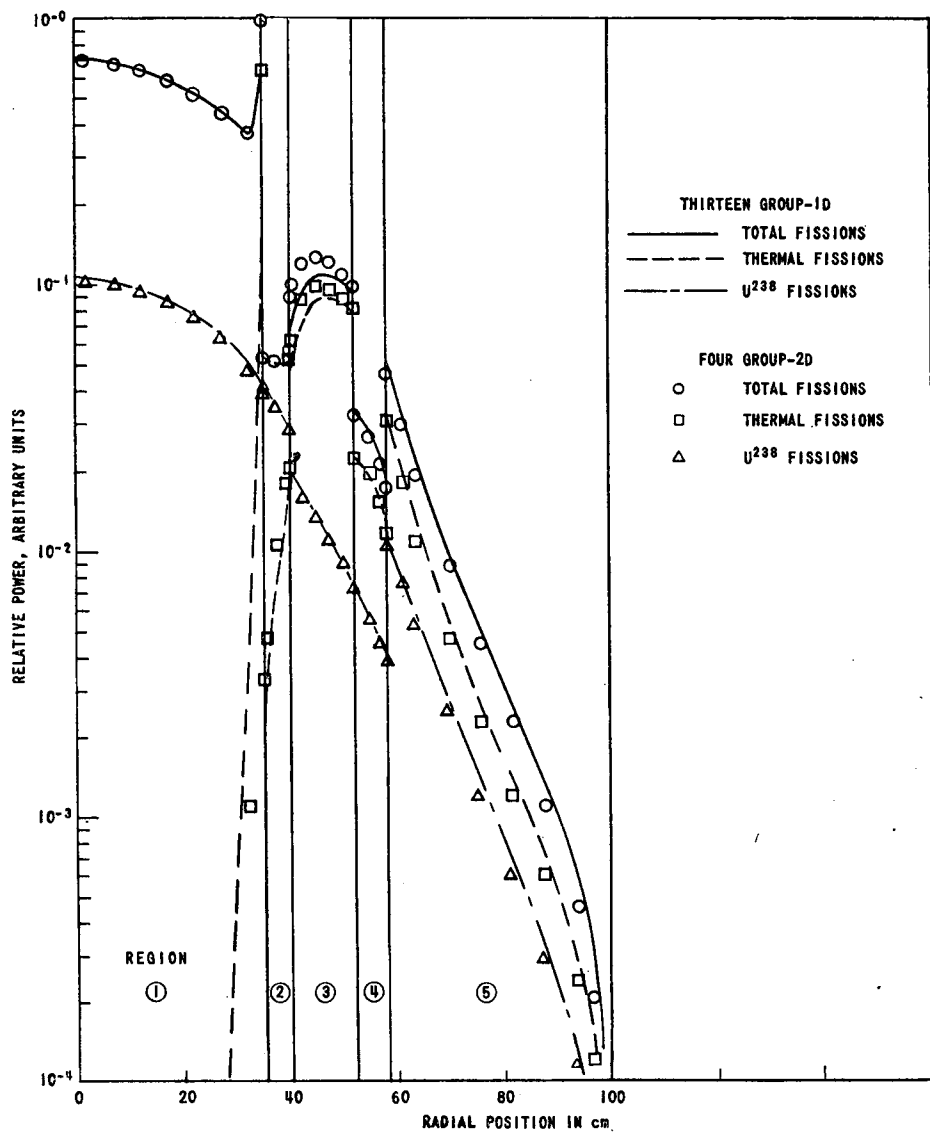


Fig. 16  
Comparison of 4-group and 13-group power distributions at midplane.

was used to calculate  $\varepsilon$  for a mixture having the composition of the contents of a pressure tube and for a mixture corresponding to homogenizing the entire pressure-tube region. The calculated values of  $\varepsilon$  for the thermal core were respectively 1.091 and 1.070. The correct value would be expected to lie within these two limiting values. The value deduced from the 2D calculation for the thermal core (region 3) was 1.083. The neutron inventory and quoted initial breeding ratio given in Tables XVIII and XIX are based on the 2D calculation.

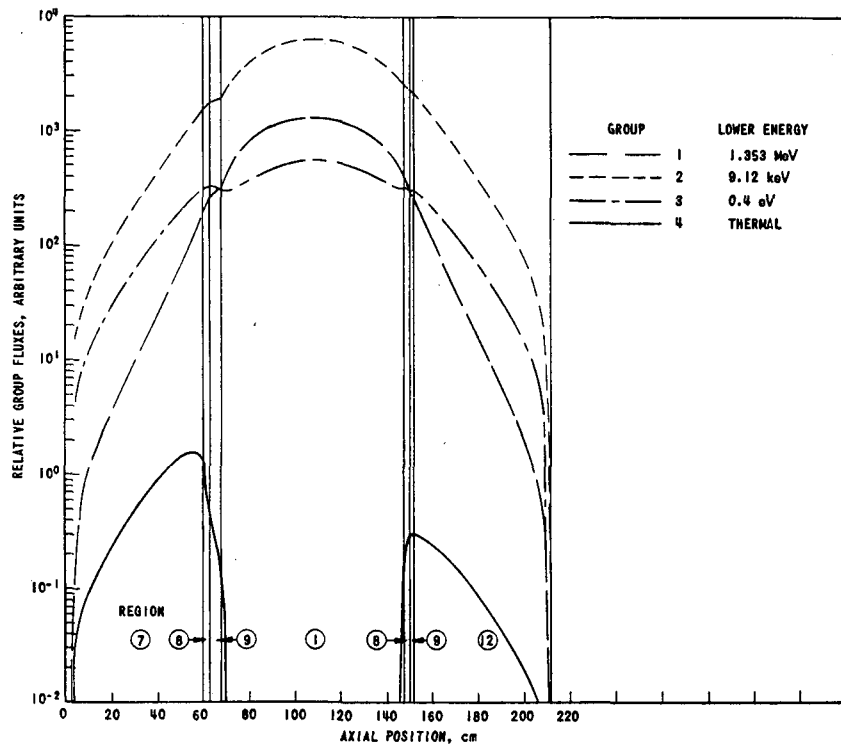


Fig. 17  
Axial flux distribution at central axis.

The rather tight limits on  $\epsilon$  indicate that the quoted values cannot be seriously in error owing to use of the 2D results.

The influence of an assumed 0.635-cm stainless-steel separator on the neutron inventory was estimated using the calculated fluxes at radial position 40.0 cm (the radial outerbound of the separator). The neutron inventory in Table XIX includes the estimated effect of the steel-separator captures.

## RESULTS

### *Static characteristics*

The 13-group fluxes have been collapsed to the equivalent 4-group structure. Thus

$$\sum_{j=2}^6 \varphi_j = \Phi_2 \quad \text{and} \quad \sum_{j=7}^{12} \varphi_j = \Phi_3 .$$

The highest energy and thermal groups are the same in the 13- and 4-group structure. Fig. 15 gives the calculated radial 13-groups 1D flux distributions at the axial midplane compared with the 4-group, 2D results. The agreement is seen to be very good except for group 3. The 4-group thermal flux at the fast core-buffer interface is also seen to be higher than the 13-group thermal value.

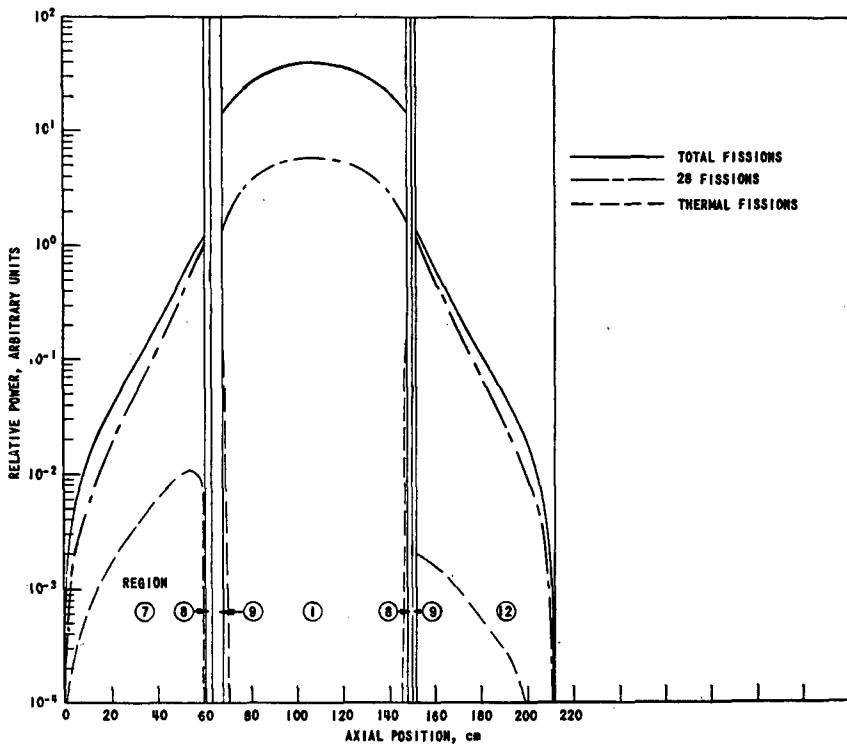


Fig. 18  
Axial power distribution at central axis.

This is reflected in the much higher power spike at the core outer edge seen in Fig. 16, which compares the power distributions for the two calculations. The thermal (and total) power in the thermal core is also higher in the 4-group calculation. These discrepancies may indicate that the resonance-capture considerations in the 4-group calculation need to be refined. In particular, the  $\Sigma_{3 \rightarrow 4}$  cross-section in the fast core appears to be too large, causing a depression of  $\Phi_3$  and an increase in  $\Phi_4$ .

The calculated critical plutonium masses for the 13-group, 1D and 4-group, 2D were respectively 222 kg and 242 kg. Not all of this 9% discrepancy need be due to inconsistencies in the cross-sections, since the assumed reflector savings of 15 cm at each end for the 1D calculation may be in error.

Figs. 17 and 18 show respectively the 4-group, 2D axial flux and power distributions at the central axis. Figs. 19 and 20 show the axial flux and power distributions at a radial position of 45.0 cm which is near the centre (radially) of the thermal core. The asymmetry seen in Figs. 17 and 18 is due to the difference in water content in the upper and lower fast axial blankets (regions 7 and 12) resulting from different steam conditions.

Table XVIII gives a summary of the 4-group, 2D results and Table XIX gives the neutron inventory as calculated using the 4-group, 2D problem. As seen in Table XIX, the water and zirconium contribute approximately equally to the parasitic losses in the water-cooled zones.

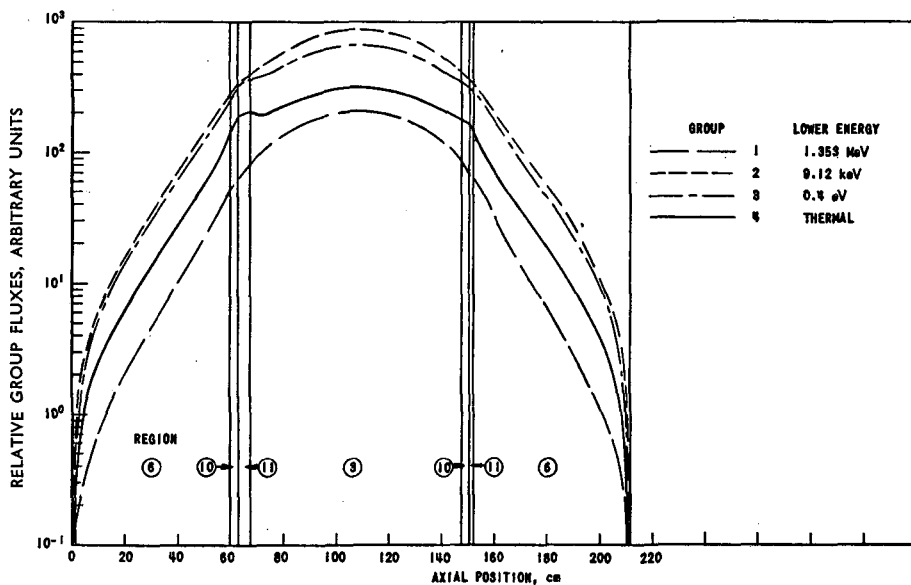


Fig. 19  
Axial flux distribution at 45.0 cm radial position.

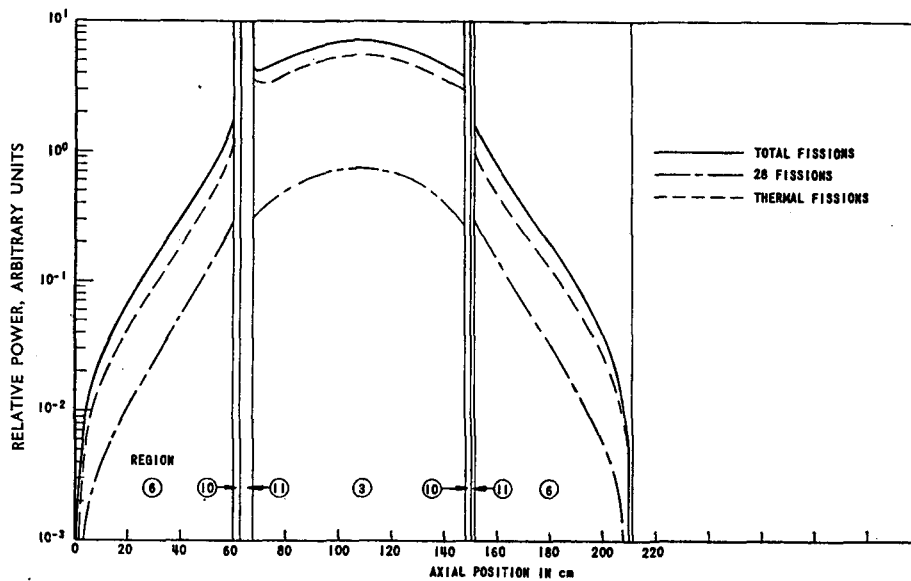


Fig. 20  
Axial power distribution at 45.0 cm radial position.

#### *Reactivity characteristics*

Table XX summarizes the reactivity characteristics of the system. The prompt-neutron lifetime as before was calculated by uniform insertion of a  $1/v$  poison.

TABLE XX  
REACTIVITY CHARACTERISTICS OF CONCEPTUAL DESIGN

Prompt neutron lifetime, ( $\mu$ s)	$\frac{\delta k}{k} \left( \frac{\delta M}{M} \right)$ fast core water	$\frac{\delta k}{k} \left( \frac{\delta M}{M} \right)$ thermal core water	Coupling parameters			
			$k_{F \leftarrow F}$	$k_{S \leftarrow S}$	$k_{F \leftarrow S}$	$k_{S \leftarrow F}$
4.5	0.028	0.019	0.930	0.257	0.391	0.133

The coupling parameters [1, 2] in Table XX were obtained using a 13-group, 1D calculation with a source iterative technique [2]. This method of calculation will of course yield only approximate values for the coupling parameters. Other investigations [2] have indicated discrepancies in some cases of as much as 30% compared with the rigorous values which would be obtained using a 2D calculation and adjoint-flux weighting.

The coupling parameters given in Table XX correspond to fast and thermal fractions of reactivity [2] of respectively 0.914 and 0.086.

#### CONCLUSIONS ON CONCEPTUAL DESIGN

The results given above indicate that the present concept exhibits a breeding ratio of the order of 1.4. Some of the factors contributing to this result as mentioned earlier in Section I are the large power fraction in the fast part of the coupled system, the small water density in the steam zones, and the relatively small water-volume ratio in the water-moderated thermal parts of the system.

The small water density of the steam zones results in a sufficiently hard spectrum, so that the plutonium capture-to-fission ratio ( $\alpha$ ) is still quite low. In particular, the spatially integrated fluxes for the fast core from the 13-group calculation yield an average plutonium- $\alpha$  for the fast core of 0.227. Fundamental mode calculations have shown that steam-cooled systems having a water density comparable to the present system yield spectra not very different from equivalent metal-cooled systems.

The water and zirconium captures in the water regions are rather small owing to the small water-volume fraction as compared, say, with a conventional light-water-moderated thermal reactor. This relatively low parasitic loss of course contributes to the high breeding ratio.

The advantage offered by using the present arrangement (a water-moderated thermal zone) as compared with using a solid moderator in the thermal zone [1] is that if a power excursion occurs, the water will increase its void content and tend to limit the excursion. This is indicated in Table XX by the thermal-core water reactivity coefficient.

The fast-core water reactivity coefficient (Table XX) calls attention to the necessity of considering the consequences of water addition to the portions of the system normally occupied by the steam coolant. Further detailed studies will be needed to verify the feasibility of start-up and shut-down performance with particular emphasis on the hazards associated with flooding and voiding of various regions.

## REFERENCES

- [1] AVERY, R., *Nucl. Sci. Engng* **3** (1958) 129.
- [2] AVERY, R. *et al.*, Proc. 2nd UN Int. Conf. PUAE **12** (1958) 151.
- [3] TOPPEL, B. J. and AVERY, R., *Trans. Amer. nucl. Soc.* **2** (1959) 149.
- [4] BUTLER, M. K. and COOK, J. M., ANL-5437.
- [5] BILODEAU, G. G. *et al.*, WAPD-TM-70 (1957).
- [6] HELLSTRAND, E., *J. appl. Phys.* **28** (1957) 1493.
- [7] GLASSTONE, S. and EDLUND, M. C., *The Elements of Nuclear Reactor Theory*, D. Van Nostrand, Inc., Princeton, N. J. (1952) 270.
- [8] DANCOFF, M. and GINSBURG, M., CP-2157 (1944).
- [9] CARLVIK, I. and PERSHAGEN, B., AE-16 (1959).
- [10] THIE, J., *Nucl. Sci. Engng* **5** (1959) 75.
- [11] WHEELER, J., unpublished code.
- [12] CARLVIK, I. and PERSHAGEN, B., AEFI-58 (1957).
- [13] Reactor Physics Constants, ANL-5800 (1958) 83.
- [14] *Ibid.*, p. 132.
- [15] WEINBERG, A. M. and WIGNER, E. P., *The Physical Theory of Neutron Chain Reactors*, The University of Chicago Press, Chicago (1958) 706.
- [16] *Ibid.*, p. 705.
- [17] *Ibid.*, p. 712.
- [18] *Ibid.*, p. 600.

INTERNATIONAL  
ATOMIC ENERGY AGENCY,  
VIENNA 1962

PRICE (A): North America: US \$9.00  
Elsewhere: Sch 109,-  
(54s.stg; NF 36 ; DM 31.50)